

**Antibacterial Secondary Metabolites from Four Endophytic
Fungi, *Eupenicillium* sp., *Diaporthe* sp.,
Fusarium decemcellulare and *Alternaria* sp.**

DISSERTATION

Submitted for the degree of Dr. rer. nat. (*rerum naturalium*)

To the
Department of Chemistry and Chemical Biology
Technische Universität Dortmund

by
Gang Li
2016

**Antibacterial Secondary Metabolites from Four Endophytic
Fungi, *Eupenicillium* sp., *Diaporthe* sp.,
Fusarium decemcellulare and *Alternaria* sp.**

APPROVED DISSERTATION

Doctoral Committee

Chairman: Prof. Dr. Daniel Rauh

Reviewers:

1. Prof. Dr. Dr. h.c. Michael Spiteller
2. Prof. Dr. Oliver Kayser

Date of defense examination: April 28, 2016

DECLARATION

I hereby declare that I have completed this thesis independently without any undue assistance. Wherever contributions of other are involved, every effort is made to indicate this clearly, with due reference to the literature(s), and acknowledgement of collaborative research and discussions.

This work was done under the guidance and supervision of Professor Dr. Dr. h.c. Michael Spiteller, at the Institute of Environmental Research (INFU), Department of Chemistry and Chemical Biology, Chair of Environmental Chemistry and Analytical Chemistry, TU Dortmund, Germany.

Gang Li

Dated: March, 2016

Place: Dortmund, Germany

In my capacity as supervisor of the candidate's thesis, I certify that the above statements are true to the best of my knowledge.

Prof. Dr. Dr. h.c. Michael Spiteller

Dated: March, 2016

Place: Dortmund, Germany

LIST OF ORIGINAL CONTRIBUTIONS

Parts of the work reported in this thesis have already been published, presented and/or are intended for publications.

Peer-reviewed articles

1. Li, G.; Kusari, S.; Kusari, P.; Kayser, O.; Spiteller, M. Endophytic *Diaporthe* sp. LG23 produces a potent antibacterial tetracyclic triterpenoid. *J. Nat. Prod.* **2015**, *78*, 2128–2132.
2. Li, G.; Kusari, S.; Lamshöft, M.; Schöffler, A.; Laatsch, H.; Spiteller, M. Antibacterial secondary metabolites from an endophytic fungus, *Eupenicillium* sp. LG41. *J. Nat. Prod.* **2014**, *77*, 2335–2341.
3. Li, G.; Kusari, S.; Spiteller, M. Natural products containing ‘decalin’ motif in microorganisms. *Nat. Prod. Rep.* **2014**, *31*, 1175–1201.

PRESENTATIONS

Poster presentations

1. Paraconic acids and alkylitaconic acids from endophytic *Eupenicillium* sp. LG41. At the 6th Junges Chemie Symposium Ruhr (JCS Ruhr); Universität Essen, Germany (17th September 2015).
2. *Eupenicillium* sp. LG41, an endophytic fungus harbored in the medicinal plant *Xanthium sibiricum* produces new antimicrobial compounds. At the 7th Tag der Chemie (Chemistry Day); the Faculty of Chemistry and Chemical Biology, TU Dortmund, Germany (7th February 2014).

ACKNOWLEDGEMENTS

It is a very pleasant opportunity to express my sincere gratitude and appreciation to all the people who supported me during my doctoral research program.

I would like to express my deepest gratitude to my supervisor **Prof. Dr. Dr. h.c. Michael Spiteller** (Institute of Environmental Research, INFU, Department of Chemistry and Chemical Biology, Chair of Environmental Chemistry and Analytical Chemistry, TU Dortmund) for his patient guidance and continuous support of my Ph.D. research. I wish to thank him for giving me the opportunity to study at INFU, Germany under his supervision, his kind assistance and efforts which enabled me to adapt a new culture and country. His immense knowledge, critical review, scientific discussions and kind guidance encouraged me to move forward and will remain thought-provoking for the rest of my life.

I would also like to express my sincere appreciation to my co-supervisor **Dr. Souvik Kusari** (INFU, Department of Chemistry and Chemical Biology, TU Dortmund) for his constructive criticisms, suggestions and support to ensure that my research was carried out efficiently. His scientific knowledge and motivation towards science inspired me to move forward.

I wish to express my gratitude to **Dr. Sebastian Zühlke** (INFU, Department of Chemistry and Chemical Biology, TU Dortmund) and **Dr. Marc Lamshöft** (Bayer Crop Science, Monheim, Germany; formerly at INFU), not only for their excellent comments and valuable suggestions, but also for their guidance in mass spectral interpretation. I thank **Dr. Ferdinand Mouafo Talontsi** (formerly at INFU, Department of Chemistry and Chemical Biology, TU Dortmund) for valuable discussions and assistance.

I gratefully acknowledge **Prof. Dr. Hartmut Laatsch** (Institute for Organic and Biomolecular Chemistry, Georg-August University) for the calculation of ECD and the critical review of my manuscript before we formally submitted to the respective journals. I would like to specially thank **Prof. Dr. Oliver Kayser** (Department of Biochemical and Chemical Engineering, Chair of Technical Biochemistry, TU Dortmund) for collaborating on the identification of fungi and bacteria. I am grateful to **Dr. Parijat Kusari** (Department of Biochemical and Chemical Engineering, TU Dortmund) and **Dr. Anja Schöffler** (Institute of Biotechnology and Drug Research, Kaiserslautern) for the identification of

fungi. I thank **Prof. Dr. Carsten Strohmann** and **Mr. Christopher Golz** for realization of the X-ray diffraction measurement.

I am thankful to all my colleagues at INFU for their constant support. I thank **Mr. Dennis Eckelmann**, **Mrs. Anke Bullach**, **Mr. Selahaddin Sezgin** for measuring the LC-MS and Maldi-MS. My sincere thanks to **Mr. James Oppong Kyekyeku**, **Ms. Evelyn Mireku**, and **Mr. Wen-Xuan Wang** for reading this thesis and their kind assistance. **Mr. Jean-Bosco Jouda** (formerly at INFU), and **Mr. Gervais Mouthé Happi** (formerly at INFU) are acknowledged for their generous assistance. I wish to thank **Mr. Ulrich Schoppe**, **Mrs. Cornelia Stolle**, **Mrs. Gabriele Hardes**, and **Mr. Jürgen Jünemann** for technical assistance for my work. I am grateful to **Mrs. Brigitte Apitius** for her suggestions which were invaluable for my cultural adaptation. I also thank my friend **Ms. Zongyi Chen** for kind support.

I gratefully acknowledge the **China Scholarship Council** (CSC) for a doctoral fellowship. I am grateful to the **Ministry of Innovation, Science, Research and Technology of the State of North Rhine-Westphalia**, Germany and the **German Research Foundation** (DFG) for funding a high-resolution mass spectrometer.

I express my deep thanks to **my family** for their unconditional support and love.

Table of Contents

		Page
I	Abstract	X
II	Zusammenfassung	XII
Chapter 1	INTRODUCTION	1
1.1	Antibiotics-state of the art	2
1.1.1	Antibiotic resistance	2
1.1.2	Discovery of antibiotics	2
1.1.3	Antibiotics-future challenge	7
1.1.4	Global strategy	7
1.2	Endophytes	8
1.2.1	Endophytic microorganisms	8
1.2.2	The origin of endophytes	9
1.2.3	The evolution and biodiversity of endophytes	9
1.2.4	Rationale for plant selection	10
1.2.5	Rationale for bioprospecting of endophytes for antibiotics	12
Chapter 2	AIMS AND OBJECTIVES	13
Chapter 3	MATERIALS AND METHODS	15
3.1	Collection of plant samples	16
3.2	Isolation, cultivation and storage of endophytic isolates	16
3.3	Pre-screening, selection of fungi and large-scale fermentation	18
3.4	Identification of selected endophytic fungi	19
3.5	Fungal extraction	20
3.6	Isolation and purification of secondary metabolites	20
3.6.1	Chromatography	23
3.6.1.1	Thin layer chromatography	23
3.6.1.2	Column chromatography	24

3.6.2	LC-MS	25
3.7	Structural elucidation	26
3.7.1	Determination of planar structure and relative configuration	26
3.7.1.1	LC-MS	26
3.7.1.2	NMR	26
3.7.1.3	¹³ C NMR calculation	26
3.7.1.4	X-ray diffraction study	27
3.7.1.5	Other methods	27
3.7.2	Determination of absolute configuration	27
3.7.2.1	Optical rotation and CD	27
3.7.2.2	ECD and ORD calculations	28
3.7.2.3	Marfey's method	29
3.7.2.4	X-ray diffraction study	30
3.8	Maldi-MS	31
3.9	Semi-synthesis for paraconic acids	31
3.9.1	Esterification	31
3.9.2	Thermodynamic equilibration	31
3.10	Bioassay	32
3.10.1	Compounds and microorganisms used for antimicrobial assay	32
3.10.2	Antibacterial assay	32
3.10.3	Cytotoxicity assay	33
Chapter 4	RESULTS AND DISCUSSION	34
4.1	Secondary metabolites isolated from <i>Eupenicillium</i> sp. LG41	35
4.1.1	Eujavanicol A (1 , known compound)	37
4.1.2	Eupenicinicol A (2 , new compound)	38
4.1.3	Eupenicinicol B (3 , new compound)	41
4.1.4	Eupenicinicol C (4 , new compound)	42
4.1.5	Eupenicinicol D (5 , new compound)	44
4.1.6	Eupenicinicol E (6 , new compound)	47

4.1.7	Eupenicisirenin A (7 , new compound)	48
4.1.8	Eupenicisirenin B (8 , new compound)	50
4.1.9	Xanthomegnin (9 , known compound)	51
4.1.10	7'- <i>O</i> -Desmethyl-viomellein (10 , new compound)	53
4.1.11	Viridicatumtoxin (11 , known compound)	54
4.1.12	(2 <i>S</i> ,3 <i>R</i> ,4 <i>S</i>)-4-Methyl-5-oxo-2-pentyl-tetrahydro-furan-3-carboxylic acid (12 , new natural product)	56
4.1.13	(2 <i>S</i> ,3 <i>R</i> ,4 <i>S</i>)-4-Methyl-5-oxo-2-pentyl-tetrahydro-furan-3-carboxylic acid methyl ester (13 , semi-synthetic compound)	58
4.1.14	(2 <i>R</i> ,3 <i>R</i> ,4 <i>S</i>)-4-Methyl-5-oxo-2-pentyl-tetrahydro-furan-3-carboxylic acid (14 , new natural product)	59
4.1.15	(2 <i>R</i> ,3 <i>R</i> ,4 <i>S</i>)-4-Methyl-5-oxo-2-pentyl-tetrahydro-furan-3-carboxylic acid methyl ester (15 , semi-synthetic compound)	60
4.1.16	(2 <i>S</i> ,3 <i>R</i> ,4 <i>R</i>)-4-Methyl-5-oxo-2-pentyl-tetrahydro-furan-3-carboxylic acid (16 , new natural product)	61
4.1.17	(2 <i>S</i> ,3 <i>R</i> ,4 <i>R</i>)-4-Methyl-5-oxo-2-pentyl-tetrahydro-furan-3-carboxylic acid methyl ester (17 , semi-synthetic compound)	62
4.1.18	(2 <i>R</i> ,3 <i>S</i> ,4 <i>S</i>)-4-Methyl-5-oxo-2-pentyl-tetrahydro-furan-3-carboxylic acid methyl ester (18 , semi-synthetic compound)	63
4.1.19	(2 <i>S</i>)-2,5-Dihydro-4-methyl-5-oxo-2-pentyl-furan-3-carboxylic acid (Striatisorolide A, 19 , known compound)	65
4.1.20	(2 <i>S</i>)-2,5-Dihydro-4-methyl-5-oxo-2-pentyl-furan-3-carboxylic acid methyl ester (20 , semi-synthetic compound)	66
4.1.21	(2 <i>S</i>)-Hexylitaconic acid (21 , known compound)	67
4.1.22	(2 <i>R</i>)-Hexylitaconic acid (22 , known compound)	68
4.1.23	(2 <i>S</i>)-Hexylitaconic acid mono methyl ester (23 , known compound)	68
4.1.24	(2 <i>S</i>)-Butylitaconic acid (24 , known compound)	69
4.1.25	Cyclo (N ^δ -(α,α -dimethylallyl)-L-Trp-6a'-(α,α -dimethylallyl)-L-Trp) (25 , known compound)	70

4.1.26	7-Hydroxy-2-[2-hydroxypropyl]-5-methyl-4 <i>H</i> -1-benzopyran-4-one (26 , known compound)	72
4.1.27	2-Furancarboxylic acid (27 , known compound)	73
4.2	Secondary metabolites isolated from <i>Diaporthe</i> sp. LG23	74
4.2.1	19-Nor-lanosta-5(10),6,8,24-tetraene-1 α ,3 β ,12 β ,22 <i>S</i> -tetraol (28 , new compound)	75
4.2.2	Ergosta-5,7,22-trienol (29 , known compound)	78
4.2.3	3 β ,5 α ,9 α -Trihydroxy-(22 <i>E</i> ,24 <i>R</i>)-ergosta-7,22-dien-6-one (30 , known compound)	79
4.2.4	3 β ,5 α ,9 α ,14 α -Tetrahydroxy-(22 <i>E</i> ,24 <i>R</i>)-ergosta-7,22-dien-6-one (31 , known compound)	80
4.2.5	(22 <i>E</i> ,24 <i>R</i>)-Ergosta-7,9(11),22-triene-3 β ,5 α ,6 α -triol (32 , known compound)	82
4.2.6	Chaxine C (33 , known compound)	84
4.2.7	Demethylcisterol A ₃ (34 , known compound)	86
4.2.8	Volemolide (35 , known compound)	87
4.2.9	4-Hydroxybenzaldehyde (36 , known compound)	88
4.2.10	1 <i>H</i> -indole-3-carbaldehyde (3-formylindole) (37 , known compound)	89
4.2.11	Uridine (38 , known compound)	90
4.2.12	2-Acetyl-7-methoxy-4,6-dimethyl-1 <i>H</i> -isoindol-1-one (39 , new compound)	91
4.3	Secondary metabolites isolated from <i>Fusarium decemcellulare</i> LG53	93
4.3.1	Cyclo-(_L -Leu- _L -Leu- _D -Leu- _L -Leu- _L -Ile) (40 , new compound)	94
4.3.2	Cyclo-(_L -Leu- _L -Leu- _D -Leu- _L -Leu- _L -Val) (41 , new compound)	96
4.3.3	Cyclo-(_L -Leu- _L -Leu- _D -Leu- _L -Leu- _L -Leu) (42 , new compound)	99
4.3.4	Fusaristatin A (43 , known compound)	101
4.3.5	Fusaristatin C (44 , new compound)	102
4.3.6	Nocapyrone S (45 , new compound)	103
4.3.7	Norlichexanthone (46 , known compound)	104
4.3.8	Chaxine B (47 , known compound)	105
4.4	Secondary metabolites isolated from <i>Alternaria</i> sp. LG19	107
4.4.1	Alternarienonic acid (48 , known compound)	108

4.4.2	(-)-(2 <i>R</i> ,3 <i>R</i> ,4 <i>aR</i>)-Altenuene (49 , known compound)	109
4.4.3	Isoaltenuene (50 , known compound)	111
4.4.4	Alternariol (51 , known compound)	112
4.4.5	Altertoxin I (52 , known compound)	112
4.4.6	Isoochracinic acid (53 , known compound)	114
4.4.7	(2 <i>E</i>)-Fumaric acid (54 , known compound)	115
4.5	Structural character and proposed biosynthetic pathways	115
4.5.1	Decalin-containing compounds (1–6)	115
4.5.2	Sirenin derivatives (7 and 8)	116
4.5.3	Pigments (9–11)	117
4.5.4	Paraconic acids (12 , 14 , 16 , and 19) and alkylitaconic acids (21–23)	118
4.5.5	The tetracyclic triterpenoid (28) and steroids (29–35)	119
4.5.6	Cyclic pentapeptides (40–42) and cyclic lipopeptides (43 and 44)	121
4.5.7	Alternaria mycotoxins (49–51)	121
4.6	Biological activities	122
4.6.1	Antibacterial activity	122
4.6.1.1	Compounds isolated from <i>Eupenicillium</i> sp. LG41	122
4.6.1.1.1	Decalin-containing compounds (1–5)	123
4.6.1.1.2	Sirenin derivatives (7 and 8) and pigment (9)	124
4.6.1.1.3	Paraconic acids (12–20) and alkylitaconic acids (21–24)	124
4.6.1.2	Compounds isolated from <i>Diaporthe</i> sp. LG23	126
4.6.1.3	Compounds isolated from <i>F. decemcellulare</i> LG53	127
4.6.2	Cytotoxicity	128
4.7	Possible ecological role of endophyte	129
4.8	Discussion	132
Chapter 5	REFERENCES	136
Appendix A	MS and NMR spectra and additional figures	153
Appendix B	List of abbreviations	253
Appendix C	Curriculum vitae	257

Abstract

Endophytes are microorganisms that colonize living, internal tissues of host plants for at least a part of their life cycle without causing any immediate, visible manifestation of disease. Endophytic microorganisms as a promising source of antibacterial natural products have attracted considerable attention. The main objective of this study was isolation, identification and antibacterial evaluation of secondary metabolites from endophytic fungi harbored in Chinese medicinal plants *Xanthium sibiricum*, *Mahonia fortunei*, and *Lonicera japonica*, which have been used in Traditional Chinese Medicine (TCM) for treating bacterial infection-related ailments.

An endophyte, *Eupenicillium* sp. LG41 was isolated from the root of *X. sibiricum*. Twenty-two secondary metabolites including six decalin motif-containing compounds (five new) (**1–6**), two new sirenin derivatives (**7** and **8**), three pigments (one new) (**9–11**), eight paraconic acids and alkylitaconic acids (three new natural products) (**12, 14, 16, 19, and 21–24**), and three other known compounds (**25–27**), were isolated from the rice, PDB or modified PDB medium using the OSMAC approach. Four methylated derivatives (**13, 15, 17, and 20**) and an isomerization product (**18**) of paraconic acids were obtained for structure-activity relationship (SAR) analysis.

The endophytic fungus *Diaporthe* sp. LG23 which was isolated from the leaves of *M. fortunei* collected from Shanghai, China, produced twelve metabolites including a novel tetracyclic triterpenoid with an aromatic B-ring system (**28**), seven biosynthetically related known steroids (**29–35**), together with four aromatic or glycosylated compounds (one new) (**36–39**). Further isolation and identification of endophytic fungi from *M. fortunei* (stem) collected from a different location, Guangdong, China, afforded an endophyte, *Fusarium decemcellulare* LG53. Chemical investigation led to the identification of eight compounds: three new cyclic pentapeptides (**40–42**), two cyclic lipopeptides (one new) (**43** and **44**), a new pyrone derivative (**45**), a known xanthone derivative (**46**), and a reported triterpenoid (**47**).

Alternaria sp. LG19 was derived from the leaves of *L. japonica*. It was discovered to produce two aromatic metabolites (**48** and **53**), four well-known *Alternaria* mycotoxins including altenuene (**49**), isoaltenuene (**50**), alternariol (**51**) and altertoxin I (**52**), as well as a dicarboxylic acid (**54**).

Altogether, forty-nine compounds were isolated from the above four endophytic fungi and five semi-synthetic derivatives were experimentally produced. Among the isolated compounds, fifteen compounds have new structures and three are new natural products which were reported as synthetic products in the literature. Their planar and relative structures were determined by the interpretation of spectroscopic data, such as IR, UV, HRMSⁿ and NMR, and/or the single crystal X-ray diffraction study, and/or ¹³C NMR calculation. Their absolute configurations were deduced by one or more of following methods, ECD and optical rotation data, ECD and ORD calculations, Marfey's method, and the single crystal X-ray diffraction study with a Cu-K α radiation.

The antibacterial efficacies of new compounds were investigated against several Gram-positive and Gram-negative bacteria obtained as clinical or environmental strains. For decalin-containing metabolites, eupenicinicol B (**3**) had the same efficacy as that of gentamicin against clinically relevant bacterium *Staphylococcus aureus* at the concentration of 1.0 $\mu\text{g/mL}$, while eupenicinicol D (**5**) was more active than **3** with an MIC value of 0.1 $\mu\text{g/mL}$. These data support the notion that altering the substitution at C-11 could drastically increase the inhibitory activity. The paraconic acid (2*S*,3*R*,4*S*)-4-methyl-5-oxo-2-pentyl-tetrahydro-furan-3-carboxylic acid (**12**) was discovered to only inhibit tested *Acinetobacter* spp., especially the multi-drug resistant strain *Acinetobacter baumannii*. The above data indicated a genus-specific antibacterial compound with a preferred stereochemical configuration. The novel tetracyclic triterpenoid 19-nor-lanosta-5(10),6,8,24-tetraene-1 α ,3 β ,12 β ,22*S*-tetraol (**28**) showed pronounced antibacterial efficacy against all the tested organisms, especially against the clinical isolates *Streptococcus pyogenes* and *Pseudomonas aeruginosa*. **5** and **28** also demonstrated marked cytotoxicity against human acute monocytic leukemia cell line (THP-1), while **12** exhibited no cytotoxic activity.

The results reported in this thesis provide several antibacterial secondary metabolites worthy of further investigation, especially the paraconic acid (**12**, termed pacbactin), underlining the potential of endophytic fungi as a source of diverse antibiotics.

Zusammenfassung

Endophyten sind Mikroorganismen, die lebende innere Gewebe von Wirtspflanzen für zumindest einen Teil des Lebenszyklus besiedeln, ohne sichtbare Erkrankungen auszulösen. Endophytische Mikroorganismen haben beträchtliche Aufmerksamkeit als eine vielversprechende Quelle für antibakterielle Naturprodukte erregt. Das Ziel dieser Forschung war die Isolierung, Identifizierung, und antibakterielle Bewertung der Sekundärmetaboliten endophytischer Pilze aus den chinesischen Heilpflanzen *Xanthium sibiricum*, *Mahonia fortunei* und *Lonicera japonica*, welche in der traditionellen chinesischen Medizin (TCM) zur Behandlung von bakteriellen Infektionen verwendet werden.

Ein Endophyt, *Eupenicillium* sp. LG41 wurde aus der Wurzel von *X. sibiricum* isoliert. 22 Sekundärmetaboliten, darunter sechs Decalin Motiv-enthaltende Verbindungen (fünf neu) (**1–6**), zwei neue Sirenin-Derivate (**7** und **8**), drei Pigmente (ein neues) (**9–11**), acht Paraconsäuren und Alkylitaconsäuren (drei neue Naturprodukte) (**12, 14, 16, 19** und **21–24**), und drei weitere bekannte Verbindungen (**25–27**), wurden aus Kultivierung mit Reis, PDB oder modifiziertem PDB Medium unter Verwendung des OSMAC-Ansatzes isoliert. Vier methylierte Derivate (**13, 15, 17** und **20**) und ein Isomerisierungsprodukt (**18**) der Paraconsäure wurden zur Struktur-Aktivitäts-Beziehungs (SAR) - Analyse erhalten.

Der endophytische Pilz *Diaporthe* sp. LG23, der aus den Blättern von *M. fortunei* aus Shanghai, China isoliert wurde, produzierte zwölf Metaboliten einschließlich eines neuartigen tetracyclischen Triterpens mit einem aromatischen B-Ringsystem (**28**), sieben biosynthetisch verwandte und bekannte Steroide (**29–35**) zusammen mit vier aromatischen oder glycosylierten Verbindungen (eine neu) (**36–39**). Des Weiteren wurde der endophytische Pilz *Fusarium decemcellulare* LG53 aus *M. fortunei* (Stamm) von Guangdong, China isoliert. Chemische Untersuchungen führten zur Identifizierung von acht Verbindungen: drei neue cyclische Pentapeptide (**40–42**), zwei zyklische Lipopeptide (eins neu) (**43** und **44**), ein neues Pyron-Derivat (**45**), ein bekanntes Xanthon-Derivat (**46**) und ein Triterpenoid (**47**).

Alternaria sp. LG19 wurde aus den Blättern von *L. japonica* isoliert. Es wurde gezeigt, dass dieser Endophyt zwei aromatische Metaboliten (**48** und **53**), vier bekannte *Alternaria*-Mykotoxine

einschließlich Altenuen (**49**), Isoaltenuen (**50**), Alternariol (**51**) und Alvertoxin I (**52**), sowie eine Dicarbonsäure produziert (**54**).

Insgesamt wurden 49 Verbindungen aus den genannten endophytischen Pilzen isoliert und fünf halbsynthetische Derivate experimentell hergestellt. Unter den isolierten Verbindungen besitzen 15 Verbindungen neue Strukturen und drei Stoffe konnten als Naturprodukte identifiziert werden, die bisher als synthetische Produkte in der Literatur berichtet wurden. Ihre relativen Strukturen wurden durch die Auswertung spektroskopischer Daten, wie beispielsweise IR, UV, NMR und HRMSⁿ, Einkristall-Röntgenstrukturanalyse und/oder ¹³C-NMR-Berechnung bestimmt. Ihre absoluten Konfigurationen wurden durch eine oder mehrere Verfahren wie ECD und Drehwinkel, ECD und ORD Berechnungen, Marfey-Analyse und Einkristall-Röntgenbeugungsanalyse mit Cu-K α -Strahlung bestimmt.

Die antibakterielle Aktivität der neuen Verbindungen wurden für verschiedene Gram-positive und Gram-negative Bakterien die als klinische oder Wild-Stämme gelten untersucht. Der Decalin-haltige Metabolit Eupenicinicol B (**3**) hatte die gleiche Wirkung wie Gentamicin gegen das Bakterium *Staphylococcus aureus* in einer Konzentration von 1,0 $\mu\text{g/mL}$, während Eupenicinicol D (**5**) mit einem MIC-Wert von 0,1 $\mu\text{g/mL}$ aktiver war als **3**. Diese Daten unterstützen die Vorstellung, dass eine Änderung der Substitution an C-11 die inhibitorische Aktivität drastisch erhöht. Die Paraconsäure (2*S*,3*R*,4*S*)-4-methyl-5-oxo-2-pentyl-tetrahydro-furan-3-carbonsäure (**12**) konnte *Acinetobacter spp.*, insbesondere den resistenten Stamm *Acinetobacter baumannii*, hemmen. Die Ergebnisse zeigen eine gattungsspezifische antibakterielle Verbindung mit einer bevorzugten stereochemischen Konfiguration. Das neuartige tetracyclische Triterpenoid 19-Nor-Lanostan-5(10),6,8,24-tetraen-1 α ,3 β ,12 β ,22*S*-Tetraol (**28**) zeigte eine ausgeprägte antibakterielle Wirksamkeit gegen alle getesteten Organismen, vor allem gegen die klinisch-relevanten Stämme *Streptococcus pyogenes* und *Pseudomonas aeruginosa*. Die Stoffe **5** und **28** zeigten zusätzlich deutliche Zytotoxizität gegen die menschliche akute monozytäre Leukämie-Zelllinie (THP-1), während **12** keine zytotoxische Aktivität besaß.

Die in dieser Arbeit berichteten und strukturell aufgeklärten antibakteriellen Sekundärmetaboliten sollten weitergehend untersucht werden. Insbesondere die Paraconsäure (**12**, pacbactin) unterstreicht das Potential endophytischer Pilze als Quelle für Antibiotika.

Chapter 1:
INTRODUCTION

1.1 Antibiotics-state of the art

1.1.1 Antibiotic resistance

Antibiotics (also called antibacterials) belong to a class of antimicrobial agents and are employed to prevent or treat a bacterial infection by either killing or inhibiting the growth of bacteria (Littmann, 2014). Antibiotic resistance is the continued growth of a microorganism in the presence of antibiotics with cytotoxic concentrations that was originally effective for treatment of infections caused by it (Wright, 2007; WHO, 2014). Antibiotics have been present in the environment for millennia and are not a human invention (MacDougall and Polk, 2005). Their role is to secure the ecological niche of producers teeming with competitors and expose other species in the selection of resistance (MacDougall and Polk 2005). Antibiotic production and emerging antibiotic resistance are important to stabilize microbial communities, leading to microbial biodiversity (Kelsic *et al.*, 2015). In certain environments, bio-active molecules from fungi, plants and other microorganisms enabled bacteria to develop highly sophisticated series of counter-measures to avoid toxic compounds (Wright and Poinar, 2012). The important genes encoding resistance to several clinically useful classes of antibiotics such as β -lactam, tetracycline, glycopeptide and vancomycin are common in metagenomes of ancient sediments or samples and predate our use of antibiotics (D'Costa *et al.*, 2011). The antibiotic resistome, a collection of all the antibiotic resistance genes and their precursors in pathogenic and non-pathogenic bacteria, strongly revealed the extensive diversity of resistance (Wright, 2007; D'Costa *et al.*, 2006). Therefore, antibiotic resistance is an ancient and natural phenomenon widespread in the environment (D'Costa *et al.*, 2011; Kelsic *et al.*, 2015; Blair *et al.*, 2015).

1.1.2 Discovery of antibiotics

Most antibiotics introduced into human medicine were derived from antibiotic-producing cultivable microorganisms (Blair *et al.*, 2015). Microorganisms are occupying most of living and nonliving niches on earth (Sánchez and Olson, 2005). It has to be noted that less than 1% of bacterial species and less than 5% of fungal species are currently known, indicating that millions of microbial species are the largely untapped resource and remain to be discovered (Gunatilaka, 2006). In addition, uncultured bacteria account for approximately 99% of all species in the external environment (Ling *et al.*, 2015).

Following the discovery of best-known antibiotic penicillin from the fungus *Penicillium notatum* in 1928 by Alexander Fleming (Tan and Tatsumura, 2015) (Table 1.1.2.1 and Figure 1.1.2.2), the golden

era of discovering and using new antibiotics really began in the 1940s (Lewis, 2012). Most currently used antibacterials are derived from a natural product lead (Table 1.1.2.1 and Figure 1.1.2.2) (Butler, 2005; Butler, 2008; Torok *et al.*, 2009; Butler *et al.*, 2013; Butler *et al.*, 2014). This implies that most antibiotics can be naturally occurring metabolites (even produced synthetically for the market) (natural products, NP), semi-synthetic compounds from a natural product template (SS NP), or synthetic compounds inspired from a natural product template (NP-derived) (Butler *et al.*, 2014). “S” is totally synthetic drug. By the end of year 2014 (Butler *et al.*, 2014; Newman and Cragg, 2016), there were around 20 antibacterial classes in which 15 (75%) are derived from a NP lead (NP, SS NP or NP-derived) while 5 (25 %) are synthetically derived (Table 1.1.2.1). There are also a surprising number of representative antibiotics which are unmodified for approval as drugs (Table 1.1.2.1). Moreover, 12 (80 %) of 15 NP-derived antibiotic lead compounds (by class) were isolated from soil-dwelling actinomycetes and 3 (20 %) from fungi.

An excellent updated review on natural products as sources of new drugs from 1981 to 2014, including antibacterial drugs from 1/1/1981 to 12/31/2014, was published by Newman and Cragg (2016). During this time period, 113 small molecules were approved as antibacterial drugs with 11 unaltered natural products (corresponding to NP) and 71 natural product derivatives (corresponding to SS NP) accounting for just over 72% of them (Figure 1.1.2.1) (Newman and Cragg, 2016). Therefore, the influence of natural product structures on antibiotic discovery is quite marked.

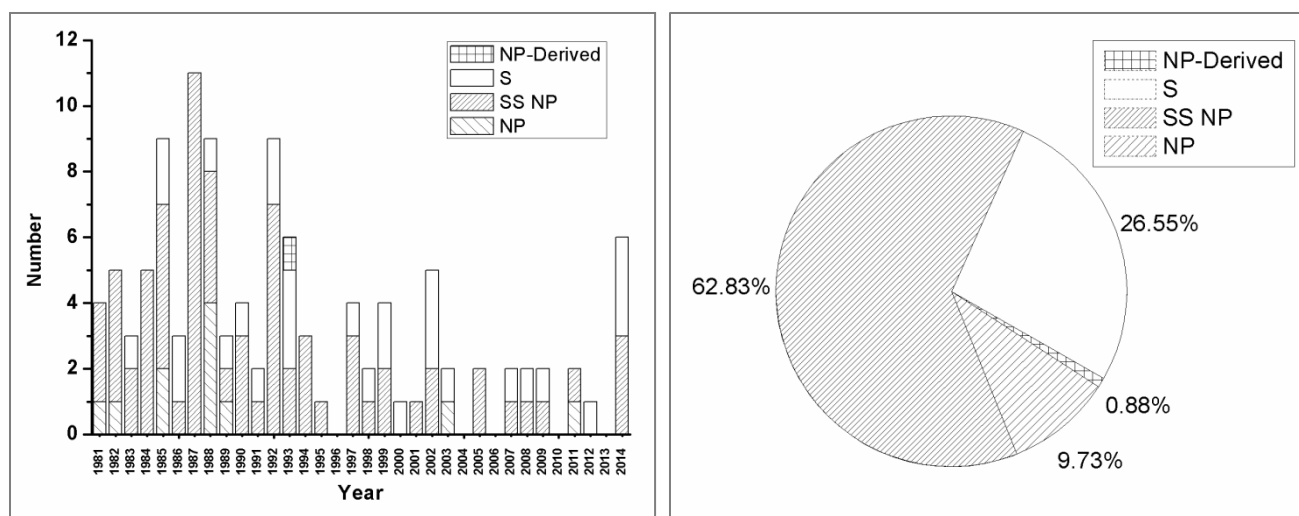


Figure 1.1.2.1 All new approved antibiotics 1981–2014 (bar graph, left; pie chart, right).

Table 1.1.2.1 Timeline of the introduction of main antibiotic classes and related antibiotics 1935-2014 (Butler, 2005; Butler, 2008; Torok *et al.*, 2009; Butler *et al.*, 2013; Butler *et al.*, 2014; Newman and Cragg, 2016).

No.	Year introduced	Drug class	Year discovered	Representative drug name	Classification	Natural product lead source
1	1935	Sulfonamide	1932	Prontosil	S	
2	1942	β -Lactam	1928	Penicillin	NP	<i>Penicillium notatum</i> (fungus)
3	1944	Aminoglycosides	1943	Streptomycin	NP	<i>Streptomyces griseus</i> (soil bacterium)
4	1948	Tetracyclines	1940s	Chlortetracycline (Aureomycin)	NP	<i>Streptomyces aureofaciens</i> (soil bacterium) (Nelson and Levy, 2011)
5	1949	Chloramphenicol	1947	Chloramphenicol	NP	<i>Streptomyces venezuelae</i> (soil bacterium)
6	1952	Macrolides	1949	Erythromycin	NP	<i>Saccharopolyspora erythraea</i> (soil bacterium)
7	1955	Streptogramins	1953	Virginiamycin	NP	<i>Streptomyces graminofaciens</i> (Charney <i>et al.</i> , 1953) (Walsh and Wright, 2005)
8	1958	Glycopeptides	1952	Vancomycin	NP	<i>Streptomyces orientalis</i> (soil bacterium) (Levine, 2006)
9	1959	5-Nitroimidazole	1950s	Metronidazole	NP-derived	Inspired from azomycin (2-nitroimidazole, 1953) isolated from an unidentified streptomyces (Dougherty and Pucci, 2012)
10	1964	Cephalosporins	1945	Cephalosporin	SS NP	Most cephalosporins are semi-synthetic derivatives of cephalosporin C from fungi of genus <i>Acremonium</i> (known as <i>Cephalosporium</i>).
11	1965	Lincosamides	1962	Lincomycin	NP	<i>Streptomyces lincolnensis</i> (soil bacterium) (de Haen, 1965; Argoudelis <i>et al.</i> , 1969)
12	1967	Quinolone	1960s	Ciprofloxacin (1987 introduced)	S	Nalidixic acid is the first member (Dougherty and Pucci, 2012)
13	1968	Rifamycins	1959	Rifampicin	SS NP	<i>Amycolatopsis mediterranei</i> (soil bacterium) (Sensi, 1983; Floss and Yu, 2005)
14	1968	Trimethoprim	1960s	Trimethoprim	S	
15	1985	Carbapenem	1976-1979	Imipenem/cilastin	SS NP	Thienamycin as the lead compound from <i>Streptomyces cattleya</i> (soil bacterium)
16	2000	Oxazolidinone	1990s	Linezolid	S	
17	2003	Lipopeptides	1980s	Daptomycin	NP	<i>Streptomyces roseosporus</i> (soil bacterium)
18	2007	Pleuromutilin	1950	Retapamulin (for human) (Novak <i>et al.</i> , 2010)	SS NP	Pleuromutilin as the lead compound from fungus <i>Clitopilus passeckerianus</i> . Tiamulin (for animals, 1979); Valnemulin (for the animal, 1999).
19	2011	Tiacumicin	1975	Fidaxomicin (Tiacumicin B)	NP	<i>Dactyloporangium aurantiacum</i> (soil bacterium) (Erb and Zhu, 2013)
20	2012	Diarylquinoline	2005	Bedaquiline	S	

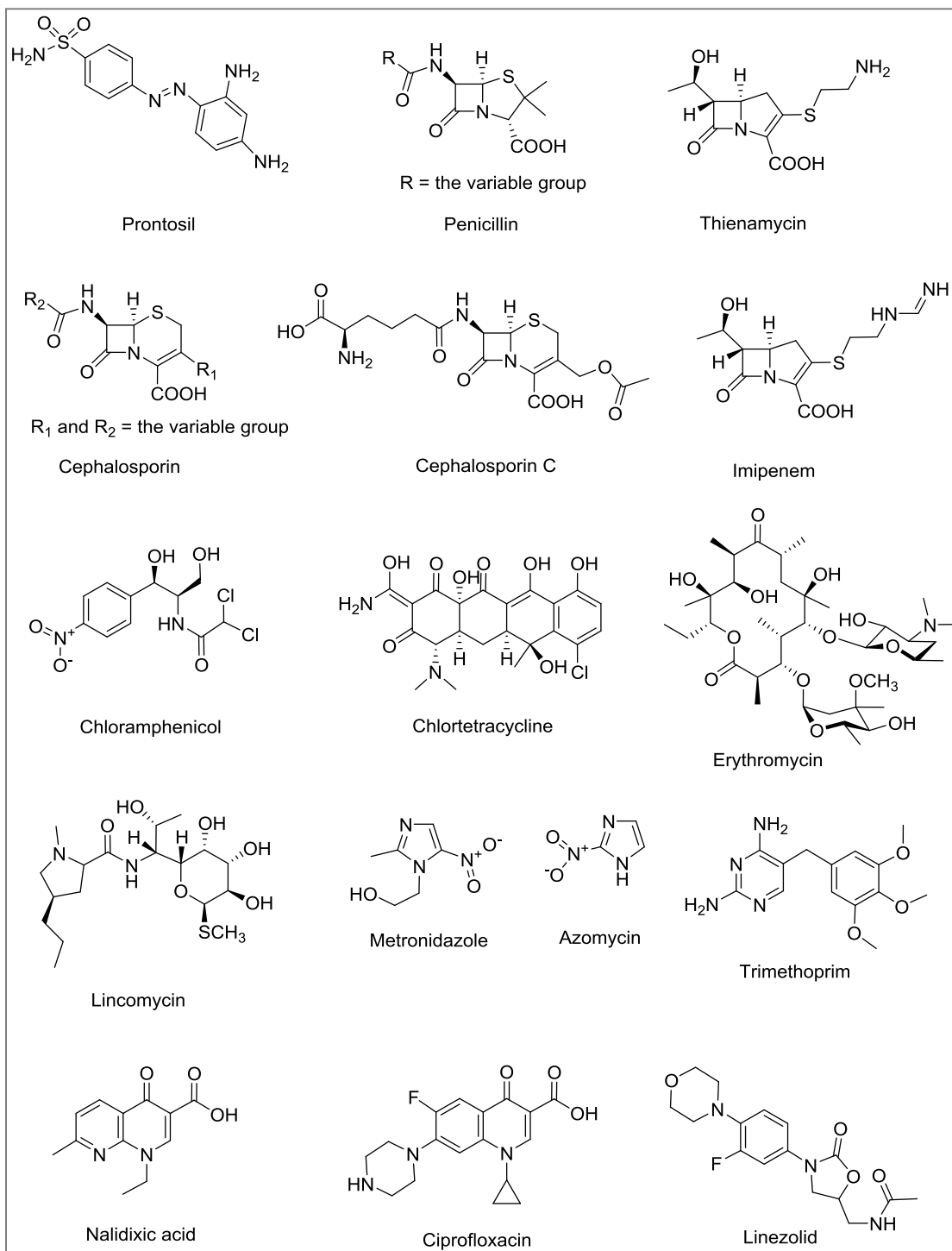


Figure 1.1.2.2 Structures of representative antibiotics as indicated in Table 1.1.3.1.

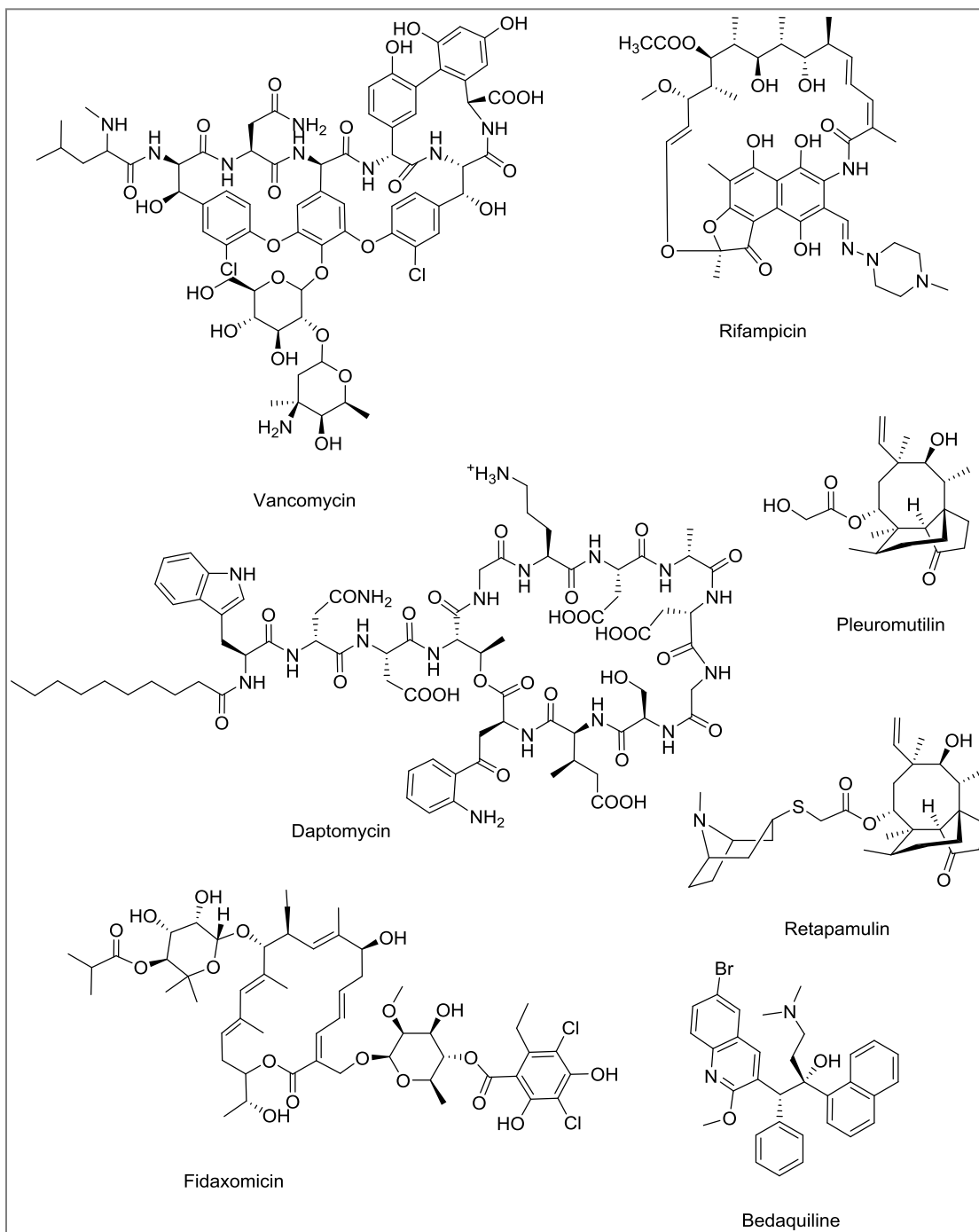


Figure 1.1.2.2 Continued.

1.1.3 Antibiotics-future challenge

As a result of the widespread use of antibiotics in human medicine, livestock or other usages, the evolutionary pressure for the emergence of antibiotic resistance is great (Blair *et al.*, 2015). Many bacteria which were previously susceptible to common or new antibiotics were reported to have acquired or developed resistance rapidly, even for antibiotics designed to evade the original mechanisms of resistance or synthesized agents (MacDougall and Polk 2005). When new antibiotics were introduced into clinical use over the past 70 years, bacteria adapted to their environment through developing resistance to newer antibiotics in the clinic, posing a major challenge in treating serious infections caused by these bacteria (Wright and Poinar, 2012; Alanis, 2005). More seriously, the indiscriminate and inappropriate use of antibacterial drugs in outpatient clinics, hospitalized patients, and animal husbandry, accelerated the emergence and selection of resistant strains. Poor sanitation and control practices enabled further emergence and spread of antibacterial resistance (Alanis, 2005; Aarestrup, 2012; Gilbert, 2012; Editor, 2013; Mole, 2013).

The threat posed by the spread of antibiotic resistance is enhanced by an alarming decline in the discovery and development of new classes of antibiotic with new biologically active pharmacophores (Editor, 2013; Butler *et al.*, 2014). There are only two new natural product-drug pharmacophores (deoxyactagardine B and PM060184) that were discovered in the last 10 years (Butler *et al.*, 2014). Considering the high cost during a decade or longer time from discovery of active molecules *in vitro* into the clinical use, as well as the broad and ancient resistome for rapid antibiotic resistance, many large pharmaceutical companies or institutes have abandoned research and development on antibiotics (Copper and Shlaes, 2011). As a result, only few new classes of antibiotics have been approved in the past 40 years (Table 1.1.3.1) (Copper and Shlaes, 2011). Finally, fewer and fewer antibiotics will remain broadly effective due to the failure to afford new drugs as quickly as their predecessors face with diverse resistance mechanisms and then lose efficacy (Carroll *et al.*, 2014; Liu *et al.*, 2016).

According to the first global report on antimicrobial resistance (AMR) released by World Health Organization (WHO, 2014), we are heading for a post-antibiotic era if the current rate of increase in antibiotic resistance continues without urgent action. As stated by WHO, in a post-antibiotic era far from being an apocalyptic fantasy, common infections and minor injuries can kill.

1.1.4 Global strategy

As antibiotic resistance is a global health crisis, it needs the global coordinated actions from

governments, companies, and academic institutions. First of all, a better framework for global surveillance of antibiotic resistance, better training about health care, and careful use of antibiotics to treat bacterial infections are crucial (Editor, 2013; WHO, 2014). More funding from governments (push) and more expertise and marketing reach from larger companies (pull) are also supportive (Copper and Shlaes, 2011). Furthermore, increasingly shared knowledge about mechanisms of resistance and their development is necessary to evaluate the potential for the emergence of resistance and facilitate the development of antibacterial molecules (Liu *et al.*, 2016). Fortunately, modern available technologies have promised us to understand the mechanisms behind the intrinsic resistance or acquiring resistance to antibiotics. Blair *et al.* (Blair *et al.*, 2015) summarized the mechanisms as three main groups: (1) the prevention of access to drug targets by minimizing the intracellular concentrations based on reduced permeability or increased efflux; (2) changes in the structure and protection of antibiotic targets by mutation or modification of targets; together with (3) the direct modification or inactivation of antibiotics through hydrolysis or addition of chemical groups to antibiotics. Moreover, concerning the antibiotic resistome and its ancient origin, Wright and Poinar (Wright and Poinar, 2012) provided several additional solutions: (1) identification of molecular targets and a systematic search for pre-existing countermeasures to develop semi-synthetic derivatives (also called generations of antibiotics) that avoid the proved resistance mechanisms; (2) synthesis of natural product-like molecules that have more penetrating ability and avoid efflux; and (3) combination use of antibiotics and/or bioactive molecules mimicking natural product complex in microbes. Finally, based on many antibacterial screening programs or available methods, global efforts are required to identify new drug pharmacophores and make them through pre-clinical drug development (Butler *et al.*, 2014). Natural products from largely untapped endophytes should be paid more attention and could be the resource of antibiotics with new pharmacophores (Newman and Cragg, 2016).

1.2 Endophytes

1.2.1 Endophytic microorganisms

Endophytes are microorganisms that colonize living, internal tissues of host plants for at least a part of their life cycle without causing any immediate, visible manifestation of disease (Stone *et al.*, 2000; Kusari *et al.*, 2012). This definition is widely accepted and broad enough to include virtually all microbes capable of occupying the intercellular spaces of leaves, twigs, stems, and roots of healthy

plants (Strobel and Long, 1998). These endophytic microbes can be divided into 11 major groups according to their plant organ source (Stone *et al.*, 2000; Bills *et al.*, 2004): (1) endophytic Clavicipitaceae; (2) fungal endophytes of dicots; (3) endophytic fungi; (4) other systemic fungal endophytes; (5) fungal endophytes of lichens; (6) endophytic fungi of bryophytes and ferns; (7) endophytic fungi of tree bark; (8) fungal endophytes of xylem; (9) fungal endophytes of root; (10) fungal endophytes of galls and cysts; (11) prokaryotic endophytes of plants (includes endophytic bacteria and actinomycetes) (Stone *et al.*, 2000; Bills *et al.*, 2004; Zhang *et al.*, 2006). As indicated by the above classification, diverse endophytic fungi, as the most frequently encountered endophytes, are ubiquitous and no study has yet reported the existence of a plant species without endophytes (Staniek *et al.*, 2008; Nisa *et al.*, 2015). Endophytes have attracted considerable attention from chemists and biologists owing to their ecological and biotechnological potential as depicted by the steady increase of publications in this field (Zhang *et al.*, 2006; Kharwar *et al.*, 2011; Kusari and Spiteller, 2011; Kusari *et al.*, 2012).

1.2.2 The origin of endophytes

The term ‘endophyte’ (Gr. *endon*, within; *phyton*, plant) was first introduced in a book by de Bary (1866). First reports regarding the presence of endophytic microbes (fungi) date back to the turn of the nineteenth and twentieth century when the regular presence of endophytic mycelium in carpels and seeds of asymptomatic plants was discovered (Guerin, 1898; Freeman, 1902; White *et al.*, 1993). Evidence of plant-associated microbes has been discovered in the fossilized tissues of stems and leaves (Taylor and Taylor, 2000; Redecker *et al.*, 2000), revealing endophyte-plant associations may have begun to evolve from the time higher plants first appeared on the earth (Strobel and Daisy, 2003). However, except for few studies, it was not until the end of the twentieth century when endophytes began to obtain more attention from chemists and biologists (Tan and Zou, 2001; Zhang *et al.*, 2006; Kusari and Spiteller, 2012).

1.2.3 The evolution and biodiversity of endophytes

Endophytes, residing in the plant tissues under a micro-environment, adapted to both biotic and abiotic selection pressures in their ecological niches over a long co-evolutionary period with hosts (Kusari *et al.*, 2013). Basic chemical communication strategies of endophytes with their host plants and with other endophytes (both fungi and bacteria) are summarized by Kusari *et al.* (2012) as follows: (1) plant-

endophyte interactions, (2) plant-endophyte interspecies crosstalk, and (3) endophyte-endophyte interspecies crosstalk. Through a long time communication, evolutionary adaptation of endophytes in plants to the complex environment enabled them to have a tremendous biosynthetic capability. There are approximately 300,000 different plant species inhabiting our planet and it can be expected that each individual one hosts a complex community of one to many endophytic microorganisms (Strobel and Daisy, 2003). The above biosynthetic capability over the co-evolutionary process as well as microbial biodiversity allowed the discovery of novel natural products with interesting biological activities. An overview of publications suggested that 51% of bioactive compounds isolated from fungal endophytes were previously unknown, compared to 38% from soil fungi (Kharwar *et al.*, 2011). Ecological aspects of endophytes (such as an antagonistic and mutualistic relationship), and endophytes as a potential source of discovery of bioactive metabolites for therapeutic agents have become the two major driving forces for better understanding and applicability of promising endophytic microorganisms (Kusari and Spiteller, 2012).

1.2.4 Rationale for plant selection

Since there are a great number of plant species, creative, imaginative and reasonable strategies should be applied to quickly narrow the search for endophytes which are novel at the genus, species or biotype level (Myers *et al.*, 2000; Strobel and Daisy, 2003). Further exploitation of these endophytes would provide the best opportunities for discovering novel bioactive secondary metabolites, and even associated plant natural products. Several reasonable methods and rational widely accepted for plant selection strategy are as follows (Strobel and Daisy, 2003; Kusari and Spiteller, 2012).

(1) Plants from distinct ecological niches, especially those with an uncommon biology, and possessing unusual strategies for subsistence are seriously considered (Strobel and Daisy, 2003). A representative case of such a plant is *Hypericum perforatum* with an uncommon biology (dark glands) (Onelli *et al.*, 2002). An endophytic fungus isolated from this plant was capable of producing plant metabolites hypericin and emodin (Kusari *et al.*, 2008; Kusari *et al.*, 2009).

(2) Plants which have an ethnobotanical history that is associated with specific practices or applications of interest (such as for treating bacterial infections) are seriously chosen (Strobel and Daisy, 2003). These plants could be used by indigenous people and are selected either via local literature or by direct touch with local people. Traditional Chinese medicine (TCM) is a system of ancient medical practice which has developed over thousands of years and plays an important role in the health maintenance of

the people in Asia (Cheung, 2011). Traditional medicinal plants are hence a source for potent endophytes producing pharmaceutical lead compounds, as is evidently supported by the increasing publications concerning bioactive metabolites from endophytes harbored in the Chinese medicinal plants (Tan and Zou, 2001; Zhang *et al.*, 2006; Miller *et al.*, 2012; Li *et al.*, 2014; Li *et al.*, 2015).

Xanthium sibiricum (Asteraceae) (Figure 1.2.4.1) could be mentioned here as a suitable example. This plant, as an important medicinal plant, has been used in TCM for decades (Kan *et al.*, 2011). *X. sibiricum* is commonly distributed in China, and its fruit (*Cang Er Zi*), leaves and roots have been utilized in TCM for treating several ailments, for example, fever and dysentery (Zhang *et al.*, 2006; Kan *et al.*, 2011). Earlier investigations of this plant have led to the isolation of sesquiterpene lactones, which are recognized as the chemical markers for *Xanthium* species (Zhang *et al.*, 2006; Li *et al.*, 2014). Another example to describe this rationale is the medicinal plant *Mahonia fortunei* (Berberidaceae) (Figure 1.2.4.1) endemic to China. *M. fortunei* (Chinese name “Shi da gong lao”), a heat-tolerant, pest-resistant plant, has been employed in TCM for treating pneumoconiosis, psoriasis and coughs, in addition to being a potent antimicrobial medicinal resource (Li *et al.*, 2007; Li *et al.*, 2015). *Lonicera japonica* (Caprifoliaceae) (Figure 1.2.4.1), as a further case, is mainly produced in eastern Asia and has been in use as traditional medicine in China for the treatment of fever and headache (Yu *et al.*, 2011; Choi *et al.*, 2007; Xiong *et al.*, 2013). The above three plants are related to bacterial infection-related ailments.



Figure 1.2.4.1 Three traditional Chinese medicinal plants: (a) *X. sibiricum* (b) *M. fortunei* (c) *L. japonica*.

An endophytic fungus isolated from *Camptotheca acuminata*, a plant used as Chinese traditional medicine for psoriasis, liver and stomach ailments and common cold (Sung *et al.*, 1998), had the

attractive capability of producing plant compounds camptothecin and analogs, which are important antineoplastic agents (Kusari *et al.*, 2009; Kusari *et al.*, 2011). The production of anticancer compound deoxypodophyllotoxin found in a medicinal plant, *Juniperus communis*, by an endophyte *Aspergillus fumigatus* in the host was also observed (Kusari *et al.*, 2009).

(3) Endemic and endangered plants that have an unusual longevity or have occupied a certain ancient land mass, are also more likely to harbor endophytes with active natural products than other plants (Strobel, 2004; Kusari and Spiteller, 2012). (4) Plants growing in areas of abundant biodiversity also have more possibility of containing endophytes with great biodiversity (Strobel, 2004; Kusari and Spiteller, 2012).

1.2.5 Rationale for bioprospecting of endophytes for antibiotics

Many natural products from endophytes harbored in traditional medicinal plants of treating bacterial infection-related ailments, have been observed to exhibit inhibitory and lethal effects on many tested bacteria (Tan and Zou, 2001; Strobel and Daisy, 2003; Strobel *et al.*, 2004; Zhang *et al.*, 2006; Li *et al.*, 2014; Li *et al.*, 2015). Several advantages of endophytic microbes as sources of new natural products are as follows (Kusari, 2010): (1) the vast diversity of endophytic microorganisms in traditional medicinal plants (Verma and Gange, 2014); (2) the considerable architectural and functional group complexity of secondary metabolites (Zhang *et al.*, 2006); (3) natural products with diverse biological functions due to co-evolution with hosts to adapt to the environmental factors or selection pressure, such as invasive bacterial pathogens (Zhang *et al.*, 2006); (4) the optimized fermentation using controlled fermentation conditions to obtain economical, environment-friendly and reproducible yield (Kusari and Spiteller, 2011); (5) combinatorial biosynthesis and biotransformation to generate the natural product libraries for drug development; (6) genome mining and metagenomics to understand the biosynthesis of natural products and manipulating the genes of antibiotic biosynthetic pathway to yield new products with novel properties and strong antibacterial efficacies (Kayser and Warzecha, 2012).

Chapter 2:
AIMS AND OBJECTIVES

The aim of this thesis focuses on isolation, identification and antibacterial evaluation of secondary metabolites from endophytic fungi harbored in Chinese medicinal plants *Xanthium sibiricum*, *Mahonia fortunei*, and *Lonicera japonica*, which are effective to bacterial infection-related ailments. Moreover, this study provides some insights into the potential pharmaceutical use of new antibacterial metabolites, and the plausible ecological roles of the endophyte.

The goals of this work are composed of the following steps:

- (1) Sampling of traditional medicinal plants *X. sibiricum*, *M. fortunei*, and *L. japonica* from different locations of China.
- (2) Isolation of endophytic fungi harbored in different tissues of the plants, and extraction of plant organs for the analysis of natural products.
- (3) Pre-screening, identification and large-scale fermentation of endophytic fungi using an OSMAC (One Strain MAny Compounds) approach, and comparison of natural products from endophytes and host plants.
- (4) Isolation, purification, and structural elucidation of secondary metabolites from fungal endophytes, as well as structural modification of targeted compounds.
- (5) Antibacterial evaluation of compounds, and cytotoxicity assessment of potential antibiotics.

Chapter 3:
MATERIALS AND METHODS

3.1 Collection of plant samples

Plant materials, which are used in TCM, were collected from different locations in the People's Republic of China. Different parts of plants, such as leaves and stems, were obtained and washed briefly using normal tap water to remove any dirt sticking to them. These fresh tissues were packed carefully and then transported to TU Dortmund, Germany within 24 h of collection. Duty Exemption Certificates for the import of plants were issued by the Chamber of Agriculture NRW under Directive 2008/61/EC. The plants have been identified and authenticated by the respective collection centers or experienced experts. Table 3.1.1 shows the detailed information regarding the names, sample codes and sampling sites of four selected plants. These plants or specimens are currently maintained at the respective collection centers.

Table 3.1.1 Names, codes, and sampling locations of four plants

Latin name	Family	Sample code	Source
<i>Xanthium sibiricum</i>	Asteraceae	X.sibiricum/Taian	Shanggang village, Taian, Shandong Province, People's Republic of China
<i>Mahonia fortunei</i>	Berberidaceae	M.fortunei/Shanghai	Shanghai Botanical Garden, Shanghai, People's Republic of China
		M.fortunei/Guangdong	South China Botanical Garden, Guangdong Province, People's Republic of China
		M.fortunei/Jinan	Quancheng Park, Jinan, Shandong Province, People's Republic of China
<i>Lonicera japonica</i>	Caprifoliaceae	L. japonica/Jinan	Shandong University campus, Jinan, Shandong Province, People's Republic of China
		L. japonica/Taian	Shanggang village, Taian, Shandong Province, People's Republic of China
<i>Isatis indigotica</i>	Brassicaceae	I.indigotica/Jinan	Shandong University campus, Jinan, Shandong Province, People's Republic of China
		I.indigotica/Taian	Shanggang village, Taian, Shandong Province, People's Republic of China

3.2 Isolation, cultivation and storage of endophytic isolates

The isolation of the endophyte was done following a previously reported method (Kusari *et al.*, 2008). The plant tissues, such as leaves, stems and roots, were thoroughly washed with normal tap water and cut into small tissue fragments, each measuring approximately 10 mm (length) by 5 mm (breadth).

Surface sterilization of these fragments was carried out by their sequential immersion in 70% ethanol for 1 min, 1.3 M sodium hypochlorite (4% available chlorine) for 3 min, 70% ethanol for 30 s and sterile double-distilled water for 1 min to avoid any possible contamination. These surface-sterilized fragments were then placed on sterile paper to remove excess water. Finally, these tissues were evenly placed on water agar (WA) medium (DIFCO, cat. no. 214530) containing 100 mg/L streptomycin in Petri dishes (Greiner Bio-One GmbH, Germany) (Figure 3.2.1). The Petri dishes were sealed with Parafilm (Bemis Company Inc., Neenah, WI, U.S.A.) and kept at 28 ± 2 °C in an incubator. The cultures in Petri dishes were checked every day to analyze the growth of endophytic fungi. After 1 or 2 weeks, fungal hyphal tips which were growing out from plant fragments, were selected and subcultured onto Sabouraud agar (SA; DIFCO, cat. no. 210950) or potato dextrose agar (PDA; DIFCO, cat. no. 213400) in Petri dishes. All fungal strains were incubated at 28 ± 2 °C in an incubator. Further purification processes were performed in case a mixture of endophytes or contamination occurred (Figure 3.2.1). Finally, many pure cultures were obtained and coded. This was followed by cryopreservation with 20% (v/v) glycerol at -80 °C in the internal culture collection at INFU, TU Dortmund, Germany for long-term storage.

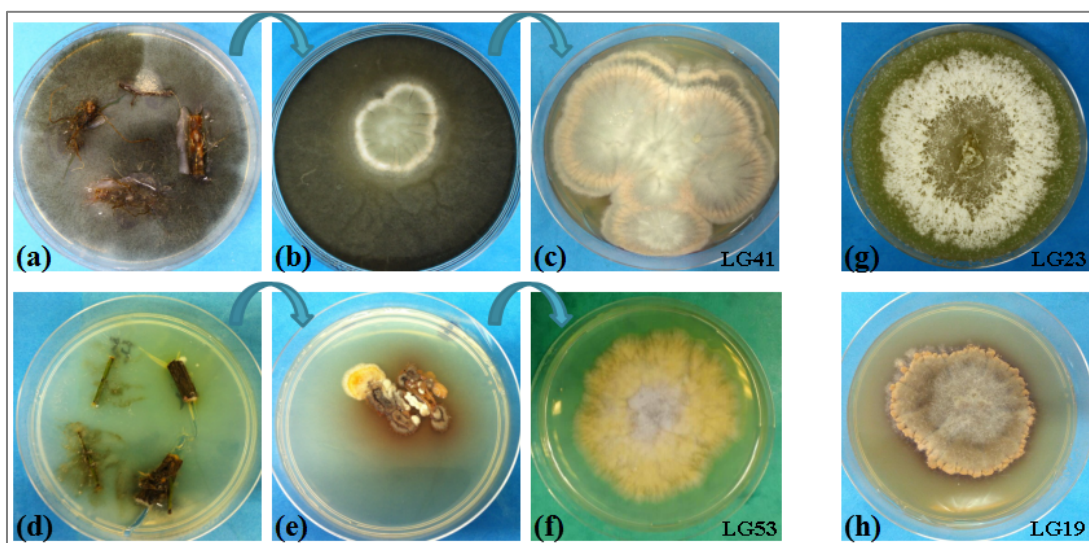


Figure 3.2.1 The isolation and culture of endophytic fungi. (a) The surface-sterilized roots of plant *X. sibiricum* (collected from Shandong) on water agar, and the growth of endophytic fungal colonies from tissue segments. (b) The sub-culture onto SA media. (c) Purified endophyte, LG41, growing on PDA media. (d) The surface-sterilized stems of plant *M. fortunei* (collected from Guangdong) on water agar, and the growth of endophytic fungal colonies from tissue segments. (e) The sub-culture onto PDA media. (f) Purified endophyte, LG53, growing on PDA media. (g) The endophytic fungus, LG23 (from the

leaves of *M. fortunei* collected from Shanghai), growing on PDA media. (h) The endophytic fungus, LG19 (from the leaves of *L. japonica* collected from Jinan, Shandong), growing on PDA media.

3.3 Pre-screening, selection of fungi and large-scale fermentation

The pre-screening for the study of metabolite profile and rapid identification of known compounds is crucial for the discovery of novel natural products. The endophytic isolates were taken from -80 °C fridge and subcultured onto PDA. After one week of incubation at 28 ± 2 °C, agar plugs were cut into small pieces under aseptic conditions. For each endophytic fungus, four pieces were used to inoculate 2 flasks (250 mL), one of which containing 100 mL potato dextrose broth (PDB) and the other one having 40 g rice and 60 mL water. The flasks containing PDB medium were maintained at 28 ± 2 °C for one month (or more based on the growth rate of cultures) in a shaker incubator (150 rpm) (INFORS HT Multitron 2, Einsbach, Germany), while others containing rice medium were incubated at room temperature for one month. These small-scale fermentation cultures afforded enough biological materials, which were extracted with EtOAc and then subjected to liquid chromatography-high resolution mass spectrometry (LC-HRMS) analysis for metabolite profiling. LC-HRMS can provide not only the reliable UV/vis spectra but also the accurate mass and rich adduct as well as the fragmentation information within the nanogram range. Sensitive LC-MS screening with ESI or APCI ionization revealed the structural information of the compounds present in a mixture. LC-HRMS data with the help of few powerful databases, such as Antibase (Laatsch, 2010) and Scifinder[®], as well as several useful literature which summarized the MS data for many secondary metabolites from microorganisms (Nielsen *et al.*, 2011; El-Elimat *et al.*, 2013), enabled the dereplication, identification and analysis of fungal metabolites. In effect, the pre-screening ensured that several fungal strains producing unknown compounds or interesting metabolites were chosen.

For the purpose of large-scale fermentation, four endophytic fungi coded LG19, LG23, LG41, and LG53 were selected based on the analysis of pre-screening (Figure 3.2.1). It has to be noted that, after new or interesting compounds were obtained from the endophytes, many different media or cultural conditions, such as using PDA and czapek-dox broth (CDB), static culture or adding chemicals, have been applied to these fungi to keep checking their metabolite profiles.

Endophytic fungus LG41 (Figure 3.2.1), was fermented for three times based on results from the pre-screening and following modification of culture media or conditions. For the first time, it was cultured in two flasks (250 mL) each containing 100 mL of PDB to get seed broth for further use. This culture was

incubated on a shaker at 150 rpm at 30 °C for 7 days. Furthermore, the seed broth (5 mL) was added to 20 flasks (500 mL) each containing 80 g of rice, 0.3 % peptone, and 120 mL of water (Li *et al.*, 2014b). The cultures were incubated for 7 weeks at room temperature (RT). This fungus LG41 was also subjected to a large-scale fermentation using PDB medium. Agar plugs were cut into small pieces and 40 pieces were selected to inoculate 40 Erlenmeyer flasks (500 mL) each containing 250 mL of PDB. The cultures were incubated at 28 °C on a rotary shaker (150 rpm) for 28 days. In the last fermentation, endophytic fungus LG41, was cultivated in 35 Erlenmeyer flasks (500 mL) each containing 250 ml of PDB supplemented with 15 mg/100 mL of nicotinamide (Sigma-Aldrich, USA) (Asai *et al.*, 2013). These flasks were maintained at 28 °C for one month under shaking (150 rpm) on a rotary shaker. For each fungus LG19, LG23, or LG53 (Figure 3.2.1), agar plugs from one week-old culture grown on PDA at 28 ± 2 °C, were cut into many small pieces under an aseptic environment, and 40 pieces were used to inoculate 20 flasks (1 L) each containing 80 g of rice, 0.3 % peptone, and 120 mL of water (Li *et al.*, 2015). The cultures were incubated at RT for up to two months.

3.4 Identification of selected endophytic fungi

The fungus, coded LG41, was identified as *Eupenicillium* sp. by Dr. Anja Schüffler on the basis of internal transcribed spacer (ITS) sequencing and morphology. The ITS sequence of the endophytic fungus was deposited at the EMBL-Bank (Accession No.: LN626295). The presence of brown cleistothecia and anamorphic conidiophores of *Penicillium* suggested that the strain LG41 belongs to the genus *Eupenicillium* (Li *et al.*, 2014b). The ITS sequence of strain LG41 exhibited high homologies of 99.8 % (in 547 bp) to *Eupenicillium brefeldianum* CBS 233.81 (GenBank Accession No.: GU981615) and 99.8 % (in 547 bp) to *Eupenicillium meridianum* CBS 443.75 (GenBank Accession No.: GU981616.1) (Li *et al.*, 2014b).

Other three selected endophytes (coded LG19, LG23, and LG53) were identified as *Alternaria* sp., *Diaporthe* sp., and *Fusarium decemcellulare* (teleomorph: *Nectria rigidiuscula*), respectively, by Dr. Parijat Kusari based on the following described method, suitably modified from case to case (Wang *et al.*, 2015). The fungal strain was cultured on PDA for one week in an incubator at 28 ± 2 °C. The total genomic DNA (gDNA) of the fungal strain was obtained from the *in vitro* cultures using peqGOLD fungal DNA mini kit (Peqlab Biotechnologie GmbH, Germany) under the manufacturer's guideline. The DNA was then utilized for PCR amplification with primers ITS4 and ITS5 (White *et al.*, 1990). ITS1, 5.8S and ITS2 regions of the rDNA were included in the amplified fragment. The PCR reaction was

carried out in 50 μL reaction mixture with 45 μL Red Taq DNA Polymerase Master Mix (1.1x), 0.5 μL forward primer (100 μM), 0.5 μL reverse primer (100 μM), 3 μL template DNA as well as 1 μL sterile double-distilled water. The PCR cycling protocol consisted of an initial denaturation at 95 °C for 2 min, 30 cycles of denaturation, annealing and elongation at 95 °C for 30 s, 54 °C for 40 s and 72 °C for 30 s. This was then performed by a final elongation step at 72 °C for 5 min. The template DNA as a negative control, was replaced by the sterile double-distilled water. The PCR amplified products spanning approximately 500-600 bp (base pairs) were monitored through gel electrophoresis. The PCR products were purified by GFX™ PCR DNA and Gel Band Purification kit (GE Healthcare Life Sciences) under the manufacturer's guidance, and sequenced from both directions at GATC Biotech (Cologne, Germany).

3.5 Fungal extraction

At the end of the fermentation, the fungal culture in solid medium (for example, rice medium) was extracted with EtOAc by sonication (20 min) at room temperature with the solvent completely submerging mycelia. The extraction procedure was repeated 3 times with fresh organic solvent. The organic solvent was then combined and evaporated to dryness under reduced pressure to afford the crude extract for further isolation and purification. For the fermentation in liquid media (for example, PDB), the culture media was filtered to remove mycelia. The filtrate was evaporated under reduced pressure to afford the concentrated broth for extraction. EtOAc with the same volume as that of the broth was added, and the solution was extracted by sonication (20 min) at RT for 3 times. The mycelia were also extracted with EtOAc under sonication. The organic solvent was pooled and evaporated under reduced pressure to give the final crude extract.

3.6 Isolation and purification of secondary metabolites

The isolation and purification of secondary metabolites from fungi were carried out by several chromatographic techniques. Chromatography is based on the concept of different partition coefficients of compounds between the mobile and stationary phases, which results in traveling at different speeds for different constituents (retention time), and finally enables the separation of substances in a mixture. In this study, the general chromatographic methods are (1) thin layer chromatography (TLC) and (2) column chromatography including silica gel column, Sephadex LH-20 column, and reversed-phase column. While progressing with isolation, nearly all the fractions and subfractions were monitored by LC-HRMS for checking their composition or purities. Figures 3.6.1–3.6.6 showed the schematic

isolation of secondary metabolites from four fungal strains (coded LG19, LG23, LG41, and LG53).

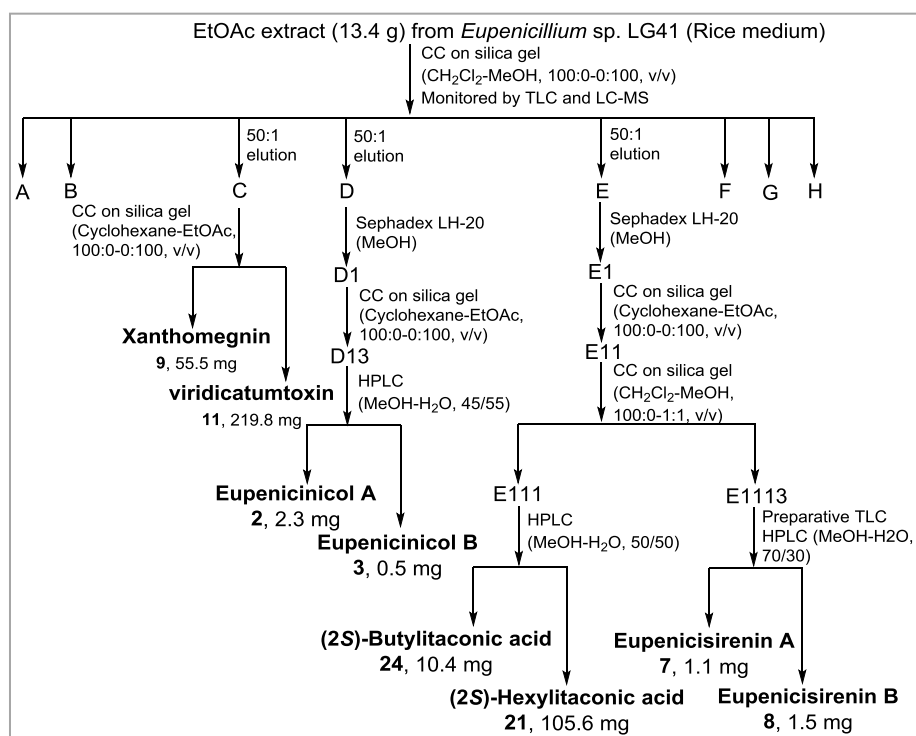


Figure 3.6.1 The schematic isolation of secondary metabolites from rice of *Eupenicillium* sp. LG41.

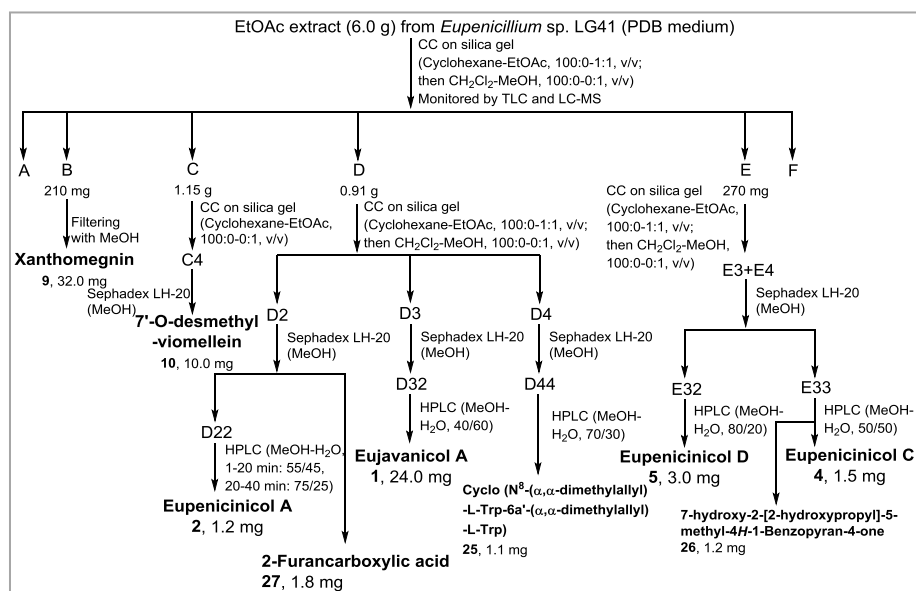


Figure 3.6.2 The schematic isolation of secondary metabolites from PDB of *Eupenicillium* sp. LG41.

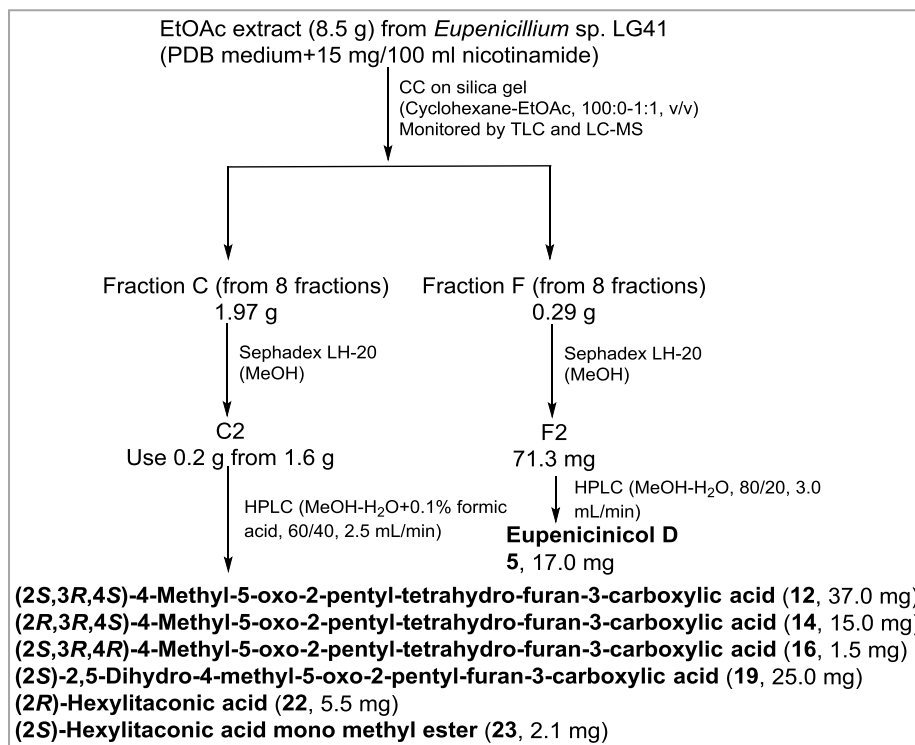


Figure 3.6.3 The schematic isolation of secondary metabolites from PDB culture with adding nicotinamide of *Eupenicillium* sp. LG41.

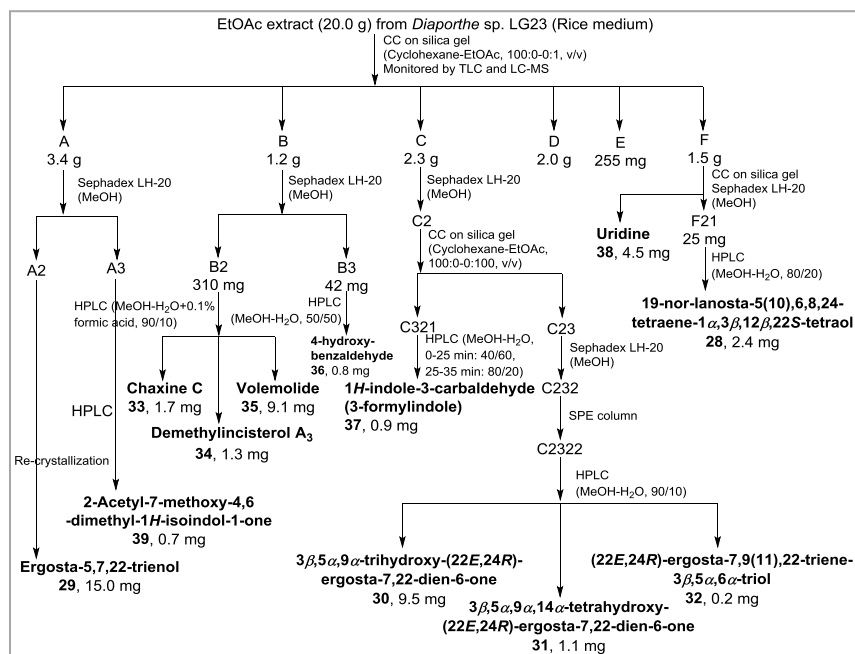


Figure 3.6.4 The schematic isolation of secondary metabolites from rice culture of *Diaporthe* sp. LG23.

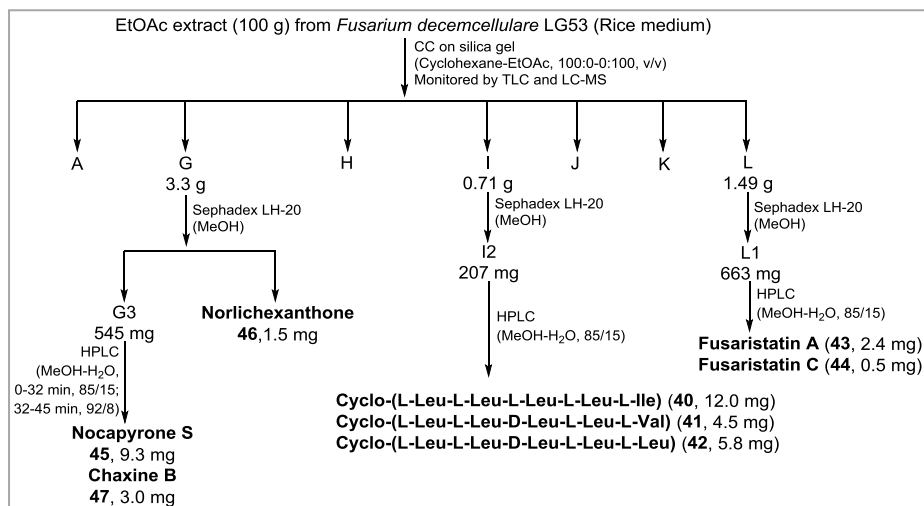


Figure 3.6.5 The schematic isolation of secondary metabolites from rice culture of *F. decemcellulare* LG53.

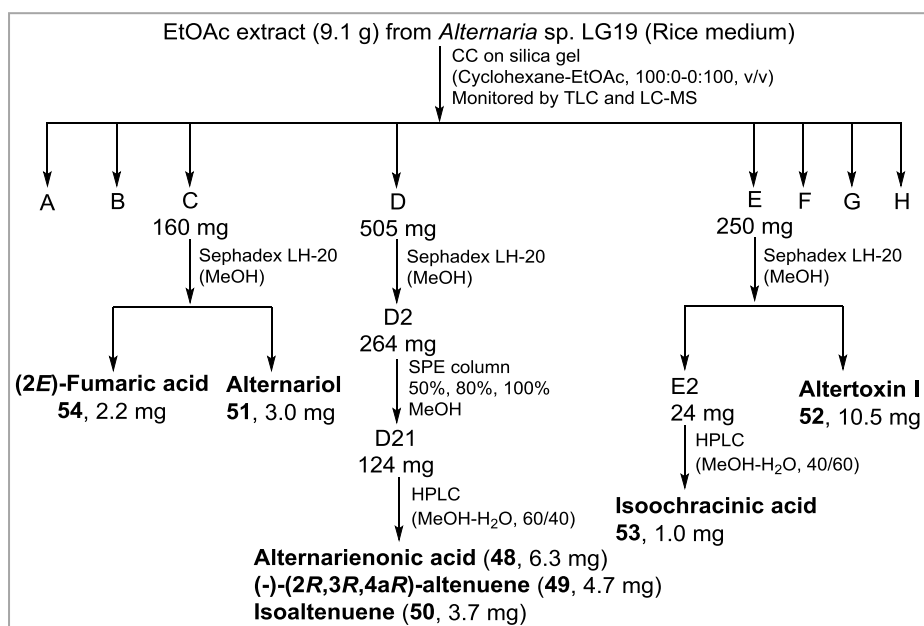


Figure 3.6.6 The schematic isolation of secondary metabolites from rice culture of *Alternaria* sp. LG19.

3.6.1 Chromatography

3.6.1.1 Thin layer chromatography

Thin layer chromatography (TLC) was performed on a piece of glass, plastic or aluminium foil, which is covered with a thin stationary phase, such as silica gel, aluminium oxide, or C₁₈-silica gel material.

Glass or aluminum TLC plates precoated with a thin layer of silica gel 60 (Merck, Darmstadt, Germany) with a fluorescent background under ultraviolet (UV) light at 254 nm due to the presence of a fluorescent dye, was employed in this study. After the separation of the mixture on TLC plate was achieved, compounds were visualized under UV light. Dark spots on the TLC plates indicated that compounds absorb UV energy but do not fluoresce while fluorescence spots suggested compounds absorb light energy and fluoresce. In addition, TLC plates were visualized by spraying with H₂SO₄-EtOH (1:9, v/v) followed by heating to reveal spots (Li *et al.*, 2014b). Retardation factor (R_f), defined as the ratio of the distance passed by the center of a targeted spot to the distance simultaneously passed by the solvent front (IUPAC, 1997), was useful for determination of similar or same components under certain solvent condition.

3.6.1.2 Column chromatography

Column chromatography (CC, also called liquid chromatography) in this thesis included silica gel CC, sephadex LH-20 CC, and reversed-phase (RP) CC. Columns were made of glass or metal tube containing an absorbent known as the stationary phase. The top of the column was loaded with the mixture of compounds and was then eluted with either a pure solvent or a mixture of different solvents. However, considering the stationary materials silica gel, sephadex LH-20, and octadecyl carbon (C₁₈)-bonded silica, the separation mechanisms for them belong to absorption chromatography (normal phase, hydrophilic stationary phase, polar interaction), size-exclusion chromatography (molecule sizes) and absorption chromatography (reversed-phase, hydrophobic stationary phase, hydrophobic interaction), respectively.

In this study, CC on silica gel 60 (70–230 mesh; AppliChem, GmbH, Darmstadt, Germany) was eluted with a gradient of CH₂Cl₂-MeOH or cyclohexane-EtOAc solvent system. The mobile phases for sephadex LH-20 column (25–100 μm; Amersham Biosciences) and RP column were methanol and methanol-water system, respectively. Two types of RP column system were used. The first one is the Bakerbond speTM polar plus C₁₈ column (J.T.Baker, no. 7466-08), and the general mobile phase was a gradient elution with 20% MeOH, 40% MeOH, 60% MeOH, 80% MeOH and 100% MeOH. The separation was performed on a Baker spe-12G apparatus (J.T.Baker, no. 7018-94) in vacuum. The other one is Nucleodex beta-PM column (10 × 250 mm, 5 μm), Gemini column (10 × 250 mm, 10 μm), or Venusil XBP C₁₈ (2) column (10 × 250 mm, 5 μm) in a semi-preparative high performance liquid chromatography (HPLC) system consisting of a Dionex Gina 50 autosampler, a Dionex DG-1210

degasser, a Gynkotech pump, and a Dionex UVD 340S detector. MeOH and H₂O were used as the mobile phase for semi-preparative HPLC. During the separation of one mixture, the percentage of mobile phase for the RP column with a certain flow rate was kept constant and was modified case-to-case before use.

3.6.2 LC-MS

The HRMS experiment was carried out on an LTQ-Orbitrap spectrometer (Thermo Fisher, USA) equipped with a heated electrospray ionization (HESI) or an atmospheric pressure chemical ionization (APCI) source. The spectrometer was equipped with an Agilent 1200 HPLC system (Santa Clara, USA) including four pumps, photodiode array (PDA) detector, column oven (30 °C), and autosampler (injection volume 5 μ L), as well as a Luna C₁₈ (2) column (3 \times 50 mm, 3 μ m) (Phenomenex, Torrance, USA). The mostly used mobile phase is a linear gradient of acetonitrile (+ 0.1 % FA; B) and H₂O (+ 0.1 % FA; A) from 20 % B to 20 % B 1.0 min, 20 % B to 100 % B 18 min, 100 % to 20 % 0.5 min, and 20 % to 20 % 5.5 min with a flow rate 0.35 mL/min. The spectrometer was operated in a positive mode (with nominal mass resolving power of 60,000 at m/z 400 with a scan rate of 1 Hz) to afford high-accuracy mass measurements within 2 ppm deviation (Talontsi *et al.*, 2013), or negative mode (ion trap). For the HESI source in positive mode, the following parameters were used for experiments: vaporizer temperature 400 °C, capillary temperature 350 °C, nitrogen sheath gas flow (arbitrary units) 60, nitrogen auxiliary gas flow (arbitrary units) 12, source voltage 4.6 kV, capillary voltage 25 V, tube lens 65 V. Moreover, the following parameters were used for APCI source in positive mode: APCI vaporizer temperature 450 °C, capillary temperature 190 °C, nitrogen sheath gas flow (arbitrary units) 50, nitrogen auxiliary gas flow (arbitrary units) 17, source voltage 6 kV, capillary voltage 35 V, tube lens 60 V. MS/MS experiments were achieved by using a fragmentation technique, collision-induced dissociation (CID, 35 eV) detected in the orbitrap mass analyzer. Ar was served as a collision gas. The LC-HRMS data was analyzed through the software Thermo Xcalibur 2.2 SP1.48 (Thermo Fisher Scientific Inc., USA). LC-HRMS can provide not only the reliable UV/vis spectra but also the accurate mass within 2 ppm deviation, and rich adduct and fragmentation information.

3.7 Structural elucidation

3.7.1 Determination of planar structure and relative configuration

3.7.1.1 LC-MS

For structural elucidation of a compound, LC-HRMS (see section 3.6.2) was employed to check the purity and provide the molecular weight and formula. MS/MS experiments were performed in CID mode to evaluate the structural features of compounds based on the fragmentation information.

3.7.1.2 NMR

The pure compounds were further submitted to nuclear magnetic resonance (NMR) measurements. Samples were analyzed with one-dimensional (1D) NMR spectroscopic techniques including ^1H and ^{13}C NMR, together with two-dimensional (2D) NMR spectroscopic techniques including correlation spectroscopy (COSY), heteronuclear single quantum correlation (HSQC), heteronuclear multiple bond correlation (HMBC), and nuclear overhauser enhancement spectroscopy (NOESY). 1D NMR, COSY, HSQC and HMBC afforded the detailed information which was applied to assign the planar structure. In addition, NOESY was used to investigate the relative configuration or three-dimensional (3D) structure of the molecule. CDCl_3 (Deutero GmbH, Kastellaun, Germany), methanol- d_4 (CD_3OD) (Deutero GmbH, Kastellaun, Germany), acetone- d_6 (Sigma-Aldrich Chemie GmbH, Germany), DMSO- d_6 (Sigma-Aldrich Chemie GmbH, Germany), or pyridine- d_5 (Sigma-Aldrich Chemie GmbH, Germany) were used as deuterated solvents and the internal locks in NMR experiments. The sample dissolved in NMR solvent was transferred to an NMR tube (5×203 mm) (Deutero GmbH, Kastellaun, Germany) and analyzed by the NMR spectroscopy. NMR spectra were recorded at 25 °C on a 400 MHz Bruker Avance DRX-400, 500 MHz Bruker Avance DRX-500, 500 MHz Varian Unity Inova 500, or 600 MHz Varian Unity Inova 600 spectrometer.

3.7.1.3 ^{13}C NMR calculation

^{13}C NMR chemical shift prediction for some compounds was achieved using a multi-standard approach (MSTD) for gauge including atomic orbitals (GIAO) ^{13}C NMR calculations (Sarotti and Pellegrinet, 2009). A general procedure and detailed information are written in section 3.7.2.2. The calculated ^{13}C NMR chemical shifts for a compound was in accordance with experimental values, supporting the

proposed planar and relative structure.

3.7.1.4 X-ray diffraction study

Single crystal X-ray diffraction experiment is used to identify the atomic and molecular 3D structure, and was performed on an Oxford diffraction Xcalibur Sapphire3 diffractometer at 150 K with graphite-monochromated Mo-K α radiation ($\lambda = 0.71073 \text{ \AA}$). With the aid of Olex2 (Dolomanov *et al.*, 2009), the crystal structure was solved with the olex2.solve (Bourhis *et al.*, 2015) structure solution program using Charge Flipping. The structure was refined with the SHELXL (Sheldrick, 2008) refinement program with the Least Squares minimisation. Molecular graphics were accomplished with Ortep-3 (for Windows, Version 2014.1) (Farrugia, 2012). Crystallographic data of compound **4** were deposited in the Cambridge Crystallographic Data Centre with a CCDC number 1440259. Copies of the data can be acquired, free of charge, from Cambridge Crystallographic Data Centre, 12 Union Road, Cambridge CB2 1EZ, UK [fax: +44(0)1223 336033 or e-mail: deposit@ccdc.cam.ac.uk].

3.7.1.5 Other methods

Infrared (IR) spectra (vibrational spectroscopy) were recorded using a Bruker Tensor 27 IR spectrometer. IR spectra exhibited many characteristic vibrational absorption bands which are associated with the absorption frequencies of functional groups. Ultraviolet-visible (UV-Vis) spectra were obtained from the photodiode array (PDA) detector in LC-HRMS. The UV-Vis absorptions in the region 200-800 nm indicated the electronic transitions from ground state to the excited state, which are related to the chromophores present in molecules.

3.7.2 Determination of absolute configuration

3.7.2.1 Optical rotation and CD

Optical rotation is a phenomenon of turning the plane of a linearly polarized light which passed through a solution containing a chiral compound. Optical rotations were carried out on an A-Krüß Optronic polarimeter at a wavelength of 589 nm. The value was calculated according to the equation $[\alpha] = (\alpha * 100) / (c * d)$. The optical path length (d) is 1 dm, and the concentration (c) is in g/100 mL. MeOH or CHCl₃ was employed as solvent at 20 °C or 22 °C.

Circular dichroism (CD), as a powerful technique for stereochemical analysis, is the differences between

the absorption of left and right circularly polarized lights, which occurs due to the chirality present in chromophore-containing molecules. CD measurements were performed using a Jasco J-715 polarimeter (Tokyo, Japan). MeOH or CHCl₃ was employed as solvent at RT to dissolve chiral molecule in a 0.1 cm quartz cuvette. The spectra ranged from 200-400 nm were obtained using a scan speed of 100 nm/min, a response time of 1 s, a resolution of 1 nm, and an accumulation of 5 scans.

3.7.2.2 ECD and ORD calculations

The calculation of electronic circular dichroism (ECD) and/or optical rotatory dispersion (ORD) is applied for absolute configuration and conformational study of compounds. The general calculation procedure is (1) to search all possible conformers which are further subjected to geometry optimization at a theory level, (2) to evaluate vibrational frequencies which afford detailed data for Boltzmann distribution at a theory level, (3) to perform ECD, ORD, and/or ¹³C NMR calculations (section 3.7.1.3) for the resultant conformers at a level of theory with or without solvent model, which gives ECD spectra of different conformers with a certain half bandwidth (eV), and (4) to simulate the overall ECD curve which are weighed by Boltzmann distribution and compare the calculated ECD spectrum with experimental one.

The absolute configurations of eupenicisirenin A (**7**) and eupenicisirenin B (**8**) were calculated using semiempirical and ab initio methods. With SPARTAN'14 (SPARTAN '14, Wavefunction, Inc., Irvine, CA, 2014) and using PM3 and the Monte Carlo technique, many starting geometries were calculated (Li *et al.*, 2014b). A further geometry optimization with Gaussian g09 (Frisch *et al.*, 2009) using density functional theory (DFT) calculations B3LYP (Becke's nonlocal three-parameter exchange and correlation functional with the Lee-Yang-Parr correlation functional)/6-311G(2d,p) afforded targeted conformers with Boltzmann factors > 0.001 (related to the states' energy difference of E < 2.5 kcal/mol). The ECD spectra for all conformers were calculated at the same level of theory and then subjected to Boltzmann averaging according to their Boltzmann factors. ORD calculations were carried out at the wB97XD/6-311G(d,p) level.

Conformational analysis, geometrical optimization, and vibrational evaluation were performed for absolute configurations of itaconic acids and paraconic acids. Conformers within a 50 kcal/mol Van der Waals (VDW) energy window from the global minimum were analyzed using Frog2 online version (Miteva *et al.*, 2010). There were 50, 43, 43, and 50 conformations calculated for molecules (2*R*,3*R*,4*S*)-4-methyl-5-oxo-2-pentyl-tetrahydro-furan-3-carboxylic acid (**14**), (2*S*,3*R*,4*S*)-4-methyl-5-oxo-2-pentyl-

tetrahydro-furan-3-carboxylic acid (**12**), (-)-phaseolinic acid, and enantiomer of (2*S*,3*R*,4*R*)-4-methyl-5-oxo-2-pentyl-tetrahydro-furan-3-carboxylic acid (**16**), respectively. For the sake of saving computational time and considering the limited effect of side chain remote from the chromophore (Berova *et al.*, 2007), we neglected the conformers due to the spin of the side chain. Therefore, 2, 3, 2, and 3 conformers from the above conformations were left and further selected for geometrical optimization using the B3LYP at 6-31G(d) basis set with the general atomic and molecular electronic structure system (GAMESS) package (Schmidt *et al.*, 1993). The program received from GAMESS distribution is 1 MAY 2013 (R1) version for 64 bit Windows. The vibrational evaluation was performed at the same level to confirm minima of conformers. The ECD calculations were performed with a DALTON program package (DALTON 2015.0) (Aidas *et al.*, 2014). Time-dependent density functional theory (TDDFT) at the B3LYP/6-31G* level was applied to calculate the singlet electronic excitation energies and rotational strengths in the gas phase and in solvation PCM model for MeOH. Finally, the ECD curve for each conformer was simulated according to the equation 8d with a half-band of 0.4 eV (Stephens and Harada, 2010).

The geometry in cartesian coordinates obtained from the above method was the basis for the calculation of NMR chemical shift. An MSTD was used for GIAO ¹³C NMR calculations (Sarotti and Pellegrinet, 2009). The NMR isotropic magnetic shielding values for a given molecule and a reference compound were calculated with a DALTON program package at an mPW1PW91/6-31G(d) level. The above magnetic shielding values were transformed to be chemical shift values according to the equation $\delta_{\text{calc}}^{\text{X}} = \delta_{\text{ref}} - \delta_{\text{x}} + \delta_{\text{ref}}$ where δ_{x} and δ_{ref} are the magnetic shielding values for the X carbon nucleus of the molecule, and the carbon atom in reference compound (sp³ for methanol, and sp-sp² for benzene), respectively (Sarotti and Pellegrinet, 2009). Finally, the individual conformer values were summed according to their Boltzmann factors to afford a Boltzmann-weighted ¹³C NMR data.

3.7.2.3 Marfey's method

The absolute configurations of three cyclic pentapeptides (**40**, **41**, and **42**) were defined by applying the Marfey's method (Marfey, 1984; Song *et al.*, 2014). Each compound (1 mg) was dissolved in 6 N HCl (1 mL) and kept in an oil bath at 110 °C for 24 h. The hydrolysates were evaporated to dryness under reduced pressure and further dissolved in 100 μ L H₂O. In addition, 1 N NaHCO₃ (50 μ L) was added to the above water solution containing hydrolysates. Further reaction with 100 μ L of 1% (10 mg/1 mL acetone) 1-fluoro-2,4-dinitrophenyl-5-L-alaninamide (FDAA, Sigma-Aldrich Chemie GmbH, Germany)

at 40 °C for 1 h to afford a yellowish mixture was carried out. After this reaction, 1N HCl (50 μ L) was employed to terminate the reaction. MeOH was finally added to the above neutral mixture to give a total volume of 1 ml, which was submitted to LC-HRMS measurement with an injection volume of 1 μ L. The LC-HRMS method was as described in previous section 3.6.2. Amino acid standards (enantiomer), such as L- and D-leucines, L- and D-isoleucines, and L- and D-valines, were purchased from Sigma-Aldrich Chemie GmbH (Steinheim, Germany) and were derivatized with FDAA in the same manner. These FDAA derivatized amino standards (diastereomers) were also submitted to LC-HRMS and had different retention time (Figure 3.7.2.3.1). The retention time for comparison of the above samples (from peptides) with standards revealed the absolute configuration of amino acids in the cyclic pentapeptides. In other words, if an LC peak (the derivatized product from the hydrolysate of peptides) had the same retention time with that for a derivatized amino acid standard, they have the same absolute configuration (see Figure 3.7.2.3.1 and Figure 4.3.1.8).

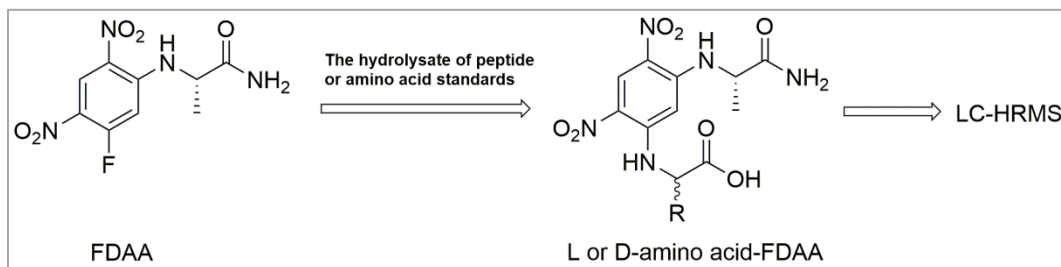


Figure 3.7.2.3.1 The general scheme for Marfey's method.

3.7.2.4 X-ray diffraction study

The single crystal X-ray diffraction analysis can also be used for assigning absolute configuration, for example, compound **40**. The experiment was carried out on a Bruker Apex Duo, which was integrated with the Bruker SAINT software package using a narrow-frame algorithm. Data was collected at 100(2) K with graphite-monochromated Cu-K α radiation ($\lambda = 1.54178$ Å). The multi-scan method (SADABS) was applied for data correction on absorption effects. The crystal structure was solved with intrinsic phasing using SHELXT2014 (Sheldrick, 2015) and refined with the SHELXL2014/7 (Sheldrick, 2008) refinement program by the full-matrix least-squares on F² method. Molecular graphics were obtained using Ortep-3 (for Windows, Version 2014.1) (Farrugia, 2012).

3.8 MALDI-MS

MALDI-imaging-HRMS were carried out with an atmospheric pressure scanning microprobe matrix-assisted laser desorption/ionization source (AP-SMALDI) (TransMIT GmbH, Germany). AP-SMALDI was coupled with a Q Exactive high resolution mass spectrometer (Thermo Scientific Inc., Bremen, Germany). UV laser was generated from a pulsed 60 Hz N₂ laser MNL 100 series (LTB Lasertechnik GmbH, Germany). An SMALDI Prep spray instrument (TransMIT GmbH, Germany) was utilized to obtain a uniform matrix layer on the sample. The images of samples were recorded on an optical microscope Leica S8APO (Leica Microsystems GmbH, Germany).

3.9 Semi-synthesis for paraconic acids

3.9.1 Esterification

A chemically engineered approach for diversification of natural product extract or fraction was applied (López *et al.*, 2007). A solution of mixture (paraconic acids and itaconic acids, 0.5 g) in 5 ml of dry acetone was added 750 mg K₂CO₃ and stirred for 0.5 h, followed by adding Me₂SO₄ (500 μL) (Chernaga *et al.*, 1999). After 0.5 h and 2 h, further Me₂SO₄ (500 μL) was added and stirring continued for 4 h. Finally, 25 % NH₃·H₂O was used to quench the reaction. The reaction solution was further evaporated to dryness and extracted with EtOAc. The resulting residue (taking 250 mg) was separated by HPLC (MeOH/H₂O containing 0.1% formic acid, 65:35, 2.5 mL/min) to afford (2*S*,3*R*,4*S*)-4-methyl-5-oxo-2-pentyl-tetrahydro-furan-3-carboxylic acid methyl ester (**13**, 120.0 mg, *t_R* = 18.4 min), (2*R*,3*R*,4*S*)-4-methyl-5-oxo-2-pentyl-tetrahydro-furan-3-carboxylic acid methyl ester (**15**, 20.0 mg, *t_R* = 14.5 min), (2*S*,3*R*,4*R*)-4-methyl-5-oxo-2-pentyl-tetrahydro-furan-3-carboxylic acid methyl ester (**17**, 13.0 mg, *t_R* = 21.9 min), and (2*S*)-2,5-dihydro-4-methyl-5-oxo-2-pentyl-furan-3-carboxylic acid methyl ester (**20**, 1.5 mg, *t_R* = 27.5 min).

3.9.2 Thermodynamic equilibration

A CH₂Cl₂ solution of 10 mg (2*S*,3*R*,4*S*)-4-methyl-5-oxo-2-pentyl-tetrahydro-furan-3-carboxylic acid methyl ester (**13**) or (2*R*,3*R*,4*S*)-4-methyl-5-oxo-2-pentyl-tetrahydro-furan-3-carboxylic acid methyl ester (**15**) (0.047 mmol) was mixed with 20 μL DBU (1,8-diazabicyclo[5.4.0]undec-7-ene) (0.13 mmol) and was stirred for 72 h at RT (Amador *et al.*, 2006; Fournier *et al.*, 2013). The reaction was monitored by LC-HRMS. The reaction mixture was evaporated to dryness and extracted with water and CH₂Cl₂.

The organic layer was collected and removed under vacuum. Based on the results of LC-HRMS, the product of **13** was directly submitted for ^1H NMR and had an enriched **17**. The organic extraction from the reaction of **15** was further purified by HPLC to afford (2*R*,3*S*,4*S*)-4-methyl-5-oxo-2-pentyl-tetrahydro-furan-3-carboxylic acid methyl ester (**18**, 0.9 mg, $t_{\text{R}} = 21.5$ min). The structure of compound **18** was confirmed by 1D and 2D NMR data (Figures 4.1.18.1 and 4.1.18.2, Appendix A) as well as the positive optical rotation and CD spectra.

3.10 Bioassay

3.10.1 Compounds and microorganisms used for antimicrobial assay

The *in vitro* antibacterial activities of the compounds were tested against a panel of standard pathogenic control strains (Leibniz-Institute DSMZ, Braunschweig, Germany). Three Gram-positive bacteria *Staphylococcus aureus* (DSM 799), *Bacillus subtilis* (DSM 1088) and *Streptococcus pyogenes* (DSM 11728), and three Gram-negative bacteria *Escherichia coli* (DSM 1116), *E. coli* (DSM 682) and *Pseudomonas aeruginosa* (DSM 22644) were used in the antibacterial assay. In addition, five Gram-negative *Acinetobacter* bacteria, *Acinetobacter* sp. (DSM 586), *Acinetobacter baylyi* (DSM 24193), *Acinetobacter calcoaceticus* (DSM 30006), *Acinetobacter baumannii* (DSM 30007) and *Acinetobacter pittii* (DSM 25618) were also included. The activation, maintenance, and preparation of working culture suspensions were carried out in accordance with established procedures (Kusari *et al.*, 2009). The compounds tested were dissolved in HPLC-grade MeOH at a concentration range of 0.1 $\mu\text{g}/\text{mL}$ to 10 $\mu\text{g}/\text{mL}$ (0.1 $\mu\text{g}/\text{mL}$, 1 $\mu\text{g}/\text{mL}$, 2 $\mu\text{g}/\text{mL}$, 5 $\mu\text{g}/\text{mL}$, and 10 $\mu\text{g}/\text{mL}$). Additionally, positive controls such as streptomycin (Sigma-Aldrich Chemie GmbH, Steinheim, Germany), gentamicin (Sigma-Aldrich Chemie GmbH, Steinheim, Germany) and/or colistin (Dr. Ehrenstorfer GmbH, Augsburg, Germany), were used simultaneously as reference standards. The standards were also prepared at the same concentration range as the tested compounds in sterile double-distilled H_2O . Furthermore, the fungi *Colletotrichum circinans* (DSM 62125) and *Aspergillus aculeatus* (DSM 2344) were used to test the antifungal activities for some compounds.

3.10.2 Antibacterial assay

According to the Clinical and Laboratory Standards Institute (CLSI) (Wikler, 2006), the disk diffusion method was applied for the determination of the antibacterial activities of the samples (Li *et al.*, 2014b).

Agar plates were prepared by 90 mm sterile Petri dishes (TPP, Trasadingen, Switzerland) containing 22 mL of agar, affording a final depth of 4 mm (nutrient agar (NA) for bacteria and PDA for fungi). Using the standard spread-plate technique, 200 μ L inoculum suspension was spread on the solid media plates. The mycelia of fungi were first thoroughly macerated and ground in a sterile mortar-pestle to give a homogeneous inoculum for spreading on the media plates. These plates were stored at 4 °C for 2 h. Sterile paper discs (Schleicher & Schuell GmbH, Dassel, Germany; 6.0 mm in diameter) were impregnated with 40 μ L of the respective working solution, air-dried under the laminar airflow hood in the clean bench and placed on the inoculated plates. The plates were then incubated at 37 °C for 24 h for bacteria or at 28 °C for 48 h for fungi (Li *et al.*, 2014b). Three negative control sets were prepared. The first control was the microorganism control and consisted of a seeded Petri dish without a sample. In addition, samples were applied to unseeded Petri dishes for checking sterility, which was used as the second control. In the third control, the solvent effect was monitored by a disk impregnated with 40 μ L of HPLC-grade MeOH or with 40 μ L of sterile double-distilled H₂O (Li *et al.*, 2014b). The standard antibiotics (see section 3.10.1) were employed to indicate the comparative antimicrobial efficacies of compounds against the tested organisms. The minimum inhibitory concentrations (MIC) of each tested compound and the reference antibiotics against each bacterium were calculated following the guidance of CLSI (Wikler, 2006). Each test was performed in triplicate.

3.10.3 Cytotoxicity assay

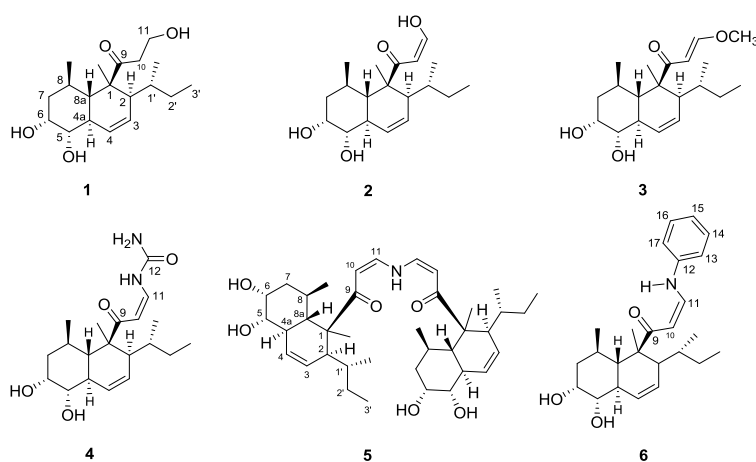
Cytotoxic assays of compounds against human acute monocytic leukemia cells (THP-1) *in vitro* were evaluated using a resazurin-based assay to measure the THP-1 mitochondrial metabolic inhibition as well as an ATPlite assay to measure the THP-1 cytoplasmic ATP depletion (Kusari *et al.*, 2009). Untreated cells were used as a negative control. The semi-logarithmic representation of the fractional survival (FS in %) of THP-1 cells as a function of concentration was provided.

Chapter 4:
RESULTS AND DISCUSSION

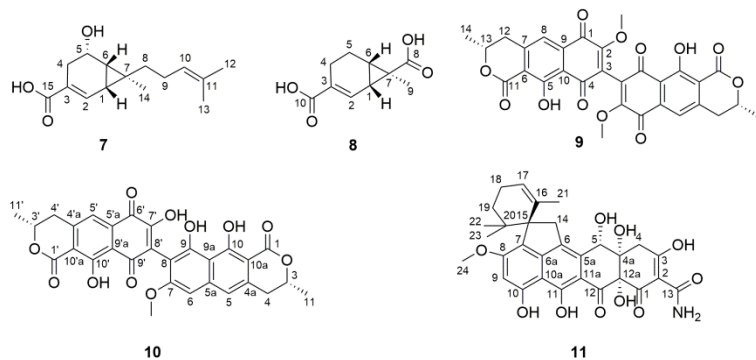
**Note: All the figures for structural elucidation of compounds 1-54
can be found in Appendix A.**

4.1 Secondary metabolites isolated from *Eupenicillium* sp. LG41

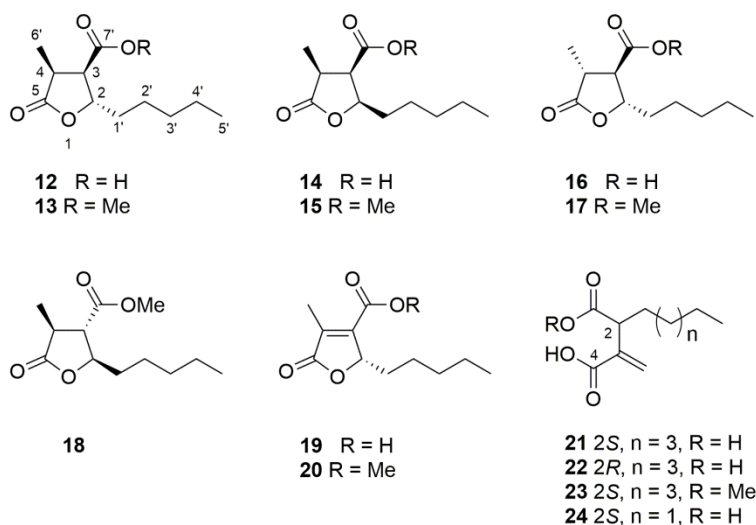
The endophytic fungus, *Eupenicillium* sp. LG41, isolated from the root of Chinese medicinal plant *X. sibiricum* (from Taian, P. R. China), was investigated using the OSMAC approach. The metabolic profiles of the endophytic strain in different conditions were monitored (see section 3.3). Detailed fermentation or isolation process was described in Chapter 3. The isolation of a known decalin-containing compound (Li *et al.*, 2014a), eujavanicol A (**1**), together with five new decalin-containing compounds, eupenicinicol A–E (**2–6**) from rice or PDB medium were achieved.



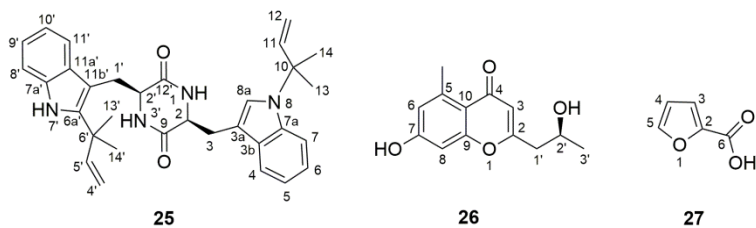
In addition to the above decalin motif-containing compounds, two new sirenin derivatives eupenicisirenin A and B (**7** and **8**) were obtained from the rice culture of *Eupenicillium* sp. LG41. Moreover, three polyketide pigments (**9–11**) including a new one (**10**), were isolated from the rice or PDB medium.



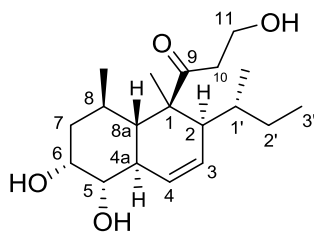
There are four paraconic acids (**12**, **14**, **16**, and **19**), which were isolated and purified from the PDB medium amended with nicotinamide (Asai *et al.*, 2013). Compounds **12**, **14**, and **16** are new naturally occurring secondary metabolites and have already been synthesized or reported as an intermediate (Amador *et al.*, 2006; Jacobi and Herradura, 1996; Drioli *et al.*, 1998). Four biologically related known alkylitaconic acids (**21–24**) were also isolated, in which **21** and **24** came from the rice culture of the endophytic strain. Furthermore, four semi-synthetic methyl esters (**13**, **15**, **17**, and **20**) and an isomerized product (**18**) were successfully obtained.



Finally, three other known compounds (**25–27**) were separated at the same time.



4.1.1 Eujavanicol A (1, known compound)



Compound **1** (code: LG41-P4312), a white powder, has a molecular formula $C_{19}H_{32}O_4$ as derived from its ESI-HRMS data ($[M+H]^+$ at m/z 325.2375, $[M+H-H_2O]^+$ at m/z 307.2271, $[M+H-2\times H_2O]^+$ at m/z 289.2166, $[M+H-3\times H_2O]^+$ at m/z 271.2059) (Figure 4.1.1.1). MS^2 spectrum (Figure 4.1.1.2) showed the successive loss of up to four water molecules ($[M+H-H_2O]^+$ at m/z 307.2269, $[M+H-2\times H_2O]^+$ at m/z 289.2160, $[M+H-3\times H_2O]^+$ at m/z 271.2053, and $[M+H-4\times H_2O]^+$ at m/z 253.1954). Furthermore, a characteristic fragment ion at m/z 217.1953 $[M+H-C_3H_8O_4]^+$ was found (Figure 4.1.1.2). 1H and ^{13}C NMR data (Figure 4.1.1.3) determined it as the known decalin-containing compound eujavanicol A which was isolated from the same genus *Eupenicillium* (Table 4.1.1.1) (Nakadate *et al.*, 2007). Moreover, compound **1** has a close optical rotation $[\alpha]^{22}_D +49.5$ (c 0.22, MeOH) compared to $[\alpha]^{22}_D +49.9$ (c 1.33, MeOH) for eujavanicol A, further supporting its known structure (Nakadate *et al.*, 2007). In the course of searching for the derivatives of compound **1** with similar MS^n pattern, we checked the pre-screening in different cultural conditions using OSMAC approach and discovered some new decalin motif-containing derivatives depicted as follows.

Table 4.1.1.1 NMR spectral data for compound **1**.

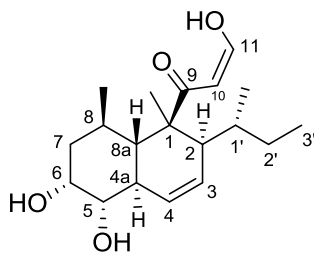
Position	Compound 1		Eujavanicol A (Nakadate <i>et al.</i> , 2007)	
	δ_C , mult. ^a	δ_H mult. ^b (J in Hz)	δ_C , mult. ^d	δ_H mult. ^e (J in Hz)
1	52.7, C_q		52.6, C_q	
2	52.4, CH	1.91 m	52.4, CH	1.94 m
3	123.9, CH	5.66 ddd (3.0, 4.5, 10.5)	124.0, CH	5.71 ddd (2.7, 4.6, 10.7)
4	126.3, CH	5.97 dt (2.5, 10.5)	126.1, CH	6.00 dt (2.0, 10.7)
4a	39.1, CH	2.10 tq (2.0, 10.5)	39.1, CH	2.14 tq (2.4, 10.4)
5	75.4, CH	3.38 dd (3.0, 10.5)	75.3, CH	3.44 br d (10.7)
6	69.7, CH	3.99 m	69.7, CH	4.04 q (3.1)
7 α	41.4, CH_2	1.80 dt (2.5, 14.5)	41.3, CH_2	1.85 dt (2.9, 14.6)

7 β		1.48 m ^c		1.52 ddd (2.6, 12.1, 14.6)
8	30.6, CH	1.68 m	30.6, CH	1.73 m
8a	43.2, CH	1.88 t (10.0)	43.1, CH	1.93 t (10.4)
9	215.8, C _q		215.7, C _q	
10a	41.2, CH ₂	2.83 ddd (4.0, 7.5, 19.0)	41.2, CH ₂	2.86 ddd (3.9, 7.3, 18.9)
10b		2.64 ddd (3.5, 6.0, 19.0)		2.66 ddd (3.7, 6.1, 18.9)
11a	58.1, CH ₂	3.80 m	58.1, CH ₂	3.84 m
11b		3.86 m		3.90 m
1'	37.3, CH	1.08 m	37.2, CH	1.13 m
2'a	24.5, CH ₂	1.44 m ^c	24.5, CH ₂	1.47 m
2'b		0.72 m ^c		0.76 m
3'	12.7, CH ₃	0.72 m ^c	12.6, CH ₃	0.76 m
1-Me	19.5, CH ₃	1.21 s	19.4, CH ₃	1.25 s
1'-Me	19.4, CH ₃	0.89 d (7.0)	19.3, CH ₃	0.93 d (6.7)
8-Me	22.5, CH ₃	0.55 d (6.5)	22.4, CH ₃	0.60 d (7.0)

^a Recorded in CDCl₃ at 100 MHz. ^b Recorded in CDCl₃ at 500 MHz. ^c Signals overlapped. ^d Recorded in CDCl₃ at 125 MHz. ^e Recorded in CDCl₃ at 500 MHz.

Eujavanicol A (1): white powder; $[\alpha]_D^{22} +49.5$ (c 0.22, MeOH); LC-UV [(Acetonitrile (aq) in H₂O/0.1% FA)] λ_{\max} 218, 288 nm; IR (film) ν_{\max} 3444, 1632, 1379, 1109, 1036 cm⁻¹; CD (MeOH) 194 ($\Delta\epsilon + 1.35$), 291 ($\Delta\epsilon - 0.04$) nm; ¹H NMR (CDCl₃, 500 MHz) and ¹³C NMR (CDCl₃, 100 MHz), see Table 4.1.1.1. Positive ESI-HRMS m/z : 325.2375 [M+H]⁺ (calcd for C₁₉H₃₃O₄, 325.2373).

4.1.2 Eupenicinicol A (2, new compound)



Eupenicinicol A (**2**, code: LG41-4133) (Li *et al.*, 2014b), was obtained from the EtOAc extract of the rice medium of the endophytic fungus *Eupenicillium* sp. It was isolated as an optically active white powder with a molecular formula C₁₉H₃₀O₄ as determined by ESI-HRMS ([M+H]⁺ at m/z 323.2216, calcd. 323.2217) and its fragment information ([M+H-H₂O]⁺ at m/z 305.2111, [M+H-2×H₂O]⁺ at m/z

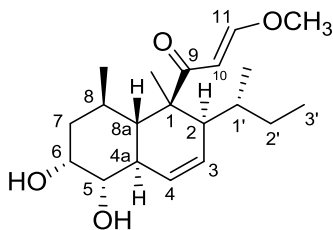
287.2006, and $[M+H-3\times H_2O]^+$ at m/z 269.1898; Figure 4.1.2.1). Moreover, MS^2 data shown in Figure 4.1.2.2 reveals the successive loss of up to four water molecules and/or a CO group ($[M+H-2\times H_2O]^+$ at m/z 287.2005, $[M+H-3\times H_2O]^+$ at m/z 269.1898, $[M+H-4\times H_2O]^+$ at m/z 251.1790; or $[M+H-2\times H_2O]^+$ at m/z 287.2005, $[M+H-2\times H_2O-CO]^+$ at m/z 259.2055, $[M+H-3\times H_2O-CO]^+$ at m/z 241.1949), indicating that there should be at least three hydroxyl functional groups and/or a carbonyl moiety in **2** (Li *et al.*, 2014b). Moreover, like compound **1**, a characteristic fragment ion at m/z 217.1951 $[M+H-C_3H_6O_4]^+$ in MS^2 spectrum was found. The 1H NMR data (Figure 4.1.2.3 and Table 4.1.2.1) suggested the presence of four methyls, two oxygenated methines, and four protons related to two double bonds. The 1D NMR data (Figure 4.1.2.3) with the help of the HSQC spectrum (Figure 4.1.2.4) showed four methyls, two methylenes, seven methines (two oxygenated), two *cis*-disubstituted double bonds (one oxygenated carbon), and two quaternary carbons. Interpretation of 1H - 1H COSY NMR spectrum (Figures 4.1.2.4 and 4.1.2.5) revealed the proton spin systems from C-2 to C-7, C-2 to C-3', 8-Me to C-4a, and C-10 to C-11 (Li *et al.*, 2014b). Key HMBC correlations of Me-8/C-7, C-8 and C-8a, and Me-1/C-1, C-2 and C-8a implied the connection of C-7 to C-8, and C-1 to C-2 and C-8a, and assigned Me-1 and Me-8 at C-1 and C-8 respectively (Li *et al.*, 2014b). Therefore, a decalin ring system was successfully determined (Li *et al.*, 2014a). The remaining side chain was determined by the HMBC correlations of Me-1 and two protons of the Δ^{10} -double bond to C-9 (Figure 4.1.2.5). Three hydroxy groups were located at C-5 (δ_H 3.47, δ_C 75.4), C-6 (δ_H 4.06, δ_C 69.7), and C-11 (δ_H 7.97, δ_C 175.4), respectively based on their chemical shifts, which was also in accordance with its MS requirement. Accordingly, the planar structure of compound **2** was unambiguously determined as depicted. The relative configuration of **2** was verified by the NOESY correlations (Figure 4.1.2.6) of Me-1/H-2, H-4a, H-8, and H-10, H-8a/H-2'b and H-5, H-5/H-6 and H-7 β . The above conclusions support that compound **2** has the same relative configuration with its analog, eujavanicol A (**1**) (Nakadate *et al.*, 2007). Compound **2** exhibited an optical rotation of $[\alpha]_D^{22} +47.8$ (*c* 0.23, MeOH) compared to $[\alpha]_D^{22} +49.9$ (*c* 1.33, MeOH) for **1** (Nakadate *et al.*, 2007) and $[\alpha]_D +30.3$ (*c* 0.11, MeOH) for tandyukisin (Yamada *et al.*, 2014) (Li *et al.*, 2014b). Considering the same biosynthetic origin for **1** and **2**, the absolute configuration of **2** should be same as that of **1** and tandyukisin.

Table 4.1.2.1 NMR spectral data for compound **2**.

Position	δ_C , mult. ^a	δ_H mult. ^b (<i>J</i> in Hz)	COSY ^b	HMBC ^b
1	49.4, C _q			
2	54.0, CH	1.84 m ^c	1', 3, 4	1', 2', 1, 3, 4, 8a, 1-Me
3	124.9, CH	5.75 dd (10.0, 3.0)	2, 4	1, 2, 4a
4	126.3, CH	6.02 d (10.0)	2, 3, 4a	2, 4a, 5, 8a
4a	39.1, CH	2.18 m	4, 5, 6, 8a	3, 4, 5
5	75.4, CH	3.47 m	4a, 6	
6	69.7, CH	4.06 br s	5, 7	8
7 α	41.4, CH ₂	1.88 m	6	5, 6, 8, 8a
7 β		1.52 m		
8	30.3, CH	1.78 m	8a, 8-Me	
8a	43.3, CH	1.94 t (10.0)	4a, 8	1, 4a, 5, 7, 8, 1-Me
9	205.7, C _q			
10	99.7, CH	5.83 d (5.0)	11	9, 11
11	175.4, CH	7.97 d (5.0)	10	9, 10
1'	36.8, CH	1.33 m	2, 1'-Me	2', 3'
2'a	25.5, CH ₂	0.79 m ^c		
2'b		1.56 m	1', 3'	2, 1', 3', 1'-Me
3'	12.6, CH ₃	0.80 m ^c	2'	1', 2'
1-Me	19.8, CH ₃	1.21 s		1, 2, 8a, 9
1'-Me	19.6, CH ₃	0.92 d (7.0)	1'	2, 1', 2'
8-Me	20.8, CH ₃	0.76 d (7.0)	8	7, 8, 8a

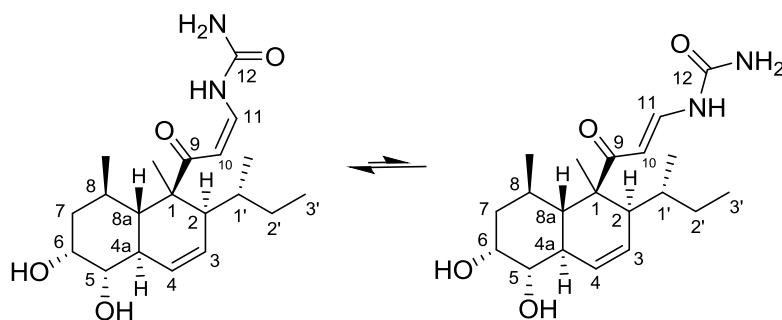
^a Recorded in CDCl₃ at 125 MHz; ¹³C multiplicities were determined by HSQC experiment. ^b Recorded in CDCl₃ at 500 MHz. ^c Signals overlapped.

Eupenicinicol A (2): white powder; $[\alpha]_D^{22}$ +47.8 (*c* 0.23, MeOH); LC-UV [(Acetonitrile (aq) in H₂O/0.1% FA)] λ_{\max} 226, 274 nm; IR (film) ν_{\max} 3452, 1632, 1114 cm⁻¹; CD (MeCN) 194 ($\Delta\epsilon$ + 4.21), 290 ($\Delta\epsilon$ - 0.09), 343 ($\Delta\epsilon$ + 0.11) nm; ¹H NMR (CDCl₃, 500 MHz) and ¹³C NMR (CDCl₃, 125 MHz), see Table 4.1.2.1; Positive ESI-HRMS *m/z*: 323.2216 [M+H]⁺ (calcd for C₁₉H₃₁O₄, 323.2217) (Li *et al.*, 2014b).

4.1.3 Eupenicinicol B (**3**, new compound)

The minor component **3** (code: LG41-4135) was also purified as a white powder (Li *et al.*, 2014b). A molecular formula of $C_{20}H_{32}O_4$ was determined from its quasimolecular ion at m/z 337.2373 $[M+H]^+$ and its fragment information ($[M+H-H_2O]^+$ at m/z 319.2268 and $[M+H-2\times H_2O]^+$ at m/z 301.2162, Figure 4.1.3.1). The MS^2 pattern of **3** was very close to that of compound **2**, especially in the abundant fragment ion at m/z 217.1948 $[M+H-C_4H_8O_4]^+$, except that a lost CH_3OH molecule was observed ($[M+H-CH_3OH]^+$ at m/z 305.2111, or $[M+H-H_2O]^+$ at m/z 319.2262, $[M+H-H_2O-CH_3OH]^+$ at m/z 287.2001, Figure 4.1.3.2). The fragmentation pattern suggested that the structure of compound **3** was similar to that of **2**, except for an additional methoxy group in **3** (Li *et al.*, 2014b). Unlike compound **2**, the 1H NMR spectrum of **3** (Figure 4.1.3.3) exhibited a large coupling constant ($J = 12.0$ Hz in **3**; $J = 5.0$ Hz in **2**) between H-10 and H-11, and a methoxy singlet (δ_H 3.77), indicating a *trans*-disubstituted double bond and locating the methoxy group at C-11. Unfortunately, due to the limited amount of **3** available for NMR experiment, ^{13}C , HSQC, and HMBC spectra were not clear for structural elucidation. However, for the moiety substituted by the methoxy group, assigning the NMR data to **3** (for OMe-11, δ_H 3.77, δ_C 58.0; for C-11, δ_H , 7.59, δ_C 163.5) is still possible from key HMBC correlations of OMe-11 to C-11, and H-11 to OMe-11. 1H - 1H COSY NMR spectrum also supported the whole structure (Figure 4.1.3.3). From a biosynthetic view, compound **3** should have the same absolute configuration as **2**.

Eupenicinicol B (3): white powder; $[\alpha]_D^{22} +16.0$ (c 0.05, MeOH); LC-UV [(Acetonitrile (aq) in $H_2O/0.1\%$ FA)] λ_{max} 226, 258 nm; IR (film) ν_{max} 3444, 1640, 1109 cm^{-1} ; 1H NMR ($CDCl_3$, 500 MHz) see Figure 4.1.3.3; Positive ESI-HRMS m/z : 337.2373 $[M+H]^+$ (calcd for $C_{20}H_{33}O_4$, 337.2379) (Li *et al.*, 2014b).

4.1.4 Eupenicinicol C (**4**, new compound)

In the course of searching for compounds with similar MSⁿ pattern as that of **1–3**, we noted that a pure compound (**4**, code: LG41-P5334) interestingly displayed two peaks with different retention times in semi-preparative HPLC and LC-HRMS systems (Figure 4.1.4.1). In addition, each collected single peak reinjected immediately changed to two signals, which was in accordance with the original chromatographic profile. Both signals shared the same molecular formula, C₂₀H₃₂O₄N₂ (6 double bond equivalents), as established by ESI-HRMS ([M+H]⁺ 365.2438, calcd. 365.2435, Figure 4.1.4.1). Therefore, a proposed kinetic equilibrium between two diastereomers was noted to be strongly favored. The MS² spectrum (Figure 4.1.4.1) of **4** also possessed the characteristic fragment ion at *m/z* 217.1949, which was present in co-occurring decalin motif-containing secondary metabolites **1–3**. The above MS data revealed a preferred cleavage of the side chain located at C-1 in **4** to give a fragment [M+H-C₄H₈O₄N₂]⁺ without any nitrogen. Further detailed analysis of MS² spectrum (Figure 4.1.4.1) supported the presence of an urea moiety in the above side chain from fragment ions at *m/z* 348.2168 [M+H-NH₃]⁺, 322.2381 [M+H-CHON]⁺, and 305.2114 [M+H-CH₄ON₂]⁺, and two hydroxyl groups from other product ions at *m/z* 287.2006 [M+H-CH₄ON₂-H₂O]⁺, and 269.1900 [M+H-CH₄ON₂-2×H₂O]⁺. The 1D NMR spectra of **4** (Figures 4.1.4.2 and 4.1.4.5) showed similar structural features to those of **1–3**, except for the observed chemical shift differences due to the side chain. The construction of side chain of **4** was determined from its ¹H-¹H COSY data and key HMBC correlations of 1-Me with C-9, and H-10 and H-11 with C-9, together with HMBC correlations from H-11 (δ_H 7.38) to C-12 (δ_C 157.5) and the chemical shifts of C-11 (δ_C 140.7) and C-12, placing the urea moiety at C-11 (Figures 4.1.4.3-4.1.4.5). Specifically, the chemical equilibrium between isomeric forms of **4** as suggested by the LC-MS was further confirmed by ¹H NMR spectrum coupled with ¹H-¹H COSY spectrum. The coupling constants

between H-10 and H-11 supported the *cis* ($J = 9.0$)- or *trans* ($J = 13.5$)-di-substituted double bond at C-10 (Figure 4.1.4.2 and Table 4.1.4.1). It would be convincing that the formation of hydrogen bond between the carbonyl group at C-9 and the nitrogen of urea is responsible for forming the dominant conformation. The relative configuration of **4** was same as that of **1–3** based on the NOESY correlations of Me-1/H-2, H-4a, H-8 and H-10, H-8a/H-2'b and H-5, H-6/H-5 and H-7 β (Figure 4.1.4.4). Finally, a single-crystal diffraction experiment further confirmed its gross structure and relative configuration (Figure 4.1.4.6). **4** should have same absolute configurations as **1–3** considering their optical rotation data and biosynthetic pathway. Therefore, the structure of compound **4** was established and named as eupenicinicol C.

Table 4.1.4.1 The NMR data for compound **4** (in CD₃OD).

Position	4	
	δ_C , mult. ^a	δ_H mult. ^b (J in Hz)
1	52.8, C _q	
2	54.4, CH	1.89 m ^c
3	125.5, CH	5.72 br d (10.0)
4	128.7, CH	6.05 br d (10.0)
4a	40.2, CH	2.17 br t (10.5)
5	76.7, CH	3.32 m ^c
6	70.9, CH	3.94 m
7 α	42.9, CH ₂	1.78 m
7 β		1.43 br t (12.0)
8	31.2, CH	1.76 m
8a	44.1, CH ^d	1.92 m ^c
9	208.2, C _q	
10	99.6, CH (80%)	5.79 d (9.0); 6.23 d (13.5) ^e
11	140.7, CH (80%)	7.38 d (8.5); 7.95 d (13.5) ^e
12	157.5, C _q	
1'	37.7, CH	1.32 m
2'a	26.5, CH ₂	0.78 m ^c
2'b		1.58 m
3'	13.0, CH ₃	0.78 m ^c
1-Me	20.4, CH ₃	1.26 s
1'-Me	20.0, CH ₃	0.90 d (7.0)
8-Me	22.2, CH ₃	0.66 d (6.5)

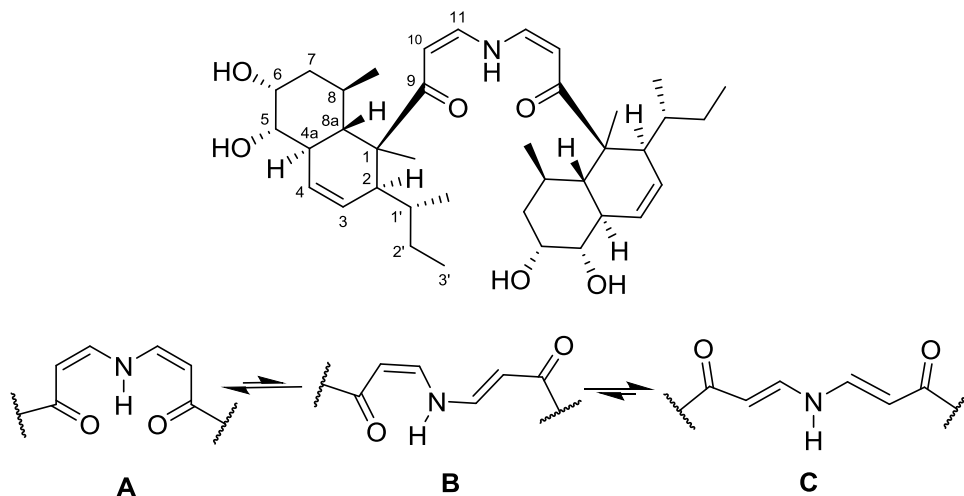
^a Recorded at 125 MHz; ¹³C multiplicities were determined by HSQC experiment. ^b Recorded at 500 MHz. ^c Signals overlapped. ^d Proposed by HMBC correlation. ^e Observed from Δ^{10} -*E*-configuration.

Eupenicinicol C (4): white powder; $[\alpha]_D^{20} +87.3$ (c 0.15, MeOH); LC-UV [(Acetonitrile (aq) in H₂O/0.1% FA)] λ_{\max} 222, 292 nm; IR (film) ν_{\max} 3333, 1645, 1568 cm⁻¹; ¹H NMR (CD₃OD, 500 MHz)

and ^{13}C NMR (CD_3OD , 125 MHz), see Table 4.1.4.1. Positive ESI-HRMS m/z : 365.2438 $[\text{M}+\text{H}]^+$ (calcd for $\text{C}_{20}\text{H}_{33}\text{O}_4\text{N}_2$, 365.2435).

Crystal data of eupenicinicol C (4): the colorless crystals were obtained from an acetone solution; crystal size $0.15 \times 0.10 \times 0.05 \text{ mm}^3$, orthorhombic crystal system, space group $P2_12_12_1$, $a = 9.0781(4) \text{ \AA}$, $b = 9.8882(5) \text{ \AA}$, $c = 26.0188(13) \text{ \AA}$, $V = 2335.60(19) \text{ \AA}^3$; $Z = 4$, $T = 150 \text{ K}$, $\mu(\text{Mo K}\alpha) = 0.084 \text{ mm}^{-1}$, $D_{\text{calc}} = 1.202 \text{ g/cm}^3$; 20307 reflections measured with 2θ ranged from 4.406 to 51.994° ; 4579 unique reflections ($R_{\text{int}} = 0.0483$, $R_{\text{sigma}} = 0.0396$). $R_1 = 0.0446$, $wR_2 = 0.1041$ (all data). Crystallographic data of eupenicinicol C (4) was deposited in the Cambridge Crystallographic Data Centre with supplementary publication number CCDC 1440259. Copies of the data can be acquired, free of charge, from Cambridge Crystallographic Data Centre, 12 Union Road, Cambridge CB2 1EZ, UK [fax: +44(0)1223 336033 or e-mail: deposit@ccdc.cam.ac.uk].

4.1.5 Eupenicinicol D (5, new compound)



Similar to compound 4, eupenicinicol D (5, code: LG41-P532, LG41-C2, or LG41-626), which was purified as a white powder, showed three un-isolated diastereomers observed in LC-HRMS experiment (Figure 4.1.5.1). All of them exhibited the same molecular formula of $\text{C}_{38}\text{H}_{59}\text{O}_6\text{N}$ (10 double bond equivalents) as verified by a positive ESI-HRMS pseudomolecular ion at m/z 626.4427 $[\text{M}+\text{H}]^+$ (Figure 4.1.5.1). In order to get clear 1D NMR data of 5, we tried several common NMR solvents acetone- d_6 , CD_3OD and $\text{DMSO}-d_6$ except for CDCl_3 where it was not soluble (Figure 4.1.5.2). Unfortunately, the

signals of three isomeric forms were always observed as exhibited by the overlapping or several minor signals (especially chemical shifts ranged from δ_{H} 5.5 to 8.0) in ^1H NMR spectrum (Figure 4.1.5.2) and some triple-splitting signals in ^{13}C NMR spectrum of **5**. However, these 1D NMR data and further 2D NMR experiments of **5** led us to roughly figure out its structural characters as similar to that of compound **4**. Therefore, we predicted that two monomers like **4** were coupled through their side chains to form a dimer structure **5**, which was also partly supported by its MS^2 analysis (Figure 4.1.5.1). Finally, we selected pyridine- d_5 as NMR solvent and recognized that only one major isomer was observed in ^1H NMR spectrum (Figure 4.1.5.2). Surprisingly, after the sample was dried, it could be easily dissolved in CDCl_3 to obtain clear NMR spectra (Figure 4.1.5.3). The above solvent optimization and results indicated that the pyridine- d_5 and CDCl_3 can be used to obtain a single molecule diastereomer (in this case, the most stable isomer). Considering that NMR data of compounds **1–3** were measured in CDCl_3 , herein we mainly described the structural elucidation of **5** using NMR data in CDCl_3 . The 1D NMR data (Figure 4.1.5.3 and Table 4.1.5.1) with the help of HSQC spectrum (Figure 4.1.5.4), revealed the presence of four methyls, two methylenes, seven methines (two oxygenated), two *cis*-disubstituted double bonds, and the remaining two quaternary carbons, accounting for 27 ^1H and 19 ^{13}C signals. A dimeric structure for **5** was constructed based on the requirement of MS data. The above analysis indicated very similar structural features as that of **1–4**, except for the significant differences due to the side chain. The side chain was assembled by ^1H - ^1H COSY correlations of H-10/H-11 and the HMBC correlations from Me-1 to C-1 and C-9, from H-10 to C-9 (Figures 4.1.5.4 and 4.1.5.5). The coupling constant of H-10/H-11 ($J = 8.4$ Hz) implied a *Z*-configured double bond (Table 4.1.5.1). The key ^1H - ^1H COSY correlation between H-11 and NH and MS requirement suggested the connection of two monomers through a nitrogen linkage, which is further supported by MS^2 spectrum with abundant fragment information in the mass range 250–400 Da (Figure 4.1.5.1). Based on this proposed structure, two hydrogen bonds should play a very important role in the stability of this *cis* isomer. This also led us to further explain the occurrence of three isomers in other solvents. Taking the NMR experiment in acetone- d_6 as an example, detailed analysis of the side chain at C-1 using ^1H NMR and ^1H - ^1H COSY data showed that **5** existed as a mixture of three isomers derived from the *cis*- or *trans*-disubstituted double bonds (Figure 4.1.5.6). Therefore, the planar structure of compound **5** was confirmed as depicted. The relative configuration of **5** was assigned through the NOESY correlations (Figure 4.1.5.7) of Me-1/H-2, H-4a, H-8, and H-10, H-8a/H-2'b and H-5, H-6/H-5, which was consistent with that of compounds **1–4**. Compound **5** was optically active with $[\alpha]_{\text{D}}^{20} +37.3$ (c 0.60, CHCl_3), excluding the

possibility of mesomer. Considering its optical rotation data and the biosynthetic pathway, **5** should have the same absolute configuration as **1–4**.

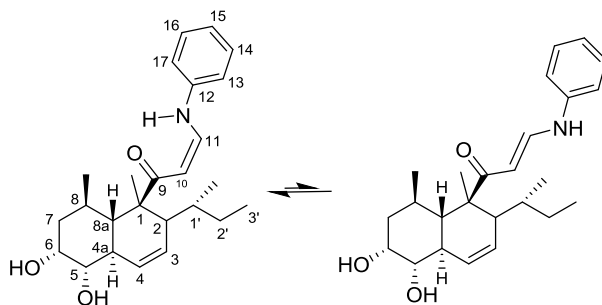
Table 4.1.5.1 The NMR data for compound **5** (in CDCl₃).

Position	5	
	δ_C , mult. ^a	δ_H mult. ^b (<i>J</i> in Hz)
1	51.3, C _q	
2	53.3, CH	1.84 m ^c
3	125.4, CH	5.74 m
4	126.4, CH	5.99 d (10.2)
4a	39.5, CH	2.12 br t (9.0)
5	75.7, CH	3.46 dd (3.0, 10.2)
6	70.0, CH	4.03 m
7 α	41.3, CH ₂	1.81 br d (13.8)
7 β		1.56 m ^c
8	30.5, CH	1.70 m
8a	43.3, CH	2.12 m ^c
9	203.5, C _q	
10	99.2, CH	5.66 d (8.4)
11	144.6, CH	6.58 t (8.4)
12		
1'	36.8, CH	1.27 m ^c
2'a	25.3, CH ₂	0.72 m ^c
2'b		1.59 m ^c
3'	12.9, CH ₃	0.73 m ^c
1-Me	20.6, CH ₃	1.24 s
1'-Me	19.9, CH ₃	0.86 d (6.6)
8-Me	21.7, CH ₃	0.65 d (6.0)
NH		13.35 br s

^a Recorded at 150 MHz; ¹³C multiplicities were determined by HSQC experiment. ^b Recorded at 600 MHz. ^c Signals overlapped.

Eupenicinicol D (5): white powder; $[\alpha]_D^{20} +37.3$ (*c* 0.60, CHCl₃), $[\alpha]_D^{20} -64.0$ (*c* 0.10, MeOH); LC-UV [(Acetonitrile (aq) in H₂O/0.1% FA)] λ_{\max} 218, 358 nm; IR (film) ν_{\max} 3376, 2956, 2918, 2849, 1644, 1577, 1465, 1061 cm⁻¹; CD (CHCl₃) 245 ($\Delta\epsilon +0.86$), 261 ($\Delta\epsilon -0.78$), 278 ($\Delta\epsilon +0.99$), 295 ($\Delta\epsilon +0.46$), 326 ($\Delta\epsilon +1.10$), 349 ($\Delta\epsilon -0.05$), 355 ($\Delta\epsilon +0.22$), 366 ($\Delta\epsilon -0.23$), 382 ($\Delta\epsilon +0.91$) nm; CD (MeOH) 238 ($\Delta\epsilon +3.99$), 314 ($\Delta\epsilon +1.80$), 361 ($\Delta\epsilon -1.70$) nm; ¹H NMR (CDCl₃, 600 MHz) and ¹³C NMR (CDCl₃, 150 MHz), see Table 4.1.5.1. Positive ESI-HRMS *m/z*: 626.4427 [M+H]⁺ (calcd for C₃₈H₆₀O₆N, 626.4415).

4.1.6 Eupenicinicol E (6, new compound)

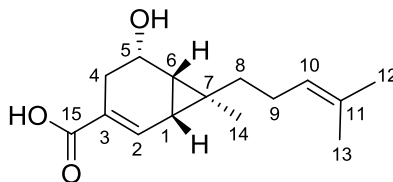


Compound **6** (code: LG41-P4222) was isolated as a white powder with a molecular formula $C_{25}H_{35}O_3N$ deduced from APCI-HRMS ($[M+H]^+$ at m/z 398.2693, calcd. 398.2690) (Figure 4.1.6.1). MS^2 spectrum showed the loss of two water molecules (m/z 380.2587 $[M+H-H_2O]^+$ and 362.2483 $[M+H-2\times H_2O]^+$) and an abundant product ion at m/z 146.0600 $[M+H-C_{16}H_{28}O_2]^+$ (Figure 4.1.6.1). 1H NMR spectrum exhibited similar structural features to those of compounds **1–5** (Figure 4.1.6.2). The differences between them were found and attributed to the side chain. Unfortunately, due to the limited amount of **6** available for NMR experiment, ^{13}C , HSQC, and HMBC spectra were not clear for structural elucidation. However, compared to compounds **2–4**, an aniline motif attached to C-11 as the structural difference in the side chain, was established on the basis of the 1H NMR and 1H - 1H COSY spectra (Figure 4.1.6.2). A chemical equilibrium of two isomers due to a hydrogen bond was also indicated by the 1H - 1H COSY spectrum and the coupling constant ($J = 8.0$ or 12.5 Hz) between H-10 and H-11 in 1H NMR spectrum (Figure 4.1.6.2 and Table 4.1.6.1). The whole structure was proposed as shown, which was supported by MS^2 spectrum with a key fragment ion $[M+H-C_{16}H_{28}O_2]^+$ ($= [C_9H_8ON]^+$) (Figure 4.1.6.1).

Table 4.1.6.1 1H NMR data for compound **6** (in CD_3OD).

Position	6
	δ_H mult. ^a (J in Hz)
3	5.69 m ^b
4	6.05 br d (9.0)
5	3.35 m ^b
6	3.94 m
10	5.73 m, ^{b,c} or 6.15 d (12.5)
11	7.56 d (8.0), ^c or 8.09 d (12.5)
13, 17	6.98-7.14 m ^b
14, 16	7.29-7.36 m ^b
15	6.98-7.14 m ^b

^a Recorded at 500 MHz. ^b Overlapped. ^c Main isomer.

4.1.7 Eupenicisirenin A (**7**, new compound)

The molecular formula of compound **7** (code: LG41-511331) (Li *et al.*, 2014b) was determined as $C_{15}H_{22}O_3$ with 5 double bond equivalents on the basis of ESI-HRMS (m/z 251.1638, $[M+H]^+$, calcd. 251.1642; m/z 233.1536, $[M+H-H_2O]^+$, calcd. 233.1536, Figure 4.1.7.1). The ESI-HRMS² spectrum of **7** (Figure 4.1.7.1) indicated the presence of a carboxyl or lactone group from fragment ions at m/z 215.1426 $[M+H-2\times H_2O]^+$, 197.1320 $[M+H-3\times H_2O]^+$ and 187.1477 $[M+H-H_2O-CH_2O_2]^+$, and of a 2- (or 3)-methylpent-2-ene moiety corresponding to other product ions at m/z 177.0907 $[M+H-H_2O-C_4H_8]^+$, 163.0751 $[M+H-H_2O-C_5H_{10}]^+$ and 149.0598 $[M+H-H_2O-C_6H_{12}]^+$ (Li *et al.*, 2014b). 1D NMR spectra in combination with HSQC data of **7** (Figures 4.1.7.2 and 4.1.7.3, and Table 4.1.7.1) verified the presence of three methyls, three methylenes, three methines (one oxygenated), one quaternary carbon signal, and four olefinic carbons. Detailed HMBC correlations of H-4 β to C-2, C-3, and C-15, and H-2 to C-15 (Figure 4.1.7.4), indicated an α,β -unsaturated carboxylic acid or lactone, supported partly by MS² analysis (Figure 4.1.7.1). Furthermore, the ¹H-¹H COSY correlations of H-1/H-2, H-1/H-6, H-5/H₂-4, and H-5/H-6 confirmed the presence of a six-membered ring system in **7** (Figure 4.1.7.4). Another ¹H-¹H spin system of CH₂(8)-CH₂(9)-CH(10) as well as the HMBC correlations of H₃-12/C-10, C-11 and C-13, and H₃-13/C-10, C-11 and C-12 verified a 2-methylpent-2-ene moiety as suggested by MS² data (Figure 4.1.7.4). The connection of C-7 to C-1, C-6, C-8 and C-14 was revealed by the HMBC correlations from H₃-14 (δ_H 1.04, s) to C-1, C-6, C-7, and C-8. Finally, a hydroxy and a carboxyl group were located at C-5 and C-3, respectively through the analysis of chemical shift of C-5 (δ_C 65.6) and the MS requirement. Thus, the planar structure was confirmed. The key NOESY correlations of H-4 α (δ_H 1.83)/H₃-14, H-10/H₃-12, and the strong NOESY correlation between H-4 β (δ_H 3.01) and H-5 enabled the determination of its relative configuration as depicted (Figure 4.1.7.5) (Li *et al.*, 2014b).

The absolute configuration of **7** was calculated using semiempirical and *ab initio*-methods (Li *et al.*, 2014b). With SPARTAN'14 (SPARTAN '14, Wavefunction, Inc., Irvine, CA, 2014) and using PM3 and

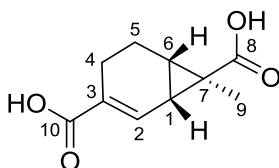
the Monte Carlo technique, 648 starting geometries were calculated, affording 100 conformers within 6.9 kcal above the global minimum. 53 conformers with Boltzmann factors >0.001 (corresponding to an energy difference of $E < 2.5$ kcal/mol) were further obtained by the geometry optimization with Gaussian g09 (Frisch *et al.*, 2009) using DFT calculations B3LYP/6-311G(2d,p). At the same theoretical level, the ECD spectra (Figure 4.1.7.6) of all conformers were calculated. The ECD values of individual conformer were summed according to their Boltzmann factors. The calculated ECD spectrum reflected the experimental CD data correctly (Figure 4.1.7.6), so that the absolute configuration of **7** is confirmed as depicted. Furthermore, ORD calculations with WB97XD/6-311G(d,p) showed a positive optical rotation of $[\alpha]_D +1.06^\circ$ (measured ($[\alpha]_D +2.7^\circ$) and confirmed the absolute configuration.

Table 4.1.7.1 ^1H and ^{13}C NMR data for compound **7** (in CDCl_3).

Position	7	
	δ_{C} , mult. ^a	δ_{H} mult. ^b (J in Hz)
1	28.1, CH	1.66 m ^c
2	141.4, CH	7.37 dd (3.0, 5.5)
3	124.6, C _q	
4 α	32.1, CH ₂	1.83 ddd (3.0, 8.5, 17.5)
4 β		3.01 dd (8.5, 17.5)
5	65.6, CH	4.28 ddd (5.5, 8.5)
6	32.8, CH	1.54 m ^c
7	34.7, C _q	
8	43.5, CH ₂	1.54 m ^c , 1.28 m
9	25.7, CH ₂	2.16 m
10	123.9, CH	5.14 t (7.0)
11	131.9, C _q	
12	25.6, CH ₃	1.72 s
13	17.7, CH ₃	1.65 s
14	13.4, CH ₃	1.04 s
15	169.5, C _q	

^a Recorded at 125 MHz; ^{13}C multiplicities were determined by HSQC experiment. ^b Recorded at 500 MHz. ^c Signals overlapped.

Eupenicisirenin A (7): white powder; $[\alpha]_D^{22} +2.7$ (c 0.11, MeOH); LC-UV [(Acetonitrile (aq) in $\text{H}_2\text{O}/0.1\%$ FA)] λ_{max} 250 nm; IR (film) ν_{max} 3415, 1643, 1375, 1321, 1101 cm^{-1} ; CD (MeOH) 209 ($\Delta\epsilon -1.11$), 260 ($\Delta\epsilon +1.54$) nm; ^1H NMR (CDCl_3 , 500 MHz) and ^{13}C NMR (CDCl_3 , 125 MHz), see Table 4.1.7.1; Positive ESI-HRMS m/z : 251.1638, $[\text{M}+\text{H}]^+$ (calcd for $\text{C}_{15}\text{H}_{23}\text{O}_3$, 251.1642); 233.1536 $[\text{M}+\text{H}-\text{H}_2\text{O}]^+$ (calcd for $\text{C}_{15}\text{H}_{21}\text{O}_2$, 233.1536) (Li *et al.*, 2014b).

4.1.8 Eupenicisirenin B (**8**, new compound)

Compound **8** (code: LG41-511332) (Li *et al.*, 2014b) was isolated as a white solid. Product ions at m/z 195.06, 151.07 and 107.03 in negative ESI-MS, MS² and MS³ (Figure 4.1.8.1) corresponded to [M-H]⁻, [M-H-COO]⁻ and [M-H-2×COO]⁻ respectively, indicating two carboxyl or lactone groups in **8**. Thus, based on the ¹H NMR data (Table 4.1.8.1 and Figure 4.1.8.2), its molecular formula was assigned as C₁₀H₁₂O₄. Like **7**, a similar ring system was also found in compound **8**, which was confirmed by the ¹H-¹H COSY correlations of H-1/H-2, H-1/H-6, and H-4β/H-5α and the HMBC correlations from H-1 to C-3 and C-7, from H-2 to C-1 and C-4, from H₂-5 to C-3 and C-6, and from H₃-9 to C-6 and C-7 (Figures 4.1.8.3 and 4.1.8.4) (Li *et al.*, 2014b). Two carboxylic acids (δ_C 170.5 and 178.2) suggested by MS analysis, were placed at C-3 and C-7, respectively. The above assignment was supported by the HMBC correlations of H-1 to C-8, H-2 to C-10, and H₃-9 to C-8. NOESY correlations of H₃-9/H-4α (δ_H 2.05), H₃-9/H-5α (δ_H 1.88), and H-1/H-6 (Figure 4.1.8.5) revealed the relative configuration of **8**.

As fewer degrees of freedom for internal rotations observed in compound **8** compared to **7**, SPARTAN'14 calculation obtained only 12 conformers. All were within a range of 2.1 kcal above the global minimum. A further optimization of the individual geometries with Gaussian g09 (Frisch *et al.*, 2009) using the same DFT calculation as that for compound **7** reduced the energy range to < 1 kcal. Based on the relative configuration, the identical curve trends of experimental and calculated ECD spectra (Figure 4.1.8.6) determined that the new compound **8** is (1*R*,6*S*,7*R*)-configured (Figure 4.1.8.6). This was further confirmed by the negative sign of the calculated optical rotation ($[\alpha]_D -43^\circ$) compared to experimental value ($[\alpha]_D^{22} -27.3^\circ$).

Regarding the NOE data of compounds **7** and **8**, the chirality centers in them share the same relative configuration. As the hydroxy group in **7** had no effect on the chromophoric system, the similar experimental and calculated ECD spectra of **7** and **8** were expected. However, their optical rotations showed opposite signs and also differed strongly in their absolute values (Li *et al.*, 2014b). Out of the 53 conformers populated at RT in **7**, 26 with a negative sign contributed -1.54° to the optical rotation. This

was compensated by 27 conformers with a positive rotation value, contributing to $+2.60^\circ$ to the optical rotation. Finally, the above data resulted in a positive optical rotation of $[\alpha]_D +1.06^\circ$ for compound **7**. As shown in Figure 4.1.8.7, the conformation of the prenyl side chain in **7** is responsible for this effect. Obviously, exciton interactions of these chromophores can significantly influence the optical rotation of **7**. An even stronger effect has been discovered for the *E*- and *Z*-nitriles calyculins A and B and was termed as π -mediated intramolecular communication between the chiral centers and the terminal nitrile group (Kondru *et al.*, 2000; Li *et al.*, 2014b).

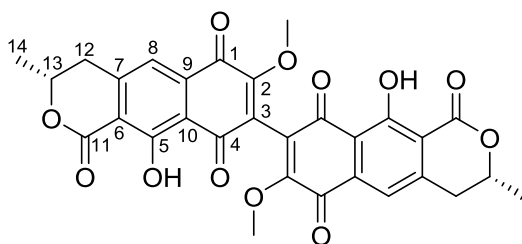
Table 4.1.8.1 ^1H and ^{13}C NMR data for compound **8** (in CD_3OD).

Position	8	
	δ_{C} , mult. ^a	δ_{H} mult. ^b (<i>J</i> in Hz)
1	26.1, CH	2.18 dd (5.5, 8.5)
2	136.5, CH	7.10 m
3	132.5, C _q ^d	
4 α	22.3, CH ₂	2.05 m
4 β		2.39 m
5	17.2, CH ₂	2.01 m ^c , 1.88 α , m
6	25.7, CH	1.97 m ^c
7	34.0, C _q ^d	
8	178.2, C _q ^d	
9	10.1, CH ₃	1.15 s
10	170.5, C _q ^d	

^a Recorded at 125 MHz; ^{13}C multiplicities were determined by HSQC experiment. ^b Recorded at 500 MHz. ^c Signals overlapped. ^d Proposed by HMBC correlations.

Eupenicisirenin B (8): white solid; $[\alpha]_D^{22} -27.3$ (*c* 0.15, MeOH); LC-UV [(Acetonitrile (aq) in $\text{H}_2\text{O}/0.1\%$ FA)] λ_{max} 246 nm; IR (film) ν_{max} 3452, 1627, 1380 cm^{-1} ; CD (MeOH) 207 ($\Delta\epsilon - 4.80$), 253 ($\Delta\epsilon + 1.19$) nm; ^1H NMR (CD_3OD , 500 MHz) and ^{13}C NMR (CD_3OD , 125 MHz), see Table 4.1.8.1; Negative ESI *m/z*: 195.06 $[\text{M}-\text{H}]^-$, 151.07 $[\text{M}-\text{H}-\text{CO}_2]^-$, and 107.03 $[\text{M}-\text{H}-2\times\text{CO}_2]^-$ (Li *et al.*, 2014b).

4.1.9 Xanthomegnin (9, known compound)

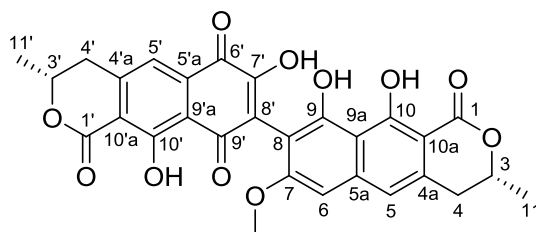


Compound **9** (code: LG41-31), a red powder, had the molecular formula $C_{30}H_{22}O_{12}$ as determined by ESI-HRMS (m/z 575.1191, $[M+H]^+$, calculated 575.1184, Δ 1.1773, Figure 4.1.9.1). However, there were only fifteen carbon signals (some split) in ^{13}C NMR spectrum (Figure 4.1.9.2), indicating that compound **9** is dimeric. In 1H NMR spectrum (Figure 4.1.9.2), two methyls (one oxygenated), a methylene, an oxygenated methine and an olefinic proton, as well as an exchangeable proton around δ_H 13.1 were found. After checking several MS databases (Nielsen *et al.*, 2011) and comparing its NMR data (Table 4.1.9.1) with that in the literature (Höfle *et al.*, 1978), compound **9** was established as xanthomegnin.

Table 4.1.9.1 1H and ^{13}C NMR data for compound **9** (in $CDCl_3$).

Position	9		Xanthomegnin (Höfle <i>et al.</i> , 1978)
	δ_C , mult. ^a (splitting signals)	δ_H mult. ^b (J in Hz)	δ_C ^c
1	180.2, C _q		179.7
2	158.3, C _q		157.9
3	123.1, C _q (123.3)		122.7
4	186.3, C _q		186.1
5	163.0, C _q		162.0
6	117.8, C _q (117.9)		117.2
7	148.4, C _q (148.5)		148.2
8	117.1, CH	7.49 s	116.8
9	134.9, C _q (135.0)		134.6
10	114.9, C _q (115.0)		114.5
11	162.5, C _q		161.9
12	36.3, CH ₂ (36.4)	3.04 m	35.8
13	74.6, CH	4.67 m	74.4
14	20.7, CH ₃ (20.8)	1.54 d (6.0)	20.4
2-OMe	61.7, CH ₃	4.15 s	61.2
OH		13.14 (13.16) s	

^a Recorded at 100 MHz; ^{13}C multiplicities were determined by HSQC experiment. ^b Recorded at 500 MHz. ^c Recorded at 67.88 MHz (Bruker WH 270 spectrometer) in $DMSO-d_6$ - $CDCl_3$ (1:4).

4.1.10 7'-O-Desmethyl-viomellein (**10**, new compound)

Compound **10** (code: LG41-P342) was also isolated as a red powder. Its molecular formula $C_{29}H_{22}O_{11}$ was determined through ESI-HRMS (m/z 547.1244, $[M+H]^+$, calculated 547.1235, Δ 1.6992). In 1H NMR spectrum (Figure 4.1.10.1), two secondary methyls (δ_H 1.58, d, $J = 6.0$ Hz; 1.59, d, $J = 6.0$ Hz), one oxygenated methyl group (δ_H 4.16), two methylenes (δ_H 3.07), two oxygenated methines (δ_H 4.72 and 4.81) and three olefinic protons (δ_H 6.94, 7.07 and 7.67) were present in **10**. The above analysis indicated that compound **10** was also a naphthoquinone derivative like compound **9**. Analysis of its HSQC and HMBC spectra (Figures 4.1.10.2 and 4.1.10.3) confirmed the key structural units as exhibited in a known compound viomellein. Further analysis of HMBC correlation from 7-OMe to C-7 (Figure 4.1.10.3) and the comparison of their NMR data (Table 4.1.10.1) established the structure of compound **10** (Stack *et al.*, 1979). The difference between compound **10** and the known compound viomellein is the hydroxy group at C-7' in **10** instead of a methoxy in viomellein.

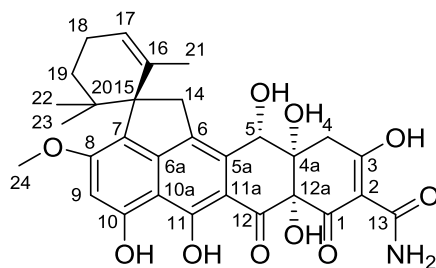
Table 4.1.10.1 1H and ^{13}C NMR data for compound **10** (in $CDCl_3$).

10						Viomellein (Stack <i>et al.</i> , 1979)					
No.	δ_C , mult. ^a	δ_H mult. ^b (J in Hz)	No.	δ_C , mult. ^a	δ_H mult. ^b (J in Hz)	No.	δ_C , mult. ^c	δ_H mult. ^d (J in Hz)	No.	δ_C , mult. ^c	δ_H mult. ^d (J in Hz)
1	170.6		1'	-		1	171.2		1'	162.4	
2			2'			2			2'		
3	76.2	4.81 m	3'	74.7	4.72 m	3	76.5	4.63	3'	74.1	4.63
4	35.3	3.07 m	4'	36.3	3.07 m	4	34.6	3.02	4'	36.3	3.02
4a	137.3		4'a	148.8		4a	134.0		4'a	147.9	
5	115.7	7.07 s	5'	117.1	7.67 s	5	116.0	6.96	5'	116.4	7.50
5a	-		5'a	-		5a	140.5		5'a	134.4	
6	103.2	6.94 s	6'	172.8		6	97.8	6.66	6'	180.1	
7	156.4		7'	-		7	160.1		7'	158.2	
8	113.5		8'	-		8	99.9		8'	123.6	
9	158.3		9'	-		9	161.3		9'	188.3	
9a	106.9		9'a	116.6		9a	105.1		9'a	114.8	
10	161.3		10'	164.0		10	155.3		10'	162.8	
10a	102.6		10'a	117.8		10a	107.9		10'a	117.6	

11	21.0	1.59 d (6.0)	11'	20.8	1.58 d (6.0)	11	20.7	1.56	11'	20.7	1.34
10-OH		12.81 s	10'-OH		13.40 s	9-OH		9.80	10'-OH		13.44
7-OMe	56.5	4.16 s				10-OH		13.88	2 xOMe	55.9, 60.3	3.84, 3.90

^a Recorded at 100 MHz; ¹³C multiplicities were determined by HSQC experiment. ^b Recorded at 500 MHz. ^c Recorded at 25.2 MHz in CDCl₃. ^d Recorded at 100 MHz in CDCl₃.

4.1.11 Viridicatumtoxin (11, known compound)



Compound **11** (code: LG41-22) was purified by column chromatography on silica gel and afforded a red powder. ESI-HRMS was applied to assign its molecular formula C₃₀H₃₁NO₁₀ based on MS information (m/z 565.1940, [M]⁺, calcd. 565.1943, Δ -0.4660, Figure 4.1.11.1). The ¹H NMR spectrum (Figure 4.1.11.2) of **11** displays signals for four tertiary methyls (one oxygenated) (δ_{H} 0.47, 0.91, 1.53, and 3.87) and several methylenes or methines. The ¹³C NMR spectrum (Figure 4.1.11.2) of **11** exhibited 30 signals. Compound **11** was confirmed as viridicatumtoxin through a detailed comparison of NMR data of **11** with that of viridicatumtoxin (Table 4.1.11.1) (Inokoshi *et al.*, 2013).

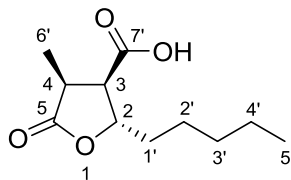
Table 4.1.11.1 ¹H and ¹³C NMR data for compound **11** (in CDCl₃).

Position	11		Viridicatumtoxin (Inokoshi <i>et al.</i> , 2013)	
	δ_{C} , mult. ^a	δ_{H} mult. ^b (J in Hz)	δ_{C} , mult. ^a	δ_{H} mult. ^b (J in Hz)
1	190.6, C _q		190.4, C _q	
2	99.7, C _q		99.5, C _q	
3	193.0, C _q		192.8, C _q	
4	40.5, CH ₂	2.75 dd (19.2) 2.82 dd (18.8)	40.3, CH ₂	2.76 dd (20.0) 2.82 dd (18.0)
4a	71.7, C _q		71.5, C _q	
5	71.8, CH	4.50 br s	71.6, CH	4.50 br s
5a	124.0, C _q		123.8, C _q	

6	137.2, C _q		137.0, C _q	
6a	147.3, C _q		147.1, C _q	
7	122.8, C _q		122.6, C _q	
8	160.9, C _q		160.7, C _q	
9	100.0, CH	6.65 s	99.9, CH	6.65 s
10	158.1, C _q		157.9, C _q	
10a	105.6, C _q		105.4, C _q	
11	166.1, C _q		165.9, C _q	
11a	105.2, C _q		105.0, C _q	
12	195.3, C _q		195.2, C _q	
12a	80.3, C _q		80.1, C _q	
13	172.9, C _q		172.7, C _q	
14	41.3, CH ₂	2.93 d (17.2) 3.47 d (16.8)	41.1, CH ₂	2.93 d (20.0) 3.44 d (20.0)
15	60.2, C _q		60.1, C _q	
16	136.7, C _q		136.6, C _q	
17	121.5, CH	5.51 br s	121.3, CH	5.51 br s
18	23.0, CH ₂	2.03 m 2.21 m	22.8, CH ₂	2.02 m 2.20 m
19	34.0, CH ₂	1.34 dd (6.0, 13.6) 1.83 ddd (6.4, 13.6, 13.6)	33.8, CH ₂	1.34 dd (6.0, 13.0) 1.84 ddd (3.0, 13.0, 13.0)
20	38.7, C _q		38.5, C _q	
21	24.1, CH ₃	1.53 s	23.9, CH ₃	1.53 s
22	25.6, CH ₃	0.47 s	25.4, CH ₃	0.47 s
23	21.2, CH ₃	0.91 s	20.9, CH ₃	0.91 s
24	55.7, CH ₃	3.87 s	55.5, CH ₃	3.87 s
3-OH		-		17.9 s
4a-OH		4.10 br s		4.15 s
5-OH		3.01 br s		3.04 br d (10.0)
10-OH		8.68 br s		8.68 br s
11-OH		14.78 br s		14.79 br s
12a-OH		5.30 s		5.28 br s
13-NH ₂		5.98 br s, 9.07 br s		5.92 br s, 9.08 br s

^a Recorded at 100 MHz in CDCl₃. ^b Recorded at 400 MHz in CDCl₃.

4.1.12 (2*S*,3*R*,4*S*)-4-Methyl-5-oxo-2-pentyl-tetrahydro-furan-3-carboxylic acid (**12**, new natural product)



Compound **12** (code: LG41-C322) was obtained as a white solid. Its molecular formula was determined as $C_{11}H_{18}O_4$ according to ESI-HRMS at m/z 215.1277 $[M+H]^+$ (Figure 4.1.12.1), indicating 3 double bond equivalents. The 1H NMR spectrum (Figure 4.1.12.2) of **12** suggested the presence of a changeable proton, two methyl groups, and three methine protons (one oxygenated). The 1D NMR data (Figure 4.1.12.2) coupled with HSQC spectrum (Figure 4.1.12.3) of **12** revealed two methyls, four methylenes, three methines (one oxygenated), and two carbonyl groups, accounting for 2 of the 3 degrees of unsaturation. The remaining double-bond equivalent was due to a multi-substituted furan ring, a γ -lactone, which was confirmed by the HMBC correlations (Figures 4.1.12.3 and 4.1.12.4) from $H_{3-6'}$ to C-3, C-4 and C-5, from H-3 and H-4 to C-2 and C-5, and from H-2 to C-5, and the chemical shifts of C-2 (δ_C 79.8) and C-5 (δ_C 177.8). The strong correlations of both $H_{2-2'}$ and $H_{3-5'}$ with C-3' and C-4', $H_{2-1'}$ with C-2' and C-3' in the HMBC spectrum verified the presence of a pentyl side chain (Figure 4.1.12.4). In addition, this side chain was located at C-2 through the analysis of HMBC correlations from H-2 and H-3 to C-1'. A carboxyl acid group was positioned at C-3 based on the HMBC correlations between H-2, H-3 and H-4 and C-7', and the MS requirement. Compound **12** possesses three asymmetric carbon centers: C-2, C-3, and C-4. The stereochemical relationships within **12** were mainly assigned by the analysis of 1D NOE and NOESY experiments (Figures 4.1.12.5-4.1.12.7). The key and significant correlations of H-2/ $H_{3-6'}$, H-2/ $H_{2-1'}$, and H-3/ $H_{2-1'}$ indicated that the Me-6', carboxyl acid and H-2 are in the same orientation. The absolute configuration of **12** was determined by comparing its optical rotation sign and value with those reported for similar structures (Figure 4.1.12.8) (Amador *et al.*, 2006; Drioli *et al.*, 1998; Banks *et al.*, 1995; Jacobi *et al.*, 2001; Huneck *et al.*, 1992; Mulzer *et al.*, 1993; Howell *et al.*, 2006; Mulzer *et al.*, 1991; Maier *et al.*, 1999; Deska *et al.*, 2009). The major difference between them is the length of side chain, which exhibited limited influence on their optical rotation. It should be emphasized that the short-side-chain as possessed in naturally occurring compounds sotolon

and maple furanone, resulted in the opposite optical rotation signs (Nakahashi *et al.*, 2011). In order to support the assignment of absolute configuration for this compound, we applied the TDDFT CD calculation and found it shows a positive cotton effect which is consistent with the experimental or literature data (Figure 4.1.12.9). The above analysis for the CD band around 220 nm conceivably allied with the $n-\pi^*$ transition of lactone chromophore, is in accordance with the empirical chirality rule of the γ -lactone ring (Beecham, 1968). Therefore, compound **12** was determined to be (2*S*,3*R*,4*S*)-4-methyl-5-oxo-2-pentyl-tetrahydro-furan-3-carboxylic acid. To the best of our knowledge, **12** was isolated as a natural product for the first time even though its synthesis (as a mixture) was achieved in 2006 (Amador *et al.*, 2006).

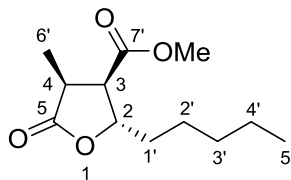
Table 4.1.12.1 ^1H and ^{13}C NMR data for compound **12** (in CDCl_3).

Position	12	
	δ_{C} , mult. ^a	δ_{H} mult. ^b (Hz)
2	79.8, CH	4.68 dt (6.0)
3	50.0, CH	3.14 dd (6.0, 8.0)
4	37.1, CH	3.02 qd (8.0)
5	177.8, C _q	
1'	34.7, CH ₂	1.66 m
2'	25.1, CH ₂	1.38 m, 1.46 m
3'	31.4, CH ₂	1.29 m ^c
4'	22.5, CH ₂	1.29 m ^c
5'	14.0, CH ₃	0.87 t (6.0)
6'	11.9, CH ₃	1.27 d (7.5)
7'	175.4, C _q	
COOH		9.23 s

^a Recorded in CDCl_3 at 125 MHz. ^b Recorded in CDCl_3 at 500 MHz. ^c Signals overlapped.

(2*S*,3*R*,4*S*)-4-Methyl-5-oxo-2-pentyl-tetrahydro-furan-3-carboxylic acid (12): white solid; $[\alpha]_{\text{D}}^{20}$ -77.1 (*c* 0.21, CHCl_3); LC-UV [(Acetonitrile (aq) in $\text{H}_2\text{O}/0.1\%$ FA)] λ_{max} 218 nm; IR (solid) ν_{max} 3164, 2955, 2928, 1760, 1729, 1180 cm^{-1} ; CD (MeOH) 215 ($\Delta\epsilon$ + 1.93) nm; ^1H NMR (CDCl_3 , 500 MHz) and ^{13}C NMR (CDCl_3 , 125 MHz), see Table 4.1.12.1. Positive ESI-HRMS m/z : 215.1277 $[\text{M}+\text{H}]^+$ (calcd for $\text{C}_{11}\text{H}_{19}\text{O}_4$, 215.1278, Δ -0.4376 ppm).

4.1.13 (2*S*,3*R*,4*S*)-4-Methyl-5-oxo-2-pentyl-tetrahydro-furan-3-carboxylic acid methyl ester (**13**, semi-synthetic compound)



Compound **13** (code: LG41-C32M3), as a methyl ester, was obtained by the reaction between dimethyl sulfate in acetone and a fraction (containing compounds **12**, **14**, **16**, and **19**) using a chemically engineered approach for diversification of natural product extract or fraction (section 3.9.1). Its molecular formula $C_{12}H_{20}O_4$ was determined on the basis of ESI-HRMS (m/z 229.1436, $[M+H]^+$, calculated 229.1434, Δ 0.5184 ppm, Figure 4.1.13.1). Detailed analysis of its 1D NMR spectra of **13** (Figure 4.1.13.2 and Table 4.1.13.1) in comparison with those of compound **12** confirmed its structure as a methyl ester of compound **12**. Thus, the preparation of methyl ester of carboxyl acid group was achieved, which was also supported by the MS/MS analysis (Figure 4.1.13.1). Its absolute configuration was further assigned using the same way as that for compound **12** (Figure 4.1.12.8).

Table 4.1.13.1 1H and ^{13}C NMR data for compound **13** (in $CDCl_3$).

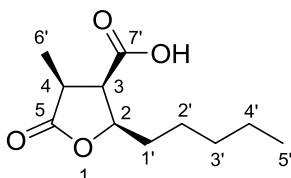
Position	13	
	δ_C , mult. ^a	δ_H mult. ^b (Hz)
2	79.5, CH	4.63 m
3	50.0, CH	3.07 dd (6.0, 9.0)
4	37.1, CH	2.91 m
5	177.2, C _q	
1'	34.7, CH ₂	1.60 m
2'	25.0, CH ₂	1.34 m, 1.43 m
3'	31.4, CH ₂	1.26 m ^c
4'	22.4, CH ₂	1.26 m ^c
5'	13.9, CH ₃	0.83 t (7.5)
6'	11.9, CH ₃	1.15 d (7.5)
7'	170.6, C _q	
OMe	52.1, CH ₃	3.69 s

^a Recorded in $CDCl_3$ at 125 MHz. ^b Recorded in $CDCl_3$ at 500 MHz. ^c Signals overlapped.

(*2S,3R,4S*)-4-Methyl-5-oxo-2-pentyl-tetrahydro-furan-3-carboxylic acid methyl ester (**13**): oil; $[\alpha]_D^{20}$ -63.4 (c 0.88, $CHCl_3$); LC-UV [(Acetonitrile (aq) in $H_2O/0.1\%$ FA)] λ_{max} 222 nm; IR (liquid) ν_{max} 2954, 2931, 2860, 1774, 1736, 1200, 1173 cm^{-1} ; 1H NMR ($CDCl_3$, 500 MHz) and ^{13}C NMR ($CDCl_3$, 125

MHz), see Table 4.1.13.1. Positive ESI-HRMS m/z : 229.1436 $[M+H]^+$ (calcd for $C_{12}H_{21}O_4$, 229.1434).

4.1.14 (2*R*,3*R*,4*S*)-4-Methyl-5-oxo-2-pentyl-tetrahydro-furan-3-carboxylic acid (**14**, new natural product)



Compound **14** (code: LG41-C321 or LG41-C3212), a white solid, showed a pseudomolecular ion peak at m/z 215.1276 $[M+H]^+$ in ESI-HRMS (Figure 4.1.14.1), indicating the molecular formula $C_{11}H_{18}O_4$ with 3 double bond equivalents. Analysis of its 1D NMR data (Figure 4.1.14.2) revealed the same structural characters to those observed in **12**, except for several minor chemical shift differences arising from the influence of stereochemical relationship. 1D NOE studies showed significant interactions of H-2/H-3, H-3/H-4, H-4/H-2, and no NOE interaction between H-3 and H₂-1', verifying that the Me-6', carboxyl acid, and side chain are on the same side of furan ring (Figures 4.1.14.3 and 4.1.14.4). Furthermore, considering the optical rotation of **14** compared to its analogs and enantiomers (Figure 4.1.12.8), the structure of **14** was established to be (2*R*,3*R*,4*S*)-4-methyl-5-oxo-2-pentyl-tetrahydro-furan-3-carboxylic acid. Finally, ECD calculation (Figure 4.1.14.5) was applied to further support its absolute configuration. As far as we know, compound **14**, as a reported synthetic intermediate (Jacobi and Herradura, 1996), is a new natural product isolated from a natural source.

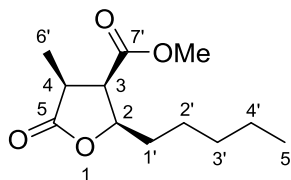
Table 4.1.14.1 1H and ^{13}C NMR data for compound **14** (in $CDCl_3$).

Position	14	
	δ_C , mult. ^a	δ_H mult. ^b (Hz)
2	79.1, CH	4.43 m
3	50.5, CH	3.32 dd (5.5, 7.0)
4	39.3, CH	2.94 m
5	177.2, C _q	
1'	31.0, CH ₂	1.67 m, 1.83 m
2'	25.7, CH ₂	1.42 m, 1.53 m
3'	31.6, CH ₂	1.30 m ^c
4'	22.6, CH ₂	1.30 m ^c
5'	14.1, CH ₃	0.89 t (7.0)
6'	10.5, CH ₃	1.30 d (7.0)
7'	175.1, C _q	
COOH		7.46 br s

^a Recorded in $CDCl_3$ at 125 MHz. ^b Recorded in $CDCl_3$ at 500 MHz. ^c Signals overlapped.

(2R,3R,4S)-4-Methyl-5-oxo-2-pentyl-tetrahydro-furan-3-carboxylic acid (14): white solid; $[\alpha]_D^{20} + 78.7$ (*c* 0.21, CHCl₃); LC-UV [(Acetonitrile (aq) in H₂O/0.1% FA)] λ_{\max} 218 nm; IR (solid) ν_{\max} 3000, 2936, 2873, 1766, 1694, 1233, 1185 cm⁻¹; CD (MeOH) 211 ($\Delta\epsilon + 0.82$) nm; ¹H NMR (CDCl₃, 500 MHz) and ¹³C NMR (CDCl₃, 125 MHz), see Table 4.1.14.1. Positive ESI-HRMS *m/z*: 215.1276 [M+H]⁺ (calcd for C₁₁H₁₉O₄, 215.1278).

4.1.15 (2R,3R,4S)-4-Methyl-5-oxo-2-pentyl-tetrahydro-furan-3-carboxylic acid methyl ester (15, semi-synthetic compound)



Compound **15** (code: LG41-C32M2), as a methyl ester, was obtained by the same strategy as compound **13**. Its molecular formula C₁₂H₂₀O₄ was determined on the basis of ESI-HRMS (*m/z* 229.1435, [M+H]⁺, calculated 229.1434, Δ 0.1021 ppm), which was same to that for compound **13** (Figure 4.1.13.1). Further analysis of its 1D NMR spectra of **15** (Figure 4.1.15.1 and Table 4.1.15.1) in comparison with that of compound **14** confirmed its structure as a methyl ester of compound **14**. Its relative configuration was supported through the analysis of 1D NOE correlations of H-2/H-3, H-3/H-4, H-4/H-2 (Figure 4.1.15.2 and 4.1.15.3). Furthermore, the same strategy as compound **12** was applied to determine its absolute configuration (Figure 4.1.12.8).

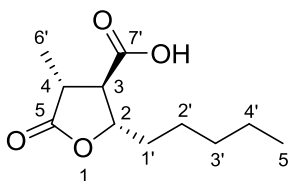
Table 4.1.15.1 ¹H and ¹³C NMR data for compound **15** (in CDCl₃).

Position	15	
	δ_C , mult. ^a	δ_H mult. ^b (Hz)
2	79.2, CH	4.39 m
3	50.9, CH	3.30 dd (5.4, 7.8)
4	39.3, CH	2.89 m
5	177.3, C _q	
1'	31.1, CH ₂	1.56 m, 1.72 m
2'	25.7, CH ₂	1.38 m, 1.50 m
3'	31.6, CH ₂	1.29 m ^c
4'	22.6, CH ₂	1.29 m ^c
5'	14.1, CH ₃	0.87 t (7.2)
6'	10.5, CH ₃	1.22 d (6.6)
7'	170.3, C _q	
OMe	51.9, CH ₃	3.72 s

^a Recorded in CDCl₃ at 150 MHz. ^b Recorded in CDCl₃ at 600 MHz. ^c Signals overlapped.

(2R,3R,4S)-4-Methyl-5-oxo-2-pentyl-tetrahydro-furan-3-carboxylic acid methyl ester (15): white solid; $[\alpha]_D^{20} + 71.6$ (c 0.10, CHCl_3); LC-UV [(Acetonitrile (aq) in $\text{H}_2\text{O}/0.1\%$ FA)] λ_{max} 222 nm; IR (liquid) ν_{max} 2950, 2929, 2866, 1777, 1729, 1176, 1130 cm^{-1} ; ^1H NMR (CDCl_3 , 600 MHz) and ^{13}C NMR (CDCl_3 , 150 MHz), see Table 4.1.15.1. Positive ESI-HRMS m/z : 229.1435 $[\text{M}+\text{H}]^+$ (calcd for $\text{C}_{12}\text{H}_{21}\text{O}_4$, 229.1434).

4.1.16 (2S,3R,4R)-4-Methyl-5-oxo-2-pentyl-tetrahydro-furan-3-carboxylic acid (16, new natural product)



Compound **16** (code: LG41-C323) has the molecular formula $\text{C}_{11}\text{H}_{18}\text{O}_4$ as determined by the same strategy as above (Figure 4.1.16.1). As indicated in reference (Amador *et al.*, 2006), this kind of compounds was sometimes isolated as a mixture. Under the progress of repeated purification of compound **16**, we obtained it as a mixture with **13** (**16:13** = 1:2) (Amador *et al.*, 2006) and submitted it for NMR measurement. Analysis of the 1D NMR data (Figures 4.1.16.2 and 4.1.16.3, and Table 4.1.16.1) indicated that compound **16** was also a γ -lactone derivative. 2D NMR data (Figures 4.1.16.4 and 4.1.16.5) confirmed that it possessed the same planar structure as shown in **12** or **14**. The key NOE interactions between H-2 and H-4, and between H-3 and H₂-1' in 1D NOE spectra of **16** allowed us to determine its stereo-configuration as 2S*, 3R*, and 4R* (Figures 4.1.16.6 and 4.1.16.7). For the purpose of verifying the absolute configuration of compound **16**, we tried many methods and finally succeeded in purifying it using a different HPLC column (Venusil XBP C₁₈ (2) column) and then measured ^1H NMR to further confirm its structure as proposed (Figure 4.1.16.3). **16** was pure enough and utilized for the optical rotation measurement to compare with natural products (-)-roccellaric acid and (-)-nephrosteranic acid, as well as the structurally related synthetic product (Figure 4.1.12.8). Finally, ECD calculation (Figure 4.1.16.8) was applied to further support its absolute configuration. Thus, the structure of **16** was assigned as (2S,3R,4R)-4-methyl-5-oxo-2-pentyl-tetrahydro-furan-3-carboxylic acid.

And the NMR data of **16** as a new and pure natural isolate are consistent with its reported synthetic data (Amador *et al.*, 2006; Drioli *et al.*, 1998).

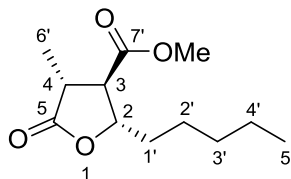
Table 4.1.16.1 ^1H and ^{13}C NMR data for compound **16** (in CDCl_3).

Position	16	
	δ_{C} , mult. ^a	δ_{H} mult. ^b (<i>J</i> in Hz)
2	79.6, CH	4.47 m
3	54.1, CH	2.68 dd (9.6, 11.4)
4	40.0, CH	2.97 m
5	177.0, C _q	
1'	35.0, CH ₂	1.70 m, 1.81 m
2'	25.1, CH ₂	1.39 m, 1.48 m
3'	31.5, CH ₂	1.30 m ^c
4'	22.6, CH ₂	1.30 m ^c
5'	14.1, CH ₃	0.88 t (7.2)
6'	14.7, CH ₃	1.35 d (7.2)
7'	175.1, C _q	

^a Recorded in CDCl_3 at 100 MHz. ^b Recorded in CDCl_3 at 600 MHz. ^c Signals overlapped.

(2*S*,3*R*,4*R*)-4-Methyl-5-oxo-2-pentyl-tetrahydro-furan-3-carboxylic acid (16): white solid; $[\alpha]_{\text{D}}^{20}$ -31.0 (*c* 0.15, MeOH); LC-UV [(Acetonitrile (aq) in $\text{H}_2\text{O}/0.1\%$ FA)] λ_{max} 218 nm; IR (liquid) ν_{max} 3403, 2932, 2861, 1746, 1173 cm^{-1} ; CD (MeOH) 217 ($\Delta\epsilon$ - 0.42) nm; ^1H NMR (CDCl_3 , 600 MHz) and ^{13}C NMR (CDCl_3 , 100 MHz), see Table 4.1.16.1. Positive ESI-HRMS m/z : 215.1277 $[\text{M}+\text{H}]^+$ (calcd for $\text{C}_{11}\text{H}_{19}\text{O}_4$, 215.1278).

4.1.17 (2*S*,3*R*,4*R*)-4-Methyl-5-oxo-2-pentyl-tetrahydro-furan-3-carboxylic acid methyl ester (**17**, semi-synthetic compound)



Compound **17** (code: LG41-C32M4), a colorless oil, was obtained through the same strategy as that for compound **13**. Similarly, it has the similar MS and MS² spectra as that for compounds **13** (Figure 4.1.13.1). The same molecular formula of $\text{C}_{12}\text{H}_{20}\text{O}_4$ with 3 double bond equivalents and same substructures were easily deduced from ESI-HRMS (m/z 229.1435 $[\text{M}+\text{H}]^+$; calcd. 229.1434, Δ 0.2524 ppm) and its MS² spectra. Detailed analysis of its 1D NMR spectra of **17** (Figure 4.1.17.1 and Table

4.1.17.1) in comparison with that of compound **16** confirmed its structure as a methyl ester of **16**. Its NOE spectra (Figures 4.1.17.2 and 4.1.17.3) showed the key interactions between H-2 and H-4, and between H-3 and H₂-1', further supporting that it has the same stereo-configuration as that of compound **16**. Finally, optical rotations (Figure 4.1.12.8) of **16**, **17**, and their known derivatives was used for comparison to assign the absolute configuration of compound **17** as 2*S*, 3*R*, and 4*R*.

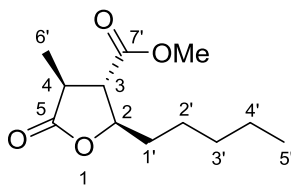
Table 4.1.17.1 ¹H and ¹³C NMR data for compound **17** (in CDCl₃).

Position	17	
	δ _C , mult. ^a	δ _H mult. ^b (J in Hz)
2	79.8, CH	4.44 m
3	54.4, CH	2.64 dd (9.6, 11.4)
4	40.1, CH	2.95 m
5	177.0, C _q	
1'	35.0, CH ₂	1.69 m, 1.77 m
2'	25.1, CH ₂	1.39 m, 1.49 m
3'	31.6, CH ₂	1.30 m ^c
4'	22.6, CH ₂	1.30 m ^c
5'	14.1, CH ₃	0.88 t (6.6)
6'	14.7, CH ₃	1.32 d (7.2)
7'	171.4, C _q	
OMe	52.8, CH ₃	3.77 s

^a Recorded in CDCl₃ at 150 MHz. ^b Recorded in CDCl₃ at 600 MHz. ^c Signals overlapped.

(2*S*,3*R*,4*R*)-4-Methyl-5-oxo-2-pentyl-tetrahydro-furan-3-carboxylic acid methyl ester (**17**): oil; [α]_D²⁰ -32.6 (*c* 0.10, CHCl₃); LC-UV [(Acetonitrile (aq) in H₂O/0.1% FA)] λ_{max} 222 nm; IR (liquid) ν_{max} 2931, 2859, 1779, 1738, 1201, 1174 cm⁻¹; ¹H NMR (CDCl₃, 600 MHz) and ¹³C NMR (CDCl₃, 150 MHz), see Table 4.1.17.1. Positive ESI-HRMS *m/z*: 229.1435 [M+H]⁺ (calcd for C₁₂H₂₁O₄, 229.1434).

4.1.18 (2*R*,3*S*,4*S*)-4-Methyl-5-oxo-2-pentyl-tetrahydro-furan-3-carboxylic acid methyl ester (**18**, semi-synthetic compound)



Thermodynamic equilibration of **15** with DBU led to a major isomer, compound **18** (code: LG41-C32M2-DBU-4), which displayed similar MS and NMR (Figures 4.1.17.1 and 4.1.18.1) features to that

of compound **17**. The detailed comparison of their 1D NMR data (Table 4.1.18.1) indicated that they have the same planar structure and relative configuration. 2D NMR spectra (Figure 4.1.18.2) of compound **18** supported its structure. However, the signs of optical rotation for compound **17** and **18** are opposite, suggesting that they are enantiomers.

In order to investigate the absolute configuration of this kind of paraconic acids, we went back to check the optical rotations of compounds **12–18** and (–)-phaseolinic acid reported in the literature (Figure 4.1.12.8). In addition, their CD spectra were also measured or collected from literature for their stereochemical analysis. Figure 4.1.18.3 showed all the possible eight structures based on compounds **12**, **14** and **16** (also suitable for compounds **13**, **15**, **17** and **18**). These eight compounds are four pairs of enantiomers with stereo-configurational differences in the γ -lactone ring. Through the above data, we were able to obtain an empirical conclusion regarding the relationship between chiroptical data and stereochemical assignments for this type of paraconic acids (Figure 4.1.18.3). The stereo-configuration at C-2 appears to relate to the sign of optical rotation while the stereochemistry at C-4 influences the sign of cotton effect. In order to support our assignments of absolute configuration for this kind of compounds, the TDDFT CD calculation is consistent with the experimental or literature data (Figures 4.1.12.9, 4.1.14.5 and 4.1.16.8). The above analysis for the CD band around 220 nm conceivably allied with the $n\text{-}\pi^*$ transition of lactone chromophore, is in accordance with the empirical chirality rule of the γ -lactone ring (Beecham, 1968).

Table 4.1.18.1 ^1H and ^{13}C NMR data for compound **18** (in CDCl_3).

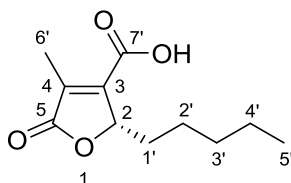
Position	17		18	
	δ_{C} , mult. ^a	δ_{H} mult. ^b (J in Hz)	δ_{C} , mult. ^a	δ_{H} mult. ^b (J in Hz)
2	79.8, CH	4.44 m	79.7, CH	4.45 (4.2, 8.4, 9.6)
3	54.4, CH	2.64 dd (9.6, 11.4)	54.4, CH	2.65 dd (9.6, 11.4)
4	40.1, CH	2.95 m	40.1, CH	2.96 m
5	177.0, C _q		176.9, C _q	
1'	35.0, CH ₂	1.69 m, 1.77 m	35.0, CH ₂	1.69 m, 1.77 m
2'	25.1, CH ₂	1.39 m, 1.49 m	25.1, CH ₂	1.40 m, 1.51 m
3'	31.6, CH ₂	1.30 m ^c	31.5, CH ₂	1.31 m ^c
4'	22.6, CH ₂	1.30 m ^c	22.6, CH ₂	1.31 m ^c
5'	14.1, CH ₃	0.88 t (6.6)	14.1, CH ₃	0.89 t (7.2)
6'	14.7, CH ₃	1.32 d (7.2)	14.6, CH ₃	1.32 d (7.2)
7'	171.4, C _q		171.4, C _q	
OMe	52.8, CH ₃	3.77 s	52.7, CH ₃	3.78 s

^a Recorded in CDCl_3 at 150 MHz. ^b Recorded in CDCl_3 at 600 MHz. ^c Signals overlapped.

(2R,3S,4S)-4-Methyl-5-oxo-2-pentyl-tetrahydro-furan-3-carboxylic acid methyl ester (18): oil; $[\alpha]_{\text{D}}^{20} +28.0$ (c 0.10, MeOH); LC-UV [(Acetonitrile (aq) in $\text{H}_2\text{O}/0.1\%$ FA)] λ_{max} 224 nm; IR (liquid) ν_{max} 2956,

1742, 1175 cm^{-1} ; CD (MeOH) 219 ($\Delta\epsilon + 0.93$) nm; ^1H NMR (CDCl_3 , 600 MHz) and ^{13}C NMR (CDCl_3 , 600 MHz), are in consistent with its enantiomer, compound **17** (Figure 4.1.18.2). Positive ESI-HRMS m/z : 229.1435 $[\text{M}+\text{H}]^+$ (calcd for $\text{C}_{12}\text{H}_{21}\text{O}_4$, 229.1434).

4.1.19 (2S)-2,5-Dihydro-4-methyl-5-oxo-2-pentyl-furan-3-carboxylic acid (Striatisorolide A, **19**, known compound)



The molecular formula of compound **19** (code: LG41-C21) was $\text{C}_{11}\text{H}_{16}\text{O}_4$, which was determined by ESI-HRMS at m/z 213.1124 $[\text{M}+\text{H}]^+$ (calcd. 213.1121, Δ 1.0086 ppm, Figure 4.1.19.1). The MS of compound **19** showed that it should also be a paraconic acid derivative and have one more double bond equivalents than compounds **12–18**. Its ^1H NMR spectrum (Figure 4.1.19.2) revealed the absence of two significant proton signals for C-3 and C-4 in compounds **12–18**. Further analysis of ^1H NMR spectrum indicated a down-field shift of the methyl signal at C-6'. The above analysis suggested a double bond between C-3 and C-4, which indicated the known compound named striatisorolide A (Stewart *et al.*, 2005). Finally, the structure was readily confirmed on the basis of comparison of its 1D NMR data (Table 4.1.19.1 and Figure 4.1.19.2) with those reported in the literature (Stewart *et al.*, 2005). Compound **19** showed an optical rotation of $[\alpha]_{\text{D}}^{20} -45.0$ (c 0.10, CHCl_3) compared to $[\alpha]_{\text{D}}^{20} -25.2$ (c 0.40, MeOH) for synthetic (*S*)-striatisorolide A (Deska and Bäckvall, 2009) and $[\alpha]_{\text{D}} -24$ (c 0.40, MeOH) for natural striatisorolide A (Stewart *et al.*, 2005), confirming its absolute configuration as shown.

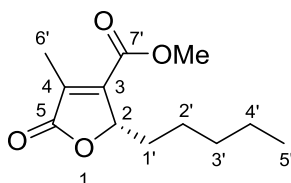
Table 4.1.19.1 ^1H and ^{13}C NMR data for compound **19** (in CDCl_3).

Position	19		Striatisorolide A (Stewart <i>et al.</i> , 2005; Deska and Bäckvall, 2009)	
	δ_{C} , mult. ^a	δ_{H} mult. ^b (J in Hz)	δ_{C} , mult. ^d	δ_{H} mult. ^e (J in Hz)
2	81.8, CH	5.12 dt (2.4, 8.0)	81.4, CH	5.12 br d (7.9)
3	147.4, C_q		146.7, C_q	
4	139.6, C_q		140.1, C_q	

5	173.3, C _q		172.7, C _q	
1'	32.7, CH ₂	1.58 m, 2.11 m	32.7, CH ₂	1.60 m, 2.12 m
2'	24.5, CH ₂	1.38 m	24.4, CH ₂	1.40m
3'	31.4, CH ₂	1.27 m ^c	31.3, CH ₂	1.30 m ^c
4'	22.5, CH ₂	1.27 m ^c	22.4, CH ₂	1.30 m ^c
5'	14.0, CH ₃	0.84 t (6.8)	13.9, CH ₃	0.87 t (6.5)
6'	11.1, CH ₃	2.21 d (2.0)	11.1, CH ₃	2.24 s
7'	166.6, C _q		166.6, C _q	
COOH		10.76, s		

^a Recorded in CDCl₃ at 100 MHz. ^b Recorded in CDCl₃ at 400 MHz. ^c Signals overlapped. ^d Recorded in CDCl₃ at 150 MHz. ^e Recorded in CDCl₃ at 600 MHz.

4.1.20 (2S)-2,5-Dihydro-4-methyl-5-oxo-2-pentyl-furan-3-carboxylic acid methyl ester (**20**, semi-synthetic compound)



Compound **20** (code: LG41-C21-Re or LG41-C32M5) was obtained from the methylation reaction which was same to that for compounds **13**, **15** and **17**. Its MS and MS/MS (Figure 4.1.20.1), as well as NMR data (Figure 4.1.20.2 and Table 4.1.20.1) were in accordance with that for the synthetic product reported in the literature (Bang *et al.*, 2015).

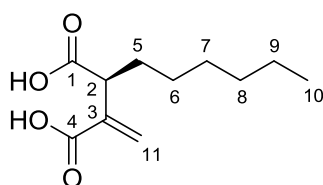
Table 4.1.20.1 ¹H and ¹³C NMR data for compound **20** (in CDCl₃).

Position	20		Literature (Bang <i>et al.</i> , 2015)	
	δ _C , mult. ^a	δ _H mult. ^b (J in Hz)	δ _C , mult. ^d	δ _H mult. ^e (J in Hz)
2	81.6, CH	5.10 m	81.5, CH	5.07-5.10 m
3	147.8, C _q		147.7, C _q	
4	137.7, C _q		137.5, C _q	
5	173.2, C _q		173.0, C _q	
1'	32.9, CH ₂	1.56 m, 2.07 m	32.8, CH ₂	2.04-2.07 m
2'	24.6, CH ₂	1.39 m	24.5, CH ₂	1.25-1.58 m
3'	31.6, CH ₂	1.30 m ^c	31.4, CH ₂	1.25-1.58 m
4'	22.6, CH ₂	1.30 m ^c	22.5, CH ₂	1.25-1.58 m
5'	14.1, CH ₃	0.88 t (6.5)	14.0, CH ₃	0.86 t (6.9)
6'	11.1, CH ₃	2.19 d (1.5)	10.9, CH ₃	2.18 d (2.1)
7'	162.9, C _q		162.7, C _q	
OMe	52.6, CH ₃	3.89 s	52.4, CH ₃	3.87 s

^a Recorded in CDCl₃ at 75 MHz. ^b Recorded in CDCl₃ at 500 MHz. ^c Signals overlapped. ^d Recorded in CDCl₃ at 75 MHz. ^e Recorded in CDCl₃ at 300 MHz.

(2*S*)-2,5-Dihydro-4-Methyl-5-oxo-2-pentyl-furan-3-carboxylic acid methyl ester (**20**): oil; $[\alpha]_D^{20} -14.2$ (*c* 0.15, CHCl₃); LC-UV [(Acetonitrile (aq) in H₂O/0.1% FA)] λ_{\max} 224 nm; IR (liquid) ν_{\max} 2955, 2927, 2858, 1765, 1725, 1224 cm⁻¹; ¹H NMR (CDCl₃, 500 MHz) and ¹³C NMR (CDCl₃, 75 MHz), see Table 4.1.20.1. Positive ESI-HRMS *m/z*: 227.1275 [M+H]⁺ (calcd for C₁₂H₁₉O₄, 227.1278).

4.1.21 (2*S*)-Hexylitaconic acid (**21**, known compound)



For compound **21** (code: LG41-511X1), the fragment ions at *m/z* 215.1278 [M+H]⁺, 197.1173 [M+H-H₂O]⁺, 169.1225 [M+H-CH₂O₂]⁺, 151.1120 [M+H-CH₂O₂-H₂O]⁺, and 123.1171 [M+H-2×CH₂O₂]⁺ in APCI-HRMS, indicated the molecular formula C₁₁H₁₈O₄ and two carboxylic acid moieties in the structure (Figure 4.1.21.1). 1D NMR spectra (Figure 4.1.21.2) of **21** showed the presence of a double bond with two olefinic protons, a down-field shift of C-2 (δ_H 3.42, δ_C 47.3), two carboxyl groups, and a side chain. With the help of databases, its 1D NMR spectral data (Figure 4.1.21.2) confirmed its structure as a known compound, hexylitaconic acid (Isogai *et al.*, 1984). The absolute configuration at C-2 was established as *S* based on the value of the optical rotation ($[\alpha]_D^{22} +3.2$ (*c* 0.96, MeOH) and the R(-)/S(+) relationship (Nakahashi *et al.*, 2009).

Table 4.1.21.1 ¹H and ¹³C NMR data for compound **21** (in CDCl₃).

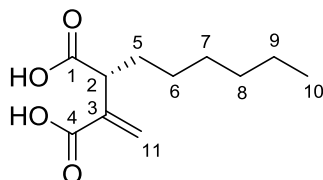
Position	21		(2 <i>S</i>)-Hexylitaconic acid (Isogai <i>et al.</i> , 1984)	
	δ_C , mult. ^a	δ_H mult. ^b (<i>J</i> in Hz)	δ_C , mult. ^d	δ_H mult. ^e (<i>J</i> in Hz)
1	179.3, C _q		179.6, C _q	
2	47.3, CH	3.42 t (7.5)	47.0, CH	3.35 t (7.0)
3	137.8, C _q		137.5, C _q	
4	171.5, C _q		171.7, C _q	
5	30.2, CH ₂	1.72 m, 1.93 m	29.9, CH ₂	1.80 m
6	27.5, CH ₂	1.29 m ^c	27.4, CH ₂	1.25 m ^c
7	29.2, CH ₂	1.29 m ^c	29.0, CH ₂	1.25 m ^c
8	31.8, CH ₂	1.29 m ^c	31.7, CH ₂	1.25 m ^c
9	22.8, CH ₂	1.29 m ^c	22.6, CH ₂	1.25 m ^c

10	14.2, CH ₃	0.87 t (7.0)	14.1, CH ₃	0.83 t (6.0)
11	129.4, CH ₂	5.82 s, 6.50 s	129.6, CH ₂	5.80 s, 6.40 s
2×COOH		6.12 br s		9.60 br s

^a Recorded in CDCl₃ at 125 MHz. ^b Recorded in CDCl₃ at 500 MHz. ^c Signals overlapped. ^d Recorded in CDCl₃ at 100 MHz. ^e Recorded in CDCl₃ at 100 MHz.

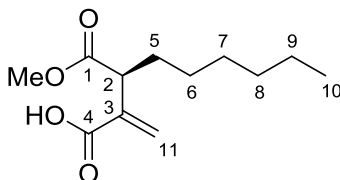
(*2S*)-Hexylitaconic acid (**21**): white solid; $[\alpha]_D^{22} +3.2$ (*c* 0.96, MeOH); LC-UV [(Acetonitrile (aq) in H₂O/0.1% FA)] λ_{\max} 228 nm; IR (film) ν_{\max} 3428, 1635, 1112 cm⁻¹; ¹H NMR (CDCl₃, 500 MHz) and ¹³C NMR (CDCl₃, 125 MHz), see Table 4.1.21.1. Positive APCI-HRMS *m/z*: 215.1278 [M+H]⁺ (calcd for C₁₁H₁₉O₄, 215.1278).

4.1.22 (*2R*)-Hexylitaconic acid (**22**, known compound)



Compound **22** (code: LG41-C326) has the similar MS and NMR data with that of compound **21** (Figure 4.1.22.1). They should be the same compound or enantiomers. However, Compared to the $[\alpha]_D^{23} -17.9$ (*c* 0.50, MeOH) for (–)-hexylitaconic acid and $[\alpha]_D^{20} +15.3$ (*c* 2.0, MeOH) for (+)-hexylitaconic acid (Klemke *et al.*, 2004), the value of $[\alpha]_D^{20} -16.5$ (*c* 0.65, CHCl₃) for compound **22** indicated that it is *R*-configured.

4.1.23 (*2S*)-Hexylitaconic acid mono methyl ester (**23**, known compound)



Compound **23** (code: LG41-C328) has the molecular formula C₁₂H₂₀O₄ as determined by ESI-HRMS at *m/z* 229.1434 [M+H]⁺; calcd. 229.1434, Δ -0.2495 ppm (Figure 4.1.23.1). Its fragment information ([M+H-H₂O]⁺ at *m/z* 211.1330, [M+H-CH₃OH]⁺ at *m/z* 197.1173) revealed the possible presence of OH

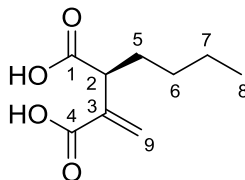
and CH₃O groups. The 1D NMR data (Figure 4.1.23.2) of **23** are very similar to those of **21**, except for an oxygenated methyl (δ_{H} 3.68). Key HMBC correlations (Figure 4.1.23.3) confirmed that this methoxy due to the esterification of carboxylic acid was located at C-1, which was also supported by the down-field shift of C-1 from δ_{C} 179.3 in **21** to 174.2 in **23**, and the comparison of NMR data with that in literature (Table 4.1.23.1) (Isogai *et al.*, 1984). Finally, Small $[\alpha]_{\text{D}}^{20} +0.48$ (c 0.41, CHCl₃) may indicate compound **23** was a mixture of two enantiomers, even through the R-(-)/S-(+) relationship (Nakahashi *et al.*, 2009) suggested it was *S*-configured.

Table 4.1.23.1 ¹H and ¹³C NMR data for compound **23** (in CDCl₃).

Position	23		(2 <i>S</i>)-Hexylitaconic acid mono methyl ester (Isogai <i>et al.</i> , 1984)	
	δ_{C} , mult. ^a	δ_{H} mult. ^b (<i>J</i> in Hz)	δ_{C} , mult. ^a	δ_{H} mult. ^b (<i>J</i> in Hz)
1	174.2, C _q		173.8, C _q	
2	46.7, CH	3.49 t (7.5)	46.5, CH	3.35 t (7.0)
3	138.4, C _q		138.1, C _q	
4	170.9, C _q		171.5, C _q	
5	31.4, CH ₂	1.67 m, 1.89 m	31.6, CH ₂	1.80 m
6	27.6, CH ₂	1.29 m ^c	27.5, CH ₂	1.20 m ^c
7	29.2, CH ₂	1.29 m ^c	29.0, CH ₂	1.20 m ^c
8	31.8, CH ₂	1.29 m ^c	31.4, CH ₂	1.20 m ^c
9	22.8, CH ₂	1.29 m ^c	22.6, CH ₂	1.20 m ^c
10	14.2, CH ₃	0.87 t (7.0)	14.1, CH ₃	0.82 t (6.0)
11	128.7, CH ₂	5.83 s, 6.46 s	129.1, CH ₂	5.80 s, 6.40 s
OMe	52.3, CH ₃	3.68 s	52.1, CH ₃	3.55 s

^a Recorded in CDCl₃ at 125 MHz. ^b Recorded in CDCl₃ at 500 MHz. ^c Signals overlapped. ^d Recorded in CDCl₃ at 100 MHz. ^e Recorded in CDCl₃ at 100 MHz.

4.1.24 (2*S*)-Butylitaconic acid (**24**, known compound)



The molecular formula C₉H₁₄O₄ was assigned to compound **24** (code: LG41-511X2) by HR-MS (Figure 4.1.24.1). It was observed that compound **24** had similar HR-MS fragment ions as **21**, and one C₂H₄-group less than **21** (Figure 4.1.24.1). Moreover, the 1D NMR data of compound **24** (Figure 4.1.24.2 and Table 4.1.24.1) revealed that its structure was similar to that of **21**, except for the *n*-butyl side chain in

24, instead of the *n*-hexyl moiety in **21**. Finally, concerning the optical rotation ($[\alpha]_D^{22} +10.3$ (*c* 1.04, MeOH)), the structure of **24** was determined as (2*S*)-2-butyl-3-methylene-succinic acid [(2*S*)-butylitaconic acid] (Turner and Aldridge, 1983).

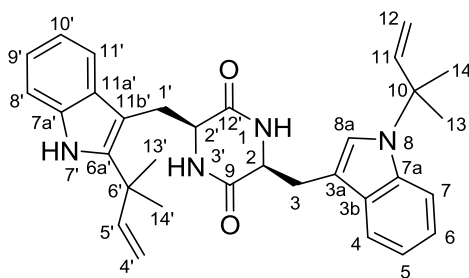
Table 4.1.24.1 ^1H and ^{13}C NMR data for compound **24** (in CDCl_3).

Position	δ_{C} , mult. ^a	δ_{H} mult. ^b (<i>J</i> in Hz)
1	179.8, C _q	
2	47.1, CH	3.43 t (7.5)
3	137.5, C _q	
4	171.8, C _q	
5	29.3, CH ₂	1.76 m, 1.95 m
6	29.5, CH ₂	1.36 m ^c
7	22.4, CH ₂	1.36 m ^c
8	13.9, CH ₃	0.92 t (6.5)
9	129.5, CH ₂	5.84 s, 6.54 s
	2 × COOH	9.32 br s

^a Recorded in CDCl_3 at 125 MHz. ^b Recorded in CDCl_3 at 500 MHz. ^c Signals overlapped.

(2*S*)-Butylitaconic acid (**24**): white solid; $[\alpha]_D^{22} +10.3$ (*c* 1.04, MeOH); LC-UV [(Acetonitrile (aq) in $\text{H}_2\text{O}/0.1\%$ FA)] λ_{max} 214 nm; IR (film) ν_{max} 3401, 1641, 1112 cm^{-1} ; ^1H NMR (CDCl_3 , 500 MHz) and ^{13}C NMR (CDCl_3 , 125 MHz), see Table 4.1.24.1. Positive ESI-HRMS m/z : 187.0966 $[\text{M}+\text{H}]^+$ (calcd for $\text{C}_9\text{H}_{15}\text{O}_4$, 187.0965).

4.1.25 Cyclo (N⁸-(α,α -dimethylallyl)-L-Trp-6a'-(α,α -dimethylallyl)-L-Trp) (**25**, known compound)



ESI-HRMS (m/z 509.2926 $[\text{M}+\text{H}]^+$; calcd. 509.2911, Δ 2.8846 ppm; Figure 4.1.25.1) coupled with 1D NMR spectrum (Figures 4.1.25.2 and 4.1.25.3) of compound **25** (code: LG41-P4413) revealed the molecular formula $\text{C}_{32}\text{H}_{36}\text{N}_4\text{O}_2$ for **25**. Interpretation of ^1H - ^1H COSY spectrum (Figures 4.1.25.3 and 4.1.25.5) indicated the connections from N-1 to C-3, from C-1' to N-3', between C-11 and C-12,

between C-4' and C-5', from C-4 to C-7, and from C-8' to C-11'. HMBC correlations (Figure 4.1.25.4, and Figure 4.1.25.5) of 1-NH/C-12', H-2'/C-12', H-2/C-9, and 3'-NH/C-9 determined a six-membered ring with two nitrogens in **25**. Further analysis of HMBC spectrum indicated the correlations from H-8a to C-3, C-3a, C-3b and C-7a, from H-5 to C-3b, and from H-6 to C-7a, establishing an indole ring system. The nitrogen was substituted by an isoprene-derived unit, which was supported through HMBC correlations from H₃-13 to C-10, C-11 and C-14, and from H₃-14 to C-10, C-11 and C-13. Using a similar strategy for assigning the remaining substructure for **25** (Figure 4.1.25.5), the whole structure was finally constructed as shown. Compound **25** was Cyclo (N⁸-(α,α -dimethylallyl)-L-Trp-6a'-(α,α -dimethylallyl)-L-Trp) (Shiono *et al.*, 1999), which was also suggested by the comparison of its NMR data with that in the literature (Table 4.1.25.1).

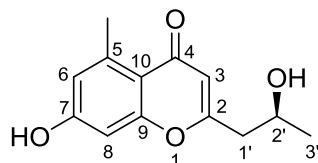
Table 4.1.25.1 ¹H and ¹³C NMR data for compound **25** (in CDCl₃).

No.	25			Literature (Shiono <i>et al.</i> , 1999)	
	δ_C , mult. ^a	δ_H mult. ^b (J in Hz)	δ_H mult. ^c (J in Hz)	δ_C , mult. ^d	δ_H mult. ^e (J in Hz)
2	55.3, CH	4.27 br d (9.5)	4.24 t (4.0)	56.8, CH	4.24 m
3	30.5, CH ₂	2.92 dd (14.5, 9.5) 3.56 dd (14.5, 3.5)	3.20 m 3.25 dd (14.5, 4.0)	30.9, CH ₂	3.20 dd (14.4, 6.1) 3.25 dd (14.4, 4.3)
3a	107.4, C _q			108.6, C _q	
3b	128.9, C _q			130.6, C _q	
4	121.7, CH	7.15 m ^e	7.68 d (7.5)	120.2, CH	7.67 dd (7.0, 1.2)
5	114.3, CH	7.52 m	7.04-7.12	119.6, CH	7.08 td (7.0, 1.2)
6	119.1, CH	7.63 m	7.04-7.12	121.6, CH	7.05 ddd (8.2, 7.0, 1.2)
7	119.7, CH	7.14 m ^e	7.45 d (8.0)	114.5, CH	7.44 dd (8.2, 1.2)
7a	136.1, C _q			136.3, C _q	
8a	124.8, CH	7.12 s	7.27 s	126.3, CH	7.26 s
9	167.0, C _q			167.3, C _q	
10	59.4, C _q			59.7, C _q	
11	144.1, CH	6.13 dd (17.5, 10.5)	6.13 dd (17.5, 10.5)	145.2, CH	6.11 dd (17.4, 10.7)
12	112.8, CH ₂	5.17-5.24	5.13 d (11.0) 5.16 d (17.0)	113.7, CH ₂	5.12 dd (10.7, 1.2) 5.15 dd (17.4, 1.2)
13	28.0 or 28.1 or 28.2, CH ₃	1.77 s	1.75 s	28.4, CH ₃	1.73 s
14	28.0 or 28.1 or 28.2, CH ₃	1.75 s	1.73 s	28.3, CH ₃	1.71 s
1'	29.7, CH ₂	2.95 dd (14.5, 10.5) 3.65 dd (15.0, 3.5)	2.26 ddd (6.0, 10.0, 16.5) 3.42 dd (14.5, 2.5)	31.6, CH ₂	2.24 dd (14.7, 10.4) 3.42 dd (14.7, 2.8)
2'	55.6, CH	4.31 br d (11.0)	4.06 br d (10.0)	57.9, CH	4.06 dt (10.4, 2.8)
4'	113.9, CH ₂	5.17-5.24	5.03 d (10.5) 5.04 d (17.5)	111.9, CH ₂	5.02 dd (10.7, 1.2) 5.04 dd (17.4, 1.2)
5'	145.9, CH	6.14 dd (17.5, 10.5)	6.13 dd (17.5, 10.5)	147.2, CH	6.12 dd (17.4, 10.7)
6'	39.3, C _q			39.9, C _q	
6a'	141.6, C _q			141.7, C _q	
7a'	134.4, C _q			135.7, C _q	

8'	110.8, CH	7.30 d (8.0)	7.23 d (8.0)	111.3, CH	7.24 dd (8.2, 1.2)
9'	122.3, CH	7.16 m ^e	6.98 t (7.0)	121.6, CH	6.97 ddd (8.2, 7.0, 1.2)
10'	120.4, CH	7.06 t (7.0)	6.82 t (7.5)	119.9, CH	6.81 ddd (7.9, 7.0, 1.2)
11'	118.5, CH	7.24 d (8.0)	6.75 d (4.5, 8.0)	119.3, CH	6.73 d (7.9)
11a'	129.2, C _q			130.5, C _q	
11b'	104.9, C _q			106.5, C _q	
12'	167.8, C _q			168.2, C _q	
13'	28.0 or 28.1 or 28.2, CH ₃	1.55 s	1.51 s	28.1, CH ₃	1.51 s
14'	28.0 or 28.1 or 28.2, CH ₃	1.55 s	1.51 s	28.2, CH ₃	1.51 s
1-NH		5.71 s			7.24 br s
3'-NH		5.85 s			6.30 d (2.8)
7'-NH		8.03 s			9.79 br s

^a Recorded in CDCl₃ at 125 MHz. ^b Recorded in CDCl₃ at 500 MHz. ^c Recorded in acetone-*d*₆ at 500 MHz. ^d Recorded in acetone-*d*₆ at 125 MHz. ^e Signals overlapped.

4.1.26 7-Hydroxy-2-[2-hydroxypropyl]-5-methyl-4*H*-1-benzopyran-4-one (26, known compound)



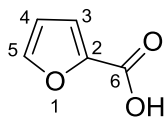
Compound **26** (code: LG41-P5333) has a molecular formula C₁₃H₁₄O₄ as determined by ESI-HRMS (*m/z* 235.0964, [M+H]⁺; calcd. 235.0965, Δ -0.3320 ppm, Figure 4.1.26.1). ¹H NMR spectrum (Figure 4.1.26.2) exhibited the signals for two methyls (δ_H 1.28 and 2.72), a methylene, an oxygenated methine (δ_H 4.20), and three aromatic/olefinic protons (δ_H 6.07, 6.64 and 6.67). A carbon signal at δ_C 182.0 indicated an unsaturated carbonyl (Figure 4.1.26.2). Three oxygenated aromatic/olefinic carbons are suggested to be present in **26** based on the ¹³C signals at δ_C 161.5, 163.0 and 167.1. A further search of database and comparison of NMR data (Table 4.1.26.1) of **26** with that in literature confirmed that it is 7-hydroxy-2-[2-hydroxypropyl]-5-methyl-4*H*-1-benzopyran-4-one (Kashiwada *et al.*, 1984; Xu *et al.*, 2009; Huang *et al.*, 2014).

Table 4.1.26.1 ^1H and ^{13}C NMR data for compound **26** (in CD_3OD).

Position	26		7-Hydroxy-2-[2-hydroxypropyl]-5-methyl-4 <i>H</i> -1-Benzopyran-4-one (Kashiwada <i>et al.</i> , 1984; Xu <i>et al.</i> , 2009; Huang <i>et al.</i> , 2014)	
	δ_{C} , mult. ^a	δ_{H} mult. ^b (<i>J</i> in Hz)	δ_{C} , mult. ^c (DMSO- <i>d</i> ₆)	δ_{H} mult. ^d (<i>J</i> in Hz) (CD_3OD)
1				
2	167.1, C _q		165.3, C _q	
3	112.5, CH	6.07 s	112.0, CH	5.97 s
4	182.0, C _q		178.8, C _q	
5	143.7, C _q		141.9, C _q	
6	118.0, CH	6.64 d (2.4)	116.9, CH	6.47 s
7	163.0, C _q		161.3, C _q	
8	101.7, CH	6.67 d (2.4)	101.1, CH	6.50 s
9	161.5, C _q		159.7, C _q	
10	115.9, C _q		114.9, C _q	
1'	44.2, CH ₂	2.67 m	43.3, CH ₂	2.65 m
2'	66.4, CH	4.20 m	64.6, CH	4.17 m
3'	23.5, CH ₃	1.28 d (6.0)	23.9, CH ₃	1.25 d (6.3)
5-CH ₃	23.1, CH ₃	2.72 s	22.9, CH ₃	2.66 s

^a Recorded in CD_3OD at 125 MHz. ^b Recorded in CD_3OD at 400 MHz. ^c Recorded in DMSO-*d*₆ at 125 MHz. ^d Recorded in CD_3OD at 500 MHz.

4.1.27 2-Furancarboxylic acid (**27**, known compound)



Compound **27** (code: LG41-P423) was isolated as a white powder. Its ^1H NMR spectrum (Figure 4.1.27.1) only displayed three aromatic/olefinic protons with a small coupling constant for each one. The ^{13}C NMR spectrum showed five aromatic/olefinic carbon signals. Key HMBC correlations (Figure 4.1.27.2) from H-3 to C-2, C-4, and C-5, from H-4 to C-3 and C-5, and from H-5 to C-2 and C-6 and considering the chemical shifts of C-2 (δ_{H} 147.7), C-5 (δ_{H} 147.3) and C-6 (δ_{H} 162.9) determined compound **27** as a known compound, 2-furancarboxylic acid (Table 4.1.27.1).

Table 4.1.27.1 ^1H and ^{13}C NMR data for compound **27** (in CD_3OD).

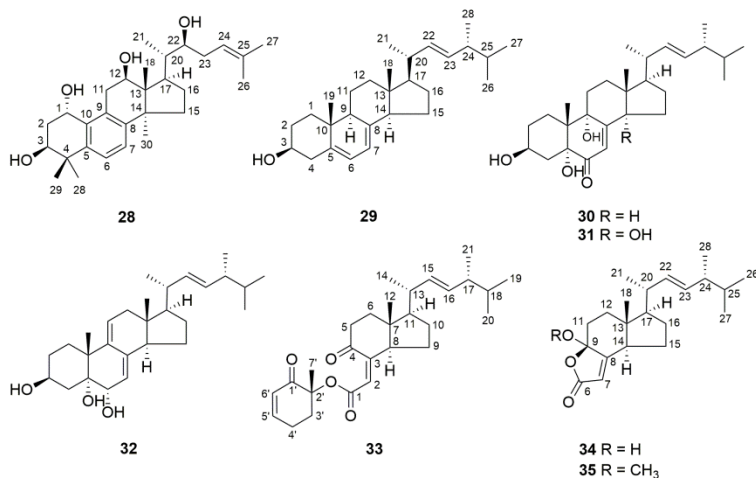
27		
Position	δ_{C} , mult. ^a	δ_{H} mult. ^b (<i>J</i> in Hz)
1		
2	147.7, C _q	
3	118.1, CH	7.14 dd (0.5, 3.5)
4	112.8, CH	6.55 dd (2.0, 3.5)

5 147.3, CH 7.67 m
6 162.9, C_q

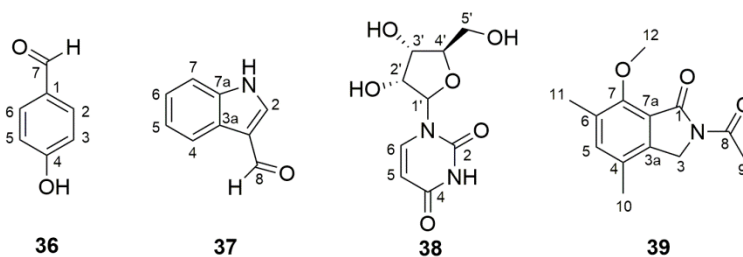
^a Recorded in CD₃OD at 100 MHz. ^b Recorded in CD₃OD at 500 MHz.

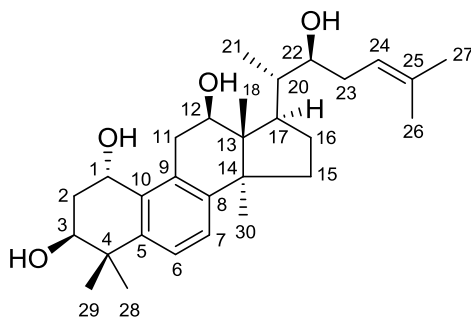
4.2 Secondary metabolites isolated from *Diaporthe* sp. LG23

A novel lanostanoid, 19-nor-lanosta-5(10),6,8,24-tetraen-1 α ,3 β ,12 β ,22 S -tetraol (**28**), characterized by the presence of an aromatic B ring and hydroxylated at C-1, C-3, C-12, and C-22, was isolated from the rice culture of an endophytic fungus *Diaporthe* sp. LG23, inhabiting leaves of the Chinese medicinal plant *M. fortunei* (from Shanghai, P. R. China). Seven biosynthetically-related known steroids (**29–35**) were also isolated in parallel.



Four aromatic or glycosylated compounds (**36–39**) including a new isoindole derivative (**39**) were also obtained.



4.2.1 19-Nor-lanosta-5(10),6,8,24-tetraene-1 α ,3 β ,12 β ,22 S -tetraol (**28**, new compound)

Compound **28** (code: LG23-621-1) (Li *et al.*, 2015) was obtained as a white powder with the molecular formula $C_{29}H_{44}O_4$ (8 double bond equivalents) as assigned from the ESI-HRMS data ($[M+H-H_2O]^+$ at m/z 439.3207, $[M+H-2\times H_2O]^+$ at m/z 421.3102, $[M+H-3\times H_2O]^+$ at m/z 403.2995, and $[M+H-4\times H_2O]^+$ at m/z 385.2889; $[2M+H]^+$ at m/z 913.6559, and $[2M+H-2\times H_2O]^+$ at m/z 877.6342; $[3M+H]^+$ at m/z 1369.9796, and $[3M+Na]^+$ at m/z 1391.9616, Figure 4.2.1.1). The mass spectrum exhibits the loss of four water molecules, indicating the presence of four hydroxy groups in **28**. The above analysis was also supported by the proposed fragmentation pathway on the basis of MS^2 data (Figures 4.2.1.2 and 4.2.1.3) (Cabrera *et al.*, 2007; Wang *et al.*, 2015). The 1H and ^{13}C NMR spectra (Figure 4.2.1.7 and Table 4.2.1.1) of **28** showed the presence of six tertiary methyls (δ_H 0.70, 1.10, 1.14, 1.46, 1.70 and 1.78), one secondary methyl (δ_H 1.16, d, $J = 7.0$ Hz) and four oxygenated methines (δ_C 65.7, 70.7, 71.8 and 75.0) (Li *et al.*, 2015). In addition to these structural characters, the 1D NMR data with the aid of 2D NMR spectra assigned five methylenes, two deoxygenated methines, three quaternary carbon signals, and eight aromatic/olefinic carbons including a *cis*-di-substituted double bond and a methine carbon (Li *et al.*, 2015). These data revealed a tetracyclic triterpene skeleton of **28** (Ríos *et al.*, 2012; Ríos *et al.*, 2011; Liu, 2014). Detailed analysis of 1H - 1H COSY NMR data confirmed the connection from C-1 to C-3, from C-6 to C-7, from C-11 to C-12, between C-15, 16, 17, 20, 22, 23 and 24, and from C-20 to C-21 (Figures 4.2.1.4 and 4.2.1.8). HMBC NMR spectrum was further employed to determine the planar structure of **28** (Figures 4.2.1.4 and 4.2.1.9). In **28**, the side chain with the connection to C-17 was verified from key HMBC correlations of H_3 -21 to C-17, C-20 and C-22, H_3 -26 to C-24, C-25 and C-27, as well as H_3 -27 to C-24, C-25 and C-26 (Li *et al.*, 2015). The C and D rings of the tetracyclic skeleton of **28** were deduced on the basis of HMBC correlations from H-11 to C-8, C-9 and C-13, H_3 -18 to C-12,

C-13, C-14 and C-17, and H₃-30 to C-8, C-13, C-14 and C-15. A benzene ring unit in the tetracyclic skeleton of **28** was determined and assigned as the B-ring by the correlations of H-6/C-8, H-6/C-10, H-7/C-5, H-7/C-9 and H-11/C-10 in the HMBC spectrum (Figure 4.2.1.4). HMBC correlations of H₃-28 to C-3, C-4, C-5 and C-29, H₃-29 to C-3, C-4, C-5 and C-28, together with H-6 to C-4 in combination with the MS requirement identified an A-ring fusing to B-ring. Four hydroxy groups were placed at C-1, C-3, C-12 and C-22, which were consistent with MS data and the chemical shifts of oxygenated methines. Therefore, the planar structure of compound **28** was confirmed as shown.

The relative stereochemistry of **28** was characterized by analysis of the coupling constants and NOESY experiment (Table 4.2.1.1 and Figure 4.2.1.5) (Li *et al.*, 2015). The NOESY correlations of H₃-28/H-3, H₃-29/H-2, and the coupling constants of H₂-2/H-1 ($J = 2.5$) and H₂-2/H-3 ($J = 4.0, 12.0$), together with the absence of NOESY correlation between H-1 and H-3 determined that two hydroxy groups located at C-1 and C-3 in A-ring are α and β configured, respectively (Kubota *et al.*, 2012). The strong NOESY correlations of H-1/H-11 β (δ_{H} 2.69), and H₃-18/H-11 β , H₃-18/H-15 β (δ_{H} 1.97), and H₃-18/H-16 β (δ_{H} 1.81) suggested the β -orientations of these protons. Furthermore, H-12 and H₃-30 were located on opposite sides based on their cross correlations (Li *et al.*, 2015). The key NOE correlations of H₃-30/H-17, H-12/H-17, and H₃-18/H-20 revealed the β -orientation of the side chain and the S configuration of C-20 (Hsu *et al.*, 2011), which were in accordance with general characteristics for the naturally occurring lanostane-type triterpenoids (Ríos *et al.*, 2011; Ríos *et al.*, 2012; Li *et al.*, 2015). From a biosynthetic standpoint, compounds possessing structural features similar to **28** (lanostane triterpenoids) are derived from a common intermediate lanosterol (Brown, 1998; Ríos *et al.*, 2012; Quin *et al.*, 2014; Li *et al.*, 2015). The conversion of lanosterol into steroid derivatives in fungi has been investigated and reviewed (Brown, 1998; Quin *et al.*, 2014; Li *et al.*, 2015), which implies their general stereo-configurations. The 22*S* absolute configuration of **28** in the side chain was supported by the relatively small coupling constant of H-20/H-22 ($J = 5.0$ Hz) (Figure 4.2.1.6) (Isaka *et al.*, 2013; Li *et al.*, 2015), as well as the significant differences of ¹³C NMR values of the same side chain between **28** and fungus-derived 22*R* inotodiol (Table 4.2.1.2) (Yusoo *et al.*, 2002; Nakata *et al.*, 2007; Li *et al.*, 2015). Accordingly, compound **28** was determined as 19-nor-lanosta-5(10),6,8,24-tetraene-1 α ,3 β ,12 β ,22*S*-tetraol.

Table 4.2.1.1 ^1H and ^{13}C NMR data for 19-nor-lanosta-5(10),6,8,24-tetraene-1 α ,3 β ,12 β ,22 S -tetraol (**28**).

Position	Compound 28			
	δ_{C} , mult. ^a	δ_{H} mult. ^b (J in Hz)	COSY	HMBC
1	65.7, CH	5.04 t (2.5)	2	
2	37.0, CH ₂	2.13 m	1, 3	
3	70.7, CH	4.15 dd (4.0, 12.0)	2	
4	39.7, qC			
5	142.5, qC			
6	124.5, CH	7.21 d (8.0)	7	4, 8, 10
7	125.5, CH	7.01 d (8.0)	6	5, 9, 14
8	144.1, qC			
9	134.6, qC			
10	132.2, qC			
11 α	34.1, CH ₂	3.63 dd (8.0, 18.0)	12	8, 9, 12, 13
11 β		2.69 dd (8.0, 18.0)		9, 10, 12
12	71.8, CH	4.41 t (8.0)	11	17, 18
13	49.6, qC			
14	53.2, qC			
15 α	32.4, CH ₂	1.75 m ^c	16 α	
15 β		1.97 m ^c		16
16 α	28.3, CH ₂	2.07 m ^c	15 α , 17	
16 β		1.81 m ^c	17	
17	44.6, CH	2.41 dt (6.5, 9.0)	16,20	18
18	11.4, CH ₃	0.70 s		12, 13, 14, 17
20	41.0, CH	1.86 m	17,21, 22	13, 17, 21, 22
21	15.3, CH ₃	1.16 d (7.0)	20	17, 20, 22
22	75.0, CH	3.75 dt (5.0, 7.5)	20, 23	21, 24
23	32.9, CH ₂	2.25 dd (7.5, 8.0)	22, 24	22, 24, 25
24	120.4, CH	5.21 t (8.0)	23, 26, 27	26, 27
25	136.0, qC			
26	18.1, CH ₃	1.70 s		24, 25, 27
27	26.0, CH ₃	1.78 s		24, 25, 26
28	27.1, CH ₃	1.46 s		3, 4, 5, 29
29	23.7, CH ₃	1.14 s		3, 4, 5, 28
30	28.0, CH ₃	1.10 s		8, 13, 14, 15

^a Recorded in CDCl₃ at 125 MHz; ¹³C multiplicities were determined by HSQC experiment. ^b Recorded in CDCl₃ at 500 MHz. ^c Signals overlapped.

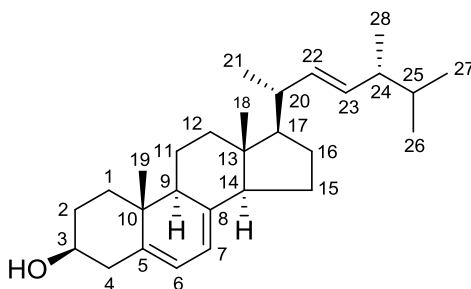
Table 4.2.1.2 The comparison of the NMR data between compound **28** and inotodiol.

Position	Compound 28		Inotodiol (Yusoo <i>et al.</i> , 2002)	
	δ_{C} , mult. ^a	δ_{H} mult. ^b (J in Hz)	δ_{C} , mult. ^a	δ_{H} mult. ^b (J in Hz)
17	44.6, CH	2.41 dt (6.5, 9.0)	47.3	1.57 m
18	11.4, CH ₃	0.70 s	15.7	0.72 s
20	41.0, CH	1.86 m	41.8	1.80 m
21	15.3, CH ₃	1.16 d (7.0)	12.6	0.94 d (1.23)
22	75.0, CH	3.75 dt (5.5, 7.5)	73.5	3.65 m
23	32.9, CH₂	2.25 dd (7.5, 8.0)	27.3	---
24	120.4, CH	5.21 t (8.0)	121.4	5.19 t
25	136.0, qC		135.0	
26	18.1, CH ₃	1.70 s	18.0	1.66 s
27	26.0, CH ₃	1.78 s	26.0	1.57 s

^a Recorded in CDCl₃ at 125 MHz. ^b Recorded in CDCl₃ at 500 MHz.

19-Nor-lanosta-5(10),6,8,24-tetraene-1 α ,3 β ,12 β ,22S-tetraol (28): white powder; $[\alpha]_D^{20} +18.3$ (c 0.24, MeOH); LC-UV [(acetonitrile (aq) in H₂O/0.1% formic acid)] λ_{\max} 222 nm; IR (solid) ν_{\max} 3352, 2929, 1638, 1454, 1413, 1379, 1100, 1033 cm⁻¹; ¹H NMR (CDCl₃, 500 MHz) and ¹³C NMR (CDCl₃, 125 MHz), see Table 4.2.1.1; Positive ESI-HRMS m/z : 439.3207 [M+H-H₂O]⁺ (calcd for C₂₉H₄₃O₃, 439.3207, Δ -0.0319 ppm), [2M+H]⁺ at m/z 913.6559 (calcd for C₅₈H₈₉O₈, 913.6552, Δ 0.7386 ppm) (Li *et al.*, 2015).

4.2.2 Ergosta-5,7,22-trienol (29, known compound)



Compound **29** (code: LG23-12) was isolated as a white crystal. The ¹H NMR and ¹H-¹H COSY spectra (Figure 4.2.2.1) showed the presence of a *trans*-disubstituted double bond at δ_H 5.17 (dd, $J = 7.0, 15.0$ Hz) and 5.22 (dd, $J = 7.0, 15.0$ Hz), a *cis*-disubstituted double bond at δ_H 5.38 (m) and 5.56 (dd, $J = 2.5, 5.5$ Hz), and an oxygenated methine at δ_H 3.63 (m). Two tertiary methyls (δ_H 0.63 and 0.94) and four secondary methyls (δ_H 0.82, 0.84, 0.91, and 1.03) were also observed. ¹³C NMR spectrum (Figure 4.2.2.2) displayed twenty-eight signals including six olefinic carbons and an oxygenated carbon at δ_C 70.6. The above analysis indicated a basic sterol derivative. Further comparison with the data (Table 4.2.2.1) in reference (Zhao *et al.*, 2010) confirmed that compound **29** was ergosta-5,7,22-trienol (ergosterol).

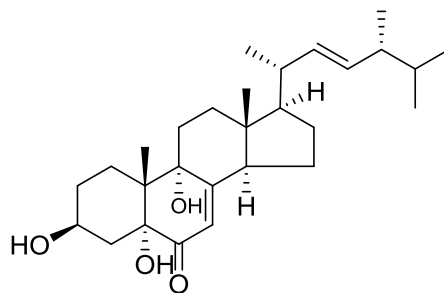
Table 4.2.2.1 ¹H and ¹³C NMR data for compound **29**.

Position	Compound 29		Ergosta-5,7,22-trienol (Zhao <i>et al.</i> , 2010)	
	δ_C , mult. ^a	δ_H mult. ^b (J in Hz)	δ_C , mult. ^a	δ_H mult. ^b (J in Hz)
1	38.6, CH ₂		38.5, CH ₂	
2	32.2, CH ₂		32.0, CH ₂	
3	70.6, CH	3.63 m	70.3, CH	3.60 m
4	41.0, CH ₂		40.8, CH ₂	
5	140.0, qC		139.8, qC	
6	119.8, CH	5.56 dd (2.5, 5.5)	119.6, CH	5.57 dd (2.5, 6.6)

7	116.5, CH	5.38 m	116.3, CH	5.36 m
8	141.5, qC		141.4, qC	
9	46.5, CH		46.3, CH	
10	37.2, qC		37.1, qC	
11	21.3, CH ₂		21.0, CH ₂	
12	39.3, CH ₂		39.5, CH ₂	
13	43.0, qC		43.0, qC	
14	54.8, CH		54.5, CH	
15	28.5, CH ₂		28.2, CH ₂	
16	23.2, CH ₂		23.0, CH ₂	
17	55.9, CH		56.0, CH	
18	12.2, CH ₃	0.63 s	12.0, CH ₃	0.63 s
19	16.5, CH ₃	0.94 s	16.3, CH ₃	0.95 s
20	40.6, CH		40.0, CH	
21	21.3, CH ₃	1.03 d (6.5)	21.1, CH ₃	1.02 d (6.6)
22	132.2, CH	5.17 dd (7.0, 15.0)	132.0, CH	5.17 dd (6.6, 15.9)
23	135.8, CH	5.22 dd (7.0, 15.0)	135.6, CH	5.24 dd (6.6, 15.9)
24	43.0, CH		42.8, CH	
25	33.3, CH		33.1, CH	
26	19.8, CH ₃	0.82 d (7.0)	19.6, CH ₃	0.82 d (6.7)
27	20.1, CH ₃	0.84 d (7.5)	20.0, CH ₃	0.84 d (6.6)
28	17.8, CH ₃	0.91 d (7.0)	17.6, CH ₃	0.92 d (6.8)

^a Recorded in CDCl₃ at 125 MHz. ^b Recorded in CDCl₃ at 500 MHz.

4.2.3 3 β ,5 α ,9 α -Trihydroxy-(22*E*,24*R*)-ergosta-7,22-dien-6-one (**30**, known compound)



Compound **30** (code: LG23-32322-2) was isolated as a white powder with a molecular formula C₂₈H₄₄O₄ assigned from the ESI-HRMS (m/z , 427.3205, calcd. for [M+H-H₂O]⁺ 427.3207, Figure 4.2.3.1). The ¹H NMR spectrum (Figure 4.2.3.2) also exhibited two tertiary methyls (δ_{H} 0.61 and 0.99) and four secondary methyls (δ_{H} 0.82, 0.84, 0.91, and 1.02) in addition to a *trans*-disubstituted double bond at δ_{H} 5.15 (dd, $J = 7.2, 15.2$ Hz) and 5.23 (dd, $J = 7.2, 15.2$ Hz). Moreover, an olefinic hydrogen at δ_{H} 5.63 (br s) was present. The ¹³C NMR spectrum (Figure 4.2.3.2) coupled with HSQC spectrum (Figure 4.2.3.3) showed an oxygenated methine and two oxygenated quaternary carbons, as well as an α,β -unsaturated carbonyl signal (δ_{C} , 198.5). These data accounted for key ¹H and ¹³C NMR resonances and revealed an ergosterol derivative. The planar structure was further constructed by HMBC

correlations with the help of ^1H - ^1H COSY data (Figure 4.2.3.4). A search in SciFinder, together with the NMR data determined compound **30** to be $3\beta,5\alpha,9\alpha$ -Trihydroxy-($22E,24R$)-ergosta-7,22-dien-6-one. The comparison of the 1D NMR data with those reported in reference (Xiong *et al.*, 2009) is shown in Table 4.2.3.1.

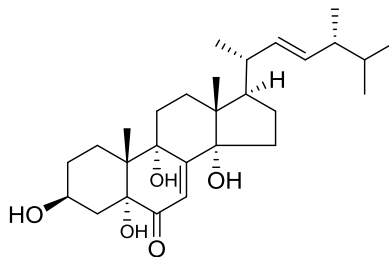
Table 4.2.3.1 ^1H and ^{13}C NMR data for compound **30**.

Position	Compound 30		$3\beta,5\alpha,9\alpha$ -Trihydroxy-($22E,24R$)-ergosta-7,22-dien-6-one (Xiong <i>et al.</i> , 2009)	
	δ_{C} , mult. ^a	δ_{H} mult. ^b (J in Hz)	δ_{C} , mult. ^c	δ_{H} mult. ^d (J in Hz)
1	25.7, CH ₂	1.49 m ^e , 2.33 t (13.2)	25.7, CH ₂	
2	30.2, CH ₂	1.44 m ^e , 1.93 m ^e	30.0, CH ₂	
3	67.4, CH	4.06 m	67.4, CH	4.04 m
4	37.1, CH ₂	1.73 m ^e , 2.08 m ^e	36.8, CH ₂	
5	79.7, qC		79.6, qC	
6	198.5, qC		199.0, qC	
7	119.9, CH	5.63 br s	119.9, CH	5.61 br s
8	165.1, qC		165.4, qC	
9	74.9, qC		74.9, qC	
10	41.9, qC		41.9, qC	
11	28.9, CH ₂	1.72 m ^e , 1.88 m ^e	29.8, CH ₂	
12	35.1, CH ₂	1.72 m ^e , 1.86 m ^e	35.1, CH ₂	
13	45.5, qC		45.5, qC	
14	52.0, CH	2.73 dd (6.4, 10.0)	52.0, CH	
15	22.6, CH ₂	1.46 m ^e , 1.57 m ^e	22.6, CH ₂	
16	28.1, CH ₂	1.34 m ^e , 1.78 m ^e	28.1, CH ₂	
17	56.2, CH	1.42 m ^e	56.2, CH	
18	12.5, CH ₃	0.61 s	12.5, CH ₃	0.61 s
19	20.6, CH ₃	0.99 s	20.5, CH ₃	0.98 s
20	40.5, CH	2.01 m ^e	40.5, CH	
21	21.3, CH ₃	1.02 d (6.4)	21.3, CH ₃	1.02 d (6.6)
22	135.3, CH	5.15 dd (7.2, 15.2)	135.5, CH	5.16 dd (6.6, 15.3)
23	132.6, CH	5.23 dd (7.2, 15.2)	132.6, CH	5.24 dd (6.9, 15.3)
24	43.0, CH	1.84 m ^e	43.0, CH	
25	33.3, CH	1.45 m ^e	33.3, CH	
26	20.2, CH ₃	0.82 d (6.8)	20.2, CH ₃	0.82 d (6.6)
27	19.9, CH ₃	0.84 d (6.8)	19.6, CH ₃	0.84 d (6.6)
28	17.8, CH ₃	0.91 d (6.8)	17.8, CH ₃	0.92 d (6.9)

^a Recorded in CDCl₃ at 100 MHz. ^b Recorded in CDCl₃ at 400 MHz. ^c Recorded in CDCl₃ at 75 MHz. ^d Recorded in CDCl₃ at 300 MHz.

^e overlapped.

4.2.4 $3\beta,5\alpha,9\alpha,14\alpha$ -Tetrahydroxy-($22E,24R$)-ergosta-7,22-dien-6-one (**31**, known compound)



Compound **31** (code: LG23-32322-1) was obtained as a white powder. Its molecular formula was deduced as C₂₈H₄₄O₅ as determined from ESI-HRMS (m/z 425.3056, calcd. for [M+H-2×H₂O]⁺ 425.3050, Figure 4.2.4.1). The ¹H NMR data coupled with HSQC spectrum of **31** (Figure 4.2.4.2) was closely related to those of **30**, except for the absence of H-14 (δ_{H} 2.73) in **30** and the downfield shift of H-7 (δ_{H} 5.63 in **30**; 5.94 in **31**). Considering the MS requirement, compound **31** was proposed to have a hydroxyl group at C-14 and should possess the same structure as 3 β ,5 α ,9 α ,14 α -tetrahydroxy-(22*E*,24*R*)-ergosta-7,22-dien-6-one, which was further confirmed through the comparison of the NMR data of **31** with reference data (Table 4.2.4.1) (Yaoita *et al.*, 1998).

Table 4.2.4.1 ¹H and ¹³C NMR data for compound **31**.

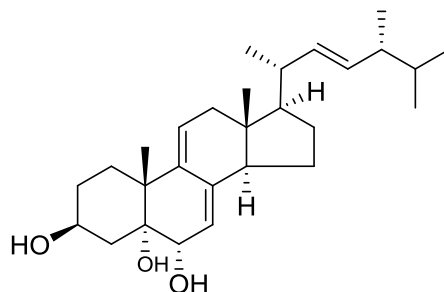
Position	Compound 31		3 β ,5 α ,9 α ,14 α -Tetrahydroxy-(22 <i>E</i> ,24 <i>R</i>)-ergosta-7,22-dien-6-one (Yaoita <i>et al.</i> , 1998)	
	δ_{C} , mult. ^a	δ_{H} mult. ^b (<i>J</i> in Hz)	δ_{C} , mult. ^c	δ_{H} mult. ^d (<i>J</i> in Hz)
1	24.7, CH ₂	2.35 ddd (14.5, 14.5, 5.0) 1.49 m	25.7, CH ₂	α 2.70 ddd (14.0, 14.0, 3.8)
2	31.3, CH ₂		31.3, CH ₂	
3	67.0, CH	4.09 m	66.6, CH	4.61 m
4	36.5, CH ₂	1.67 m, 2.10 m	37.8, CH ₂	α 2.82 dd (12.0, 5.3)
5	78.9, qC ^f		79.6, qC	
6	NS ^e		199.3, qC	
7	122.0, CH	5.94 s	122.1, CH	6.25 s
8	NS ^e		158.9, qC	
9	76.7, qC ^f		77.2, qC	
10	42.5, qC ^f		42.8, qC	
11	29.8, CH ₂		31.0, CH ₂	
12	27.5, CH ₂		28.5, CH ₂	
13	46.7, qC ^f		47.3, qC	
14	87.1, qC ^f		86.2, qC	
15	26.2, CH ₂		27.4, CH ₂	
16	28.0, CH ₂		28.0, CH ₂	
17	49.9, CH		50.5, CH	
18	16.4, CH ₃	0.71 s	16.6, CH ₃	0.73 s
19	20.1, CH ₃	1.02 s	20.2, CH ₃	1.13 s
20	39.7, CH	2.09 m	40.4, CH	2.13 m
21	21.1, CH ₃	1.03 d (8.0)	21.5, CH ₃	1.09 d (6.6)
22	134.7, CH	5.19 dd (7.5, 15.0)	135.2, CH	5.26 dd (8.1, 15.4)
23	132.5, CH	5.27 dd (7.5, 15.0)	132.4, CH	5.31 dd (7.3, 15.4)
24	42.9, CH		43.1, CH	

25	32.7, CH		33.3, CH
26	19.5, CH ₃	0.83 d (7.0)	19.9, CH ₃ 0.85 d (7.0)
27	19.8, CH ₃	0.85 d (7.5)	20.2, CH ₃ 0.86 d (6.6)
28	17.5, CH ₃	0.92 d (6.5)	17.8, CH ₃ 0.94 d (7.0)

^a Recorded in CDCl₃ at 125 MHz. ^b Recorded in CDCl₃ at 500 MHz. ^c Recorded in C₅D₅N at 150 MHz. ^d Recorded in C₅D₅N at 600 MHz.

^e Not assigned. ^f assigned from HMBC spectrum.

4.2.5 (22*E*,24*R*)-Ergosta-7,9(11),22-triene-3β,5α,6α-triol (**32**, known compound)

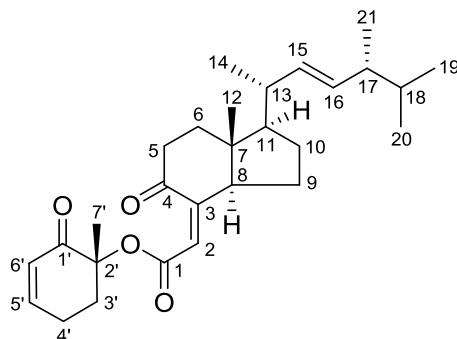


Compound **32** (code: LG23-32322-5) was purified as a white solid. A molecular formula of C₂₈H₄₄O₃ (seven double bond equivalents) was assigned from the ESI-HRMS (m/z 411.3251, calcd. for [M+H-H₂O]⁺ 411.3258, Figure 4.2.5.1). The UV spectrum showed an absorption maximum at 228 nm. The above results are similar to that of compounds **30** and **31**. Furthermore, detailed analysis of ¹H NMR spectrum (Figure 4.2.5.2) revealed similar structural features such as two tertiary methyls (δ_{H} 0.56 and 1.11) and four secondary methyls (δ_{H} 0.83, 0.85, 0.92, and 1.02). A *trans*-disubstituted double bond located in the side chain was verified by the presence of two olefinic protons at δ_{H} 5.17 (dd, $J = 8.5, 15.0$ Hz) and 5.25 (dd, $J = 7.5, 15.0$ Hz). In addition, the 3-OH was also proposed based on the observed oxygenated methine at δ_{H} 4.03. These data suggested compound **32** was also an ergosterol derivative. Unfortunately, owing to the limited amount of **32** available for further NMR measurement, clear ¹³C NMR spectrum were not obtained but the strong correlations especially based on methyl groups in HMBC spectrum (Figure 4.2.5.3) was useful to connect the proposed structural units of **32**. Therefore, according to these data and further comparison with the literature (Table 4.2.5.1) (Anastasia *et al.*, 1979; Ishizuka *et al.*, 1997), compound **32** was concluded to be (22*E*,24*R*)-ergosta-7,9(11),22-triene-3β,5α,6α-triol.

Table 4.2.5.1 ^1H and ^{13}C NMR data for compound **32**.

Position	Compound 32		<i>(22E,24R)</i> -Ergosta-7,9(11),22-triene-3 β ,5 α ,6 β -triol (Ishizuka <i>et al.</i> , 1997)		<i>(22E,24R)</i> -Ergosta-7,9(11),22-triene-3 β ,5 α ,6 α -triol (Anastasia <i>et al.</i> , 1979)
	δ_{C} , mult. ^a	δ_{H} mult. ^b (J in Hz)	δ_{C} , mult. ^c	δ_{H} mult. ^d (J in Hz)	δ_{H} mult. ^f (J in Hz)
1	30.1, CH ₂		29.7, CH ₂		
2	30.6, CH ₂		30.8, CH ₂		
3	66.7, CH	4.03 m	67.7, CH	4.12 m	4.00 m
4	37.4, ^g CH ₂		42.2, CH ₂	β 2.07 dd (12.8, 11.4)	
5	76.1, qC		75.3, qC		
6	70.4, ^g CH	3.99 m	74.0, CH	3.82 br s	
7	121.3, CH	5.17 m ^e	118.2, CH	5.45 br d (5.6)	5.14 m
8	137.2, qC		138.9, qC		
9	139.4, qC		140.0, qC		
10	41.1, qC		40.7, qC		
11	125.0, CH	5.69 br d (6.5)	126.4, CH	5.75 br d (6.3)	5.65 m
12	42.2, CH ₂		42.5, CH ₂		
13	42.4, qC		42.5, qC		
14	51.3, CH		51.4, CH		
15	22.8, CH ₂		23.1, CH ₂		
16	28.6, CH ₂		28.7, CH ₂		
17	56.1, CH		56.0, CH		
18	11.2, CH ₃	0.56 s	11.5, CH ₃	0.60 s	0.53 s
19	24.2, ^g CH ₃	1.11 s	26.3, CH ₃	1.28 s	1.06 s
20	40.5, CH		40.3, CH		
21	20.4, CH ₃	1.02 d (6.5)	20.7, CH ₃	1.02 d (6.6)	
22	135.7, CH	5.17 dd (15.0, 8.5)	135.2, CH	5.16 dd (15.2, 7.8)	5.23 m
23	132.5, CH	5.25 dd (15.0, 7.5)	132.3, CH	5.26 dd (15.2, 7.1)	5.23 m
24	42.7, CH		42.8, CH		
25	32.9, CH		33.1, CH		
26	19.4, CH ₃	0.83 d (7.0)	19.6, CH ₃	0.83 d (6.8)	
27	19.8, CH ₃	0.85 d (7.0)	19.9, CH ₃	0.84 d (6.6)	
28	17.5, CH ₃	0.92 d (6.5)	17.6, CH ₃	0.92 d (6.8)	

^a Assigned from HSQC and HMBC spectra at 500 MHz. ^b Recorded in CDCl₃ at 500 MHz. ^c Recorded in CDCl₃ at 150 MHz. ^d Recorded in CDCl₃ at 600 MHz. ^e overlapped. ^f Recorded in CDCl₃ at 100 MHz. ^g Had significant differences with that in literature.

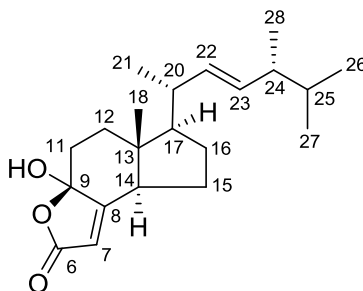
4.2.6 Chaxine C (**33**, known compound)

Compound **33** (code: LG23-222-7), as a white solid, has a molecular formula $C_{28}H_{40}O_4$ as derived from ESI-HRMS (m/z 441.3005, calcd. for $[M+H]^+$ 441.2999, Δ 1.2233 ppm) (Figure 4.2.6.1). Two characteristic fragment ions at m/z 333.2425 $[M+H-C_7H_8O]^+$ and 315.2319 $[M+H-C_7H_{10}O_2]^+$ were observed (Figure 4.2.6.1). It presented the UV absorption maximum at 224 nm. The 1H and ^{13}C NMR spectra (Figure 4.2.6.2) in combination with the HSQC spectrum (Figure 4.2.6.3) established the presence of two tertiary methyls, four secondary methyls, six methylenes, five methines, two quaternary carbons (one oxygenated), six aromatic/olefinic carbons including a *cis*-disubstituted and a *trans*-disubstituted double bonds, and three carbonyl carbons (one conjugated). These data accounted for all 1H and ^{13}C NMR resonances. Interpretation of 1H - 1H COSY spectrum (Figure 4.2.6.3) determined the connection from C-3' to C-6', from C-5 to C-6, from C-8 to C-11, and C-13 to C-17, as well as from C-18 to C-20. Key HMBC correlations (Figure 4.2.6.4) from H_3 -12 to C-6, C-7, C-8, and C-11, from H_3 -19 and H_3 -20 to C-17, from H_2 -5 to C-3 and C-4, and from H-2 to C-1, C-4, and C-8 indicated the C and D rings attached with a side chain. The above substructure is similar to that of ergosterol derivatives. However, further HMBC correlations (Figure 4.2.6.4) of H_3 -7'/C-1', H_3 -7'/C-2', H_3 -7'/C-3', H_2 -3'/C-1', and H-5'/C-1 determined a modified cyclohexanone motif. Considering the chemical shifts of C-1 (δ_C 164.4) and C-2' (δ_C 81.4) and the MS requirement, the planar structure of compound **33** was constructed through an oxygen bridge between the two substructures mentioned above, which was also supported by the MS fragment information (Figure 4.2.6.1). Finally, through comparison with the literature data (Table 4.2.6.1) (Choi *et al.*, 2009), compound **33** was elucidated as chaxine C.

Table 4.2.6.1 ^1H and ^{13}C NMR data for compound **33**.

Position	Compound 33		Chaxine C (Choi <i>et al.</i> , 2009)	
	δ_{C} , mult. ^a	δ_{H} mult. ^b (<i>J</i> in Hz)	δ_{C} , mult. ^c	δ_{H} mult. ^d (<i>J</i> in Hz)
1	164.4, qC		164.2, qC	
2	117.7, CH	5.64 d (2.5)	117.5, CH	5.65 d (1.5)
3	156.4, qC		156.2, qC	
4	204.7, qC		204.6, qC	
5 α	39.2, CH ₂	2.46 m	39.0, CH ₂	2.43 m
5 β		2.72 ddd (15.5, 13.5, 7.5)		2.70 ddd (13.4, 7.0, 7.3)
6 α	38.2, CH ₂	1.67 ddd (13.0, 13.0, 5.5)	38.0, CH ₂	1.65 ddd (13.4, 12.8, 5.5)
6 β		2.20 ddd (13.0, 7.5, 2.0)		2.18 m
7	46.7, qC		46.5, qC	
8	58.0, CH	2.48 m	57.8, CH	2.44 m
9	21.9, CH ₂	1.52 m ^e , 1.58 m ^e	21.8, CH ₂	1.46 m, 1.53 m
10	29.2, CH ₂	1.48 m ^e , 1.89 m ^e	29.0, CH ₂	1.45 m, 1.86 m
11	55.6, CH	1.42 m ^e	55.3, CH	1.38 dd (18.3, 9.0)
12	12.3, CH ₃	0.89 s	12.1, CH ₃	0.85 s
13	40.3, CH	2.08 m	40.1, CH	2.06 m
14	21.2, CH ₃	1.02 d (6.5)	21.0, CH ₃	1.00 d (6.4)
15	134.8, CH	5.15 dd (15.0, 8.5)	134.6, CH	5.12 dd (15.3, 8.5)
16	133.1, CH	5.26 dd (15.0, 8.0)	132.9, CH	5.23 dd (15.3, 7.6)
17	43.0, CH	1.85 m	42.8, CH	1.84 m
18	33.2, CH	1.47 m	33.0, CH	1.45 m
19	19.8, CH ₃	0.84 d (7.0)	19.6, CH ₃	0.82 d (7.6)
20	20.1, CH ₃	0.82 d (7.0)	19.9, CH ₃	0.80 d (7.6)
21	17.8, CH ₃	0.92 d (7.0)	17.6, CH ₃	0.90 d (6.7)
1'	195.9, qC		196.7, qC	
2'	81.4, qC		81.2, qC	
3'	32.3, CH ₂	2.02 m ^e 2.93 ddd (13.0, 11.0, 5.5)	32.1, CH ₂	2.01 m 2.91 ddd (12.1, 6.1, 5.7)
4'	25.0, CH ₂	2.43 m, 2.50 m	24.7, CH ₂	2.40 m, 2.45 m
5'	149.0, CH	6.89 m	148.1, CH	6.86 m
6'	128.3, CH	6.03 br d (10.5)	128.1, CH	6.01 d (10.5)
7'	22.1, CH ₃	1.48 s	21.9, CH ₃	1.46 s

^a Recorded in CDCl₃ at 125 MHz. ^b Recorded in CDCl₃ at 500 MHz. ^c Recorded in CDCl₃ at 125 MHz. ^d Recorded in CDCl₃ at 500 MHz. ^e overlapped.

4.2.7 Demethylincisterol A₃ (**34**, known compound)

Compound **34** (code: LG23-222-5), a white solid, has a molecular formula C₂₁H₃₂O₃ as determined by the ESI-HRMS (m/z 333.2425, calcd. for [M+H]⁺ 333.2424, Δ 0.2139 ppm) (Figure 4.2.7.1). The MS also showed the loss of one water molecule (m/z 315.2321, calcd. for [M+H-H₂O]⁺ 315.2319, Δ 0.8247 ppm), suggesting the possible presence of a hydroxy group in **34**. As expected, ¹³C NMR spectrum (Figure 4.2.7.2) showed twenty-one carbon signals. Although the MS data of **34** is quite different from those of compounds elucidated before, the ¹³C and ¹H NMR spectra (Figure 4.2.7.2) exhibited the same signals for the side chain to those of compounds **29–33**. One more methyl singlet at δ_{H} 0.61 and δ_{C} 11.9 was also observed, and one lactone group was proposed to be present in **34** on the basis of the chemical shifts (δ_{C} 170.9) and MS requirement. The above analysis enabled us to obtain several important structural characters, which were further considered in a structure search using ‘Molecular Formula’ mode in Scifinder. Finally, a compound named demethylincisterol A₃ was proposed to have the same structure as **34**, which was successfully confirmed through the comparison of 1D NMR data of **34** with that reported in the literature (Table 4.2.7.1) (Togashi *et al.*, 1998; Mansoor *et al.*, 2005).

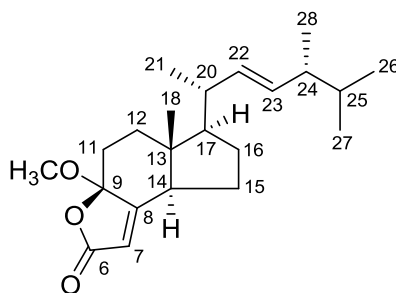
Table 4.2.7.1 ¹H and ¹³C NMR data for compound **34**.

Position	Compound 34		Demethylincisterol A ₃ (Togashi <i>et al.</i> , 1998; Mansoor <i>et al.</i> , 2005)	
	δ_{C} , mult. ^a	δ_{H} mult. ^b (J in Hz)	δ_{C} , mult. ^c	δ_{H} mult. ^d (J in Hz)
6	170.9, qC		171.8, qC	
7	112.5, CH	5.63 d (2.0)	112.0, CH	5.61 d (2.0)
8	170.7, qC		171.2, qC	
9	104.9, qC		105.4, qC	
11 α	35.5, CH ₂	2.28 ddd (2.0, 3.5, 14.0)	35.2, CH ₂	2.30 ddd (2.4, 3.9, 13.7)
11 β		NS ^f		1.84 ddd (4.9, 13.0, 13.7)

12 α	35.3, CH ₂	NS ^f	35.1, CH ₂	1.63 ddd (3.9, 13.0, 13.2)
12 β		1.98 ddd (2.5, 5.0, 13.0)		1.96 ddd (2.4, 3.9, 13.7)
13	49.0, qC		48.9, qC	
14	50.5, CH	2.65 ddd (1.5, 6.5, 11.5)	50.4, CH	2.66 ddd (2.0, 5.9, 11.2)
15	21.6, CH ₂		21.4, CH ₂	α 1.72 m, β 1.48 m
16	29.0, CH ₂		28.9, CH ₂	α 1.90 m, β 1.47 m
17	55.6, CH		55.4, CH	1.50 m
18	11.9, CH ₃	0.61 s	11.8, CH ₃	0.60 s
20	40.3, CH		40.2, CH	2.05 m
21	21.2, CH ₃	1.04 d (6.5)	21.0, CH ₃	1.04 d (6.8)
22	134.8, CH	5.17 dd (7.5, 15.0)	134.7, CH	5.17 dd (8.3, 15.2)
23	133.1, CH	5.26 dd (8.5, 15.0)	132.8, CH	5.26 dd (7.3, 15.1)
24	43.0, CH		42.9, CH	1.86 m
25	33.2, CH		33.1, CH	1.49 m
26	19.8, CH ₃	0.83 d (6.5)	19.7, CH ₃	0.83 d (6.8)
27	20.1, CH ₃	0.84 d (6.5)	20.0, CH ₃	0.84 d (6.8)
28	17.8, CH ₃	0.92 d (7.0)	17.6, CH ₃	0.92 d (6.8)

^a Recorded in CDCl₃ at 125 MHz. ^b Recorded in CDCl₃ at 500 MHz. ^c Recorded in CDCl₃ at 150 MHz. ^d Recorded in CDCl₃ at 600 MHz. ^e overlapped. ^f Not assigned.

4.2.8 Volemolide (35, known compound)



The molecular formula of compound **35** (code: LG23-222-8) was established as C₂₂H₃₄O₃ based on the ESI-HRMS information ([M+H]⁺ at *m/z* 347.2584, calcd. 347.2581, Δ 0.9240 ppm; [M+H-CH₃OH]⁺ at *m/z* 315.2322, calcd. 315.2319, Δ 1.2119 ppm) (Figure 4.2.8.1). The comparison of UV and MS data between compounds **34** and **35** indicated that compound **35** was similar to **34**. Further comparison of their ¹H and ¹³C NMR spectra (Figure 4.2.8.2) enabled us to find a significant difference due to the existence of one methoxy in **35**. As indicated in MS/MS data ([M+H-H₂O]⁺ 315.2318 in **34**; [M+H-CH₃OH]⁺ 315.2321 in **35**), the hydroxy group in **34** was replaced by the methoxy in **35**. The whole

structure was confirmed by the comparison of 1D NMR data with literature data (Table 4.2.8.1) (Kobata *et al.*, 1994) and was identical with the known compound volemolide (Kobata *et al.*, 1994).

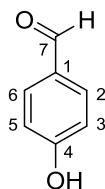
Table 4.2.8.1 ^1H and ^{13}C NMR data for compound **35**.

Position	Compound 35		Volemolide (Kobata <i>et al.</i> , 1994)	
	δ_{C} , mult. ^a	δ_{H} mult. ^b (<i>J</i> in Hz)	δ_{C} , mult. ^c	δ_{H} mult. ^d (<i>J</i> in Hz)
6	170.9, qC		170.7, qC	
7	114.4, CH	5.75 d (1.5)	114.2, CH	5.75 d (1.7)
8	169.3, qC		169.1, qC	
9	108.0, qC		107.8, qC	
11 α	34.7, CH ₂	2.33 ddd (3.0, 4.0, 14.5)	34.5, CH ₂	2.33 ddd (2.2, 3.5, 13.3)
11 β		NS ^e		1.77 m
12 α	35.2, CH ₂		35.0, CH ₂	1.57 m
12 β				1.93 m
13	49.1, qC		48.9, qC	
14	50.8, CH	2.41ddd (1.5, 6.5, 11.5)	50.6, CH	2.41ddd (1.7, 6.0, 9.4)
15	21.5, CH ₂		21.3, CH ₂	α 1.73 m, β 1.49 m
16	29.0, CH ₂		28.9, CH ₂	α 1.90 m, β 1.48 m
17	55.7, CH		55.5, CH	1.50 m
18	12.1, CH ₃	0.61 s	11.9, CH ₃	0.61 s
20	40.3, CH		40.1, CH	2.06 m
21	21.2, CH ₃	1.03 d (6.5)	21.0, CH ₃	1.03 d (6.6)
22	134.8, CH	5.16 dd (8.5, 15.0)	134.7, CH	5.16 dd (7.3, 15.3)
23	133.0, CH	5.25 dd (7.5, 15.0)	132.9, CH	5.26 dd (7.3, 15.3)
24	43.0, CH		42.8, CH	1.87 m
25	33.2, CH		33.0, CH	1.48 m
26	19.8, CH ₃	0.82 d (7.0)	19.6, CH ₃	0.82 d (6.7)
27	20.1, CH ₃	0.84 d (7.0)	20.0, CH ₃	0.84 d (6.7)
28	17.8, CH ₃	0.92 d (7.0)	17.6, CH ₃	0.92 d (6.8)
OMe	50.3, CH ₃	3.12, s	50.1, CH ₃	3.12, s

^a Recorded in CDCl₃ at 125 MHz. ^b Recorded in CDCl₃ at 500 MHz. ^c Recorded in CDCl₃ at 62.5 MHz. ^d Recorded in CDCl₃ at 250 MHz.

^e Not assigned.

4.2.9 4-Hydroxybenzaldehyde (**36**, known compound)



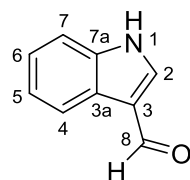
Compound **36** (code: LG23-232) was obtained as a white powder. It has the well-resolved UV bands with maxima at 222 and 282 nm. ESIMS in the negative mode (Figure 4.2.9.1) provided an ion peak at m/z 120.70, corresponding to $[M-H]^-$. The ^1H NMR spectrum revealed a possible symmetrical structure owing to the double-integration of signals at δ_{H} 6.91 and 7.77 compared to proton at δ_{H} 9.76. Key HMBC correlations of H-2 and H-6 to C-4 and C-7, as well as H-3 and H-5 to C-1, is shown in Figure 4.2.9.2. Accordingly, the structure of compound **36** was established as the known compound 4-hydroxybenzaldehyde which has the identical NMR data with that of **36** (Table 4.2.9.1) (Shi *et al.*, 2014).

Table 4.2.9.1 ^1H and ^{13}C NMR data for compound **36**.

Position	Compound 36		4-Hydroxybenzaldehyde (Shi <i>et al.</i> , 2014)
	δ_{C} , mult. ^a	δ_{H} mult. ^b (J in Hz)	δ_{H} mult. ^c (J in Hz)
1	130.0, qC		
2, 6	133.3, CH	7.77 d (8.5)	7.77 d (8.5)
4	165.0, qC		
3, 5	116.8, CH	6.91 d (8.5)	6.91 d (8.5)
7	192.5, CH	9.76 s	9.76 s

^a Assigned from HMBC spectrum in CD_3OD at 500 MHz. ^b Recorded in CD_3OD at 500 MHz. ^c Recorded in CDCl_3 at 500 MHz.

4.2.10 1H-indole-3-carbaldehyde (3-formylindole) (**37**, known compound)



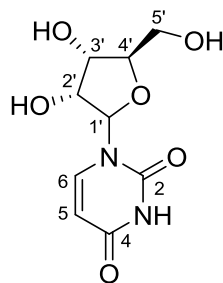
Compound **37** (code: LG23-3213) was isolated as a white powder. The interpretation of ^1H - ^1H COSY spectrum (Figure 4.2.10.1) indicated the connection from C-4 to C-7. The benzene ring was constructed by HMBC correlations of H-4/C-7a and H-7/C-3a (Figure 4.2.10.2). The proton signal of aldehyde was correlated to C-3 and C-3a in HMBC spectrum (Figure 4.2.10.2). In addition, HMBC correlations from H-2 to C-3 and C-7a were observed. Considering the chemical shifts of C-2 and C-7a, and through the comparison of NMR data with that of reference data (Table 4.2.10.1), the structure was determined to be the known compound 1H-indole-3-carbaldehyde (Wang *et al.*, 2013).

Table 4.2.10.1 ^1H and ^{13}C NMR data for compound **37**.

Position	Compound 37		^1H -indole-3-carbaldehyde (3-formylindole) (Wang <i>et al.</i> , 2013)	
	δ_{C} , mult. ^a	δ_{H} mult. ^b (<i>J</i> in Hz)	δ_{C} , mult. ^c	δ_{H} mult. ^d (<i>J</i> in Hz)
1				
2	139.8, CH	8.09 s	139.4, CH	8.26 d (2.3)
3	119.9, qC		118.4, qC	
3a	125.7, qC		124.7, qC	
4	122.3, CH	8.16 d (7.5)	121.5, CH	8.07 d (7.6)
5	123.6, CH	7.24 dd (7.0)	123.1, CH	7.19 dd (7.8, 7.6)
6	124.8, CH	7.28 dd (7.5)	124.4, CH	7.24 dd (8.0, 7.8)
7	113.0, CH	7.48 d (8.0)	113.2, CH	7.49 d (8.0)
7a	138.9, qC		137.6, qC	
8	187.3, CH	9.89 s	185.5, CH	9.91 s

^a Assigned from HMBC spectrum in CD_3OD at 500 MHz. ^b Recorded in CD_3OD at 500 MHz. ^c Recorded in $\text{DMSO}-d_6$ at 150 MHz. ^d Recorded in $\text{DMSO}-d_6$ at 600 MHz.

4.2.11 Uridine (**38**, known compound)



Compound **38** (code: LG23-633) was isolated as a white powder with a molecular formula $\text{C}_9\text{H}_{12}\text{O}_6\text{N}_2$ as derived from ESI-HRMS (m/z 245.0771, calcd. for $[\text{M}+\text{H}]^+$ 245.0768, Δ 1.0591 ppm, Figure 4.2.11.1). ^1H NMR spectrum (Figure 4.2.11.2) showed eight signals for *cis*-double bond protons at δ_{H} 5.70 (d, $J = 8.0$ Hz) and 7.99 (d, $J = 8.0$ Hz), together with six oxygenated protons including a down-field shifted signal at δ_{H} 5.90 (d, $J = 5.0$ Hz). Interpretation of ^1H - ^1H COSY spectrum (Figures 4.2.11.2 and 4.2.11.3) revealed the connection from C-5 to C-6, from C-1' to 2', and from C-3' to C-5'. Further analysis of HMBC spectrum (Figure 4.2.11.3) afforded the whole structure as a known compound uridine on the basis of key HMBC correlations of H-5/C-4, H-6/C-4, H-6/C-2, H-6/C-1', H-1'/C-2, H-

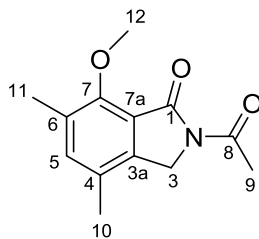
1'/C-3', and H-1'/C-4'. The NMR data of compound **38** was consistent with that of known compound (Table 4.2.11.1) (Mantsch and Smith, 1973).

Table 4.2.11.1 ^1H and ^{13}C NMR data for compound **38**.

Position	Compound 38		Uridine (Mantsch and Smith, 1973)
	δ_{C} , mult. ^a	δ_{H} mult. ^b (<i>J</i> in Hz)	δ_{C} , mult. ^c
2	151.9, qC		152.3, qC
4	165.7, qC		164.6, qC
5	102.1, CH	5.70 d (8.0)	103.3, CH
6	142.2, CH	7.99 d (8.0)	142.3, CH
1'	90.0, CH	5.90 d (5.0)	89.3, CH
2'	75.1, CH	4.18 t (5.0)	75.1, CH
3'	70.7, CH	4.15 t (5.0)	71.4, CH
4'	86.1, CH	4.01 m	86.3, CH
5'	62.1, CH ₂	3.73 dd (2.5, 12.0) 3.84 dd (3.0, 12.0)	62.4, CH ₂

^a Recorded in CD₃OD at 125 MHz. ^b Recorded in CD₃OD at 500 MHz. ^c Recorded in DMSO-*d*₆ at 25.16 MHz.

4.2.12 2-Acetyl-7-methoxy-4,6-dimethyl-1*H*-isoindol-1-one (**39**, new compound)



Compound **39** (code: LG23-133) was isolated as a white solid with a molecular formula C₁₃H₁₅NO₃ as determined by ESI-HRMS (*m/z* 234.1123, calcd. for [M+H]⁺ 234.1125, Δ -0.6404 ppm, Figure 4.2.12.1). 1D NMR data (Figure 4.2.12.2 and Table 4.2.12.1) coupled with HSQC spectrum revealed the presence of four methyl groups (one oxygenated), one methylene, six aromatic/olefinic carbons including an oxygenated quaternary carbon (δ_{C} 155.7) and a methine carbon (δ_{H} 7.26, δ_{C} 138.4), and two amide carbonyls (δ_{C} 166.6 and 171.6). The above data accounted for all NMR resonances. HMBC correlations (Figures 4.2.12.3 and 4.2.12.4) of H₃-10 with C-3a, C-4 and C-5, H₃-11 with C-5, C-6 and C-7, and H-5 with C-3a and C-7 determined a benzene ring with two methyl groups. Furthermore, a methoxy group located at C-7 was confirmed by the HMBC correlation between H₃-12 and C-7. Key HMBC cross-peaks

(Figure 4.2.12.4) from H₂-3 to C-1, C-3a and C-7a, together with the chemical shifts of C-1 and C-3 (δ_{H} 4.63, δ_{C} 47.0) indicated a γ -lactam fused with the benzene ring. The nitrogen was further substituted with an acetyl unit, which was proved by the HMBC correlation from H₃-9 to C-8, and the MS requirement. Finally, we applied the quantum chemical calculations to predict the ¹³C NMR chemical shifts (Sarotti and Pellegrinet, 2009). A comparison of the calculated ¹³C NMR values by GIAO method (gauge including atomic orbitals) at the B3LYP/6-31+G(d,p)//mPW1PW91/6-31+G(d) level and the corresponding experimental chemical shifts for compound **39** was shown in Table 4.2.12.1. A good matching between the experimental and calculated ¹³C NMR values supports the structure of **39**. Accordingly, the structure of compound **39** was determined as shown.

Table 4.2.12.1 ¹H and ¹³C NMR data for compound **39**.

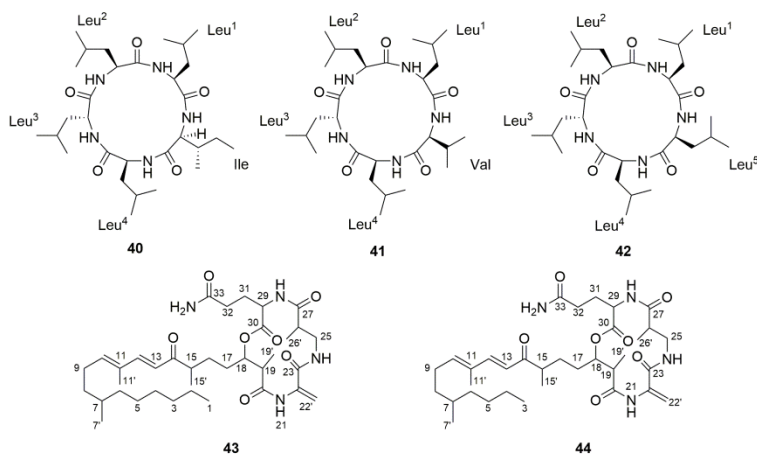
Position	Compound 39		NMR calculation	
	δ_{C} , mult. ^a	δ_{H} mult. ^b (<i>J</i> in Hz)	δ_{C} , mult. ^c	deviation ^d
1	166.6, qC		166.9	0.3
2				
3	47.0, CH ₂	4.63 s	47.6	0.6
3a	139.5, qC		141.5	2.0
4	128.0, qC		127.9	-0.1
5	138.4, CH	7.26 s	138.8	0.4
6	131.9, qC		133.2	1.3
7	155.7, qC		156.0	0.3
7a	122.3, qC		123.3	1.0
8	171.6, qC		171.7	0.1
9	25.1, CH ₃	2.68 s	26.4	1.3
10	17.0, CH ₃	2.26 s	18.2	1.2
11	15.5, CH ₃	2.30 s	18.2	2.7
12	62.1, CH ₃	3.97 s	59.1	-3

^a Recorded in CDCl₃ at 150 MHz. ^b Recorded in CDCl₃ at 600 MHz. ^c Calculated ¹³C NMR data. ^d The deviation between calculated and experimental ¹³C NMR data.

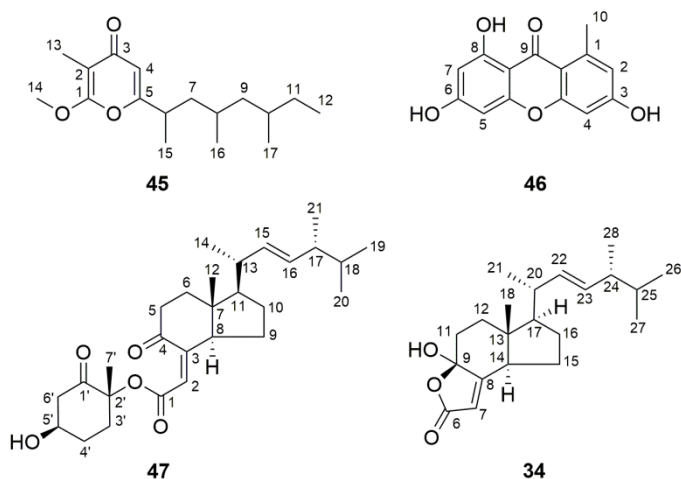
2-Acetyl-7-methoxy-4,6-dimethyl-1H-isoindol-1-one (39): white powder; LC-UV [(acetonitrile (aq) in H₂O/0.1% formic acid)] λ_{max} 218, 306 nm; ¹H NMR (CDCl₃, 600 MHz) and ¹³C NMR (CDCl₃, 150 MHz), see Table 4.2.12.1. Positive ESI-HRMS *m/z*: 234.1123 [M+H]⁺ (calcd for C₁₃H₁₆NO₃, 234.1125, Δ -0.6404 ppm).

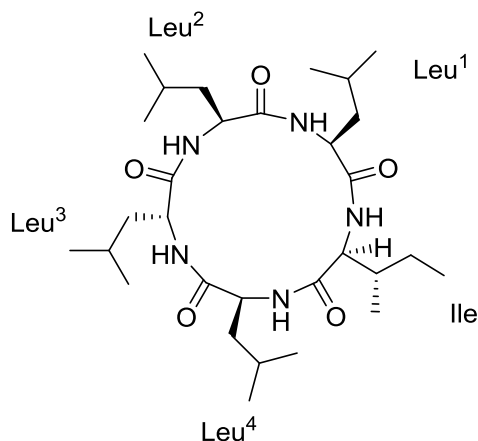
4.3 Secondary metabolites isolated from *Fusarium decemcellulare* LG53

Three new cyclic pentapeptides (**40–42**), together with two cyclic lipopeptides (**43** and **44**) in which **44** is a new compound, were isolated from the rice culture of an endophytic fungus, *F. decemcellulare* LG53, harbored in the stem of a traditional medicinal plant *M. fortunei* collected from Guangdong, P. R. China.



A new pyrone derivative (**45**), a known xanthone derivative (**46**), as well as a known triterpenoid (**47**) were also isolated and purified in parallel. Moreover, compound **34** previously obtained from *Diaporthe* sp. LG23, was also found and isolated from *F. decemcellulare* LG53.



4.3.1 Cyclo-(L-Leu-L-Leu-D-Leu-L-Leu-L-Ile) (**40**, new compound)

Compound **40** (code: LG53-924) was isolated as a white amorphous powder with a molecular formula $C_{30}H_{55}O_5N_5$ (six double bond equivalents) as established from the ESI-HRMS information (m/z : 566.4282 $[M+H]^+$, calcd. 566.4276, Δ 1.1058 ppm, Figure 4.3.1.1). MS^2 spectrum (Figure 4.3.1.1) showed three leucine/isoleucine (Leu/Ile) residues and an important fragment ion at m/z 227.1752 $[M+H-3\times C_6H_{11}ON]^+$ from the pseudomolecular ion at m/z 566.43 $[M+H]^+$, which was same with that of cyclo-(L-Leu-L-Leu-L-Leu-L-Leu-L-Ile) (Taontsi *et al.*, 2012). At the beginning of NMR measurement, we used $CDCl_3:CD_3OD$ (1:3) as the NMR solvent. The 1H and ^{13}C NMR data (Figure 4.3.1.2) displayed the similar structural features as that for cyclo-(L-Leu-L-Leu-L-Leu-L-Leu-L-Ile). Five amide carbonyls and five α -methines were clearly observed. In order to finally confirm the structure and considering the importance of NH groups for assigning the amino acids sequence, we measured NMR data of **40** in $DMSO-d_6$ and found five down-field signals corresponding to amide protons (Figure 4.3.1.3 and Table 4.3.1.1). Furthermore, four Leu residues and one Ile were defined based on correlations from amide protons, α -proton, and butyl groups in 1H - 1H COSY and TOCSY spectra (Figure 4.3.1.4). Key HMBC correlations (Figures 4.3.1.5 and 4.3.1.6) of the α -proton and/or NH of one amino acid residue with the carbonyl carbon of the neighboring residue were observed for determining the amino acids sequence, which was also supported by the NOESY correlations (Figure 4.3.1.6). According to the requirement of MS, compound **40** as a peptide, should be cyclic. Finally, a single-crystal X-ray diffraction study allowed the assignment of its relative configuration as shown (Figure 4.3.1.7). The absolute configuration of **40** was also verified on the basis of the Flack parameter $\chi = 0.02$ (7). Interestingly, the

crystal lattice displayed that three monomers were coupled together through several hydrogen bonds, affording a fascinating three-dimensional structure containing a channel inside. The absolute configuration of five amino acid residues was also defined by applying the Marfey's method. The acid hydrolysate of **40** and amino acid standards were derivatized with Marfey's reagent (FDAA). LC-MS analysis (Figure 4.3.1.8) showed that the configuration of one Leucine residue was D while that for others were L. The above analysis finally confirmed this pentapeptide as cyclo-(L-Leu-L-Leu-D-Leu-L-Leu-L-Ile).

Table 4.3.1.1 ^1H and ^{13}C NMR data (in DMSO- d_6) of compound **40**.

Unit	No.	δ_{C} , mult. ^{a,d}	δ_{H} mult. ^b (J in Hz)	Selected HMBC ^b	Selected COSY ^b	NOE
Leu ¹	1	171.3, C _q				
	2	52.2, CH	4.32, m	1, 3	3, Leu ¹ -NH	
	3	40.5, CH ₂	1.44, m ^c	1	2	
			1.54, m ^c	1		
	4	24.8, CH	1.44, m ^c	2, 3, 5, 6		
	5	22.9, CH ₃	0.88, m ^c			
	6	22.7, CH ₃	0.90, m ^c	3, 4, 5		
NH			7.20, d (6.5)	Leu ² -1 (weak)	2	2
Leu ²	1	171.7, C _q				
	2	52.5, CH	4.07, m	1, 3	3, Leu ² -NH	
	3	40.2, CH ₂	1.50, m ^c		2	
			1.59, m ^c	3, 5, 6		
	5	21.0, CH ₃	0.77, d (6.0)	3, 4, 6		
	6	23.4, CH ₃	0.86, m ^c	3		
	NH			8.60, d (8.0)	Leu ³ -1	2
Leu ³	1	172.0, C _q				
	2	52.4, CH	4.15, m	1, 3	3, Leu ³ -NH	Leu ² -NH
	3	39.0, CH ₂	1.37, m ^c	1, 2, 4, 5	2	
			1.49, m ^c	1		
	4	25.1, CH	1.49, m ^c			
	5	22.9, CH ₃	0.83, d (6.5)	3, 4, 6		
	6	22.5, CH ₃	0.88, m ^c	3		
NH			8.73, d (6.0)	Leu ⁴ -1	2	Leu ⁴ -2
Leu ⁴	1	173.1, C _q				
	2	50.6, CH	4.44, m	1, 3, Ile-1	3, Leu ⁴ -NH	
	3	42.1, CH ₂	1.36, m ^c	1, 2, 4	2	
	4	25.0, CH	1.52, m ^c	2, 3		
	5	23.6, CH ₃	0.88, m ^c	3, 4, 6		
	6	22.2, CH ₃	0.88, m ^c	3, 4, 6		
	NH			7.86, d (8.5)	Ile-1 (weak)	2
Ile	1	171.6, C _q				
	2	63.5, CH	3.30, m	1, 3, 4 (weak), 6 (weak)	3, Ile-NH	
	3	33.6, CH	2.30, m		2	

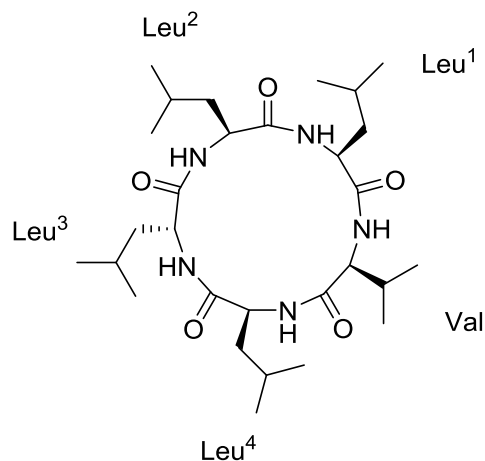
4	25.7, CH ₂	1.03, m 1.41, m ^c	3, 5, 6		
5	10.3, CH ₃	0.79, t (6.5)	3, 4		
6	15.9, CH ₃	0.80, d (6.5)	2, 3, 4		
NH		8.38, br s		2	2, Leu ¹⁻² (weak)

^a Recorded in DMSO-*d*₆ at 125 MHz; ¹³C multiplicities were determined by HSQC experiment. ^b Recorded in DMSO-*d*₆ at 500 MHz. ^c Signals overlapped. ^d Assigned by 2D NMR in DMSO-*d*₆ together with the help of ¹³C NMR spectrum in CD₃OD.

Cyclo-(L-Leu-L-Leu-D-Leu-L-Leu-L-Ile) (40): white powder; $[\alpha]_D^{20}$ -95.8 (*c* 0.12, MeOH); LC-UV [(Acetonitrile (aq) in H₂O/0.1% FA)] λ_{\max} 224 nm; IR (liquid) ν_{\max} 3317, 2956, 1633, 1532, 1021 cm⁻¹; ¹H NMR (DMSO-*d*₆, 500 MHz) and ¹³C NMR (DMSO-*d*₆, 125 MHz), see Table 4.3.1.1; ¹H NMR (CDCl₃:CD₃OD 1:3, 500 MHz) and ¹³C NMR (CDCl₃:CD₃OD 1:3, 125 MHz), see Figure 4.3.1.2. Positive ESIHRMS *m/z*: 566.4282 [M+H]⁺ (calcd for C₃₀H₅₆O₅N₅, 566.4276, Δ 1.1058 ppm).

Crystal data of 40: the colorless crystals were obtained from an CH₂Cl₂:DMSO (1:1, v/v) solution; crystal size 0.060 × 0.108 × 0.153 mm³, triclinic crystal system, space group *P1*, unit cell dimensions *a* = 13.594(4) Å, *b* = 14.583(3) Å, *c* = 15.223(3) Å, Volume 2477.2(10) Å³; *Z* = 3, *T* = 100(2) K, μ (Cu *K* α) = 0.620 mm⁻¹, *D*_{calc} = 1.138 g/cm³; 62098 reflections collected with θ angel ranged from 3.35 to 67.99°; 17320 independent reflections (*R*_{int} = 0.0418). *R*₁ = 0.0461, *wR*₂ = 0.1187 (all data); absolute structure parameter (Flack parameter) 0.02 (7) (Parsons *et al.*, 2013). Crystallographic data of **40** was deposited in the Cambridge Crystallographic Data Centre with a CCDC number. Copies of the data can be acquired, free of charge, from Cambridge Crystallographic Data Centre, 12 Union Road, Cambridge CB2 1EZ, UK by fax: +44(0)1223 336033 or e-mail: deposit@ccdc.cam.ac.uk.

4.3.2 Cyclo-(L-Leu-L-Leu-D-Leu-L-Leu-L-Val) (41, new compound)



The molecular formula of **41** (code: LG53-922), $C_{29}H_{53}O_5N_5$ with six degrees of unsaturation, was established from ESI-HRMS at m/z 552.4124 $[M+H]^+$ (calcd for $C_{29}H_{54}O_5N_5$, 552.4120, Δ 0.8478 ppm, Figure 4.3.2.1). Each five α -protons, α -methine carbons, and amide carbonyls were present in 1H and ^{13}C NMR (in CD_3OD) spectra (Figure 4.3.2.2). The high N content of **41** and its five NH signals ranging from δ_H 7.0 to 9.0 in 1H NMR spectrum (in $DMSO-d_6$) also indicated a pentapeptide (Figure 4.3.2.3 and Table 4.3.2.1). The interpretation of 1H - 1H COSY and TOCSY data revealed the spin systems due to the amine protons (NH), α -protons, and additional high-field signals including methines, methylenes and methyl protons, defining one valine (Val) and four Leu residues (Figures 4.3.2.4 and 4.3.2.6). Moreover, these Val and Leu fragments were clearly observed in HR-CID (collision induced dissociation)- MS^2 experiment of **41** (Figure 4.3.2.1). Based on the requirement of molecular formula, the pentapeptide should also be cyclic.

The amino acids sequence was confirmed by analysis of HMBC and NOESY data of **41** (Figures 4.3.2.5, 4.3.2.6 and 4.3.2.7). Key HMBC correlations of the α -proton and/or NH of one amino acid residue with the carbonyl carbon of the neighboring residue were observed from δ_H 8.59 (Leu^2_{NH}) to 172.1 (Leu^3_{C-1}), from δ_H 8.71 (Leu^3_{NH}) and δ_H 4.17 (Leu^3_{H-2}) to 173.3 (Leu^4_{C-1}), from δ_H 7.86 (Leu^4_{NH}) and δ_H 4.43 (Leu^4_{H-2}) to 171.7 (Val_{C-1}), and from δ_H 8.42 (Val_{NH}) to 171.5 (Leu^1_{C-1}). Cross-peaks of Leu^1_{NH}/Leu^2_{NH} , Leu^2_{NH}/Leu^3_{H-2} , Leu^3_{NH}/Leu^4_{H-2} , Leu^4_{NH}/Val_{H-3} , and Val_{NH}/Leu^1_{H-2} in the NOESY spectrum of **41** finally determined the sequence as cyclo-(Leu^1 - Leu^2 - Leu^3 - Leu^4 -Val). The configuration of five amino acid residues was defined through applying the Marfey's method. The acid hydrolysate of **41** and amino acid standards were derivatized with Marfey's reagent (FDAA). LC-MS analysis showed that the configurations of Val and three Leu residues were L (Figure 4.3.2.8). The remaining Leucine unit was D-configured and located between Leu-2 and Leu-4, which was same as that of compound **40** and supported by the key NOE cross peaks of Leu^1_{NH}/Leu^2_{NH} and Leu^2_{NH}/Leu^3_{H-2} (Figure 4.3.2.7). Finally, the structure of **41** was established as cyclo-(L-Leu-L-Leu-D-Leu-L-Leu-L-Val).

Table 4.3.2.1 ^1H and ^{13}C NMR data (in $\text{DMSO-}d_6$) of compound **41**.

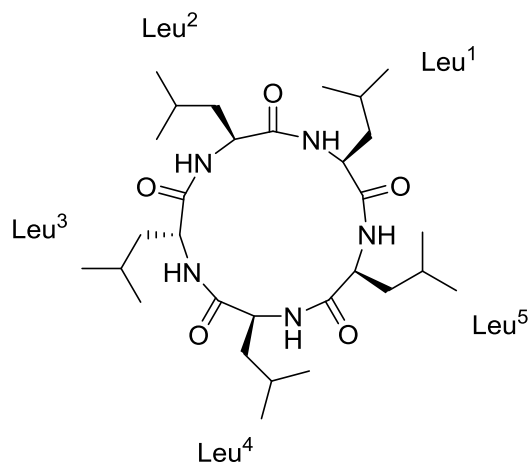
Unit	No.	δ_{C} , mult. ^{a,d}	δ_{H} mult. ^b (J in Hz)	Selected HMBC ^b	Selected COSY ^b	NOE
Leu ¹	1	171.5, C _q				
	2	52.2, CH	4.32, m	1, 3, 4	3, Leu ¹ -NH	NH, Val-NH
	3	40.6, CH ₂	1.44, m ^c	1, 2, 4, 5	2	
			1.55, m ^c	1, 2, 4, 5	2	
	4	25.1, CH	1.44, m ^c	2, 3, 5, 6		
	5	22.6, CH ₃	0.90, m ^c	3, 4, 6		
	6	23.1, CH ₃	0.86, m ^c	3, 5		
NH			7.21, br s		2	2, Leu ² -NH
Leu ²	1	172.0, C _q				
	2	52.6, CH	4.07, m	1, 3, 4	3, Leu ² -NH	
	3	40.4, CH ₂	1.51, m ^c	1, 2, 5	2	
	4	24.8, CH	1.59, m ^c	2, 3, 5, 6		
	5	21.1, CH ₃	0.78, d (6.5)	3, 4, 6		
	6	23.5, CH ₃	0.87, m ^c	3, 5		
	NH			8.59, d (8.0)	Leu ³ -1, 2, 3	2
Leu ³	1	172.1, C _q				
	2	52.5, CH	4.17, m	1, 3, 4, Leu ⁴ -1	3, Leu ³ -NH	Leu ² -NH
	3	39.2, CH ₂	1.37, m ^c	1, 2, 4	2	
			1.48, m ^c			
	4	24.8, CH	1.45, m ^c	2, 3, 5		
	5	22.9, CH ₃	0.83, d (6.0)	3, 4, 6		
	6	22.5, CH ₃	0.88, m ^c	3		
NH			8.71, d (6.5)	Leu ⁴ -1, 2, 3	2	Leu ⁴ -2
Leu ⁴	1	173.3, C _q				
	2	50.7, CH	4.43, m	1, 3, 4, Val-1	3, Leu ⁴ -NH	NH, Leu ³ -NH
	3	42.2, CH ₂	1.37, m ^c	1, 2	2	
	4	25.1, CH	1.51, m ^c	2, 3		
	5	23.3, CH ₃	0.88, m ^c	3, 6		
	6	22.3, CH ₃	0.88, m ^c	3, 5		
	NH			7.86, d (8.5)	Val-1	2
Val	1	171.7, C _q				
	2	65.6, CH	3.20, t (8.5)	1, 3, 4, 5	3, Val-NH	NH
	3	28.2, CH	2.50, m	1 (weak), 2, 4, 5	2, 4, 5	Leu ⁴ -NH
	4	19.8, CH ₃	0.83, d (6.0)	2, 3, 5	3	
	5	20.1, CH ₃	0.83, d (6.0)	2, 3, 4	3	
	NH			8.42, d (5.5)	Leu ¹ -1	2

^a Recorded in $\text{DMSO-}d_6$ at 125 MHz; ^{13}C multiplicities were determined by HSQC experiment. ^b Recorded in $\text{DMSO-}d_6$ at 500 MHz. ^c Signals overlapped. ^d Assigned by 2D NMR in $\text{DMSO-}d_6$ together with the help of ^{13}C NMR spectrum in CD_3OD .

Cyclo-(L-Leu-L-Leu-D-Leu-L-Leu-L-Val) (41): white powder; $[\alpha]_{\text{D}}^{20}$ -87.4 (c 0.43, MeOH); LC-UV [(Acetonitrile (aq) in $\text{H}_2\text{O}/0.1\%$ FA)] λ_{max} 224 nm; IR (liquid) ν_{max} 3306, 2957, 2928, 1634, 1532, 1037 cm^{-1} ; ^1H NMR ($\text{DMSO-}d_6$, 500 MHz) and ^{13}C NMR ($\text{DMSO-}d_6$, 125 MHz), see Table 4.3.2.1; ^1H

NMR (CD₃OD, 600 MHz) and ¹³C NMR (CD₃OD, 150 MHz), see Figure 4.3.2.2. Positive ESIHRMS *m/z*: 552.4124 [M+H]⁺ (calcd for C₂₉H₅₄O₅N₅, 552.4120, Δ 0.8478 ppm).

4.3.3 Cyclo-(L-Leu-L-Leu-D-Leu-L-Leu-L-Leu) (**42**, new compound)



For compound **42** (code: LG53-923) as a white powder, its quasimolecular ion at *m/z* 566.4281 [M+H]⁺ (calcd for C₃₀H₅₆O₅N₅, 566.4276, Δ 0.8903 ppm, Figure 4.3.3.1) in ESI-HRMS spectrum indicated a molecular formula of C₃₀H₅₆O₅N₅, corresponding to the same molecular formula as **40** and one CH₂ group more than **41**. In addition, HR-CID-MS² spectrum (Figure 4.3.3.1) of **42**, which showed the same fragment information as that of **40**, exhibited the presence of five Leu/Ile residues without a Val moiety. ¹H and ¹³C NMR data (in CD₃OD, Figure 4.3.3.2) of **42** revealed similar structural features to those of **40** and **41**. Based on further comparison of NMR data (in DMSO-*d*₆) for **41** and **42**, the significant differences can be observed in the downfield shift of H-2 (Leu⁵, δ_H 3.77 in **42**; Val, δ_H 3.20 in **41**) in ¹H NMR spectrum of **42**, as well as the upfield shift of C-2 (Leu⁵, δ_C 56.3 in **42**; Val, δ_C 65.6 in **41**) and an additional methylene carbon signal (Leu⁵, δ_C 39.0 in **42**) in ¹³C NMR spectrum (in DMSO-*d*₆, Figures 4.3.3.3 and 4.3.3.5, together with Table 4.3.3.1) of **42**. The analysis above supported a pentapeptide made of five Leu/Ile residues. By utilizing the same strategy as **40** and **41**, a combination of COSY, TOCSY, HSQC, HMBC, and NOESY analysis (Figures 4.3.3.4-4.3.3.7) and the Marfey's method (Figure 4.3.3.7) determined the final structure of **42** as Cyclo-(L-Leu-L-Leu-D-Leu-L-Leu-L-Leu).

Table 4.3.3.1 ^1H and ^{13}C NMR data (in $\text{DMSO-}d_6$) of compound **42**.

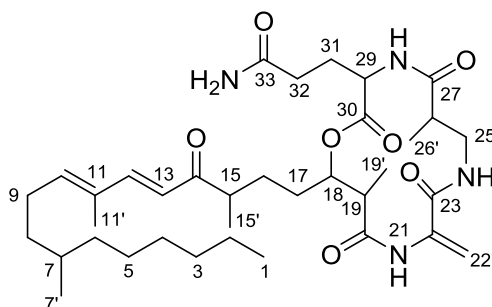
Unit	No.	δ_{C} , mult. ^{a,d}	δ_{H} mult. ^b (J in Hz)	Selected HMBC ^b	Selected COSY ^b	NOE
Leu ¹	1	171.5, C _q				
	2	51.8, CH	4.31, m	1, 3, 4	3, Leu ¹ -NH	Leu ⁵ -NH
	3	40.1, CH ₂	1.54, m ^c	1	2	
	4	25.0, CH	1.47, m ^c	2, 3		
	5	22.4, CH ₃	0.86, m ^c	3		
	6	23.1, CH ₃	0.90, m ^c	3, 4, 5		
	NH			7.27, br s		2
Leu ²	1	172.1, C _q				
	2	52.4, CH	4.10, m	1, 3, 4	3, Leu ² -NH	
	3	40.4, CH ₂	1.50, m ^c	1	2	
	4	24.7, CH	1.60, m ^c	2, 3, 5, 6		
	5	21.1, CH ₃	0.78, d (6.5)	3, 4, 6		
	6	23.6, CH ₃	0.86, m ^c	4, 5		
	NH			8.57, d (8.5)	Leu ³ -1, 2, 3	2
Leu ³	1	172.1, C _q				
	2	52.5, CH	4.16, m	1, 3, 4, Leu ⁴ -1	3, Leu ³ -NH	Leu ² -NH
	3	39.1, CH ₂	1.38, m ^c	1, 2, 4	2	
			1.50, m ^c	2		
	4	24.8, CH	1.46, m ^c	3		
	5	22.9, CH ₃	0.83, d (5.5)	3, 4, 6		
	6	22.5, CH ₃	0.88, m ^c	3		
NH			8.74, d (6.5)	Leu ⁴ -1, 2, 3	2	Leu ⁴ -2
Leu ⁴	1	173.2, C _q				
	2	50.8, CH	4.38, m	1, 3, 4	3, Leu ⁴ -NH	NH, Leu ³ -NH
	3	42.3, CH ₂	1.37, m ^c	1, 2, 4	2	
	4	25.1, CH	1.49, m ^c	2, 3		
	5	23.3, CH ₃	0.88, m ^c	3, 4		
	6	22.5, CH ₃	0.88, m ^c	3, 4		
	NH			7.65, d (8.0)	Leu ⁵ -1	2
Leu ⁵	1	172.8, C _q				
	2	56.3, CH	3.77, m	1, 3, 4 (weak), Leu ¹ -1	3, Leu ⁵ -NH	NH
	3	39.0, CH ₂	1.54, m ^c	2	2	
			1.82, m	1, 2, 4, 5, 6	2	
	4	25.2, CH	1.53, m ^c	3		
	5	22.0, CH ₃	0.83, d (5.5)	3		
	6	23.1, CH ₃	0.88, m ^c	3		
NH			8.21, d (6.0)	Leu ¹ -1	2	2, Leu ¹ -2

^a Recorded in $\text{DMSO-}d_6$ at 125 MHz; ^{13}C multiplicities were determined by HSQC experiment. ^b Recorded in $\text{DMSO-}d_6$ at 500 MHz. ^c Signals overlapped. ^d Assigned by 2D NMR in $\text{DMSO-}d_6$ together with the help of ^{13}C NMR spectrum in CD_3OD .

Cyclo-(L-Leu-L-Leu-D-Leu-L-Leu-L-Leu) (42): white powder; $[\alpha]_{\text{D}}^{20}$ -90.6 (c 0.35, MeOH); LC-UV [(Acetonitrile (aq) in $\text{H}_2\text{O}/0.1\%$ FA)] λ_{max} 224 nm; IR (liquid) ν_{max} 3300, 2930, 2871, 1630, 1540, 1050 cm^{-1} ; ^1H NMR ($\text{DMSO-}d_6$, 500 MHz) and ^{13}C NMR ($\text{DMSO-}d_6$, 125 MHz), see Table 4.3.3.1; ^1H

NMR (CD₃OD, 500 MHz) and ¹³C NMR (CD₃OD, 125 MHz), see Figure 4.3.3.2. Positive ESIHRMS *m/z*: 566.4281 [M+H]⁺ (calcd for C₃₀H₅₆O₅N₅, 566.4276, Δ 0.8903 ppm).

4.3.4 Fusaristatin A (43, known compound)



Compound **43** (code: LG53-121-8) was obtained as an amorphous white powder with a molecular formula C₃₆H₅₈N₄O₇ as revealed through ESI-HRMS (*m/z*: 659.4387 [M+H]⁺, calcd. 659.4378, Δ 1.3559 ppm, Figure 4.3.4.1). SciFinder search indicated that it may be fusaristatin A, which was supported by the possible presence of amino acids glutamine, dehydroalanine, and aminoisbutyric acid from fragment ions at *m/z* 513.3679, 428.3158 and 359.2941 in the ESI-MS² spectrum (Figure 4.3.4.1). Finally, comparison of 1D NMR data (Figure 4.3.4.2 and Table 4.3.4.1) of **43** with that of fusaristatin A confirmed that they are the same compound (Shiono *et al.*, 2007; Chaesung *et al.*, 2010).

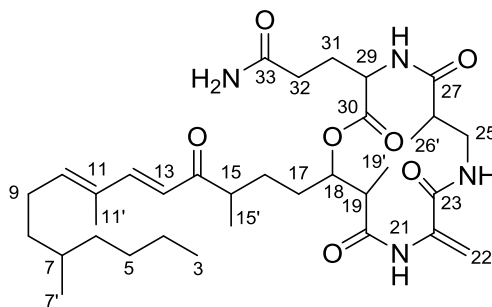
Table 4.3.4.1 ¹H and ¹³C NMR data (in CDCl₃:CD₃OD = 1:3) of compound **43**.

No.	43		Fusaristatin A (in C ₅ D ₅ N) (Shiono <i>et al.</i> , 2007)		Fusaristatin A (in CD ₃ CN) (Chaesung <i>et al.</i> , 2010)	
	δ _C , mult. ^a	δ _H mult. ^b (J in Hz)	δ _C , mult. ^c	δ _H mult. ^d (J in Hz)	δ _C , mult. ^e	δ _H mult. ^f (J in Hz)
1	12.7, CH ₃		14.2, CH ₃	0.85 t (7.0)	14.5, CH ₃	0.88 m
2	21.8, CH ₂		22.9, CH ₂	1.20-1.33	23.5, CH ₂	1.27 m
3	30.7, CH ₂		32.1, CH ₂	1.20-1.33	32.2, CH ₂	2.25 m
4	25.8, CH ₂		27.2, CH ₂	1.20-1.33	27.4, CH ₂	2.25 m
5	28.8, CH ₂		29.9, CH ₂	1.20-1.33	30.4, CH ₂	1.27 m
6	36.1, CH ₂		37.1, CH ₂	1.07-1.11 1.20-1.33	37.6, CH ₂	1.27 m
7	31.8, CH		32.8, CH	1.36-1.44	33.3, CH	1.27 m
7'	18.2, CH ₃		19.7, CH ₃	0.87 d (6.4)	19.9, CH ₃	0.88 m
8	35.4, CH ₂		36.5, CH ₂	1.20-1.33 1.36-1.44	36.9, CH ₂	1.41 m
9	25.7, CH ₂		26.9, CH ₂	2.13-2.22 m	27.3, CH ₂	2.25 m
10	144.0, CH	6.03 t (7.0)	143.9, CH	6.00 t (7.2)	145.0, CH	6.02 t (7.8)

11	132.5, C _q		133.5, C _q		134.2, C _q
11'	10.6, CH ₃	1.82 s	12.2, CH ₃	1.80 s	12.5, CH ₃
12	148.2, CH	7.27 d (15.5)	147.9, CH	7.50 d (15.7)	148.5, CH
13	121.9, CH	6.20 d (15.5)	123.5, CH	6.36 d (15.7)	124.0, CH
14	204.7, C _q		203.3, C _q		204.8, C _q
15	42.9, CH	2.75 m	44.3, CH	2.95-3.04 m	44.6, CH
15'	15.9, CH ₃	1.17 d (7.0)	17.2, CH ₃	1.09 d (6.9)	17.3, CH ₃
16	26.7, CH ₂		28.3, CH ₂	1.49-1.61 m	28.8, CH ₂
17	28.2, CH ₂		30.1, CH ₂	1.88-2.00 m	30.5, CH ₂
18	75.8, CH	5.00 m	77.1, CH	5.36-5.41 m	77.6, CH
19	42.3, CH	2.88 m	44.2, CH	2.80-2.86 m	44.5, CH
19'	13.6, CH ₃	1.20 d (7.5)	15.3, CH ₃	1.28 d (7.1)	15.1, CH ₃
20	173.7, C _q		173.2, C _q		173.3, C _q
22	136.2, C _q		138.9, C _q		138.1, C _q
22'	114.9, CH ₂	5.89 s, 5.38 s 6.18 s	114.1, CH ₂	5.58 s, 6.18 s 6.18 s	115.1, CH ₂
23	164.4, C _q		164.8, C _q		164.7, C _q
25	41.2, CH ₂	3.51 m	42.5, CH ₂	3.70-3.79 m 3.82-3.90 m	42.8, CH ₂
26	40.8, CH	2.61 m	42.3, CH	2.80-2.86 m	42.5, CH
26'	13.1, CH ₃	1.11 d (7.0)	15.0, CH ₃	1.30 d (7.1)	14.6, CH ₃
27	174.4, C _q		174.5, C _q		174.7, C _q
29	51.4, CH	4.47 dd (8.5, 6.0)	53.2, CH	5.05 dd (14.0, 7.6)	53.6, CH
30	170.0, C _q		171.9, C _q		172.3, C _q
31	26.1, CH ₂		27.4, CH ₂	2.54-2.59 m	27.7, CH ₂
32	31.1, CH ₂		32.4, CH ₂	2.66-2.71 m	32.7, CH ₂
33	175.8, C _q		175.4, C _q		175.6, C _q

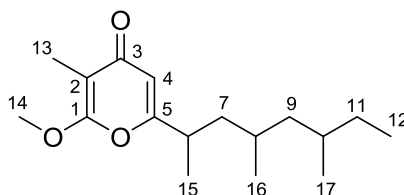
^a Recorded in CDCl₃:CD₃OD (1:3) at 125 MHz; Assignment of many signals might be interchangeable. ^b Recorded in CDCl₃:CD₃OD (1:3) at 500 MHz. ^c Recorded in C₅D₅N at 100 MHz. ^d Recorded in C₅D₅N at 400 MHz. ^e Recorded in CD₃CN at 150 MHz. ^f Recorded in CD₃CN at 600 MHz.

4.3.5 Fusaristatin C (44, new compound)



Compound **44** (code: LG53-121-5) was obtained as an amorphous white powder with a molecular formula $C_{34}H_{54}N_4O_7$ as revealed through ESI-HRMS (m/z : 631.4074 $[M+H]^+$, calcd. 631.4081, Δ 1.3988 ppm, Figure 4.3.5.1). The above MS data indicated compound **44** has a C_2H_4 group less than that for compound **43**. Amino acids glutamine, dehydroalanine, and aminoisbutyric acid was also present from fragment ions at m/z 485.3367, 400.2843, and 331.2628 in the ESI-MS² spectrum (Figure 4.3.5.1). Finally, detailed HMBC correlations (Figures 4.3.5.2 and 4.3.5.3) confirmed its structure as shown. The difference between **43** and **44** was due to the side chain.

4.3.6 Nocapyrone S (**45**, new compound)



Compound **45** (code: LG53-731), was isolated as a white powder, possessed a molecular formula $C_{17}H_{28}O_3$. Its molecular formula was deduced through ESI-HRMS at m/z 281.2107 $[M+H]^+$ (calcd. 281.2111, -1.6302 ppm, Figure 4.3.6.1). Two tertiary methyls (δ_H 1.83, 3.98), three secondary methyls (δ_H 1.21, 0.84, 0.79), and one triplet methyl (δ_H 0.86) were observed in 1H NMR spectrum of **45** (Figure 4.3.6.2 and Table 4.3.6.1). Only one olefinic/aromatic proton (δ_H 6.06) was present in the structure of **45**. The ^{13}C NMR spectrum (Figure 4.3.6.2) exhibited seventeen carbon signals. Interpretation of 1H - ^{13}C spectrum (Figures 4.3.6.3 and 4.3.6.4) revealed the connections from C-6 to C-10, and from C-11 to C-12. Detailed HMBC correlations (Figure 4.3.6.4) from H-4 to C-2, C-3, C-5 and C-6, from H₃-13 to C-1, C-2 and C-3, from H₃-15 to C-5, and from H₃-12 to C-10 allowed the construction of the structure of compound **45**. The methoxy was located at C-1 through a key HMBC correlation of H₃-14/C-1 (Figure 4.3.6.4). Therefore, the structure was confirmed as shown. However, the absolute configuration was still not assigned.

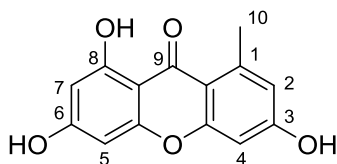
Table 4.3.6.1 ^1H and ^{13}C NMR data (in CDCl_3) of compound **45**.

Position	δ_{C} , mult. ^a	δ_{H} mult. ^b (J in Hz)
1	163.0, C _q	
2	101.1, C _q	
3	181.7, C _q	
4	110.7, CH	6.06 s
5	167.1, C _q	
6	35.6, CH	2.68 m
7	43.0, CH ₂	1.40 m ^c , 1.48 m ^c
8	28.0, CH	1.51 m ^c
9	44.6, CH ₂	1.07 m
10	31.9, CH	1.37 m ^c
11	30.6, CH ₂	1.15 m, 1.26 m ^c
12	11.6, CH ₃	0.86 t (7.5)
13	6.8, CH ₃	1.83 s
14	55.7, CH ₃	3.98 s
15	18.6, CH ₃	1.21 d (7.0)
16	19.7, CH ₃	0.84 d (6.5)
17	19.1, CH ₃	0.79 d (6.5)

^a Recorded in CDCl_3 at 125 MHz; ^{13}C multiplicities were determined by HSQC experiment. ^b Recorded in CDCl_3 at 500 MHz.

Nocapyrone S (45): white powder; $[\alpha]_{\text{D}}^{20}$ -19.0 (c 0.93, MeOH); LC-UV [(Acetonitrile (aq) in $\text{H}_2\text{O}/0.1\%$ FA)] λ_{max} 222 nm; IR (liquid) ν_{max} 2926, 1664, 1628, 1035 cm^{-1} ; ^1H NMR (CDCl_3 , 500 MHz) and ^{13}C NMR (CDCl_3 , 125 MHz), see Table 4.4.6.1; Positive ESIHRMS m/z : 281.2107 $[\text{M}+\text{H}]^+$ (calcd for $\text{C}_{17}\text{H}_{29}\text{O}_3$, 281.2111, Δ -1.6302 ppm).

4.3.7 Norlichexanthone (46, known compound)



Compound **46** (code: LG53-76) was isolated as a yellow powder with a molecular formula $\text{C}_{14}\text{H}_{10}\text{O}_5$ as established by ESI-HRMS information (m/z 259.0597, $[\text{M}+\text{H}]^+$; calcd. 259.0601, Δ -1.4554, Figure 4.3.7.1). Its UV spectrum displayed absorption maxima at 240 and 312 nm. The ^1H NMR spectrum (Figure 4.3.7.2) showed four signals for aromatic protons ranging from δ_{H} 6.0 to 7.0 and one signal for an additional methoxy group at δ_{H} 2.77. With the help of ^{13}C NMR spectrum (Figure 4.3.7.2) and

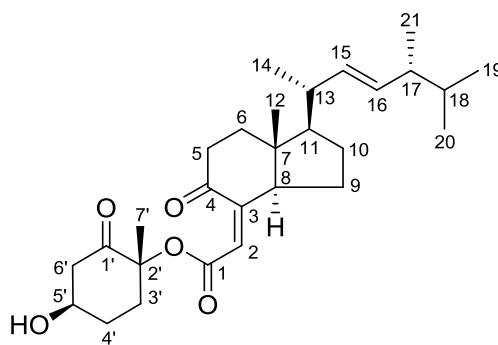
SciFinder search, compound **46** was a known compound named norlichexanthone. The comparison for their 1D NMR data is listed in Table 4.3.7.1.

Table 4.3.7.1 ^1H and ^{13}C NMR data (in CD_3OD) of compound **46**.

Position	Compound 46		Norlichexanthone (Qin <i>et al.</i> , 2014)	
	δ_{C} , mult. ^a	δ_{H} mult. ^b (<i>J</i> in Hz)	δ_{C} , mult. ^a	δ_{H} mult. ^b (<i>J</i> in Hz)
1	144.7, C _q		143.3, C _q	
2	117.0, CH	6.59 s ^c	115.6, CH	6.61 s
3	160.8, C _q		159.3, C _q	
4	101.6, CH	6.59 s ^c	100.1, CH	6.61 s
4a	164.1, C _q		163.4, C _q	
5	94.2, CH	6.22 d (2.0)	92.8, CH	6.21 d (2.0)
5a	166.0, C _q		164.6, C _q	
6	158.6, C _q		157.1, C _q	
7	98.8, CH	6.11 d (2.0)	97.3, CH	6.11 d (2.0)
8	164.8, C _q		163.4, C _q	
8a	104.0, C _q		102.5, C _q	
9	183.5, C _q		182.0, C _q	
10	23.5, CH ₃	2.77 s	22.1, CH ₃	2.77 s

^a Recorded in CD_3OD at 125 MHz. ^b Recorded in CD_3OD at 500 MHz.

4.3.8 Chaxine B (**47**, known compound)



Compound **47** (code: LG53-735), as a white solid, has a molecular formula $\text{C}_{28}\text{H}_{42}\text{O}_5$ as derived from ESI-HRMS information (m/z 459.3111, $[\text{M}+\text{H}]^+$; 481.2927, $[\text{M}+\text{Na}]^+$, Figure 4.3.8.1). Two characteristic fragment ions at m/z 333.2425 $[\text{M}+\text{H}-\text{C}_7\text{H}_{10}\text{O}_2]^+$ and 315.2318 $[\text{M}+\text{H}-\text{C}_7\text{H}_{12}\text{O}_3]^+$ were observed (Figure 4.3.8.1). The above MS pattern was very similar to that for chaxine C isolated from fungus *Diaporthe* sp. LG23 (Figure 4.2.6.1), and indicated that compound **47** was a derivative of chaxine C. The ^1H and ^{13}C NMR spectra (Figure 4.3.8.2) in combination with the HSQC spectrum (Figure 4.3.8.3 and Table 4.3.8.1) established the presence of two tertiary methyls, four secondary

methyls, seven methylenes, six methines (one oxygenated), two quaternary carbons (one oxygenated), four aromatic/olefinic carbons including a *trans*-disubstituted double bonds, together with three carbonyl carbons. These data accounted for all ^1H and ^{13}C NMR resonances. Interpretation of ^1H - ^1H COSY spectrum (Figure 4.3.8.3) determined the connection as highlighted in Figure 4.3.8.4. Key HMBC correlations (Figure 4.3.8.4) from H₃-12 to C-6, C-7, C-8 and C-11, from H₃-19 and H₃-20 to C-17, from H₂-5 to C-3 and C-4, and from H-2 to C-1, C-4 and C-8 indicated the C and D rings attached with a side chain. The above substructure is closely related to that of chaxine C. However, the further HMBC correlations (Figure 4.3.8.4) of H₃-7'/C-1', H₃-7'/C-2', H₃-7'/C-3' and H-6'/C-1 determined a modified cyclohexanone motif. Considering the chemical shifts of C-1 (δ_{C} 165.5), and C-2' (δ_{C} 82.8), as well as the MS requirement, a connection between C-1 and C-2' was proposed for the planar structure of compound **47**, which was also supported by the MS fragment information (Figure 4.3.8.1). Finally, a hydroxyl group was located at C-5' (δ_{C} 70.3). The comparison of NMR data of **47** with that in the literature (Table 4.3.8.1) (Choi *et al.*, 2009) confirmed that compound **47** was chaxine B.

Table 4.3.8.1 ^1H and ^{13}C NMR data (in CDCl_3) of compound **47**.

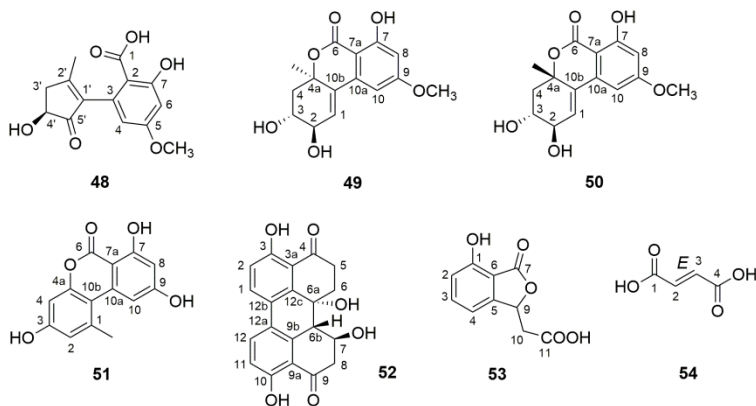
Position	Compound 47		Chaxine B (Choi <i>et al.</i> , 2009)	
	δ_{C} , mult. ^a	δ_{H} mult. ^b (<i>J</i> in Hz)	δ_{C} , mult. ^c	δ_{H} mult. ^d (<i>J</i> in Hz)
1	165.5, qC		165.3, qC	
2	117.6, CH	5.58 d (2.5)	117.4, CH	5.55 d (2.4)
3	156.1, qC		155.9, qC	
4	203.6, qC		203.5, qC	
5 α	38.9, CH ₂	2.51 m	38.4, CH ₂	2.48 m
5 β		2.69 m		2.67 m
6 α	37.9, CH ₂	1.70 m	37.7, CH ₂	1.68 ddd (13.1, 13.1, 5.2)
6 β		2.23 m		2.20 m
7	46.4, qC		46.2, qC	
8	57.7, CH	2.52 m	57.5, CH	2.50 m
9	22.2, CH ₂	1.51 m, 1.60 m	22.0, CH ₂	1.47 m, 1.59 m
10	29.1, CH ₂	1.48 m, 1.91 m	28.9, CH ₂	1.47 m, 1.89 m
11	55.6, CH	1.44 m	55.4, CH	1.40 m
12	12.3, CH ₃	0.88 s	12.1, CH ₃	0.86 s
13	40.3, CH	2.08 m	40.1, CH	2.07 m
14	21.2, CH ₃	1.04 d (6.5)	21.0, CH ₃	1.01 d (6.7)
15	134.7, CH	5.16 dd (15.0, 7.5)	134.5, CH	5.13 dd (15.3, 8.5)
16	133.2, CH	5.27 dd (15.0, 8.5)	133.0, CH	5.25 dd (15.3, 7.9)

17	43.0, CH	1.87 m	42.8, CH	1.84 m
18	33.2, CH	1.48 m	33.0, CH	1.46 m
19	20.1, CH ₃	0.84 d (6.5)	19.9, CH ₃	0.82 d (7.0)
20	19.8, CH ₃	0.83 d (7.0)	19.6, CH ₃	0.80 d (7.0)
21	17.8, CH ₃	0.92 d (7.0)	17.6, CH ₃	0.90 d (7.0)
1'	204.7, qC		204.5, qC	
2'	82.8, qC		82.6, qC	
3'	33.4, CH ₂	1.55 m, 2.35 m	33.2, CH ₂	1.53 m, 2.32 m
4'	29.8, CH ₂	1.94 m	29.6, CH ₂	1.90 m, 1.95 m
5'	70.3, CH	3.95 m	70.1, CH	3.93 m
6'	47.9, CH ₂	2.68 m, 2.88 (dd 13.0, 9.0)	47.7, CH ₂	2.67 m, 2.86 (dd 13.1, 8.9)
7'	20.5, CH ₃	1.45 s	20.3, CH ₃	1.43 s

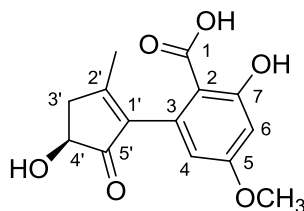
^a Recorded in CDCl₃ at 125 MHz. ^b Recorded in CDCl₃ at 500 MHz. ^c Recorded in CDCl₃ at 125 MHz. ^d Recorded in CDCl₃ at 500 MHz. ^e overlapped.

4.4 Secondary metabolites isolated from *Alternaria* sp. LG19

Four well-known *Alternaria* mycotoxins including altenuene (**49**), isoaltenuene (**50**), alternariol (**51**) and altertoxin I (**52**), and their derivative (**48**), as well as two known compounds (**53** and **54**) were isolated from the rice culture of an endophytic fungus *Alternaria* sp. LG19, occurring in the leaves of *L. japonica* collected from Jinan, Shandong, P. R. China.



4.4.1 Alternarienic acid (**48**, known compound)



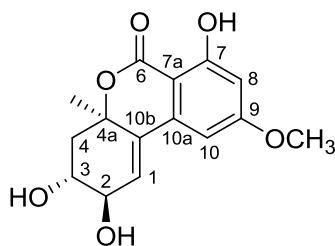
Compound **48** (code: LG19-4211) was isolated as a white solid with a molecular formula $C_{14}H_{14}O_6$ as determined by ESI-HRMS with a pseudomolecular ion $[M+H]^+$ at m/z 279.0864 (calcd. 279.0863, Δ 0.1795 ppm, Figure 4.4.1.1). The 1H NMR spectrum (Figure 4.4.1.2) displayed signals for two methyls (one oxygenated), a methylene, an oxygenated methine, together with two aromatic/olefinic protons. Interpretation of 1H - 1H COSY spectrum (Figure 4.4.1.3) revealed correlations between C-3' and C-4'. A tetra-substituted benzene ring was constructed based on HMBC correlations from H-6 to C-2, C-4, C-5, and C-7, from H-4 to C-2 and C-6 (Figure 4.4.1.4). Meanwhile, a methoxy and a hydroxyl group were located at C-5 and C-7 respectively, through the analysis of chemical shifts at C-5 (δ_C 165.5) and C-7 (δ_C 166.7), and HMBC correlation from 5-OCH₃ to C-5. Further interpretation of the HMBC spectrum suggested key correlations of Me-2'/C-1', Me-2'/C-2', Me-2'/C-3', and H-3'/C-5', indicating a cyclopentenone substructure with a methyl and a hydroxy group located at C-2' and C-4' respectively. A key HMBC correlation (Figure 4.4.1.4) between H-4 and C-1' was used to link benzene ring and cyclopentenone. Based on the MS requirement of **48** and chemical shift values at C-1 (δ_C 173.4) and C-2 (δ_C 106.3), a carboxyl group was attached to C-2. Finally, a comparison of NMR data with that for alternarienic acid in the literature (Aly *et al.*, 2008) confirmed that they share the same planar structure (Table 4.4.1.1). However, it has to be noted that the ^{13}C NMR spectrum of **48** showed some doublet signals, indicating compound **48** may be the mixture of two isomers as shown in Figure 4.4.1.5. ECD calculation at B3LYP/6-31G(d)//B3LYP/6-31G(d) level using the GAMESS and DALTON program packages, was applied to assign the absolute configuration of **48**. The CD values of five conformers were calculated and weighted according to their Boltzmann factors. Figure 4.4.1.6 shows that the calculated ECD curve is consistent with experimental one.

Table 4.4.1.1 ^1H and ^{13}C NMR data (in CD_3OD) of compound **48**.

Position	Compound 48		Alternarienonic acid (Aly <i>et al.</i> , 2008)	
	δ_{C} , mult. ^a	δ_{H} mult. ^b (<i>J</i> in Hz)	δ_{C} , mult. ^c	δ_{H} mult. ^d (<i>J</i> in Hz)
1	173.4, ^e C _q		164.3, C _q	
2	106.3, ^e C _q		109.9, C _q	
3	137.5, C _q		137.3, C _q	
4	111.5, CH	6.16 br s	110.2, CH	6.07 d (2.5)
5	165.5, C _q		164.3, C _q	
6	101.6, CH	6.48 d (2.0)	101.4, CH	6.40 d (2.5)
7	166.7, C _q		166.0, C _q	
1'	141.9, C _q		142.5, C _q	
2'	167.1, C _q		165.2, C _q	
3'	41.8, CH ₂	3.03 dd (7.6, 18.0) 2.50 br d (18.0)	41.8, CH ₂	3.00 dd (6.9, 17.3) 2.49 br d (17.0)
4'	73.1, CH	4.31 dd (3.2, 6.4)	73.2, CH	4.38 dd (2.8, 6.3)
5'	208.6, C _q		209.0, C _q	
2'-CH ₃	17.8, CH ₃	2.03 s	17.8, CH ₃	1.99 s
5-OCH ₃	56.0, CH ₃	3.82 s	55.8, CH ₃	3.78 s

^a Recorded in CD_3OD at 100 MHz. ^b Recorded in CD_3OD at 400 MHz. ^c Recorded in CD_3OD at 125 MHz. ^d Recorded in CD_3OD at 500 MHz. ^e Corrected values compared to that in literature.

4.4.2 (-)-(2*R*,3*R*,4*aR*)-Altenuene (**49**, known compound)



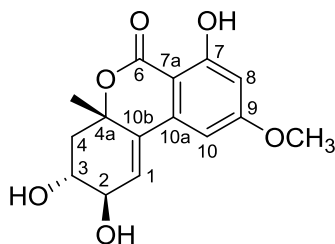
ESI-HRMS of **49** (code: LG19-4212) showed the pseudomolecular ion $[\text{M}+\text{H}]^+$ at m/z 293.1020 (calcd. 293.1020, Δ 0.1895 ppm, Figure 4.4.2.1), confirming its molecular formula as $\text{C}_{15}\text{H}_{16}\text{O}_6$. 1D NMR data (Figure 4.4.2.2) with the help of HSQC spectrum (Figure 4.4.2.3) indicated the presence of two methyls (one oxygenated), a methylene, two oxygenated methines, a quaternary carbon, three aromatic/olefinic methine carbons, and six aromatic/olefinic/carbonyl carbon signals. The observed correlations in ^1H - ^1H COSY spectrum allowed the connection from C-1 to C-4 (Figure 4.4.2.4). In the HMBC spectrum (Figure 4.4.2.4), a methyl at C-4a was found to correlate to C-4, C-4a, and C-10b. Similarly, the proton

signal at δ_{H} 6.23 exhibited correlation with C-4a, which allowed the assignment for a six-membered ring. A further benzene ring was confirmed to be present on the basis of HMBC correlations from H-8 to C-7, C-7a, C-9 and C-10, and from H-10 to C-7a and C-8 (Figure 4.4.2.4). Two rings were connected through a C-10a/C-10b bond from the analysis of key HMBC correlations from H-1 to C-10a, and from H-10 to C-10b. Three hydroxyl groups and a methoxy were proposed and located at C-2, C-3, C-7 and C-9, respectively due to their corresponding chemical shifts and the HMBC correlation of 9-OCH₃/C-9. Finally, a six-member lactone ring was placed in the middle of the ring system of **49**, which was supported by the HMBC correlations from H-8 and H-10 to C-6, and the chemical shifts of C-6 (δ_{C} 170.4) and C-4a (δ_{C} 82.5), as well as the MS requirement. Accordingly, compound **49** was identified to have the same planar structure as altenuene, and they also have similar 1D NMR data (He *et al.*, 2012) (Table 4.4.2.1). The sign of optical rotation and the CD curve of **49** were identical to that for (-)-(2*R*,3*R*,4*aR*)-altenuene (Altemöller *et al.*, 2006) (Figure 4.4.2.5).

Table 4.4.2.1 ¹H and ¹³C NMR data (in CD₃OD) of compound **49**.

Position	Compound 49		Altenuene (He <i>et al.</i> , 2012)	
	δ_{C} , mult. ^a	δ_{H} mult. ^b (<i>J</i> in Hz)	δ_{C} , mult. ^c	δ_{H} mult. ^d (<i>J</i> in Hz)
1	131.4, CH	6.23 d (2.8)	131.0, CH	6.30 d (3.3)
2	72.3, CH	4.08 dd (5.6, 2.8)	69.5, CH	3.95 m
3	70.7, CH	3.78 m	68.7, CH	3.70 dddd (8.0, 7.4, 3.8, 3.5)
4	40.8, CH ₂	2.41 dd (14.4, 3.6) 2.00 dd (14.4, 5.2)	38.6, CH ₂	2.26 dd (14.0, 3.5) 1.95 dd (14.0, 7.4)
4a	82.5, C _q		81.2, C _q	
6	170.4, C _q		168.2, C _q	
7	165.2, C _q		163.0, C _q	
7a	101.6, C _q		100.0, C _q	
8	101.8, CH	6.48 d (2.4)	100.9, CH	6.50 d (2.3)
9	168.0, C _q		165.8, C _q	
10	103.7, CH	6.67 d (2.4)	102.3, CH	6.74 d (2.3)
10a	140.8, C _q		139.2, C _q	
10b	134.8, C _q		131.8, C _q	
4a-CH ₃	28.0, CH ₃	1.51 s	27.4, CH ₃	1.47 s
9-OCH ₃	56.3, CH ₃	3.88 s	55.8, CH ₃	3.86 s

^a Recorded in CD₃OD at 100 MHz. ^b Recorded in CD₃OD at 400 MHz. ^c Recorded in DMSO-*d*₆ at 100 MHz. ^d Recorded in DMSO-*d*₆ at 400 MHz.

4.4.3 Isoaltenuene (**50**, known compound)

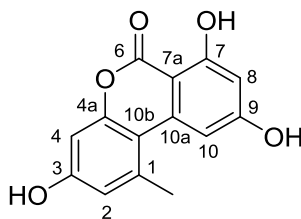
By the same strategy as above, compound **50** (code: LG19-4213) has the same molecular formula $C_{15}H_{16}O_6$ as that for **49** (Figure 4.4.3.1). Its 1H NMR spectrum (Figure 4.4.3.2) was close to that of **49** except for small differences observed for the chemical shifts and coupling constants from H-1 to H₂-4. The above analysis indicated that compounds **49** and **50** shared the same planar structure but had different relative configurations. 1D NOESY technique (Figures 4.4.3.2 and 4.4.3.3) was applied to assign the relative configuration of **50** as shown based on the 1D NOESY correlations of CH_3 -4a/H-3, CH_3 -4a/H-4 β , and H-2/H-4 α (Figure 4.4.3.4), together with their coupling constants (Table 4.4.3.1). Hence, **50** was established as a known compound isoaltenuene (Altemöller *et al.*, 2006).

Table 4.4.3.1 1H NMR data (in CD_3OD) of compound **50**.

Position	Compound 50	Isoaltenuene (Altemöller <i>et al.</i> , 2006)	Compound 49
	δ_H mult. ^a (J in Hz)	δ_H mult. ^b (J in Hz)	δ_H mult. ^c (J in Hz)
1	6.19 d (2.4)	6.12 d (2.4)	6.23 d (2.8)
2	4.22 dd (7.8, 2.4)	4.39 dd (8.0, 2.4)	4.08 dd (5.6, 2.8)
3	3.75 ddd (12.0, 8.4, 3.6)	3.79-3.90 m	3.78 m
4	β , 2.27 dd (12.0, 3.6) α , 2.17 t (12.0)	β , 2.37 dd (12.5, 3.8) α , 2.31 dd (12.5, 6.7)	2.41 dd (14.4, 3.6) 2.00 dd (14.4, 5.2)
8	6.49 d (2.4)	6.46 d (2.3)	6.48 d (2.4)
10	6.66 d (2.4)	6.56 d (2.3)	6.67 d (2.4)
4a- CH_3	1.56 d (0.6)	1.62 d (0.7)	1.51 s
9-O CH_3	3.87 s	3.79-3.90 m	3.88 s

^a Recorded in CD_3OD at 600 MHz. ^b Recorded in $CDCl_3$ at 500 MHz. ^c Recorded in CD_3OD at 400 MHz.

4.4.4 Alternariol (51, known compound)



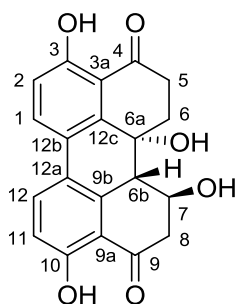
The molecular formula $C_{14}H_{10}O_5$ was assigned to compound **51** (code: LG19-35) through the analysis of ESI-HRMS information (m/z 259.0600, $[M+H]^+$; calcd. 259.0601, Δ -0.2774, Figure 4.4.4.1). The 1H NMR spectrum (Figure 4.4.4.2) displayed five signals including four aromatic protons and a methyl at δ_H 2.66. It showed UV maximum absorption at 258, 288, 300 and 340 nm. The above analyses were in accordance with the data for alternariol (Nielsen *et al.*, 2011; Gu, 2009) (Table 4.4.4.1).

Table 4.4.4.1 1H NMR data (in DMSO- d_6) of compound **51**.

Position	Compound 51	Alternariol (Gu, 2009) In DMSO- d_6	Alternariol (Aly <i>et al.</i> , 2008) In CD $_3$ OD	Alternariol (Tan <i>et al.</i> , 2008) In acetone- d_6
	δ_H mult. ^a (J in Hz)	δ_H mult. ^b (J in Hz)	δ_H mult. ^c (J in Hz)	δ_H mult. ^d (J in Hz)
2	6.61 m	6.62 d (2.5)	6.65 d (2.5)	6.78 d (2.4) ^e
4	6.69 m	6.70 d (2.4)	6.55 d (2.5)	6.69 d (2.4) ^e
8	6.35 m	6.36 d (1.5)	6.32 d (2.0)	6.44 d (2.1)
10	7.19 m	7.23 d (1.5)	7.20 d (2.0)	7.33 d (2.1)
1-CH $_3$	2.66 d (4.5)	2.69 s	2.71 s	2.77 s

^a Recorded in DMSO- d_6 at 500 MHz. ^b Recorded in DMSO- d_6 at 300 MHz. ^c Recorded in CD $_3$ OD at 500 MHz. ^d Recorded in acetone- d_6 at 300 MHz. ^e Maybe interchangeable.

4.4.5 Alvertoxin I (52, known compound)

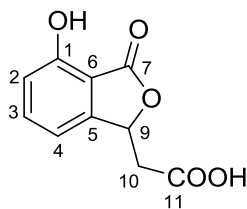


Compound **52** (code: LG19-53), a pigment, has a molecular formula $C_{20}H_{16}O_6$ as established by a pseudomolecular ion at m/z 353.1017 $[M+H]^+$ (calcd. 353.1020, Δ -0.7934) in ESI-HRMS spectrum (Figure 4.4.5.1). The 1H NMR spectrum (Figure 4.4.5.2) exhibited the signals for two pairs of aromatic ortho hydrogens, an oxygenated methine, and seven saturated protons. The ^{13}C NMR spectrum (Figure 4.4.5.2) showed twenty carbon signals including two carbonyl groups and two oxygenated aromatic carbons. Interpretation of 1H - 1H COSY spectrum (Figure 4.4.5.3) of **52** revealed correlations from C-1 to C-2, from C-5 to C-6, from C-6b to C-8, and from C-11 to C-12. The above analysis indicated compound **52** was alvertoxin I, which was often found in the fungus *Alternaria* spp. And its 1D NMR data are consistent with that for alvertoxin I (Table 4.4.5.1) (Stack *et al.*, 1986).

Table 4.4.5.1 1H NMR data (in DMSO- d_6) of compound **52**.

Position	Compound 52		Alvertoxin I (Stack <i>et al.</i> , 1986)	
	δ_C , mult. ^a	δ_H mult. ^b (J in Hz)	δ_C , mult. ^c	δ_H mult. ^d (J in Hz)
1	132.8, CH	8.03 d (8.5)	132.9, CH	8.1 d
2	118.2, CH	7.03 d (8.5)	117.8, CH	7.1 d
3	160.9, C _q		161.0, C _q	
3a	114.0, C _q		113.8, C _q	
4	206.2, C _q		206.0, C _q	
5	33.8, CH ₂	2.57 br d (17.5), Ca. 3.0 m ^e	33.5, CH ₂	2.59 dt, Ca. 3.0 m
6	34.9, CH ₂	2.29 dt (14.5, 3.0), Ca. 3.0 m ^e	34.8, CH ₂	2.30 dt, Ca. 3.0 m
6a	68.2, C _q		68.0, C _q	
6b	51.6, CH	2.90 m ^e	51.4, CH	2.86 m
7	64.8, CH	4.51 m	64.7, CH	4.50 d
8	47.6, CH ₂	Ca. 3.0 m ^e 2.86 dd (15.5, 4.0)	47.5, CH ₂	Ca. 3.0 m 2.86 m
9	204.3, C _q		204.2, C _q	
9a	116.8, C _q		116.5, C _q	
9b	140.9, C _q		140.7, C _q	
10	160.4, C _q		160.4, C _q	
11	115.9, CH	6.94 d (8.5)	115.5, CH	6.9 d
12	132.2, CH	8.00 d (8.5)	132.5, CH	8.0 d
12a	125.2, C _q		124.8, C _q	
12b	123.9, C _q		123.5, C _q	
12c	138.5, C _q		138.4, C _q	

^a Recorded in DMSO- d_6 at 125 MHz. ^b Recorded in DMSO- d_6 at 500 MHz. ^c Recorded in DMSO- d_6 at 75 MHz. ^d Recorded in DMSO- d_6 at 300 MHz. ^e Signals overlapped.

4.4.6 Isochracinic acid (**53**, known compound)

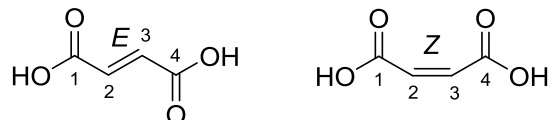
The molecular formula of compound **53** (code: LG19-522) was confirmed by ESI-HRMS (m/z 209.0443 $[M+H]^+$; calcd. 209.0444, Δ -0.5888 ppm, Figure 4.4.6.1). Three proton signals (6.95, d, $J = 7.8$; 7.60, t, $J = 8.4$, 7.15, d, $J = 7.8$) in ^1H NMR spectrum indicated a trisubstituted benzene ring (Figure 4.4.6.2). Detailed HMBC correlations from H-2 to C-4 and C-6, from H-3 to C-1 and C-5, and from H-4 to C-2 and C-6 supported above analysis. HMBC correlations (Figure 4.4.6.3) observed from H-9 to C-5 and C-6 supported above analysis. HMBC correlations (Figure 4.4.6.3) observed from H-9 to C-5 and C-11, and from H₂-10 to C-5, C-9 and C-11 allowed the connection of C-5/C-9/C-10/C-11 or C-5/C-10/C-9/C-11. The HMBC correlation of H-2/C-7, and the chemical shifts (Table 4.4.6.1) of C-7 (δ_{C} 169.6) and C-9 (δ_{C} 77.7) enabled us to confirm a five- or six-membered lactone ring fusing to the benzene ring. The last hydroxyl group was attached to C-1 based on its chemical shift (δ_{C} 156.7), which was in accordance with the MS requirement. Finally, compound **53** was identified as a known compound, isochracinic acid with a five-membered lactone ring (Fan *et al.*, 2012).

Table 4.4.6.1 ^1H and ^{13}C NMR data (in acetone- d_6) of compound **53**.

Position	Compound 53		Isochracinic acid (Fan <i>et al.</i> , 2012)	
	δ_{C} , mult. ^a	δ_{H} mult. ^b (J in Hz)	δ_{C} , mult. ^c	δ_{H} mult. ^d (J in Hz)
1	156.7, C _q		156.4, C _q	
2	115.9, CH	6.95 d (7.8)	115.8, CH	6.93 d (8.2)
3	136.9, CH	7.60 t (8.4)	136.5, CH	7.58 t (7.8)
4	113.7, CH	7.15 d (7.8)	113.4, CH	7.12 d (7.5)
5	151.0, C _q		150.6, C _q	
6	111.7, C _q		111.5, C _q	
7	169.6, C _q		169.5, C _q	
8	-		-	
9	77.7, CH	5.86 dd (7.8, 4.8)	77.5, CH	5.84 dd (7.9, 4.8)
10	38.8, CH ₂	3.10 ddd (16.8, 4.8, 1.2) 2.86 ddd (16.8, 7.8, 0.6)	38.7, CH ₂	3.07 dd (16.8, 4.9) 2.83 dd (16.8, 7.9)
11	170.4, C _q		170.2, C _q	

^a Assigned based on data from the HSQC and HMBC spectra at 600 MHz. ^b Recorded in acetone- d_6 at 600 MHz. ^c Recorded in acetone- d_6 at 100 MHz. ^d Recorded in acetone- d_6 at 400 MHz.

4.4.7 (2E)-Fumaric acid (**54**, known compound)



Compound **54** (code: LG19-32) was confirmed as a known compound (2E)-fumaric acid based on the comparison of its 1D NMR data (Figure 4.4.7.1) with that reported in the literature (Table 4.4.7.1).

Table 4.4.7.1 ^1H and ^{13}C NMR data (in CD_3OD) of compound **54**.

Position	Compound 54		(2E)-Fumaric acid		(2Z)-Fumaric acid	
	δ_{C} , mult. ^a	δ_{H} mult. ^b (J in Hz)	δ_{C} , mult. ^c	δ_{H} mult. ^d (J in Hz)	δ_{C} , mult. ^e	δ_{H} mult. ^f (J in Hz)
1,4	168.1, C _q		Ca. 168.0, C _q		Ca. 167.0, C _q	
2,3	135.2, CH	6.76 s	Ca. 135.0, CH	Ca. 6.75 s	Ca. 130.0, CH	Ca. 6.25 s

^a Recorded in CD_3OD at 125 MHz. ^b Recorded in CD_3OD at 500 MHz. ^c Recorded in CD_3OD at 100 MHz obtained from Advanced Chemistry Development Inc. ^d Recorded in CD_3OD at 400 MHz obtained from Advanced Chemistry Development Inc. ^e Recorded in $\text{DMSO}-d_6$ at 75 MHz obtained from Advanced Chemistry Development Inc. ^f Recorded in $\text{DMSO}-d_6$ at 300 MHz obtained from Advanced Chemistry Development Inc.

4.5 Structural character and proposed biosynthetic pathways

4.5.1 Decalin-containing compounds (1–6)

Natural products containing a ‘decalin’ motif occur frequently in microorganisms and show diverse biological activities, including antimicrobial and anticancer activities (Li *et al.*, 2014a). Compounds **1–6** are polyketide decalin-derived secondary metabolites with a double bond between C-3 and C-4. A enzymatic or non-enzymatic intramolecular Diels-Alder (IMDA) cycloaddition could be responsible for the formation of decalin motif (Figure 4.5.1.1) (Li *et al.*, 2014a). The unusual incorporation of an urea or aniline substructure into **2** might be a key biosynthetic step for the occurrence of new compounds **4–6** (Ding *et al.*, 2008).

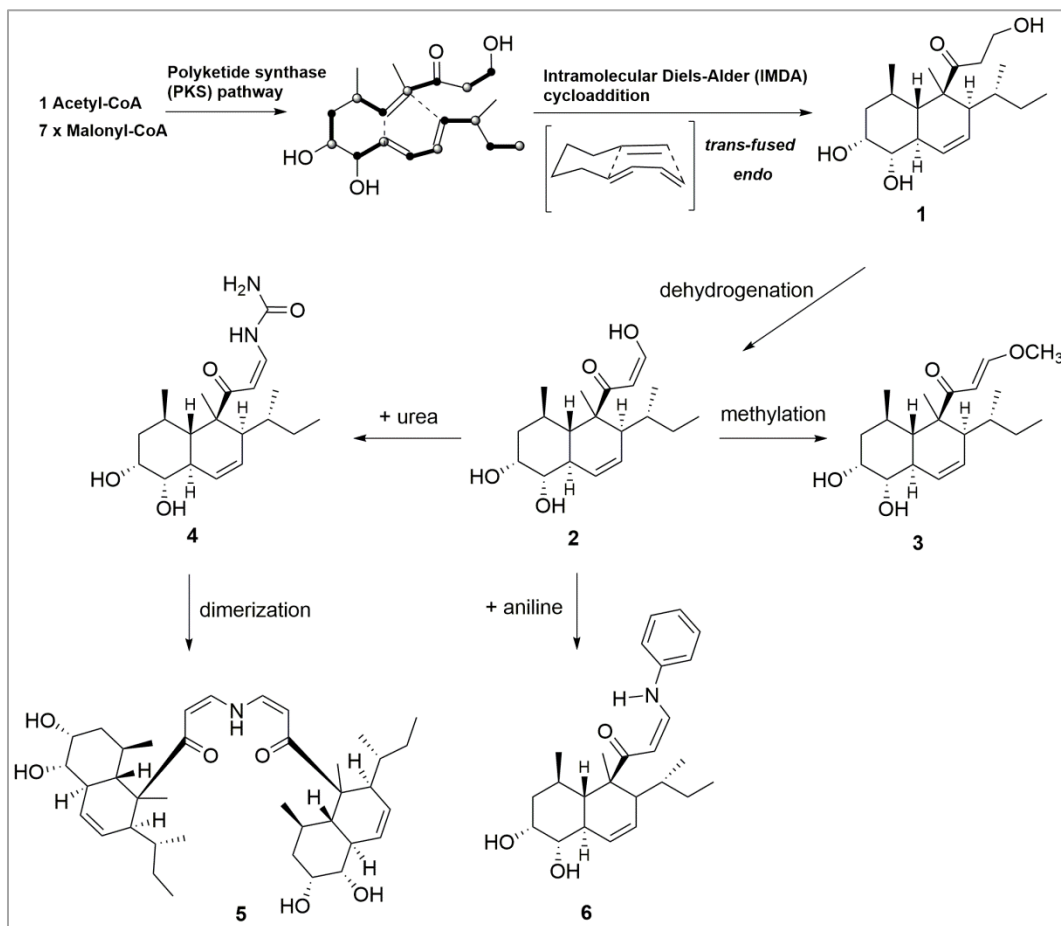


Figure 4.5.1.1 Plausible biosynthetic pathway of compounds 1–6 (Li *et al.*, 2014a; Ding *et al.*, 2008).

4.5.2 Sirenin derivatives (7 and 8)

Sirenin acts as a fungal sexual pheromone as a low concentration (Nutting *et al.*, 1968). It belongs to the class of sesquiterpenes (Nutting *et al.*, 1968). Obviously, compounds 7 and 8 are the derivatives of sirenin (Figure 4.5.2.1). Three isoprenoid units were condensed into farnesyl pyrophosphate, followed by the cyclization and consequent oxidation to afford sirenin, as well as compounds 7 and 8. However, it is also possible that the new compound 8 was formed through the condensation, cyclization and oxidation of two isoprenoid building blocks, and is a monoterpene.

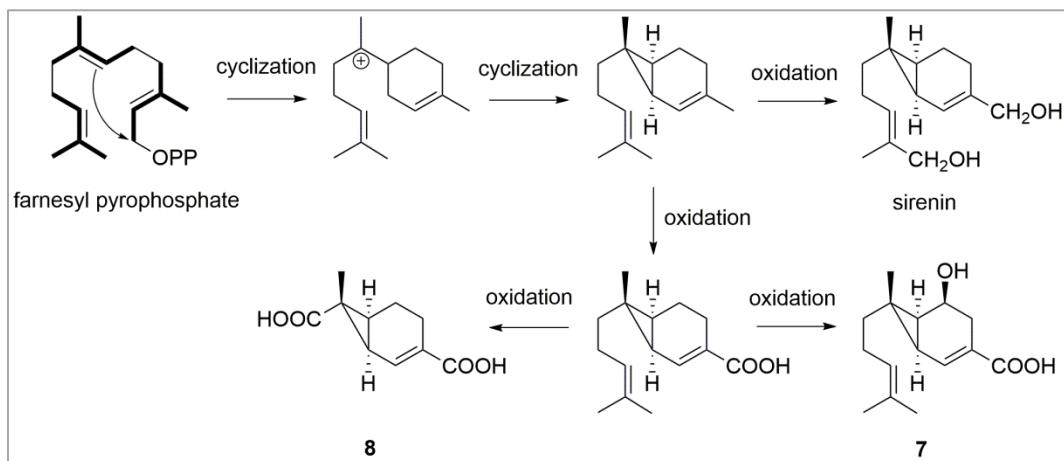


Figure 4.5.2.1 Plausible biosynthetic pathway of sirenin derivatives **7** and **8** (Nutting *et al.*, 1968).

4.5.3 Pigments (9–11)

Natural products that have a naphthopyranone (1*H*-naphtho[2,3-*c*]pyran-1-one) core structure are widely found in fungi and bacteria (Donner, 2015). The class belongs to the family of polyketide and exhibited a diverse range of identified bio-activities, such as antimicrobial, cytotoxic and antioxidant activities (Donner, 2015). Generally, they are biosynthesized from acyl CoA precursors through polyketide synthases (PKSs). There are three types of bacterial PKSs are well-known to date (Shen, 2003). PKSs as the multienzyme complexes with a single set of iteratively acting activities, should be responsible for the biosynthesis of **9–11** (polycyclic and aromatic polyketides) (Shen, 2003). As shown in figure 4.5.3.1, seven building blocks (acetyl-CoA and malonyl-CoA) formed core structures 3-alkyl naphthopyranone and 6,9-naphthoquinone. Further methylation followed by oxidative coupling (dimerization) afforded compounds **9** and **10** (Bode *et al.*, 2007). Viridicatumtoxin (**11**) is a rare fungal compound that is similar to the bacterial tetracycline antibiotics (Chooi, *et al.*, 2010). It is a polyketide-isoprenoid hybrid product with a polyketide-derived tetracyclic scaffold and a spirobicyclic ring of geranyl origin (Chooi, *et al.*, 2012). A key prenyl transferase VrtC was proved to be involved in alkylation of the tetracyclic intermediate (Figure 4.5.3.2) (Chooi, *et al.*, 2012). Further cyclization yielded the product **11**.

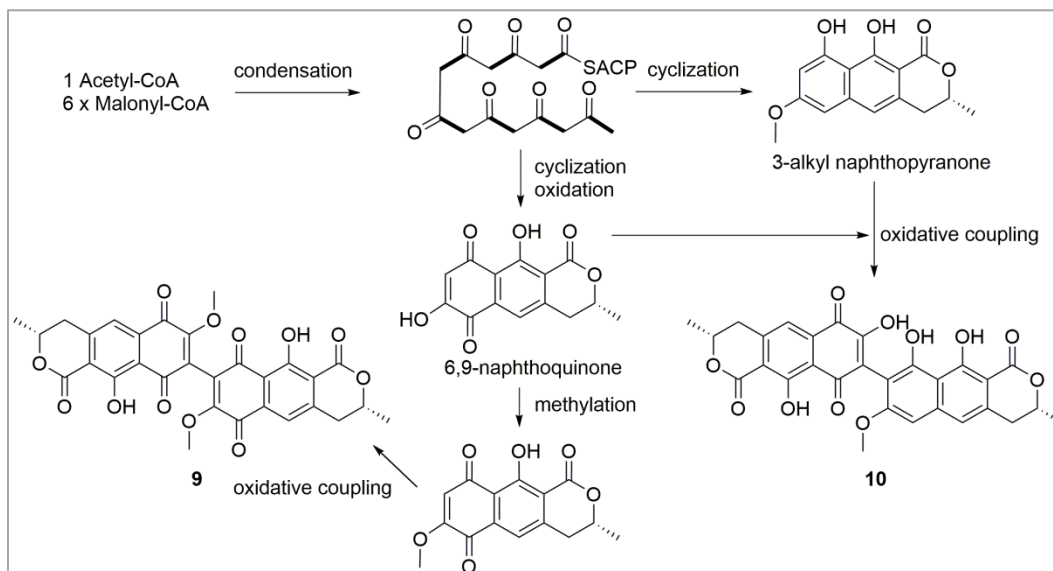


Figure 4.5.3.1 Plausible biosynthetic pathway of **9** and **10** (Bode *et al.*, 2007; Donner, 2015).

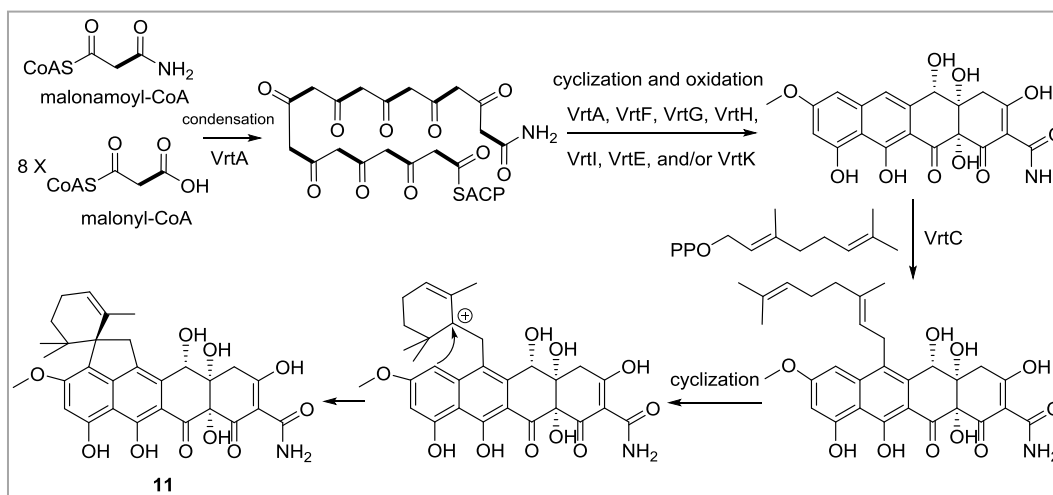


Figure 4.5.3.2 Plausible biosynthetic pathway of **11** (Chooi, *et al.*, 2010; Chooi, *et al.*, 2012).

4.5.4 Paraconic acids (**12**, **14**, **16**, and **19**) and alkylitaconic acids (**21–23**)

Paraconic acids, as naturally occurring trisubstituted γ -butyrolactones (Seitz and Reiser, 2005), have attracted considerable attention from organic and medicinal chemists owing to their interesting structural and biological properties (Amador *et al.*, 2006). The γ -butyrolactone scaffold is generally substituted with a methyl or methylene group at α -position, a carboxyl group at β -position, and an alkyl chain at γ -position. The alkyl chain of various lengths as well as the stereochemical relationship between these

substituents contribute to the significant structural differences (Amador *et al.*, 2006). Biosynthetically, paraconic acids (for example, compound **19**) might be assigned as cyclic products of corresponding alkylitaconic acids (Stewart *et al.*, 2005) (Figure 4.5.4.1). For the backbone construction of bioactive alkylitaconic acids **21** or **22**, it may include two steps (Figure 4.5.4.1) (Fujii *et al.*, 2015). Firstly, fatty acid synthase or highly reducing iterative polyketide synthase (HR-PKS) might be involved in the formation of C8 fatty acyl chain. Furthermore, an oxaloacetic acid was proposed to be incorporated into the above fatty acyl chain by the citrate synthase homologue.

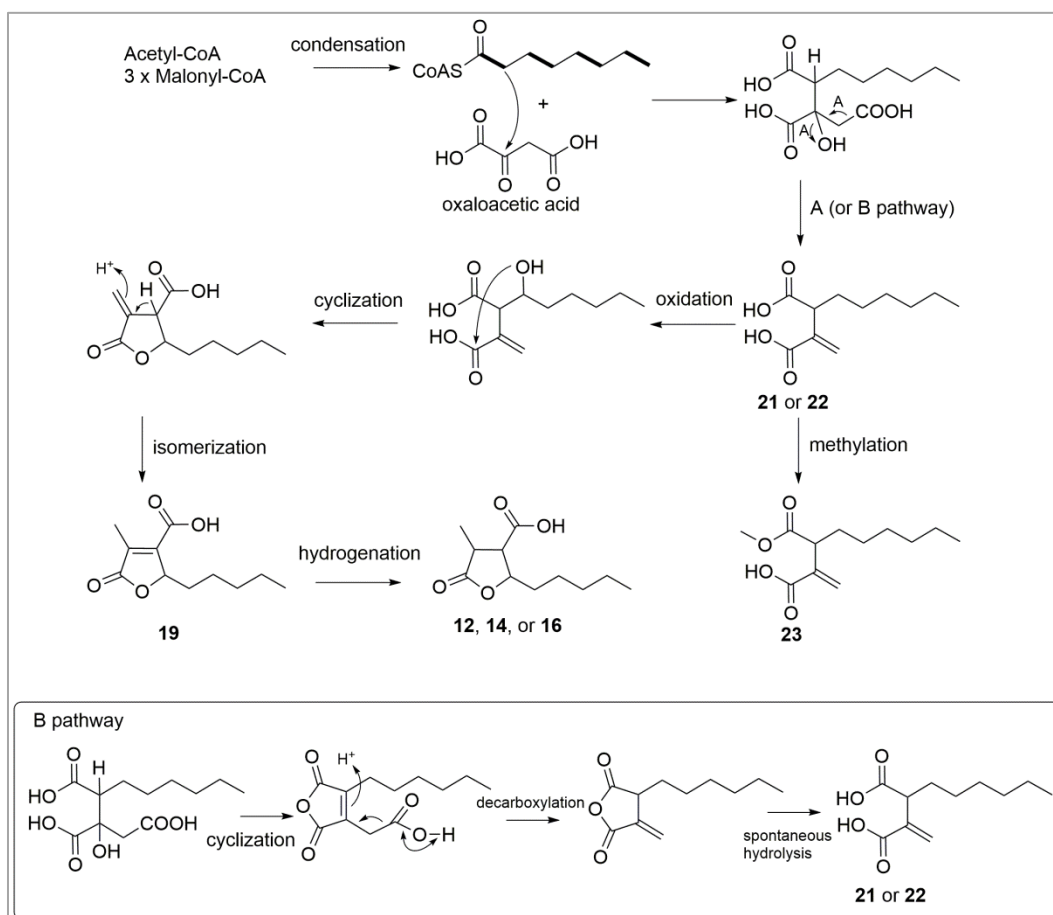


Figure 4.5.4.1 Plausible biosynthetic pathway of alkylitaconic acids and paraconic acids (Fujii *et al.*, 2015).

4.5.5 The tetracyclic triterpenoid (**28**), and steroids (**29–35**)

Compound **28** represents an unusual fungus-derived 19-nor-lanostane tetracyclic triterpene with an aromatic B-ring (Li *et al.*, 2015). Furthermore, it seems that there is only one further natural

lanostane/cucurbitane derivative (19-nor-cucurbita-5(10),6,8,22(*E*),24-pentaen-3 β -ol from plant) with an aromatized B ring (Hsu *et al.*, 2011; Li *et al.*, 2015). Compounds possessing structural features similar to **28** are biosynthesized from a common intermediate lanosterol (Figure 4.5.5.1) (Brown, 1998; Ríos *et al.*, 2012; Quin *et al.*, 2014). The “6-6-6-5” tetracyclic lanosterol is biosynthesized via cyclization of 2,3-oxidosqualene followed by sequential backbone rearrangement (two methyl migrations and hydride shifts). It has to be noted that a stable intermediate with “6-6-5” rings is followed by the C-ring expansion concomitant with the formation of the D-ring to yield the “6-6-6-5” scaffold in lanosterol (Chen *et al.*, 2015). Subsequent aromatization of the B-ring of lanosterol skeleton may be responsible for the loss of Me-19, followed by hydroxylation at C-1, C-12 and C-22 to afford **28** (Figure 4.5.5.1). The conversion of lanosterol into steroid derivatives **29–35** in fungi is shown in figure 4.5.5.1 (Brown, 1998; Quin *et al.*, 2014).

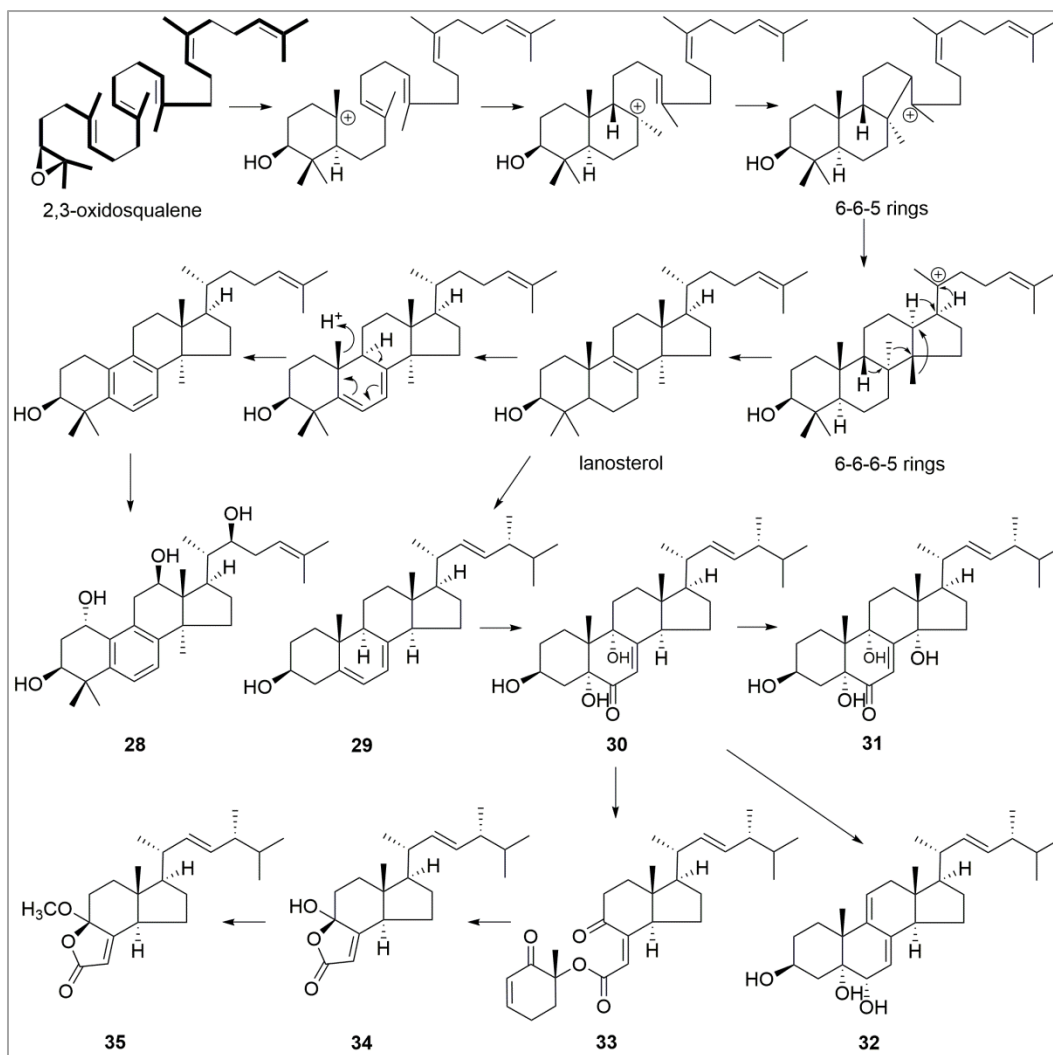


Figure 4.5.5.1 Plausible biosynthetic pathway of tetracyclic triterpenoid (**28**), and steroids (**29–35**) (Chen *et al.*, 2015; Quin *et al.*, 2014; Mansoor *et al.*, 2005; Brown, 1998).

4.5.6 Cyclic pentapeptides (**40–42**) and cyclic lipopeptides (**43** and **44**)

Nonribosomal peptides (NRPs) are a group of biologically active peptides, which were biosynthesized by large multimodular enzymes, nonribosomal peptide synthetases (NRPSs) (Strieker *et al.*, 2010). The substrates for building the structures are not limited to the 20 proteinogenic amino acids. The nonproteinogenic building blocks or other acids are also frequently found and contribute to structural diversity of NRPs (Strieker *et al.*, 2010). Cyclic pentapeptides (**40–42**) are polypeptide chains with five amino acids, which were biosynthesized without free N- and C-terminal because of the cyclization from head to tail (Joo, 2012). The D-leucine discovered in NRPs (**40–42**) can arise from the direct incorporation of D-amino acids or in situ epimerization of an L-aminoacyl C- α center (the more general route) (Stachelhaus and Walsh, 2000). Cyclic lipopeptides (**43** and **44**) consist of two parts, the peptide and the lipid. The first part was constructed by proteinogenic and nonproteinogenic amino acids, which was achieved by NRPSs (Sørensen *et al.*, 2014). The second part was a fatty acid chain linked to the peptidyl backbone, which was formed by HR-PKS. Therefore, compounds **43** and **44** are hybrid peptide-polyketide natural products (Sørensen *et al.*, 2014).

4.5.7 *Alternaria* mycotoxins (**49–51**)

Compounds **49–51**, as important mycotoxins from the *Alternaria* fungi, not only caused significant economic losses in agriculture, but also posed serious health risks to humans and livestock (Chooi *et al.*, 2015). The PKS gene is responsible for their biosynthesis (Saha *et al.*, 2012). Figure 4.5.7.1 showed that the polyketide chain was converted to target products by two types of cyclization.

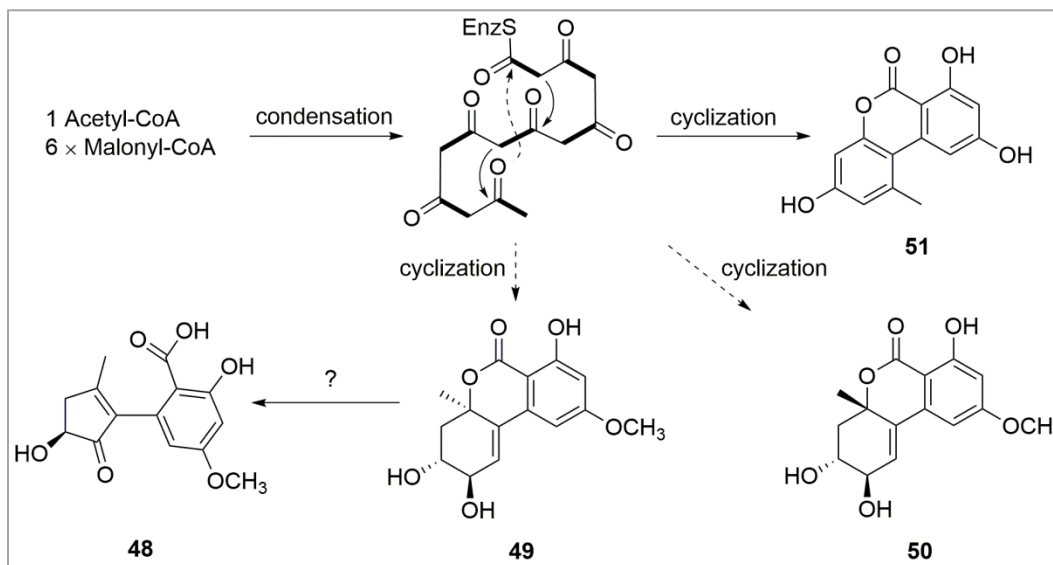


Figure 4.5.7.1 Proposed biosynthetic pathway for **48–51** (Chooi *et al.*, 2015; Saha *et al.*, 2012).

4.6 Biological activities

Given an extensive use of the host plants in TCM, we embarked on a traditional knowledge-based de-replication of the functional roles of the compounds isolated from endophytes (Li *et al.*, 2015). Our focus was to correlate the traditional usage of the plant in TCM to the bioactivity of the actually isolated compounds produced by the endophytic fungi residing inside the host plant (Li *et al.*, 2015). Chinese medicinal plants *X. sibiricum*, *M. fortunei*, and *L. japonica* for the isolation of endophytic fungi, have been used in TCM for treating bacterial infection-related ailments (see section 1.2.4). Therefore, the antibacterial efficacies of new compounds and selected known metabolites were investigated against several Gram-positive and Gram-negative bacteria obtained from clinical or environmental strains. Furthermore, in order to correctly interpret the high antibacterial efficacies of several compounds, a resazurin-based assay to measure the THP-1 mitochondrial metabolic inhibition and an ATPlite assay to measure the THP-1 cytoplasmic ATP depletion were used to evaluate the cytotoxicity of potential antibiotics.

4.6.1 Antibacterial activity

4.6.1.1 Compounds isolated from *Eupenicillium* sp. LG41

4.6.1.1.1 Decalin-containing compounds (1–5)

Table 4.6.1.1.1.1 shows the minimum inhibitory concentrations (MIC) of five decalin-containing compounds against five bacteria [*S. aureus*, *E. coli* (DSM 1116, Risk-group 1, RG1), *E. coli* (DSM 682, RG2), *B. subtilis*, and *Acinetobacter* sp.] compared to the standard references streptomycin and gentamicin. Compound **3** had the same efficacy as that of gentamicin against clinically relevant RG2 bacterium *S. aureus* at the concentration of 1.0 $\mu\text{g/mL}$ (Table 4.6.1.1.1.1). Moreover, compound **5** was more active than **3** against *S. aureus* with an MIC value of 0.1 $\mu\text{g/mL}$ (Table 4.6.1.1.1.1 and Figure 4.6.1.1.1.1). An SAR investigation was explored. By comparing **5** with **2** and **3**, the substitution at C-11 could be noted to play an important role in increasing the antibacterial activity against the selected bacterium (Li *et al.*, 2014b). These results reveal not only the importance of substitution at C-11, but also the potential of compounds **3** and **5** as potent compounds that could be developed into new derivatives to increase the antimicrobial efficacy. Decalin-motif containing compounds had weak or no antibacterial activities against other four selected Gram-positive and Gram-negative bacteria.

Table 4.6.1.1.1.1 MIC of the compounds **1–5** (see page 35) against Gram-positive and Gram-negative bacteria compared to standard references (streptomycin and gentamicin).^a

organism (DSMZ no.)	1	2	2^b	3	4	5	streptomycin	gentamicin
<i>Staphylococcus aureus</i> (DSM 799)	>10.0	>10.0	>10.0	1.0	>10.0	0.1	5.0	1.0
<i>Escherichia coli</i> (DSM 1116)	5.0	5.0	>10.0	5.0	>10.0	>10.0	1.0	1.0
<i>Escherichia coli</i> (DSM 682)	>10.0	nt	>10.0	nt	>10.0	>10.0	1.0	1.0
<i>Bacillus subtilis</i> (DSM 1088)	>10.0	>10.0	10.0	>10.0	>10.0	>10.0	5.0	1.0
<i>Acinetobacter</i> sp. (DSM 586)	>10.0	10	>10.0	>10.0	>10.0	>10.0	10.0	5.0

^aAll values are in $\mu\text{g/mL}$ and derived from experiments in triplicate. ^bThe second time to test. nt: not tested.

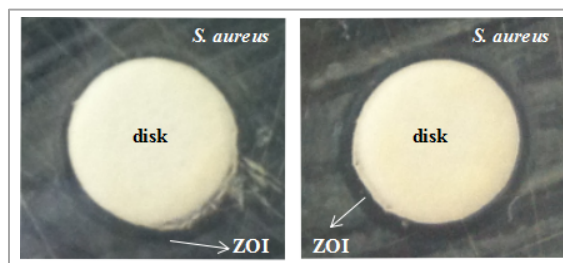


Figure 4.6.1.1.1.1 The observed zones of inhibition (ZOIs) of compound **5** against *S. aureus* at the concentration of 0.1 $\mu\text{g/mL}$.

4.6.1.1.2 Sirenin derivatives (7 and 8) and pigment (9)

Table 4.6.1.1.2.1 exhibits the MIC of sirenin derivatives (7 and 8) and pigment (9) against four bacteria [*S. aureus*, *E. coli* (RG1), *B. subtilis*, and *Acinetobacter* sp.] compared to the standard references streptomycin and gentamicin. Compounds 7–9 exhibited strong efficacy against the soil bacterium *Acinetobacter* sp., being more potent than streptomycin and having the same efficacy as gentamicin. Figure 4.6.1.1.2.1 exhibits the zones of inhibition (ZOIs) of compound 9 against *B. subtilis* and *Acinetobacter* sp.

Table 4.6.1.1.2.1 MIC of the compounds 7–9 (see page 35) against Gram-positive and Gram-negative bacteria compared to standard references (streptomycin and gentamicin).^a

organism (DSMZ no.)	7	8	9	streptomycin	gentamicin
<i>Staphylococcus aureus</i> (DSM 799)	>10.0	>10.0	nt	5.0	1.0
<i>Escherichia coli</i> (DSM 1116)	5.0	10.0	nt	1.0	1.0
<i>Bacillus subtilis</i> (DSM 1088)	>10.0	>10.0	10.0	5.0	1.0
<i>Acinetobacter</i> sp. (DSM 586)	5.0	5.0	5.0	10.0	5.0

All values are in $\mu\text{g/mL}$ and derived from experiments in triplicate. nt: not tested.

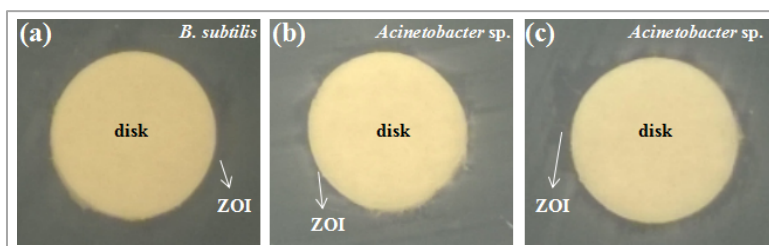


Figure 4.6.1.1.2.1 The observed ZOIs of compound 9 against *B. subtilis* (a, 10 $\mu\text{g/mL}$) and *Acinetobacter* sp. (b, 5 $\mu\text{g/mL}$; c, 10 $\mu\text{g/mL}$).

4.6.1.1.3 Paraconic acids (12–20) and alkylitaconic acids (21–24)

The antibacterial activities of paraconic acids and alkylitaconic acids against Gram-positive and negative pathogenic bacteria such as *S. aureus*, *S. pyogenes*, and *E. coli*, as well as the soil-dwelling bacteria *B. subtilis* and *Acinetobacter* sp. were evaluated (Table 4.6.1.1.3.1). Most of paraconic acids and alkylitaconic acids selectively inhibited the soil bacterium *Acinetobacter* sp. and exhibited no inhibitory

activities against the other four Gram-positive and negative bacteria *S. aureus*, *S. pyogenes*, *B. subtilis* and *E. coli* (Table 4.6.1.1.3.1). Compounds **12**, **17**, **21**, and **24** exhibited the most pronounced inhibitory effects on the soil bacterium *Acinetobacter* sp. at the concentration of 1.0 $\mu\text{g/mL}$, being more potent than that of both reference antibiotics streptomycin (10 $\mu\text{g/mL}$) and gentamicin (5 $\mu\text{g/mL}$) (Table 4.6.1.1.3.1). By comparing compound **13** with **12**, and **15** with **14**, as well as **23** with **21**, the free carboxyl group was beneficial for the high inhibitory activity against *Acinetobacter* sp. The contrary was observed from the comparison of compound **20** with **19**.

Table 4.6.1.1.3.1 MIC of the compounds (**12–17**, and **19–24**) (see page 36) against Gram-positive and Gram-negative bacteria compared to standard references (streptomycin and gentamicin).^a

organism (DSMZ no.)	12	13	14	15	16^b	17	19	20	21	22	23	24	streptomycin	gentamicin
<i>Staphylococcus aureus</i> (DSM 799)	>10	>10	>10	>10	>10	>10	>10	>10	>10	>10	>10	>10	5.0	1.0
<i>Escherichia coli</i> (DSM 682)	>10	>10	>10	>10	>10	>10	>10	>10	10	>10	>10	>10	1.0	1.0
<i>Bacillus subtilis</i> (DSM 1088)	>10	>10	>10	5.0	>10	>10	>10	>10	>10	>10	>10	>10	5.0	1.0
<i>Acinetobacter</i> sp. (DSM 586)	1.0	5.0	10	>10	2.0	1.0	>10	5.0	1.0	>10	>10	1.0	10	5.0
<i>Streptococcus pyogenes</i> (DSM 11728)	>10	>10	>10	>10	>10	>10	>10	>10	>10	>10	>10	>10	>10	10

^a All values are in $\mu\text{g/mL}$ and derived from experiments in triplicate. ^b a mixture (**16:13** = 1:2)

In order to further understand the inhibitory effects of paraconic acids and alkylitaconic acids on *Acinetobacter* species, four more *Acinetobacter* species (Table 4.6.1.1.3.2), of them *A. baylyi* and *A. calcoaceticus* were isolated from soil or water, and *A. baumannii* and *A. pittii* from the clinic, were tested. The soil bacterium *Acinetobacter* sp. was also included and parallelly tested (Table 4.6.1.1.3.2). A last-resort antibiotic colistin, as one of currently the best options for multi-drug resistant *A. baumannii* (Jung and Park, 2015), was employed as the positive control.

Table 4.6.1.1.3.2 MIC of the compounds (**12–24**) (see page 36) against five different strains of Gram-negative *Acinetobacter* bacteria compared to a standard reference (colistin).^a

organism (DSMZ no.)	12	13	14	15	16	17	18	19	20	21	22	23	24	colistin	
<i>Acinetobacter baylyi</i> (DSM 24193)	2.0	5.0	>10	>10	>10	5.0	>10	>10	>10	>10	>10	>10	>10	2.0	10
<i>Acinetobacter calcoaceticus</i> (DSM 30006)	5.0	>10	>10	>10	>10	>10	>10	>10	>10	>10	>10	>10	>10	>10	5.0
<i>Acinetobacter baumannii</i> (DSM 30007)	5.0	>10	>10	>10	>10	>10	>10	>10	>10	>10	>10	>10	>10	>10	5.0
<i>Acinetobacter pittii</i> (DSM 25618)	2.0	5.0	>10	>10	>10	>10	>10	>10	>10	>10	>10	>10	>10	>10	5.0
<i>Acinetobacter</i> sp. (DSM 586)	1.0	5.0	>10	>10	5.0	2.0	>10	>10	5.0	2.0	>10	>10	2.0	1.0	

^a All values are in $\mu\text{g/mL}$ and derived from experiments in triplicate.

As indicated by results in table 4.6.1.1.3.2, compound **12** was found to be highly active against all five Gram-negative *Acinetobacter* spp. (*Acinetobacter* sp., *A. baylyi*, *A. calcoaceticus*, *A. baumannii* and *A. pittii*), qualitatively effective in the same range as that of the last-resort antibiotic colistin. Therefore, compound **12** should be a genus-specific bioactive paraconic acid. Compound **13**, as the methyl ester of **12**, showed the inhibitory activity against *A. baylyi*, *A. pittii* and *Acinetobacter* sp. at the concentration of 5 $\mu\text{g/mL}$ (Table 4.6.1.1.3.2). On the basis of compound **12**, the SAR for acids **12–24** is investigated. A γ -lactone motif and a free carboxylic acid functional group are pivotal for the antibacterial efficacy of compound **12** against *Acinetobacter* spp. Furthermore, a critical comparison among metabolites **12–20** with a γ -lactone ring revealed that the stereo-configuration relationship at C-2, C-3 and C-4 are really important for their antibacterial effects. Fortunately, in the current work, a preferred stereochemical configuration (2*S*, 3*R*, 4*S*) exhibited in compound **12** was discovered and it would be worthy of further structural modification for studying the selective antibacterial activity. *Acinetobacter*, as a genus of gram-negative, oxidase-negative and strictly aerobic bacteria, live in diverse natural environments (Jung and Park, 2015). In this genus, *A. baumannii*, a species with a multi-drug resistance trait and rapid resistance development is reported to have caused a wide range of infections, especially in hospital intensive care units (ICU) (Jung and Park, 2015; McConnell et al., 2013). The discovery and development of new antimicrobial agents are urgent (WHO, 2014). Admittedly, our results obtained from the disc diffusion assay only depict a qualitative *in vitro* susceptibility of the tested organisms against the isolated compounds, comparable to the standard reference antibiotics. In particular, it was interesting to note the sensitivity of the *Acinetobacter* species against compound **12** on solid agar medium as per the latest guidelines of the CLSI. However, it is important to consider the general drawbacks of the disc diffusion assay, in addition to its advantages, when interpreting the obtained results. Therefore, more *in vitro* as well as *in vivo* assays must be preformed to determine the therapeutic efficacy of compound **12** in actual practice before considering it as a lead compound for treating *Acinetobacter* infections. Nevertheless, our results provide a starting point for considering compound **12** (termed pacbactin) as a promising lead compound for the treatment of *Acinetobacter* spp.

4.6.1.2 Compounds isolated from *Diaporthe* sp. LG23

The antibacterial efficacies of a tetracyclic triterpene (**28**) as well as six biosynthetically-related known ergosterol derivatives (**30–35**) against the clinical risk-group 2 (RG2) human pathogens were evaluated

(Table 4.6.1.2.1). Gram-positive bacteria (*S. aureus* and *S. pyogenes*) as well as Gram-negative bacteria (*E. coli* and *P. aeruginosa*) were used. The Gram-positive soil bacterium *B. subtilis* (RG1) was also included.

Table 4.6.1.2.1 MIC of the compounds **28**, and **30–35** (see page 74) against Gram-positive and Gram-negative bacteria compared to standard references (streptomycin and gentamicin).^a

organism (DSMZ no.)	28	30	31	32	33	34	35	streptomycin	gentamicin
<i>Staphylococcus aureus</i> (DSM 799)	5.0	>10	>10	>10	1.0	>10	>10	5.0	1.0
<i>Escherichia coli</i> (DSM 682)	5.0	>10	>10	>10	>10	>10	>10	1.0	1.0
<i>Bacillus subtilis</i> (DSM 1088)	2.0	5.0	>10	>10	5.0	>10	>10	5.0	1.0
<i>Pseudomonas aeruginosa</i> (DSM 22644)	2.0	>10	>10	>10	>10	>10	>10	10.0	1.0
<i>Streptococcus pyogenes</i> (DSM 11728)	0.1	>10	>10	>10	>10	>10	>10	>10	10.0

^aAll values are in $\mu\text{g/mL}$ and derived from experiments in triplicate.

Compound **28**, an unusual fungus-derived 19-nor-lanostane tetracyclic triterpenoid with an aromatic B-ring system, showed marked antibacterial efficacy against both Gram-positive and Gram-negative bacteria, especially the clinical isolates of *S. pyogenes* and *P. aeruginosa* as well as a human pathogenic strain of *S. aureus* (Table 4.6.1.2.1) (Li *et al.*, 2015). Our results, therefore, indicate that **28** is a potent antibacterial compound. Compounds **30** and **33** were active against *B. subtilis* having a similar efficacy as that of the reference standard streptomycin. Compound **31**, the hydroxylated product of **30** at C-14, showed no inhibitory activity, indicating that the substitution by a hydroxyl group is not beneficial to the activity. Compound **33** showed the same antibacterial efficacy as gentamicin against *S. aureus* with an MIC value of 1.0 $\mu\text{g/mL}$. Comparison of the MIC values of **33** with those of **30–32**, **34**, and **35** suggested that the A ring and/or seco-ring B system observed in **33** has a significant effect on the antibacterial efficacy.

4.6.1.3 Compounds isolated from *F. decemcellulare* LG53

The Gram-positive bacteria *S. aureus* and *B. subtilis*, as well as Gram-negative bacteria *E. coli* and *Acinetobacter* sp. were employed for biological test. Table 4.6.1.3.1 shows the MIC values of new cyclic pentapeptides **40–42** compared to both standard antibiotics, streptomycin and gentamicin. None of the new cyclic pentapeptides **40–42** exhibited inhibitory efficacies against the selected bacteria (Table

4.6.1.3.1). The cyclic lipopeptide, fusaristatin A (**43**), was well-known to be inactive against many tested bacteria and several fungi (Hegge *et al.*, 2015). However, as indicated by the work on several cyclopeptides employed as “cross-talk” agents in plant (Wang *et al.*, 2015), a further investigation is warranted to examine their functions in cross-talk.

Table 4.6.1.3.1 MIC of the compounds **40–42** (see page 93) against Gram-positive and Gram-negative bacteria compared to standard references (streptomycin and gentamicin).^a

organism (DSMZ no.)	40	41	42	streptomycin	gentamicin
<i>Staphylococcus aureus</i> (DSM 799)	>10.0	>10.0	>10.0	5.0	1.0
<i>Escherichia coli</i> (DSM 1116)	>10.0	>10.0	>10.0	1.0	1.0
<i>Escherichia coli</i> (DSM 682)	>10.0	>10.0	>10.0	1.0	1.0
<i>Bacillus subtilis</i> (DSM 1088)	>10.0	>10.0	>10.0	5.0	1.0
<i>Acinetobacter</i> sp. (DSM 586)	>10.0	>10.0	>10.0	10.0	5.0

^aAll values are in $\mu\text{g/mL}$ and derived from experiments in triplicate.

4.6.2 Cytotoxicity

In order to correctly interpret the antibacterial efficacies of compounds, a resazurin-based assay to measure the THP-1 mitochondrial metabolic inhibition and an ATPlite assay to measure the THP-1 cytoplasmic ATP depletion were used to evaluate the cytotoxicity of selected highly active compounds **5**, **12**, **13**, and **28**. Semi-logarithmic representations of the fractional survival (FS in %) of THP-1 cells in response to the concentration (μM) are as shown below (Figures 4.6.2.1-4.6.2.4). Compounds **5** and **28** were highly cytotoxic *in vitro* against THP-1 cells (Figure 4.6.2.1 and 4.6.2.4). Because of the high cytotoxicities of **5** and **28**, they cannot be used as antibacterial agents. Surprisingly, none of compounds **12** and **13** displayed potential cytotoxic effects on THP-1 cells at high concentrations (Figures 4.6.2.2 and 4.6.2.3). The above results indicated the potential of **12** as a promising lead compound.

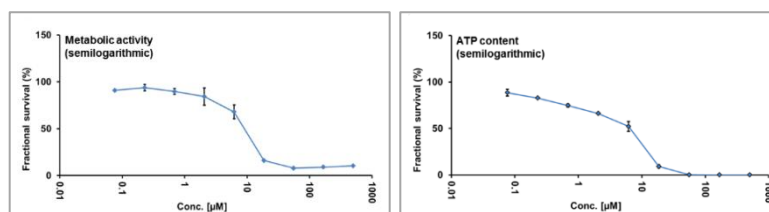


Figure 4.6.2.1 *In vitro* cytotoxic assays of compound **5** against THP-1 cells.

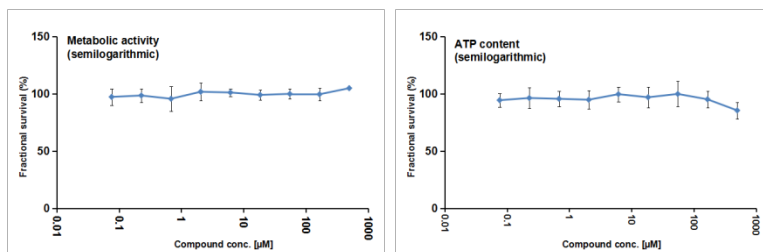


Figure 4.6.2.2 *In vitro* cytotoxic assays of compound **12** against THP-1 cells.

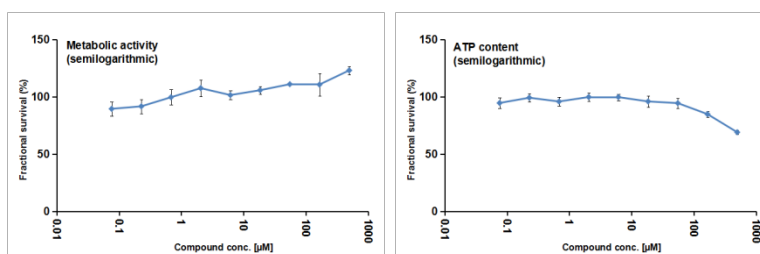


Figure 4.6.2.3 *In vitro* cytotoxic assays of compound **13** against THP-1 cells.

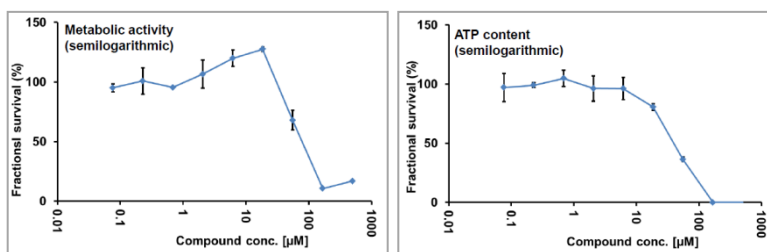


Figure 4.6.2.4 *In vitro* cytotoxic assays of compound **28** against THP-1 cells.

4.7 Possible ecological role of endophyte

Microorganisms rarely live in axenic conditions in nature and endophytes are no exception (Li *et al.*, 2015). Endophytic microorganisms typically co-evolve a plethora of ‘traits’ for surviving and functioning in their diverse ecological niches (Kusari *et al.*, 2012). These traits emerge as a result of multifaceted multispecies interaction of endophytes with associated organisms (other endophytes, invading phytopathogens, invading pests and parasites, as well as the host plant), and range from production of antimicrobial chemical defense compounds to triggers for activating cryptic biosynthetic pathways, production of precursors, quorum sensing molecules, epigenetic modulators, and even direct physical organismal interactions (Kusari *et al.*, 2013; Kusari *et al.*, 2014; Kusari *et al.*, 2015; Li *et al.*,

2015). In the laboratory, all these chemical or molecular crosstalks between several organisms are really difficult to investigate *in vitro*. Normally, *in vitro* culture conditions are mostly different from *in planta* micro-environment where endophytic microorganisms live. Hence, there is no direct significance for quantitative estimation of production of a secondary metabolite by an endophyte *in vitro* and *in planta* (Kusari *et al.*, 2014; Li *et al.*, 2015). In addition, the *in planta* metabolic activity of an endophyte is mostly dictated by the interactions or communication strategies with coexisting microorganisms (Li *et al.*, 2015). Therefore, endophytic microorganisms are known to stop or reduce production of certain secondary metabolites over repeated subculturing, mostly due to loss of suitable *in planta* triggers (Kusari *et al.*, 2012; Li *et al.*, 2015).

Since the endophytic fungus *Eupenicillium* sp. LG41, was isolated from the roots of *X. sibiricum*, the ecological role of the endophyte was proposed (Li *et al.*, 2014b). Some isolated compounds (for example, compound **12**) exhibited significant inhibitory activities against the Gram-positive bacterium *B. subtilis* and the Gram-negative bacterium *Acinetobacter* sp., which typically inhabit soil and the rhizosphere (see section 4.6.1.1). Soil, especially the rhizosphere, is a microbial hot spot where multipartite interactions are intensified (Li *et al.*, 2014b). It is thus reasonable to propose that the root-endophyte provides defense to the host plant against specific soil bacteria. Our data also reveal the potential of *Diaporthe* sp. LG23 in aiding host plant defense against invading pathogens by secreting active antibacterial compounds (Li *et al.*, 2015). Without a doubt, a further study is needed to evaluate the endophyte's *in planta* metabolic processes to exemplify its true function in host plant.

As indicated by the work on several cyclopeptides employed as “cross-talk” agents in plant (Wang *et al.*, 2015), an investigation for the possible functions of cyclopeptides **40–43** from *F. decemcellulare* LG53, was carried out. As shown in figure 4.7.1A, antifungal evaluation against fungus LG52 (isolated from the same plant tissue with *F. decemcellulare* LG53) using PDA medium amended with compounds **40–43** with different concentrations showed that the growth of fungus LG52 was only inhibited on PDA medium containing fusaristatin A (**43**). It has to be noted that the inhibition was concentration-dependent (Figure 4.7.1B). Moreover, MALDI-Imaging-HRMS was applied and showed that compound **43** was secreted into the PDA medium around the fungal mycelia of *F. decemcellulare* LG53 (Figure 4.7.2). More interestingly, compound **43** was accumulated outside *F. decemcellulare* LG53 with a higher ion intensity when the mycelia of two endophytic fungi came in physical contact (Figure 4.7.2). Thus, we assumed that compound **43** was secreted into the endophytic community *in planta* and might be employed to maintain the balance in the ecological niche.

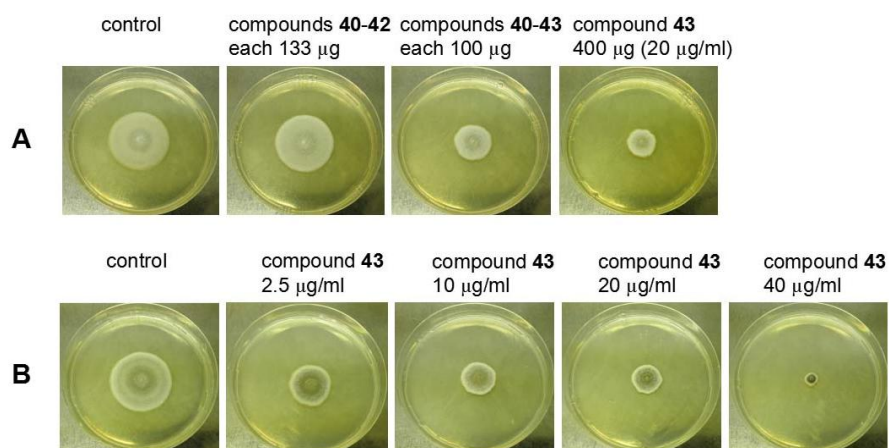


Figure 4.7.1 Fungus LG52 was grown on PDA medium amended with compounds **40–43**. A: For each petri dish, there are total 400 μg pure compounds or mixture in 20 mL PDA medium (final concentration: 20 $\mu\text{g}/\text{mL}$). B: Compound **43** with different concentrations was added into 20 mL PDA medium.

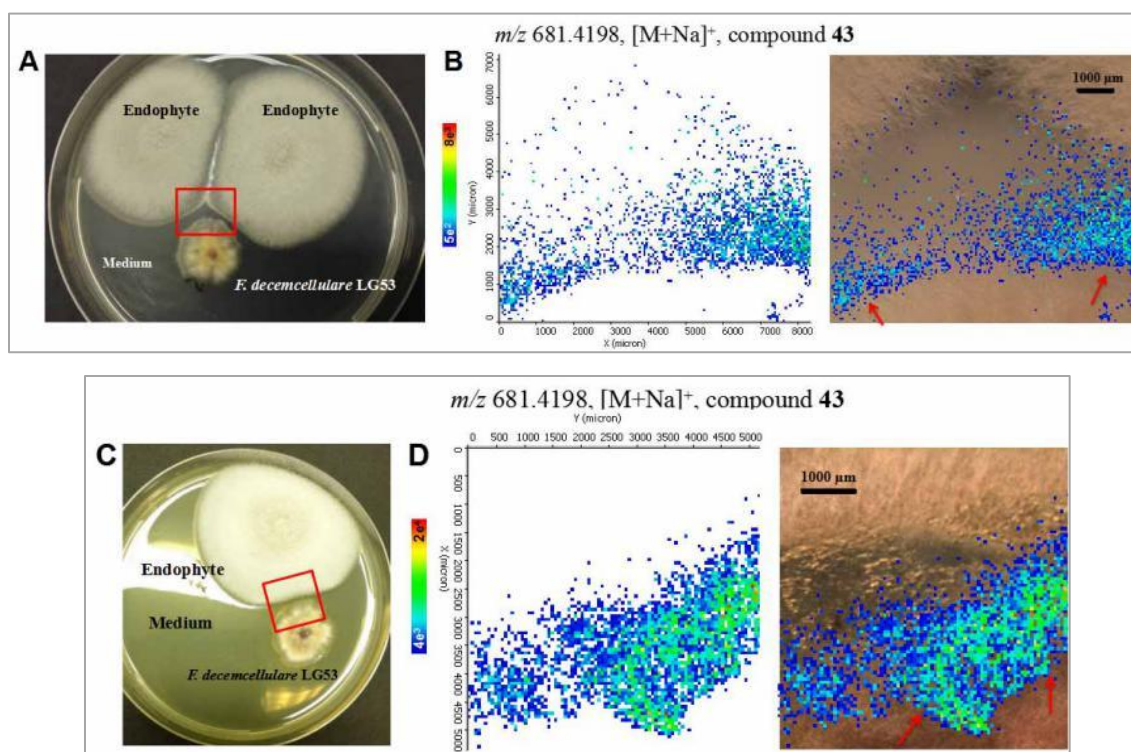


Figure 4.7.2 Localization of compound **43** detected in MALDI-imaging-HRMS scan of the endophytic fungi isolated from the same plant tissue after 7 days. A,C The picture of co-culture between two endophytes and the area (red frame) selected for MS measurement. B,D Ion intensity map of mass m/z 681.4198, $\text{C}_{36}\text{H}_{58}\text{O}_7\text{N}_4\text{Na}$, $[\text{M}+\text{Na}]^+$ (compound **43**).

Endophytes as one of ubiquitous, yet cryptic communities, show less manifest phenomena. The regulation of host defense, fungal virulence, and other environmental factors is complex, and difficult to investigate (Kusari *et al.*, 2012). The fundamental aspects of their interactions with hosts and other inhabitants are poorly understood (Arnold *et al.*, 2003; Kusari *et al.*, 2012; Kusari *et al.*, 2014b). Wang *et al.* (2015) discovered several cyclopeptides which were employed as “cross-talk” agents between two endophytes. Fusaristatin A (**43**), a cyclic lipopeptide, is well-known to be inactive against many tested bacteria and fungi (Hegge *et al.*, 2015). However, compound **43** showed a concentration-dependent inhibition of the growth of an endophytic fungus (Figure 4.7.1), which was isolated from the same community with the producer of **43**. It can be induced by a neighbor and then secreted into the environment (Figure 4.7.2). The above evidence strongly indicates a balanced antagonism in fungal endophytes of the host, which might also explain the presence of antimicrobial metabolites that endophytes synthesize (Schulz *et al.*, 2015).

4.8 Discussion

In 1945, Alexander Fleming received the Nobel Prize in Physiology or Medicine for his discovery of penicillin, a fungus-derived antibiotic (Tan and Tatsumura, 2015). The golden era of discovering and using new antibiotics started then (Lewis, 2012). In 1952, Selman Waksman was awarded the same Nobel Prize for his contribution in the discovery of streptomycin, a bacterium-derived antibiotic active against tuberculosis (Woodruff, 2014). After 63 years, the prestigious Nobel Prize in Physiology or Medicine in 2015 was awarded to natural products discoverers again. The prize was shared by Youyou Tu for her discovery of the antimalarial agent artemisinin, and William Cecil Campbell and Ōmura Satoshi for their discovery of avermectin, which acts against infections caused by roundworm parasites (Kong and Tan, 2015). It has to be noted that the discovery of artemisinin was inspired by traditional Chinese medicine (TCM), while the avermectin was discovered from a soil streptomycete (Kong and Tan, 2015). The above facts not only promote the renaissance of natural products chemistry, but also attract more attention and enthusiasm on traditional medical practice and/or promising microorganisms in certain ecological niches to discover new drugs (Shen, 2015). With the recent advances in microbial genomics and metagenomics, a new golden age of natural products drug discovery is drawing (Shen, 2015).

Since the emergence and spread of antibiotic resistance, the discovery and development of antibacterial agents with new natural product-drug pharmacophores are urgent (WHO, 2014). Endophytes, a distinct group of microorganisms, asymptotically colonize living, internal tissues of host plants (Kusari *et al.*, 2012). They have been proved to have enormous biological diversity and a variety of biosynthetic capabilities due to their complex association with host plants and other organisms in their ecological niches (Kusari *et al.*, 2012; Zhang *et al.*, 2006). For example, they can produce bioactive plant compounds including the valuable anti-cancer agent paclitaxel (Taxol) (Stierle *et al.*, 1993; Kharwar *et al.*, 2011; Kusari *et al.*, 2012). Traditional medicinal plants have an ethnobotanical history that is associated with specific medical practices or applications of interest (Strobel and Daisy, 2003). They harbor certain endophytic microorganisms that adapt to the environmental factors or selection pressure *in planta* over the co-evolutionary process, and might have desirable biosynthetic capabilities related to host plant (Zhang *et al.*, 2006; Kusari and Spiteller, 2011; Kusari *et al.*, 2012). From a traditional knowledge-based strategy (Li *et al.*, 2015), endophytes isolated from traditional medicinal plants used for treating bacterial infection-related diseases could be a promising source for new antibiotics, as exemplified by the results in this thesis.

The aim of this thesis focuses on the isolation, identification and antibacterial evaluation of secondary metabolites from four endophytes harbored in the traditional medicinal plants *X. sibiricum*, *M. fortunei*, and *L. japonica*, which were effective in the treatment of bacterial infection-related ailments (Zhang *et al.*, 2006; Choi *et al.*, 2007; Li *et al.*, 2007; Kan *et al.*, 2011; Yu *et al.*, 2011; Xiong *et al.*, 2013). More than fifty endophytic fungi were isolated from the above mentioned plants, supporting the evidence of the vast diversity of endophytic microorganisms (Verma and Gange, 2014). It has to be mentioned herein that the plant tissues collected from different locations in gardens or wild places (see section 3.1) nearly have the same compositions by the analysis of LC-MS. However, the chemical profiles for endophytes from these tissues had the major differences. Regarding this, another interesting finding is that *Diaporthe* sp. LG23 and *F. decemcellulare* LG53 from the leaves and stems of *M. fortunei* respectively, can produce the same degraded triterpenoid compound **34**, in addition to the similar compound **33** or **47** with the same highly rearranged core structures. Further research to discover the possible influence of host plant *M. fortunei* on endophytes is necessary.

From the selected four fungal endophytes, forty-nine secondary metabolites with diverse structures and/or functional groups including decalin-containing polyketides, aromatic polyketides, sesquiterpenes (sirenin derivatives), tetracyclic triterpenoid, steroids, naphthopyranone derivatives (pigments),

polyketide-isoprenoid hybrid pigment, trisubstituted γ -butyrolactone, unsaturated dicarboxylic acids, cyclic pentapeptides, and cyclic lipopeptides were isolated. Five semi-synthetic derivatives were also obtained for SAR investigation. Fifteen compounds (31%) have new structures and three (6%) are new natural products which have already been synthesized (Jacobi and Herradura, 1996; Drioli *et al.*, 1998; Amador *et al.*, 2006). The new compounds including new natural products account for 37% of isolated metabolites compared to reported 51% unknown bioactive compounds from endophytic fungi and 38% from soil fungi (Kharwar *et al.*, 2011).

Many major developments have been recognized and well employed in the field of natural products isolation and structural elucidation (Sticher, 2008; Bucar *et al.*, 2013; Breton *et al.*, 2013; Seger *et al.*, 2013). The hyphenated instrumental analysis platforms (such as HPLC-MS or HPLC-NMR) have become powerful tools for the analysis and identification of constituents in raw materials (Seger *et al.*, 2013). LC-MS guided pre-screening and isolation in this thesis enabled the rapid identification of already known compounds (dereplication), and were crucial to the fast discovery of new antibiotics (Nielsen *et al.*, 2011). However, some compounds with interesting activities may be undetected, untraceable, and/or difficult to isolate by modern techniques, even under bioassay-guided isolation sometimes (Bucar *et al.*, 2013; Pettit *et al.*, 2016). In addition, many wrong structural assignments of natural products by MS, NMR or even X-ray diffraction study are commonly found in literature (Nicolaou and Snyder, 2005; Suyama *et al.*, 2011; Ayoup *et al.*, 2014; Zhang and Timmermann, 2016). Modern quantum chemical calculations including ORD, ECD, and NMR calculations are successfully used in complex molecules to assign their stereo-configurations or planar structures (Tantillo, 2013), for example the structural elucidation of compounds **7**, **8**, **12**, **14**, **16**, **39**, and **48** in this thesis. In many cases, however, combinations of approaches may be required to fully characterize secondary metabolites.

Antibacterial evaluation led to the discovery of highly active compounds **5**, **12**, and **28**. However, owing to the high cytotoxicities of **5** and **28**, they cannot be used as candidates for antibiotic development. Surprisingly, pacbactin (**12**) as a genus-specific bioactive paraconic acid, displayed no potential cytotoxic effects on THP-1 cells at high concentrations. Although the structure or configuration present in **12** ensure its high antibacterial activity against five *Acinetobacter* spp., five more stereoisomers of pacbactin (**12**) are necessary for a comprehensive SAR analysis of this kind of paraconic acids. Moreover, as indicated by its methyl ester derivative (**13**) with the attenuation of antibacterial activity, the structural modification to get a lot of semi-synthetic derivatives is needed for further determining the SAR (Nepali *et al.*, 2014). Synthesis of compound **12**-like molecules that have more penetrating ability

and avoid efflux is also preferred (Wright and Poinar, 2012; Blair *et al.*, 2015). More importantly, modern technologies in molecular biology should be applied to identify the molecular target(s) and the mechanism-of-action of interesting compounds (Schenone *et al.*, 2013). Without a doubt, a systematic analysis for pre-existing countermeasures to develop compound derivatives is needed to avoid the proved antibiotic resistance mechanisms (Wright and Poinar, 2012).

Admittedly, our results obtained from the disc diffusion assay only depict a qualitative *in vitro* susceptibility of the tested organisms against the isolated compounds as per the latest guidelines of the CLSI, comparable to the standard reference antibiotics. In particular, it was attractive to discover the sensitivity of the *Acinetobacter* species against compound **12** on solid agar medium. However, the general drawbacks of the disc diffusion assay in addition to its advantages have to be considered when interpreting the obtained results. Therefore, in order to fully determine the therapeutic efficacy of compound **12** in actual practice before considering it as a lead compound for treating *Acinetobacter* infections, more *in vitro* as well as *in vivo* assays must be preformed. Nevertheless, our results provide a starting point for considering compound **12** (termed pacbactin) as a promising lead compound for the treatment of *Acinetobacter* spp.

Chapter 5:
REFERENCES

Aarestrup, F. Sustainable farming: get pigs off antibiotics. *Nature* **2012**, *486*, 465–466.

Aidas, K.; Angeli, C.; Bak, K. L.; Bakken, V.; Bast, R.; Boman, L.; Christiansen, O.; Cimiraglia, R.; Coriani, S.; Dahle, P.; Dalskov, E. K.; Ekström, U.; Enevoldsen, T.; Eriksen, J. J.; Ettenhuber, P.; Fernández, B.; Ferrighi, L.; Fliegl, H.; Frediani, L.; Hald, K.; Halkier, A.; Hättig, C.; Heiberg, H.; Helgaker, T.; Hennem, A. C.; Hettema, H.; Hjertenæs, E.; Høst, S.; Høyvik, I. M.; Iozzi, M. F.; Jansík, B.; Jensen, H. J. A.; Jonsson, D.; Jørgensen, P.; Kauczor, J.; Kirpekar, S.; Kjærgaard, T.; Klopper, W.; Knecht, S.; Kobayashi, R.; Koch, H.; Kongsted, J.; Krapp, A.; Kristensen, K.; Ligabue, A.; Lutnæs, O. B.; Melo, J. I.; Mikkelsen, K. V.; Myhre, R. H.; Neiss, C.; Nielsen, C. B.; Norman, P.; Olsen, J.; Olsen, J. M. H.; Osted, A.; Packer, M. J.; Pawlowski, F.; Pedersen, T. B.; Provasi, P. F.; Reine, S.; Rinkevicius, Z.; Ruden, T. a.; Ruud, K.; Rybkin, V. V.; Sałek, P.; Samson, C. C. M.; de Merás, A. S.; Saue, T.; Sauer, S. P. a.; Schimmelpfennig, B.; Sneskov, K.; Steindal, A. H.; Sylvester-Hvid, K. O.; Taylor, P. R.; Teale, A. M.; Tellgren, E. I.; Tew, D. P.; Thorvaldsen, A. J.; Thøgersen, L.; Vahtras, O.; Watson, M. a.; Wilson, D. J. D.; Ziolkowski, M.; Ågren, H. The Dalton quantum chemistry program system. *Wiley Interdiscip. Rev. Comput. Mol. Sci.* **2014**, *4*, 269–284.

Alanis, A. J. Resistance to antibiotics: are we in the post-antibiotic era? *Arch. Med. Res.* **2005**, *36*, 697–705.

Altemöller, M.; Podlech, J.; Fenske, D. Total synthesis of altenuene and isoaltenuene. *Eur. J. Org. Chem.* **2006**, *2006*, 1678–1684.

Aly, A. H.; Edrada-Ebel, R.; Indriani, I. D.; Wray, V.; Müller, W. E. G.; Totzke, F.; Zirrgiebel, U.; Schächtele, C.; Kubbutat, M. H. G.; Lin, W. H.; Proksch, P.; Ebel, R. Cytotoxic metabolites from the fungal endophyte *Alternaria* sp. and their subsequent detection in its host plant *Polygonum senegalense*. *J. Nat. Prod.* **2008**, *71*, 972–980.

Amador, M.; Ariza, X.; Carcia, J. A versatile stereoselective approach to paraconic acids. *Heterocycles*, **2006**, *67*, 705–720.

Anastasia, M.; Fiecchi, A.; Scala, A. Permanganate oxidation of ergosterol. *J. Org. Chem.* **1979**, *44*, 3657–3661.

Argoudelis, A. D.; Eble, T. E.; Fox, J. A.; Mason, D. J. Biosynthesis of lincomycin. IV. origin of methyl groups. *Biochemistry* **1969**, *8*, 3408–3411.

Arnold, A. E.; Mejía, L. C.; Kyllö, D.; Rojas, E. I.; Maynard, Z.; Robbins, N.; Herre, E. A. Fungal endophytes limit pathogen damage in a tropical tree. *Proc. Natl. Acad. Sci. USA* **2003**, *100*, 15649–15654.

Asai, T.; Otsuki, S.; Taniguchi, T.; Monde, K.; Yamashita, K.; Sakurai, H.; Ozeki, T.; Oshima, Y. Structures and absolute configurations of short-branched fatty acid dimers from an endophytic fungus of *Aloe arborescens*. *Tetrahedron Lett.* **2013**, *54*, 3402–3405.

Ayoub, M. S.; Cordes, D. B.; Slawin, A. M. Z.; O'Hagan, D. Total synthesis of a reported

- fluorometabolite from *Streptomyces* sp. TC1 indicates an incorrect assignment. The isolated compound did not contain fluorine. *J. Nat. Prod.* **2014**, *77*, 1249–1251.
- Bang, J.; Kim, H.; Kim, J.; Yu, C.-M. Asymmetric aldol reaction of allenates: regulation for the selective formation of isomeric allenyl or alkynyl aldol adduct. *Org. Lett.* **2015**, *17*, 1573–1576.
- Banks, M. R.; Dawson, I. M.; Gosney, I.; Hodgson, P. K. G.; Thorburn, P. A concise synthesis of (–)-dihydroprotolichesterinic acid via consecutive stereocontrolled 1,4-conjugate addition and *syn*-aldol condensation reactions. *Tetrahedron Lett.* **1995**, *36*, 3567–3570.
- Berova, N.; Bari, L. D.; Pescitelli, G. Application of electronic circular dichroism in configurational and conformational analysis of organic compounds. *Chem. Soc. Rev.* **2007**, *36*, 914–931.
- Beecham, A. F. Circular dichroism in lactones. *Tetrahedron Lett.* **1968**, *19*, 2355–2360.
- Bills, J. K.; Christensen, M.; Powell, M.; Thorn, G.; in *Biodiversity of Fungi: Endophytic Fungi*, edited by Mueller, G. M.; Bills, G. F.; Foster, M. Elsevier Academic Press, CA, USA, 2004, p. 241.
- Blair, J. M. A.; Webber, M. A.; Baylay, A. J.; Ogbolu, D. O.; Piddock, L. J. V. Molecular mechanisms of antibiotic resistance. *Nat. Rev. Microbiol.* **2015**, *13*, 42–51.
- Bode, S. E.; Drochner, D.; Müller, M. Synthesis, biosynthesis, and absolute configuration of vioxanthin. *Angew. Chem. Int. Ed.* **2007**, *46*, 5916–5920.
- Bourhis, L. J.; Dolomanov, O. V.; Gildea, R. J.; Howard, J. A. K.; Puschmann, H. The anatomy of a comprehensive constrained, restrained refinement program for the modern computing environment - *Olex2* dissected. *Acta Cryst.* **2015**, *A71*, 59–75.
- Brown, G. D. The biosynthesis of steroids and triterpenoids. *Nat. Prod. Rep.* **1998**, *15*, 653–696.
- Bucar, F.; Wube, A.; Schmid, M. Natural product isolation-how to get from biological material to pure compounds. *Nat. Prod. Rep.* **2013**, *30*, 525–545.
- Butler, M. S. Natural products to drugs: natural product derived compounds in clinical trials. *Nat. Prod. Rep.* **2005**, *22*, 162–195.
- Butler, M. S. Natural products to drugs: natural product derived compounds in clinical trials. *Nat. Prod. Rep.* **2008**, *25*, 475–516.
- Butler, M. S.; Blaskovich, M. A.; Copper, M. A. Antibiotics in the clinical pipeline in 2013. *J. Antibiot.* **2013**, *66*, 571–591.
- Butler, M. S.; Robertson, A. A. B.; Copper, M. A. Natural product and natural product derived drugs in clinical trials. *Nat. Prod. Rep.* **2014**, *31*, 1612–1661.

- Cabrera, G. M.; Vellasco, A. P.; Levy, L. M.; Eberlin, M. N. Characterisation of fungal lanostane-type triterpene acids by electrospray ionisation mass spectrometry. *Phytochem. Anal.* **2007**, *18*, 489–495.
- Carroll, S. P.; Jørgensen, P. S.; Kinnison, M. T.; Bergstrom, C. T.; Denison, R. F.; Gluckman, P.; Smith, T. B.; Strauss, S. Y.; Tabashnik, B. E. Applying evolutionary biology to address global challenges. *Science* **2014**, *346*, 313.
- Charney, J.; Fisher, W. P.; Curran, C.; Machlowitz, R. A.; Tytell, A. A. Streptogramin, a new antibiotic. *Antibiot. Chemother.* **1953**, *3*, 1283–1286.
- Chernaga, A. N.; Davies, S. G.; Lewis, C. N.; Todd, R. S. Stereoselective Michael addition of benzylamines to homochiral methylenebutanedioates. *J. Chem. Soc. Perkin Trans. 1* **1999**, 3603–3608.
- Cheung, F. TCM: made in China. *Nature* **2011**, *480*, S82–S83.
- Choi, J.-H.; Ogawa, A.; Abe, N.; Masuda, K.; Koyama, T.; Yazawa, K.; Kawagishi, H. Chaxines B, C, D, and E from the edible mushroom *Agrocybe chaxingu*. *Tetrahedron* **2009**, *65*, 9850–9853.
- Choi, C. W.; Jung, H. A.; Kang, S. S.; Choi, J. S. Antioxidant constituents and a new triterpenoid glycoside from *Flos Lonicerae*. *Arch. Pharm. Res.* **2007**, *30*, 1–7.
- Chooi, Y.-H.; Cacho, R.; Tang, Y. Identification of the viridicatumtoxin and griseofulvin gene clusters from *Penicillium aethiopicum*. *Chem. Biol.* **2010**, *17*, 483–494.
- Chooi, Y.-H.; Wang, P.; Fang, J.; Li, Y.; Wu, K.; Wang, P.; Tang, Y. Discovery and characterization of a group of fungal polycyclic polyketide prenyltransferases. *J. Am. Chem. Soc.* **2012**, *134*, 9428–9437.
- Chooi, Y.-H.; Muria-Gonzalez, J. M.; Mead, O. L.; Solomon, P. S. *SnPKS19* encodes the polyketide synthase for alternariol mycotoxin biosynthesis in the wheat pathogen *Parastagonospora nodorum*. *Appl. Environ. Microbiol.* **2015**, *81*, 5309–5317.
- Chaesung, L.; Kim, J.; Choi, J. N.; Ponnusamy, K.; Jeon, Y.; Kim, S.-U.; Kim, J. G.; Lee, C. H. Identification, fermentation, and bioactivity against *Xanthomonas oryzae* of antimicrobial metabolites isolated from *Phomopsis longicolla* S1B4. *J. Microbiol. Biotechnol.* **2010**, *20*, 494–500.
- Chen, N.; Wang, S.; Smentek, L.; Jr. Hess, B. A.; Wu, R. Biosynthetic mechanism of lanosterol: cyclization. *Angew. Chem. Int. Ed.* **2015**, *54*, 8693–8696.
- Clay, K. Defensive symbiosis: a microbial perspective. *Func. Ecol.* **2014**, *28*, 293–298.
- Copper, M. A.; Shlaes, D. Fix the antibiotics pipeline. *Nature* **2011**, *472*, 32.
- D’Costa, V. M.; Mcgrann, K. M.; Hughes, D. W.; Wright, G. D. Sampling the antibiotic resistome. *Science* **2006**, *311*, 374–377.

- D'Costa, V. M.; King, C. E.; Kalan, L.; Morar, M.; Sung, W. W. L.; Schwarz, C.; Froese, D.; Zazula, G.; Calmels, F.; Debruyne, R.; Golding, G. B.; Poinar, H. N.; Wright, G. D. Antibiotic resistance is ancient. *Nature* **2011**, *477*, 457–461.
- de Bary, A. Morphologie und Physiologie der Pilze, Flechten, und Myxomyceten. Hofmeister's handbook of physiological botany, vol. II, 1866, Leipzig, Germany.
- de Haen, P. Drugs approved for clinical use by the food and drug administration. *The Journal of New Drugs*, **1965**, *5*, 358–364.
- Deska, J.; Bäckvall, J.-E. Enzymatic kinetic resolution of primary allenic alcohols. Application to the total synthesis and stereochemical assignment of striatisporolide A. *Org. Biomol. Chem.* **2009**, *7*, 3379–3381.
- Ding, L.; Fotso, S.; Li, F.; Qin, S.; Laatsch, H. Hualyzin, a symmetrical urea derivative isolated from *Penicillium herquei* isolate GA4. *J. Nat. Prod.* **2008**, *71*, 1068–1069.
- Donner, C. D. Naphthopyranones— isolation, bioactivity, biosynthesis and synthesis. *Nat. Prod. Rep.* **2015**, *32*, 578–604.
- Dolomanov, O. V.; Bourhis, L. J.; Gildea, R. J.; Howard, J. A. K.; Puschmann, H. OLEX2: a complete structure solution, refinement and analysis program. *J. Appl. Cryst.* **2009**, *42*, 339–341.
- Dougherty, J. T.; Pucci, M. J. *Antibiotic Discovery and Development*. New York: Springer. 2012.
- Drioli, S.; Felluga, F.; Forzato, C.; Nitti, P.; Pitacco, G.; Valentin, E. Synthesis of (+)- and (-)-phaseolinic acid by combination of enzymatic hydrolysis and chemical transformations with revision of the absolute configuration of the natural product. *J. Org. Chem.* **1998**, *63*, 2385–2388.
- Editor, Editorial: the antibiotic alarm. *Nature* **2013**, *495*, 141. doi:10.1038/495141a.
- Editor, Editorial: antibiotic threat. *Nature* **2013**, *499*, 379. doi:10.1038/499379b.
- El-Elimat, T.; Figueroa, M.; Ehrmann, B. M.; Cech, N. B.; Pearce, C. J.; Oberlies, N. H. High-resolution MS, MS/MS, and UV database of fungal secondary metabolites as a dereplication protocol for bioactive natural products. *J. Nat. Prod.* **2013**, *76*, 1709–1716.
- Erb, W.; Zhu, J. From natural product to marketed drug: the tiacumicin odyssey. *Nat. Prod. Rep.* **2013**, *30*, 161–174.
- Fan, Y. C.; Kwon, O. Phosphine/palladium-catalyzed syntheses of alkylidene phthalans, 3-deoxyisoochracinic acid, isoochracinic acid, and isoochracinol. *Org. Lett.* **2012**, *14*, 3264–3267.
- Farrugia, L. J. WinGX and ORTEP for Windows: an update. *J. Appl. Cryst.* **2012**, *45*, 849–854.

- Floss, H. G.; Yu, T.-W. Rifamycins-mode of action, resistance, and biosynthesis. *Chem. Rev.* **2005**, *105*, 621–632.
- Fournier, J.; Lozano, O.; Menozzi, C.; Arseniyadis, S.; Cossy, J. Palladium-catalyzed asymmetric allylic alkylation of cyclic dienol carbonates: efficient route to enantioenriched γ -butenolides bearing an all-carbon α -quaternary stereogenic center. *Angew. Chem. Int. Ed.* **2013**, *52*, 1257–1261.
- Freeman, E. M. The seed fungus of *Lolium temulentum*, L., the Darnel. *Phil. Trans. R. Soc. London, Ser. B*, **1902**, *196*, 1–27.
- Frisch, M. J.; Trucks, G. W.; Schlegel, H. B.; Scuseria, G. E.; Robb, M. A.; Cheeseman, J. R.; Scalmani, G.; Barone, V.; Mennucci, B.; Petersson, G. A.; Nakatsuji, H.; Caricato, M.; Li, X.; Hratchian, H. P.; Izmaylov, A. F.; Bloino, J.; Zheng, G.; Sonnenberg, J. L.; Hada, M.; Ehara, M.; Toyota, K.; Fukuda, R.; Hasegawa, J.; Ishida, M.; Nakajima, T.; Honda, Y.; Kitao, O.; Nakai, H.; Vreven, T.; Montgomery, J. A.; Peralta, J. E.; Ogliaro, F.; Bearpark, M.; Heyd, J. J.; Brothers, E.; Kudin, K. N.; Staroverov, V. N.; Kobayashi, R.; Normand, J.; Raghavachari, K.; Rendell, A.; Burant, J. C.; Iyengar, S. S.; Tomasi, J.; Cossi, M.; Rega, N.; Millam, J. M.; Klene, M.; Knox, J. E.; Cross, J. B.; Bakken, V.; Adamo, C.; Jaramillo, J.; Gomperts, R.; Stratmann, R. E.; Yazyev, O.; Austin, A. J.; Cammi, R.; Pomelli, C.; Ochterski, J. W.; Martin, R. L.; Morokuma, K.; Zakrzewski, V. G.; Voth, G. A.; Salvador, P.; Dannenberg, J. J.; Dapprich, S.; Daniels, A. D.; Farkas, O.; Foresman, J. B.; Ortiz, J. V.; Cioslowski, J., Fox, D. J. *Gaussian 09W*, Version 7.0; Gaussian: Wallingford, CT, 2009.
- Fujii, R.; Matsu, Y.; Minami, A.; Nagamine, S.; Takeuchi, I.; Gomi, K.; Oikawa, H. Biosynthetic study on antihypercholesterolemic agent phomoidride: general biogenesis of fungal dimeric anhydrides. *Org. Lett.* **2015**, *17*, 5658–5661.
- Gilbert, N. Rules tighten on use of antibiotics on farms. *Nature* **2012**, *481*, 125.
- Gu, W. Bioactive metabolites from *Alternaria brassicicola* ML-P08, an endophytic fungus residing in *Malus halliana*. *World J. Microbiol. Biotechnol.* **2009**, *25*, 1677–1683.
- Guerin, P. Sur la presence d'un champignon dans l'ivraie. *J. Botanique* **1898**, *12*: 230–238.
- Gunatilaka, A. A. L. Natural products from plant-associated microorganisms: distribution, structural diversity, bioactivity, and implications of their occurrence. *J. Nat. Prod.* **2006**, *69*, 509–526.
- He, J.-W.; Chen, G.-D.; Gao, H.; Yang, F.; Li, X.-X.; Peng, T.; Guo, L.-D.; Yao, X.-S. Heptaketides with antiviral activity from three endolichenic fungal strains *Nigrospora* sp., *Alternaria* sp. and *Phialophora* sp. *Fitoterapia* **2012**, *83*, 1087–1091.
- Hegge, A.; Lønborg, R.; Nielsen, D. M.; Sørensen, J. L. Factors influencing production of fusaristatin A in *Fusarium graminearum*. *Metabolites* **2015**, *5*, 184–191.
- Howell, G. P.; Fletcher, S. P.; Geurts, K.; Horst, B. T.; Feringa, B. L. Catalytic Asymmetric Synthesis of Acyclic Arrays by Tandem 1,4-Addition-Aldol Reactions. *J. Am. Chem. Soc.* **2006**, *128*, 14977–14985.

- Höfle, G.; Röser, K. Structure of xanthomegnin and related pigments: reinvestigation by ^{13}C nuclear magnetic resonance spectroscopy. *J. Chem. Soc., Chem. Commun.* **1978**, 611–612.
- Hsu, C.; Hsieh, C.-L.; Kuo, Y.-H.; Huang, C.-J. Isolation and identification of cucurbitane-type triterpenoids with partial agonist/antagonist potential for estrogen receptors from *Momordica charantia*. *J. Agric. Food Chem.* **2011**, *59*, 4553–4561.
- Huneck, S.; Takeda, R. Zur Chemie der Proto-und allo-Proto-lichesterinsäure/contribution to the chemistry of proto- and allo-proto-lichesterinic acids. *Z. Naturforsch.* **1992**, *47b*, 842–854.
- Huang, H.; Cao, Y.; Tian, L.; Lin, W.; Zhang, K. A new polyunsaturated acid from the marine-derived *Streptomyces violans* (No. HTTA-F04129). *Chem. Nat. Compd.* **2014**, *50*, 402–404.
- Inokoshi, J.; Nakamura, Y.; Hongbin, Z.; Uchida, R.; Nonaka, K.; Masuma, R.; Tomoda, H. Spirohexalines, new inhibitors of bacterial undecaprenyl pyrophosphate synthase, produced by *Penicillium brasilianum* FKI-3368. *J. Antibiot.* **2013**, *66*, 37–41.
- Isaka, M.; Chinthanom, P.; Kongthong, S.; Srichomthong, K.; Choeyklin, R. Lanostane triterpenes from cultures of the Basidiomycete *Ganoderma orbiforme* BCC 22324. *Phytochemistry* **2013**, *87*, 133–139.
- Ishizuka, T.; Yaoita, Y.; Kikuchi, M. Sterol constituents from the fruit bodies of *Grifola frondosa* (FR.) S. F. Gray. *Chem. Pharm. Bull.* **1997**, *45*, 1756–1760.
- Isogai, A.; Washizu, M.; Kondo, K.; Murakoshi, S.; Suzuki, A. Isolation and identification of (+)-hexylitaconic acid as a plant growth regulator. *Agric. Biol. Chem.* **1984**, *48*, 2607–2609.
- Jacobi, P. A.; Herradura, P. Enantioselective syntheses of (+)-and (–)-nephrosteranic acid employing the Nicholas-Schreiber reaction. *Can. J. Chem.* **2001**, *79*, 1727–1735.
- Jacobi, P. A.; Herradura, P. Enantioselective syntheses of (+)-and (–)-phaseolinic acid. *Tetrahedron Lett.* **1996**, *37*, 8297–8300.
- Joo, S. H. Cyclic peptides as therapeutic agents and biochemical tools. *Biomol. Ther.* **2012**, *20*, 19–26.
- Jung, J.; Park, W. *Acinetobacter* species as model microorganisms in environmental microbiology: current state and perspectives. *Appl. Microbiol. Biotechnol.* **2015**, *99*, 2533–2548.
- Kan, S.; Chen, G.; Han, C.; Chen, Z.; Song, X.; Ren, M.; Jiang, H. Chemical constituents from the roots of *Xanthium sibiricum*. *Nat. Prod. Res.* **2011**, *25*, 1243–1249.
- Kashiwada, Y.; Nonaka, G.-I.; Nishioka, I. Studies on rhubarb (*Rhei Rhizoma*). V. isolation and characterization of chromone and chromanone derivatives. *Chem. Pharm. Bull.* **1984**, *32*, 3493–3500.
- Kayser, O.; Warzecha, H. Pharmaceutical biotechnology: drug discovery and clinical applications. John

Wiley & Sons, 2012.

Kelsic, E. D.; Zhao, J.; Vetsigian, K.; Kishony, R. Counteraction of antibiotic production and degradation stabilizes microbial communities. *Nature* **2015**, *521*, 516–519.

Kharwar, R. N.; Mishra, A.; Gond, S. K.; Stierle, A.; Stierle, D. Anticancer compounds derived from fungal endophytes: their importance and future challenges. *Nat. Prod. Rep.* **2011**, *28*, 1208–1228.

Klemke, C.; Kehraus, S.; Wright, A. D.; König, G. M. New secondary metabolites from the marine endophytic fungus *Apiospora montagnei*. *J. Nat. Prod.* **2004**, *67*, 1058–1063.

Kondru, R. K.; Beratan, D. N.; Friestad, G. K.; Smith, A. B.; Wipf, P. Chiral action at a distance: remote substituent effects on the optical activity of calyculins A and B. *Org. Lett.* **2000**, *2*, 1509–1512.

Kong, L. Y.; Tan, R. X. Artemisinin, a miracle of traditional Chinese medicine. *Nat. Prod. Rep.* **2015**, *32*, 1617–1621.

Kubota, T.; Iwai, T.; Takahashi-Nakaguchi, A.; Fromont, J.; Gonoï, T.; Kobayashi, J. Agelasines O–U, new diterpene alkaloids with a 9-*N*-methyladenine unit from a marine sponge *Agelas* sp. *Tetrahedron* **2012**, *68*, 9738–9744.

Kusari, S.; Lamshöft, M.; Zühlke, S.; Spiteller, M. An endophytic fungus from *Hypericum perforatum* that produces hypericin. *J. Nat. Prod.* **2008**, *71*, 159–162.

Kusari, S.; Zühlke, S.; Kosuth, J.; Cellarova, E.; Spiteller, M. Light-independent metabolomics of endophytic *Thielavia subthermophila* provides insight into microbial hypericin biosynthesis. *J. Nat. Prod.* **2009**, *72*, 1825–1835.

Kusari, S.; Zühlke, S.; Spiteller, M. An endophytic fungus from *Camptotheca acuminata* that produces camptothecin and analogs. *J. Nat. Prod.* **2009**, *72*, 2–7.

Kusari, S.; Lamshöft, M.; Spiteller, M. *Aspergillus fumigatus* Fresenius, an endophytic fungus from *Juniperus communis* L. Horstmann as a novel source of the anticancer pro-drug deoxypodophyllotoxin. *J. Appl. Microbiol.* **2009**, *107*, 1019–1030.

Kusari, S.; Zühlke, S.; Borsch, T.; Spiteller, M. Positive correlations between hypericin and putative precursors detected in the quantitative secondary metabolite spectrum of *Hypericum*. *Phytochemistry* **2009**, *70*, 1222–1232.

Kusari, S. Endophytic fungi harbored in *Camptotheca acuminata*, *Hypericum perforatum* and *Juniperus communis* plants as promising sources of camptothecin, hypericin and deoxypodophyllotoxin. 2010, Ph.D. thesis, TU Dortmund.

Kusari, S.; Spiteller, M. Are we ready for industrial production of bioactive plant secondary metabolites utilizing endophytes? *Nat. Prod. Rep.* **2011**, *28*, 1203–1207.

- Kusari, S.; Zühlke, S.; Spiteller, M. Effect of artificial reconstitution of the interaction between the plant *Camptotheca acuminata* and the fungal endophyte *fusarium solani* on Camptothecin Biosynthesis. *J. Nat. Prod.* **2011**, *74*, 764–775.
- Kusari, S.; Hertweck, C.; Spiteller, M. Chemical ecology of endophytic fungi: origins of secondary metabolites. *Chem. Biol.* **2012**, *19*, 792–798.
- Kusari, S.; Spiteller, M. Metabolomics of endophytic fungi producing associated plant secondary metabolites: progress, challenges and opportunities. In *Metabolomics*, Editor: Roessner, U. Rijeka, Croatia: InTech, 2012, pp. 241–266.
- Kusari, S.; Pandey, S. P.; Spiteller, M. Untapped mutualistic paradigms linking host plant and endophytic fungal production of similar bioactive secondary metabolites. *Phytochemistry* **2013**, *91*, 81–87.
- Kusari, S.; Singh, S.; Jayabaskaran, C. Biotechnological potential of plant-associated endophytic fungi: hope versus hype. *Trends Biotechnol.* **2014a**, *32*, 297–303.
- Kusari, S.; Lamshöft, M.; Kusari, P.; Gottfried, S.; Zühlke, S.; Louven, K.; Hentschel, U.; Kayser, O.; Spiteller, M. Endophytes are hidden producers of maytansine in *Putterlickia* roots. *J. Nat. Prod.* **2014b**, *77*, 2577–2584.
- Kusari, P.; Kusari, S.; Spiteller, M.; Kayser, O. Implications of endophyte-plant crosstalk in light of quorum responses for plant biotechnology. *Appl. Microbiol. Biotechnol.* **2015**, *99*, 5383–5390.
- Laatsch, H. *AntiBase 2014: The natural compound identifier*; Wiley-VCH: Weinheim, Germany; <http://www.wiley-vch.de/publish/dt/books/ISBN3-527-33841-1/>. 2014.
- Levine, D. P. Vancomycin: a history. *Clin. Infect. Dis.* **2006**, *42*, S5–S12.
- Lewis, K. Antibiotics: recover the lost art of drug discovery. *Nature* **2012**, *485*, 439–440.
- Li, A.-R.; Zhu, Y.; Li, X.-N.; Tian, X.-J. Antimicrobial activity of four species of Berberidaceae. *Fitoterapia* **2007**, *78*, 379–381.
- Li, G.; Kusari, S.; Spiteller, M. Natural products containing 'decalin' motif in microorganisms. *Nat. Prod. Rep.* **2014a**, *31*, 1175–1201.
- Li, G.; Kusari, S.; Lamshöft, M.; Schöffler, A.; Laatsch, H.; Spiteller, M. Antibacterial secondary metabolites from an endophytic fungus, *Eupenicillium* sp. LG41. *J. Nat. Prod.* **2014b**, *77*, 2335–2341.
- Li, G.; Kusari, S.; Kusari, P.; Kayser, O.; Spiteller, M. Endophytic *Diaporthe* sp. LG23 produces a potent antibacterial tetracyclic triterpenoid. *J. Nat. Prod.* **2015**, *78*, 2128–2132.

- Ling, L. L.; Schneider, T.; Peoples, A. J.; Spoering, A. L.; Engels, I.; Conlon, B. P.; Mueller, A.; Schaeberle, T. F.; Hughes, D. E.; Epstein, S.; Jones, M.; Lazarides, L.; Steadman, V. A.; Cohen, D. R.; Felix, C. R.; Fetterman, K. A.; Millett, W. P.; Nitti, A. G.; Zullo, A. M.; Chen, C.; Lewis, K. A new antibiotic kills pathogens without detectable resistance. *Nature* **2015**, *517*, 455–459.
- Littmann, J. Antimicrobial resistance and distributive Justice. London: University College London, Ph.D. Thesis; 2014.
- Liu, D.-Z. A review of ergostane and cucurbitane triterpenoids of mushroom origin. *Nat. Prod. Res.* **2014**, *28*, 1099–1105.
- Liu, Y.-Y.; Wang, Y.; Walsh, T. R.; Yi, L.-X.; Zhang, R.; Spencer, J.; Doi, Y.; Tian, G.; Dong, B.; Huang, X.; Yu, L.-F.; Gu, D.; Ren, H.; Chen, X.; Lv, L.; He, D.; Zhou, H.; Liang, Z.; Liu, J.-H.; Shen, J. Emergence of plasmid-mediated colistin resistance mechanism MCR-1 in animals and human beings in China: a microbiological and molecular biological study. *Lancet Infect. Dis.* **2016**, *16*, 161–168.
- López, S. N.; Ramallo, I. A.; Sierra, M. G.; Zacchino, S. A.; Furlan, R. L. E. Chemically engineered extracts as an alternative source of bioactive natural product-like compounds. *Proc. Natl. Acad. Sci. U.S.A.* **2007**, *104*, 441–444.
- MacDougall, C.; Polk, R. E. Antimicrobial stewardship programs in health care systems. *Clin. Microbiol. Rev.* **2005**, *18*, 638–656.
- Maier, M. S.; Marimon, D. I. C.; Stortz, C. A.; Adler, M. T. A revised structure for (–)-dihydropertusaric acid, a γ -butyrolactone acid from the lichen *Punctelia microsticta*. *J. Nat. Prod.* **1999**, *62*, 1565–1567.
- Mansoor, T. A.; Hong, J.; Lee, C.-O. Bae, S.-J.; Im, K. S.; Jung, J. H. Cytotoxic sterol derivatives from a marine sponge *Homaxinella* sp. *J. Nat. Prod.* **2005**, *68*, 331–336.
- Mantsch, H. H.; Smith, I. C. P. A study of solvent effects on the ^{13}C nuclear magnetic resonance spectra of cholesterol, pyridine, and uridine. *Can. J. Chem.* **1973**, *51*, 1384–1391.
- Marfey, P. Determination of D-amino acids. II use of a bifunctional reagent, 1,5-difluoro-2,4-dinitrobenzene. *Carlsberg Res. Commun.* **1984**, *49*, 591–596.
- McConnell, M. J.; Actis, L.; Pachón, J. *Acinetobacter baumannii*: human infections, factors contributing to pathogenesis and animal models. *FEMS Microbiol. Rev.* **2013**, *37*, 130–155.
- Miteva, M. A.; Guyon, F.; Tufféry, P. Frog2: Efficient 3D conformation ensemble generator for small compounds. *Nucleic Acids Res.* **2010**, *38*, W622–W627.
- Mole, B. MRSA: farming up trouble. *Nature* **2013**, *499*, 398–400.
- Mulzer, J.; Kattner, L.; Strecker, A. R.; Schröder, C.; Buschmann, J.; Lehmann, C.; Luger, P. Highly felkin-anh selective hiyama additions of chiral allylic bromides to aldehydes. application to the first

- synthesis of nephromopsinic acid and its enantiomer. *J. Am. Chem. Soc.* **1991**, *113*, 4218–4229.
- Mulzer, J.; Salimi, N.; Hartl, H. First asymmetric synthesis of (+)- and (–)-roccellaric acid and dihydroprotolichesterinic acid. *Tetrahedron: Asymmetry*, **1993**, *4*, 457–471.
- Myers, N.; Mittermeier, R. A.; Mittermeier, C. G.; da Fonseca, G. A. B.; Kent, J. Biodiversity hotspots for conservation priorities. *Nature* **2000**, *403*, 853–858.
- Nakadate, S.; Nozawa, K.; Horie, H.; Fujii, Y.; Nagai, M.; Hosoe, T.; Kawai, K.; Yaguchi, T.; Fukushima, K. Eujavanicols A–C, decalin derivatives from *Eupenicillium javanicum*. *J. Nat. Prod.* **2007**, *70*, 1510–1512.
- Nakahashi, A.; Yaguchi, Y.; Miura, N.; Emura, M.; Monde, K. A vibrational circular dichroism approach to the determination of the absolute configurations of flavorous 5-substituted-2(5*H*)-furanones. *J. Nat. Prod.* **2011**, *74*, 707–711.
- Nakahashi, A.; Miura, N.; Monde, K.; Tsukamoto, S. Stereochemical studies of hexylitaconic acid, an inhibitor of p53–HDM2 interaction. *Bioorg. Med. Chem. Lett.* **2009**, *19*, 3027–3030.
- Nakata, T.; Yamada, T.; Taji, S.; Ohishi, H.; Wada, S.-i.; Tokuda, H.; Sakuma, K.; Tanaka, R. Structure determination of inonotsuoxides A and B and in vivo anti-tumor promoting activity of inotodiol from the sclerotia of *Inonotus obliquus*. *Bioorg. Med. Chem.* **2007**, *15*, 257–264.
- Nelson, M. L.; Levy, S. B. The history of the tetracyclines. *Ann. N. Y. Acad. Sci.* **2011**, *1241*, 17–32.
- Nepali, K.; Sharma, S.; Sharma, M.; Bedi, P. M. S.; Dhar, K. L. *Eur. J. Med. Chem.* **2014**, *77*, 422–487.
- Newman, D. J.; Cragg, G. M. Natural product as sources of new drugs from 1981 to 2014. **2016**, DOI: 10.1021/acs.jnatprod.5b01055.
- Nielsen, K. F.; Månsson, M.; Rank, C.; Frisvad, J. C.; Larsen, T. O. Dereplication of microbial natural products by LC-DAD-TOFMS. *J. Nat. Prod.* **2011**, *74*, 2338–2348.
- Novak, R.; Shlaes, D. M. The pleuromutilin antibiotics: a new class for human use. *Curr. Opin. Invest. Drugs* **2010**, *11*, 182–191.
- Nicolaou, K. C.; Snyder, S. A. Chasing molecules that were never there: misassigned natural products and the role of chemical synthesis in modern structure elucidation. *Angew. Chem. Int. Ed.* **2005**, *44*, 1012–1044.
- Nisa, H.; Kamili, A. N.; Nawchoo, I. A.; Shafi, S.; Shameem, N.; Bandh, S. A. Fungal endophytes as prolific source of phytochemicals and other bioactive natural products: A review. *Microb. Pathog.* **2015**, *82*, 50–59.

- Nutting, W. H.; Rapoport, H.; Machlis, L. The structure of sirenin. *J. Am. Chem. Soc.* **1968**, *90*, 6434–6438.
- Onelli, E.; Rivetta, A.; Giorgi, A.; Bignami, M.; Cocucci, M.; Patrignani, G. Ultrastructural studies on the developing secretory nodules of *Hypericum perforatum*. *Flora* **2002**, *197*, 92–102.
- Pettit, G. R.; Smith, T. H.; Arce, P. M.; Flahive, E. J.; Anderson, C. R.; Chapuis, J.-C.; Xu, J.-P.; Gory, T. L.; Belcher, P. E.; Macdonald, C. B. *J. Nat. Prod.* **2015**, *78*, 476–485.
- Qin, C.; Lin, X.; Lu, X.; Wan, J.; Zhou, X.; Liao, S.; Tu, Z.; Xu, S.; Liu, Y. Sesquiterpenoids and xanthenes derivatives produced by sponge-derived fungus *Stachybotry* sp. HH1 ZSDS1F1-2. *J. Antibiot.* **2015**, *68*, 121–125.
- Quin, M. B.; Flynn, C. M.; Schmidt-Dannert, C. Traversing the fungal terpenome. *Nat. Prod. Rep.* **2014**, *31*, 1449–1473.
- Redecker, D.; Kodner, R.; Graham, L. E. Glomalean fungi from the Ordovician. *Science* **2000**, *289*, 1920–1921.
- Ríos, J.-L.; Andújar, I.; Recio, M.-C.; Giner, R.-M. Lanostanoids from fungi: a group of potential anticancer compounds. *J. Nat. Prod.* **2012**, *75*, 2016–2044.
- Ríos, J.-L. Chemical constituents and pharmacological properties of *Poria cocos*. *Planta Med.* **2011**, *77*, 681–691.
- Saha, D.; Fetzner, R.; Burkhardt, B.; Podlech, J.; Metzler, M.; Dang, H.; Lawrence, C.; Fischer, R. Identification of a polyketide synthase required for alternariol (AOH) and alternariol-9-methyl ether (AME) formation in *Alternaria alternata*. *PLoS ONE* **2012**, *7*, e40564.
- Sánchez, S.; Olson, B. Ecology and industrial microbiology: microbial diversity—the bright and promising future of microbial manufacturing. *Curr. Opin. Microbiol.* **2005**, *8*, 229–233.
- Sarotti, A. M.; Pellegrinet, S. C. A multi-standard approach for GIAO ¹³C NMR calculations. *J. Org. Chem.* **2009**, *74*, 7254–7260.
- Schenone, M.; Dančík, V.; Wagner, B. K.; Clemons, P. A. Target identification and mechanism of action in chemical biology and drug discovery. *Nat. Chem. Biol.* **2013**, *9*, 232–240.
- Schmidt, M. W.; Baldrige, K. K.; Boatz, J. A.; Elbert, S. T.; Gordon, M. S.; Jensen, J. H.; Koseki, S.; Matsunaga, N.; Nguyen, K. A.; Su, S.; Windus, T. L.; Dupuis, M.; Jr. Montgomery, J. A. General atomic and molecular electronic structure system. *J. Comput. Chem.* **1993**, *14*, 1347–1363.
- Schulz, B.; Haas, S.; Junker, C.; André, N.; Schobert, M. Fungal endophytes are involved in multiple balanced antagonisms. *Curr. Sci.* **2015**, *109*, 39–45.

- Seitz, M.; Reiser, O. Synthetic approaches towards structurally diverse γ -butyrolactone natural-product-like compounds. *Curr. Opin. Chem. Biol.* **2005**, *9*, 285–292.
- Sensi, P. History of the development of rifampicin. *Rev. Infect. Dis.* **1983**, *5*, S402–S406.
- Sheldrick, G. M. A short history of *SHELX*. *Acta Cryst.* **2008**, *A64*, 112–122.
- Sheldrick, G. M. Crystal structure refinement with *SHELXL*. *Acta Cryst.* **2015**, *C71*, 3–8.
- Shen, B. Polyketide biosynthesis beyond the type I, II and III polyketide synthase paradigms. *Curr. Opin. Chem. Bio.* **2003**, *7*, 285–295.
- Shen, B. A new golden age of natural products drug discovery. *Cell* **2015**, *163*, 1297–1300.
- Shi, Y.-n.; Liu, D.-h.; Jin, H.; Yang, Y.; Zhao, D.-k.; Wang, Y.-h.; Long, C.-l. Chemical constituents from the fruits of *Dipteronia dyeriana*. *Nat. Prod. Res. Dev.* **2014**, *26*, 1207–1211.
- Shiono, Y.; Akiyama, K.; Hayashi, H. New okaramine congeners, okamines J, K, L, M and related compounds, from *Penicillium simplicissimum* ATCC 90288. *Biosci. Biotechnol. Biochem.* **1999**, *63*, 1910–1920.
- Shiono, Y.; Tsuchinari, M.; Shimanuki, K.; Miyajima, T.; Murayama, T.; Koseki, T.; Laatsch, H.; Funakoshi, T.; Takanami, K.; Suzuki, K. Fusaristatins A and B, two new cyclic lipopeptides from an endophytic *Fusarium* sp. *J. Antibiot.* **2007**, *60*, 309–316.
- Song, Y.; Li, Q.; Liu, X.; Chen, Y.; Zhang, Y.; Sun, A.; Zhang, W.; Zhang, J.; Ju, J. Cyclic hexapeptides from the deep south China sea-derived *Streptomyces scopuliridis* SCSIO ZJ46 active against pathogenic Gram-positive bacteria. *J. Nat. Prod.* **2014**, *77*, 1937–1941.
- Sørensen, J. L.; Sondergaard, T. E.; Covarelli, L.; Fuertes, P. R.; Hansen, F. T.; Frandsen, R. J. N.; Saei, W.; Lukassen, M. B.; Wimmer, R.; Nielsen, K. F.; Gardiner, D. M.; Giese, H. Identification of the biosynthetic gene clusters for the lipopeptides fusaristatin A and W493 B in *Fusarium graminearum* and *F. pseudograminearum*. *J. Nat. Prod.* **2014**, *77*, 2619–2625.
- SPARTAN '14, Wavefunction, Inc.: Irvine, CA, 2014.
- Stachelhaus, T.; Walsh, C. T. Mutational analysis of the epimerization domain in the initiation module pheATE of gramicidin S synthetase. *Biochemistry* **2000**, *39*, 5775–5787.
- Stack, M. E.; Mazzola, E. P.; Eppley, R. M. Structures of xanthoviridicatin D and xanthoviridicatin G, metabolites of *penicillium viridicatum*: application of proton and carbon-13 NMR spectroscopy. *Tetrahedron Lett.* **1979**, *52*, 4989–4992.
- Stack, M. E.; Mazzola, E. P.; Page, S. W.; Pohland, A. E.; Highet, R. J.; Tempesta, M. S.; Corley, D. G. Mutagenic perylenequinone metabolites of *Alternaria alternata*: altertoxins I, II, and III. *J. Nat. Prod.*

1986, 49, 866–871.

Staniek, A.; Woerdenbag, H. J.; Kayser, O. Endophytes: exploiting biodiversity for the improvement of natural product-based drug discovery. *J. Plant Interact.* **2008**, 3, 75–93.

Stephens, P. J.; Harada, N. ECD cotton effect approximated by the Gaussian curve and other methods. *Chirality* **2010**, 22, 229–233.

Stewart, M.; Capon, R. J.; Lacey, E.; Tennant, S.; Gill, J. H. Calbistrin E and two other new metabolites from an Australian isolate of *Penicillium striatisporum*. *J. Nat. Prod.* **2005**, 68, 581–584.

Sticher, O. Natural product isolation. *Nat. Prod. Rep.* **2008**, 25, 517–554.

Stierle, A.; Strobel, G.; Stierle, D. Taxol and taxane production by *Taxomyces andreane*, an endophytic fungus of pacific yew. *Science* **1993**, 260, 214–216.

Strieker, M.; Tanović, A.; Marahiel, M. A. Nonribosomal peptide synthetases: structures and dynamics. *Curr. Opin. Struct. Biol.* **2010**, 20, 234–240.

Stone, J. K.; Bacon, C. W.; White, J. F. in *An overview of endophytic microbes: endophytism defined*. Editors: Bacon, C. W.; White, Jr. J. F. *Microbial Endophytes*, Marcel Dekker Inc., New York, 2000, pp. 3–5.

Strobel, G. A.; Long, D. M. Endophytic microbes embody pharmaceutical potential. *ASM News* **1998**, 64, 263–268.

Strobel, G.; Daisy, B. Bioprospecting for microbial endophytes and their natural products. *Microbiol. Mol. Bio. Rev.* **2003**, 67, 491–502.

Strobel, G.; Daisy, B.; Castillo, U.; Harper, J. Natural products from endophytic microorganisms. *J. Nat. Prod.* **2004**, 67, 257–268.

Sung, C. K.; Kimura, T.; But, P. P. H.; Guo, J. X. *International collation of traditional and folk medicine: Northeast Asia*, Part III. A project of UNESCO, 1998, vol. 3, World Scientific Publishing Co. Pte. Ltd., Singapore.

Suyama, T. L.; Gerwick, W. H.; McPhail, K. L. Survey of marine natural product structure revisions: a synergy of spectroscopy and chemical synthesis. *Bioorg. Med. Chem.* **2011**, 19, 6675–6701.

Talontsi, F. M.; Facey, P.; Tatong, M. D. K.; Islam, M. T.; Frauendorf, H.; Draeger, S.; von Tiedemann, A.; Laatsch, H. Zoosporicidal metabolites from an endophytic fungus *Cryptosporiopsis* sp. of *Zanthoxylum leprieurii*. *Phytochemistry* **2012**, 83, 87–94.

Tan, R. X.; Zou, W. X. Endophytes: a rich source of functional metabolites. *Nat. Prod. Rep.* **2001**, 18, 448–459.

- Tan, N.; Tao, Y.; Pan, J.; Wang, S.; Xu, F.; She, Z.; Lin, Y.; Jones, E. B. G. Isolation, structure elucidation, and mutagenicity of four alternariol derivatives produced by the mangrove endophytic fungus No. 2240. *Chem. Nat. Compd.* **2008**, *44*, 296–300.
- Tan, S. Y.; Tatumura, Y. Alexander Fleming (1881-1955): discover of penicillin. *Singapore Med. J.* **2015**, *56*, 366–367.
- Tantillo, D. J. Walking in the woods with quantum chemistry-applications of quantum chemical calculations in natural products research. *Nat. Prod. Rep.* **2013**, *30*, 1079–1086.
- Taylor, T. N.; Taylor, E. L. *The rhynie chert ecosystem: a model for understanding fungal interactions*. Editors: Bacon, C. W.; White, Jr. J. F. *Microbial Endophytes*, Marcel Decker Inc., New York, 2000, pp. 31–48.
- Togashi, H.; Mizushima, Y.; Takemura, M.; Sugawara, F.; Koshino, H.; Esumi, Y.; Uzawa, J.; Kumagai, H.; Matsukage, A.; Yoshida, S.; Sakaguchi, K. 4-Hydroxy-17-methylincisterol, an inhibitor of DNA polymerase- α activity and the growth of human cancer cells *in vitro*. *Biochem. Pharmacol.* **1998**, *56*, 583–590.
- Torok, E.; Moran, E.; Cooke, F. *Oxford handbook of infectious diseases and microbiology*. Oxford University Press, 2009.
- Turner, W. B.; Aldridge, D. C. *Fungal metabolites II*; Academic Press: London, **1983**, p. 279.
- Verma, V. C.; Gange, A. C. *Advances in endophytic research*. Springer, New Delhi, 2014.
- Walsh, C. T.; Wright, G. Eds. Introduction: antibiotic resistance. *Chem. Rev.* **2005**, *105*, 391–394.
- Wang, C.; Yang, Y.; Mei, Z.; Yang, X. Cytotoxic compounds from *Laminaria japonica*. *Chem. Nat. Compd.* **2013**, *49*, 699–701.
- Wang, P.; Wang, B.; Xu, J.; Sun, J.; Yan, Q.; Ji, B.; Zhao, Y.; Yu, Z. Detection and chemical profiling of Ling-Gui-Zhu-Gan decoction by ultra performance liquid chromatography-hybrid linear ion trap-orbitrap mass spectrometry. *J. Chromatogr. Sci.* **2015**, *53*, 263–273.
- Wang, W.-X.; Kusari, S.; Sezgin, S.; Lamshöft, M.; Kusari, P.; Kayser, O.; Spiteller, M. Hexacyclopeptides secreted by an endophytic fungus *Fusarium solani* N06 act as crosstalk molecules in *Narcissus tazetta*. *Appl. Microbiol. Biotechnol.* **2015**, *99*, 7651–7662.
- White, T. J.; Bruns, T. D.; Lee, S.; Taylor, J. W. In *Protocols: a guide to methods and applications*. PCR Academic Press: San Diego, 1990; pp 315–322.
- White, Jr. J. F.; Morgan-Jones, G.; Morrow, A. C. Taxonomy, life cycle, reproduction and detection of Acremonium endophytes. *Agric. Ecosyst. Environ.* **1993**, *44*, 13–37.

- Wikler, M. A. *Performance standards for antimicrobial disk susceptibility tests; approved standard, Ninthed. (M2-A9)*; CLSI: Wayne, PA, **2006**.
- World Health Organization (WHO). *Antimicrobial resistance: global report on surveillance*, published April 2014, available from: <http://www.who.int/drugresistance/documents/surveillancereport/en/>.
- Woodruff, H. B. Selman A. Waksman, winner of the 1952 Nobel Prize for physiology or medicine. *Appl. Environ. Microbiol.* **2014**, *80*, 2–8.
- Wright, G. D. The antibiotic resistome: the nexus of chemical and genetic diversity. *Nature Rev. Microbiol.* **2007**, *5*, 175–186.
- Wright, G. D.; Poinar, H. Antibiotic resistance is ancient: implications for drug discovery. *Trends Microbiol.* **2012**, *20*, 157–159.
- Xiong, H.-Y.; Fei, D.-Q.; Zhou, J.-S.; Yang, C.-J.; Ma, G.-L. Steroids and other constituents from the mushroom *Armillaria lueo-virens*. *Chem. Nat. Compd.* **2009**, *45*, 759–761.
- Xiong, J.; Li, S.; Wang, W.; Hong, Y.; Tang, K.; Luo, Q. Screening and identification of the antibacterial bioactive compounds from *Lonicera japonica* Thunb. Leaves. *Food. Chem.* **2013**, *138*, 327–333.
- Xu, J.; Kjer, J.; Sendker, J.; Wray, V.; Guan, H.; Edrada, R.; Lin, W.; Wu, J.; Proksch, P. Chromones from the endophytic fungus *Pestalotiopsis* sp. isolated from the Chinese mangrove plant *Rhizophora mucronata*. *J. Nat. Prod.* **2009**, *72*, 662–665.
- Yamada, T.; Mizutani, Y.; Umebayashi, Y.; Inno, N.; Kawashima, M.; Kikuchi, T.; Tanaka, R. Tandyukisin, a novel ketoaldehyde decalin derivative, produced by a marine sponge-derived *Trichoderma harzianum*. *Tetrahedron Lett.* **2014**, *55*, 662–664.
- Yaoita, Y.; Amemiya, K.; Ohnuma, H.; Furumura, K.; Masaki, A.; Matsuki, T.; Kikuchi, M. Sterol constituents from five edible mushrooms. *Chem. Pharm. Bull.* **1998**, *46*, 944–950.
- Yu, Y.; Song, W.; Zhu, C.; Lin, S.; Zhao, F.; Wu, X.; Yue, Z.; Liu, B.; Wang, S.; Yuan, S.; Hou, Q.; Shi, J., Homosecoiridoids from the flower buds of *Lonicera japonica*. *J. Nat. Prod.* **2011**, *74*, 2151–60.
- Yusoo, S.; Yutaka, T.; Minoru, T. Triterpenoids, steroids, and a new sesquiterpene from *Inonotus obliquus* (Pers.: Fr.) Pilat. *Int. J. Med. Mushr.* **2002**, *4*, 77–84.
- Zhang, H. W.; Song, Y. C.; Tan, R. X. Biology and chemistry of endophytes. *Nat. Prod. Rep.* **2006**, *23*, 753–771.
- Zhang, X. Q.; Ye, W. C.; Jiang, R. W.; Yin, Z. Q.; Zhao, S. X.; Mak, T. C. W.; Yao, X. S. Two new eremophilanolides from *Xanthium sibiricum*. *Nat. Prod. Res.* **2006**, *20*, 1265–1270.

Zhang, H.; Timmermann, B. N. Withanolide structural revisions by ^{13}C NMR spectroscopic analysis inclusive of the α -gauche effect. *J. Nat. Prod.* **2016**, DOI: 10.1021/acs.jnatprod.5b00648.

Zhao, J.; Mou, Y.; Shan, T.; Li, Y.; Zhou, L.; Wang, M.; Wang, J. Antimicrobial metabolites from the endophytic fungus *Pichia guilliermondii* isolated from *Paris polyphylla* var. *yunnanensis*. *Molecules* **2010**, *15*, 7961–7970.

Appendix A
MS and NMR spectra, and additional figures

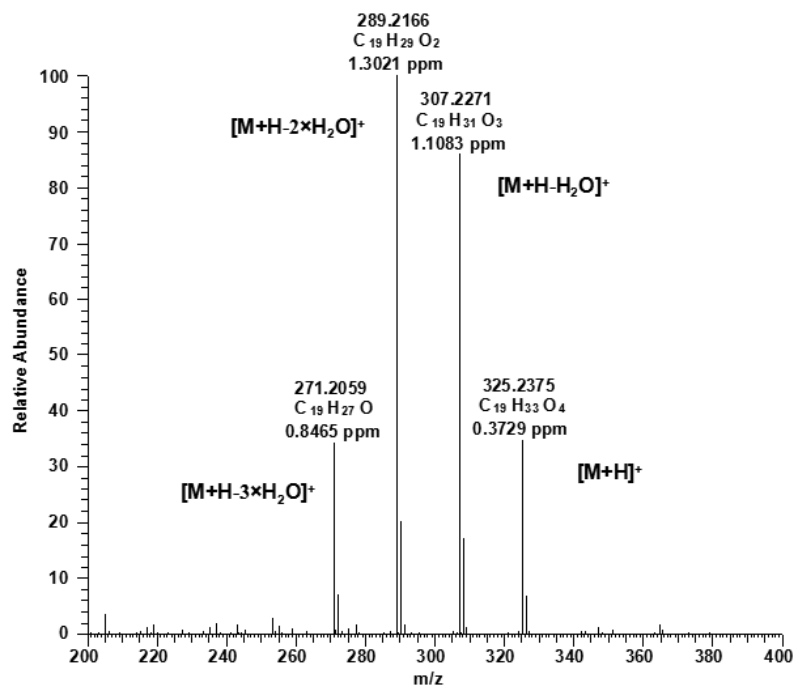


Figure 4.1.1.1 Positive ESI-HRMS spectrum of compound 1.

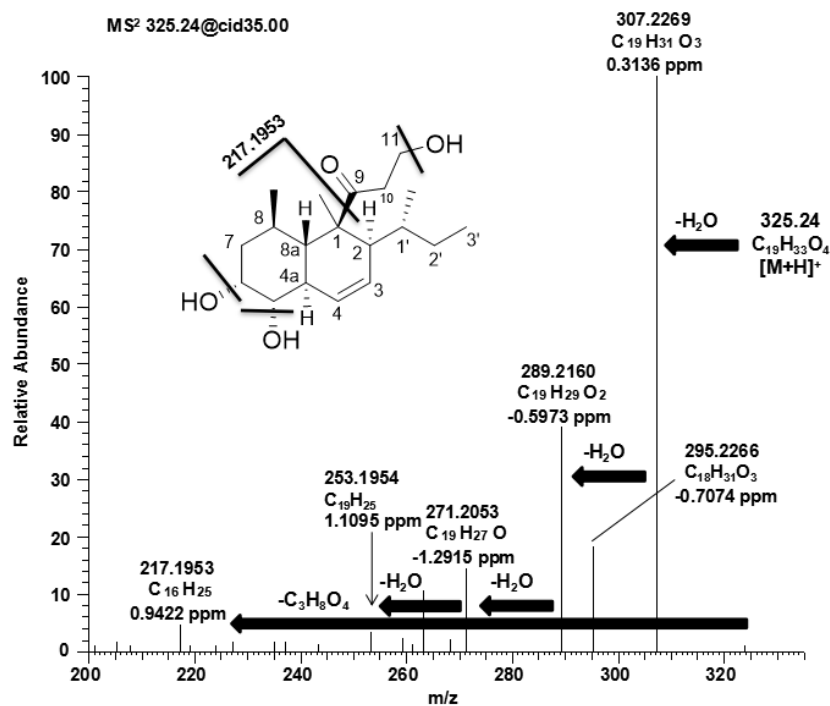


Figure 4.1.1.2 Positive ESI-HRMS/MS spectrum of compound 1.

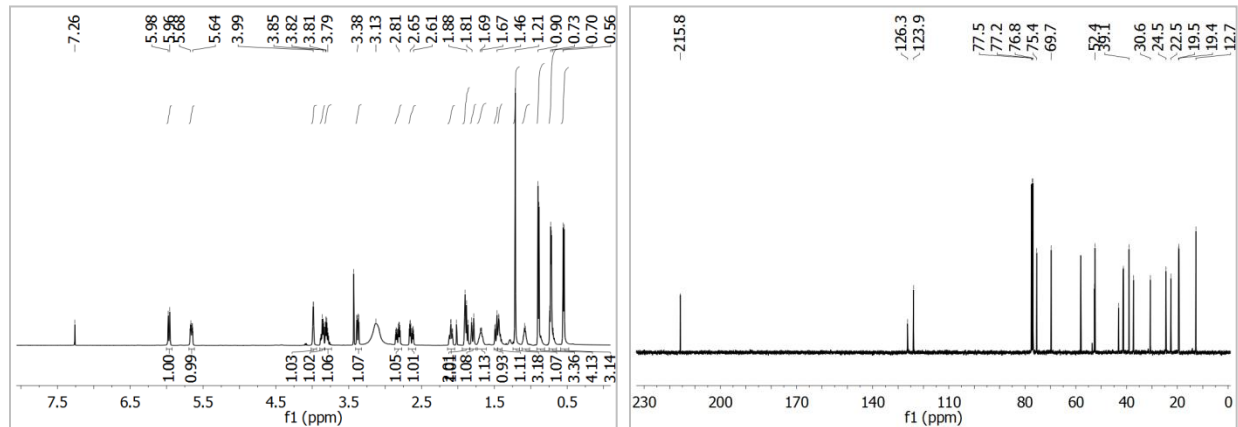


Figure 4.1.1.3 ¹H (left) and ¹³C (right) NMR spectra of compound 1 in CDCl₃.

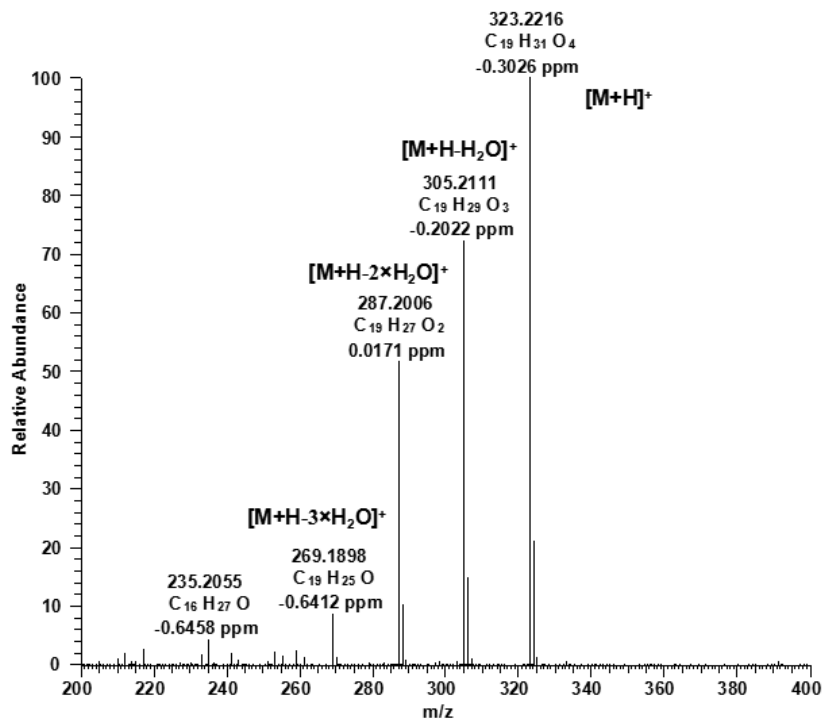


Figure 4.1.2.1 Positive ESI-HRMS spectrum of compound 2.

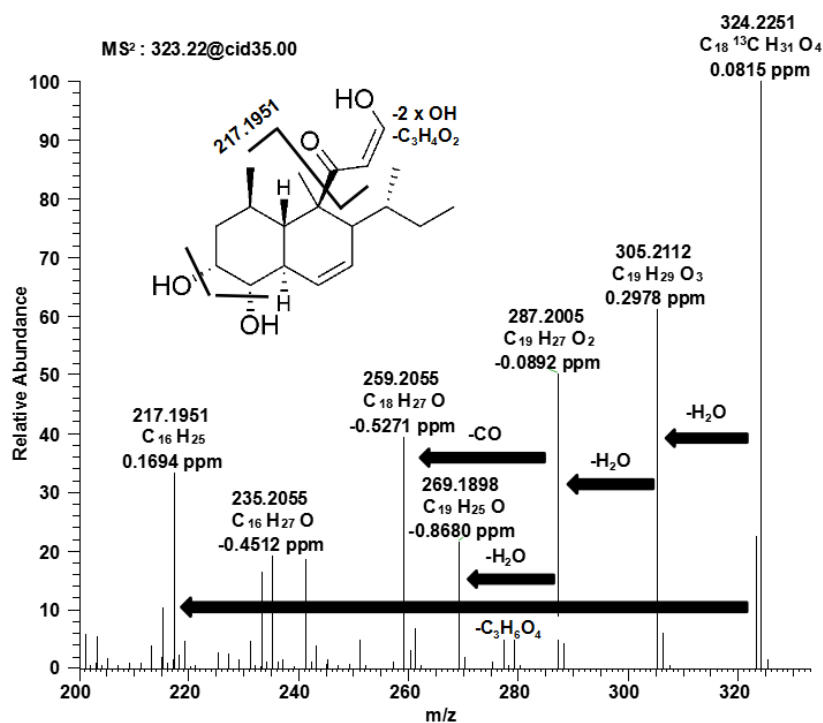


Figure 4.1.2.2 Positive ESI-HRMS/MS spectrum of compound 2.

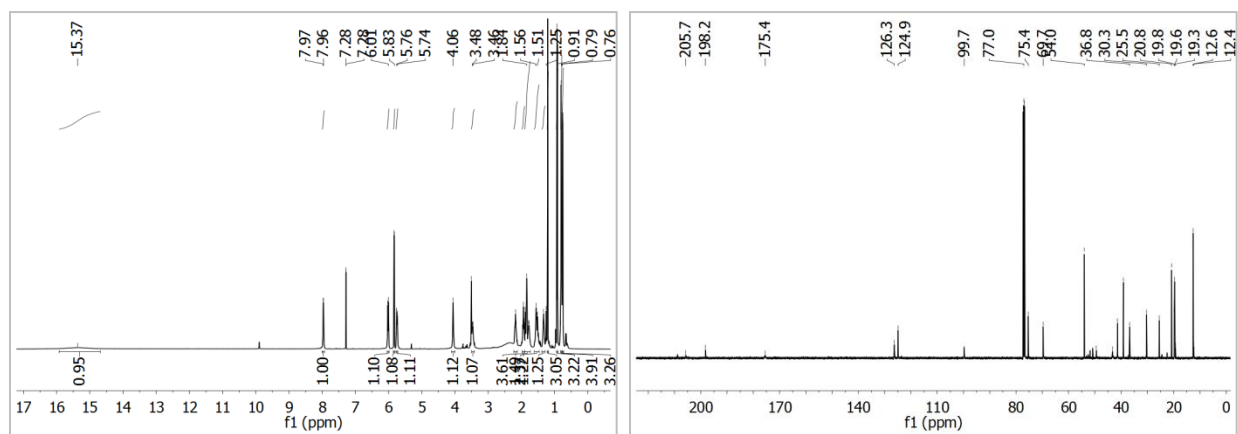


Figure 4.1.2.3 ¹H (left) and ¹³C (right) NMR spectra of compound 2 in CDCl₃.

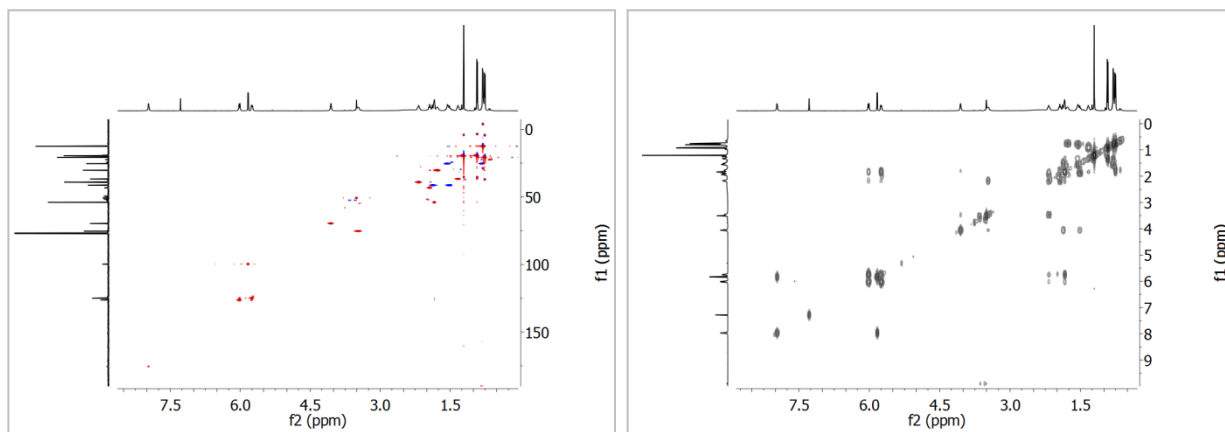


Figure 4.1.2.4 HSQC (left) and ¹H-¹H COSY (right) NMR spectra of compound **2** in CDCl₃.

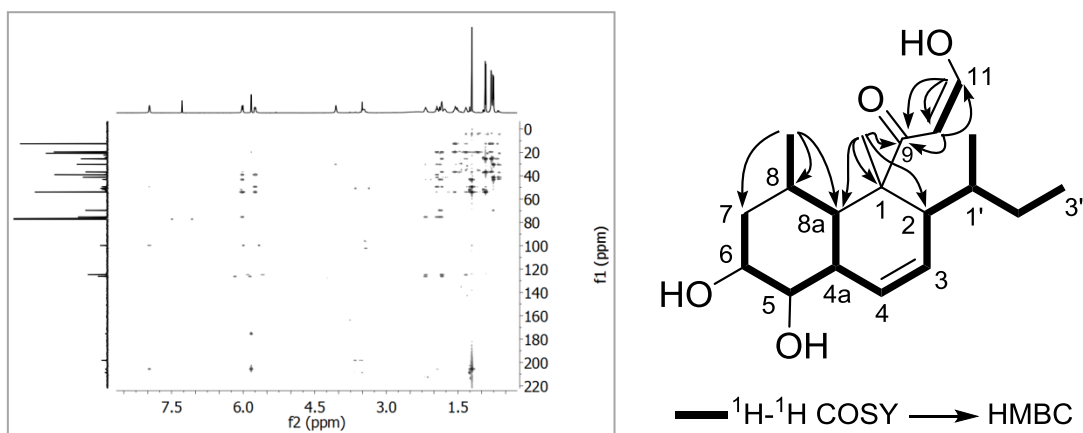


Figure 4.1.2.5 HMBC spectrum (left) and key ¹H-¹H COSY and HMBC correlations (right) of **2**.

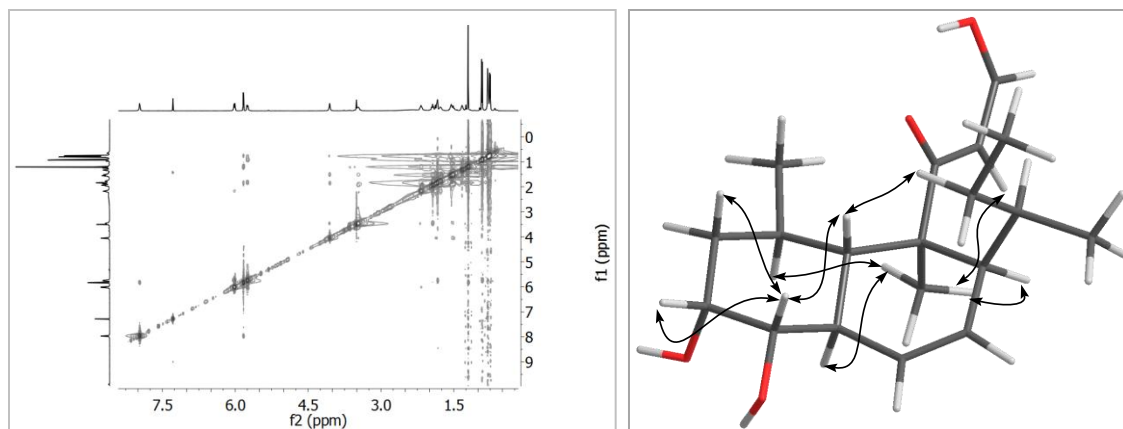


Figure 4.1.2.6 NOESY spectrum (left) and key NOESY correlations (right) of **2** in CDCl₃.

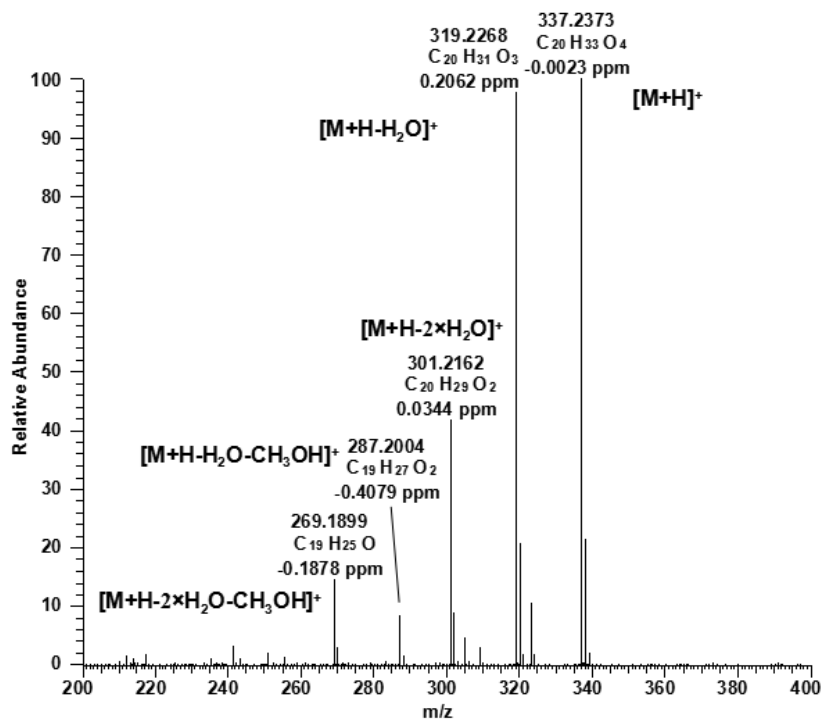


Figure 4.1.3.1 Positive ESI-HRMS spectrum of compound 3.

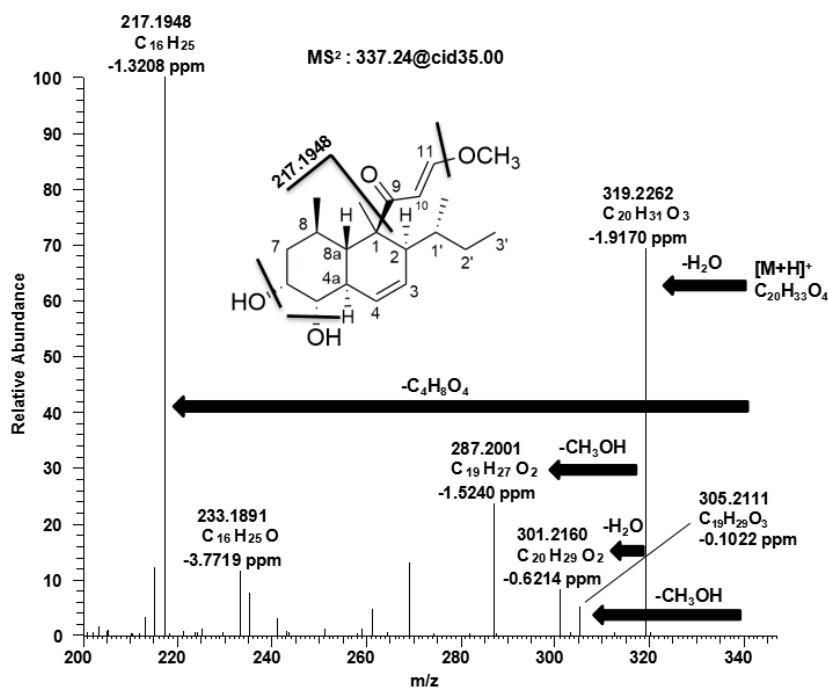


Figure 4.1.3.2 Positive ESI-HRMS/MS spectrum of compound 3.

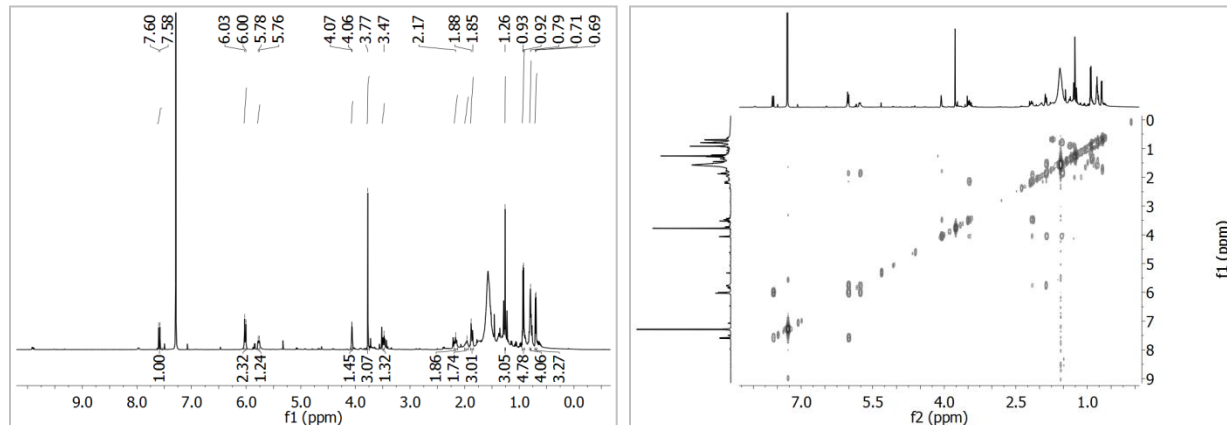


Figure 4.1.3.3 ^1H (left) and ^1H - ^1H COSY (right) NMR spectra of compound **3** in CDCl_3 .

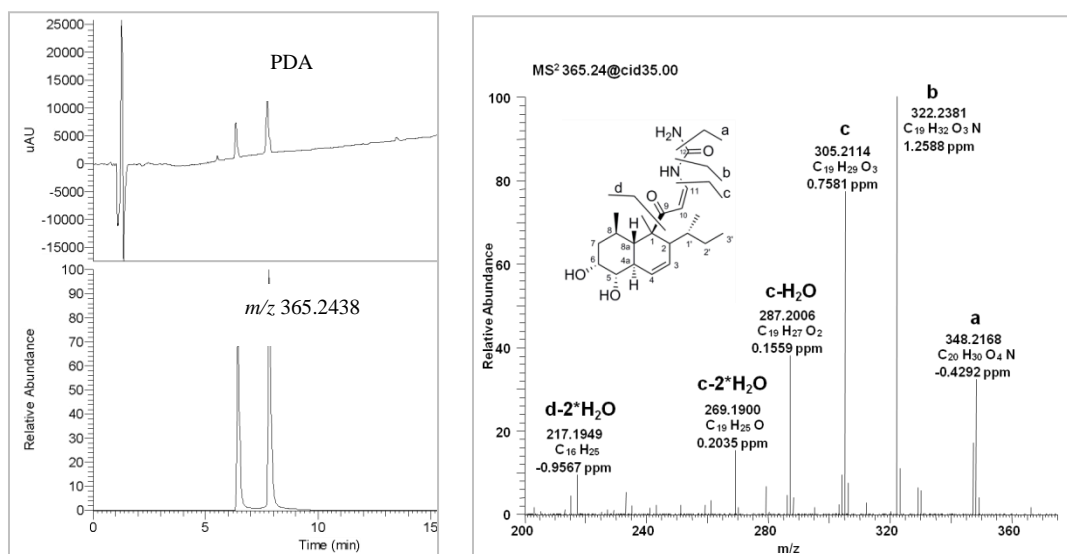


Figure 4.1.4.1 The LC-MS chromatogram (left, m/z 365.2438) of **4** and positive MS/MS spectrum (right) of **4**. The a-d indicated the proposed position of cleavage and the corresponding fragment ions.

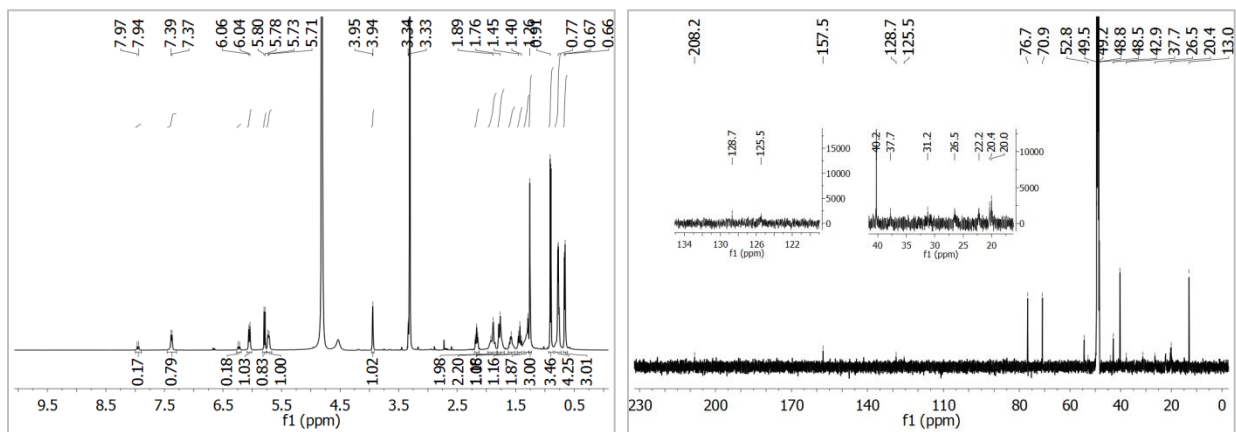


Figure 4.1.4.2 ^1H (left) and ^{13}C (right) NMR spectra of compound **4** in CD_3OD .

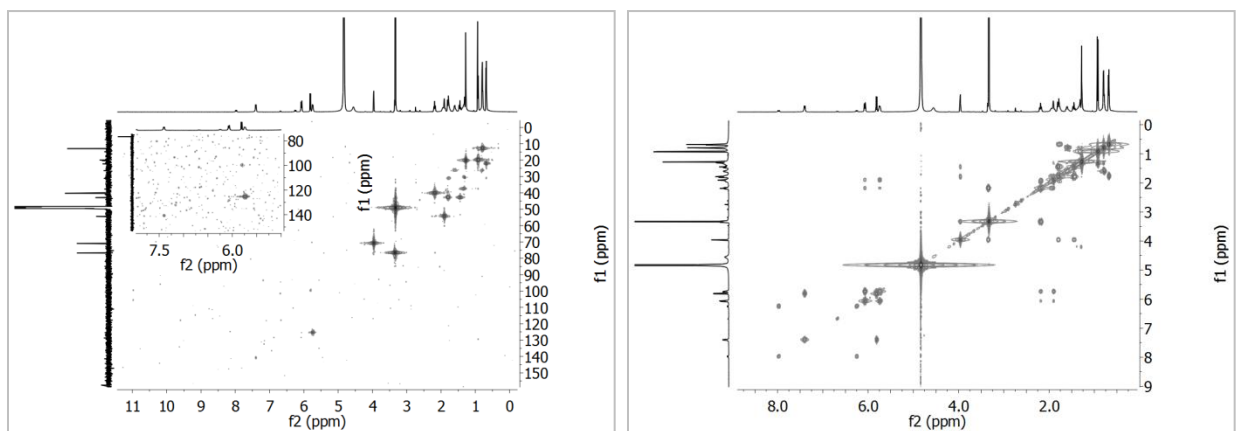


Figure 4.1.4.3 HSQC (left) and ^1H - ^1H COSY (right) NMR spectra of compound **4** in CD_3OD .

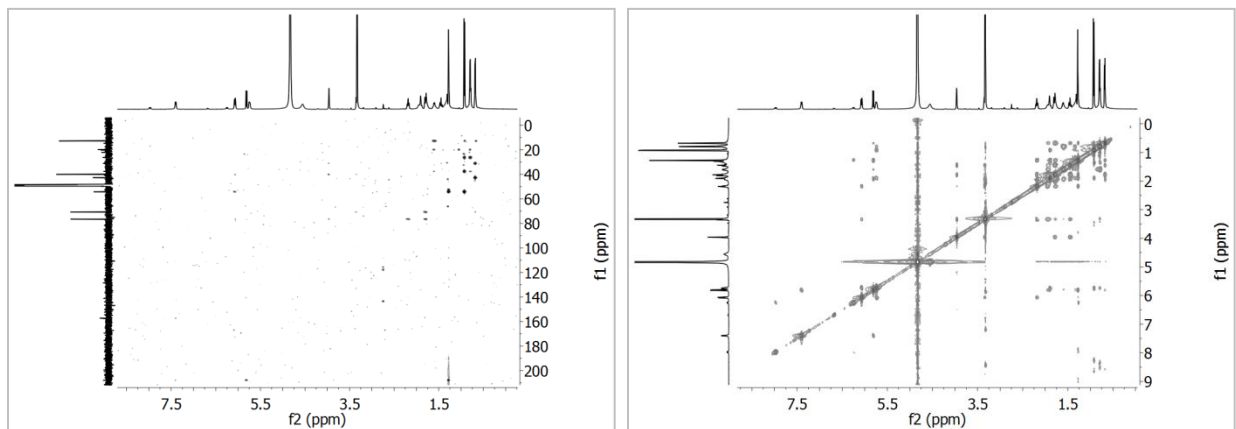


Figure 4.1.4.4 HMBC (left) and NOESY (right) NMR spectra of compound **4** in CD_3OD .

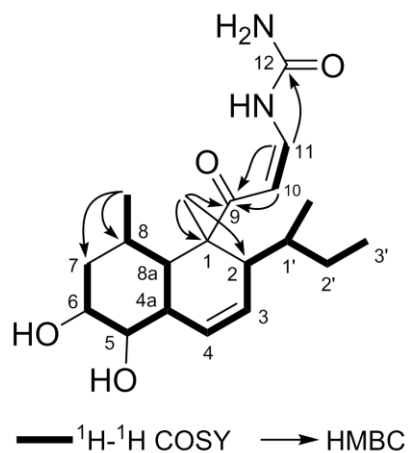


Figure 4.1.4.5 Key ¹H-¹H COSY and HMBC correlations of **4**.

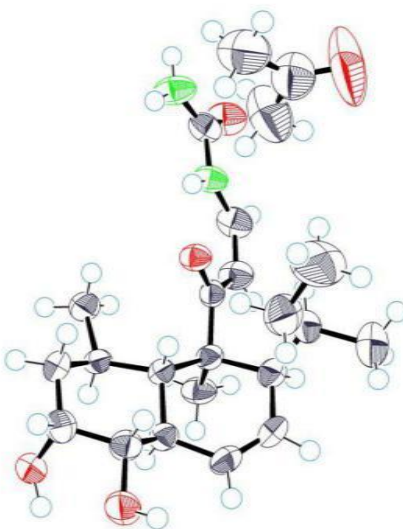


Figure 4.1.4.6 ORTEP drawing of **4**.

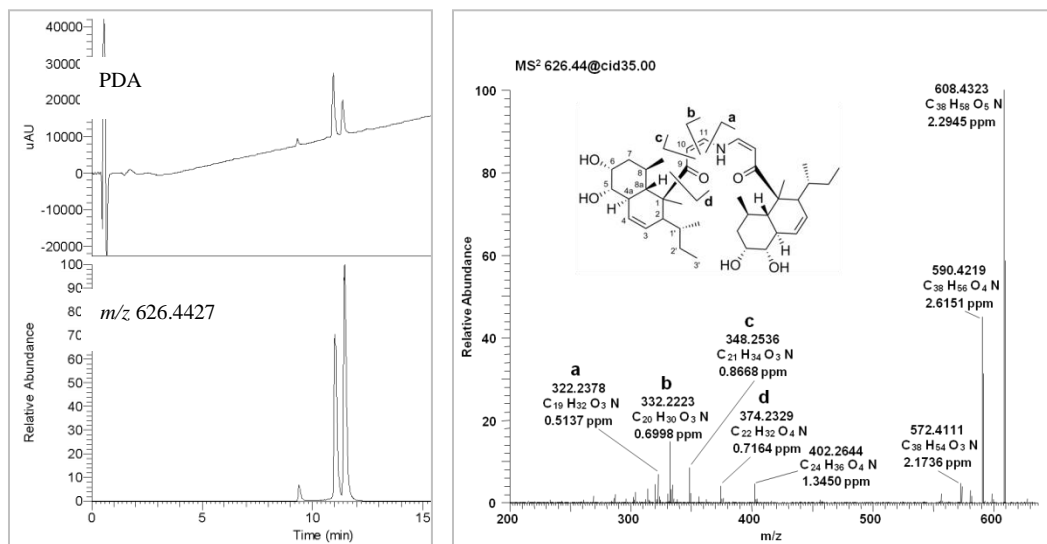


Figure 4.1.5.1 The LC-MS chromatogram (left, m/z 626.4427) of **5** and positive MS/MS spectrum (right) of **5**. The a-d indicated the proposed position of cleavage and the corresponding fragment ions.

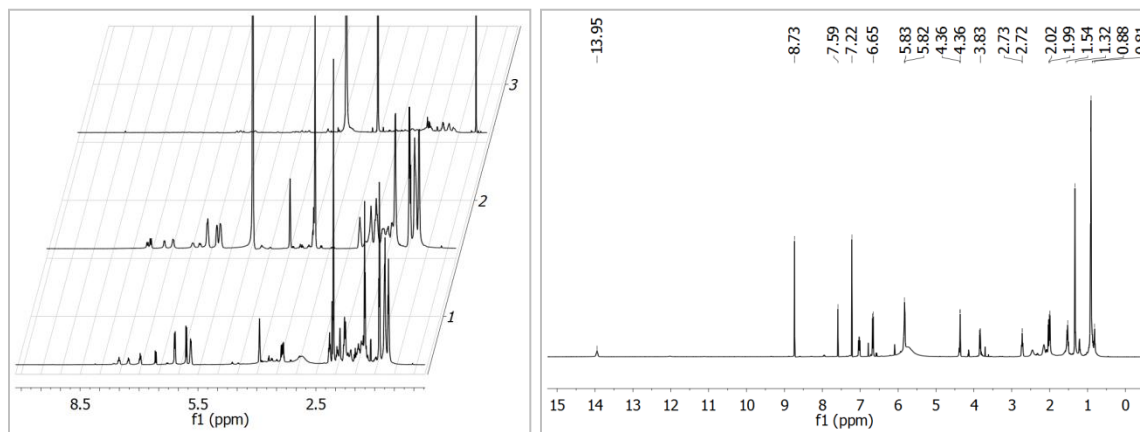


Figure 4.1.5.2 The comparison for ^1H NMR spectra in acetone- d_6 , CD_3OD , and $\text{DMSO}-d_6$ (left), as well as the ^1H NMR spectrum in pyridine- d_5 (right).

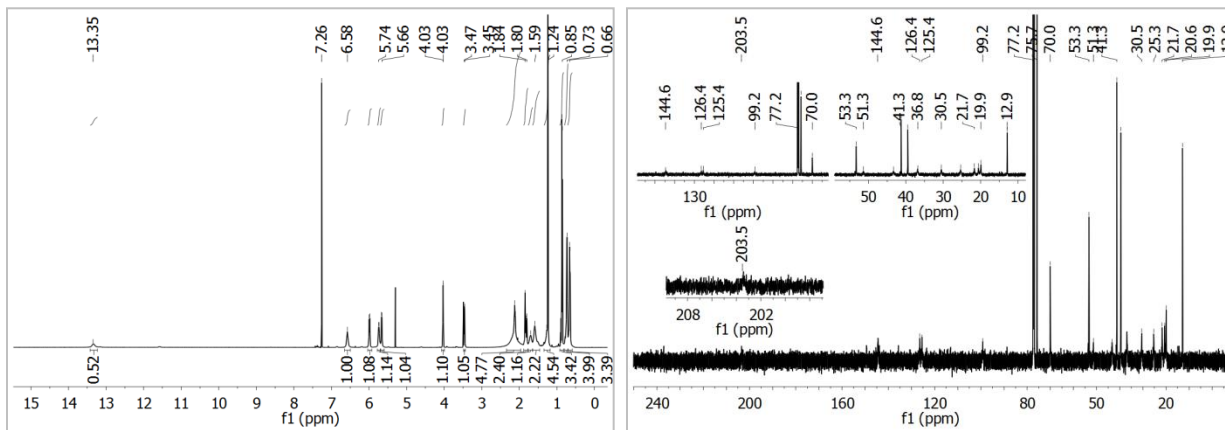


Figure 4.1.5.3 ^1H (left) and ^{13}C (right) NMR spectra (in CDCl_3) of compound **5**.

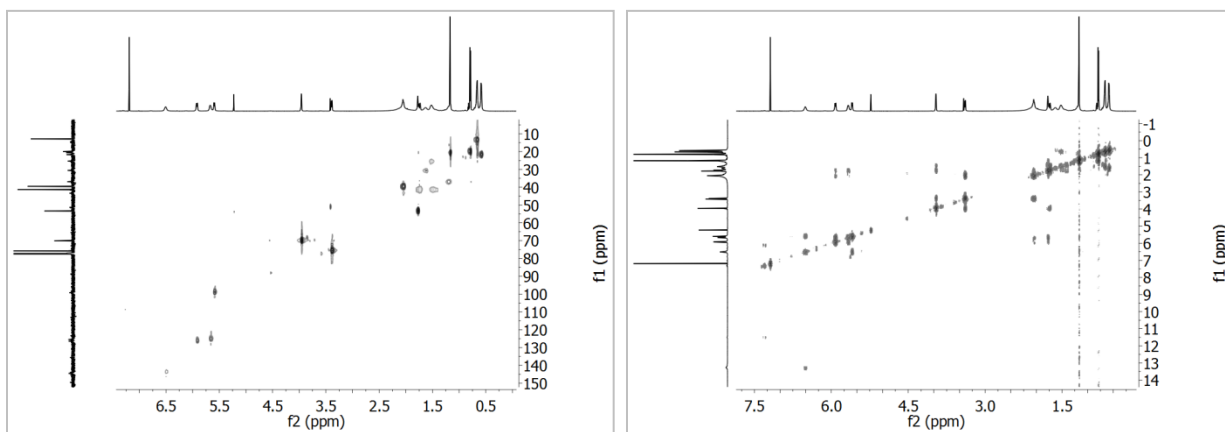


Figure 4.1.5.4 HSQC (left) and ^1H - ^1H COSY (right) NMR spectra of compound **5** in CDCl_3 .

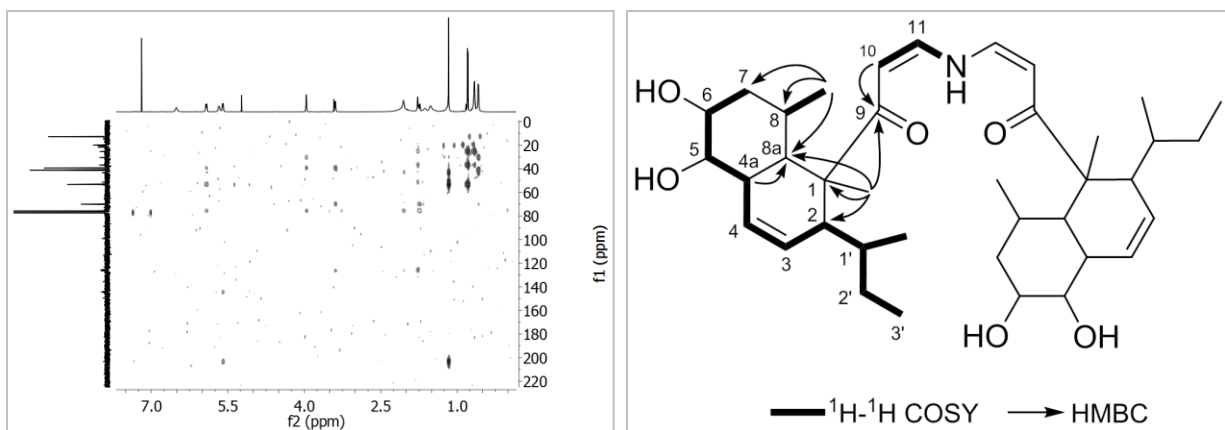


Figure 4.1.5.5 HMBC (left) and key ^1H - ^1H COSY and HMBC correlations (right) of **5**.

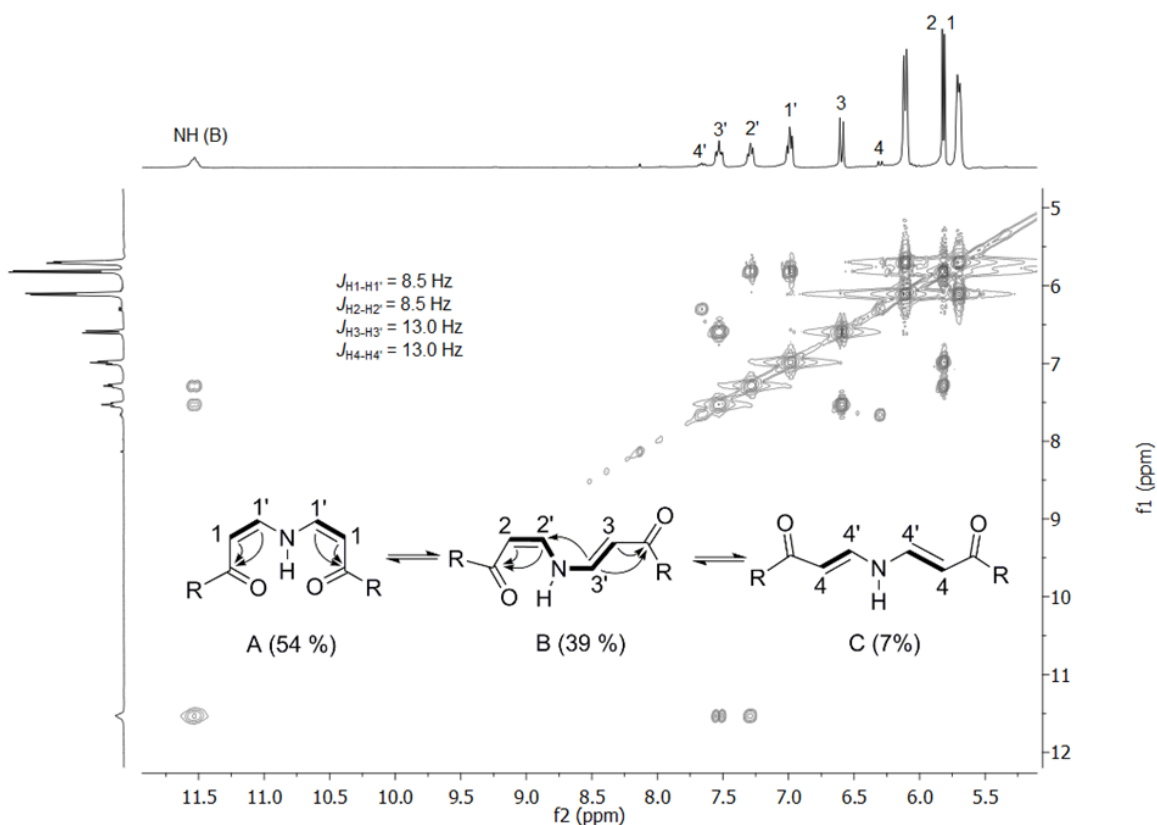


Figure 4.1.5.6 The partial ^1H - ^1H COSY spectrum (in acetone- d_6) of **5**. The coupling constants of protons at double bonds are included. Observed ^1H - ^1H COSY correlations (bold) and key HMBC correlations (arrow) are shown in the structures of three isomers (structures A, B and C in a kinetic equilibrium).

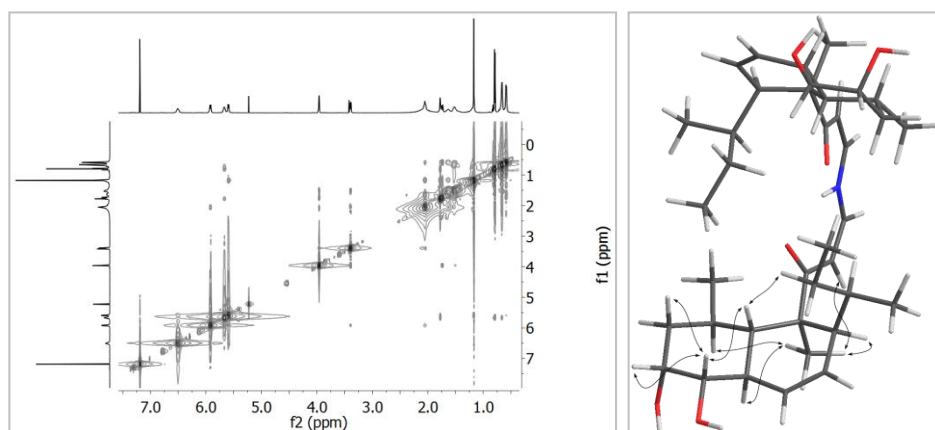
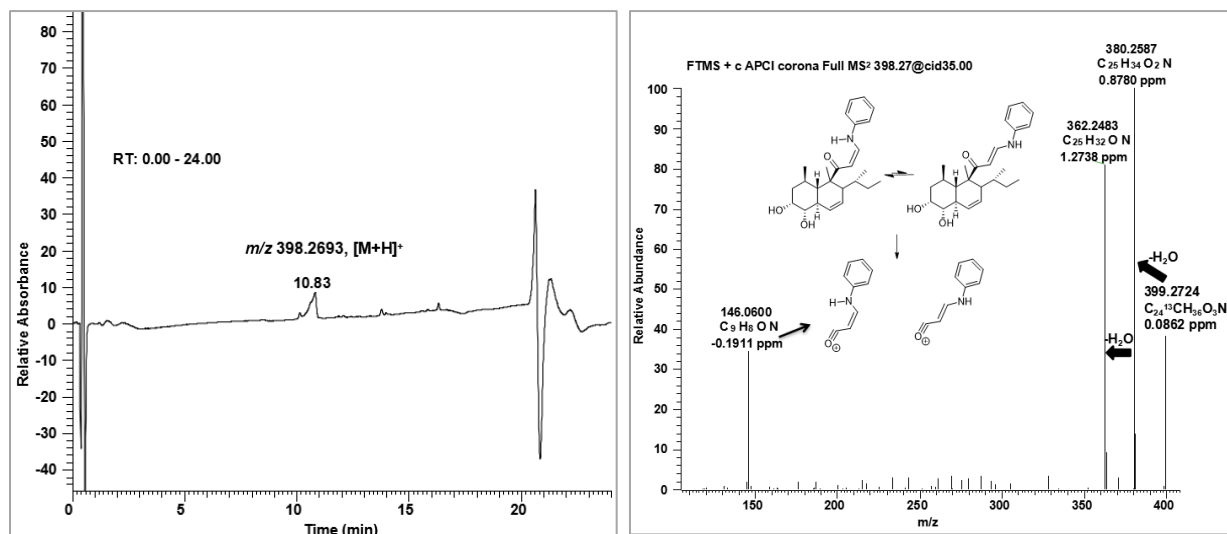
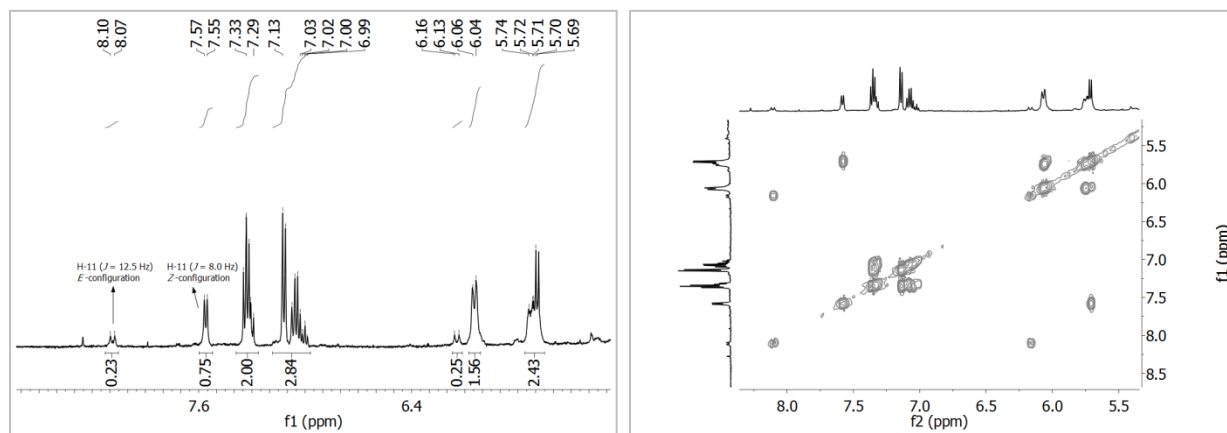


Figure 4.1.5.7 NOESY (left) spectrum and key NOESY correlations (right) of **5**.**Figure 4.1.6.1** The LC-MS chromatogram (left) and positive APCI-MS/MS spectrum (right) of **6**.**Figure 4.1.6.2** The partial 1H NMR spectrum (in CD_3OD) (left) and partial 1H - 1H COSY (in CD_3OD) (right) NMR spectra of compound **6**.

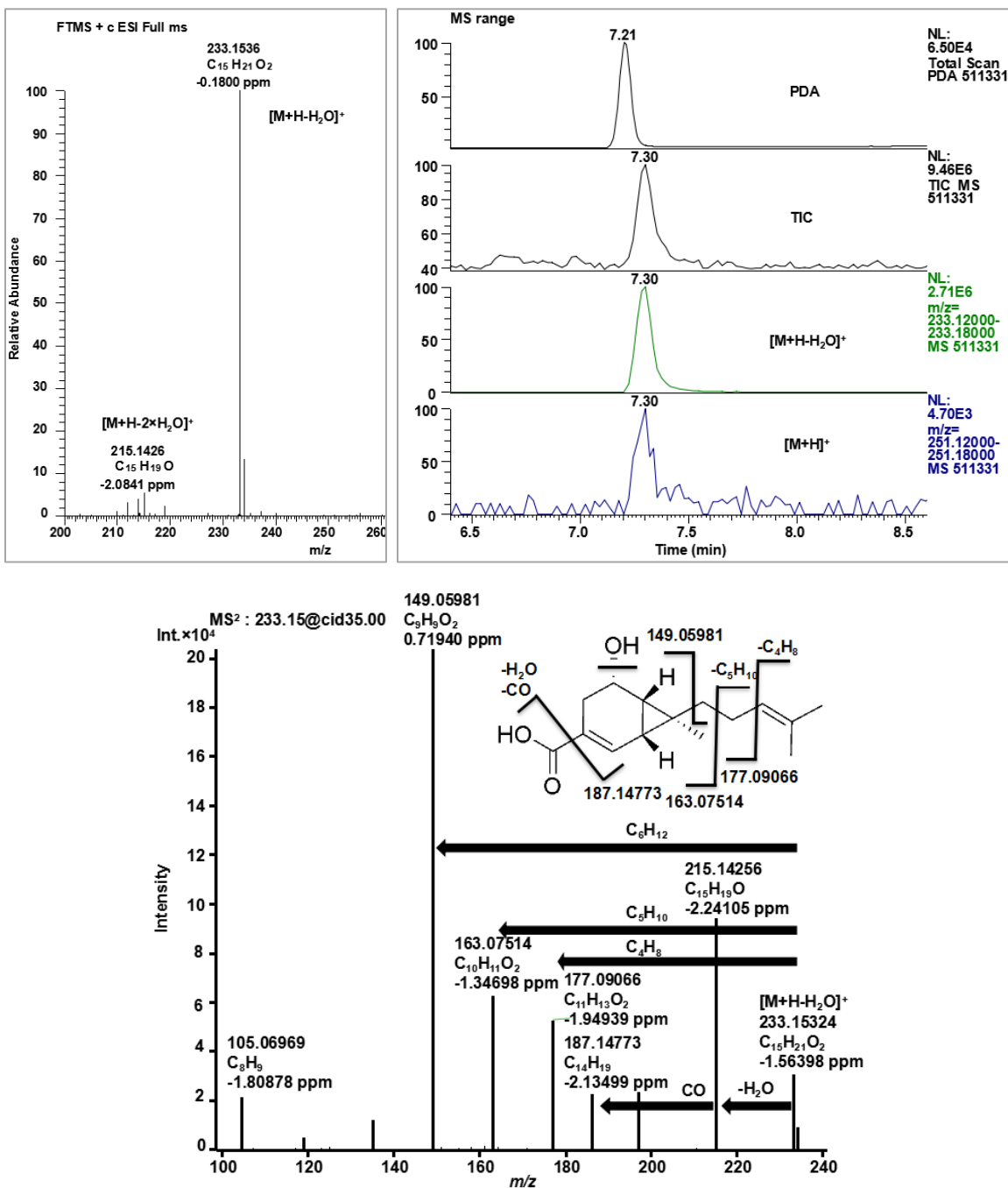


Figure 4.1.7.1 Positive ESI-HRMS (top) and MS/MS (bottom) spectra of 7.

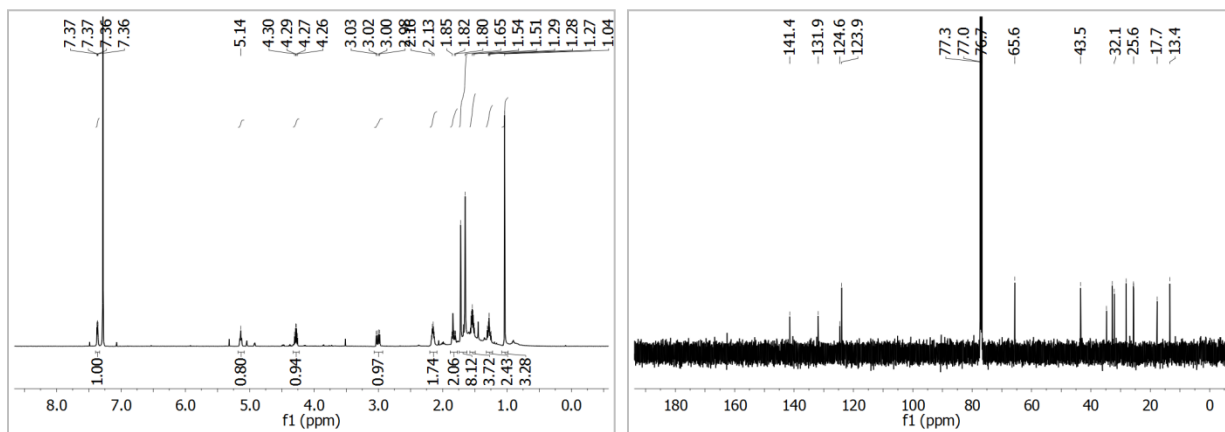


Figure 4.1.7.2 ^1H (left) and ^{13}C (right) NMR spectra (in CDCl_3) of compound 7.

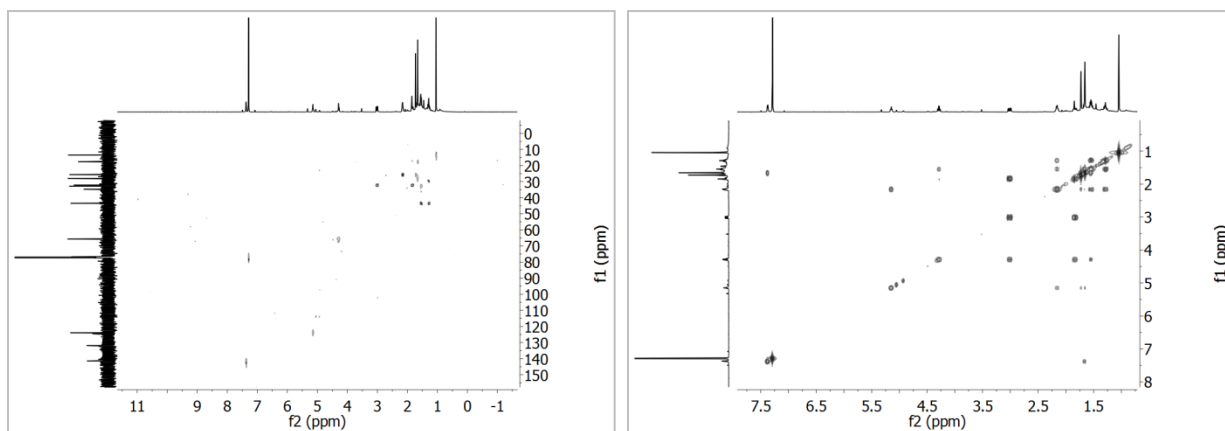


Figure 4.1.7.3 HSQC (left) and ^1H - ^1H COSY (right) NMR spectra of compound 7 in CDCl_3 .

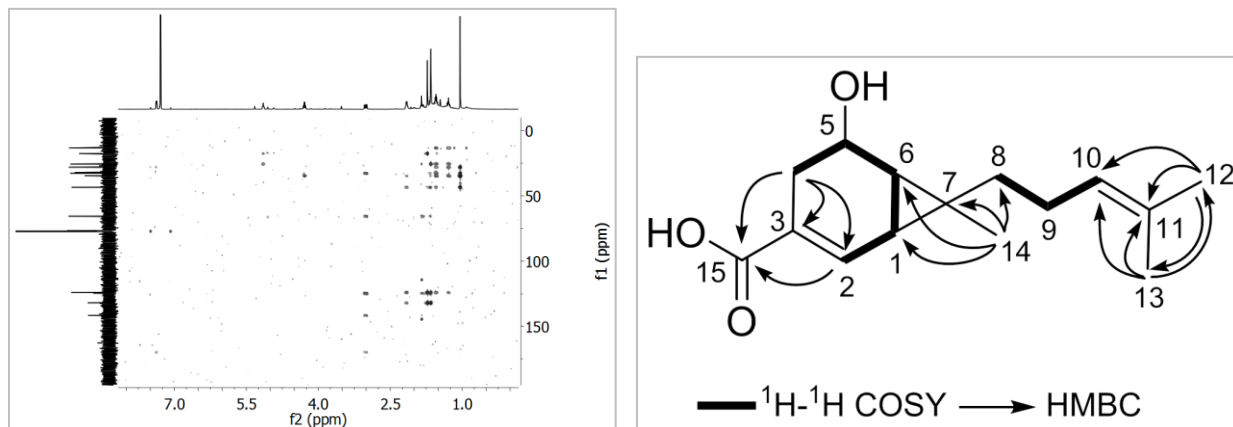


Figure 4.1.7.4 HMBC spectrum (left) and key ^1H - ^1H COSY and HMBC correlations (right) of 7.

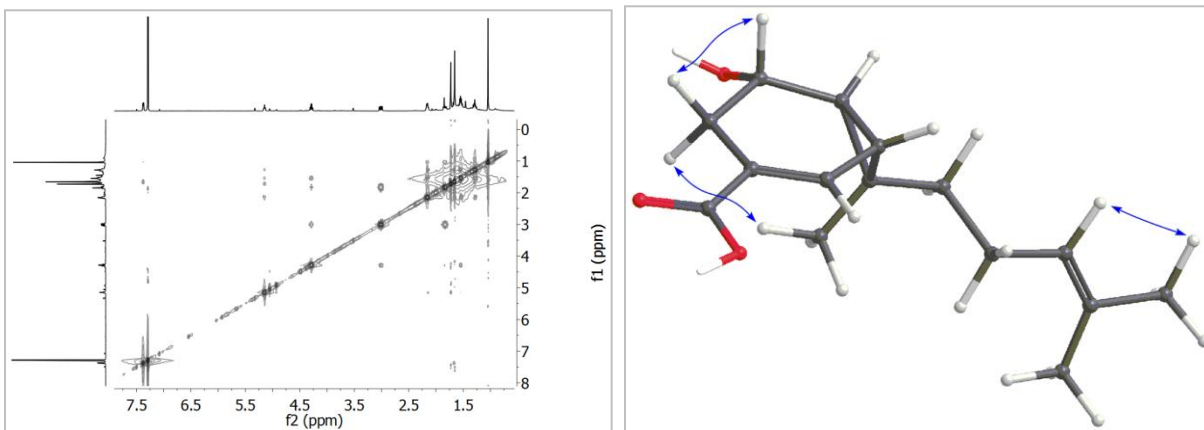


Figure 4.1.7.5 NOESY (left) spectrum and key NOESY correlations (right) of **7**.

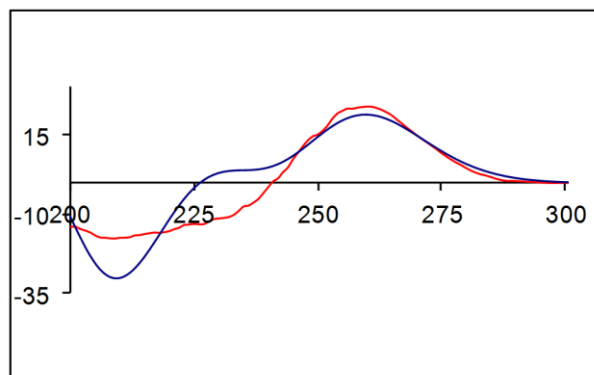
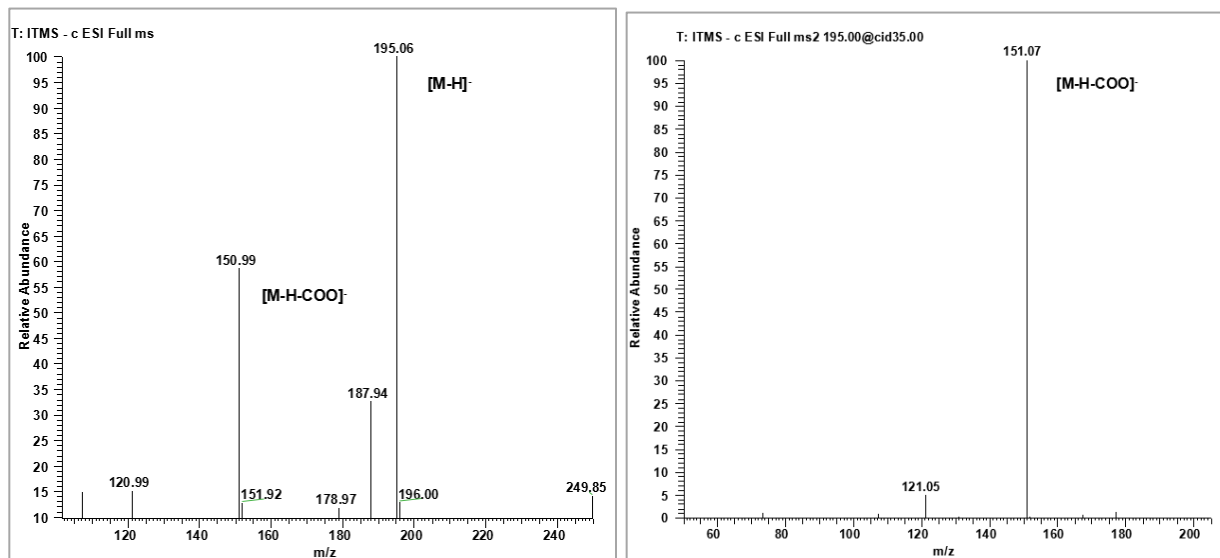


Figure 4.1.7.6 Experimental (red) and calculated (blue) ECD curves of **7**.



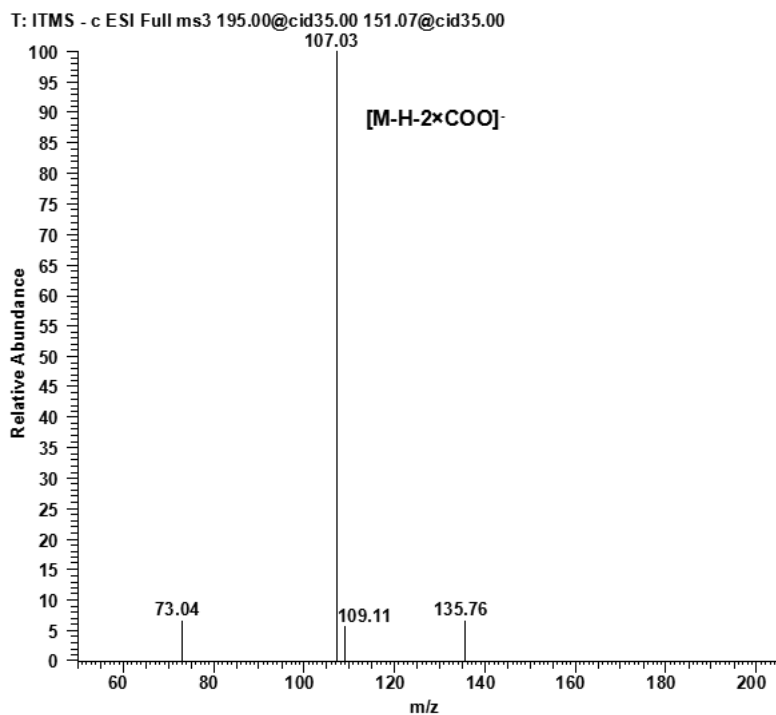


Figure 4.1.8.1 The ESIMS, MS/MS and MS³ spectra in negative mode of **8**.

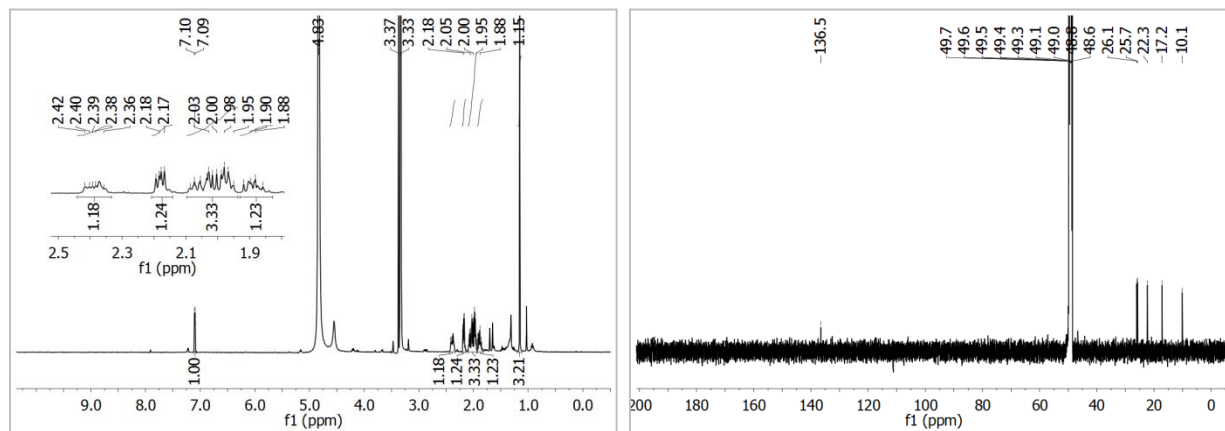


Figure 4.1.8.2 ¹H (left) and ¹³C (right) NMR spectra (in CD₃OD) of compound **8**.

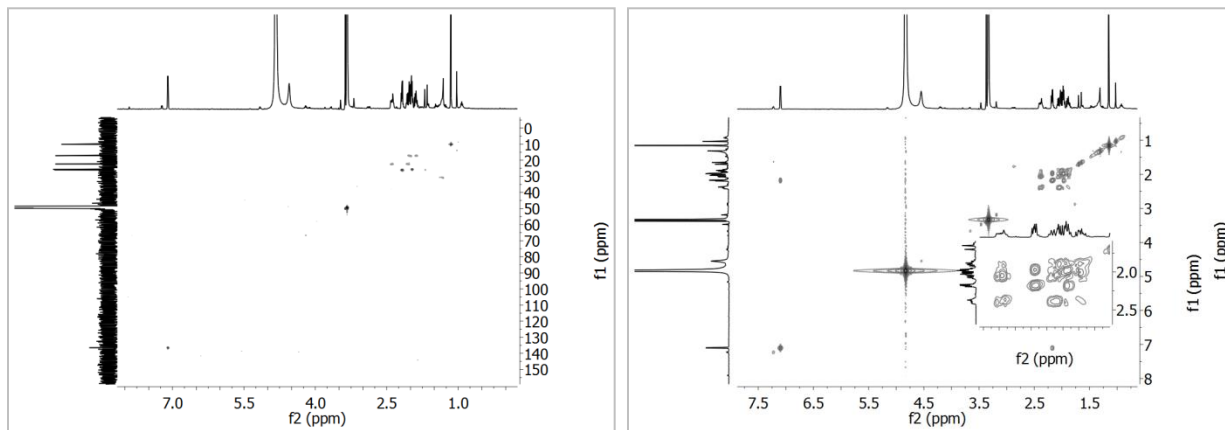


Figure 4.1.8.3 HSQC (left) and ¹H-¹H COSY (right) NMR spectra of compound 8 in CD₃OD.

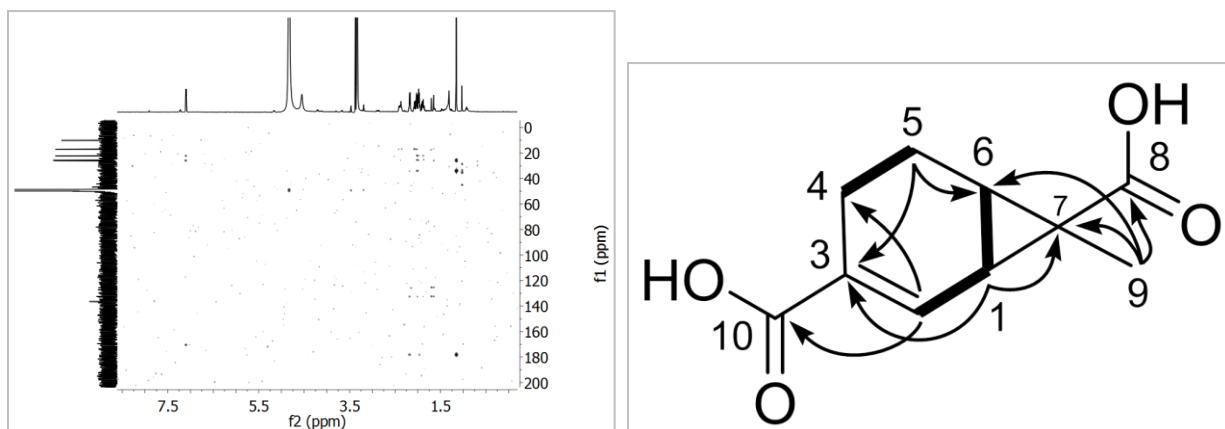


Figure 4.1.8.4 HMBC (left) spectrum and key ¹H-¹H COSY and HMBC correlations (right) of 8.

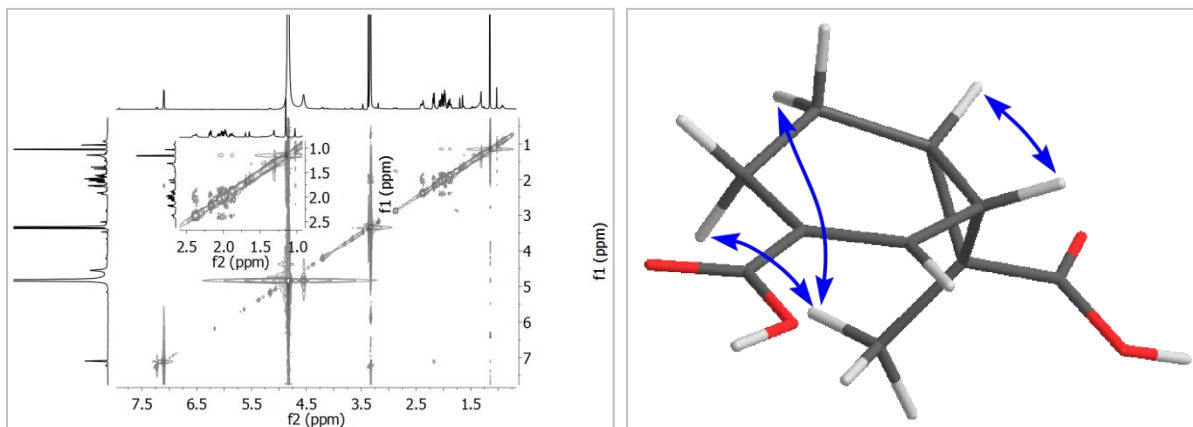


Figure 4.1.8.5 NOESY (left) spectrum and key NOESY correlations (right) of 8.

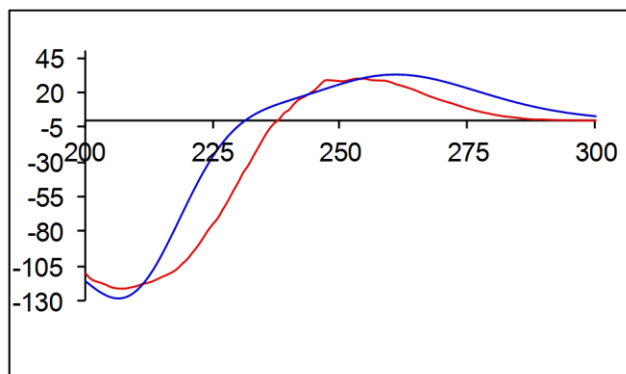


Figure 4.1.8.6 Experimental (red) and calculated (blue) ECD curves of eupenicisirenin B (**8**).

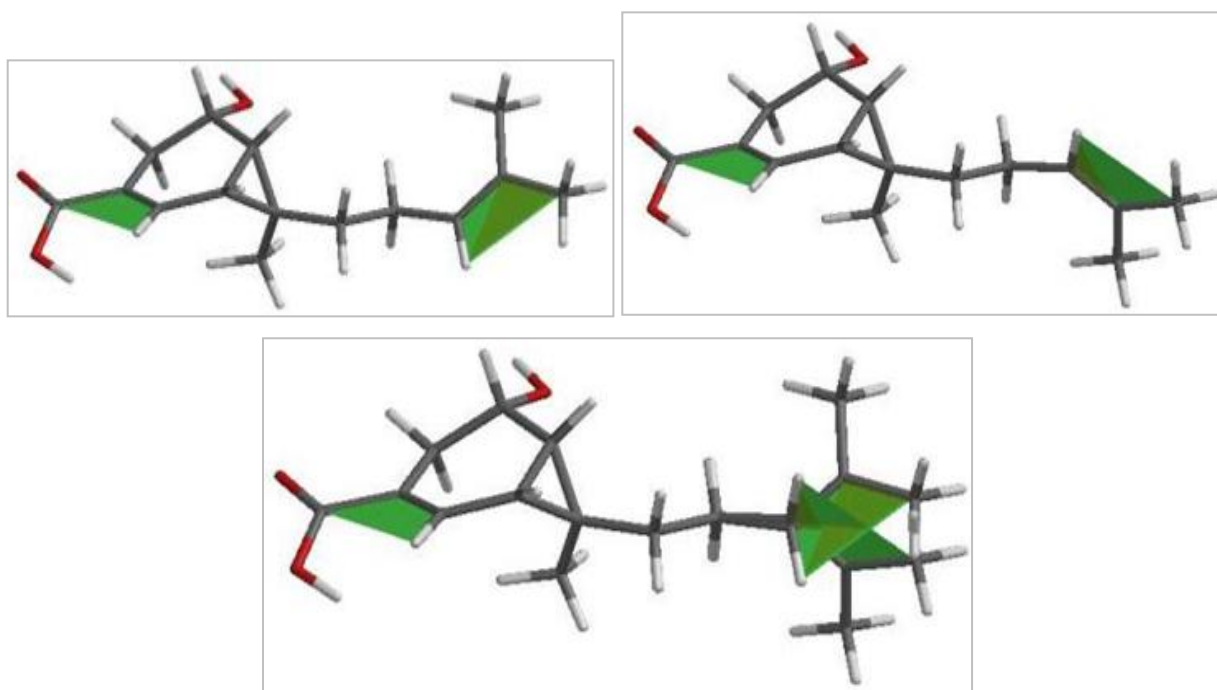


Figure 4.1.8.7 Fitting of conformer 65 (top left) with the highest positive and of 66 (top right) with the highest negative Boltzmann-weighted contribution to the calculated optical rotation of eupenicisirenin A (**7**). The green areas in the aligned structures (bottom) are marking the double bond planes; they cut each other in the side chain at an angle of 60° .

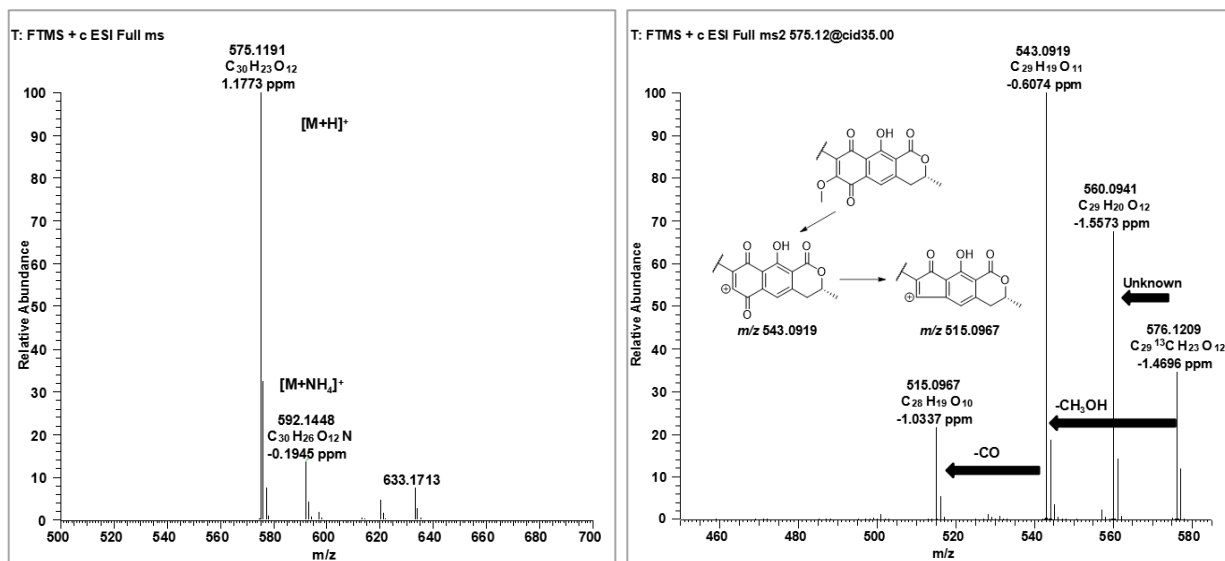


Figure 4.1.9.1 Positive ESI-HRMS (left) and MS/MS (right) spectra of compound **9**.

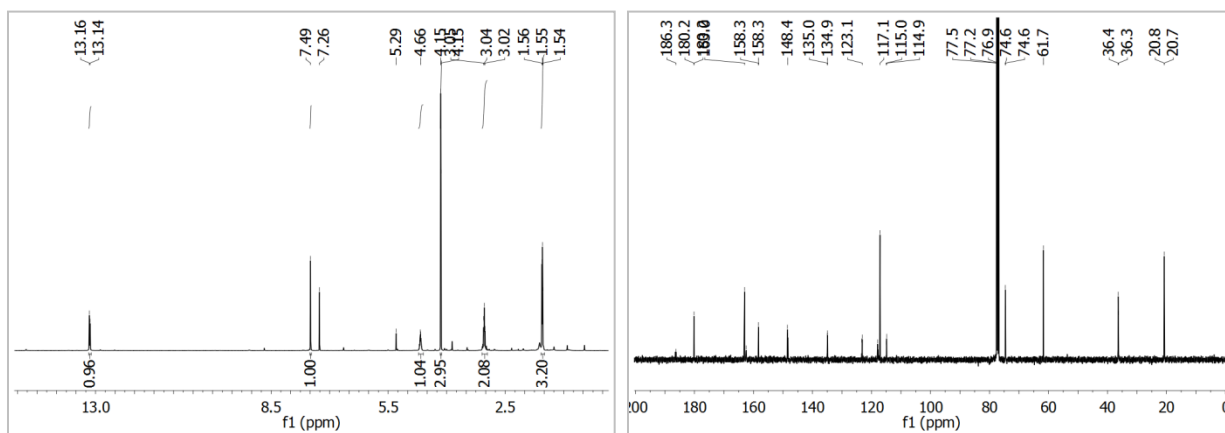


Figure 4.1.9.2 1H (left) and ^{13}C (right) NMR spectra (in $CDCl_3$) of compound **9**.

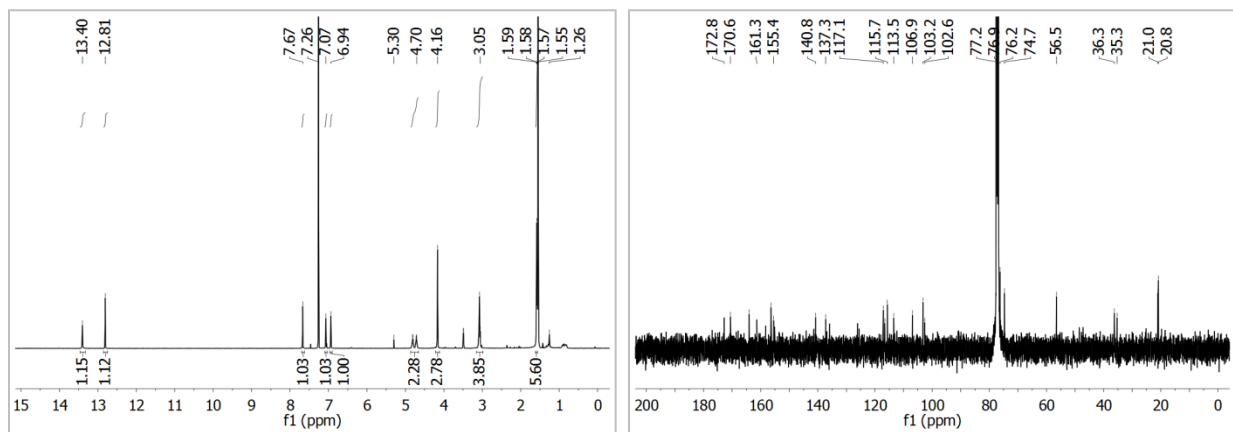


Figure 4.1.10.1 ^1H (left) and ^{13}C (right) NMR spectra (in CDCl_3) of compound **10**.

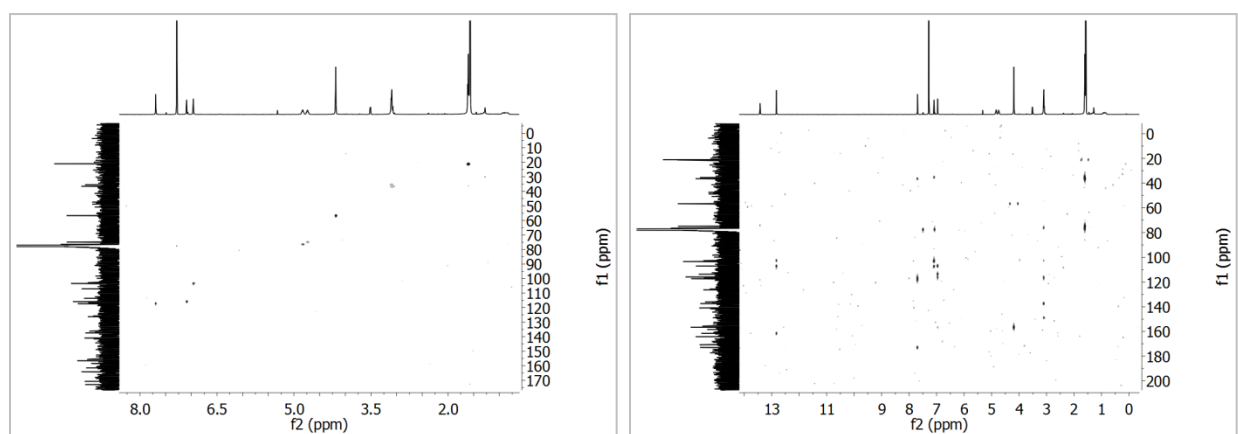


Figure 4.1.10.2 HSQC (left) and HMBC (right) NMR spectra (in CDCl_3) of compound **10**.

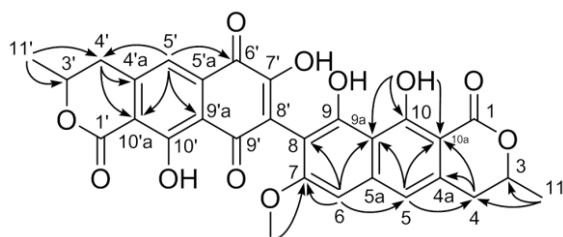


Figure 4.1.10.3 Key HMBC correlations of **10**.

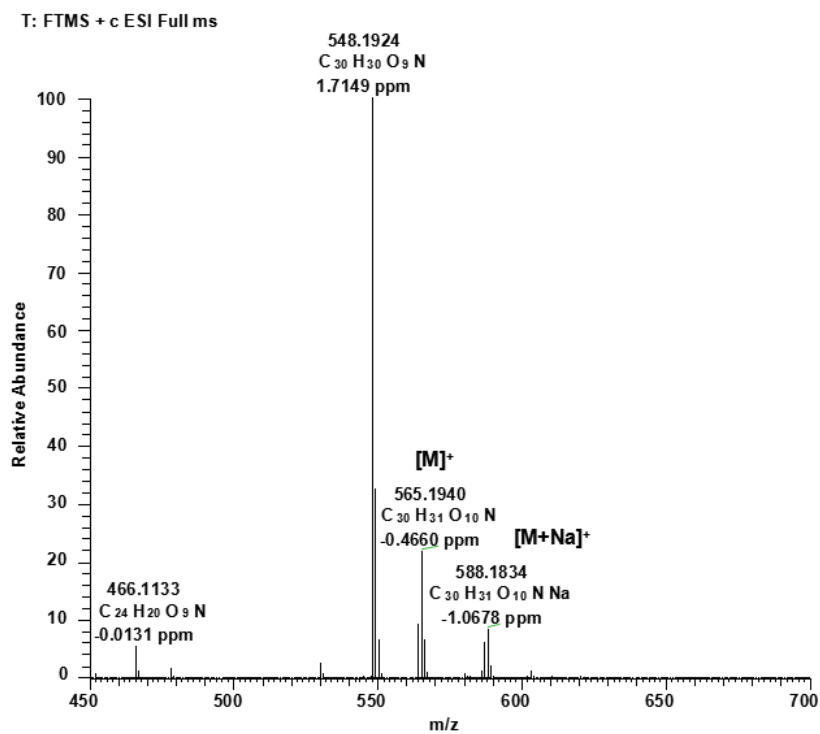


Figure 4.1.11.1 Positive ESI-HRMS spectrum of compound 11.

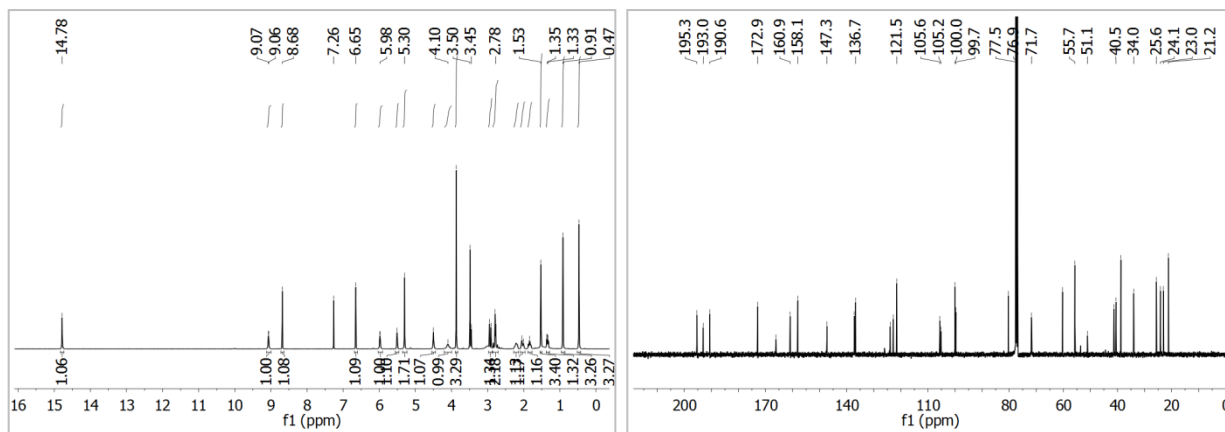


Figure 4.1.11.2 ¹H (left) and ¹³C (right) NMR spectra (in CDCl₃) of compound 11.

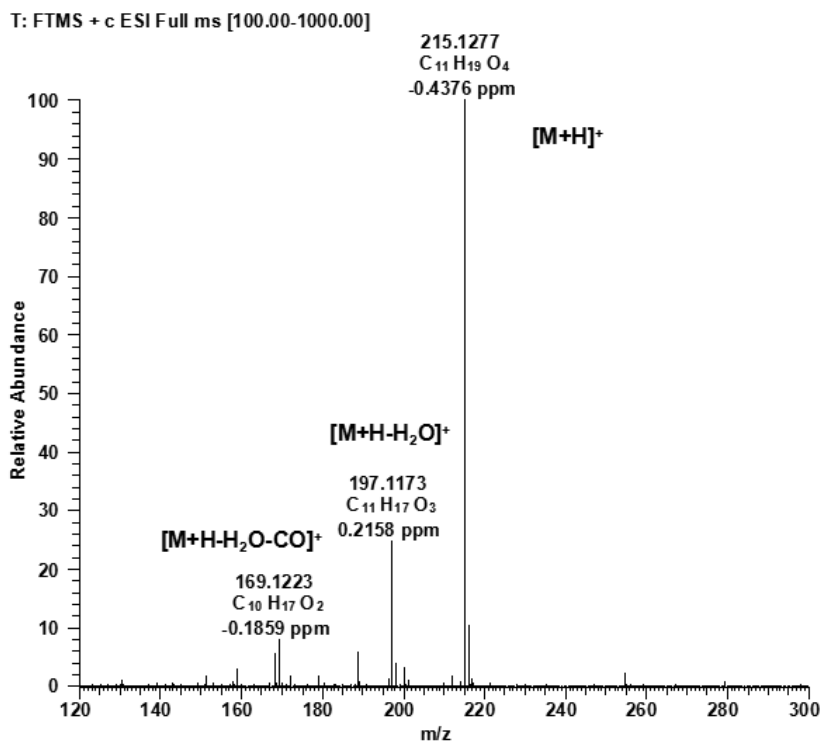


Figure 4.1.12.1 Positive ESI-HRMS spectrum of compound **12**.

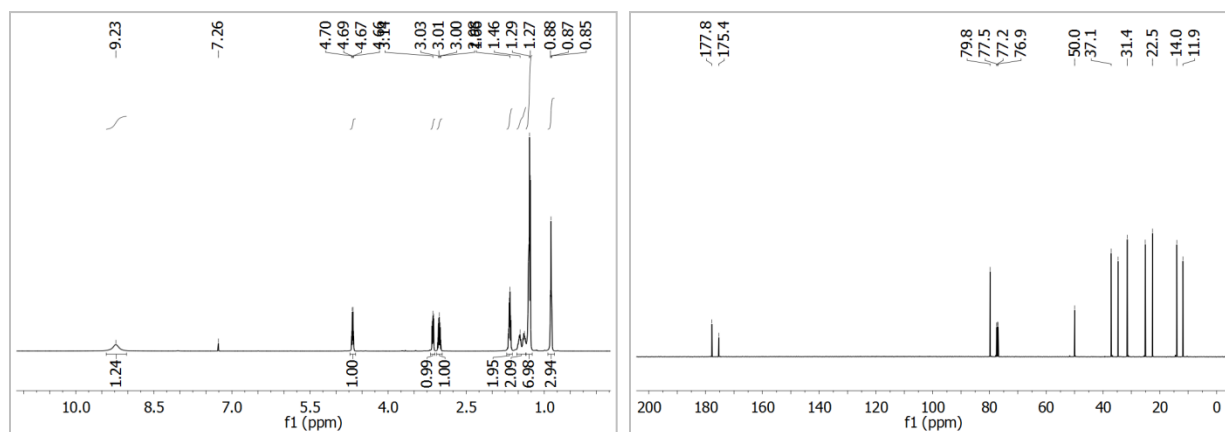


Figure 4.1.12.2 ¹H (left) and ¹³C (right) NMR spectra (in CDCl₃) of compound **12**.

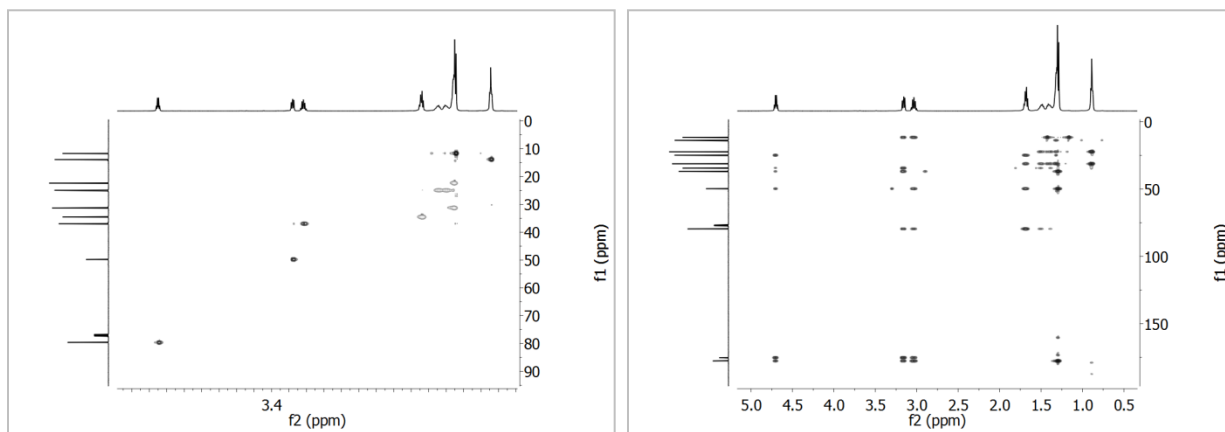


Figure 4.1.12.3 HSQC (left) and HMBC (right) NMR spectra of compound **12** in CDCl₃.

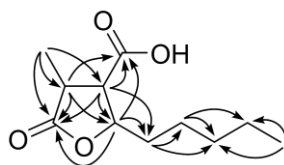


Figure 4.1.12.4 The key HMBC correlations of **12**.

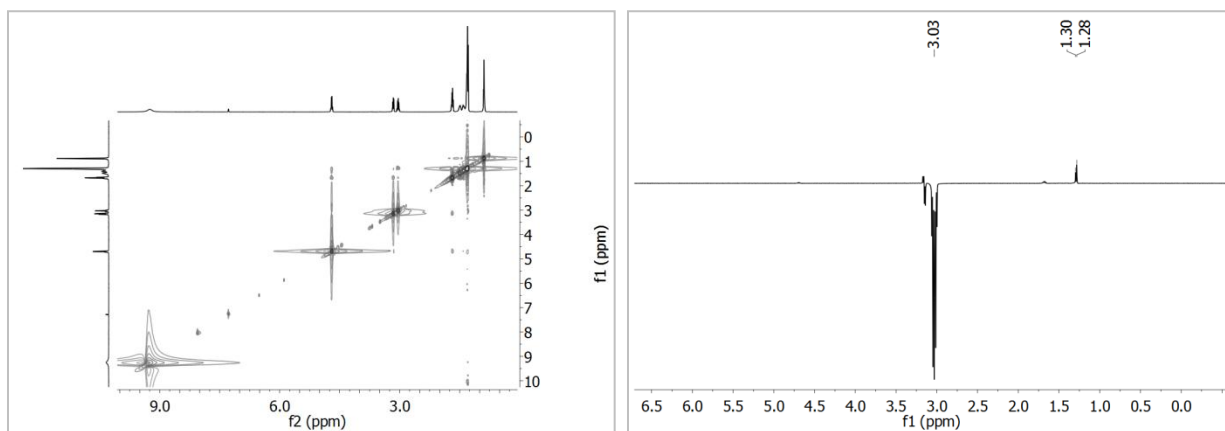


Figure 4.1.12.5 NOESY (left) and 1D NOESY (right) NMR spectra of compound **12** in CDCl₃.

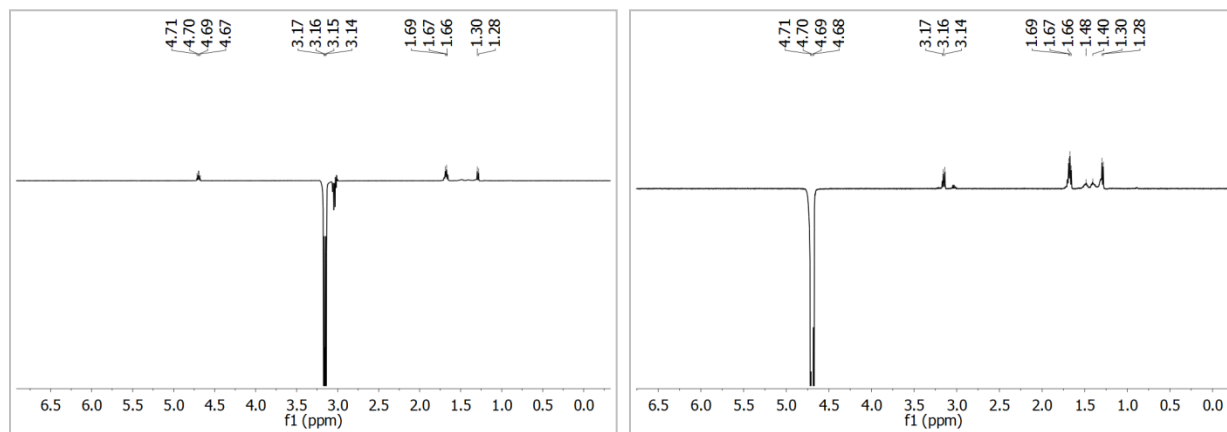


Figure 4.1.12.6 1D NOESY NMR spectra of compound **12** in CDCl₃.

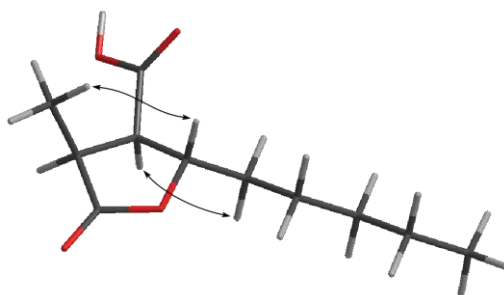


Figure 4.1.12.7 The key NOE correlations of **12**.

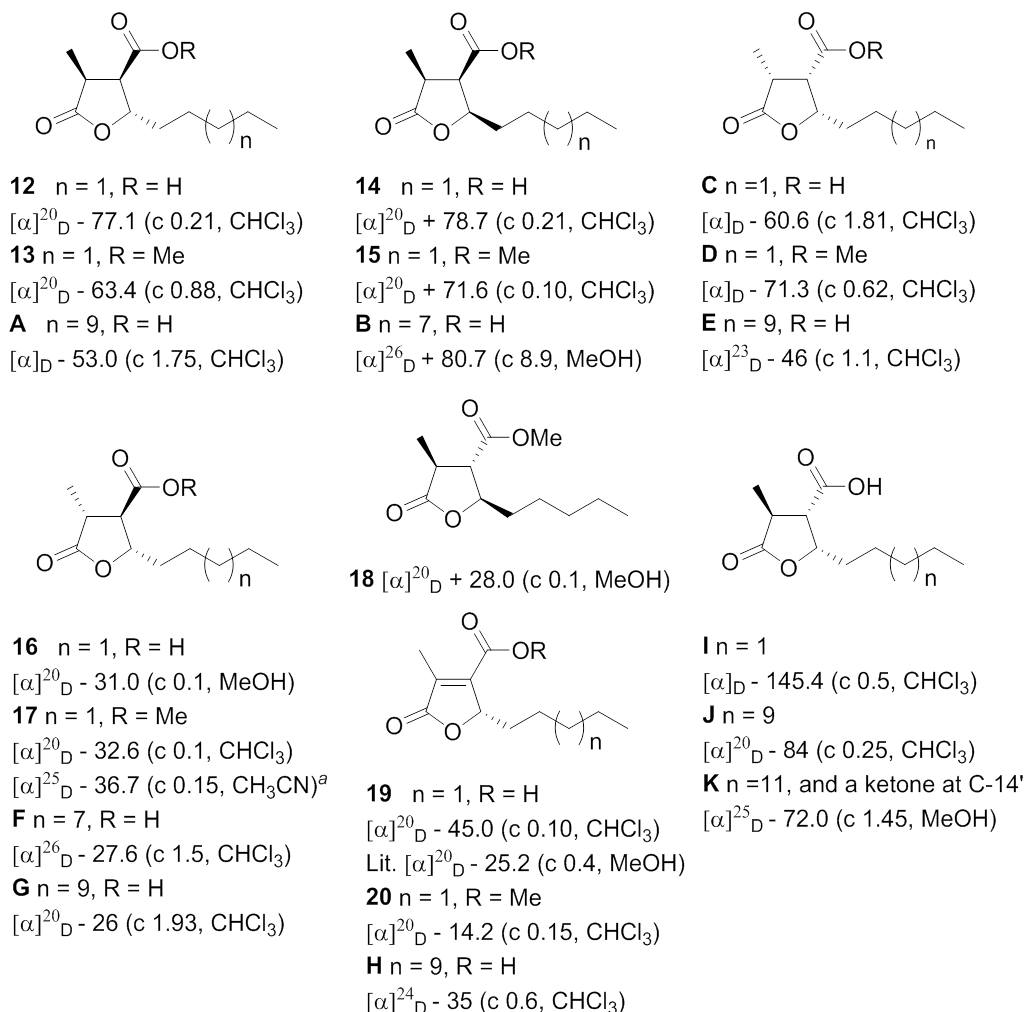
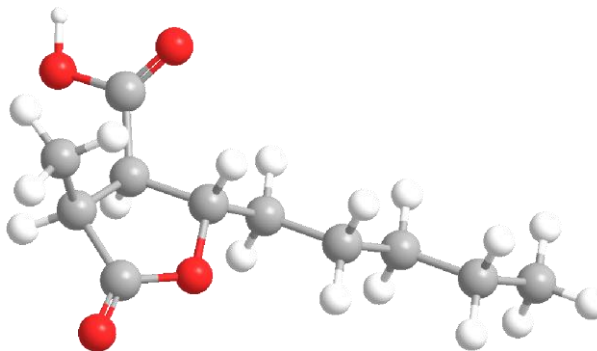
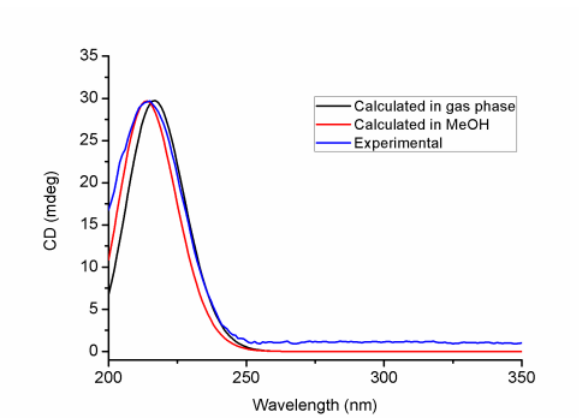
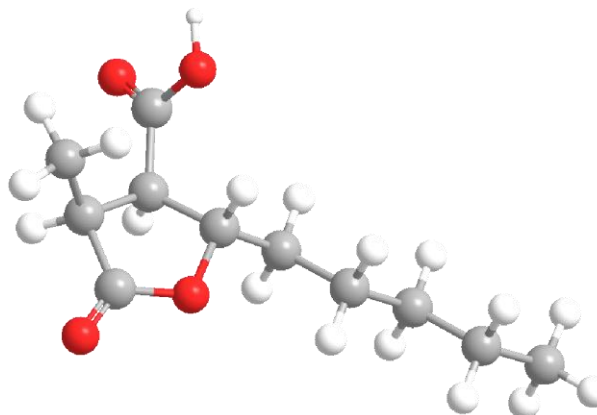
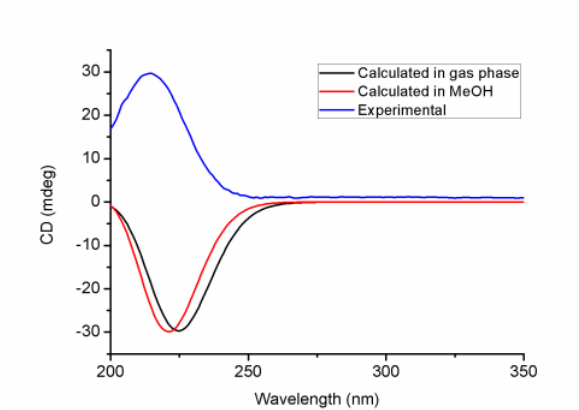


Figure 4.1.12.8 The optical rotations for **12–20** and related paraconic acid derivatives. Compound **A**: (–)-dihydroprotolichesterinic acid (Banks *et al.*, 1995); **B**: 4-(*S*)-methyl-5-oxo-2-(*R*)-undecyloxolane-3-(*R*)-carboxylic acid (Jacobi *et al.*, 2001); **C** (Amador *et al.*, 2006); **D** (Amador *et al.*, 2006); **E**: 4-(*R*)-methyl-5-oxo-2-(*S*)-undecyloxolane-3-(*S*)-carboxylic acid (Huneck *et al.*, 1992); **F**: (–)-nephrosteranic acid (Jacobi *et al.*, 2001); **G**: (–)-roccellaric acid (Mulzer *et al.*, 1993); **H**: lichesterinic acid (Huneck *et al.*, 1992); **I**: (–)-phaseolinic acid (Howell *et al.*, 2006); **J**: (–)-nephromopsinic acid (Huneck *et al.*, 1992; Mulzer *et al.*, 1991); **K**: (–)-dihydropertusaric acid (Maier *et al.*, 1999). ^athe data obtained from literature (Drioli *et al.*, 1998; Deska *et al.*, 2009).

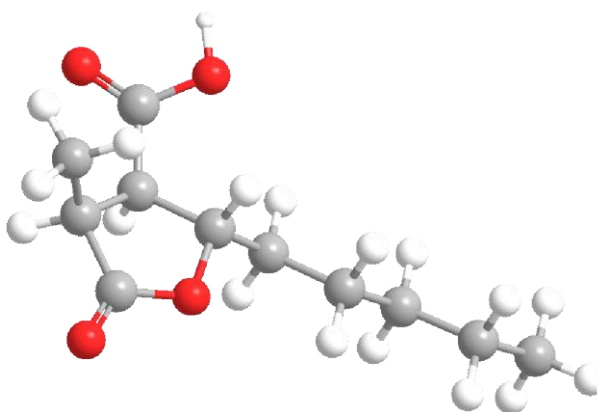
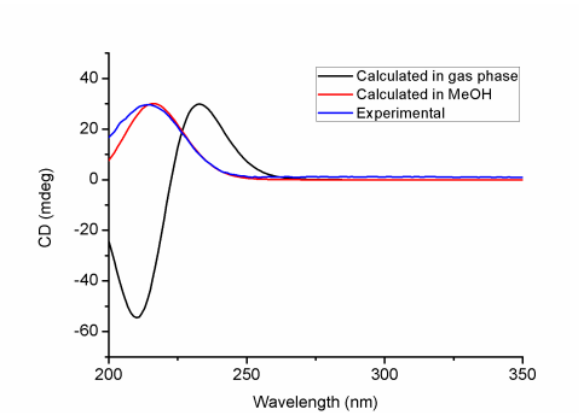
A



B



C



D

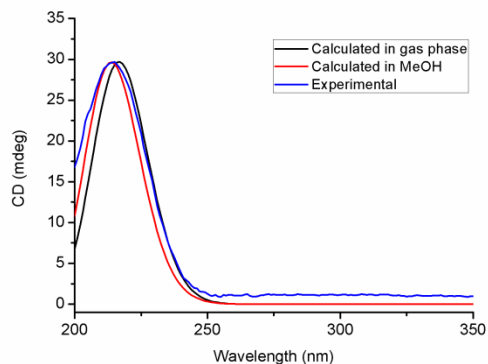
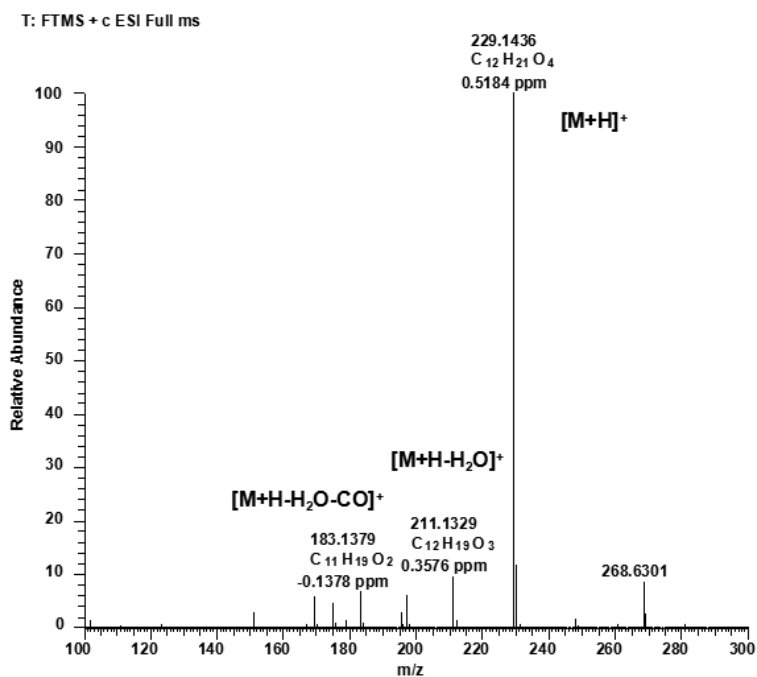


Figure 4.1.12.9 The ECD calculation for three conformers (A–C) of compound **12** and the Boltzmann-averaged calculated CD [D from A (89.99%), B (1.56%) and C (8.45%)]. Experimental ECD (blue), calculated ECD in gas phase (black) and in MeOH (red).



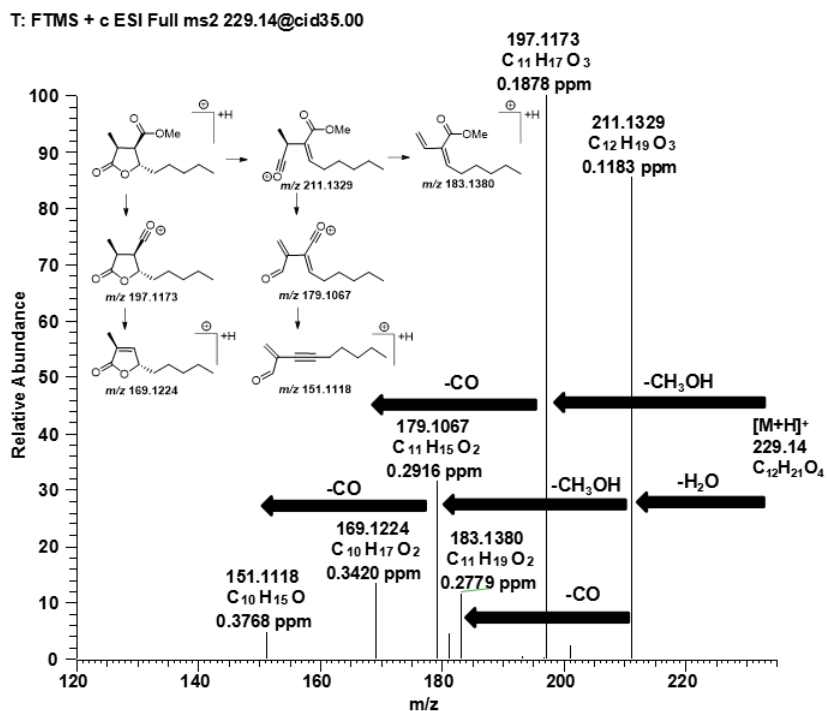


Figure 4.1.13.1 Positive ESI-HRMS (top) and MS/MS (bottom) spectra of compound **13**.

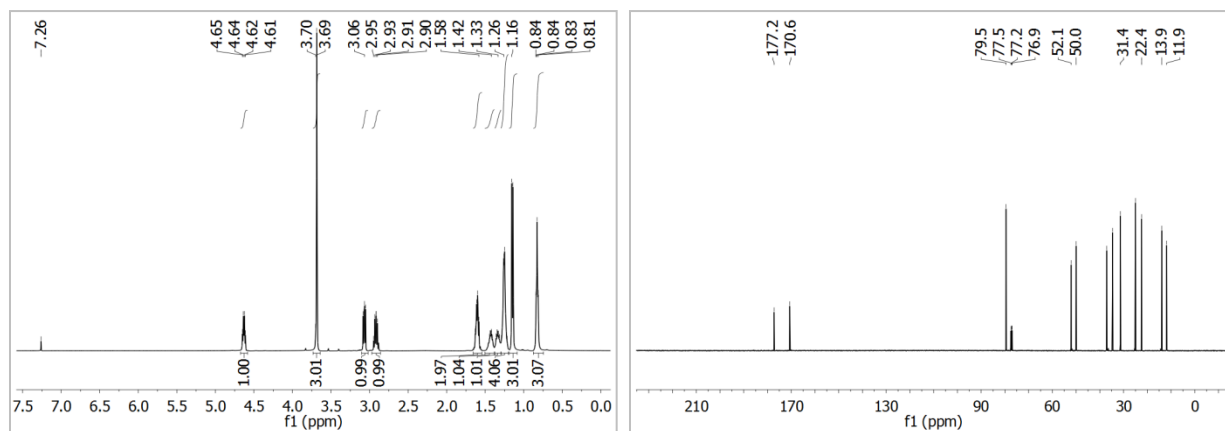


Figure 4.1.13.2 ¹H (left) and ¹³C (right) NMR spectra (in CDCl₃) of compound **13**.

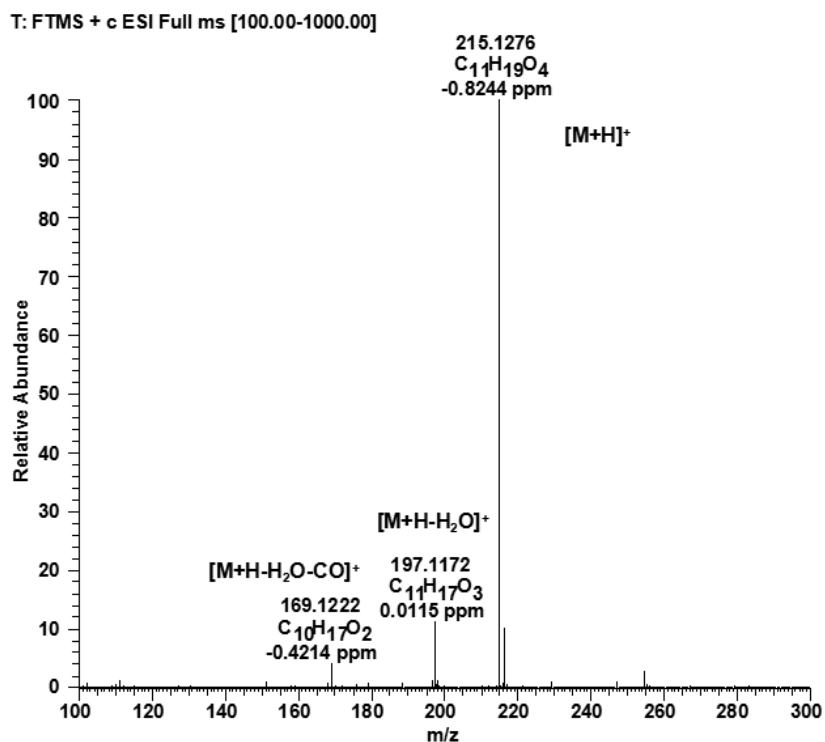


Figure 4.1.14.1 Positive ESI-HRMS spectrum of compound 14.

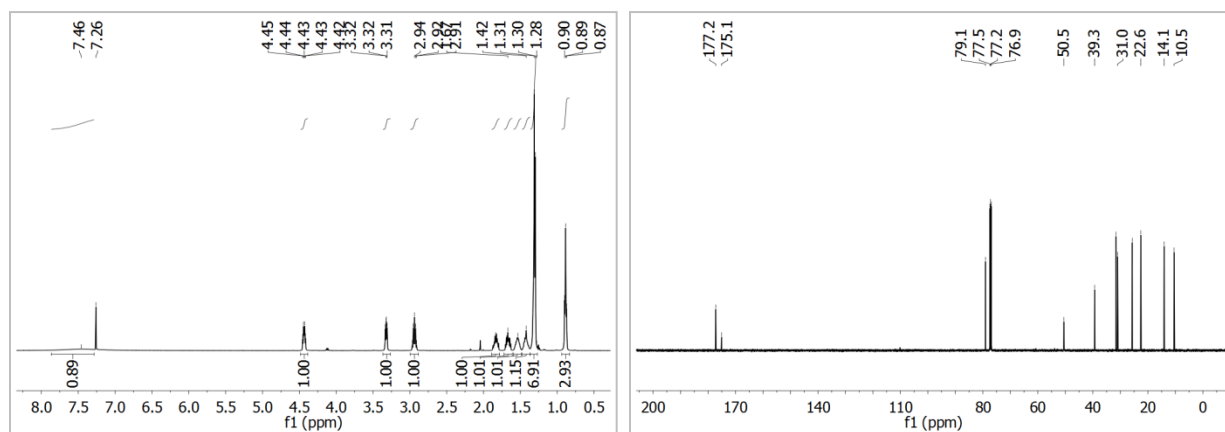


Figure 4.1.14.2 ¹H (left) and ¹³C (right) NMR spectra (in CDCl₃) of compound 14.

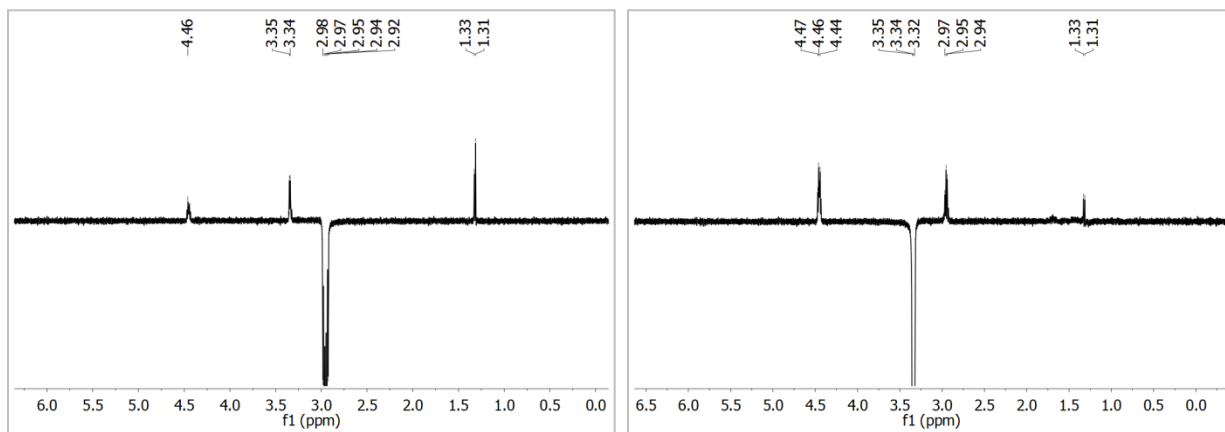


Figure 4.1.14.3 1D NOESY spectra of compound **14** in CDCl_3 .

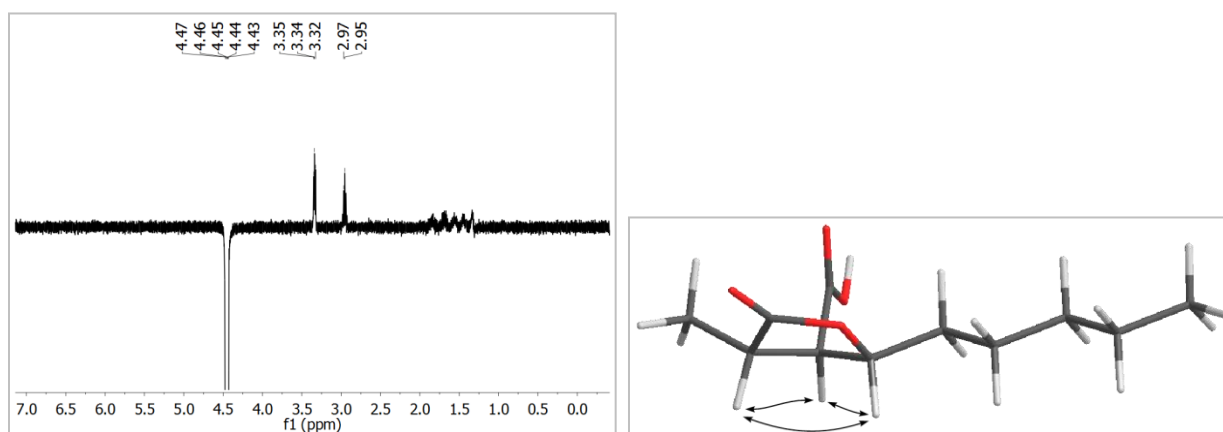
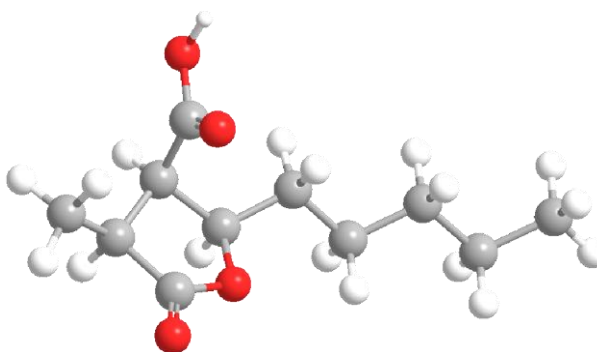
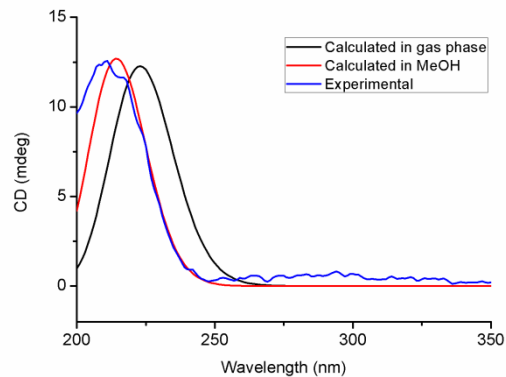


Figure 4.1.14.4 1D NOESY (left) spectrum and key NOE correlations (right) of compound **14**.

A



B

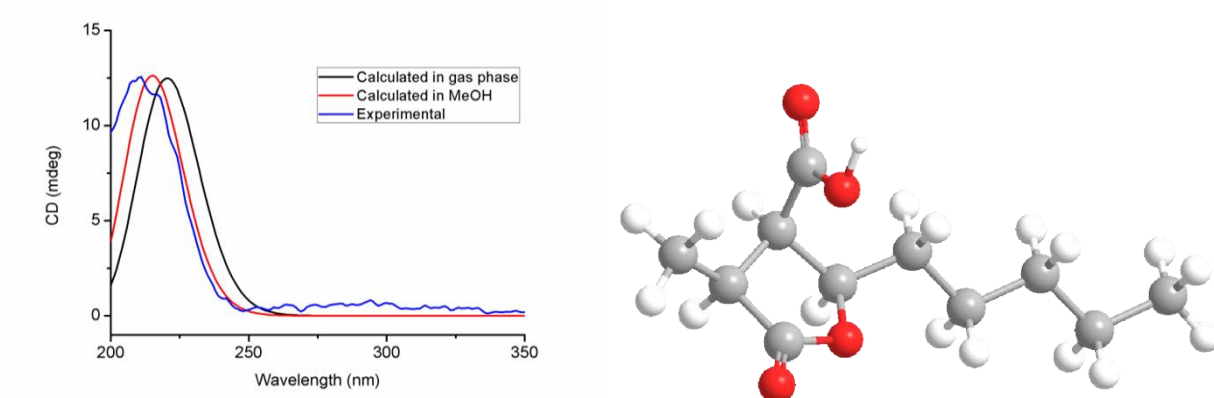


Figure 4.1.14.5 The ECD calculation for two conformers (A and B) of compound **14**. Experimental ECD (blue), calculated ECD in gas phase (black) and in MeOH (red).

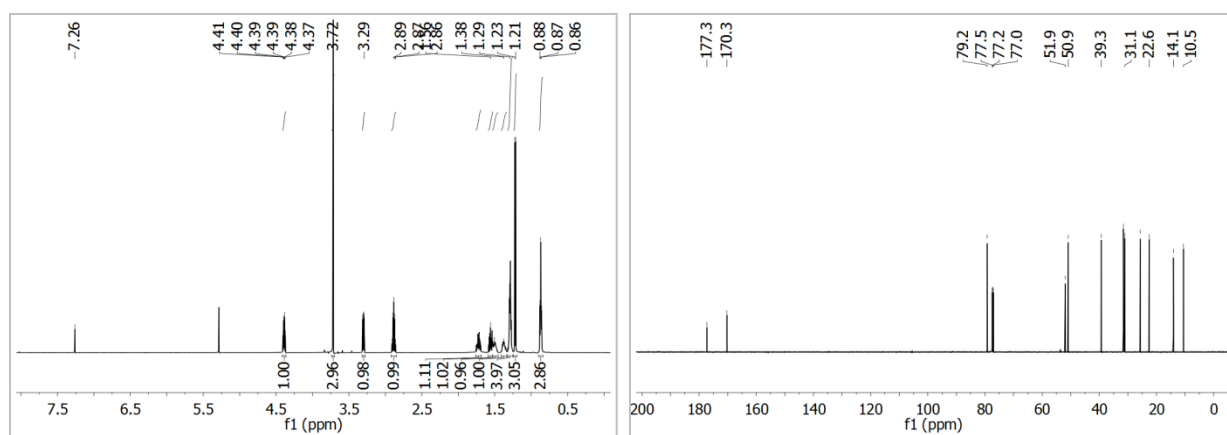


Figure 4.1.15.1 ^1H (left) and ^{13}C (right) NMR spectra (in CDCl_3) of compound **15**.

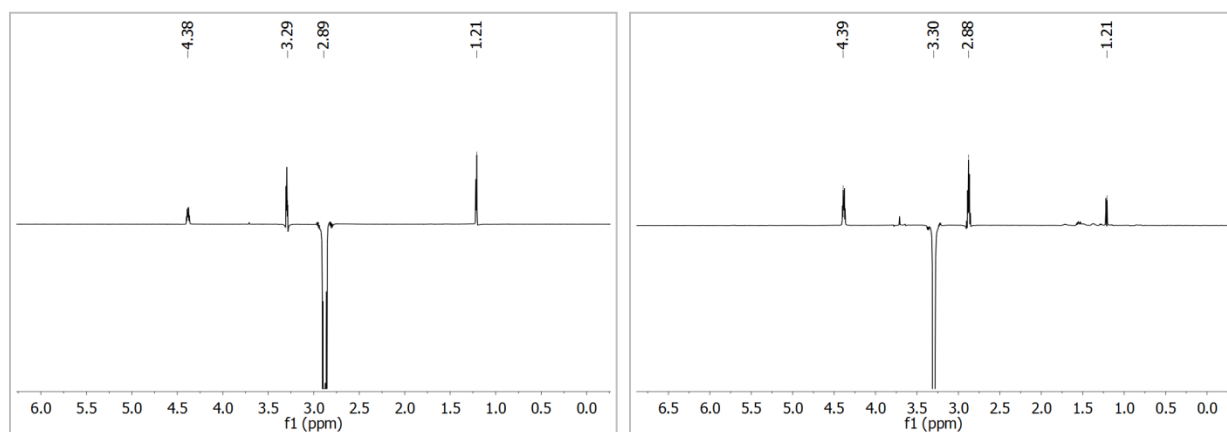


Figure 4.1.15.2 1D NOESY spectra of compound **15** in CDCl_3 .

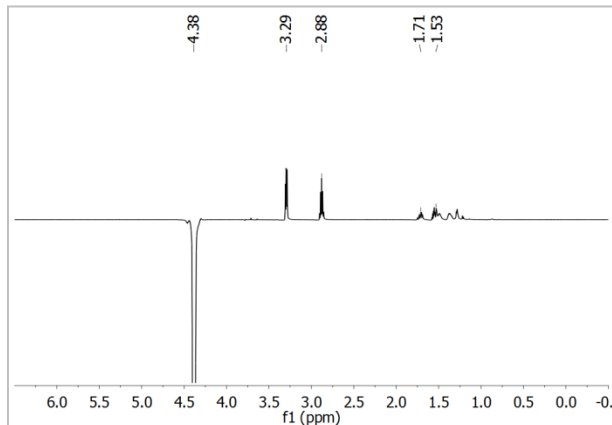


Figure 4.1.15.3 1D NOESY spectrum of compound **15** in CDCl_3 .

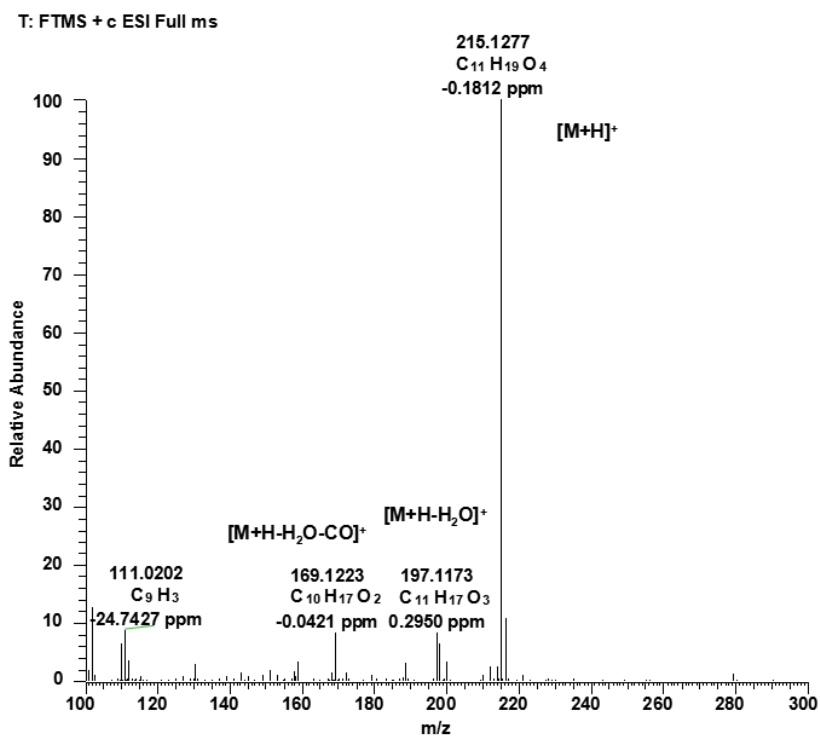


Figure 4.1.16.1 Positive ESI-HRMS spectrum of compound **16**.

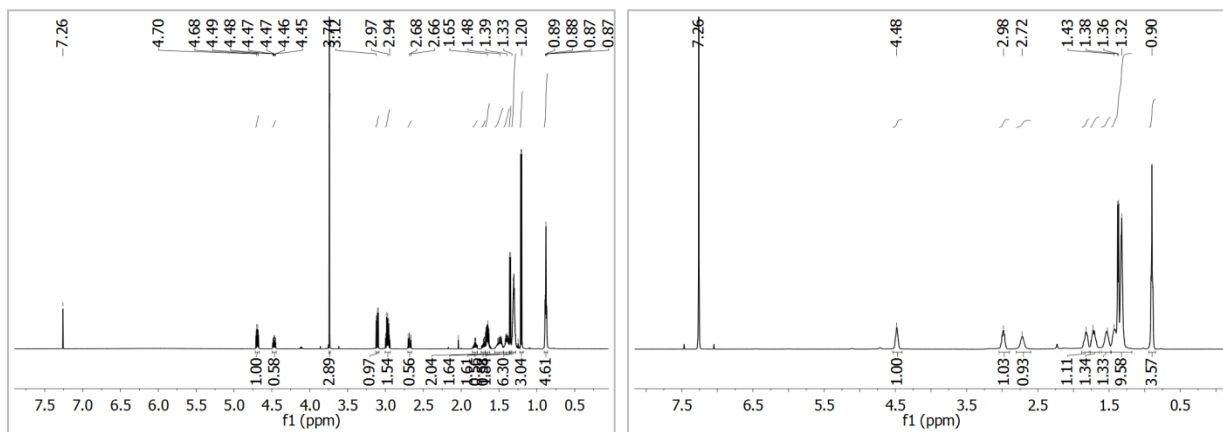


Figure 4.1.16.2 ^1H (left) and ^{13}C (right) NMR spectra (in CDCl_3) of compound **16**.

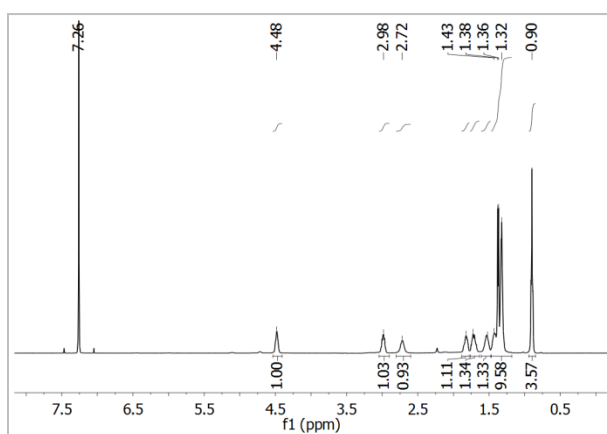


Figure 4.1.16.3 ^1H NMR spectrum of compound **16** after purification.

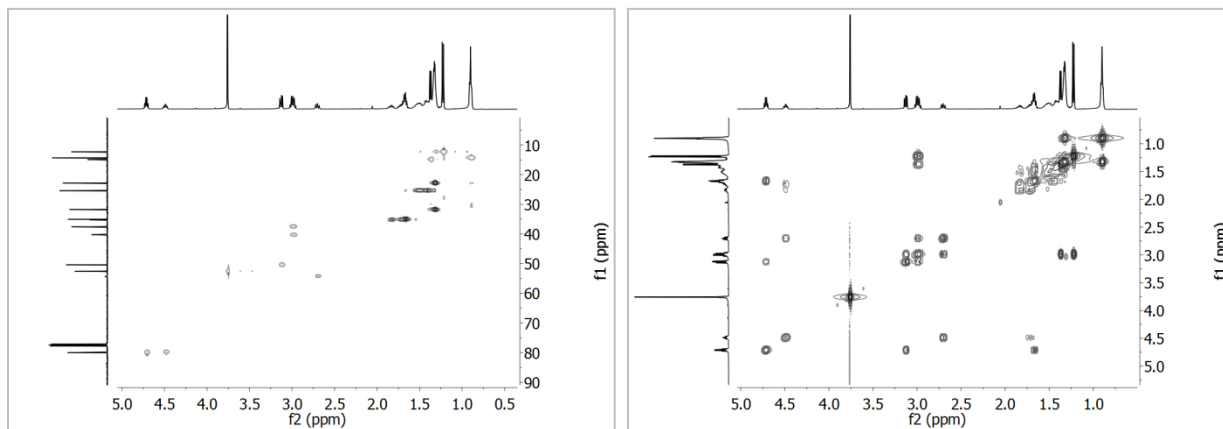


Figure 4.1.16.4 HSQC (left) and ^1H - ^1H COSY (right) NMR spectra (in CDCl_3) of compound **16**.

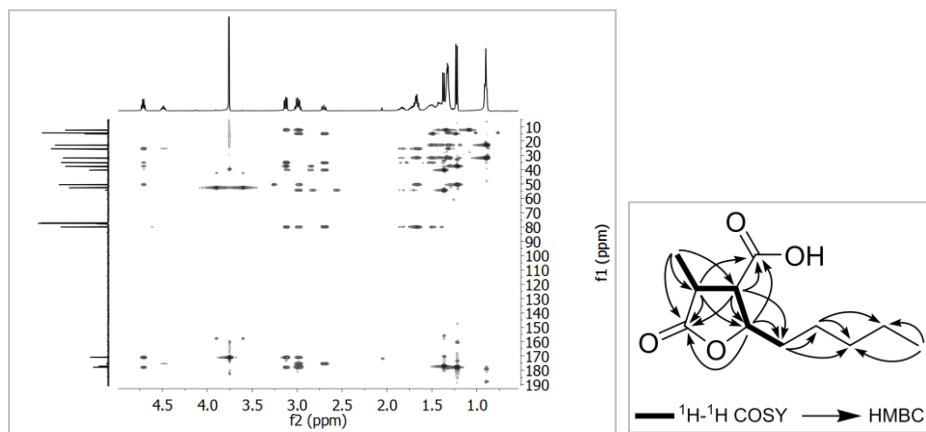


Figure 4.1.16.5 HMBC spectrum (left, in CDCl_3) and key ^1H - ^1H COSY and HMBC correlations (right) of compound **16**.

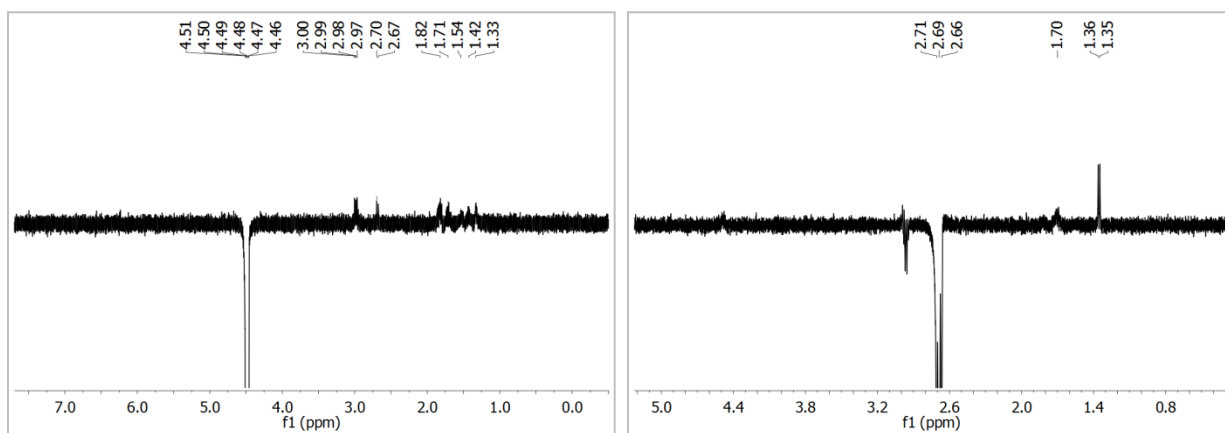


Figure 4.1.16.6 1D NOESY spectra of compound **16** in CDCl_3 .

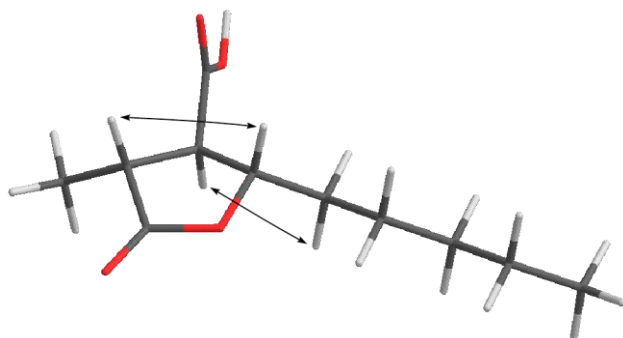
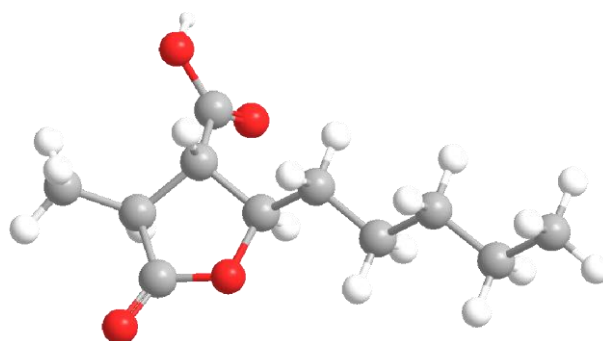
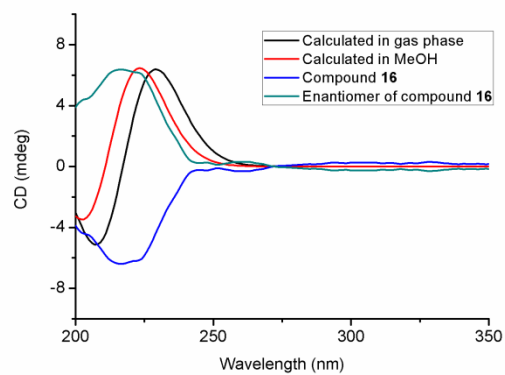
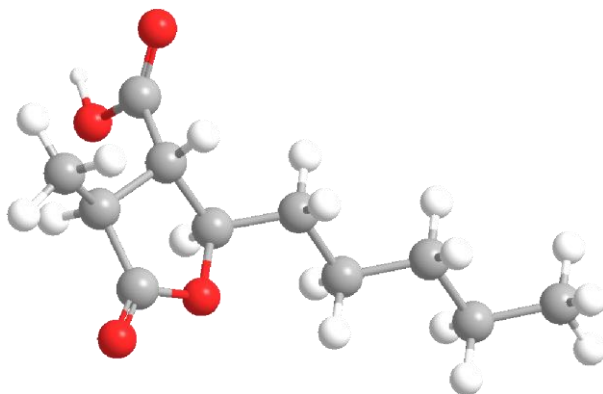
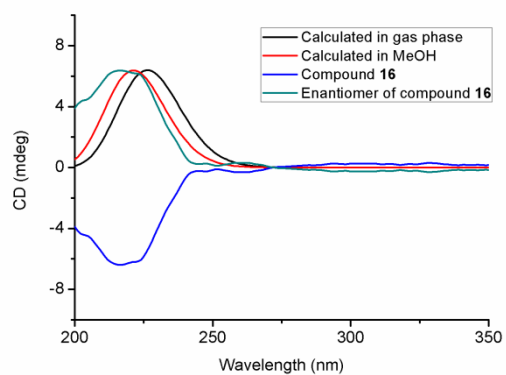


Figure 4.1.16.7 Key NOE correlations of compound **16**.

A



B



C

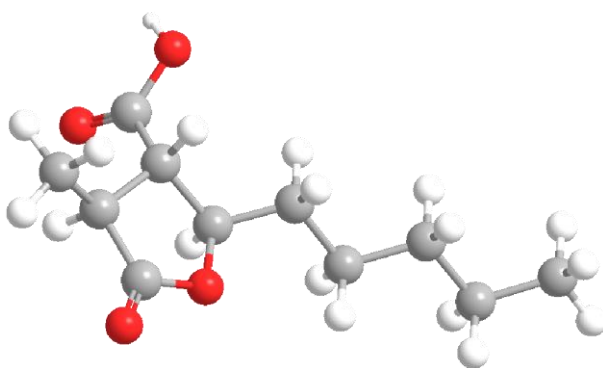
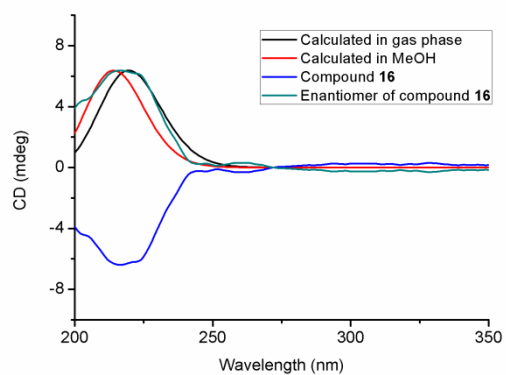


Figure 4.1.16.8 The ECD calculation for three conformers (A–C) of the enantiomer of compound **16**: experimental ECD (blue) of **16**, calculated ECD in gas phase (black) and in MeOH (red).

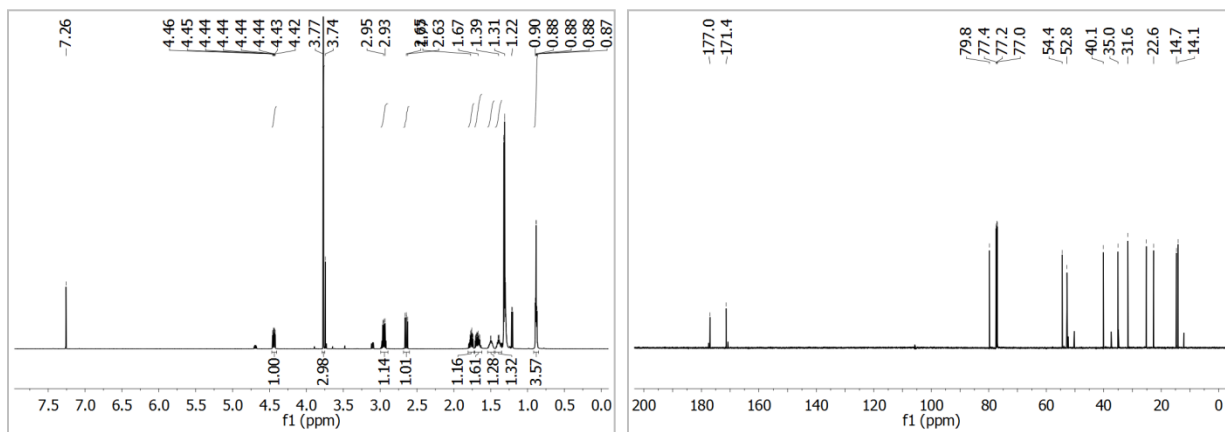


Figure 4.1.17.1 ^1H (left) and ^{13}C (right) NMR spectra (in CDCl_3) of compound **17**.

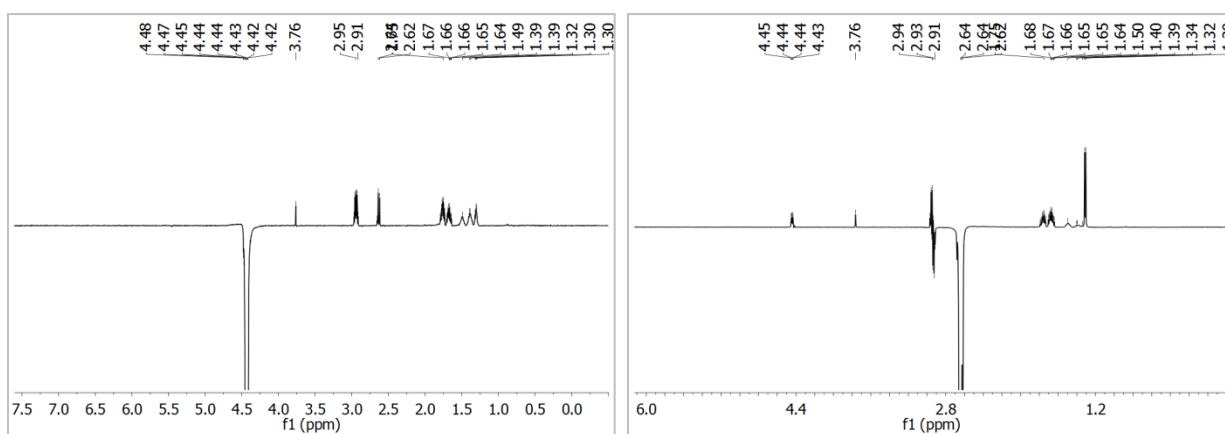


Figure 4.1.17.2 1D NOE NMR spectra of compound **17** in CDCl_3 .

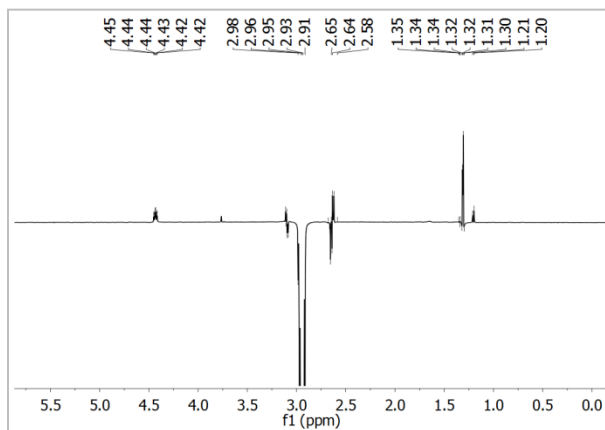


Figure 4.1.17.3 1D NOE NMR spectrum of compound **17** in CDCl_3 .

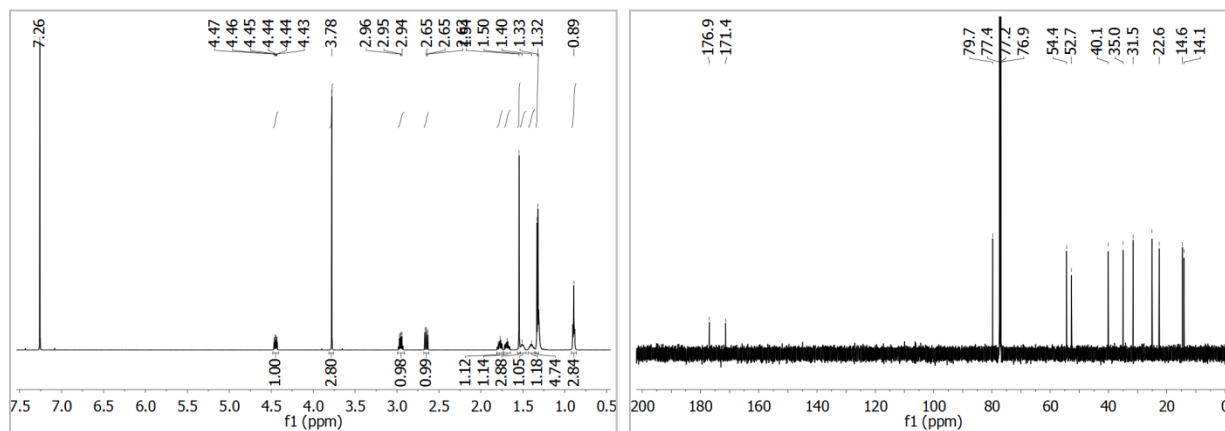


Figure 4.1.18.1 ^1H (left) and ^{13}C (right) NMR spectra (in CDCl_3) of compound **18**.

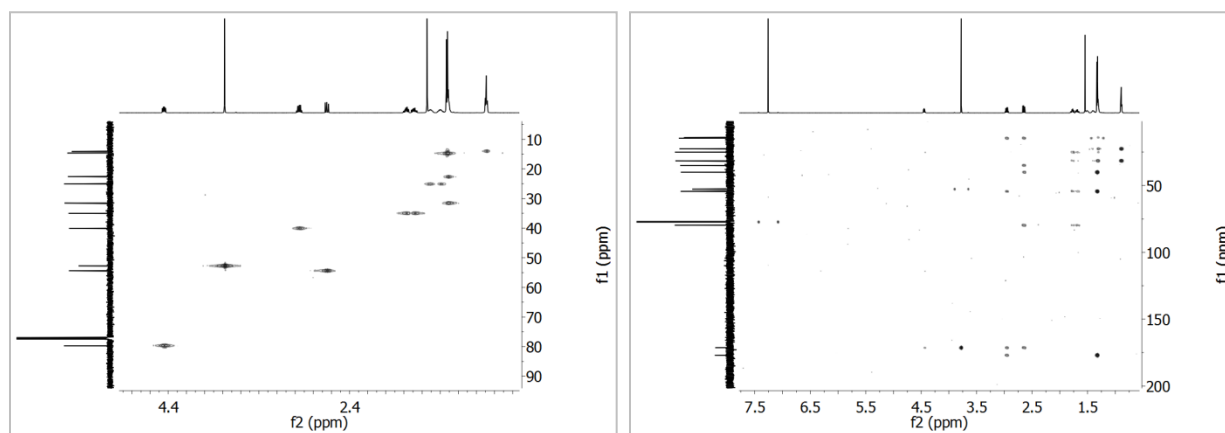


Figure 4.1.18.2 HSQC (left) and HMBC (right) NMR spectra (in CDCl_3) of compound **18**.

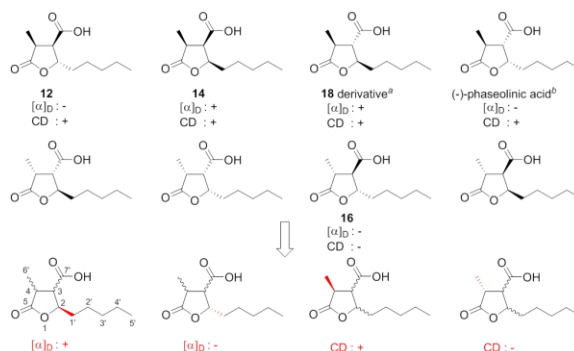


Figure 4.1.18.3 The analysis of relationship between compound configurations and chiroptical data. ^aThe signs of optical rotation and CD data were proposed from compounds **16** and **18**. ^bThe data was collected from the literature (Howell *et al.*, 2006).

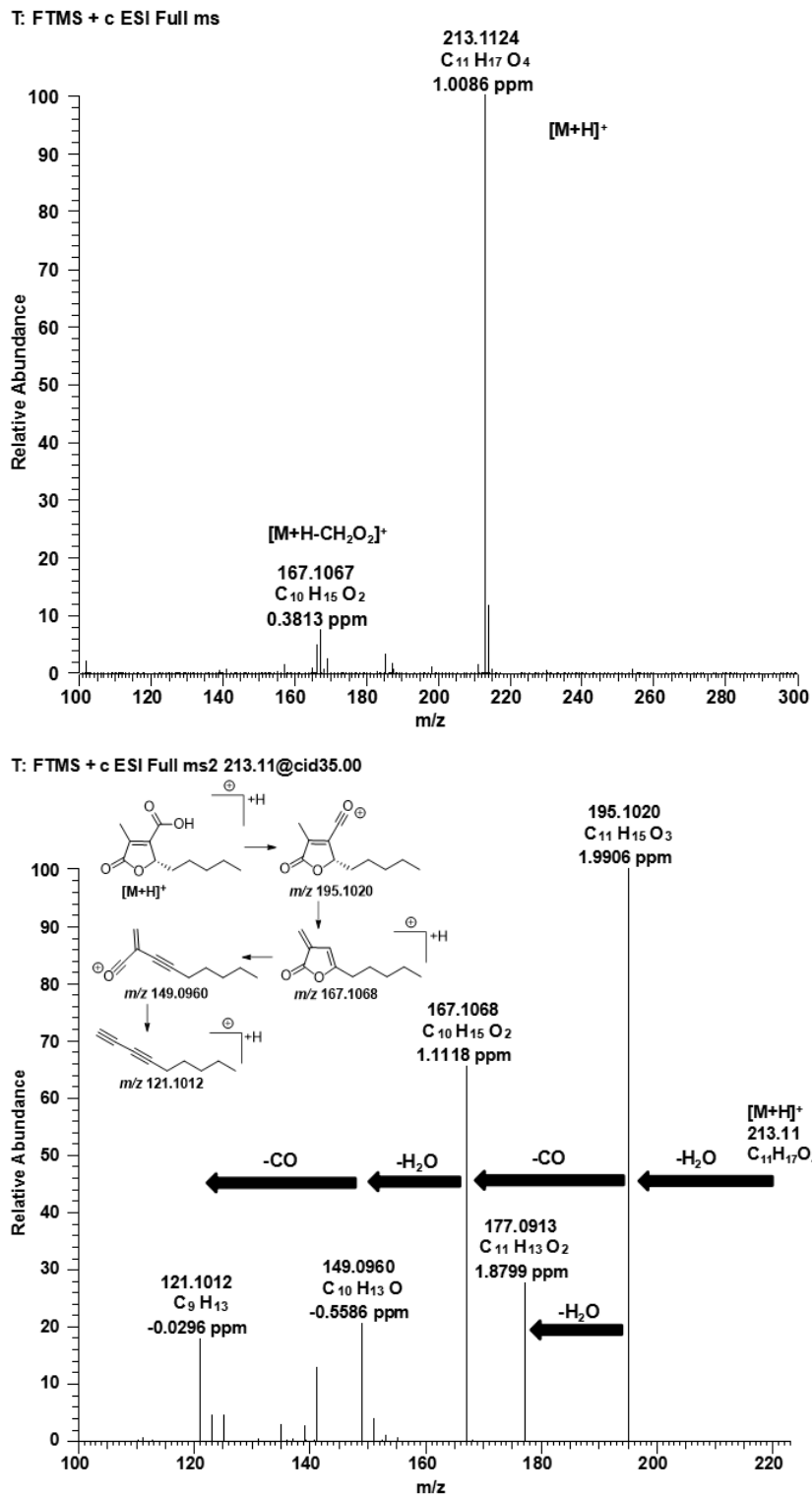


Figure 4.1.19.1 Positive ESI-HRMS (top) and MS/MS (bottom) spectra of compound 19.

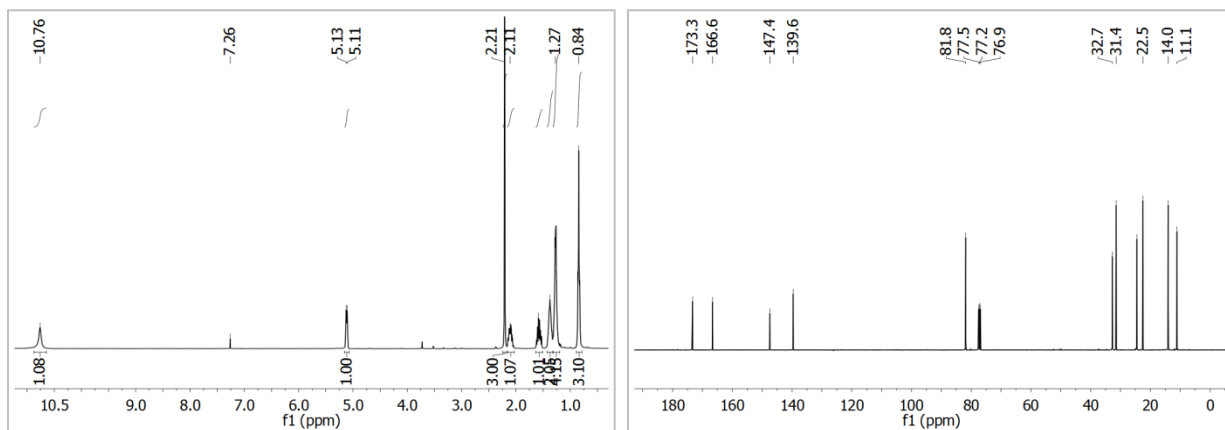


Figure 4.1.19.2 ^1H (left) and ^{13}C (right) NMR spectra (in CDCl_3) of compound **19**.

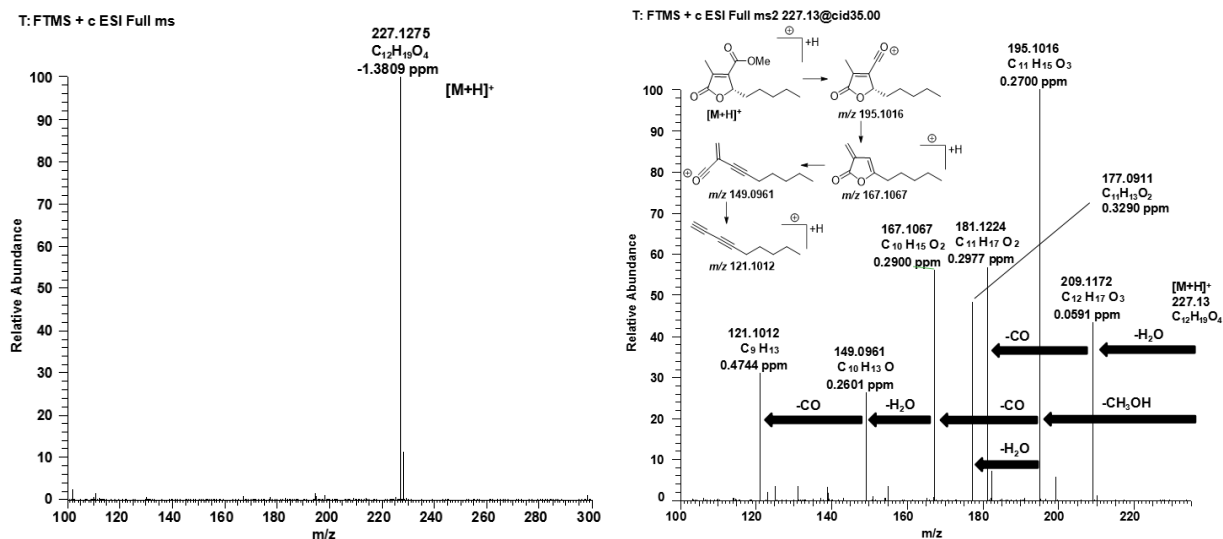


Figure 4.1.20.1 Positive ESI-HRMS (left) and MS/MS (right) spectra of compound **20**.

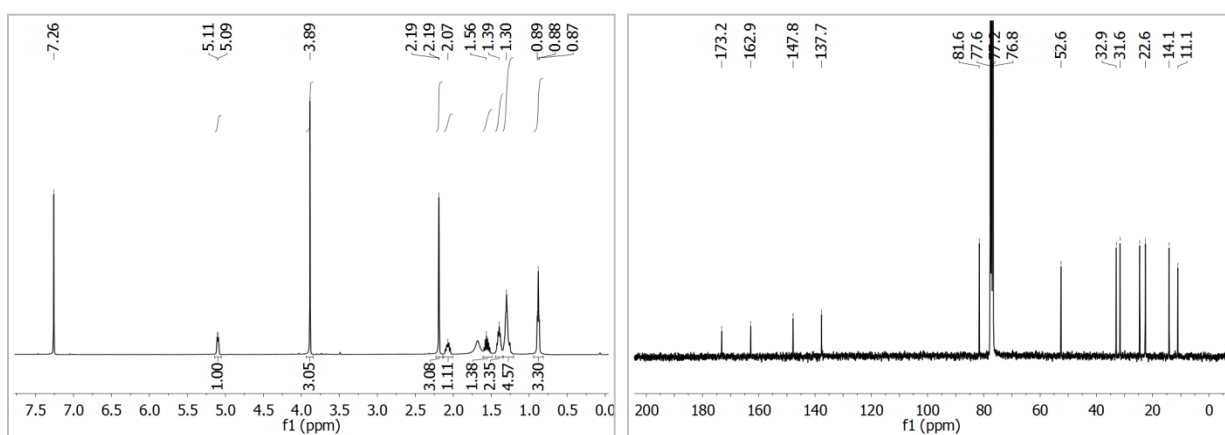


Figure 4.1.20.2 ^1H (left) and ^{13}C (right) NMR spectra (in CDCl_3) of compound **20**.

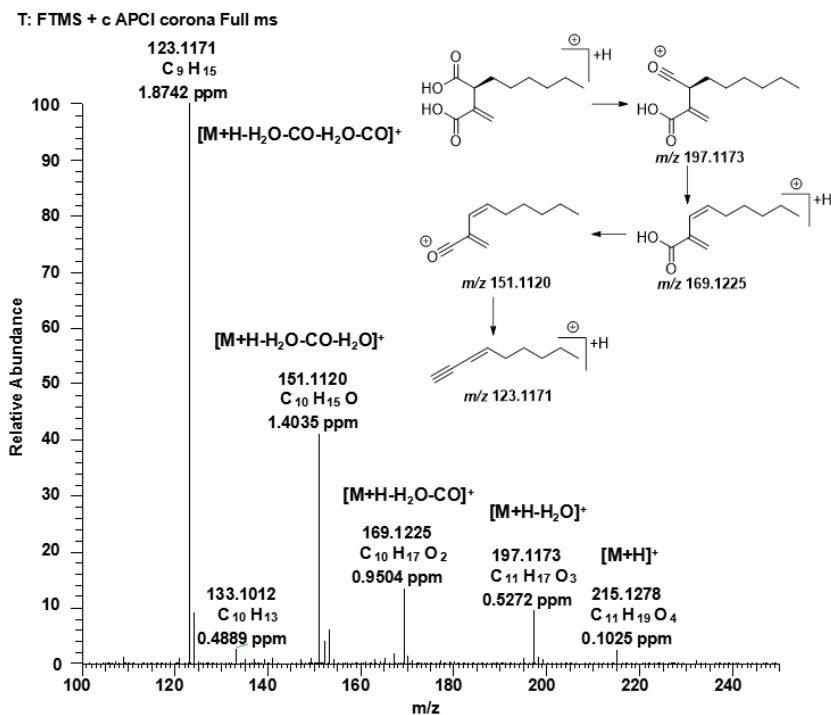


Figure 4.1.21.1 Positive APCI-HRMS spectrum of compound **21**.

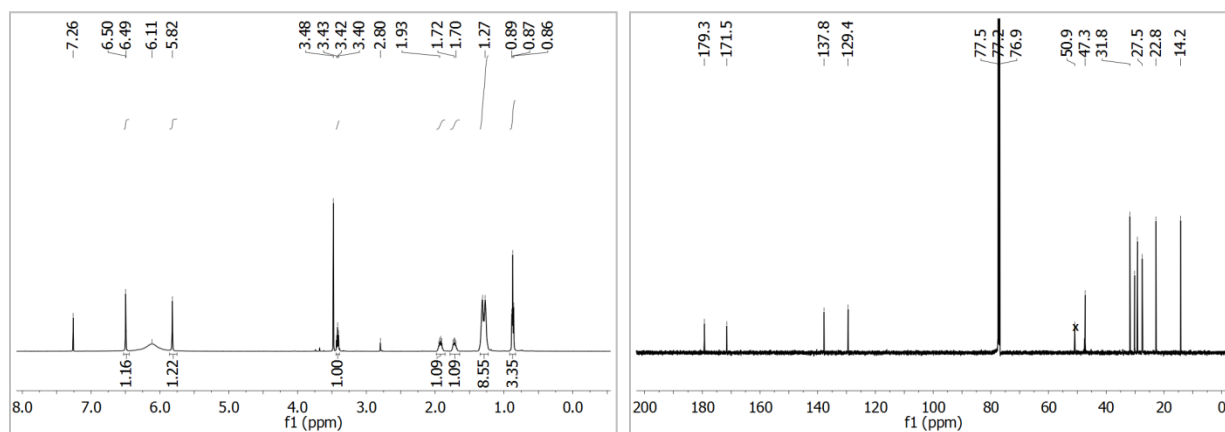


Figure 4.1.21.2 ¹H (left) and ¹³C (right) NMR spectra (in CDCl₃) of compound **21**.

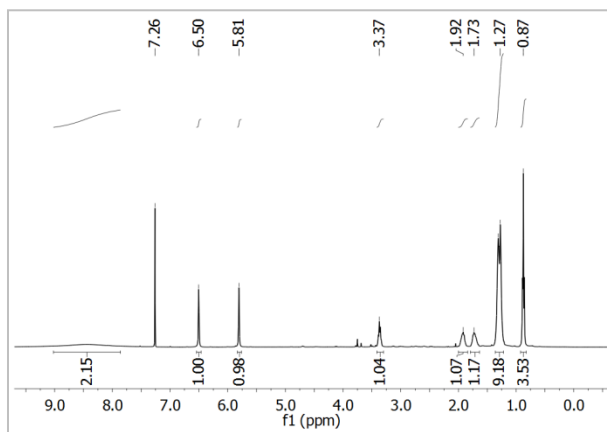


Figure 4.1.22.1 ^1H NMR spectrum (in CDCl_3) of compound **22**.

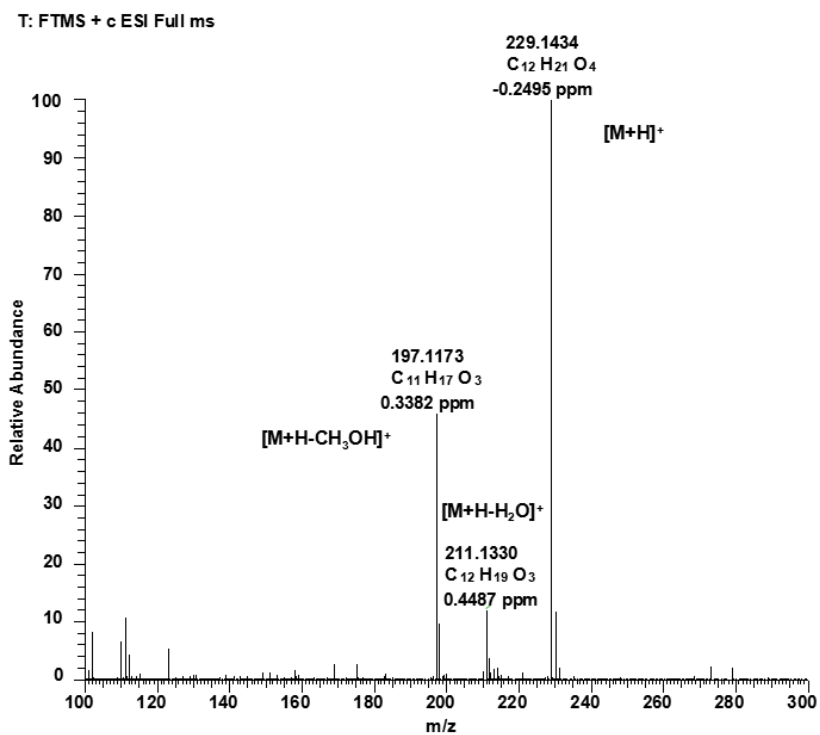


Figure 4.1.23.1 Positive ESI-HRMS spectrum of compound **23**.

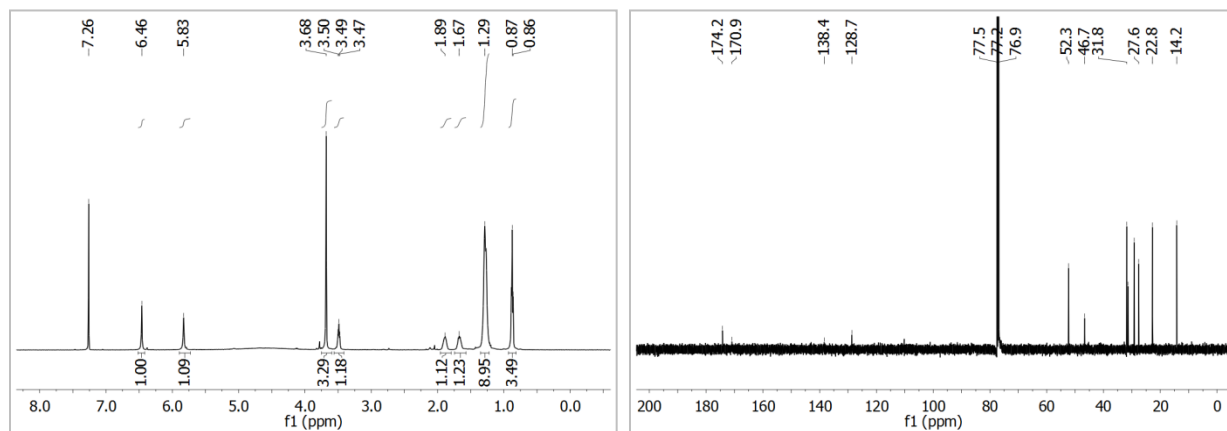


Figure 4.1.23.2 ^1H (left) and ^{13}C (right) NMR spectra (in CDCl_3) of compound 23.

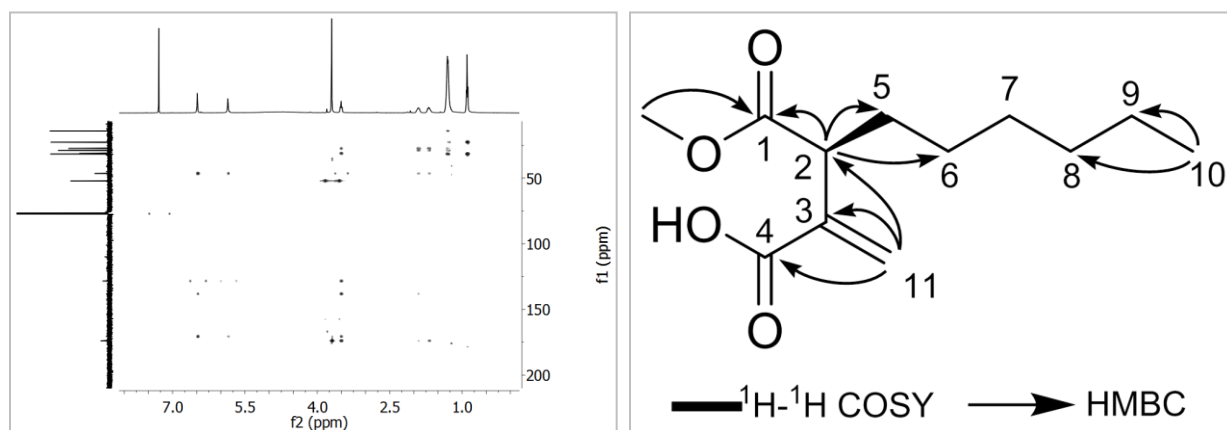


Figure 4.1.23.3 The HMBC spectrum (left, in CDCl_3) and key HMBC correlations (right) of compound 23.

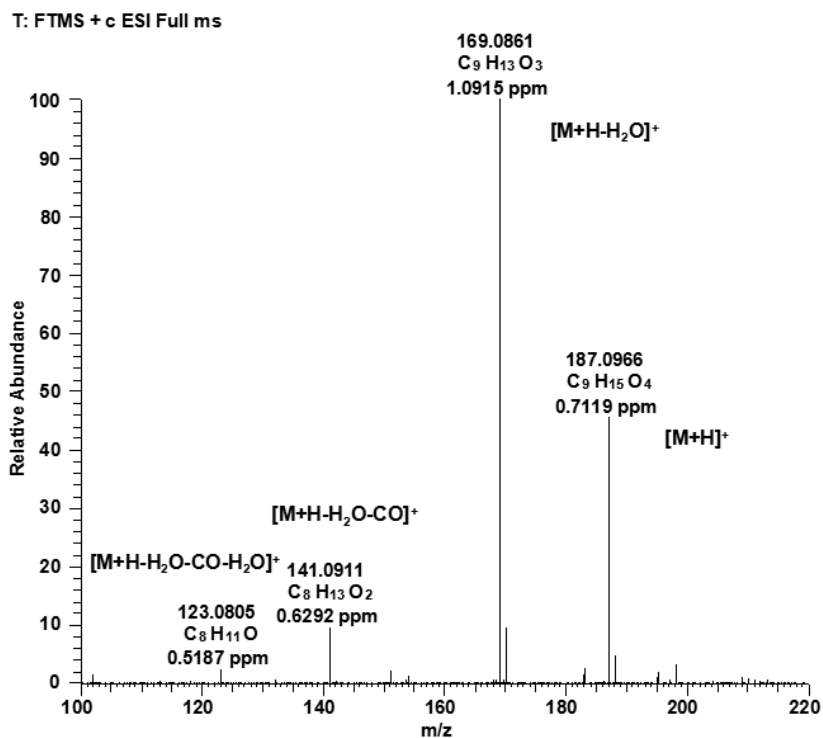


Figure 4.1.24.1 Positive ESI-HRMS spectrum of compound 24.

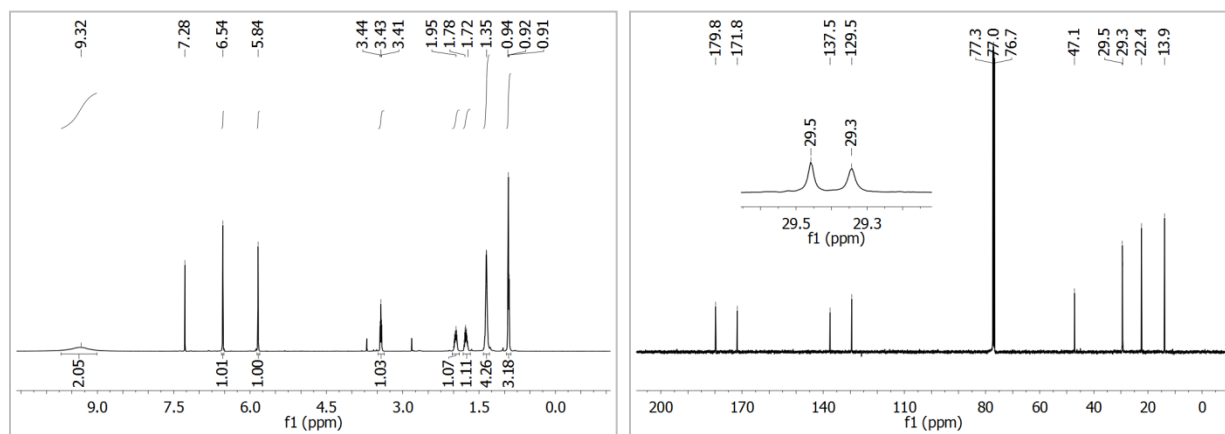


Figure 4.1.24.2 ¹H (left) and ¹³C (right) NMR spectra (in CDCl₃) of compound 24.

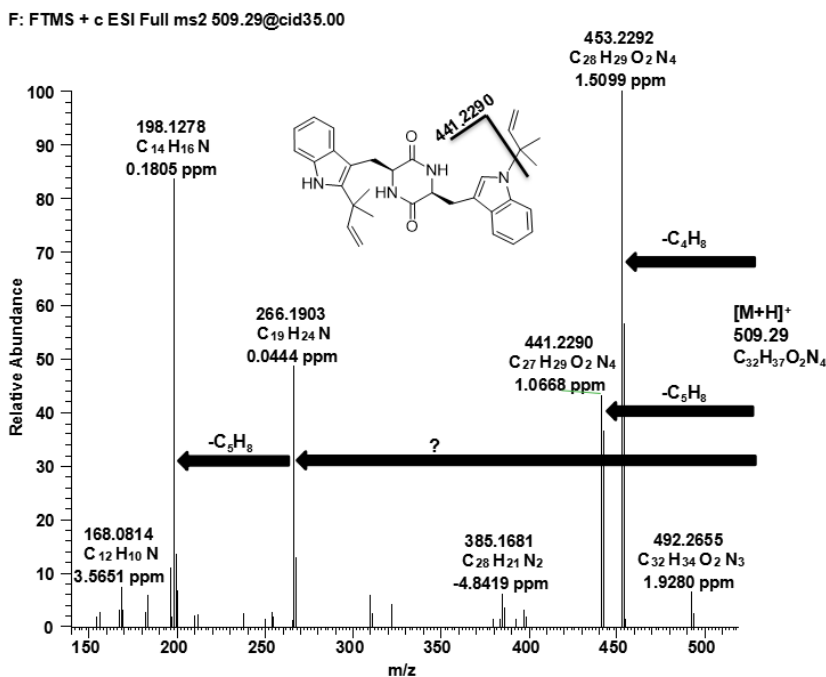
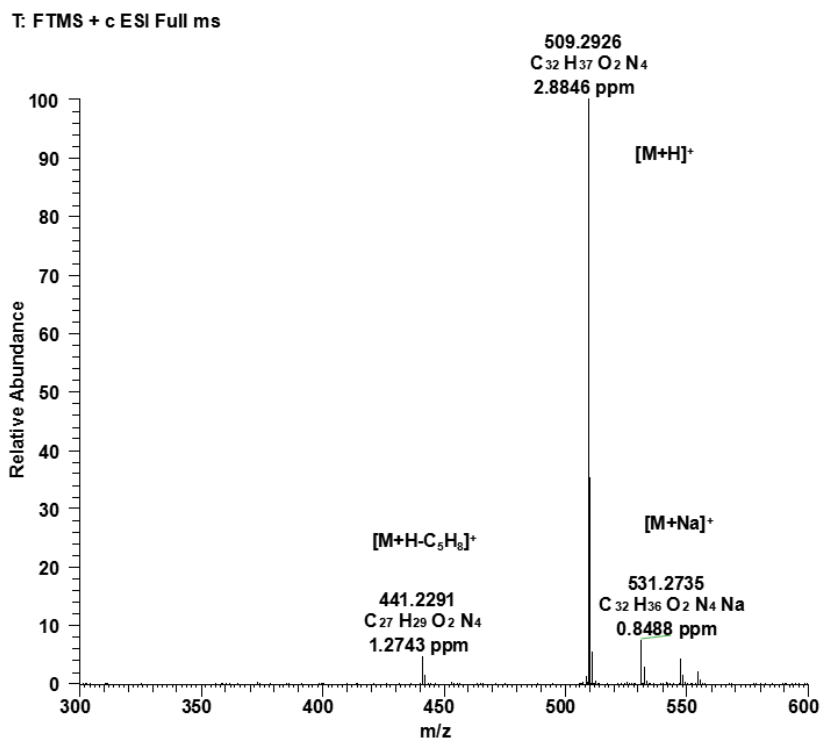


Figure 4.1.25.1 Positive ESI-HRMS (top) and MS/MS (bottom) spectra of compound 25.

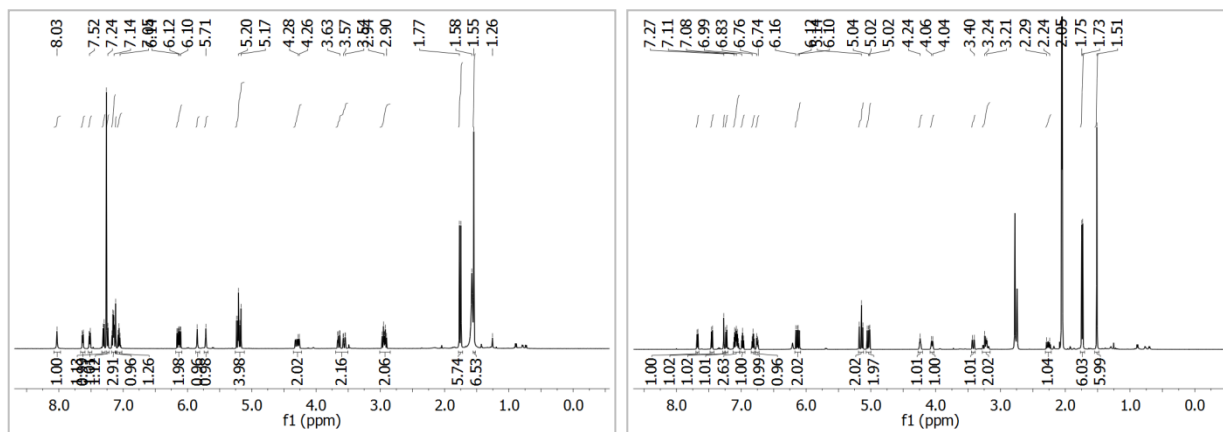


Figure 4.1.25.2 ^1H (left, in CDCl_3) and ^1H (right, in $\text{acetone-}d_6$) NMR spectra of compound 25.

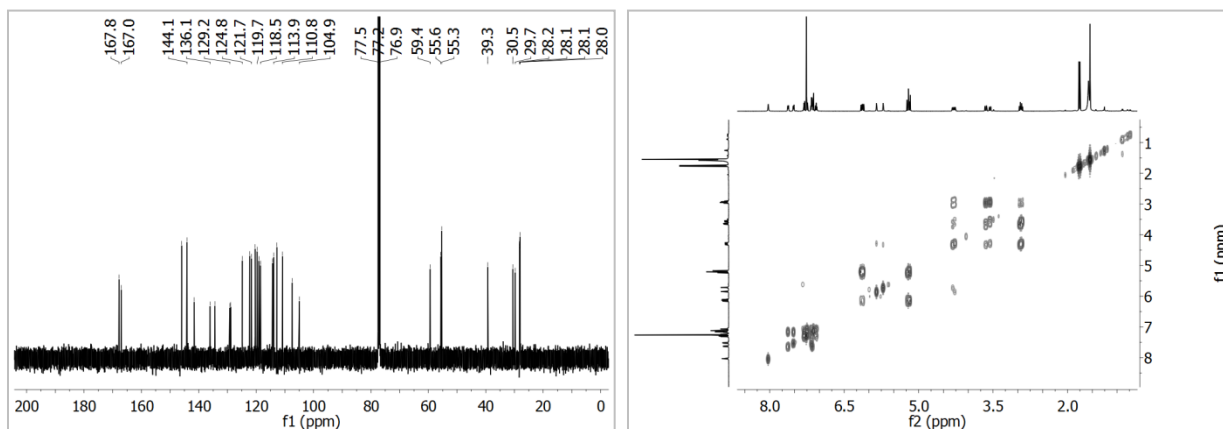


Figure 4.1.25.3 ^{13}C NMR (left) and ^1H - ^1H COSY (right) spectra (in CDCl_3) of compound 25.

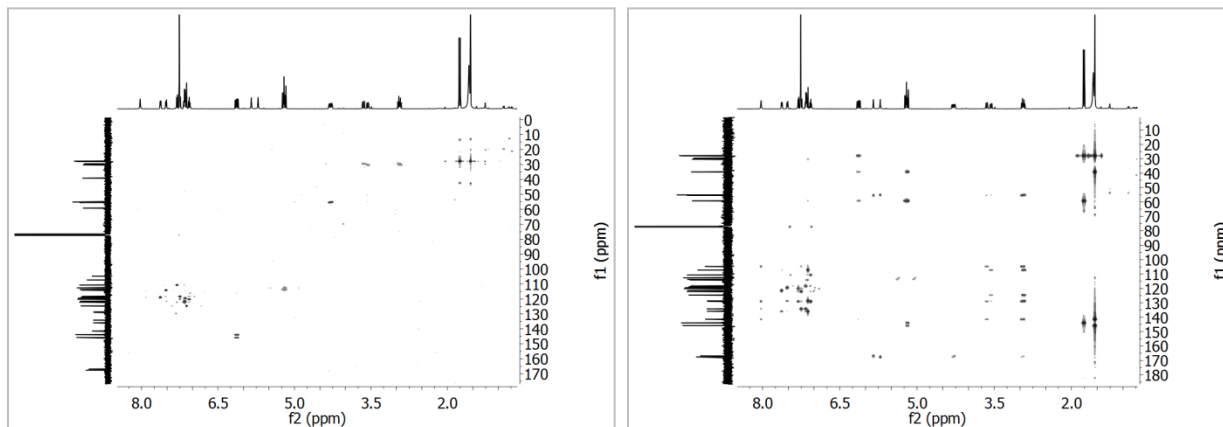


Figure 4.1.25.4 HSQC (left) and HMBC (right) NMR spectra (in CDCl_3) of compound 25.

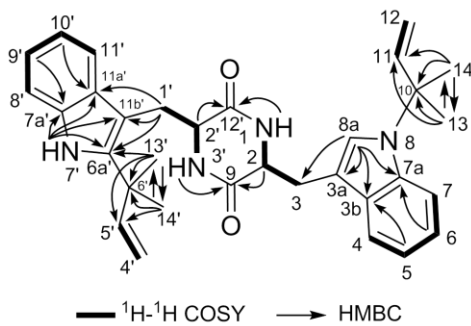


Figure 4.1.25.5 $^1\text{H}-^1\text{H}$ COSY and Key HMBC correlations of compound 25.

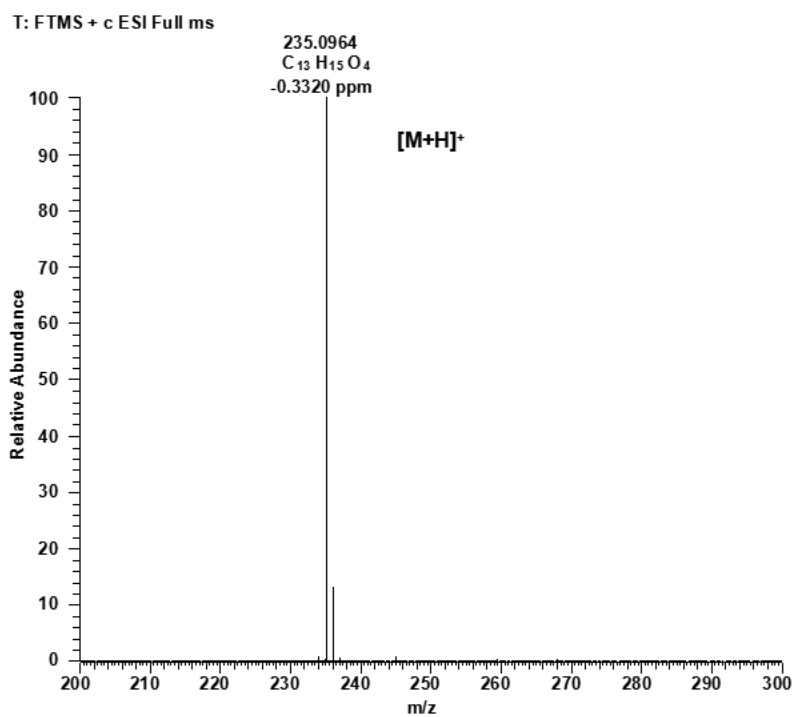


Figure 4.1.26.1 Positive ESI-HRMS spectrum of compound 26.

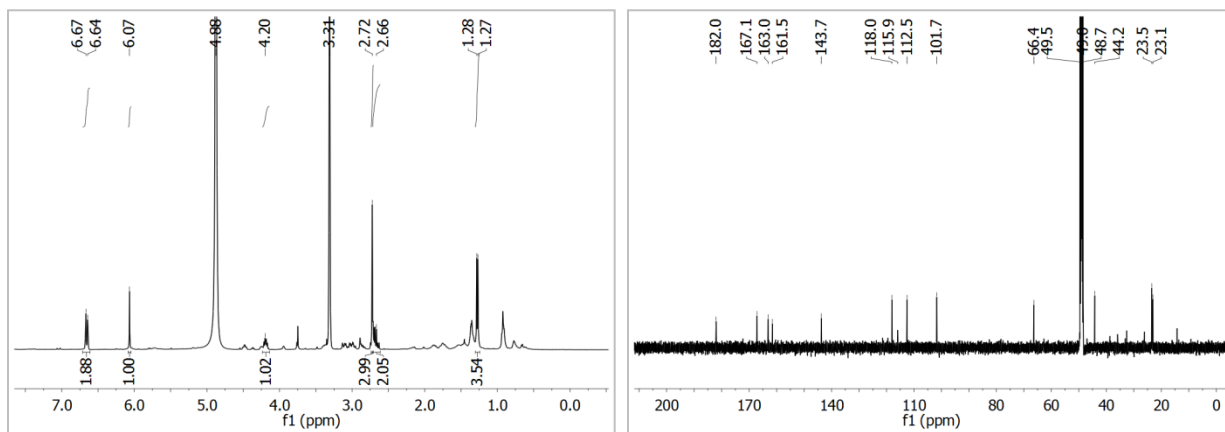


Figure 4.1.26.2 ^1H and ^{13}C NMR spectra (in CD_3OD) of compound 26.

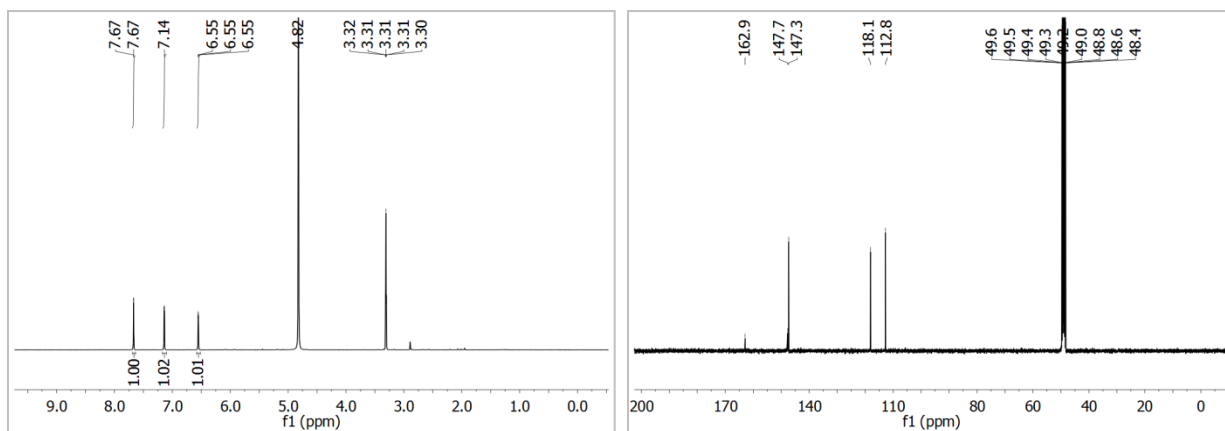


Figure 4.1.27.1 ^1H and ^{13}C NMR spectra (in CD_3OD) of compound 27.

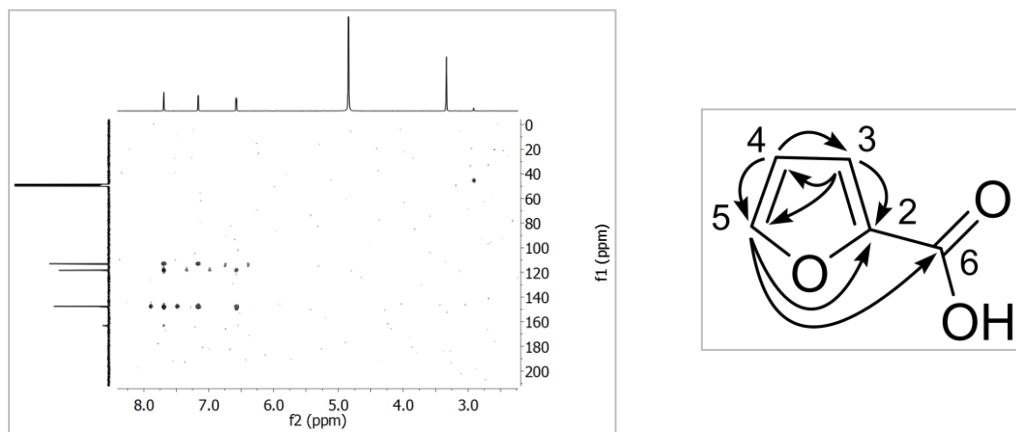


Figure 4.1.27.2 HMBC spectrum and key HMBC correlations (500 MHz) of compound 27.

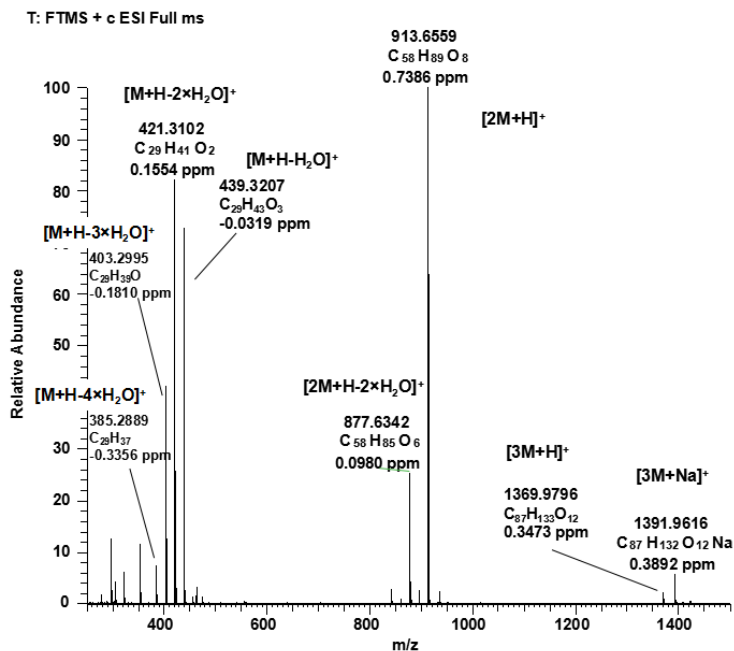
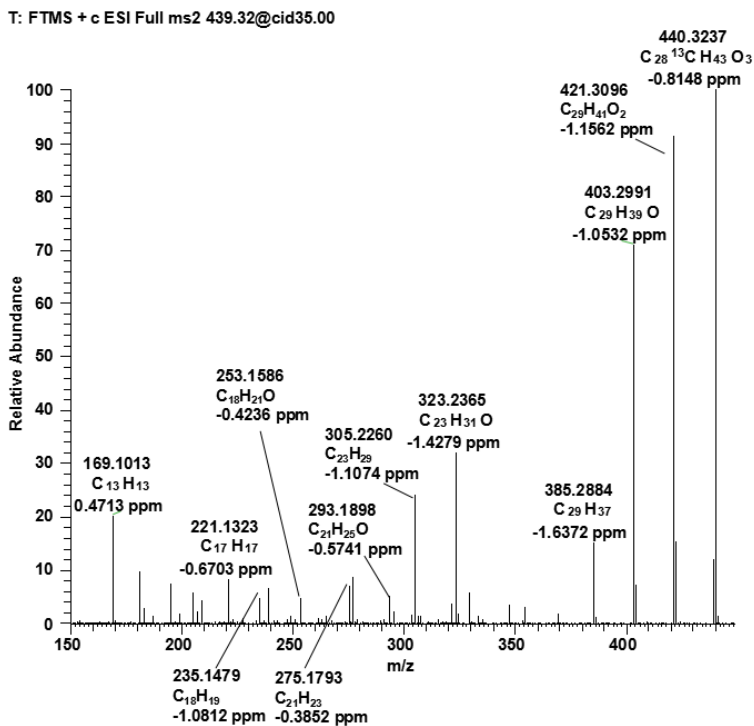


Figure 4.2.1.1 Positive ESI-HRMS spectrum of 28.

Figure 4.2.1.2 Positive ESI-HRMS/MS spectrum (MS/MS of m/z 439.32) of 28.

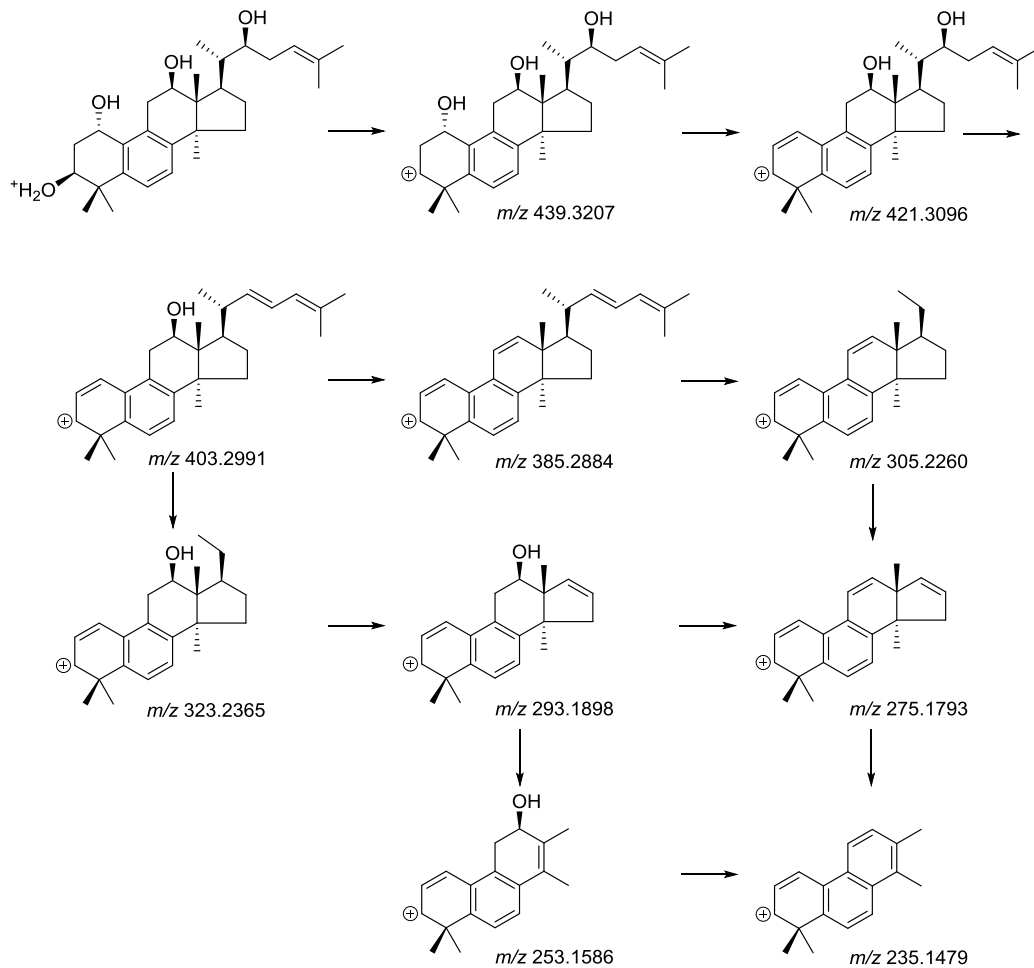


Figure 4.2.1.3 Proposed collision-induced mass spectral fragmentation pathway of **28** in positive ESI mode.

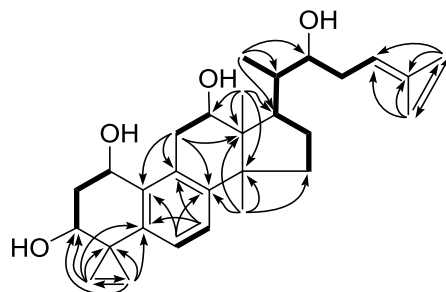


Figure 4.2.1.4 Key HMBC correlations of compound **28**.

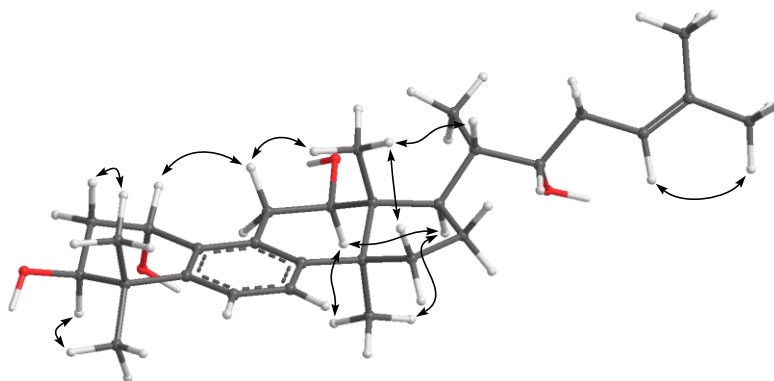


Figure 4.2.1.5 The key NOESY correlations of compound **28**.

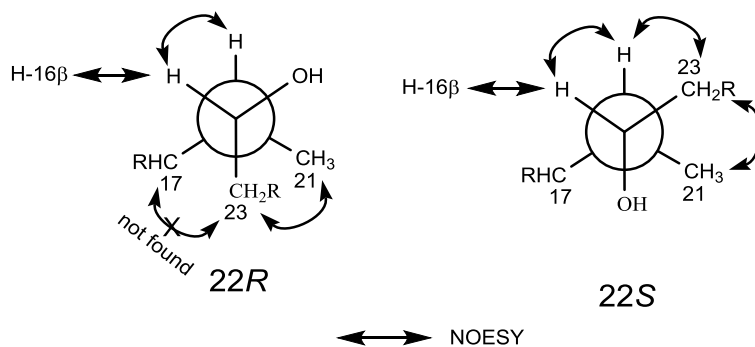


Figure 4.2.1.6 The two possible configurations of C-17, C-20, C-21, C-22, and C-23 in **28**.

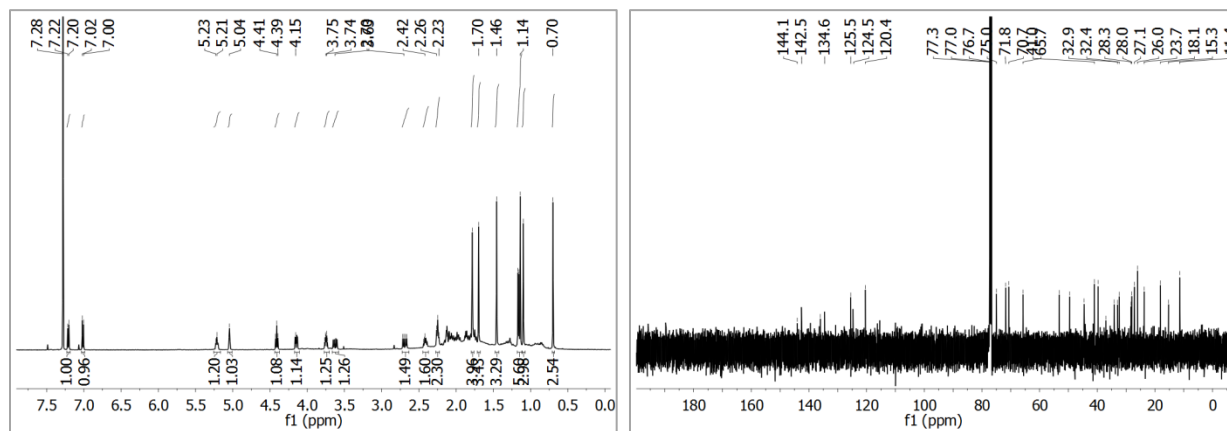


Figure 4.2.1.7 ¹H (left) and ¹³C (right) NMR spectra of compound **28** in CDCl₃.

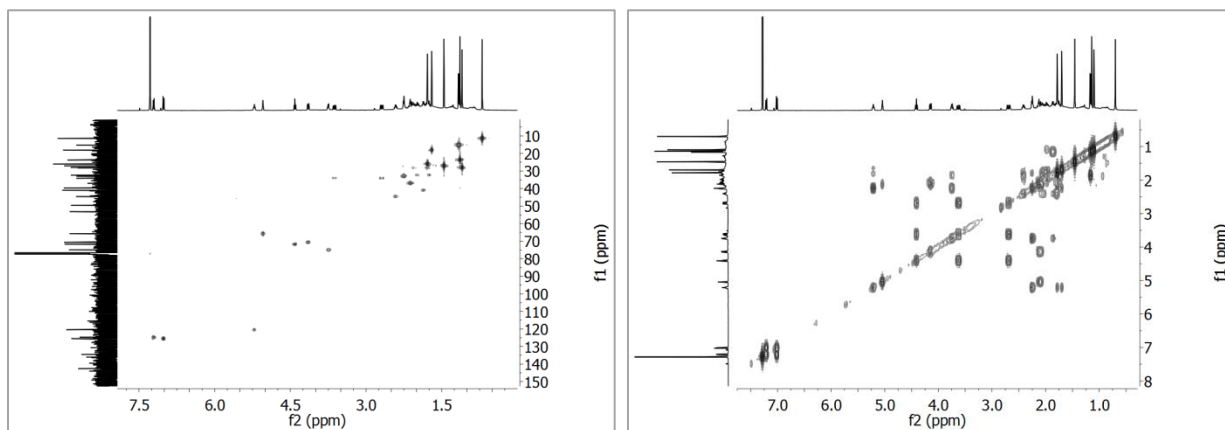


Figure 4.2.1.8 HSQC (left) and ¹H-¹H COSY (right) NMR spectra of compound **28** in CDCl₃.

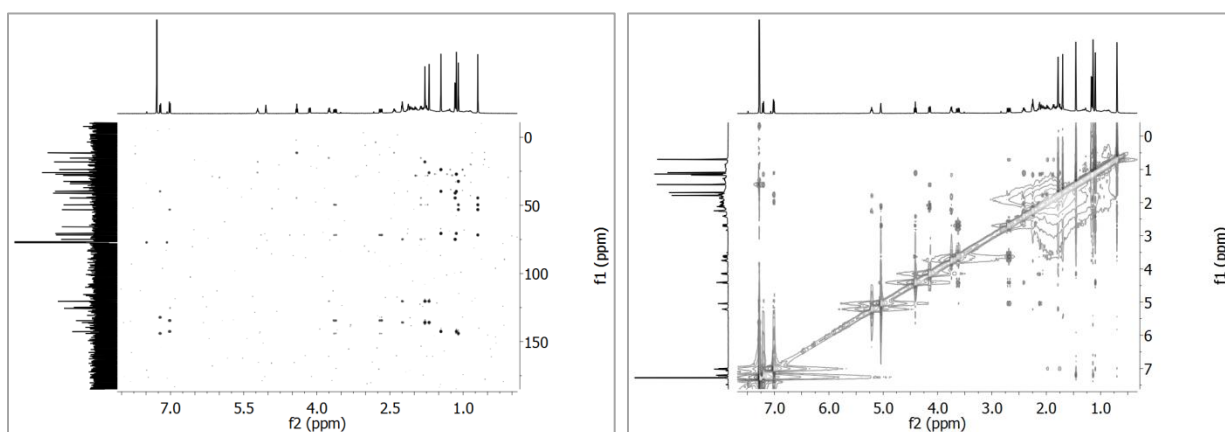


Figure 4.2.1.9 HMBC (left) and NOESY (right) NMR spectra of compound **28** in CDCl₃.

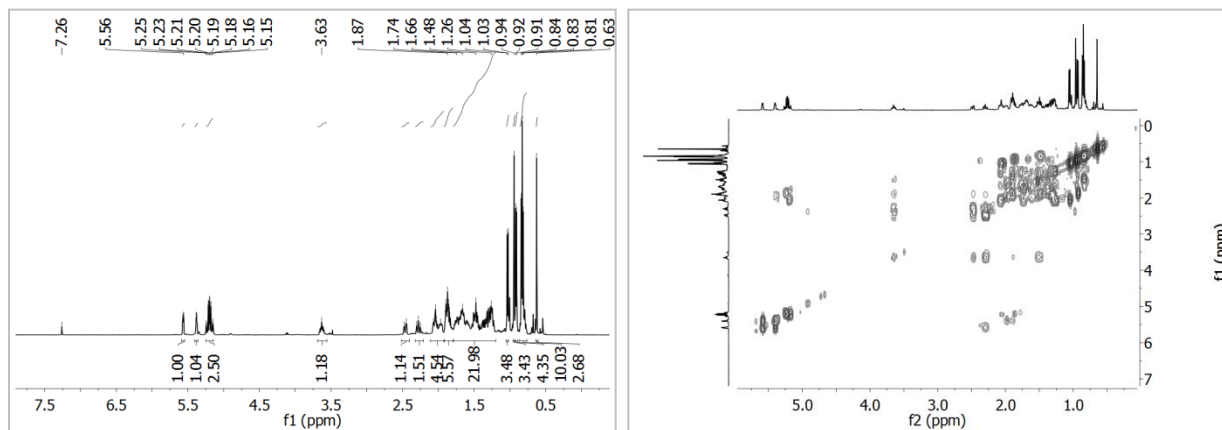


Figure 4.2.2.1 ¹H (left) and ¹H-¹H COSY (right) spectra of compound **29** in CDCl₃.

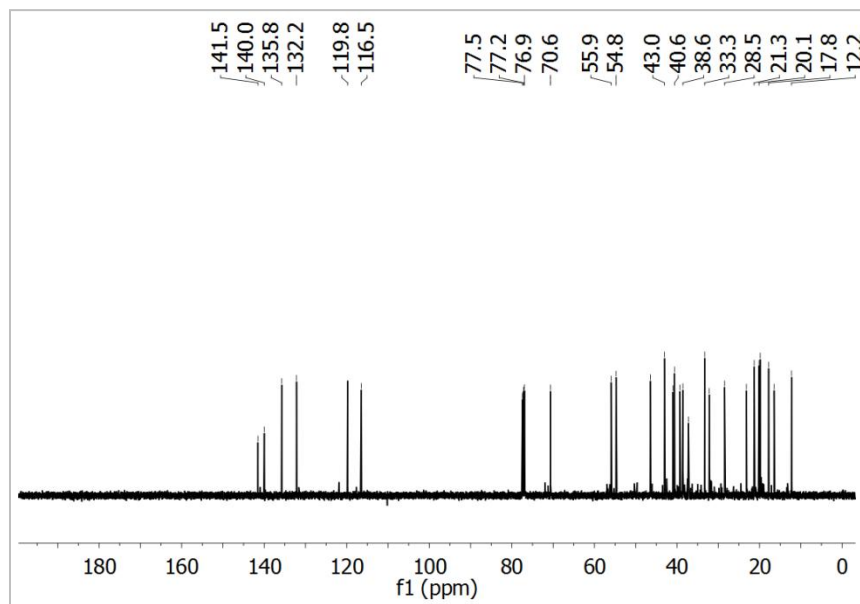


Figure 4.2.2.2 ^{13}C NMR spectrum of compound **29** in CDCl_3 .

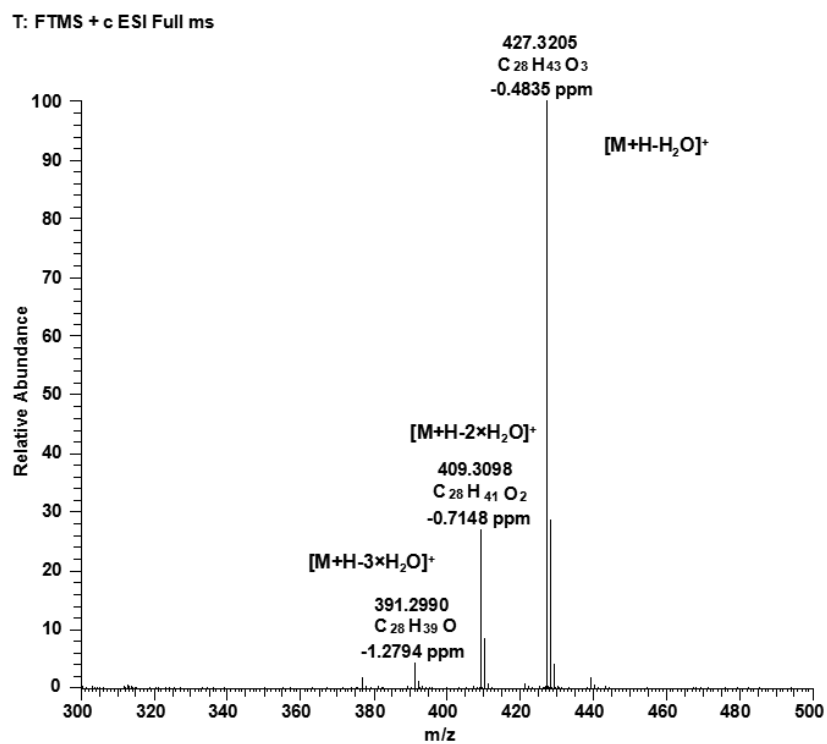


Figure 4.2.3.1 Positive ESI-HRMS spectrum of compound **30**.

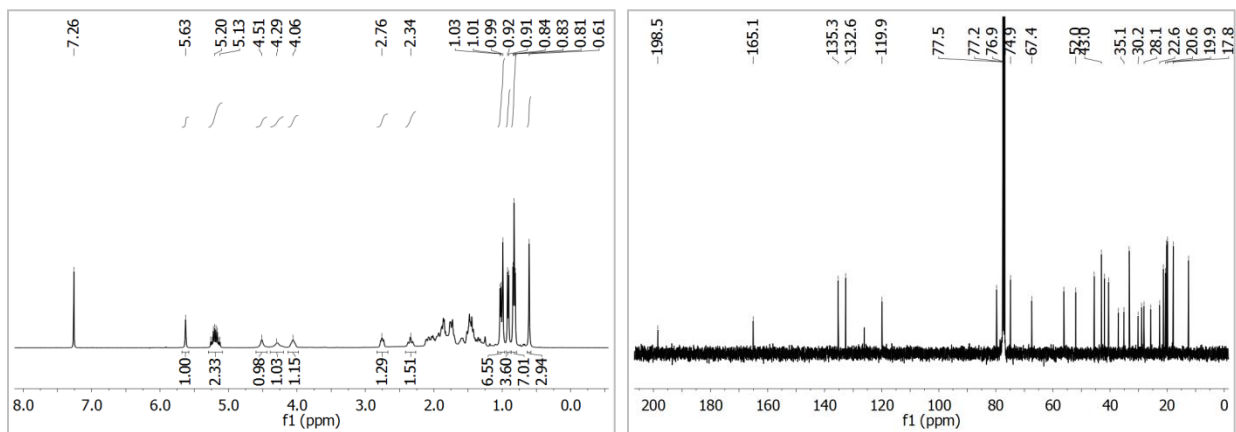


Figure 4.2.3.2 ¹H (left) and ¹³C (right) NMR spectra of compound 30 in CDCl₃.

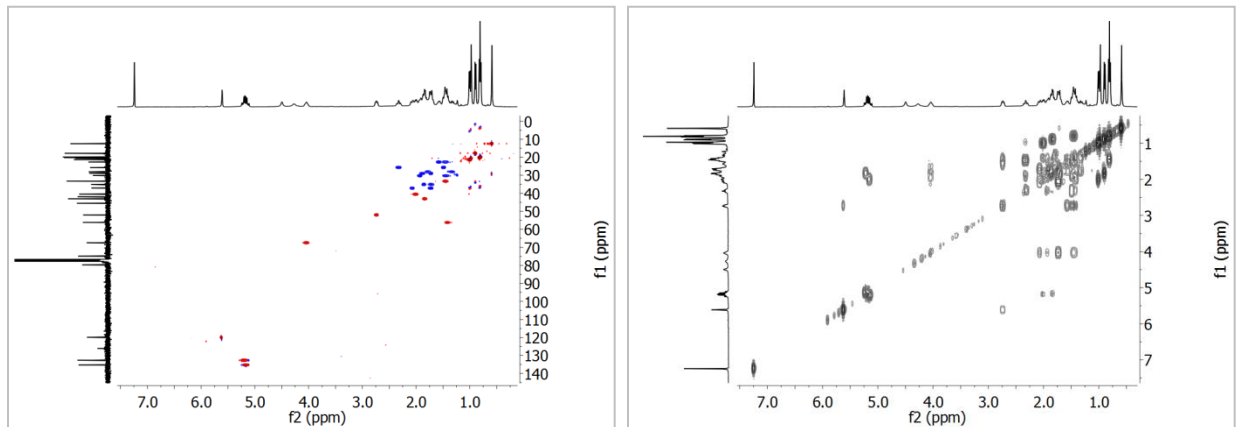


Figure 4.2.3.3 The HSQC (left) and ¹H-¹H COSY (right) spectra of compound 30 in CDCl₃.

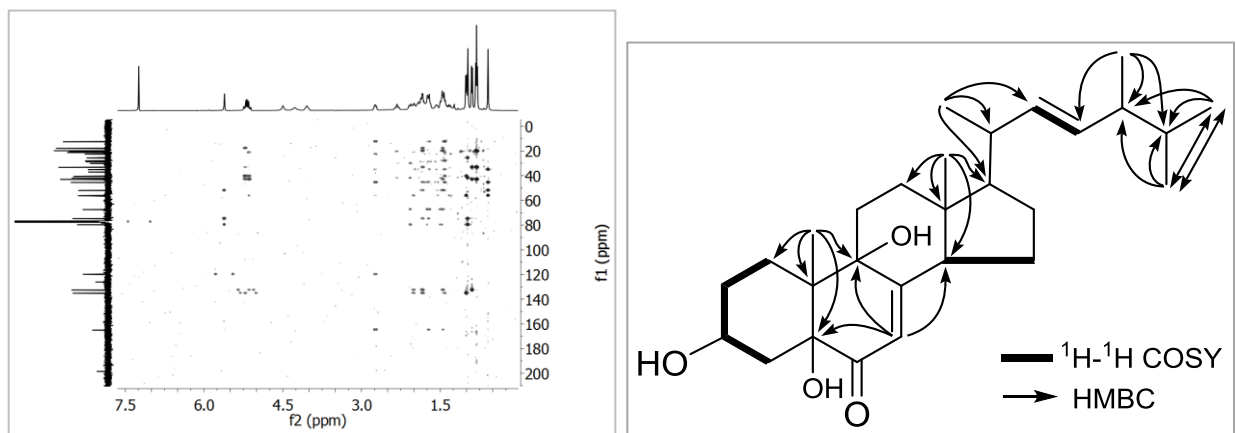


Figure 4.2.3.4 HMBC spectrum (left) and key ¹H-¹H COSY and HMBC correlations (right) of compound 30.

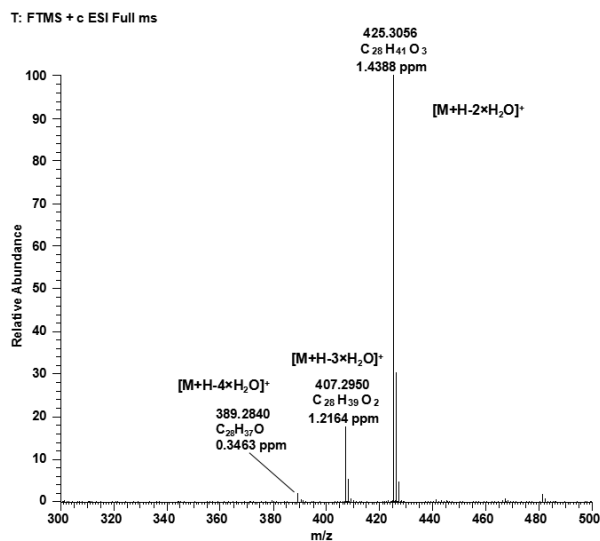


Figure 4.2.4.1 Positive ESI-HRMS spectrum of compound **31**.

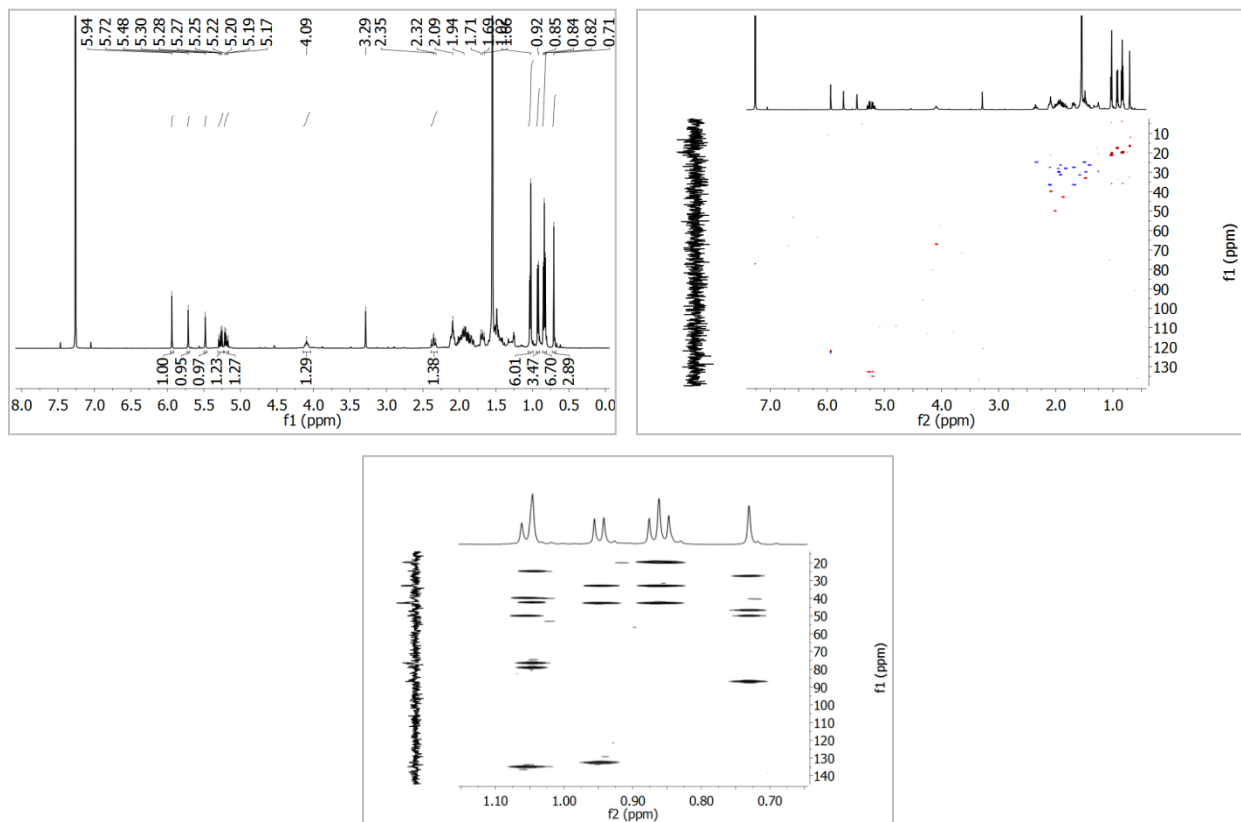


Figure 4.2.4.2 ¹H (up, left) and HSQC (up, right) spectra together with the partial HMBC (bottom) spectrum of compound **31** in CDCl₃.

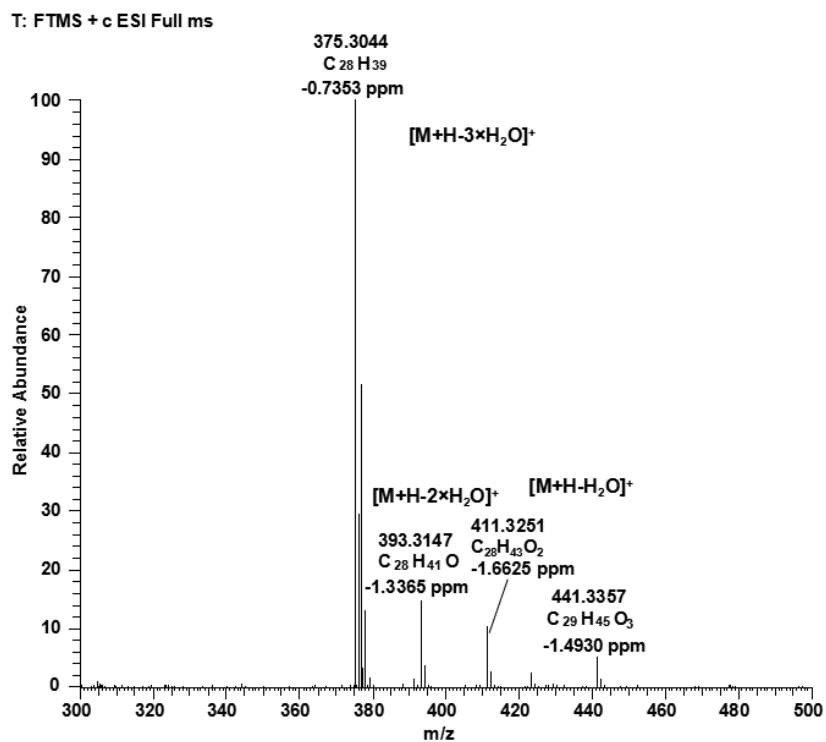


Figure 4.2.5.1 Positive ESI-HRMS spectrum of compound **32**.

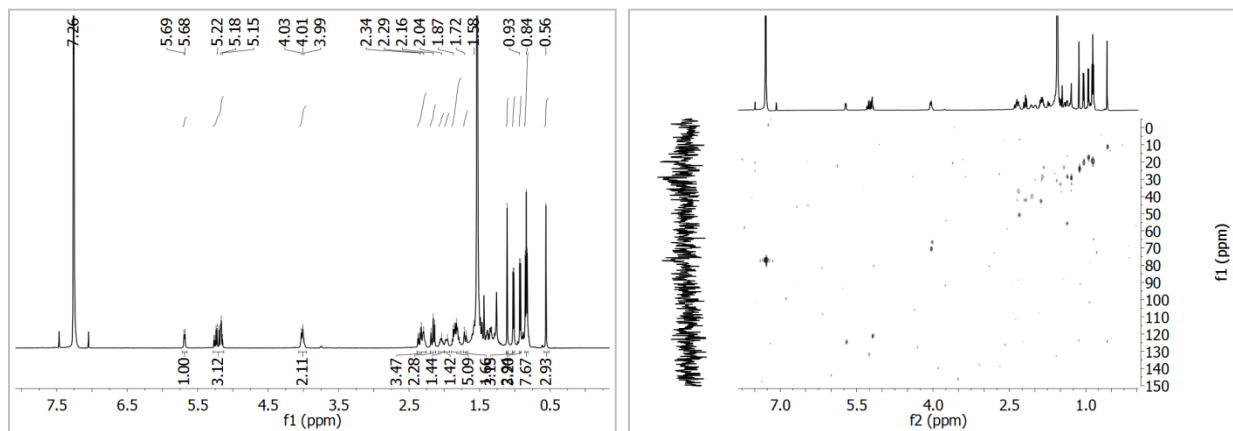


Figure 4.2.5.2 ¹H (left) and HSQC (right) spectra of compound **32** in CDCl₃.

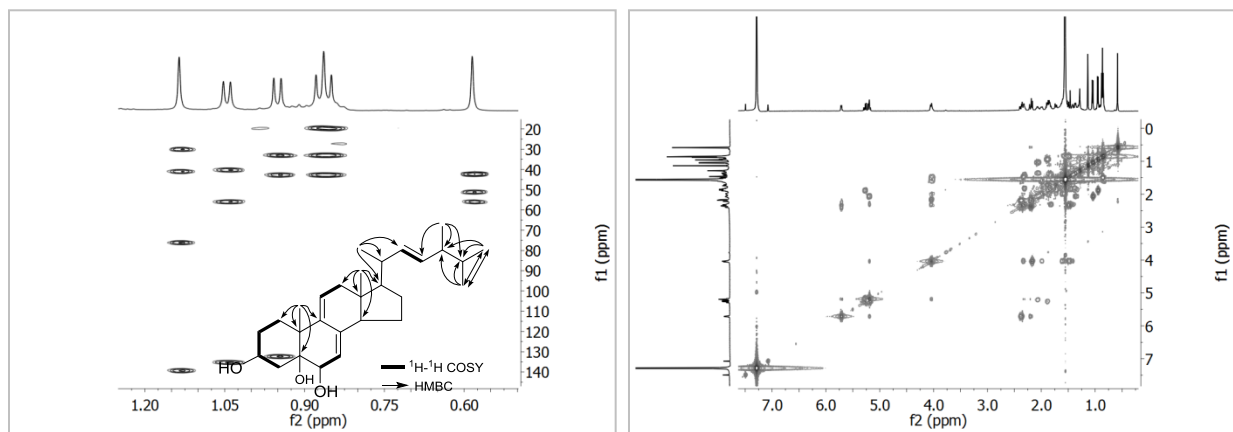


Figure 4.2.5.3 Partial HMBC (left) and ¹H-¹H COSY (right) spectra for compound **32** in CDCl₃.

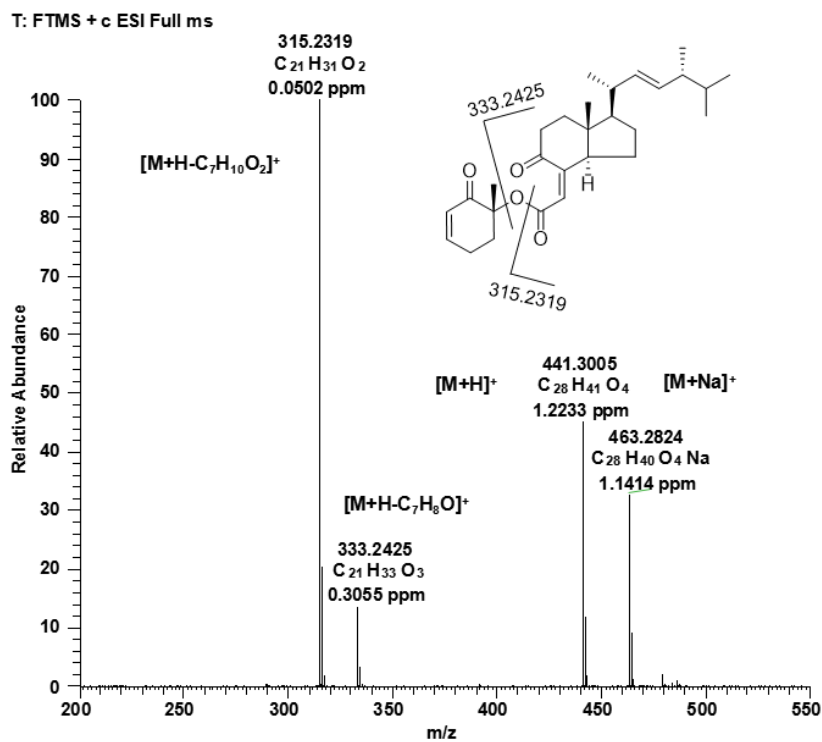


Figure 4.2.6.1 Positive ESI-HRMS spectrum of compound **33**.

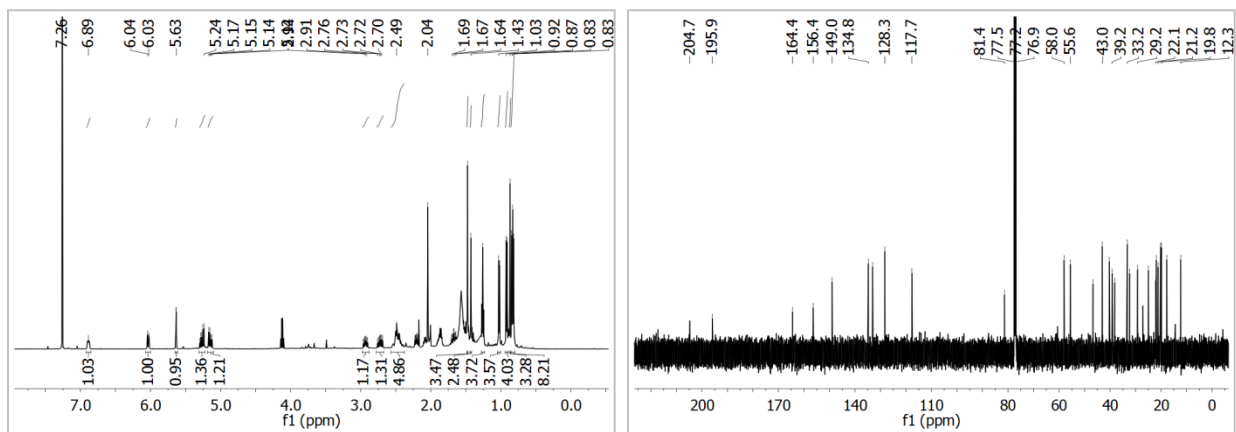


Figure 4.2.6.2 ^1H (left) and ^{13}C (right) NMR spectra of compound **33** in CDCl_3 .

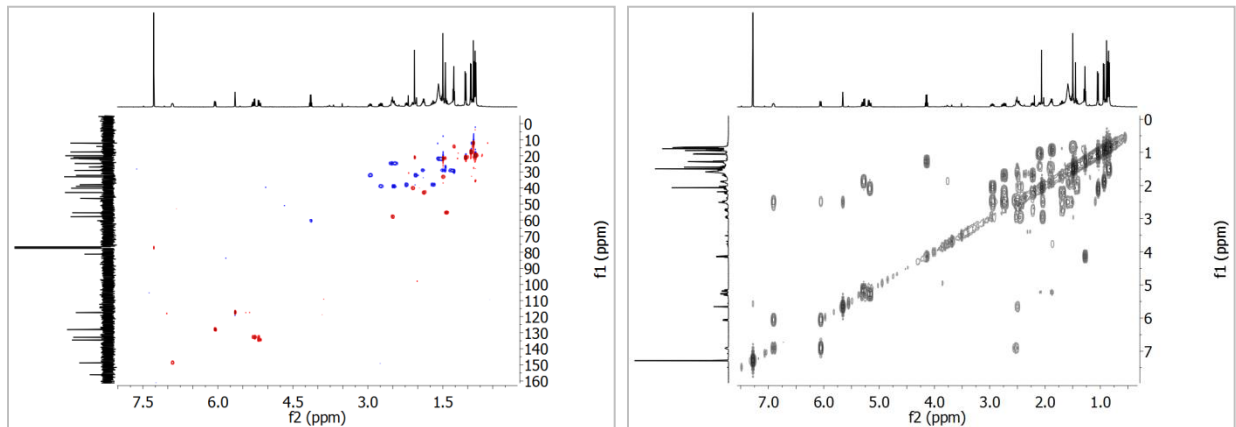


Figure 4.2.6.3 HSQC (left) and ^1H - ^1H COSY (right) spectra of compound **33** in CDCl_3 .

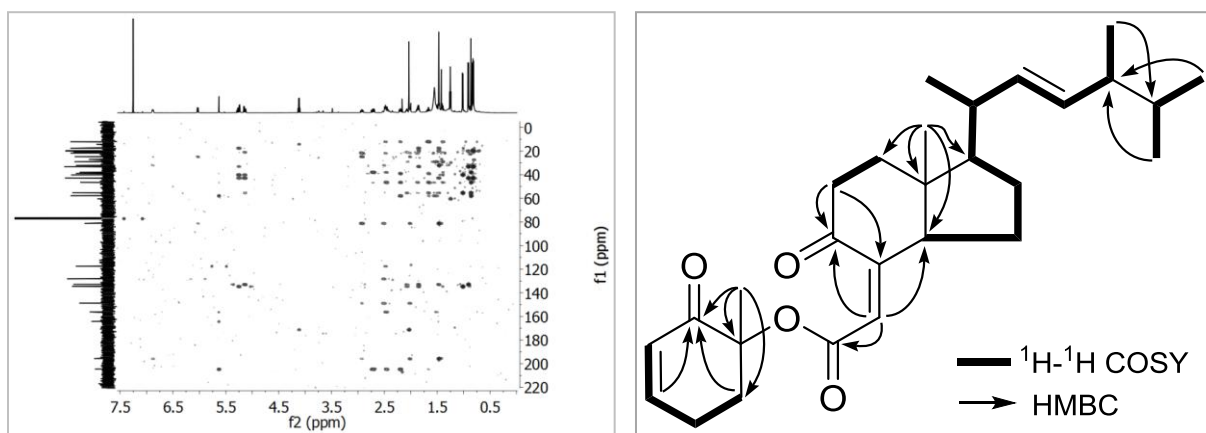


Figure 4.2.6.4 HMBC spectrum (left) , and key ^1H - ^1H COSY and HMBC correlations of compound **33**.

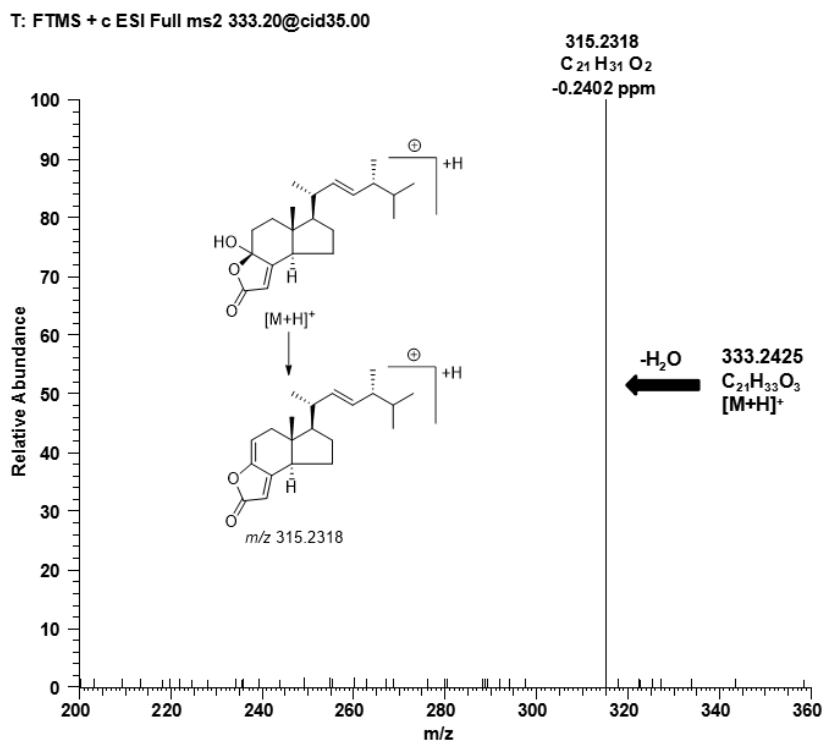
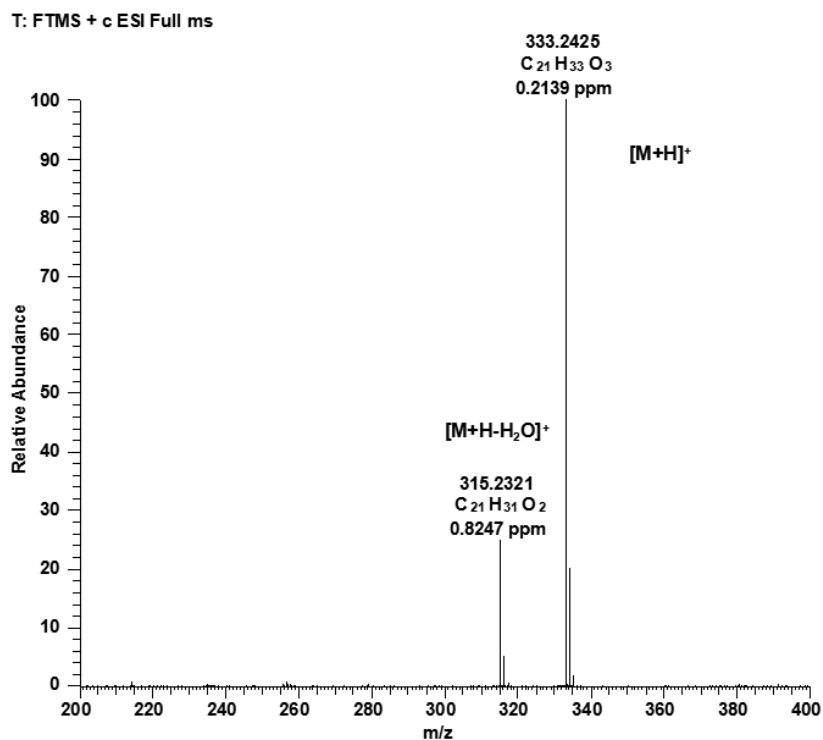


Figure 4.2.7.1 Positive ESI-HRMS (top) and MS/MS (bottom) spectra of compound 34.

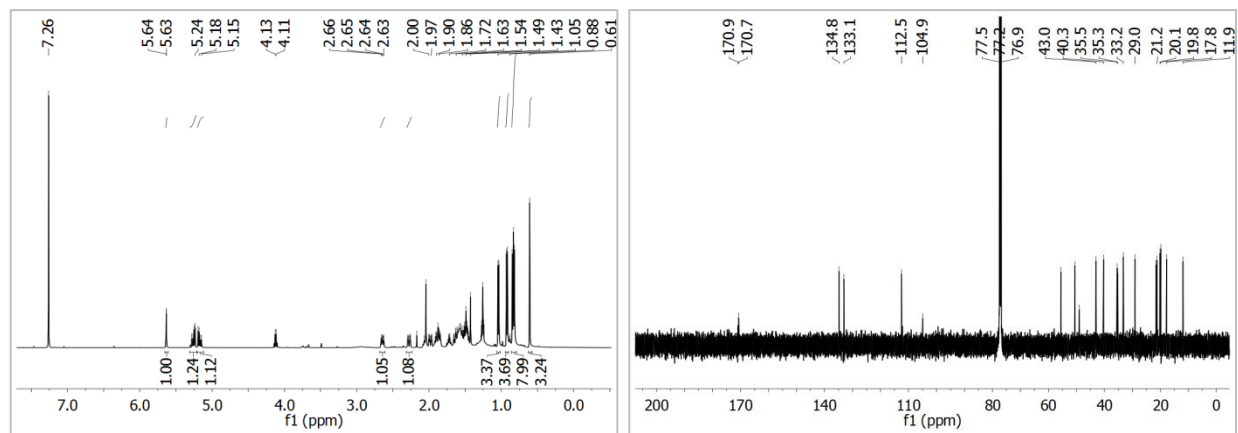
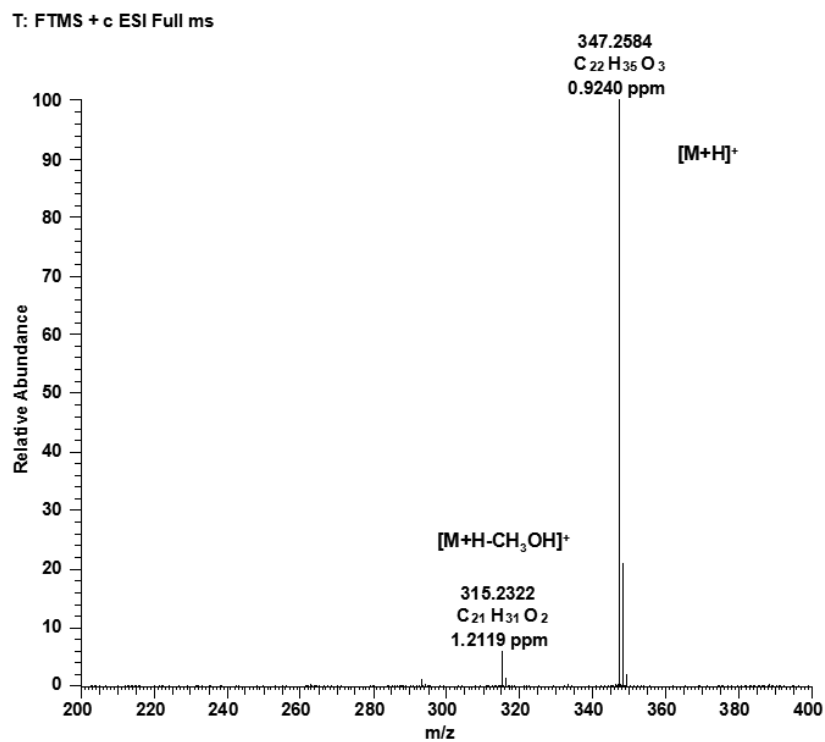


Figure 4.2.7.2 ¹H (left) and ¹³C (right) NMR spectra of compound 34 in CDCl₃.



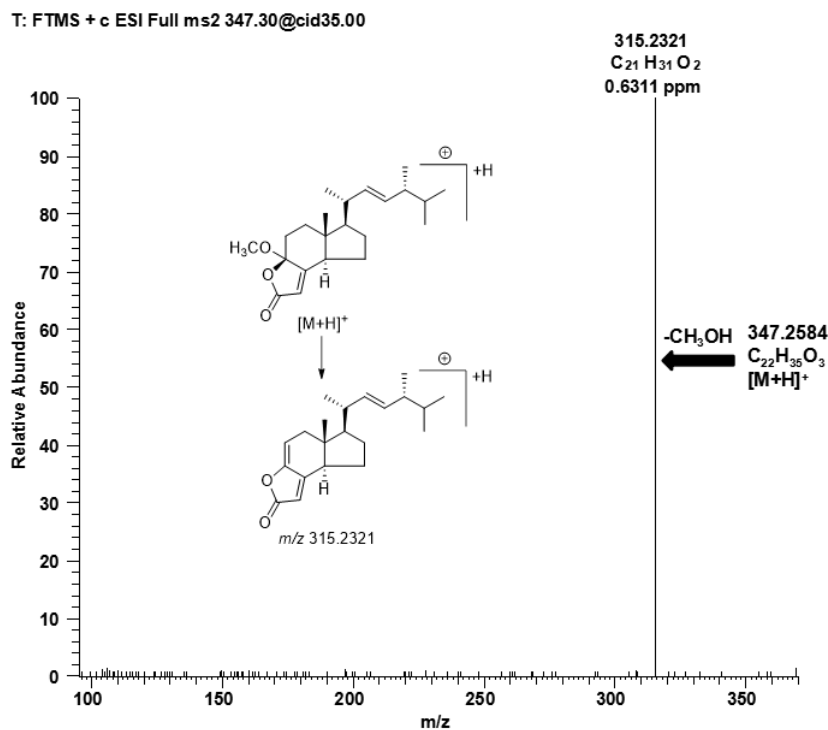


Figure 4.2.8.1 Positive ESI-HRMS (top) and MS/MS (bottom) spectra of compound **35**.

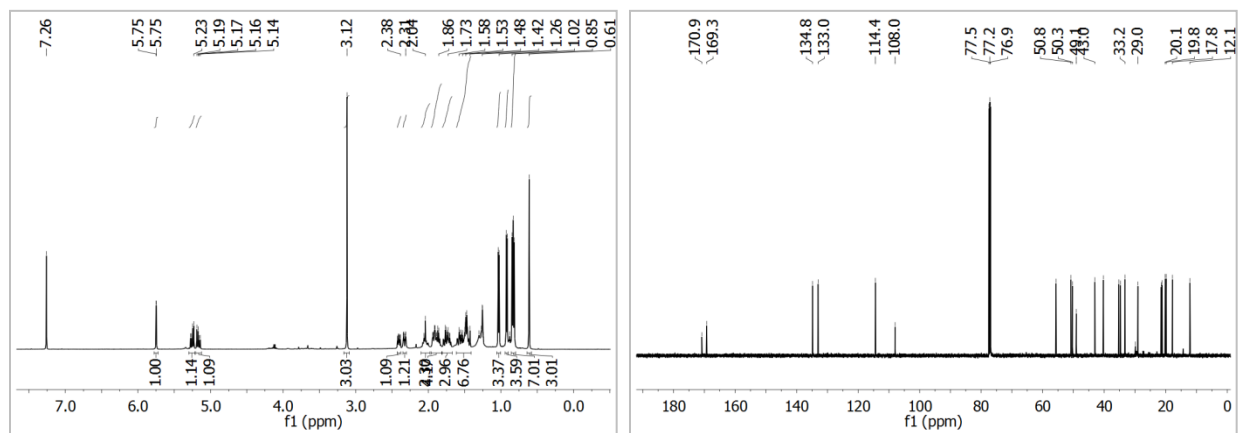


Figure 4.2.8.2 ¹H (left) and ¹³C (right) NMR spectra of compound **35** in CDCl₃.

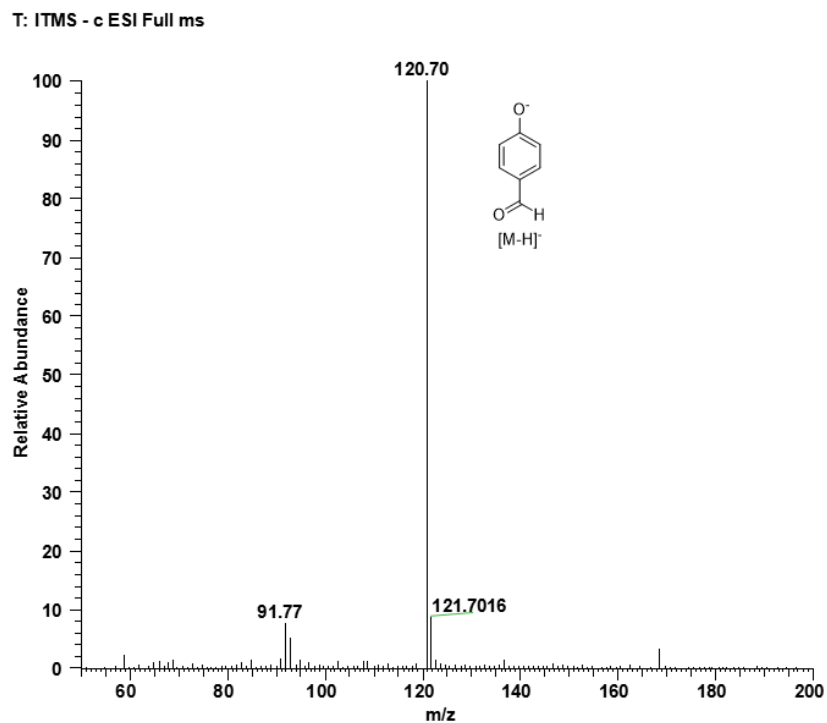


Figure 4.2.9.1 Negative ESI-HRMS spectrum of compound **36**.

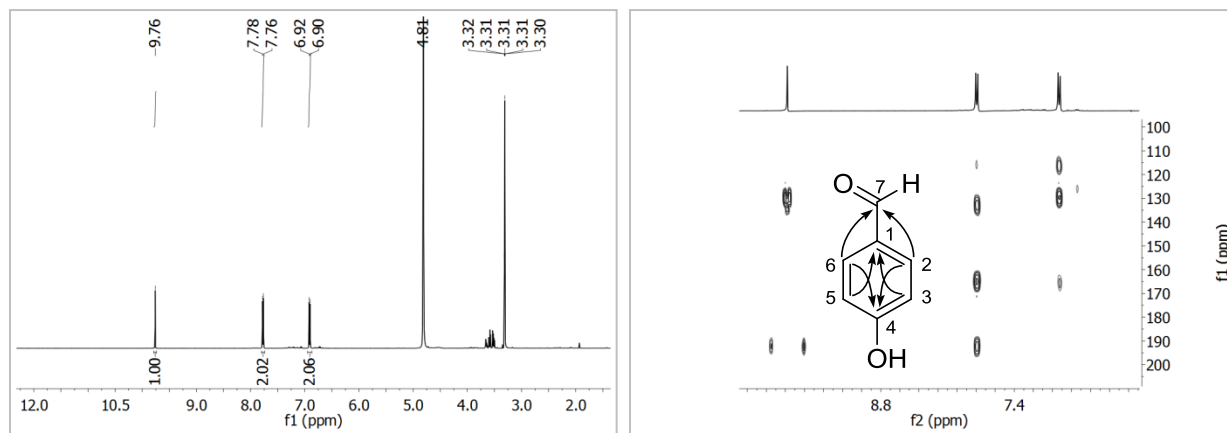


Figure 4.2.9.2 ¹H (left) and partial HMBC (right) NMR spectra of compound **36** in CD₃OD.

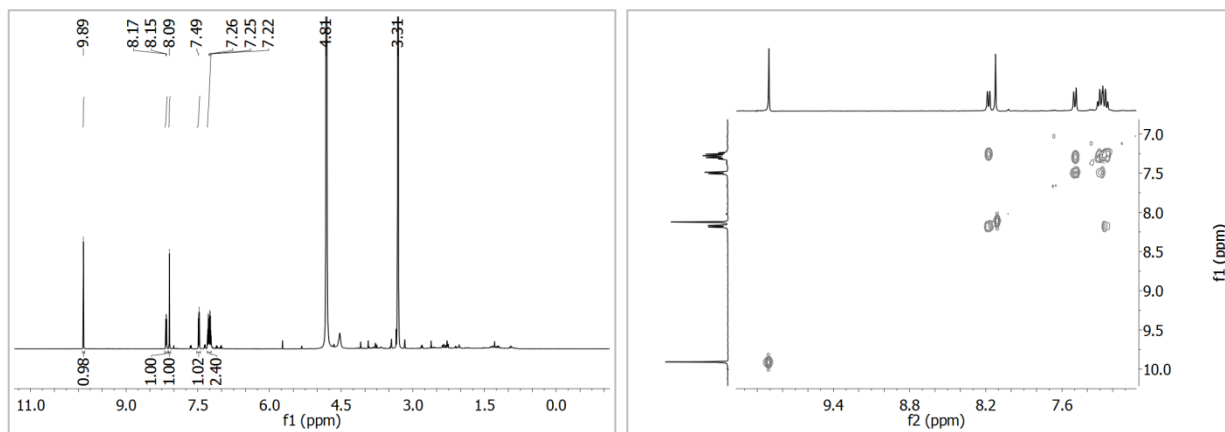


Figure 4.2.10.1 ¹H (left) and ¹H-¹H COSY (right) NMR spectra of compound **37** in CD₃OD.

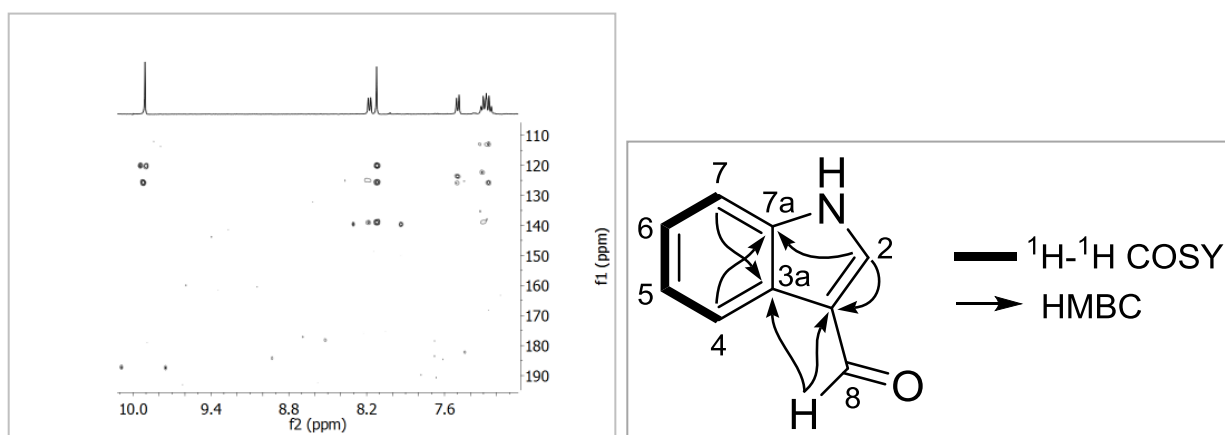


Figure 4.2.10.2 HMBC (left) spectrum and key ¹H-¹H COSY and HMBC correlations (right) of compound **37**.

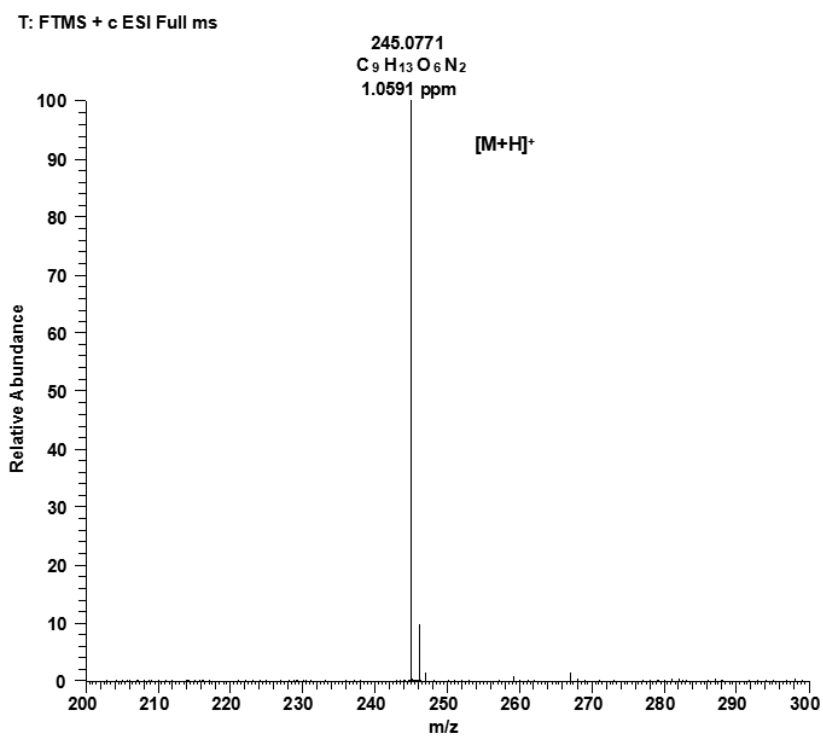


Figure 4.2.11.1 Positive ESI-HRMS spectrum of compound **38**.

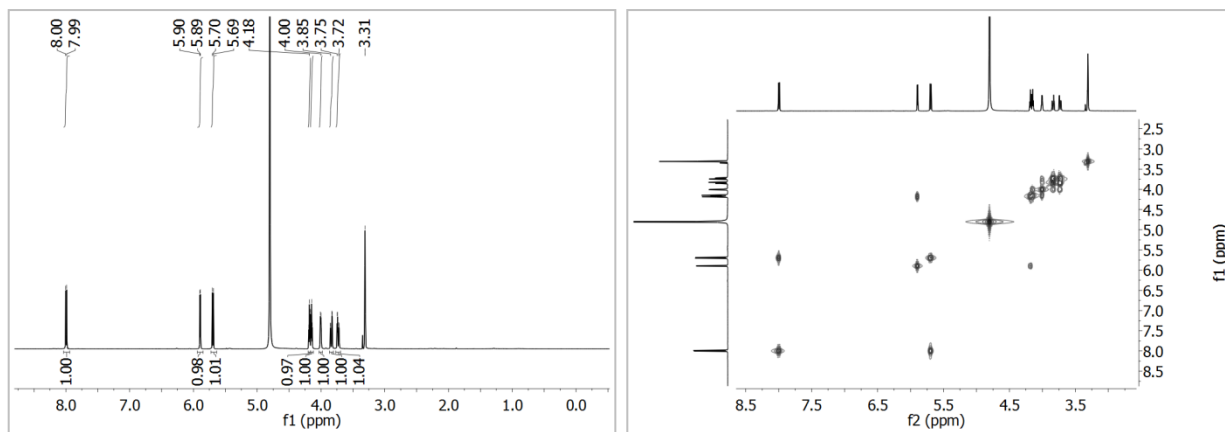


Figure 4.2.11.2 1H (left) and 1H - 1H COSY (right) NMR spectra of compound **38** in CD_3OD .

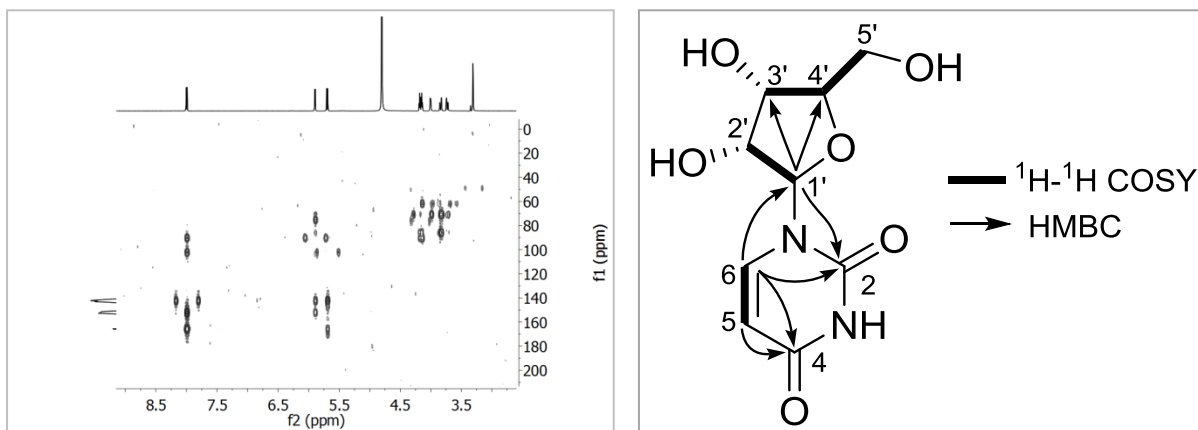


Figure 4.2.11.3 HMBC (left) spectrum and key $^1\text{H}-^1\text{H}$ COSY and HMBC correlations (right) of compound **38**.

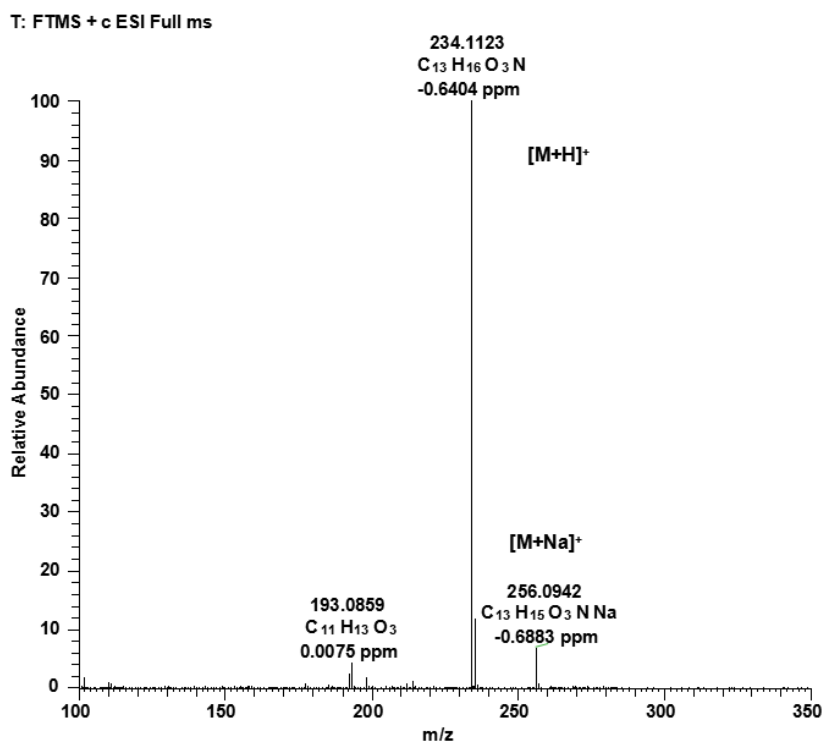


Figure 4.2.12.1 Positive ESI-HRMS spectrum of compound **39**.

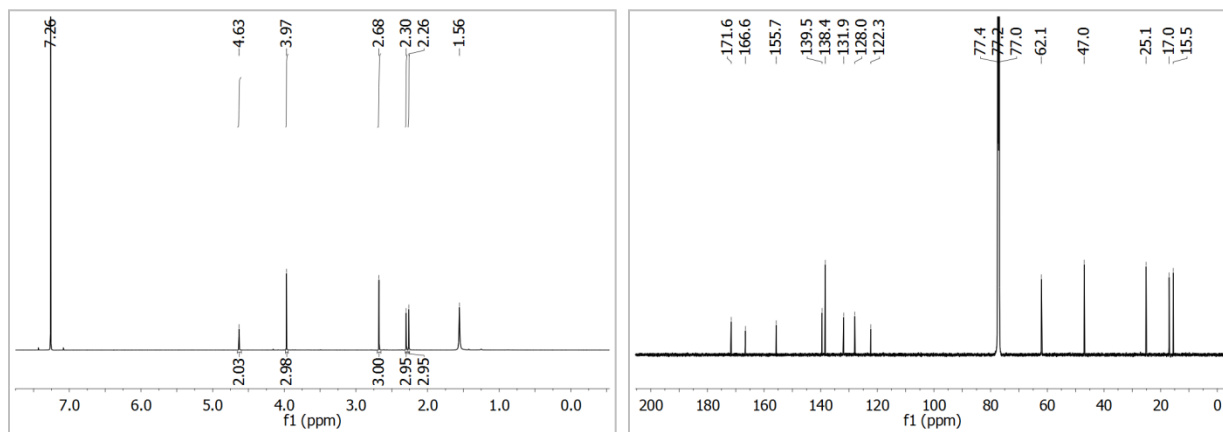


Figure 4.2.12.2 ^1H (left) and ^{13}C (right) NMR spectra of compound **39** in CDCl_3 .

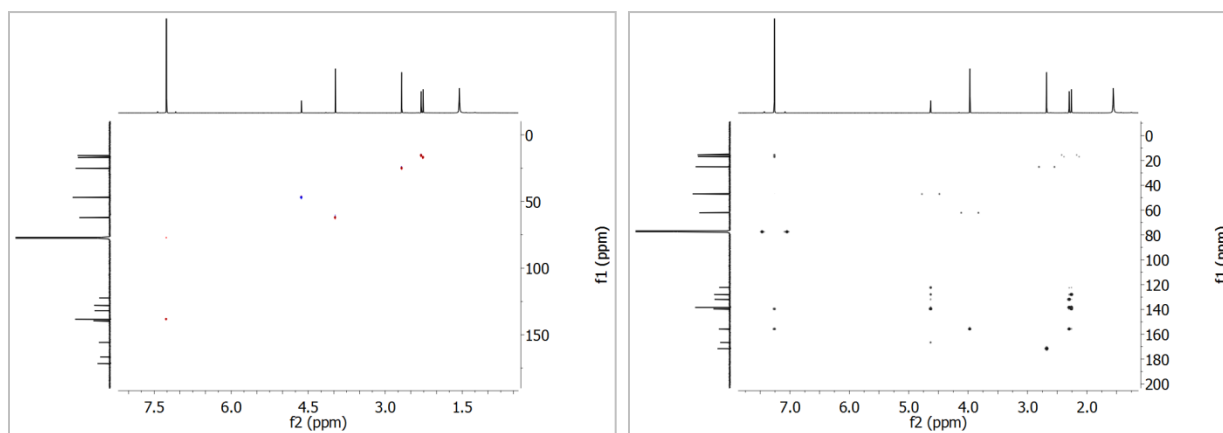


Figure 4.2.12.3 HSQC (left) and HMBC (right) NMR spectra of compound **39** in CDCl_3 .

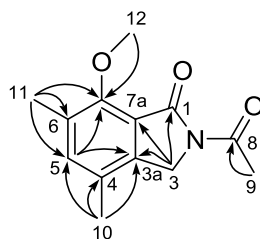


Figure 4.2.12.4 Key HMBC correlations of compound **39**.

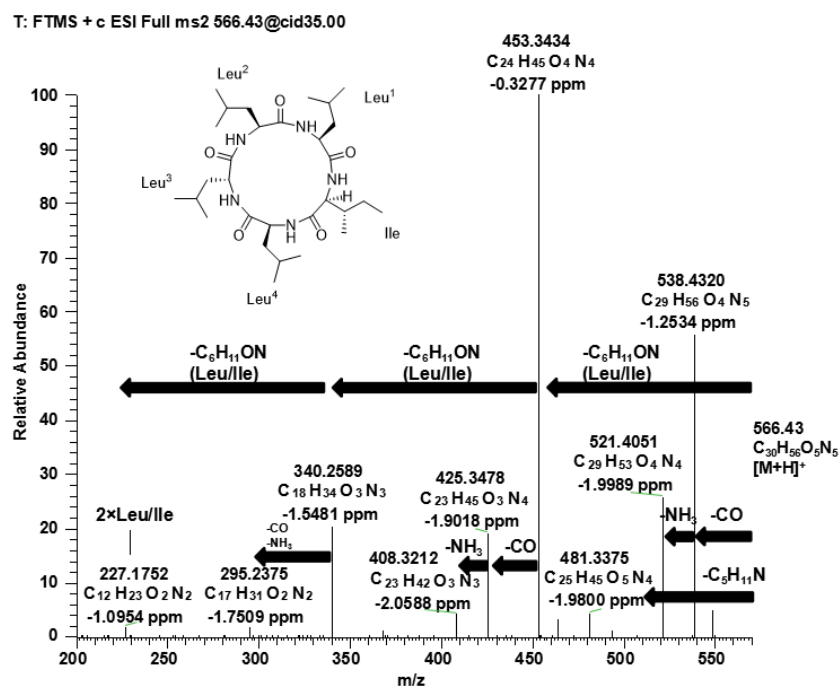
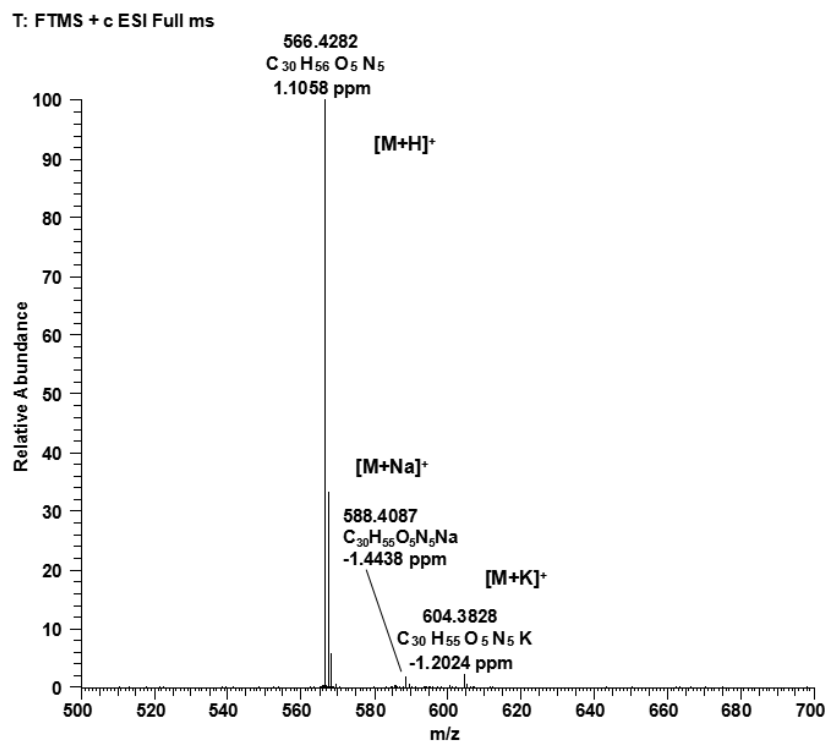


Figure 4.3.1.1 Positive ESI-HRMS (top) and MS/MS (bottom) spectra of compound 40.

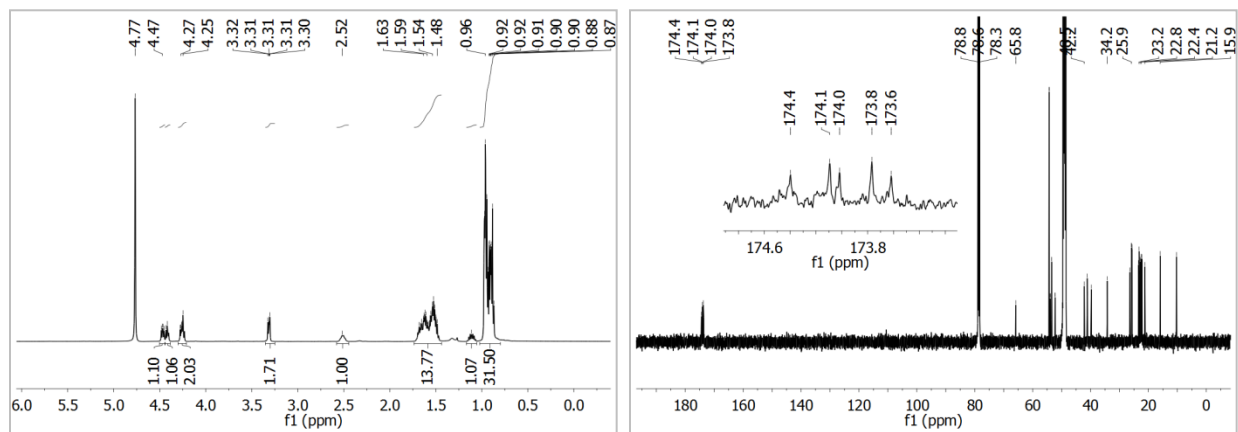


Figure 4.3.1.2 ^1H (left) and ^{13}C (right) NMR spectra (in $\text{CDCl}_3:\text{CD}_3\text{OD} = 1:3$) of compound **40**.

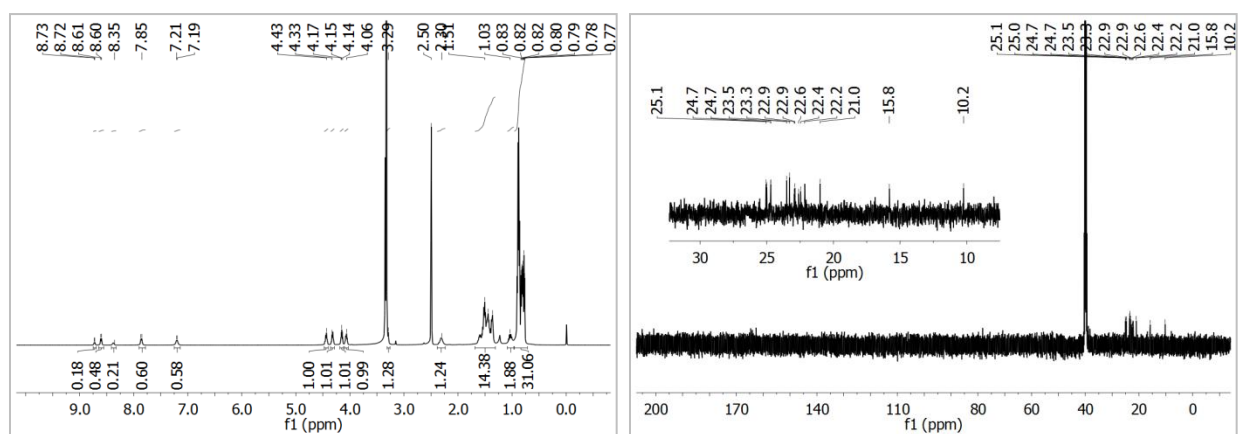


Figure 4.3.1.3 ^1H (left) and ^{13}C (right) NMR spectra (in $\text{DMSO}-d_6$) of compound **40**.

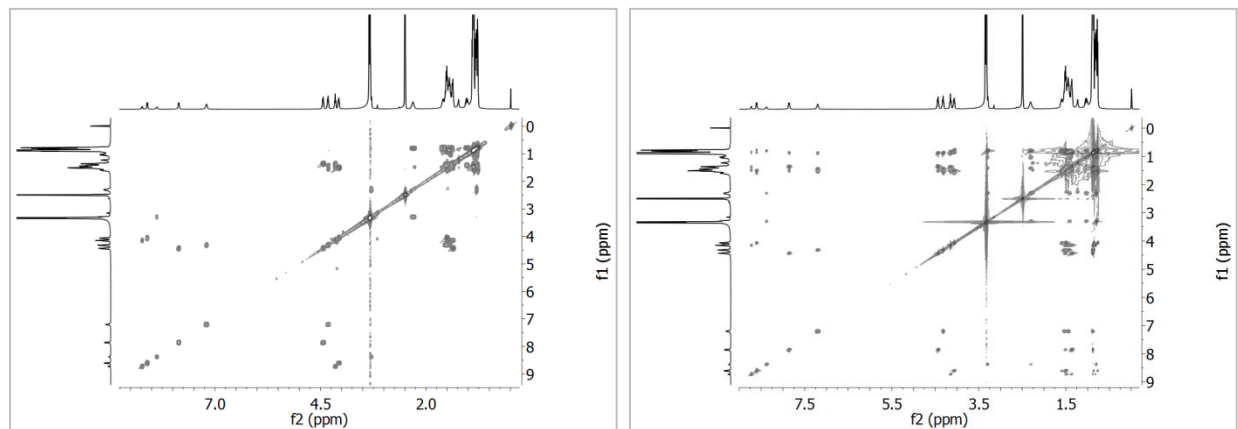


Figure 4.3.1.4 ^1H - ^1H COSY (left) and TOCSY (right) NMR spectra (in $\text{DMSO}-d_6$) of compound **40**.

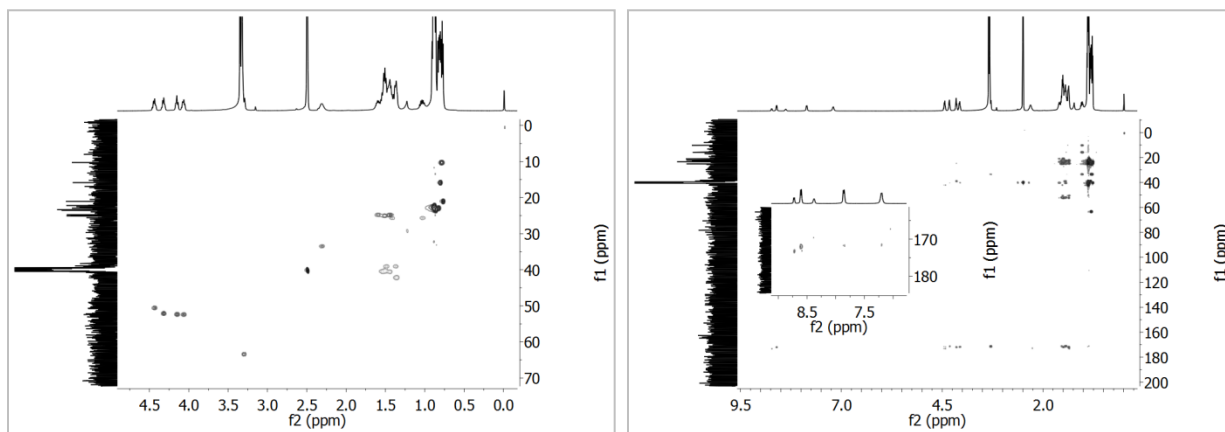


Figure 4.3.1.5 HSQC (left) and HMBC (right) spectra (in DMSO- d_6) of **40**.

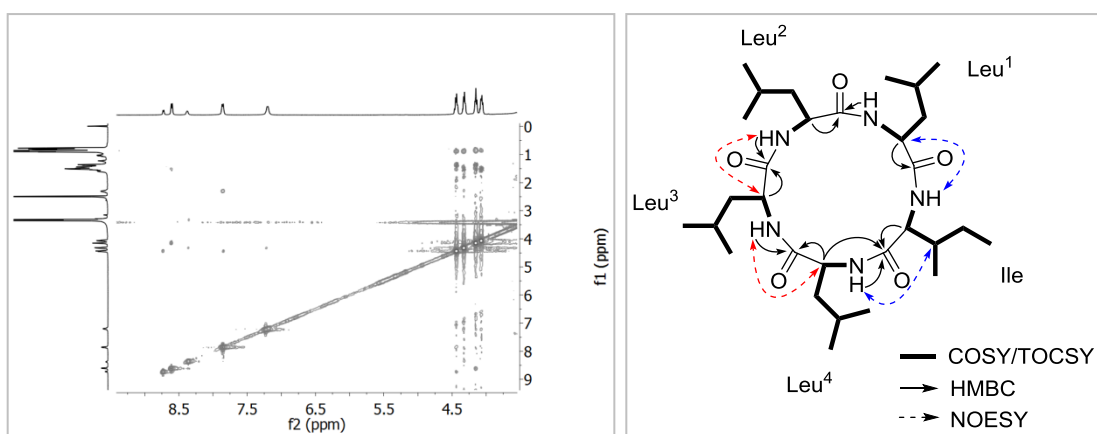


Figure 4.3.1.6 NOESY spectrum (left, in DMSO- d_6) and key ^1H - ^1H COSY, HMBC, and NOESY correlations (right) of **40**. The NOE cross-peaks marked in blue color indicated the small structural difference in solution compared to that of its crystal structure.

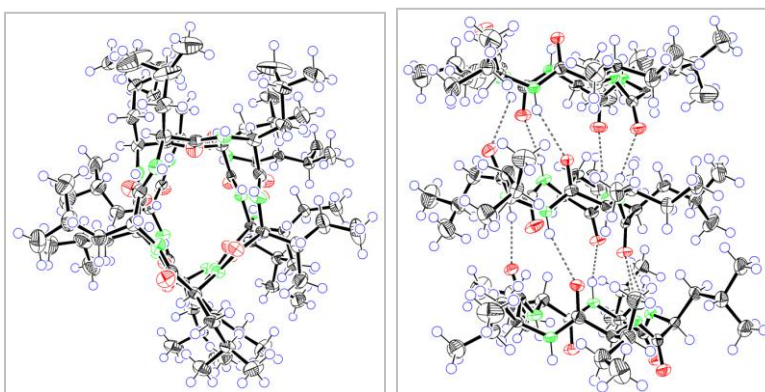
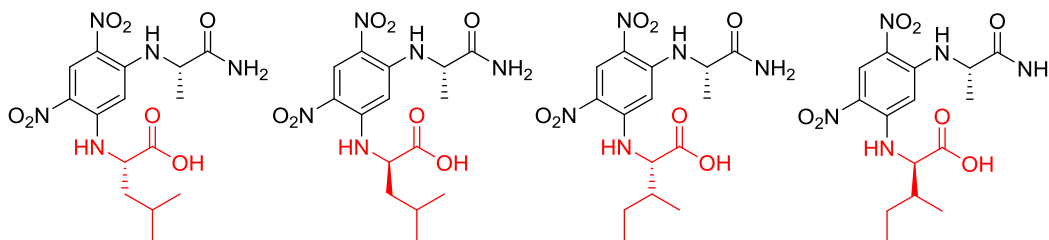


Figure 4.3.1.7 The Ortep drawing of compound **40**.

A:



B:

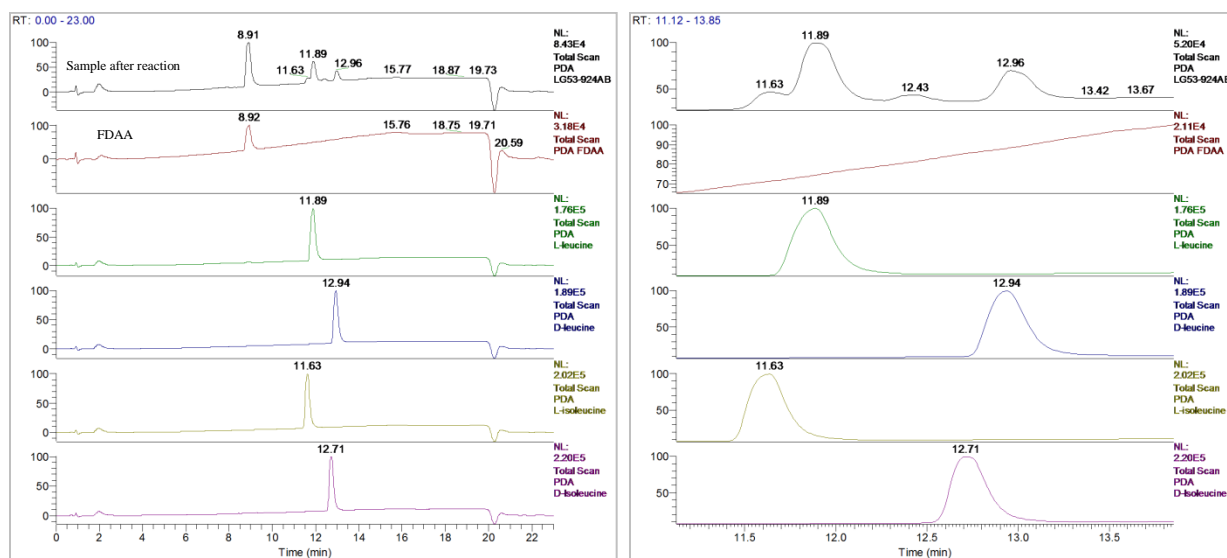


Figure 4.3.1.8 The Marfey's method for assigning the absolute configurations of amino acid residues. A: Marfey's reagent FDAA-derived amino acid standards. B: LC-MS for FDAA derivatives of the hydrolysis of **40** (left) and amino acid standards; enlarged LC-MS (right).

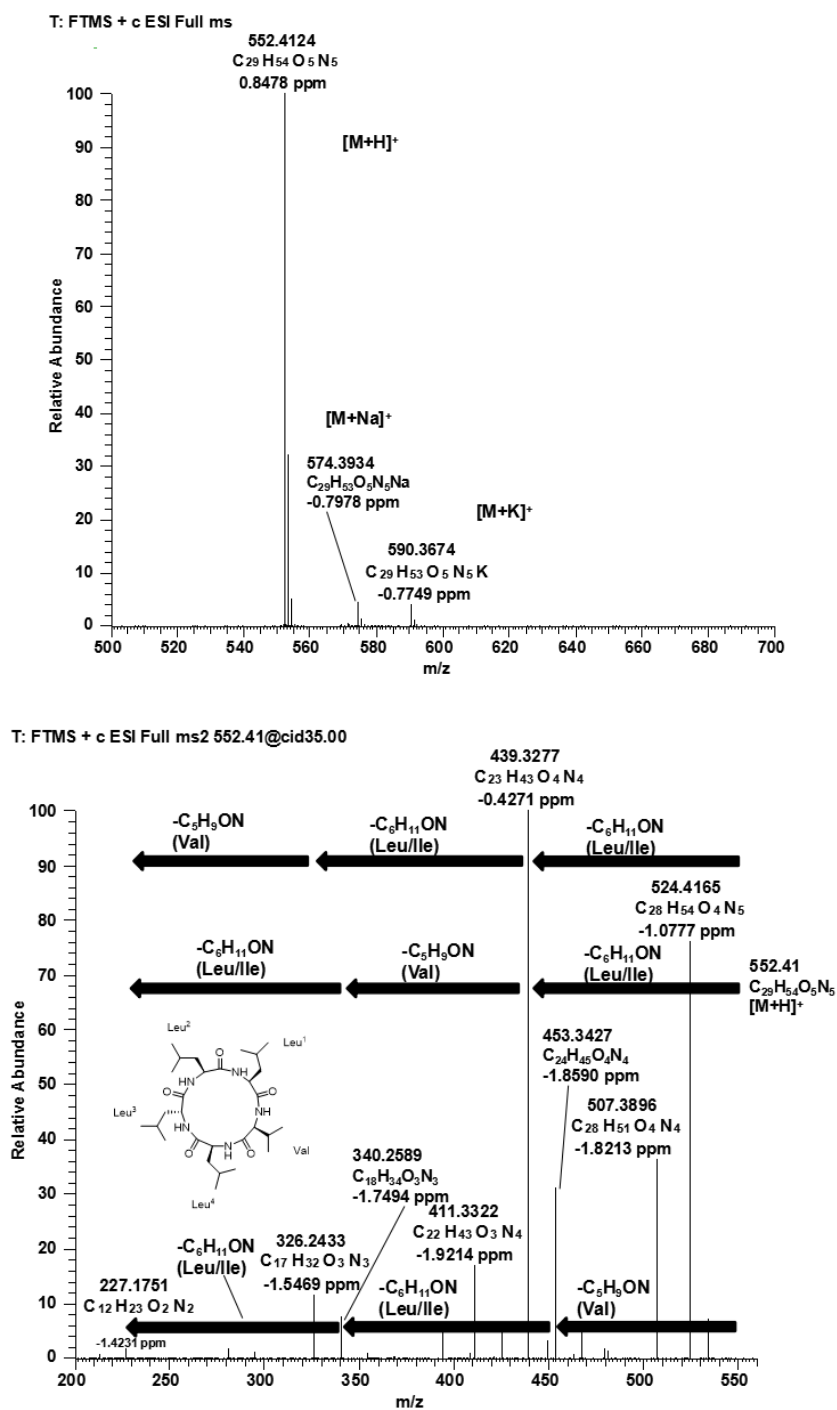


Figure 4.3.2.1 Positive ESI-HRMS (top) and MS/MS (bottom) spectra of compound 41.

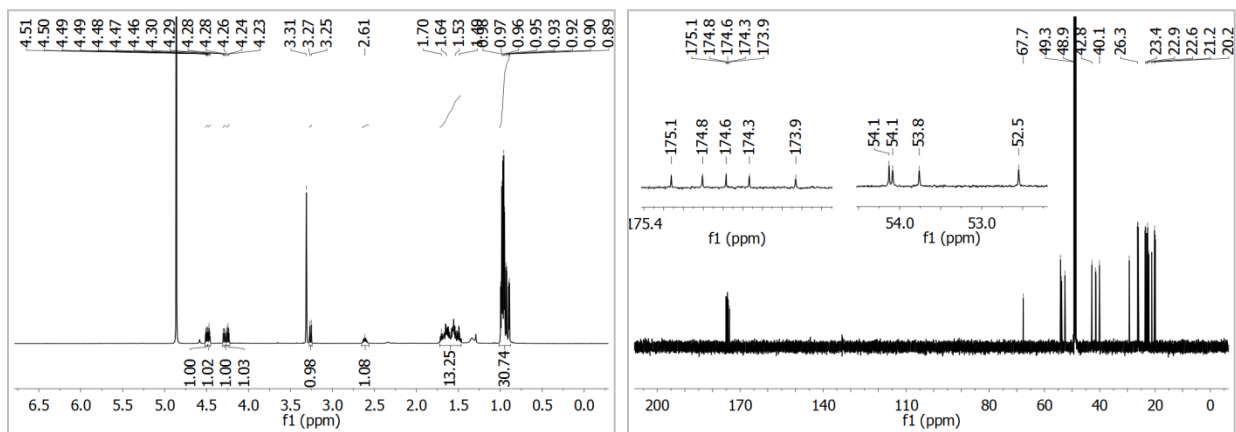


Figure 4.3.2.2 ^1H (left) and ^{13}C (right) NMR spectra (in CD_3OD) of compound **41**.

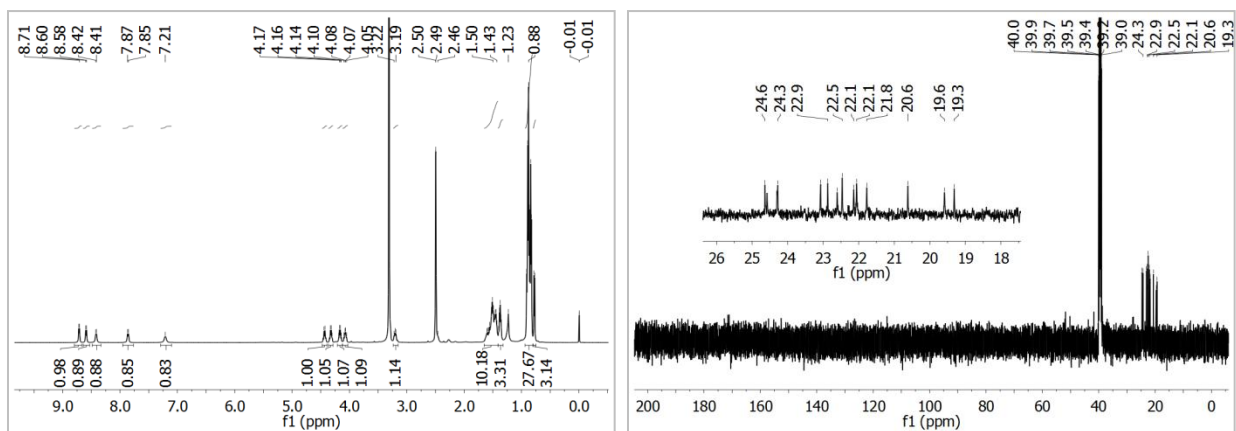


Figure 4.3.2.3 ^1H (left) and ^{13}C (right) NMR spectra (in $\text{DMSO}-d_6$) of compound **41**.

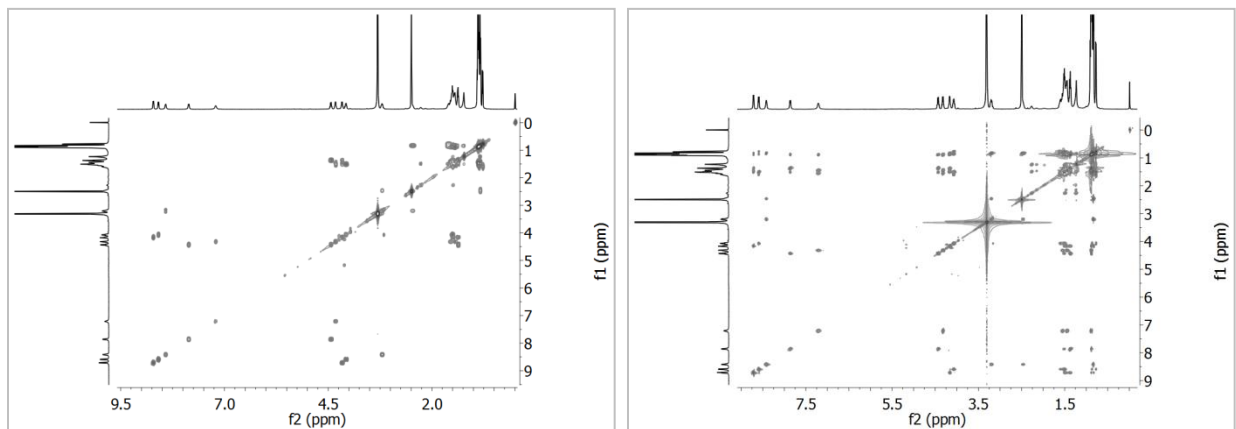


Figure 4.3.2.4 ^1H - ^1H COSY (left) and TOCSY (right) NMR spectra (in $\text{DMSO}-d_6$) of compound **41**.

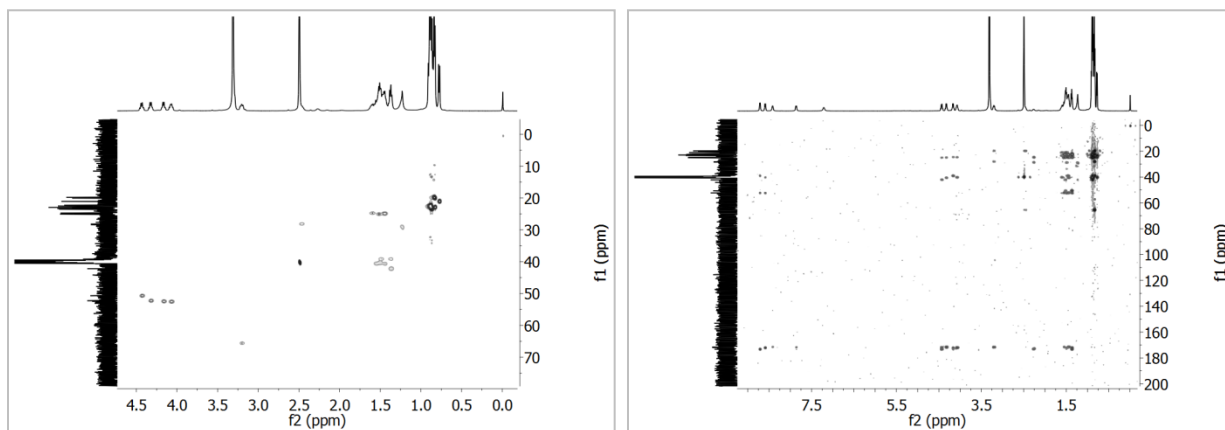


Figure 4.3.2.5 HSQC (left) and HMBC (right) spectra (in $\text{DMSO-}d_6$) of **41**.

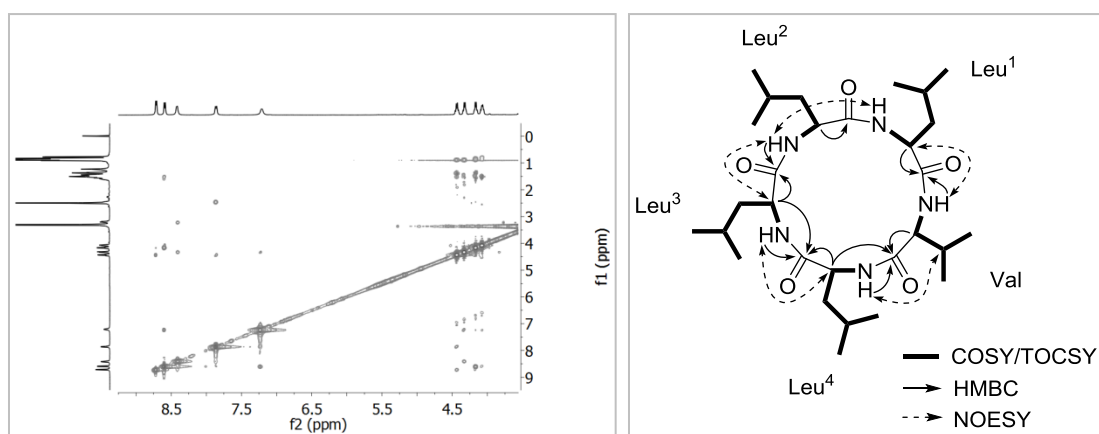


Figure 4.3.2.6 NOESY spectrum (left, in $\text{DMSO-}d_6$) and key $^1\text{H-}^1\text{H}$ COSY, HMBC, and NOESY correlations (right) of **41**.

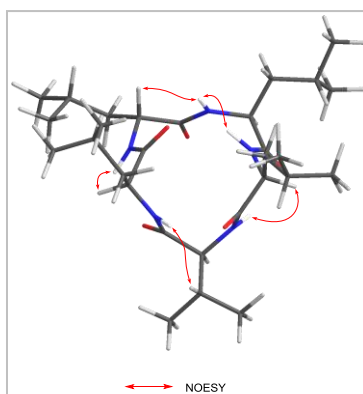
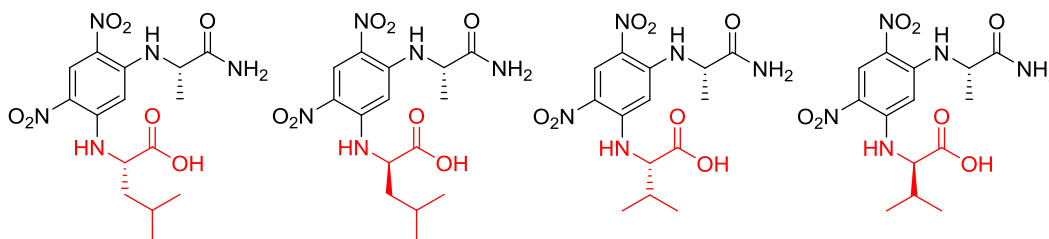


Figure 4.3.2.7 Key NOESY correlations of compound **41**.

A:



B:

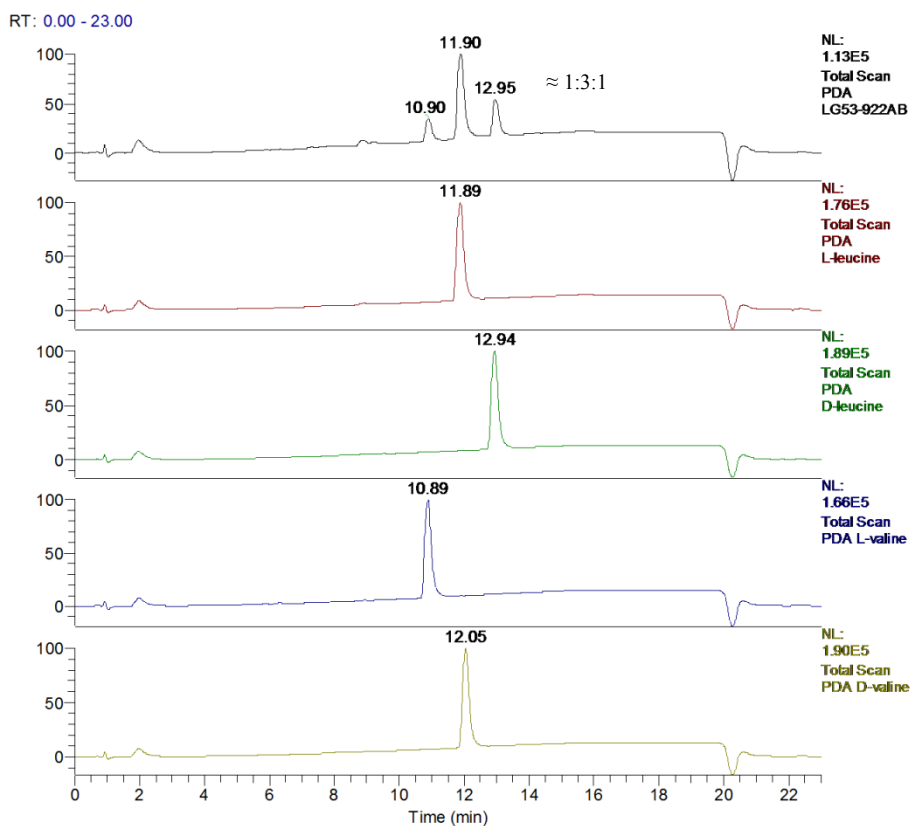


Figure 4.3.2.8 The Marfey's method for assigning the absolute configurations of amino acid residues. A: Marfey's reagent FDAA-derivatized amino acid standards. B: LC-MS for FDAA derivatives of the hydrolysis of **41** and amino acid standards.

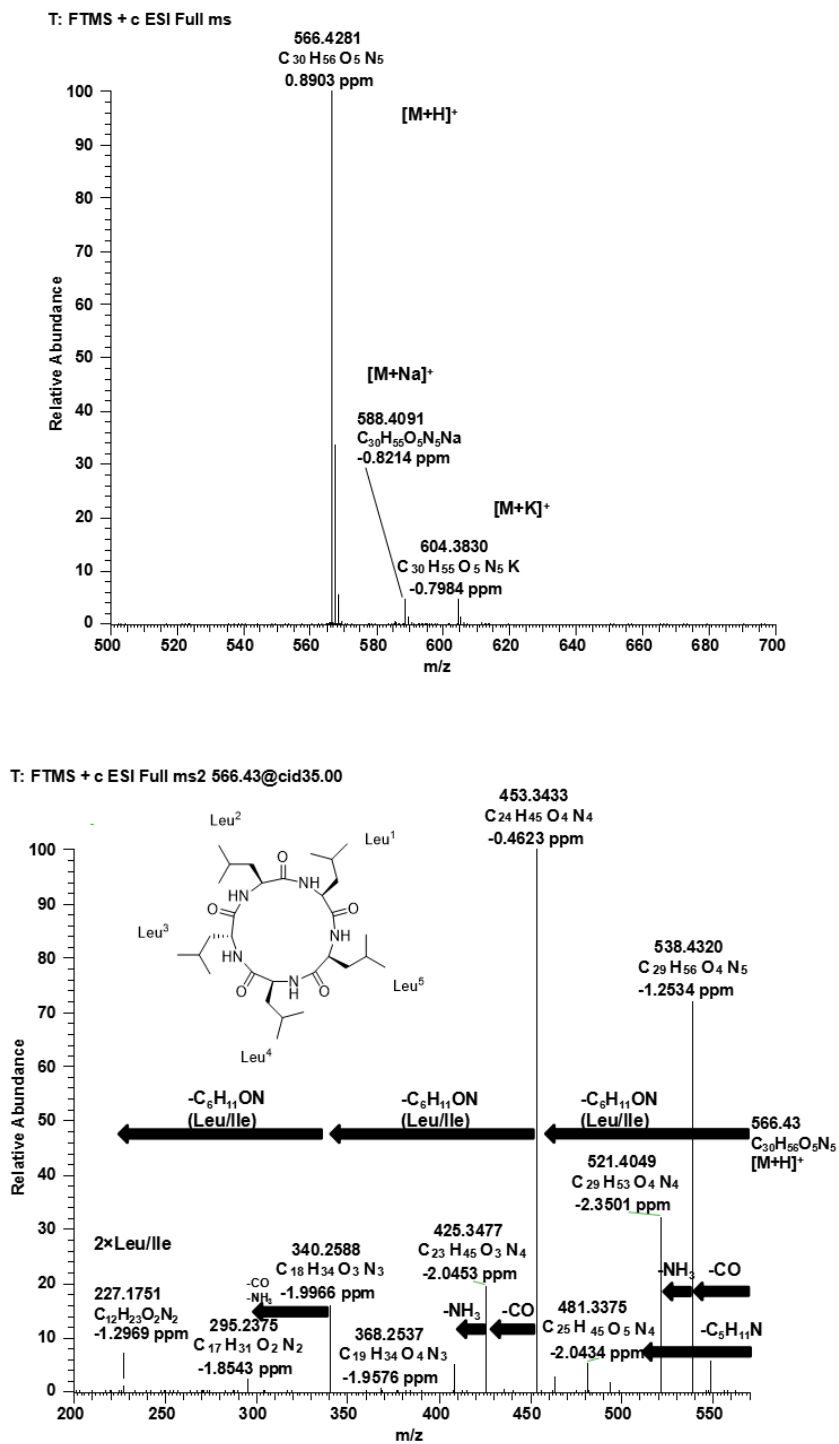


Figure 4.3.3.1 Positive ESI-HRMS (top) and MS/MS (bottom) spectra of compound 42.

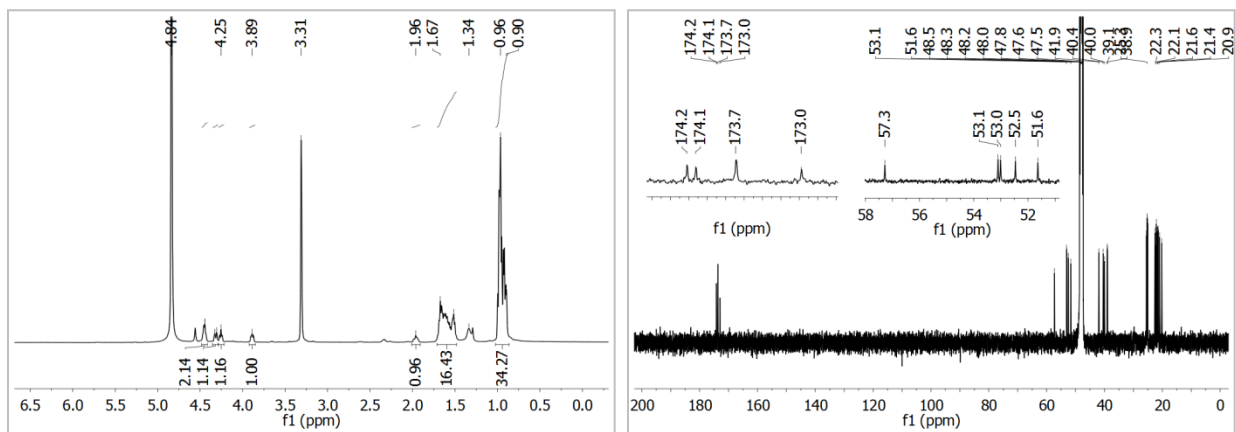


Figure 4.3.3.2 ^1H (left) and ^{13}C (right) NMR spectra (in CD_3OD) of compound **42**.

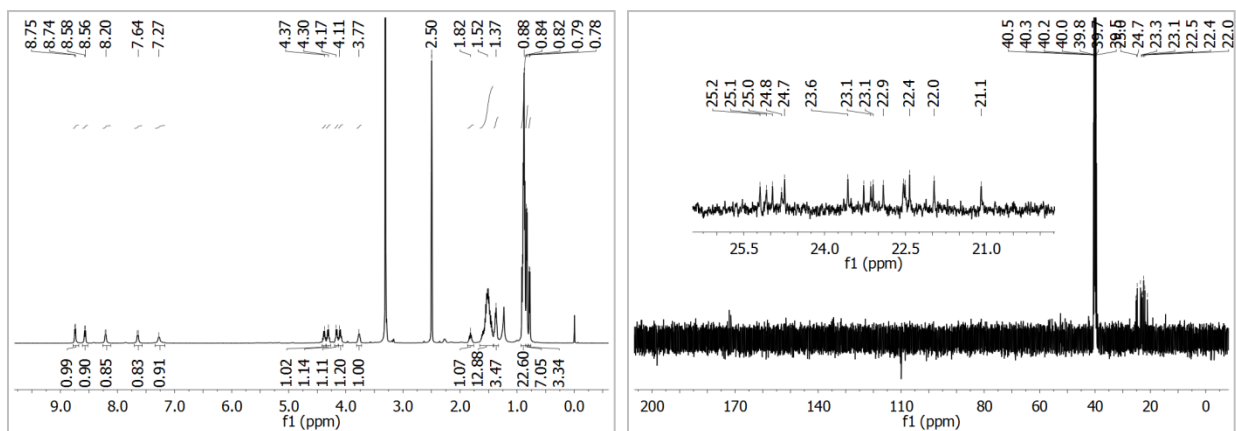


Figure 4.3.3.3 ^1H (left) and ^{13}C (right) NMR spectra (in $\text{DMSO}-d_6$) of compound **42**.

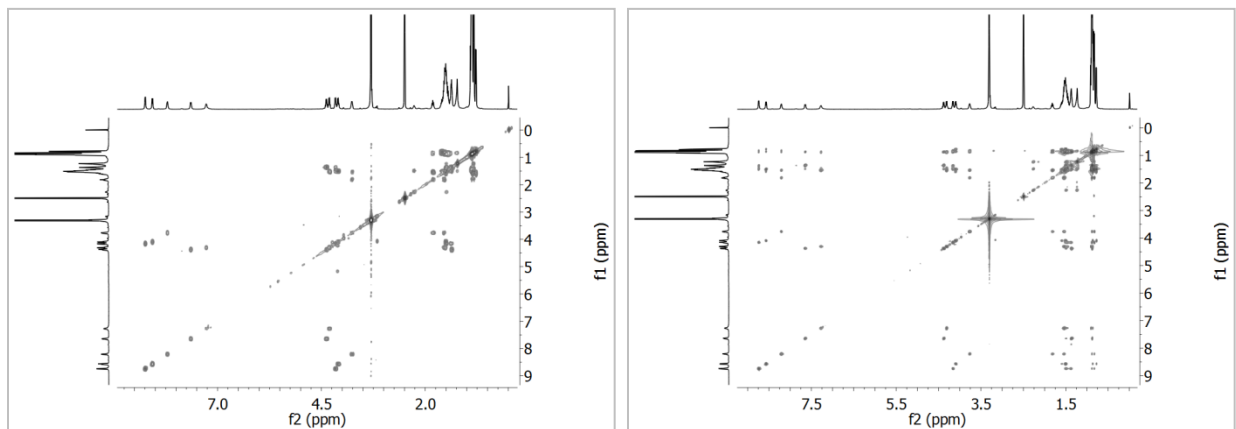


Figure 4.3.3.4 ^1H - ^1H COSY (left) and TOCSY (right) NMR spectra (in $\text{DMSO}-d_6$) of compound **42**.

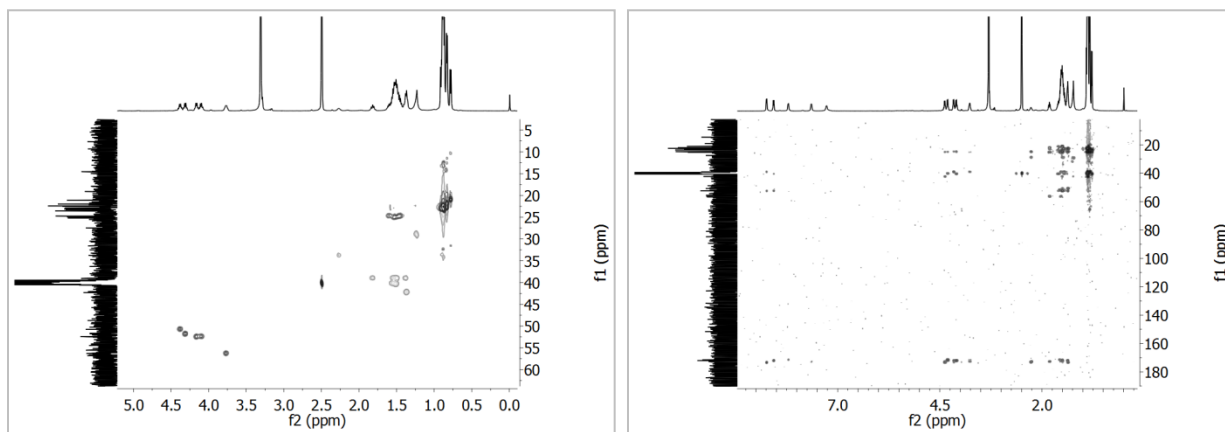


Figure 4.3.3.5 HSQC (left) and HMBC (right) spectra (in $\text{DMSO-}d_6$) of **42**.

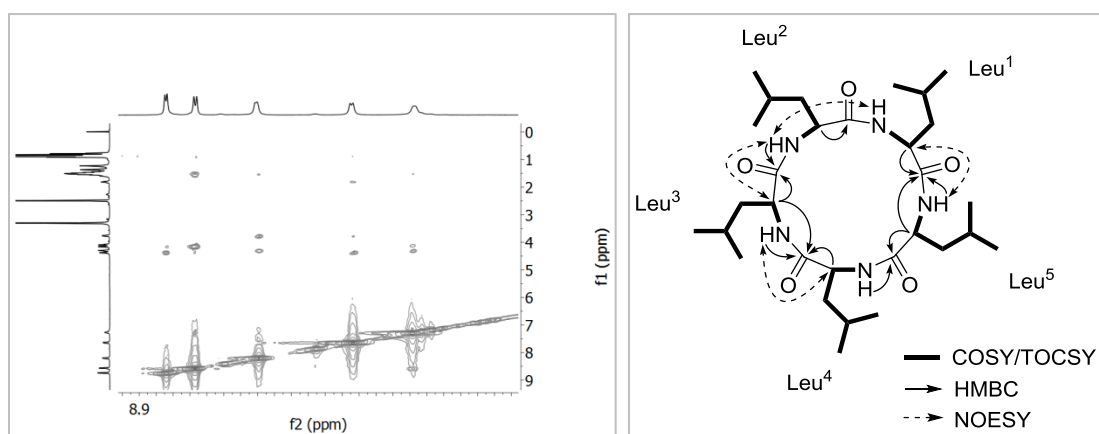
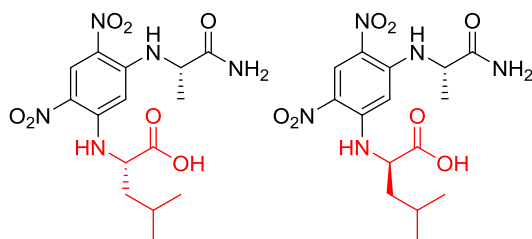


Figure 4.3.3.6 NOESY spectrum (left, in $\text{DMSO-}d_6$) and key $^1\text{H-}^1\text{H}$ COSY, HMBC, and NOESY correlations (right) of **42**.

A:



B:

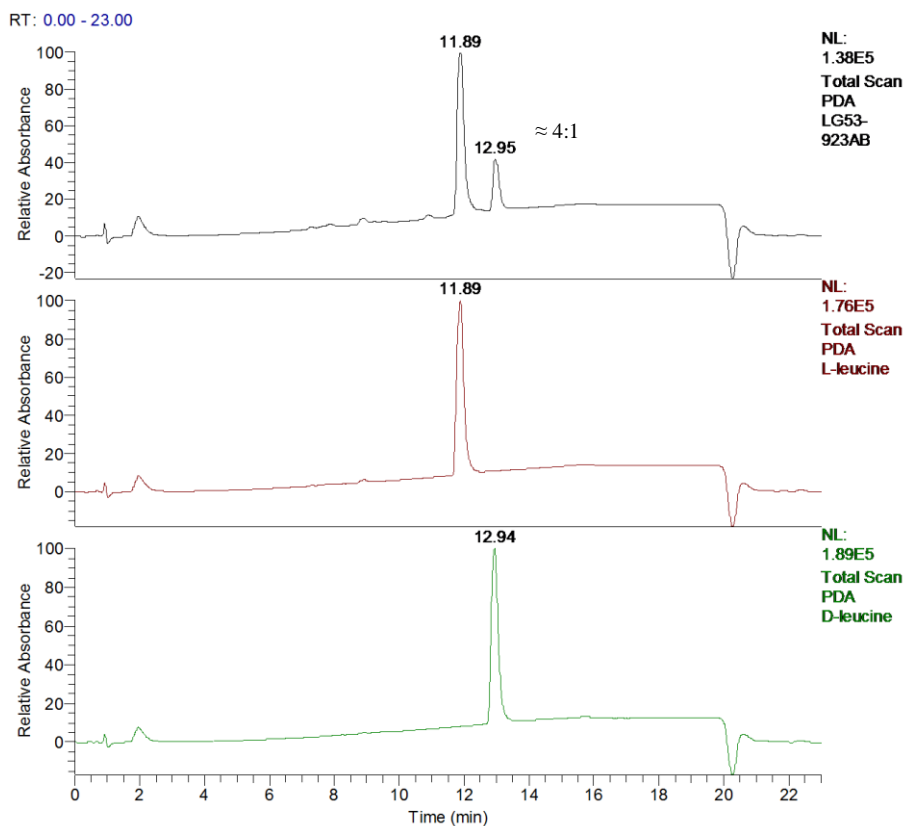
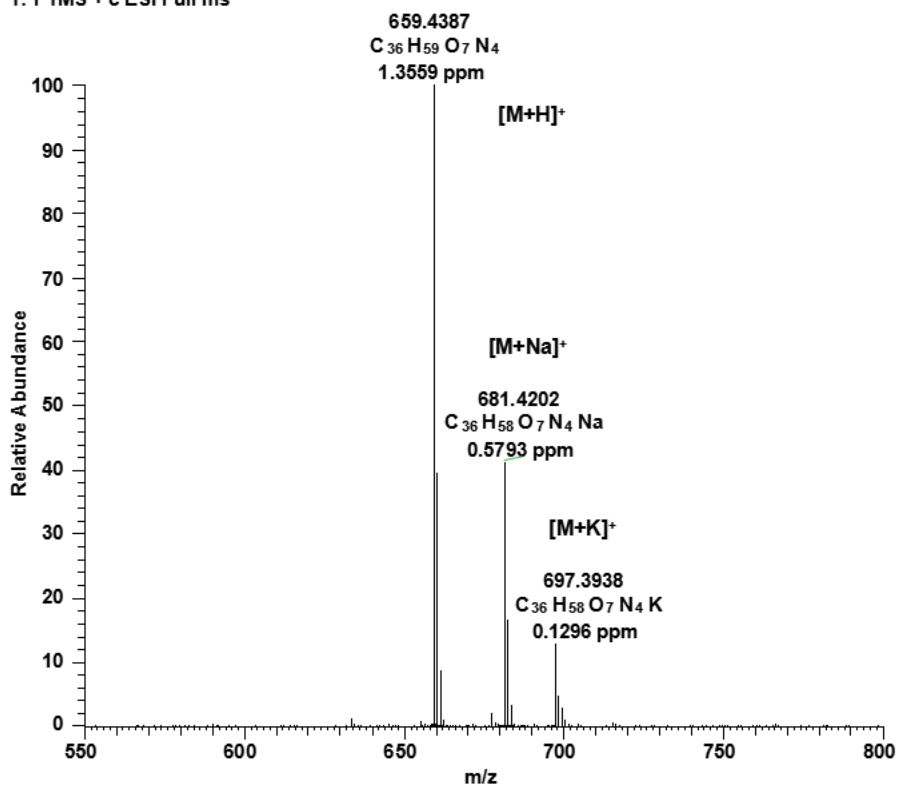
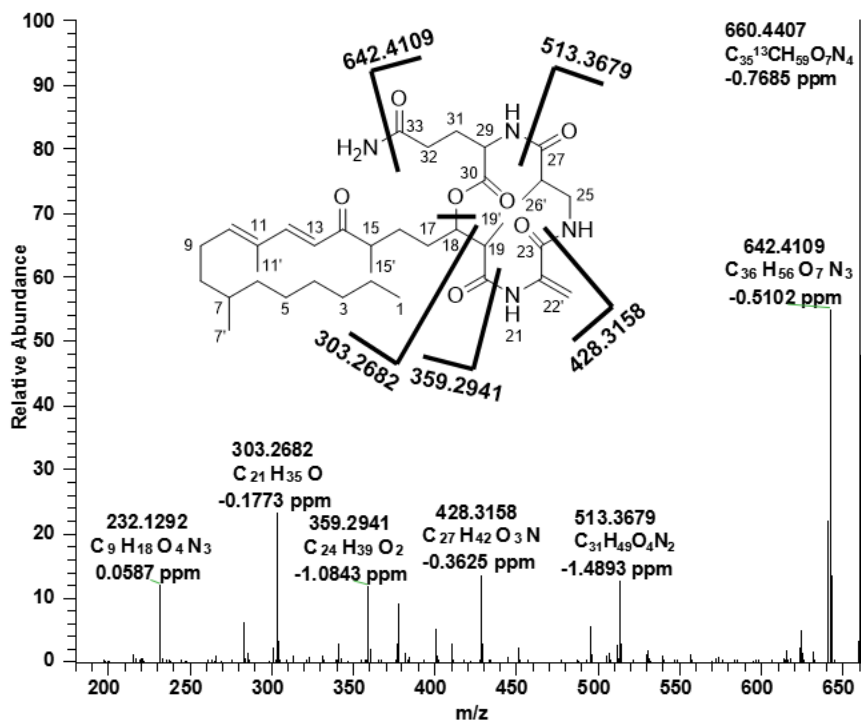


Figure 4.3.3.7 The Marfey's method for assigning the absolute configurations of amino acid residues. A: Marfey's reagent FDAA-derivatized amino acid standards. B: LC-MS for FDAA derivatives of the hydrolysis of **42** and amino acid standards.

T: FTMS + c ESI Full ms



T: FTMS + c ESI Full ms2 659.44@cid35.00



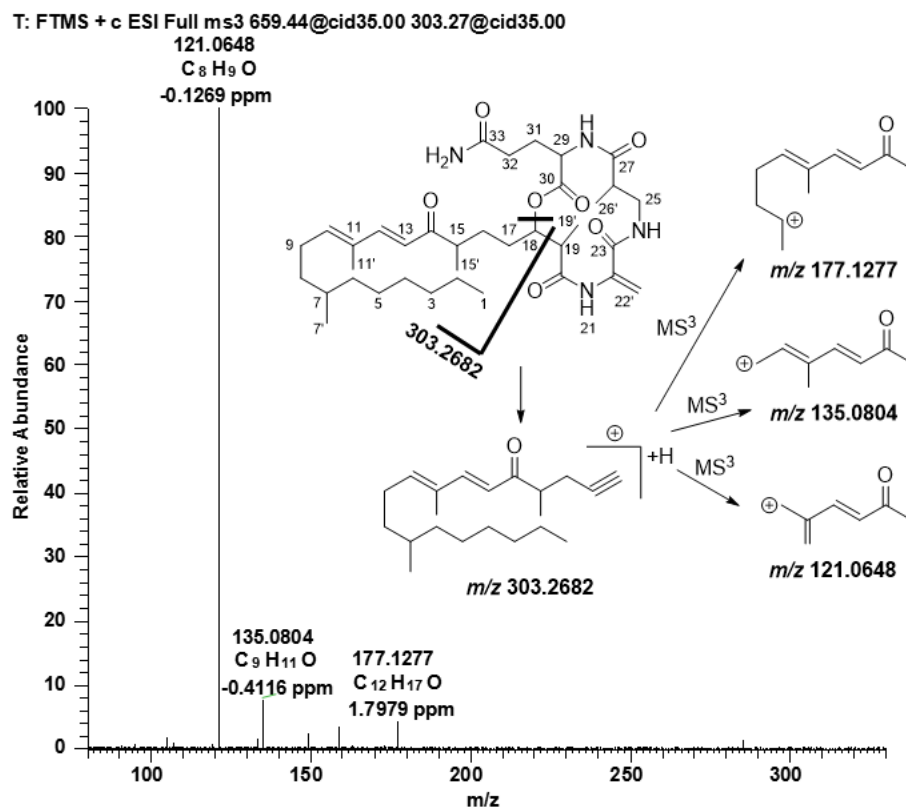


Figure 4.3.4.1 Positive ESI-HRMS (top), MS² (medium) and MS³ (bottom) spectra of compound 43.

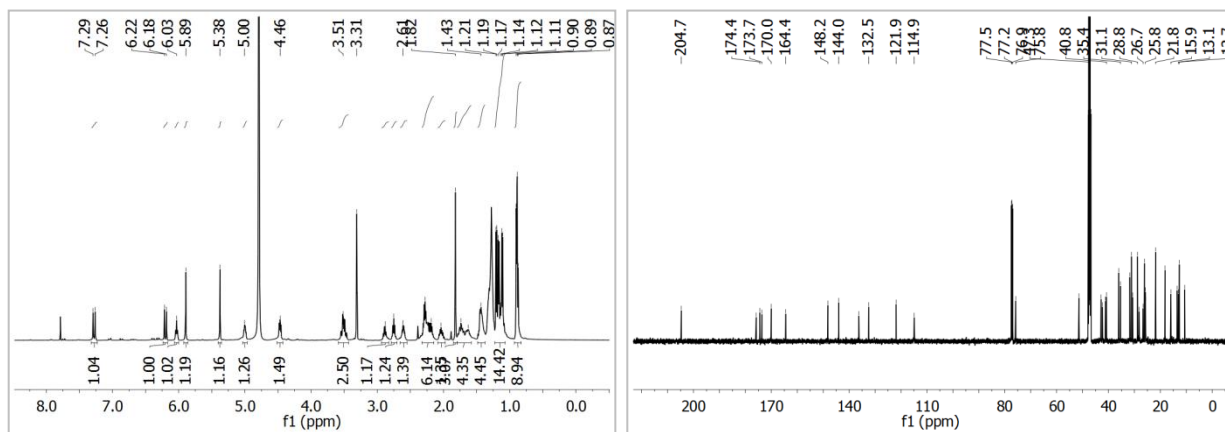
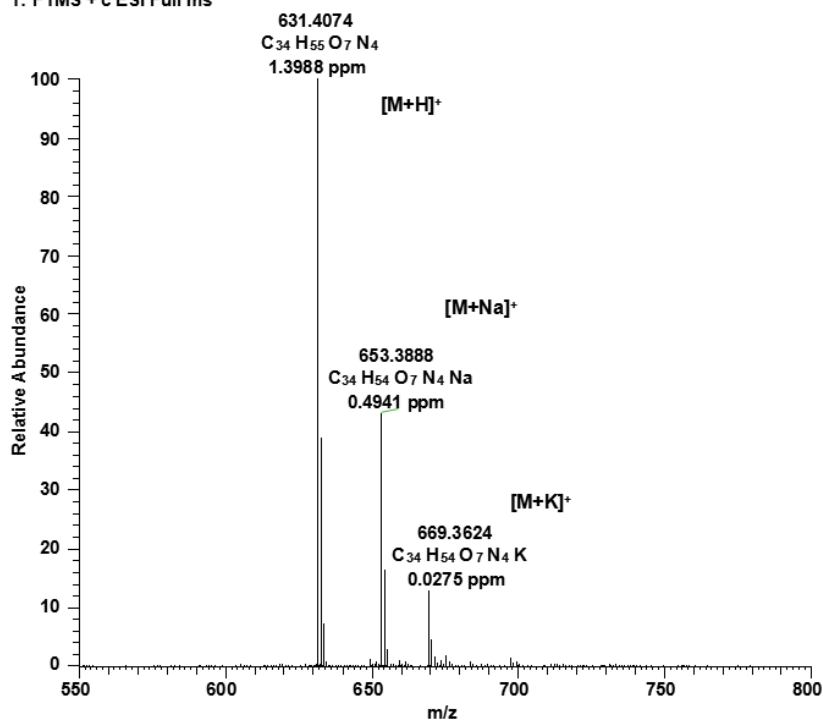
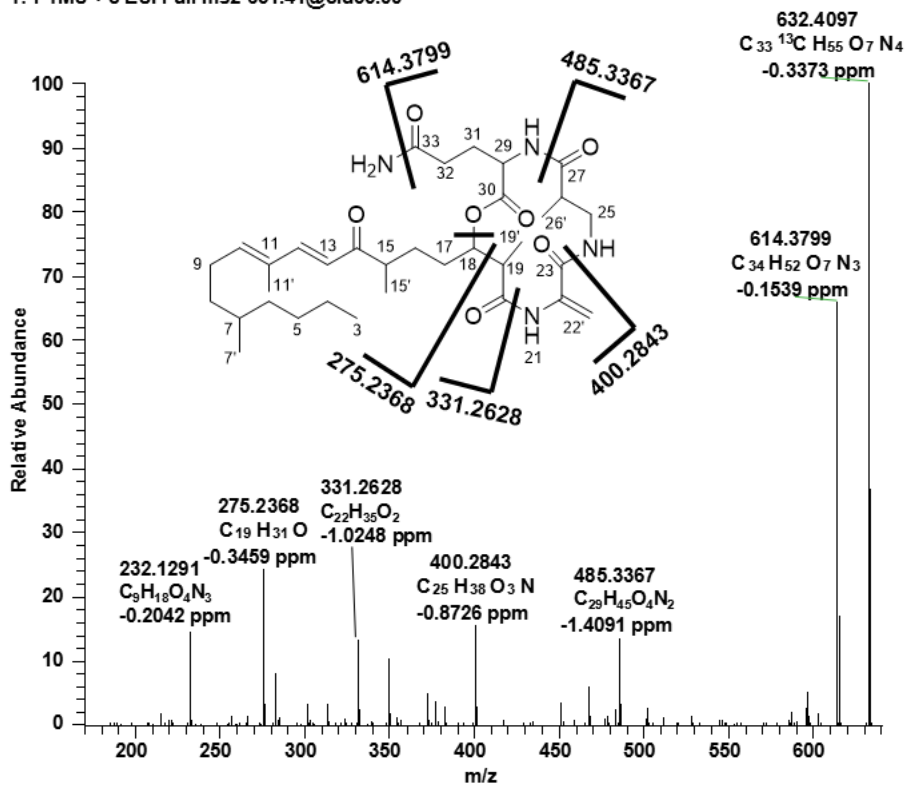


Figure 4.3.4.2 ¹H (left) and ¹³C (right) NMR spectra (in CDCl₃:CD₃OD = 1:3) of compound 43.

T: FTMS + c ESI Full ms



T: FTMS + c ESI Full ms2 631.41@cid35.00



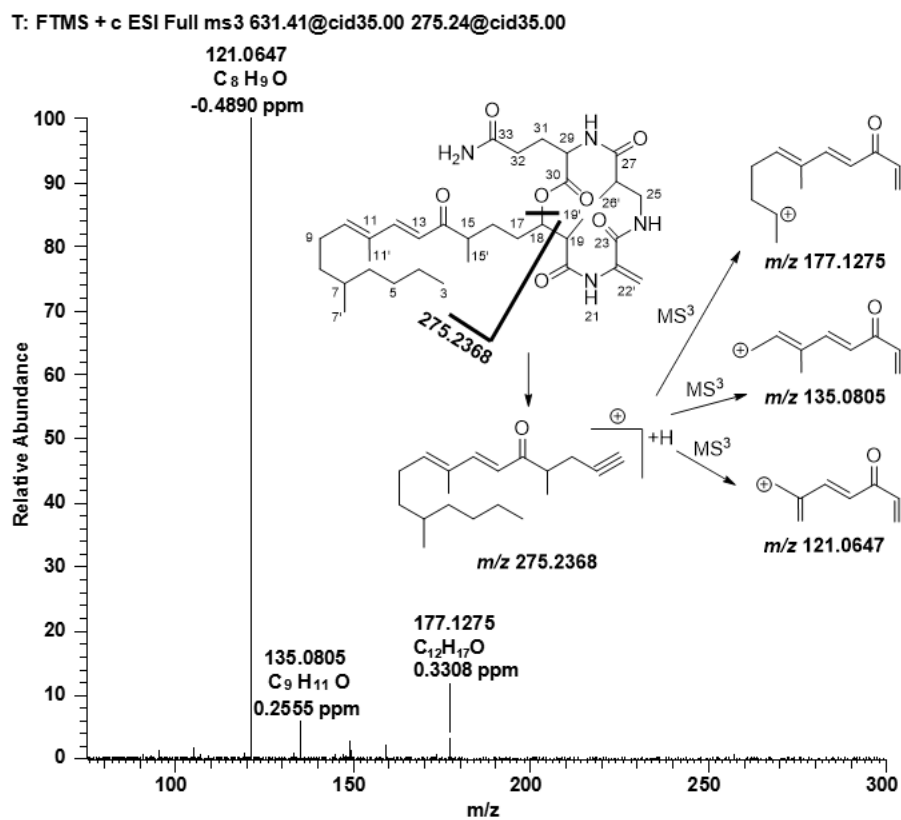


Figure 4.3.5.1 Positive ESI-HRMS (top), MS² (medium) and MS³ (bottom) spectra of compound 44.

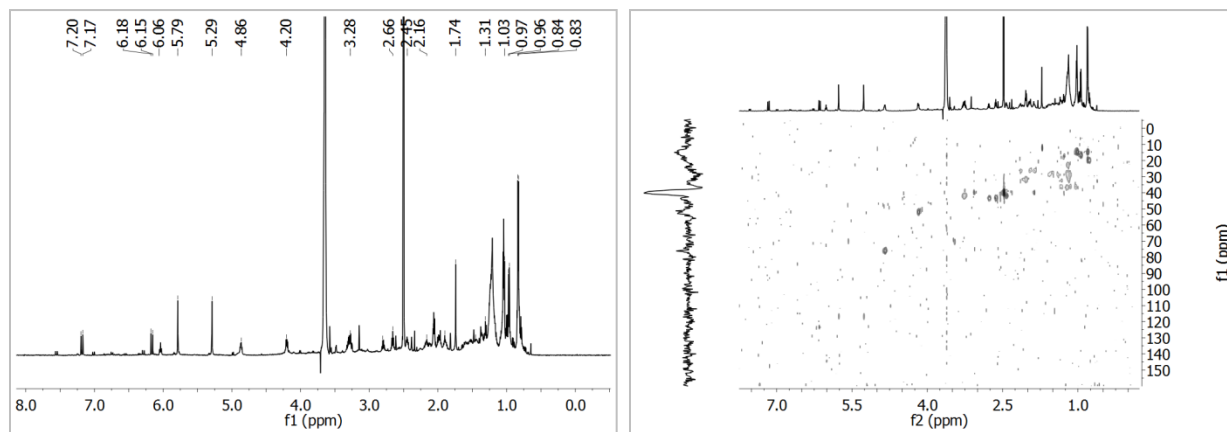


Figure 4.3.5.2 ¹H (left) and HSQC (right) NMR spectra (in DMSO-*d*₆) of compound 44.

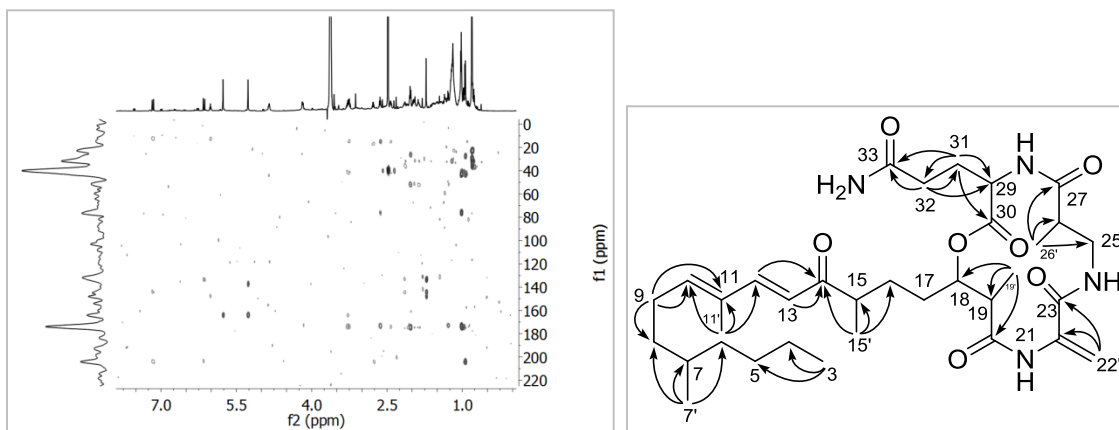
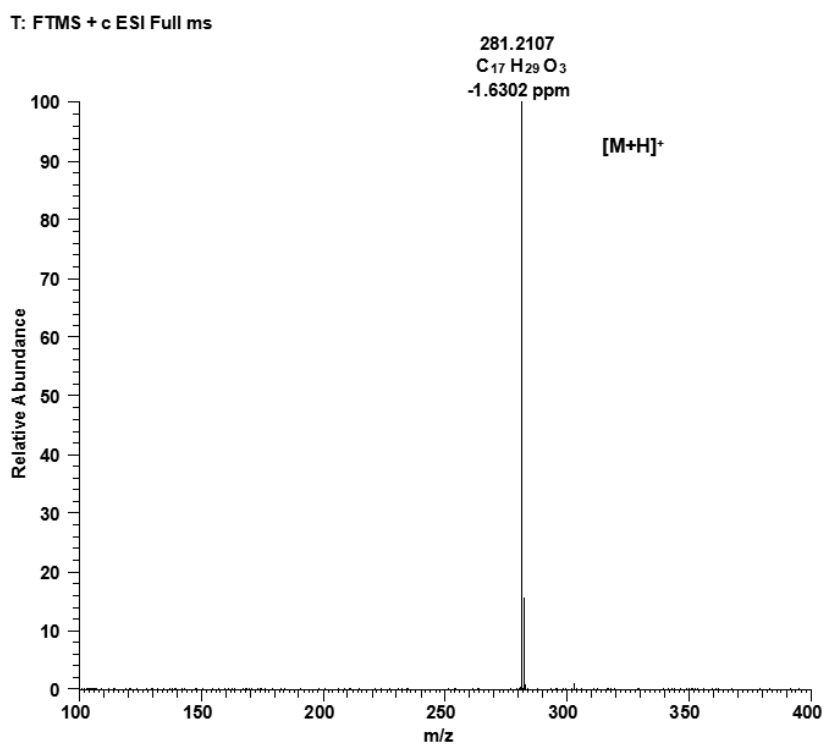


Figure 4.3.5.3 HMBC spectrum (left, in DMSO- d_6) and key HMBC correlations of **44**.



T: FTMS + c ESI Full ms2 281.21@cid35.00

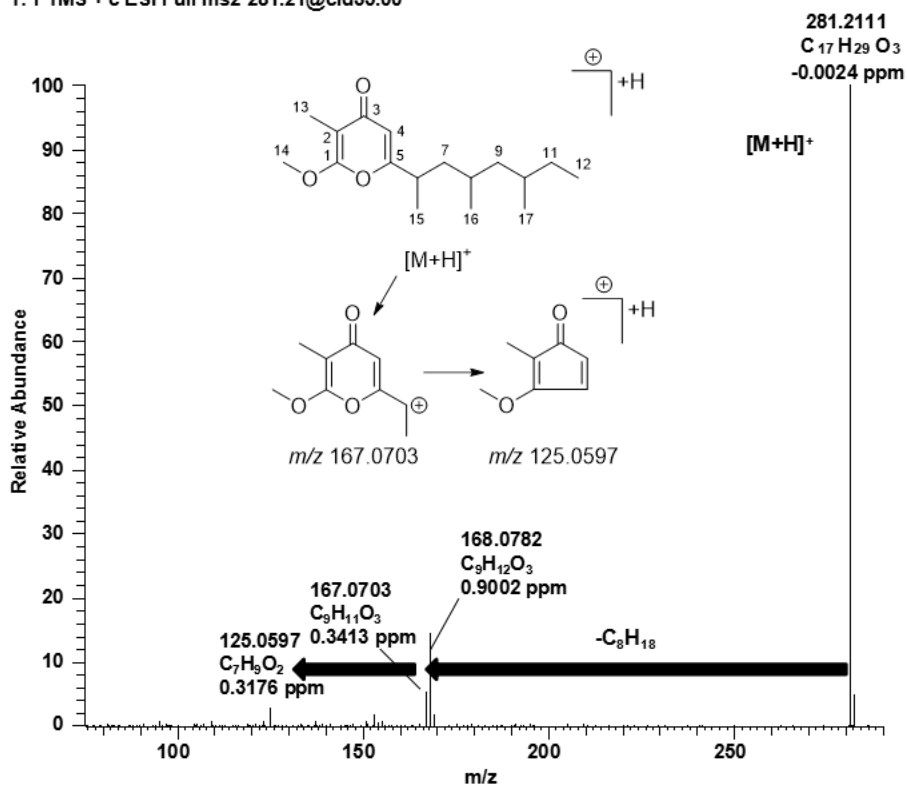


Figure 4.3.6.1 Positive ESI-HRMS (top) and MS/MS (bottom) spectra of compound 45.

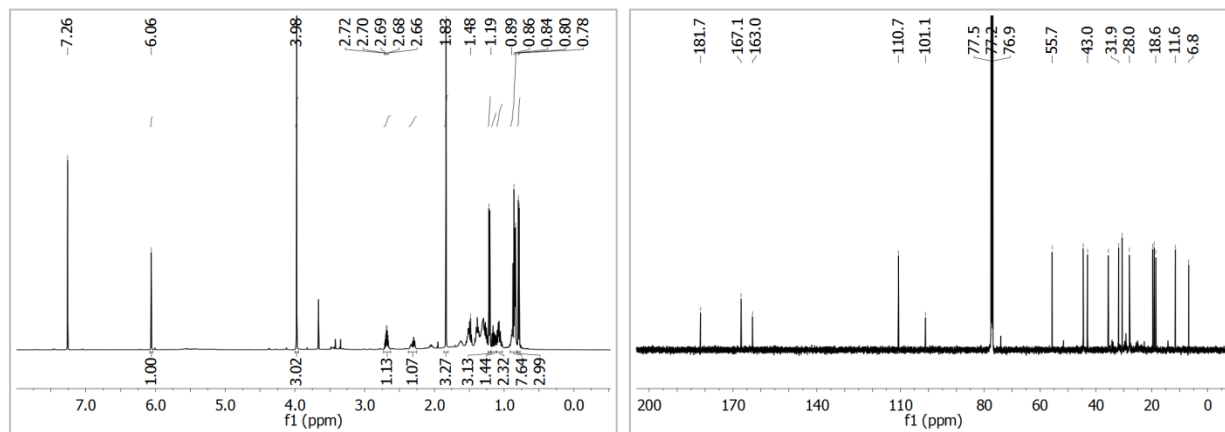


Figure 4.3.6.2 1H (left) and ^{13}C (right) NMR spectra (in $CDCl_3$) of compound 45.

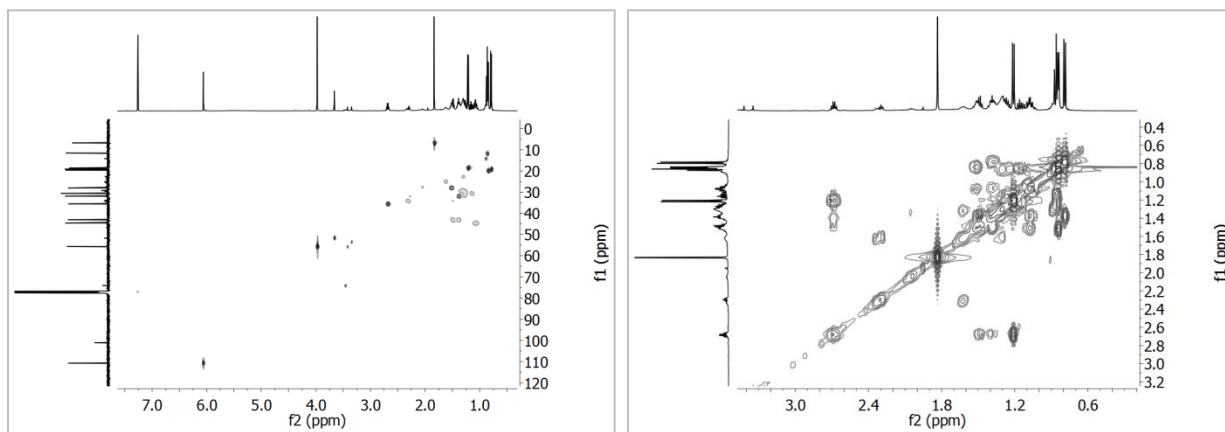


Figure 4.3.6.3 HSQC (left) and ^1H - ^1H COSY (right) NMR spectra (in CDCl_3) of compound 45.

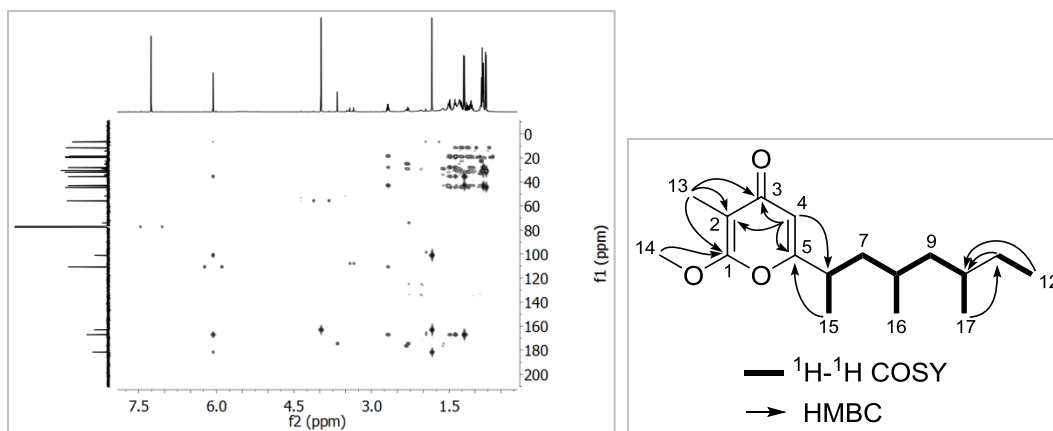


Figure 4.3.6.4 HMBC (left) spectrum (in CDCl_3) and key ^1H - ^1H COSY and HMBC correlations of 45.

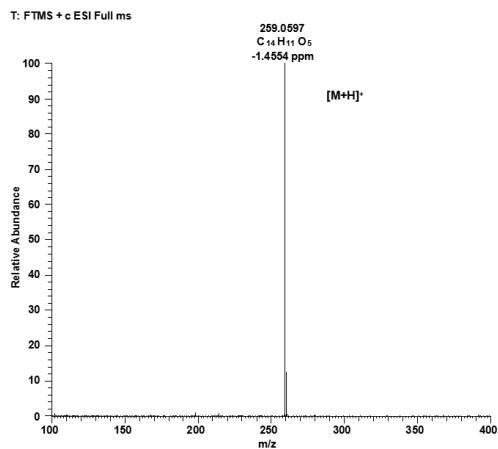


Figure 4.3.7.1 Positive ESI-HRMS spectrum of compound 46.

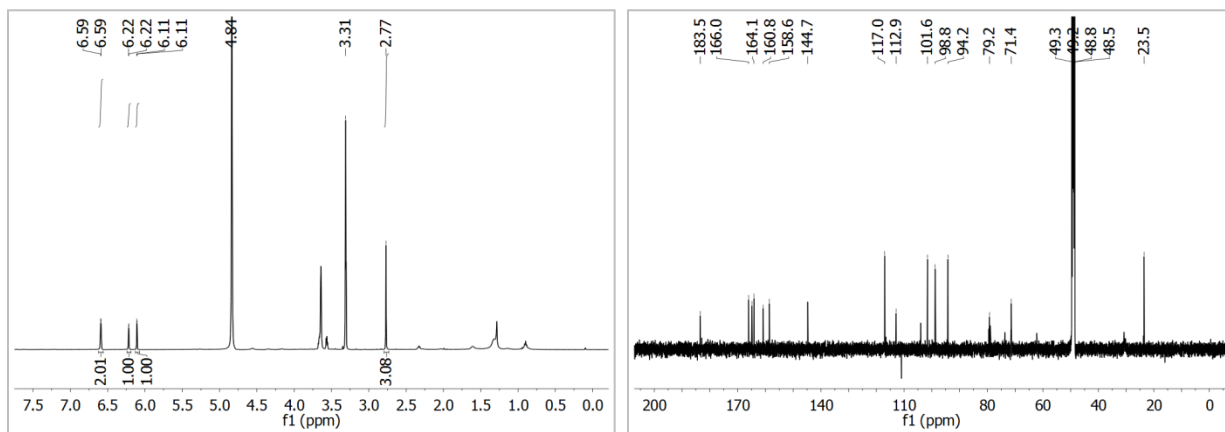


Figure 4.3.7.2 ^1H (left) and ^{13}C (right) NMR spectra (in CD_3OD) of compound 46.

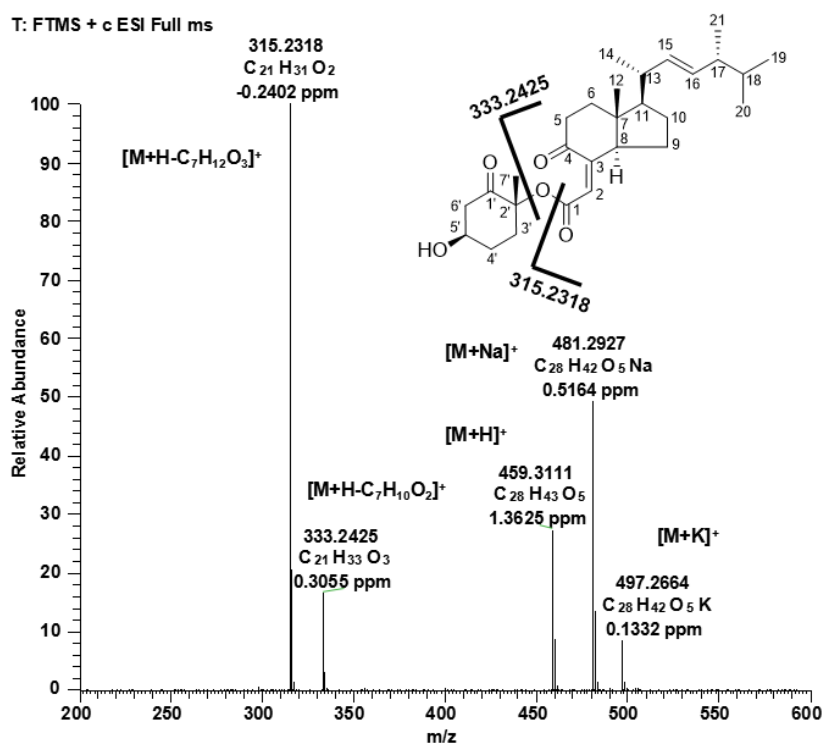


Figure 4.3.8.1 Positive ESI-HRMS spectrum of compound 47.

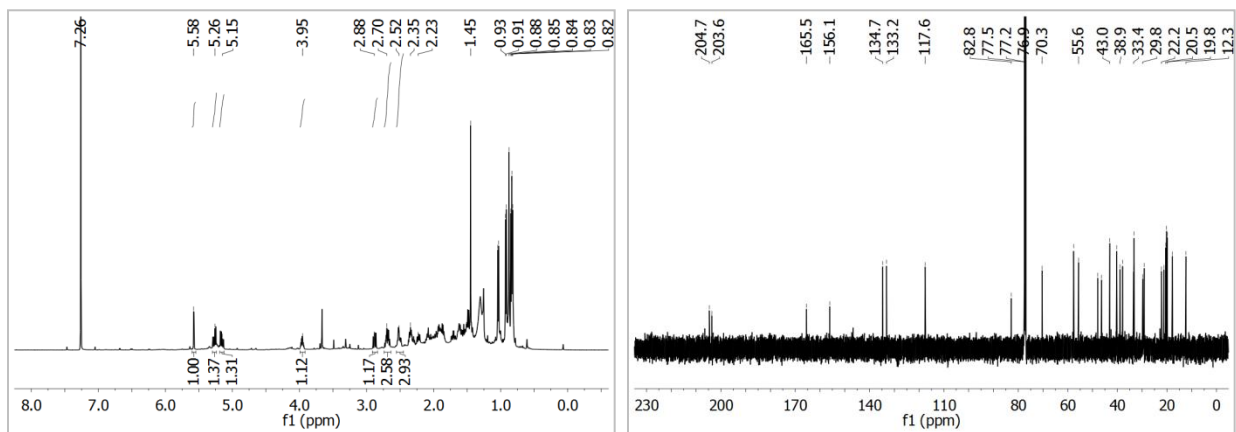


Figure 4.3.8.2 ^1H (left) and ^{13}C (right) NMR spectra (in CDCl_3) of compound 47.

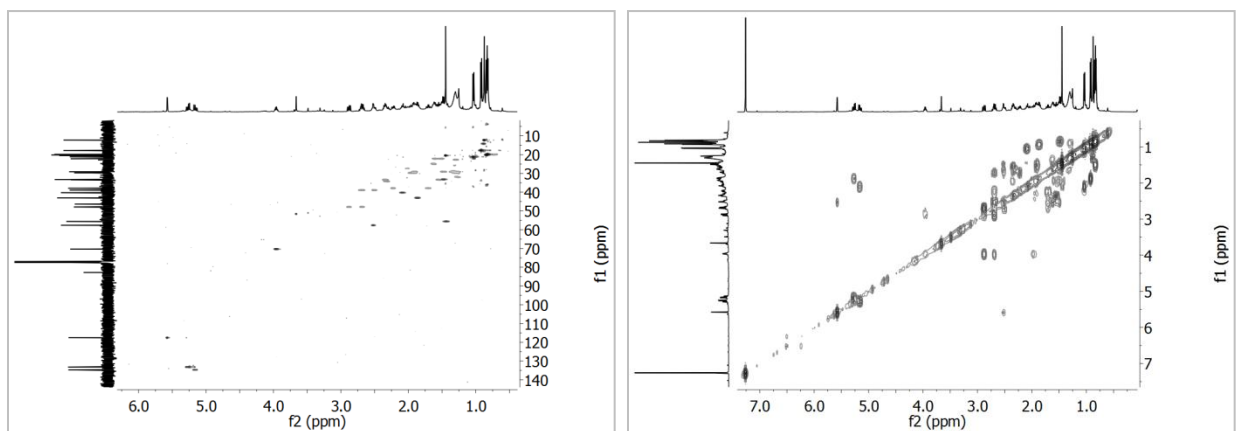


Figure 4.3.8.3 HSQC (left) and ^1H - ^1H COSY (right) NMR spectra (in CDCl_3) of compound 47.

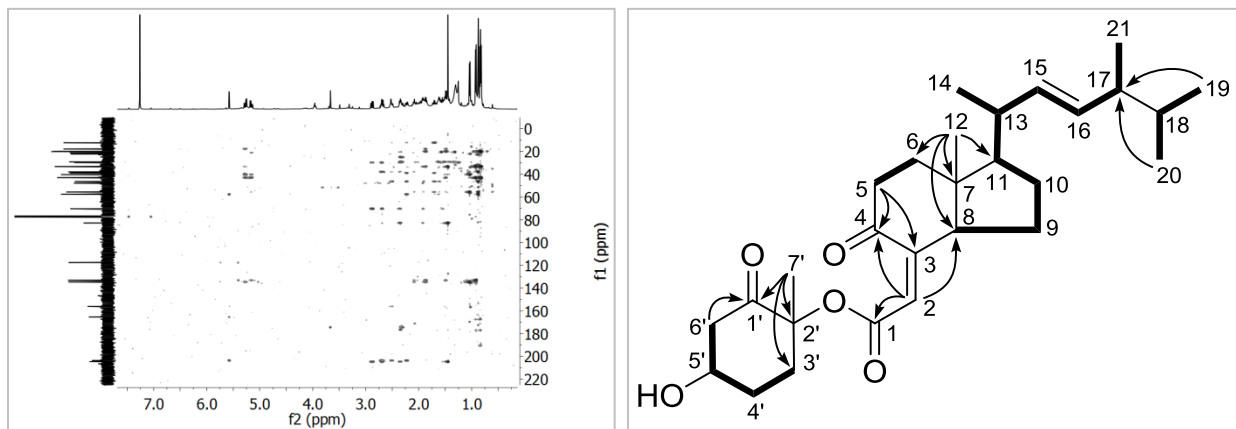


Figure 4.3.8.4 HMBC spectrum (left, in CDCl_3) and key ^1H - ^1H COSY and HMBC correlations (right) of 47.

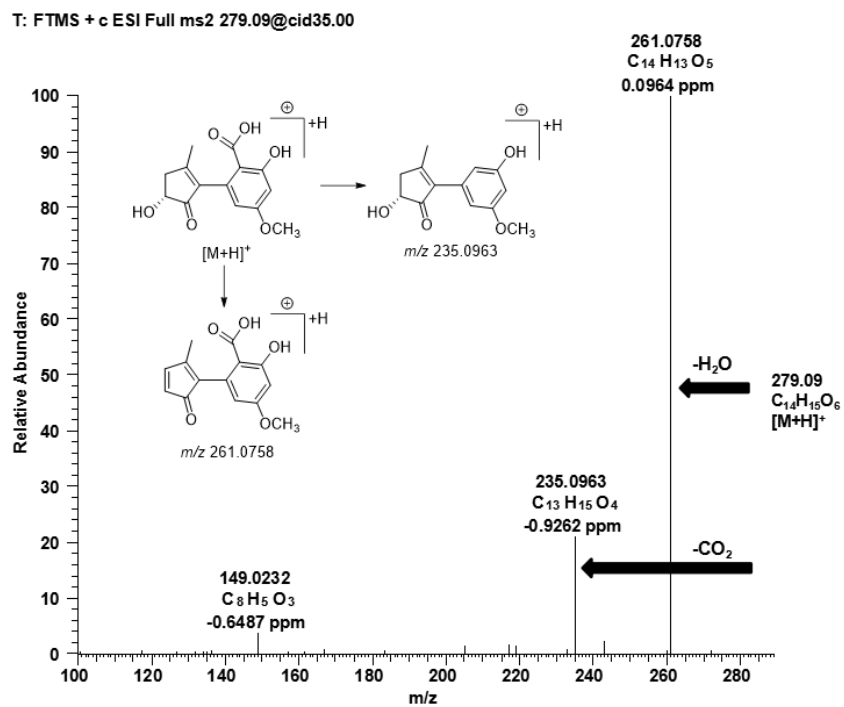
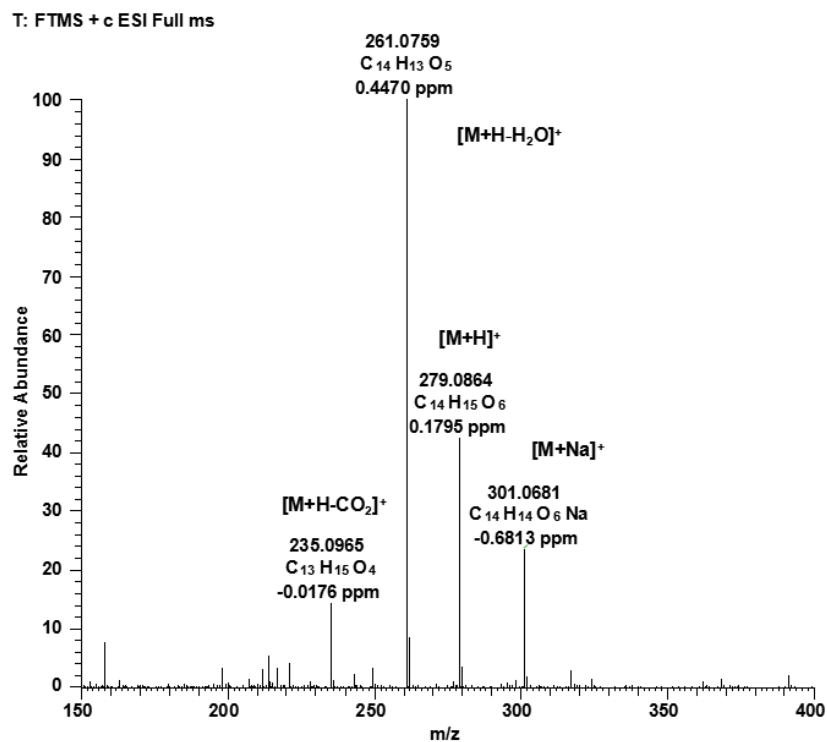


Figure 4.4.1.1 Positive ESI-HRMS (top) and MS/MS (bottom) spectra of compound 48.

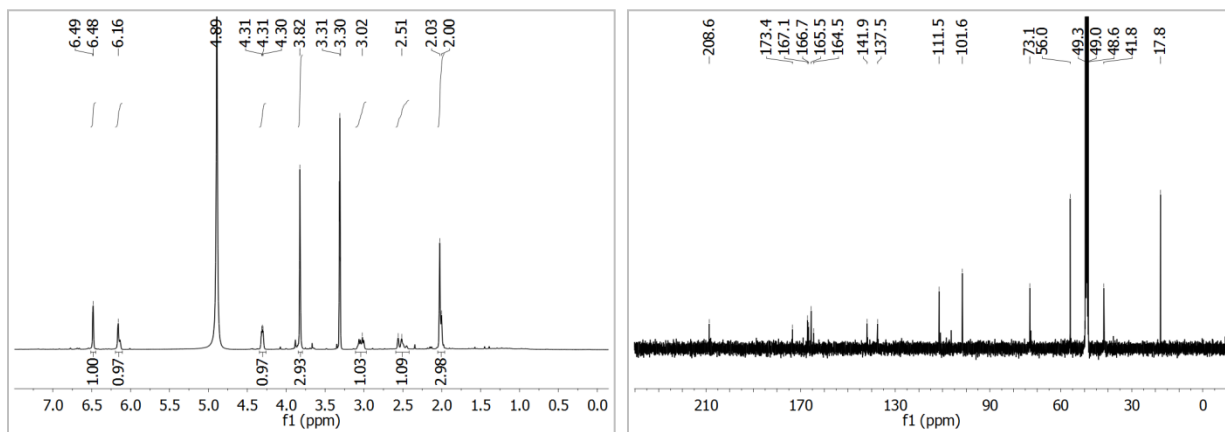


Figure 4.4.1.2 ^1H (left) and ^{13}C (right) NMR spectra (in CD_3OD) of compound 48.

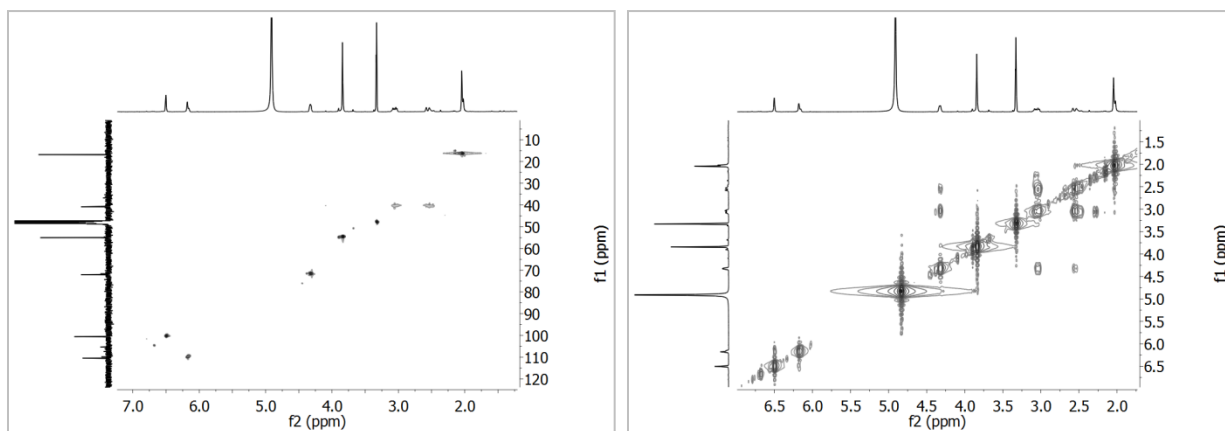


Figure 4.4.1.3 HSQC (left) and ^1H - ^1H COSY (right) spectra (in CD_3OD) of 48.

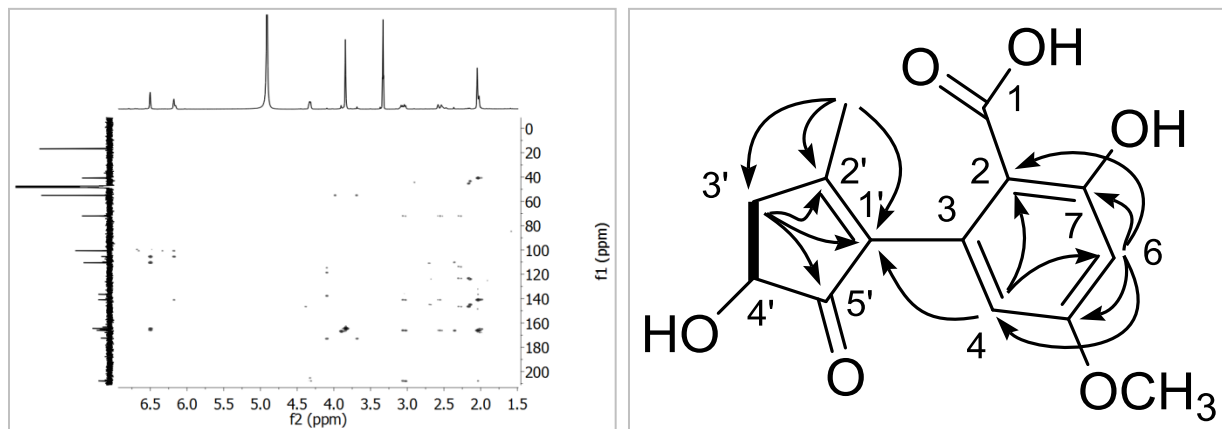


Figure 4.4.1.4 HMBC (left) spectrum and key ^1H - ^1H COSY and HMBC correlations (right) of 48.

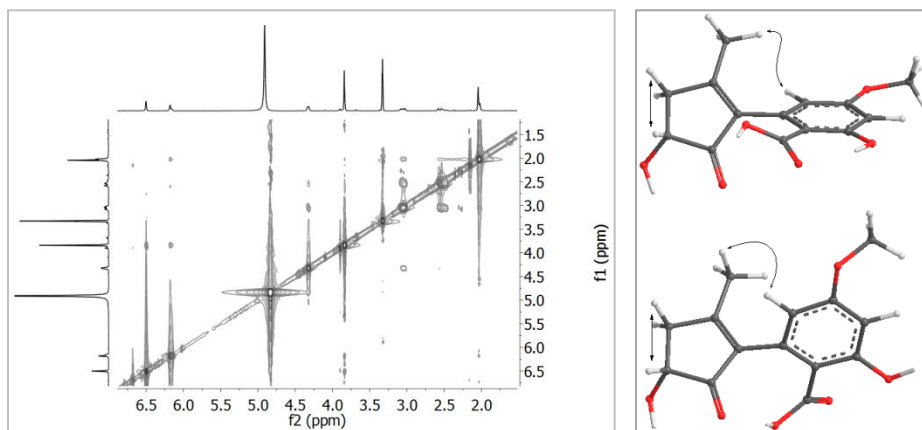


Figure 4.4.1.5 NOESY (left) spectrum and key NOESY correlations (right) of **48**.

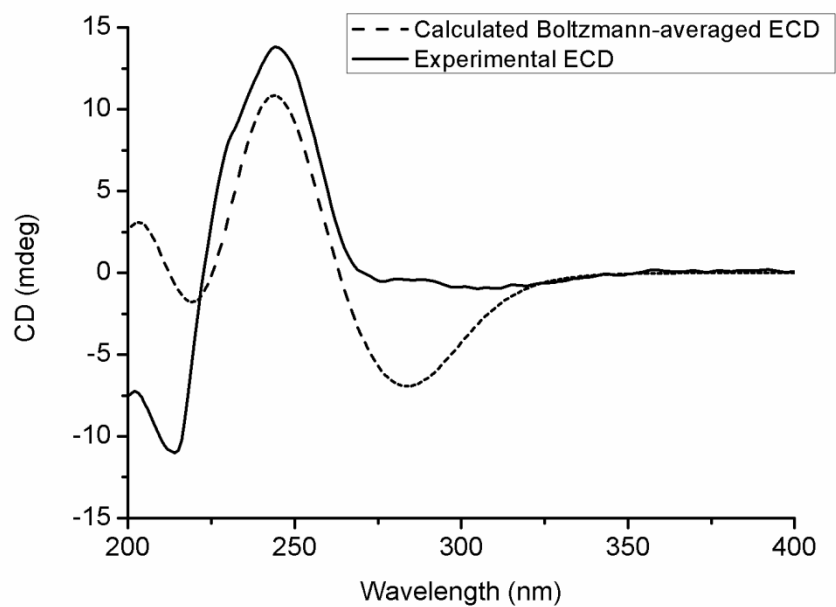


Figure 4.4.1.6 Experimental and calculated CD spectra of **48**.

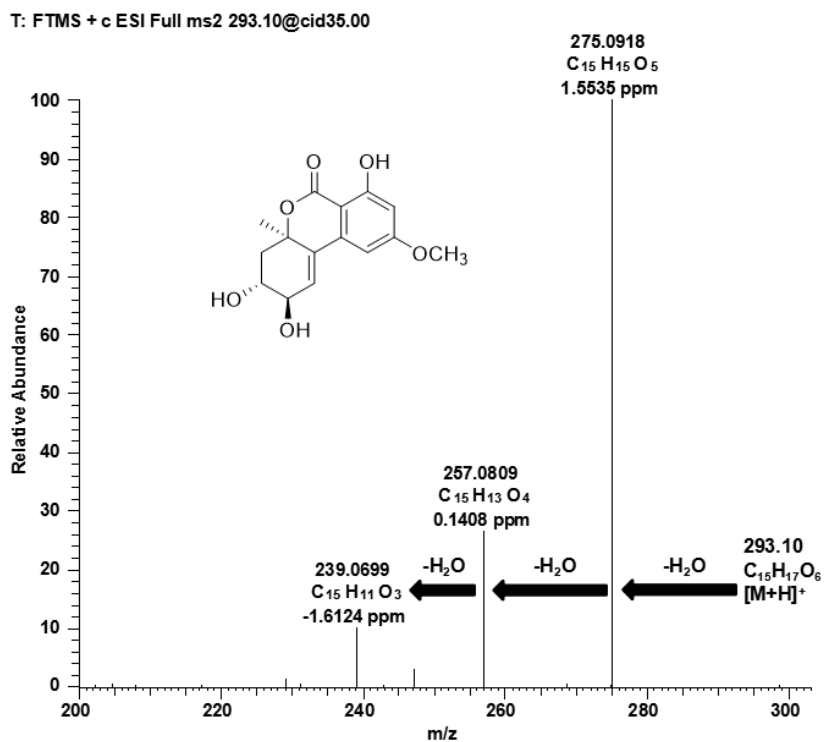
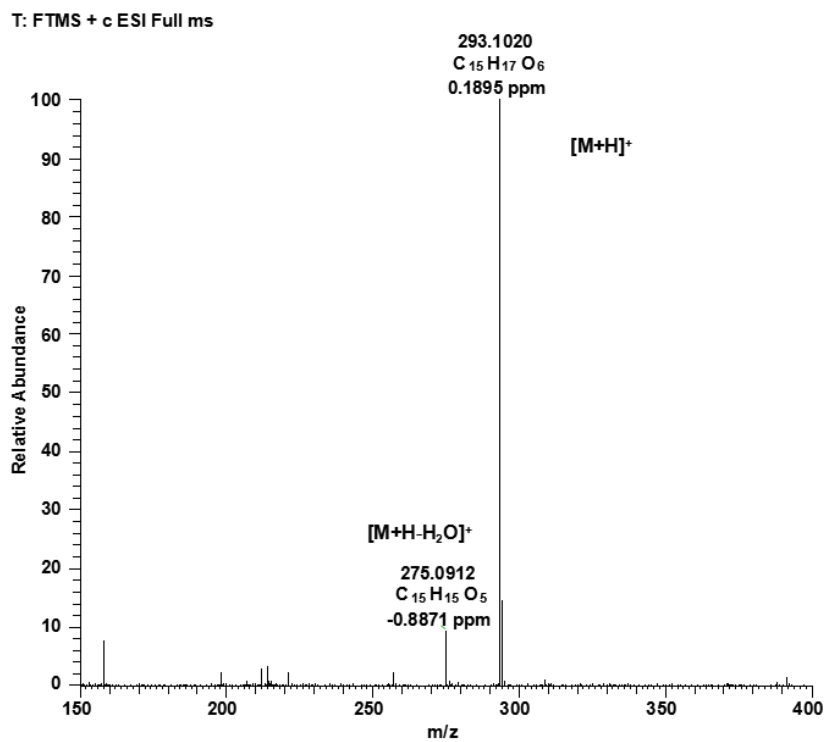


Figure 4.4.2.1 Positive ESI-HRMS (top) and MS/MS (bottom) spectra of compound 49.

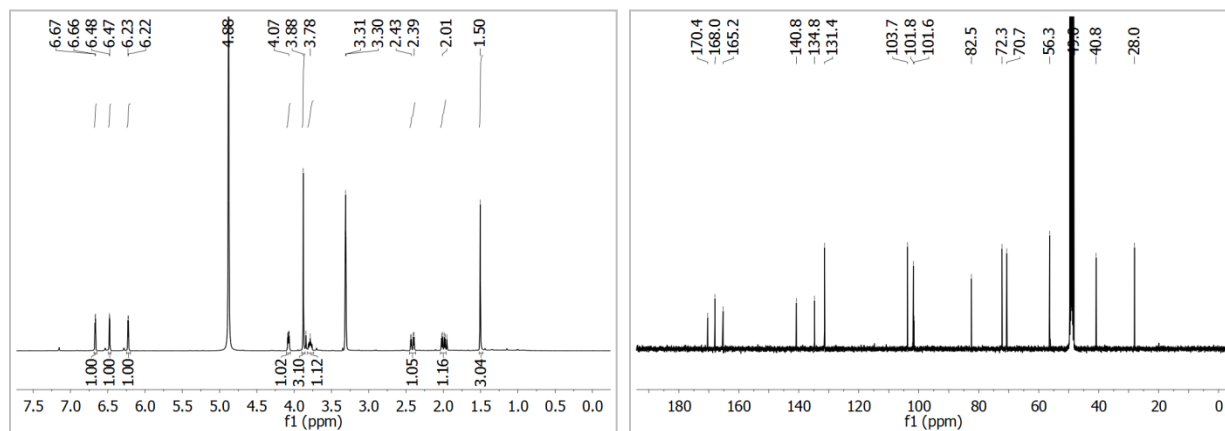


Figure 4.4.2.2 ^1H (left) and ^{13}C (right) NMR spectra (in CD_3OD) of compound **49**.

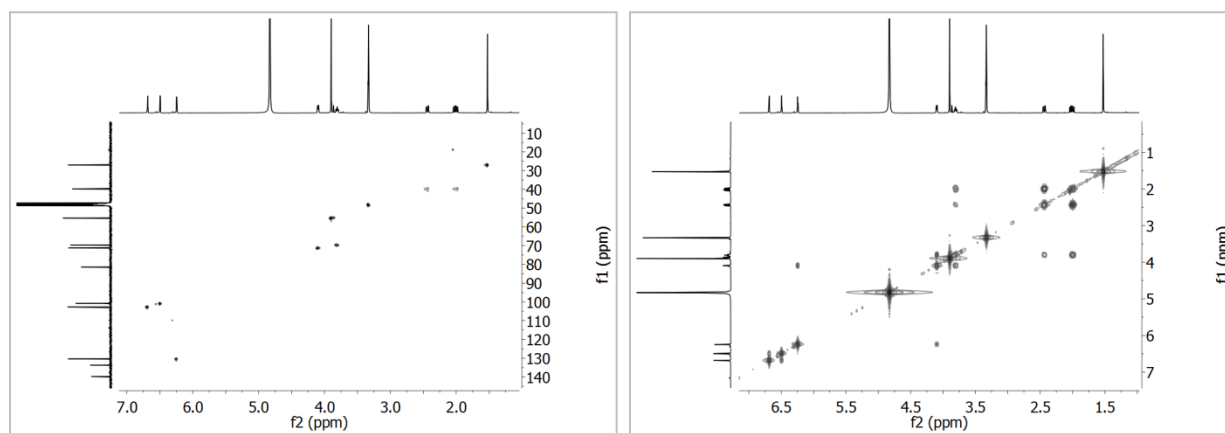


Figure 4.4.2.3 HSQC (left) and ^1H - ^1H COSY (right) spectra (in CD_3OD) of **49**.

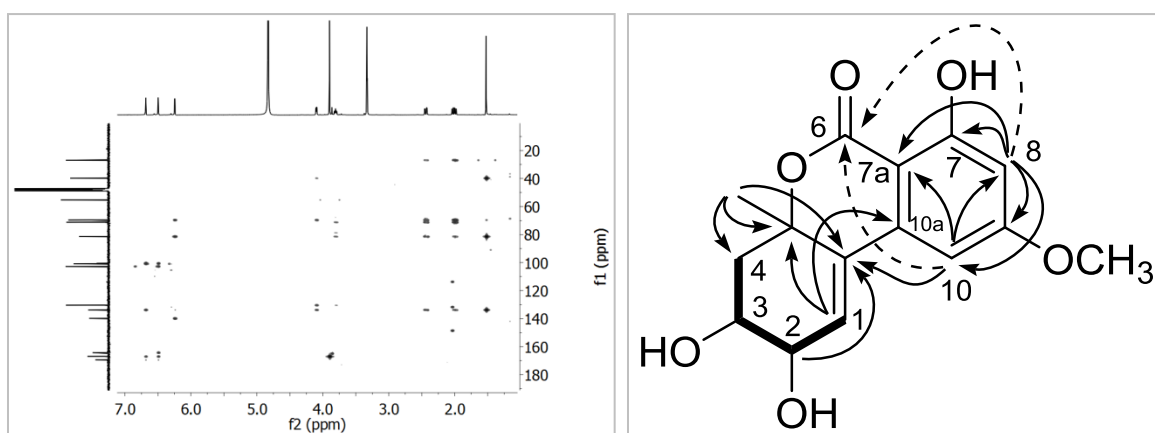


Figure 4.4.2.4 HMBC spectrum (left, in CD_3OD), and key ^1H - ^1H COSY and HMBC correlations of **49**.

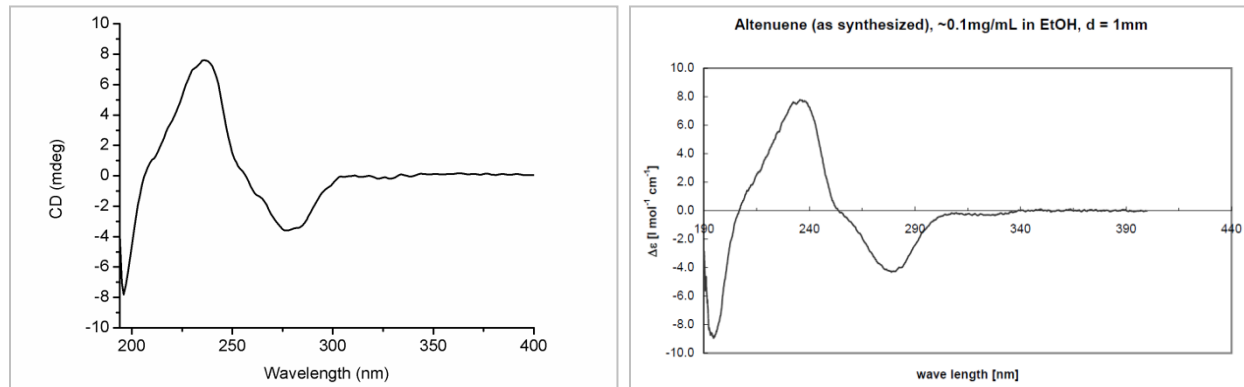
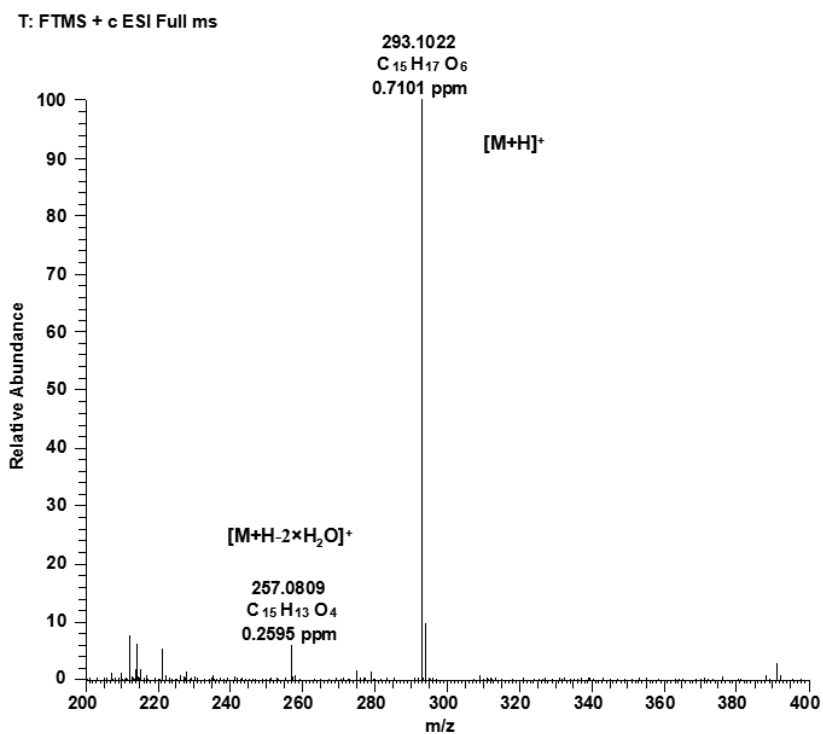


Figure 4.4.2.5 CD spectra for the natural (left) and synthesized (right, Altemöller *et al.*, 2006) **49**.



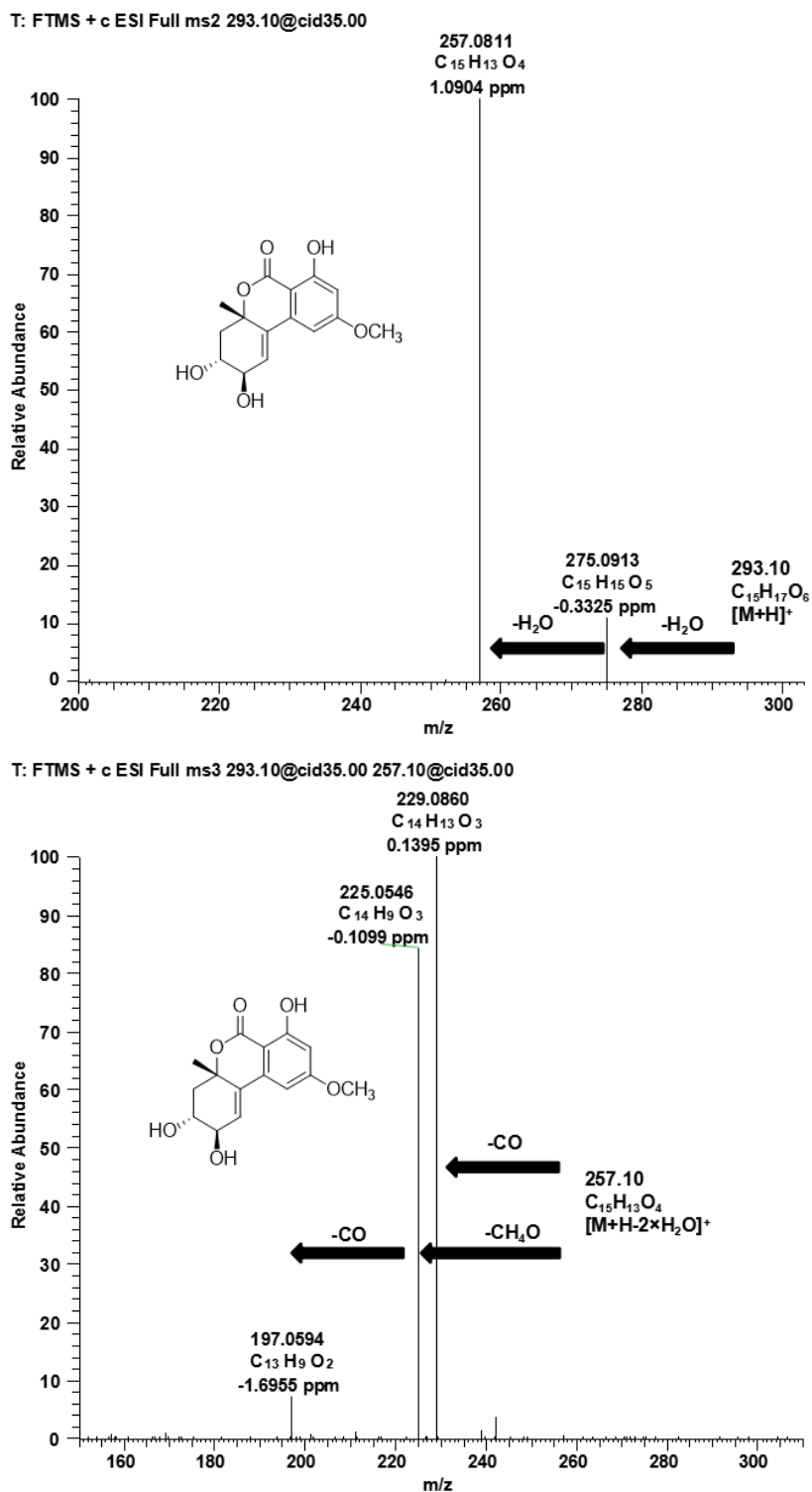


Figure 4.4.3.1 Positive ESI-HRMS (top), MS² (medium) and MS³ (bottom) spectra of compound 50.

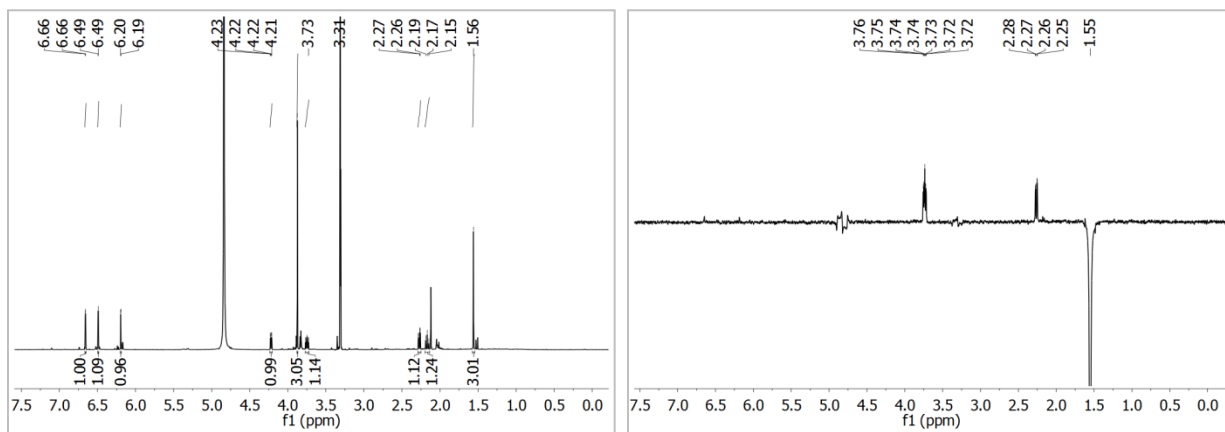


Figure 4.4.3.2 ¹H (left) and 1D NOESY spectra (right, in CD₃OD) of compound 50.

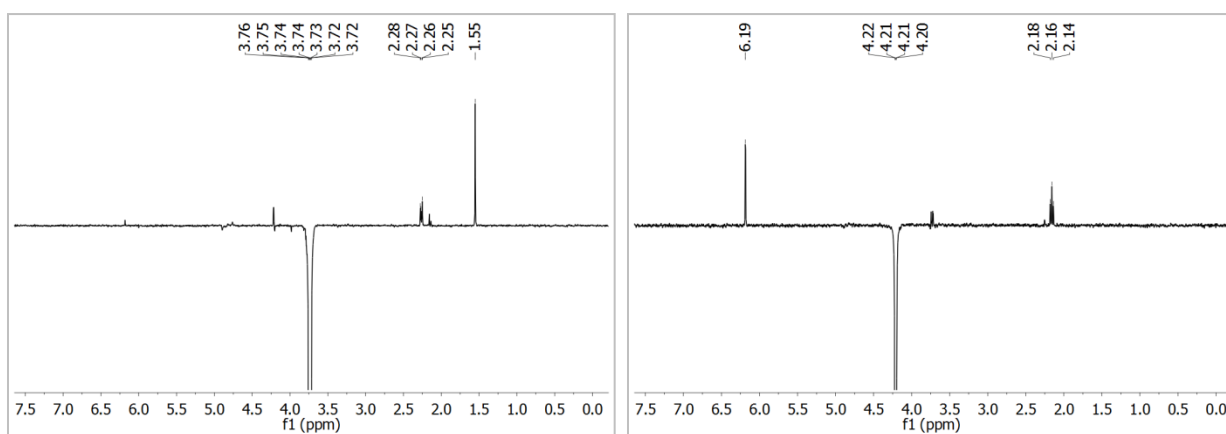


Figure 4.4.3.3 1D NOESY spectra (in CD₃OD) of compound 50.

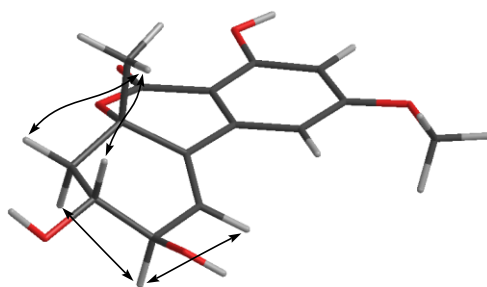


Figure 4.4.3.4 Key NOE correlations of compound 50.

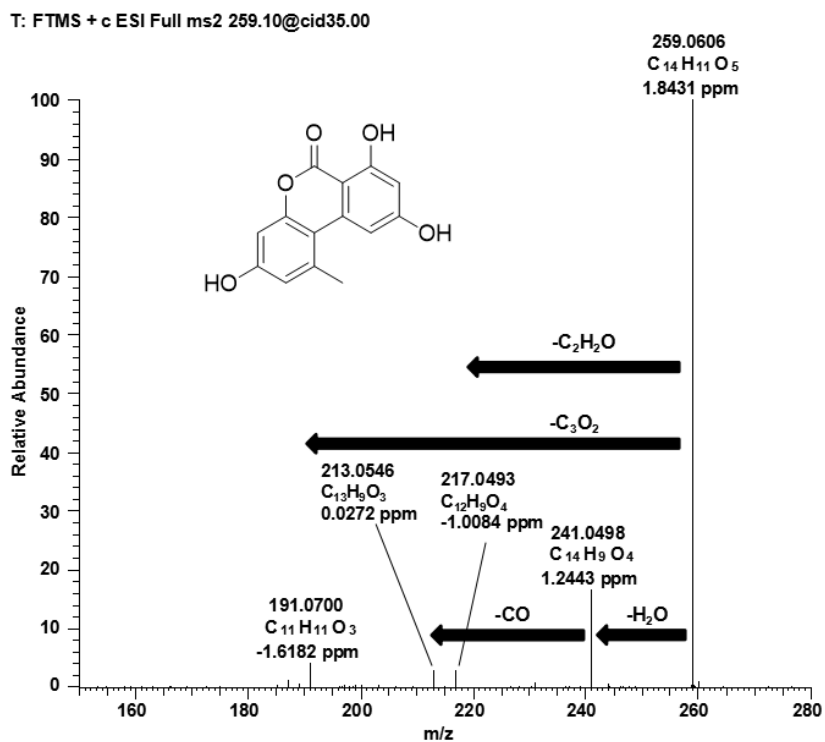
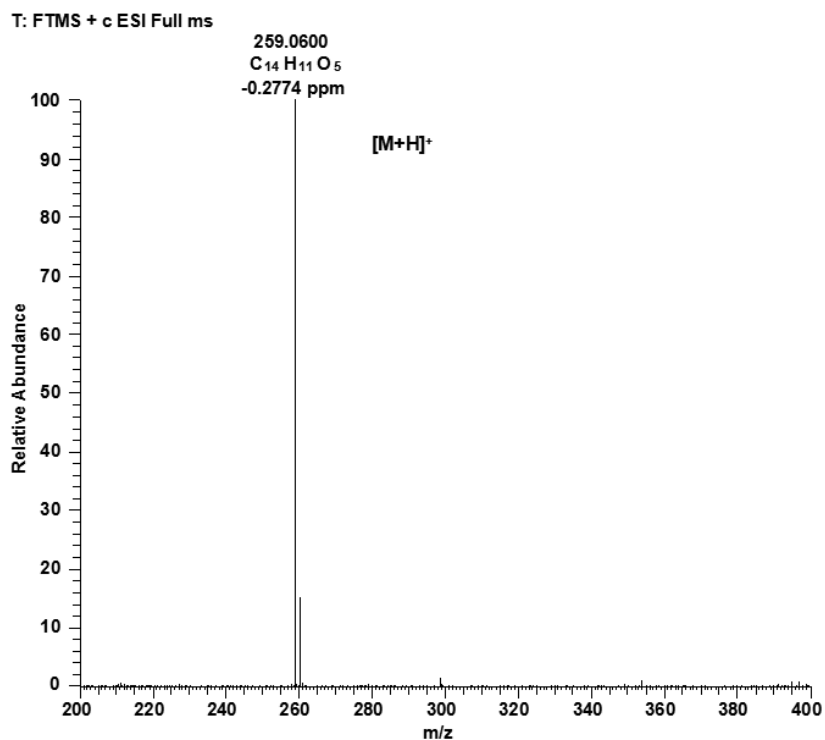


Figure 4.4.4.1 Positive ESI-HRMS (top) and MS/MS (bottom) spectra of compound 51.

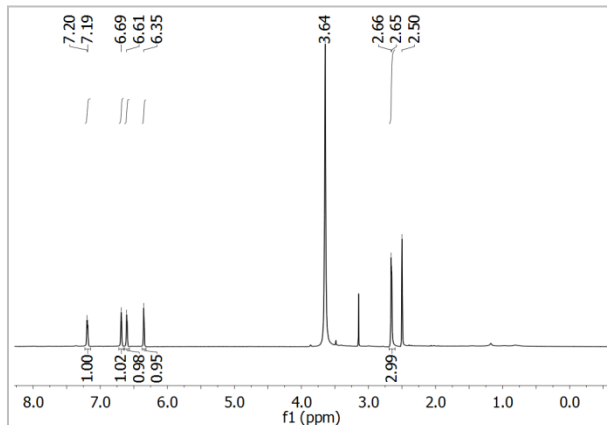
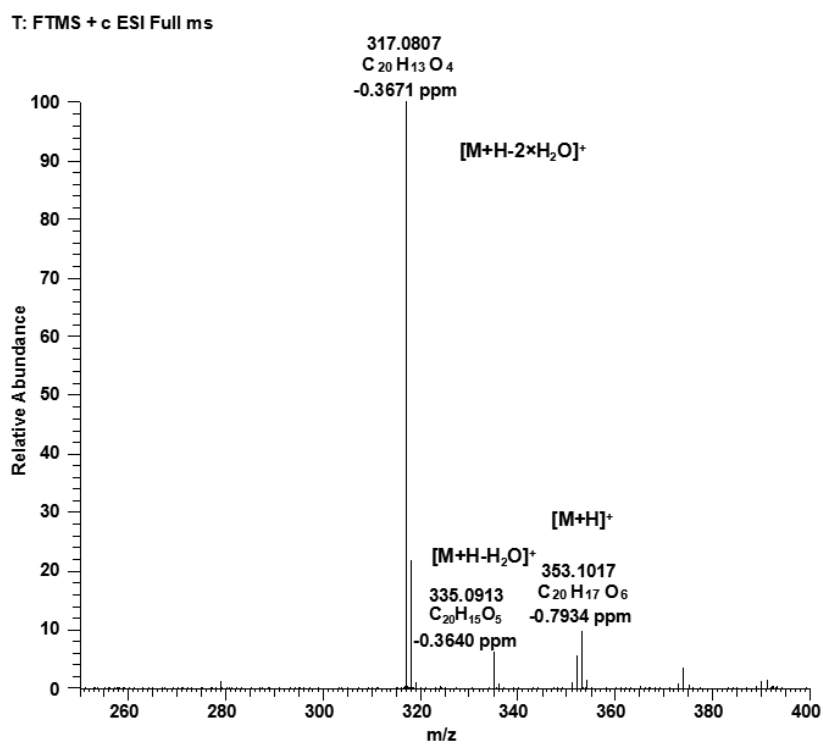


Figure 4.4.4.2 ^1H NMR spectrum (in $\text{DMSO}-d_6$) of compound **51**.



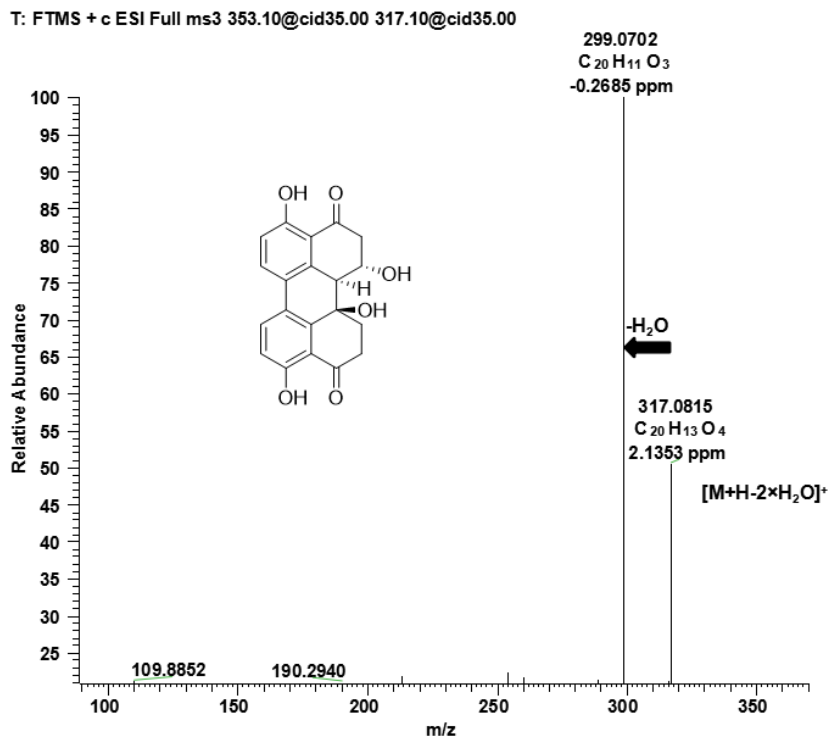


Figure 4.4.5.1 Positive ESI-HRMS (top) and MS³ (bottom) spectra of compound 52.

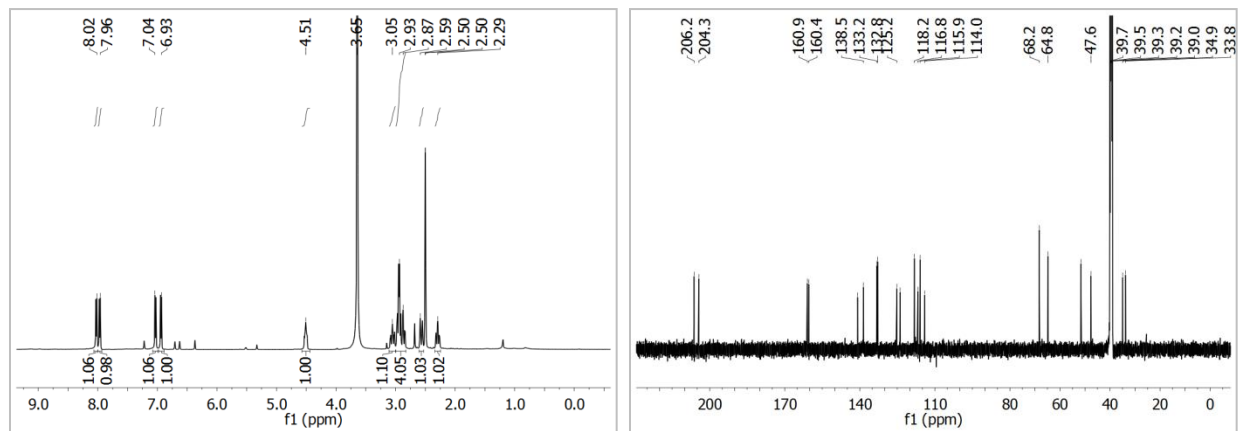


Figure 4.4.5.2 ¹H (left) and ¹³C (right) NMR spectra (in DMSO-*d*₆) of compound 52.

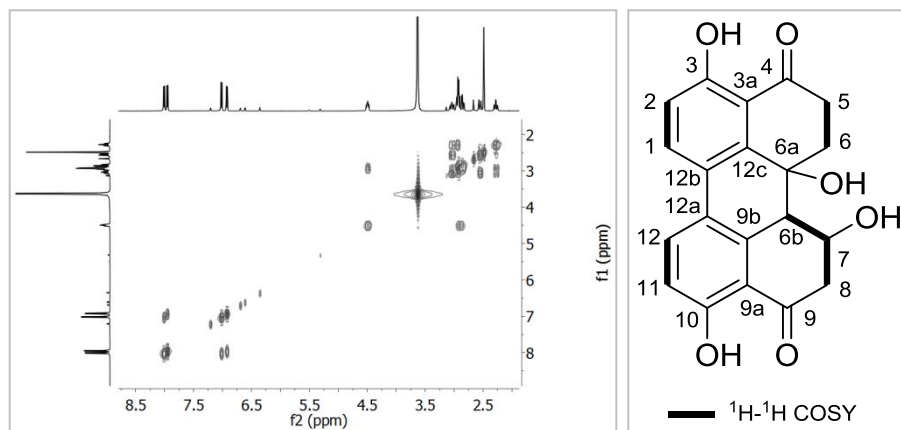


Figure 4.4.5.3 ^1H - ^1H COSY NMR spectrum (left) and ^1H - ^1H COSY correlations (right) of compound 52.

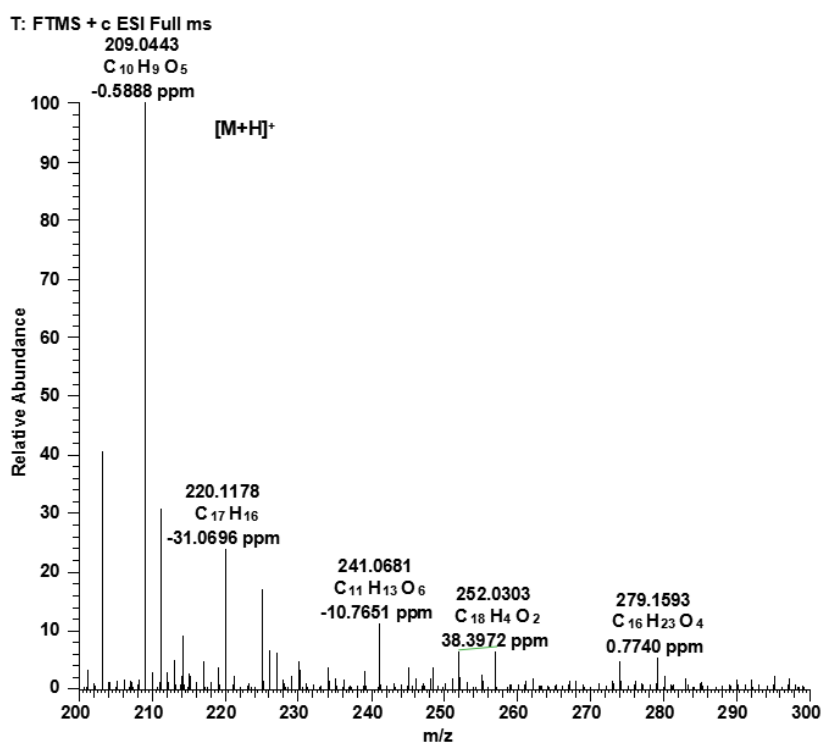


Figure 4.4.6.1 Positive ESI-HRMS spectrum of compound 53.

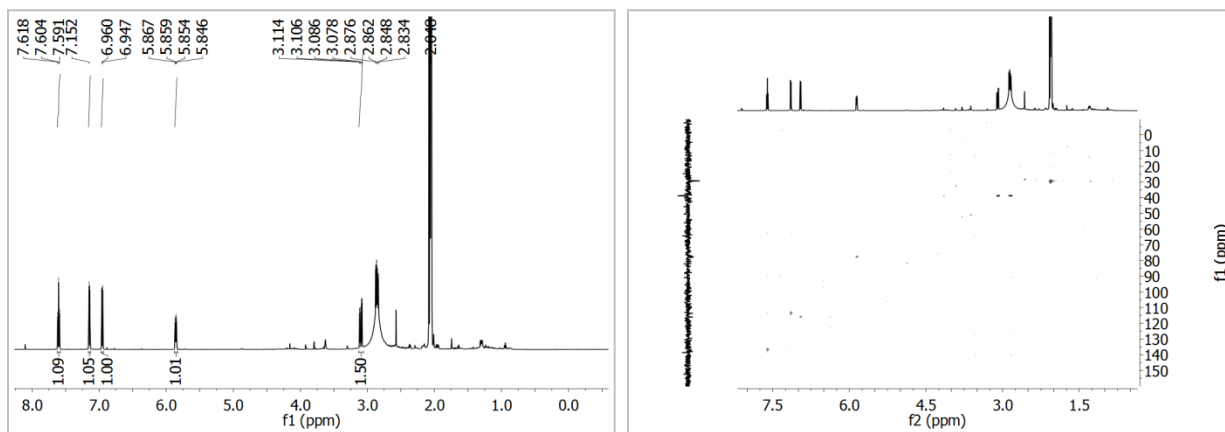


Figure 4.4.6.2 ^1H (left) and HSQC (right) NMR spectra (in acetone- d_6) of compound **53**.

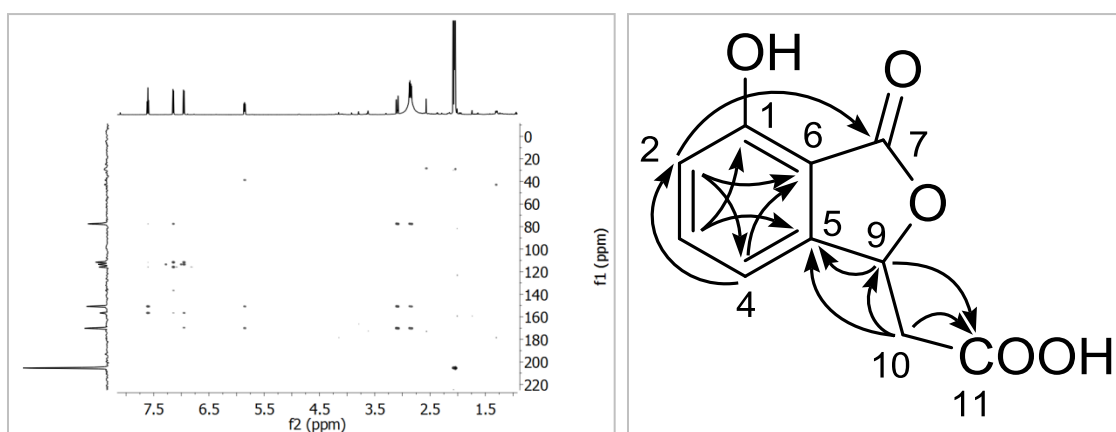


Figure 4.4.6.3 HMBC NMR spectrum (left, in acetone- d_6) and key HMBC correlations (right) of compound **53**.

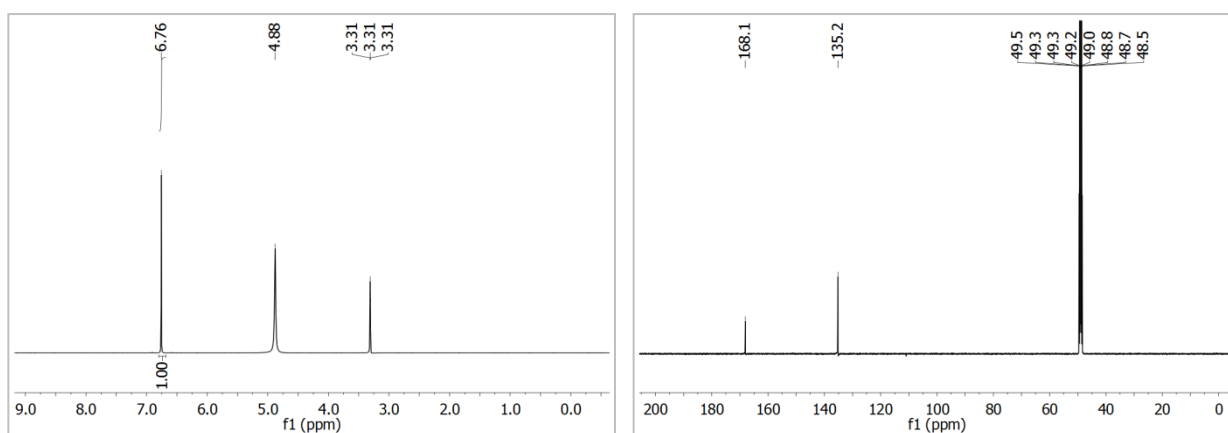


Figure 4.4.7.1 ^1H (left) and ^{13}C (right) NMR spectra (in CD_3OD) of compound **54**.

Appendix B
List of abbreviations

List of Abbreviations

Å	Angstrom
AMR	Antimicrobial resistance
APCI	Atmospheric pressure chemical ionization
bp	Base pairs
°C	Degree Celsius
CC	Column chromatography
CD	Circular dichroism
CDCl ₃	Deuterated chloroform
CD ₃ OD	Deuterated methanol
CHCl ₃	Chloroform
CH ₂ Cl ₂	Dichloromethane
CID	Collision induced dissociation
CLSI	Clinical and Laboratory Standards Institute
CoA	Coenzyme A
COSY	Correlation spectroscopy
DBU	1,8-diazabicyclo[5.4.0]undec-7-ene
DFT	Density functional theory
DMSO	Dimethyl sulfoxide
DMSO- <i>d</i> ₆	Deuterated dimethyl sulfoxide
DNA	Deoxyribonucleic acid
EtOAc	Ethyl acetate
EtOH	Ethanol
g	Gram
GAMESS	General atomic and molecular electronic structure system
GIAO	Gauge including atomic orbitals
HCl	Hydrogen chloride
HESI	Heated electrospray ionization
HMBC	Heteronuclear multiple bond correlation
H ₂ O	Water
HPLC	High performance liquid chromatography
H ₂ SO ₄	Sulfuric acid
HSQC	Heteronuclear single quantum correlation

Hz	Hertz
IR	Infrared spectra
ITS	Internal Transcript Spacer
kcal/mol	Kilocalorie per mole
K ₂ CO ₃	Potassium carbonate
L	Liter
LC-HRMS	Liquid chromatography-high resolution mass spectrometry
MALDI-imaging-HRMS	Matrix assisted laser desorption ionization imaging high-resolution mass spectrometry
MeOH	Methanol
Me ₂ SO ₄	Dimethyl sulfate
mg/mL	Milligram per milliliter
mg	Milligram
MIC	Minimum inhibitory concentration
min	Minute
mL	Milliliter
mm	Millimeter
MSTD	Multi-standard approach
<i>m/z</i>	Mass-to-charge ratio
NA	Nutrient agar
NaHCO ₃	Sodium bicarbonate
NB	Nutrient broth
NH ₃	Ammonia
nm	Nanometer
NMR	Nuclear magnetic resonance
NOESY	Nuclear overhauser enhancement spectroscopy
NP	Natural products
NRPS	Nonribosomal peptide synthetases
ORD	Optical rotatory dispersion
PCR	Polymerase chain reaction
PDA (HPLC)	Photodiode array
PDA	Potato dextrose agar
PDB	Potato dextrose broth
PKS	Polyketide synthase
rpm	Revolutions per minute
RP CC	Reversed-phase column chromatography

R _f	Retardation factor
s	Second
SA	Sabouraud dextrose agar
SAR	Structure-activity relationship(s)
SB	Sabouraud dextrose broth
SPE	Solid-phase extraction
TCM	Traditional Chinese Medicine
TDDFT	Time-dependent density functional theory
THP-1	Human acute monocytic leukemia cells
TLC	Thin layer chromatography
t _R	Retention time
μL	Microliter
μM	Micromolar
UV/vis	Ultraviolet/visible
V	Voltage
VDW	Van der Waals
v/v	Volume to volume
WA	Water agar
WHO	World Health Organization
ZOI	Zone of inhibition

Appendix C
Curriculum vitae

Curriculum Vitae

Personal information

Name: Gang Li
Date of birth: 27th, April, 1987
Gender: Male
Nationality: Chinese

Education

11.2012–2016

PhD thesis at Institute of Environmental Research (INFU), Department of Chemistry and Chemical Biology, Chair of Environmental Chemistry and Analytical Chemistry, TU Dortmund, Dortmund, Germany

09.2009–07.2012

Master in Pharmaceutical Engineering at Shandong University, Jinan, China.

09.2005–07.2009

Bachelor in Science of Chinese pharmacology, Shandong University of Traditional Chinese Medicine, Jinan, China.

Financial support

11.2015–04.2016

Wissenschaftliche Hilfskraft (WHK), TU Dortmund

11.2012–10.2015

PhD Scholarship from China Scholarship Council (CSC), Ministry of Education of China.